JET TRANSPORT PERFORMANCE METHODS

Jet Transport
Performance Methods

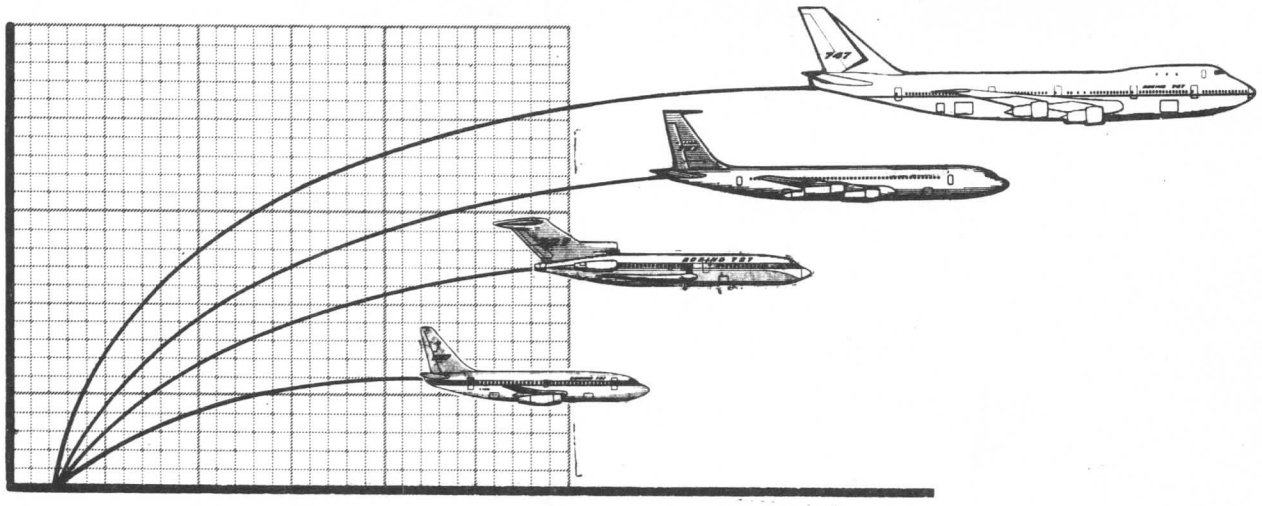

THE BOEING COMPANY
COMMERCIAL AIRPLANE GROUP
SEATTLE, WASHINGTON U.S.A.
BOEING DOCUMENT NO. D6-1420

SIXTH EDITION
MAY 1969

P R E F A C E

The purpose of this text is to provide a classroom training aid for performance courses conducted for airline customer personnel. The test contains an explanation of turbojet airplane performance methods and their application to jet-propelled aircraft. In addition, the text includes necessary background information for the specific operation and performance of Boeing jet transports.

JP-5 6.8 lb/gal 7,4805 gal/ft³ 50.87 lb/ft³

C O N T E N T S

C O N T E N T S

C O N T E N T S

C O N T E N T S

C O N T E N T S

C O N T E N T S

Airspeed Calculations (Cont'd.)

The curves on Pages 26 through 33 deserve special mention since they link V_I to M_I, V_{IN} to M_{IN}, and V_c to M_T. Actually the chart is calculated on the basis of V_c and M_T; however, for a given installation the static source pressure error is reflected in both V_{IN} and M_{IN} in proportion. Therefore, the chart gives the exact relationship between these two parameters. However, since the instrument error of the airspeed indicator and of the Machmeter are not the same, the chart will only give the approximate corresponding value. The instrument errors of standard instruments are rather small and for most practical work the chart is sufficient for converting V_I directly to M_I.

$$M_T = \left[5\left(\left[\left((.2\left(V_c/661.475\right)^2+1\right)^{3.5}-1\right)/\delta+1\right]^{.28571429}-1\right)\right]^{0,5}$$

$$V_{CAS} = \left[\left(\delta\left(\left(1+.2M_T^2\right)^{3.5}-1\right)+1\right)^{.28571429}-1\right]^{0,5} 661.475 \left(\sqrt{5}\right)$$

2,2361

VLTR:

1033 R1

It should be noted that 661.475 (KTAS) is the Standard Day/sea level speed of sound and may be denoted as A_0.

Expressions for dynamic pressure, q, are:

$$q = \frac{V_T^2 \sigma}{295.374}$$

and

$$q = 1481.34 \delta M_T^2$$

The first expression for dynamic pressure utilizes the following unit conversion:

1 knot = 1.6878 feet/second

The acceleration factor to account for climbout speeds other than constant values of true airspeed, i.e. $\frac{dV_T}{dh}$ is a non-zero value, is defined as:

$$f_{acc} \equiv 1 + \frac{V_T}{g} \frac{dV_T}{dh}$$

where g = sea level, gravitational acceleration, 32.17405 ft/second^2

The above f_{acc} factor is dependent upon the speed schedule (calibrated airspeed/Mach) and the crossover attitude.

Crossover attitude is defined as the pressure attitude at which the climb calibrated airspeed is equal to the climb Mach number and is determined from the following equation:

$$h_{crossover} = \frac{1 - \left\{ \frac{\left[1 + 0.2\left(\frac{V_c}{661.475}\right)^2\right]^{-1}}{\left[1 + 0.2 M_T^2\right]^{3.5} - 1} \right\}^{\frac{1}{5.2561}}}{6.87535 \times 10^{-6}}$$

For constant climbout calibrated airspeed below the crossover attitude values the expression for f_{acc} may be derived into a more convenient, Mach number dependent form:

$$f_{acc} = 1 + \left[(-0.2142018 M_T + 0.65667144) M_T - 0.01405534\right] M_T$$

INTRODUCTION

0-1 HISTORY AND DEVELOPMENT

In May, 1954, a new airplane was rolled out of the Renton, Washington plant. This airplane, the prototype of America's first jet transport, was an investment of the Boeing Airplane Company, and represented the company's re-entry into the field of commercial aviation. For a decade production strength was being poured into the national defense effort. Now there appeared a place on the production line for other than military aircraft.

The decision to offer a jet transport to the nation's airlines was not a new idea. Early design studies were begun in 1946 and carried on through the years. The success of the B-47 bomber instilled even more confidence in the undertaking. In late 1947 and in 1948 an appreciable amount of preliminary work was done on a commercial jet transport configuration. This was largely directed toward an investigation of the possible economics of the configuration to see if such a transport would be commercially feasible. Very little drawing board design work was attempted and the characteristics assumed for the studies were taken directly from the contempory swept wing bomber investigations. Work accomplished during 1947 and subsequent years in some cases was placed under the designation of Model 473. Some designs proposed in this era were the 473-12, 473-14, 473-19, and 473-29 models.

By mid-1949 it had become apparent that neither Boeing nor the potential users possessed sufficient knowledge of the factors which would be involved in a jet operation. Consequently, Boeing undertook a comprehensive study, based upon the performance of a hypothetical airplane. Included were not merely takeoff and landing distances and cruising speeds, but the entire picture of jet transport operation. The airplane upon which the study was based was powered by four engines having characteristics somewhat similar to those of the military J-57 engine manufactured by Pratt & Whitney aircraft. It had a wing area of 2500 square feet with a sweepback of 35 degrees, with aerodynamic characteristics similar to those of the B-52. This study constituted by far the most thoroughly-filled package of jet-transport information assembled by anyone to that time.

So favorable was the reaction of potential customers that a small project was organized to begin actual design and wind tunnel work. The most significant result was a 1950 design called the 473-60. It was similar to the airplane of earlier performance work except that it had a slightly smaller wing of 2300 square feet. The wing characteristics were virtually identical to those of the B-52. The landing gear was a tricycle type having all three gears supported in the body, resulting in a very narrow tread. The "60" was proposed in two versions: a domestic model weighing 135,000 pounds, and a transocean model offered in weights up to 180,000 pounds. A wind tunnel model was made and a full aerodynamic study carried out. In the process, it appeared that improvements should be made in certain areas, particularly the landing gear.

While the Model 473-60 study was underway, considerable preliminary design and aerodynamic work was being done on improvements to the C-97 configuration. A variety of engines were investigated including advanced versions of the Pratt and Whitney R-4360 and turboprop installations. Two of the designs that appeared on the drawing board prior to 1950 were the 367-14 and the 367-22. These models retained the then current C-97 wing and landing gear features but incorporated various engine changes. The improvements were not as great as anticipated, and the designs undertook further change.

By 1950 a configuration was proposed which was expected to remedy some of the problems encountered in attempting to improve the C-97. The model was designated 367-60 and was powered by four turboprop engines. It was characterized by a gulled-wing designed to lower the floor and to provide propeller clearance. Sweepback was beginning to look profitable and an 18 degree sweep was selected for this model. However, progress of the turboprop engine development was disappointing and serious consideration was given to the turbojet engine.

Late in 1950 work was begun on Model 367-64, a design based around a C-97 body, four jet engines and a new landing gear. The wing had an area of 2500 square feet and 25 degrees of sweepback. The increased sweep was found to give more desirable Mach number characteristics. A great deal of effort went into this design. The amount of wind tunnel testing that was done was more than many high speed airplanes have had prior to first flight. Although this design, commonly known as the "Advanced C-97," was a good airplane, it became evident by late summer of 1951 that it would not be sold. All was not lost, for the vast fund of knowledge gained from turboprop and turbojet investigations brought about a better understanding of design and operational requirements of a jet transport. The landing gear problem, which had been difficult in earlier designs had been worked out on the 367-64. In other ways, including body shape, development work on the "64" pointed to further improvements.

For example, the fuel capacity of the 367-64 was less than desired. This was partially due to the fact that the wing had been severely thinned in order to achieve Mach number objectives. In addition, the thinning had produced a wing that would be difficult to fabricate from a manufacturing standpoint. To adjust these factors, a new wing was laid out which was thicker and had a 35-degree angle of sweepback. Even here, previous efforts were not lost, as the wing was essentially the "64" wing rotated an additional 10 degrees about the root. The result of the additional sweep reduced the span from 140 feet to 130 feet but maintained the gross area at 2500 square feet, including an inboard trailing edge extension which faired the landing gear. It is this wing, with refinements to airfoil sections and trailing edge extension which is on todays 707 prototype.

Many of the drawings made at the end of 1951 were now being labeled Model 707, as they were the products of joint efforts to incorporate the work of the past months into a saleable article. It appeared also that a demonstration airplane was required to convince potential customers of the advantages of jet transportation to a degree sufficient to warrant their large investment in new equipment. Models 707-5 and 707-6 evolved to a point where a decision to build a prototype airplane was forthcoming. In May 1952, work was begun although for economic reasons the model number was changed from 707 to 367-80. It was desired also to keep the prototype light in weight and simple in design and operation. During the course of the design, a number of changes were made. The most significant of these was the change from dual engine pods to four single pods. Subsequent attempts to enlarge the body cross-section were discontinued in favor of making the change on production models.

The models discussed herein are but a few of the 150 "paper" airplanes that make up the ancestral lines of the 707. The years of research, investigation, and production ingenuity culminated on July 15, 1954 when the 367-80 prototype made the historic first flight from Renton Airport. Landing was made at Seattle, Boeing Field, after a flight of one hour and 24 minutes.

Two versions of the production 707 airplane exist: the "Stratoliner," and the "Intercontinental." The Stratoliner airplane was designed to serve the longer domestic and most intercontinental routes and has a range capability of over 3,500 nautical miles. The Intercontinental was designed to carry a 40,000 pound payload over 5,000 nautical miles. There are variations within the models and series depending upon the requirements of the customers.

Following closely on the heels of the family of 707 airplanes is the medium range Model 720. Although similar to its predecessor in appearance, it is a completely new design from a weight and structural strength viewpoint. Variations of Model 720 exist largely due to the type of power plant equipment used. The development of a turbofan engine with its higher thrust ratings and vastly improved specific fuel consumption makes the Model 720 an attractive package.

Another addition to the family of Boeing airplanes is the Model 727. It features the latest advances in jet engine technology and aerodynamics. Its smaller size and versatility provides low cost air transportation in the short-to-medium range class.

Over a period of 4 1/2 years, thousands of details and design features were studied for feasibility and checked out against specific airline objectives. Having detailed and tested a total of 68 complete airplane designs, the final form of the 727 was established. The Model 727 differs noticeably in appearance from its predecessors, in that it is equipped with three turbofan engines and a dominating empennage section. Two of the three engines are mounted in pods at each side of the rear fuselage. The cowl-enclosed third engine is suspended from a beam at the rear of the fuselage, with the air intake located at the base of the vertical fin. The engine location dictated the design of tail, such that the horizontal stabilizer is attached to the top of the fin structure. The vertical stabilizer is swept sharply aft to give the control surfaces maximum effect for minimum size and weight.

A high degree of "commonness" has been preserved in the 707/720 and the 727 airplanes. Any changes in the systems were made only on the basis of improvements possibly due to experience and to advances in the state of technology, or due to the aircraft's intended short-haul, minimum ground time use.

Low speed performance is built into the wing by means of high-lift devices. These consist of triple-slotted trailing-edge flaps and leading-edge flaps and slats. The 727 uses dual hydraulic packages to power the primary flight controls throughout complete surfact travel. Elevators and ailerons are aerodynamically balanced to allow manual operation. The rudder has a third hydraulic system available for backup purposes.

To reduce the turn-around time and make the airplane as self-sufficient as possible an aft airstair is installed as an integral part of the fuselage. In addition, a forward airstair can be installed at the option of the customer. To provide electric and pneumatic power for ground operation an airborne auxiliary power unit can be installed in the wheel well.

Advanced high-lift devices enable the 727 to operate at full payload (24,000 lbs.) from 5,000-foot runways. The 727 is capable of carrying 70 - 114 passengers at speeds up to 600 miles per hour over a distance ranging from 150 to 1,700 miles.

INTRODUCTION

The most recent addition to the family of Boeing airplanes is the Model 737. The 737 offers the public jet speed, comfort and convenience on routes as short as 100 miles. The 737 is designed to operate over short-to-medium ranges, at cruise speeds up to 580 m.p.h., from sea level runways under 5,000 feet in length. The 737 design draws heavily from its companion aircraft, the 727. Commonness between the two airplanes is apparent in the 737's wide body structure, identical doors, sidepanels, ceilings, seats, and engines.

The 737 is equipped with two wing-mounted turbofan engines, tucked close under the wing. This location gives "eye-level" engine accessibility and improved structural efficiency. The engines are located near the center of gravity which increases loading flexibility and located far enough outboard to clear a water or slush spray pattern from the nose gear.

Low speed performance is built into the wing by means of high-lift flaps that are similar to the 727 flaps; triple-slotted trailing-edge flaps, leading edge slats outboard of the engine nacelles, and Krueger-type leading-edge flaps inboard of the engine nacelles. The 737 operates at the lowest approach speed of any jet transport and exhibits excellent speed stability.

Passenger enplaning and deplaning from the 737 is provided with two entry door positioned forward and aft on the left side of the passenger cabin. All entry and service doors are of plug-type design. Two emergency exits are centrally positioned in the passenger compartment with access to the wing.

The auxiliary power unit (APU) with built-in sound suppressors installed in the tail end of the fuselage supplies electrical energy and air for engine starting and air conditioning on the ground. In flight, the APU provides air-conditioning air or electrical power in the event of an engine shutdown. To reduce the turn-around time, airstairs carried directly under the forward entry door eliminate the need for airport stairways. One novel feature is the landing gear. The main landing gear wheel wells have no separately powered doors. The wheels in their retracted position form an effective wheel-well seal. All main landing gear parts are identical for left and right hand gear, thus cutting spares inventory in half.

Fully certified 737's are scheduled for delivery beginning in late 1967.

Another recent addition to the growing family of Boeing airplanes is the Model 747 airplane. The airplane is a standard four-engine, land based, low wing passenger airplane designed for commercial transportation of passengers, but incorporating certain built-in primary structural provisions for modification to an all cargo configuration. The wide body allows ten abreast passenger seating or side by side arrangement of 8 foot cross section cargo containers in the body constant section.

The 747 has a high long-range cruise speed, and will transport a 124,000 pound payload (490 economy passengers plus baggage), approximately 4,000 nautical miles. It is designed for a maximum taxi gross weight of 683,000 pounds, and a maximum landing weight of 564,000 pounds. The landing gear, avionic equipment, and high-lift flap systems allow automatic approach to touchdown of the 747 to existing airfields with 707-300B capability. Propulsion is supplied by four newly developed, high bypass ratio turbofan engines of 42,000 pounds thrust per engine.

High efficiency primary and secondary air flow thrust reversers are installed. Variable area inlets, similar to the 300B, are used. Air for starting is supplied by either an APU, another engine, or an external air cart. Fuel is carried in integral wing tanks. Manifolded pressure refueling points are provided under each wing for pressure fueling. Overwing filler ports are provided for gravity fueling.

Powered flight controls are used for rudder, ailerons and elevators. Dual automatic flight control systems are installed.

Electrical, low pressure pneumatic and hydraulic secondary power is used. These systems have multiple power sources for high reliability. A gas turbine APU supplies all ground power requirements for ground operations and maintenance functions. The communications and navigation installations are similar to those used on the 707 type airplanes. Flight crew and passenger compartments are air conditioned and pressurized by multiple isolated air conditioning systems using air bleed from the four engines. Emergency oxygen is supplied at all passenger and crew locations. Cabin air is used for electronic equipment cooling.

Lower hold cargo volume, using containers, is approximately 5200 cubic feet. An additional 1000 cubic feet of bulk volume is available.

The flight crew consists of a captain, first officer, and a flight engineer. The operational crew also includes 16 cabin attendants. The flight deck, located above the passenger level, has seating accommodations for a check pilot or observer and a second observer.

A typical passenger arrangement consists of 54 first class passengers, 6 abreast at 42 inch pitch, 308 economy class passengers, 9 abreast at 34 inch pitch and an 8 place lounge.

0-2 PRINCIPAL DIMENSIONS

Specification information and principal dimension data for the family of 707, 720, 727, 737 and 747 airplanes follow.

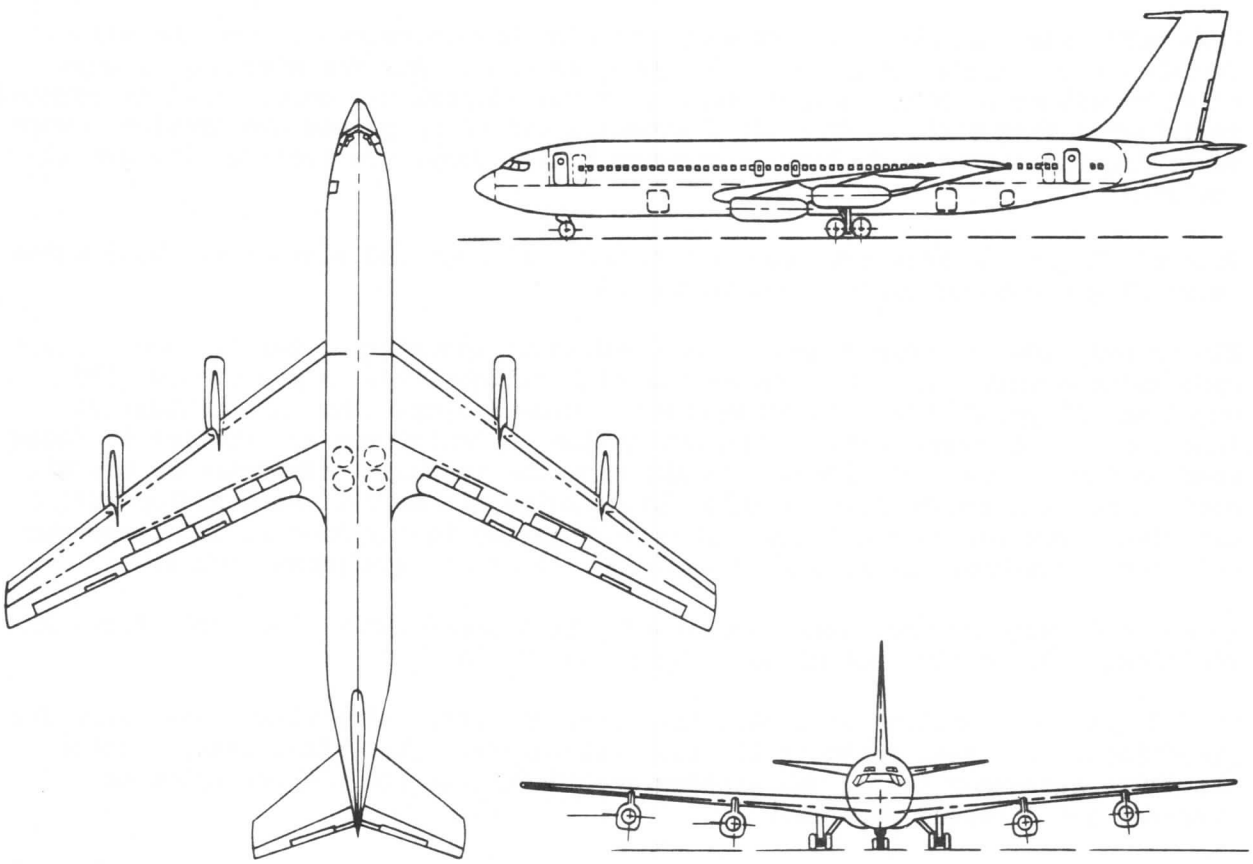

707-100 SERIES
PRINCIPAL DIMENSIONS

WING

Area	2433 Sq. Ft.
Span	130 Ft. 10 In.
Root Chord	338 In.
Tip Chord	112 In.
Taper Ratio	.342
Incidence Root	+2°
Incidence Tip	+2°
Dihedral	7°
Sweepback C/4	35°
Aspect Ratio	7.065
M.A.C.	241.88 In.
M.A.C. LOC.(Sta)	786.2

FLAP

Leading Edge Area	26.1 Sq. Ft.
Trailing Edge Area	361.65 Sq. Ft.

AILERON

Inboard Area	39.0 Sq. Ft.
Outboard Area	80.6 Sq. Ft.

HORIZONTAL TAIL

Stabilizer Area	382.7 Sq. Ft.
Elevator Area	117.6 Sq. Ft.
Span	39 Ft. 8.4 In.

VERTICAL TAIL

Dorsal Area	8.7 Sq. Ft.
Fin Area	226.4 Sq. Ft.
Rudder Area	101.9 Sq. Ft.
Ventral Fin Area	25.5 Sq. Ft.

BODY

Length	138 Ft. 10 In.

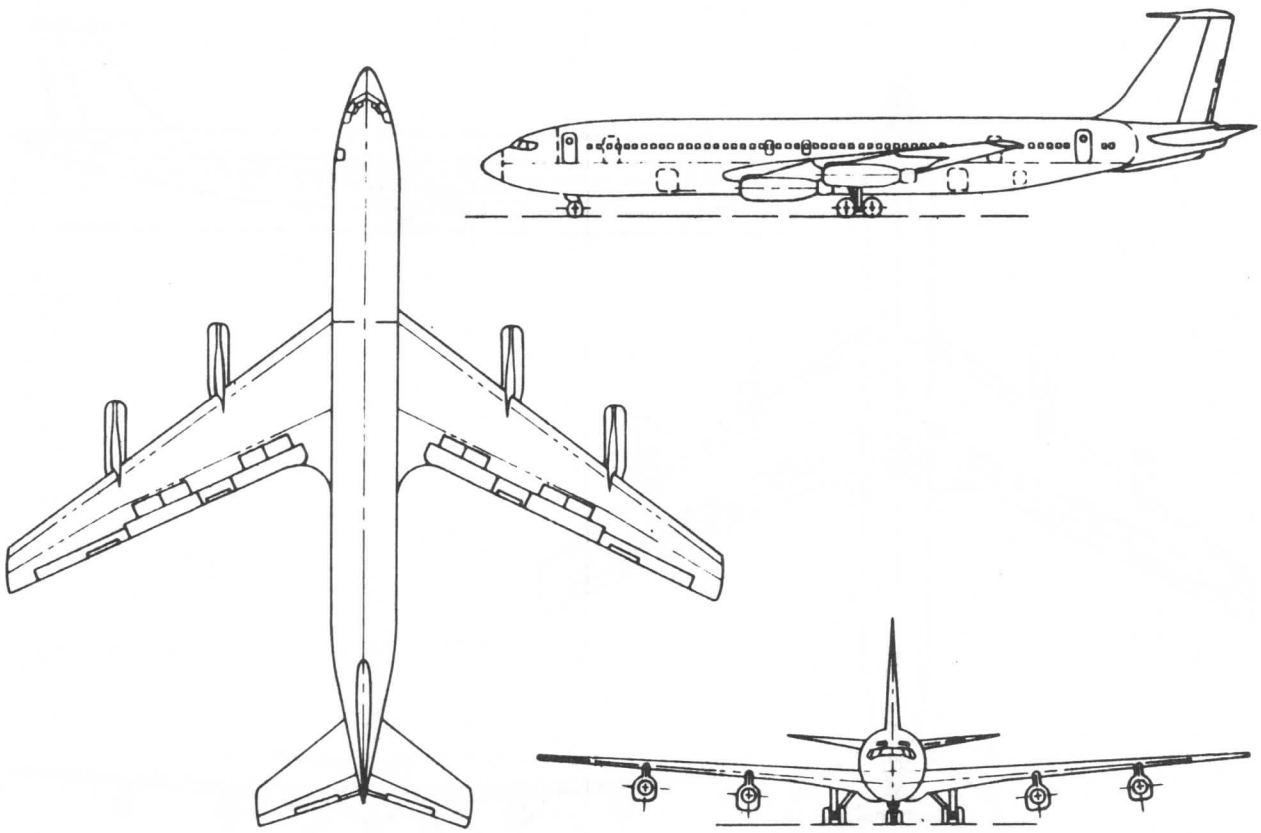

707-100B SERIES
PRINCIPAL DIMENSIONS

WING

Area	2433 Sq. Ft.
Span	130 Ft. 10 In.
Root Chord	338 In.
Tip Chord	112 In.
Taper Ratio	.342
Incidence at Root.	+2°
Incidence at Tip .	+2°
Dihedral	7°
Sweepback C/4	35°
Aspect Ratio	7.065
M.A.C.	241.88 In.
Leading Edge MAC .	Station 786.2

FLAP

Leading Edge Area	74.19 Sq. Ft.
Trailing Edge Area	361.65 Sq. Ft.

AILERON

Inboard Area	39.0 Sq. Ft.
Outboard Area	80.6 Sq. Ft.

HORIZONTAL TAIL

Stabilizer Area	427.7 Sq. Ft.
Elevator Area	117.6 Sq. Ft.
Span	43 Ft.

VERTICAL TAIL

Dorsal Area	8.7 Sq. Ft.
Fin Area	226.4 Sq. Ft.
Rudder Area	101.9 Sq. Ft.
Ventral Fin Area .	25.5 Sq. Ft.

BODY

Length	138 Ft. 10 In.
	or 128 Ft. 10 In.

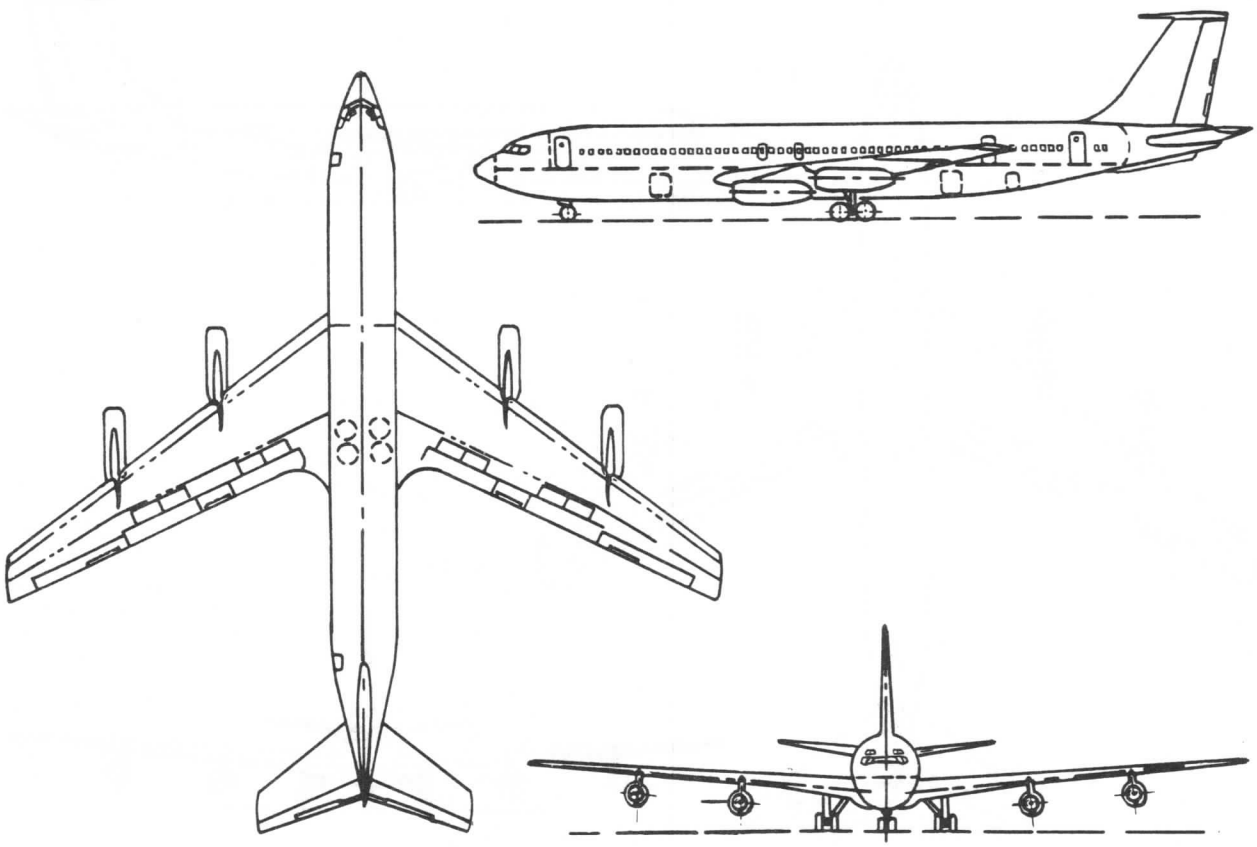

707-200 SERIES
PRINCIPAL DIMENSIONS

WING

Area	2433 Sq. Ft.
Span	130 Ft. 10 In.
Root Chord	338 In.
Tip Chord	112 In.
Taper Ratio	.342
Incidence Root	+2°
Incidence Tip	+2°
Dihedral	7°
Sweepback C/4	35°
Aspect Ratio	7.065
M.A.C.	241.88 In.
M.A.C. LOC.(Sta)	786.2

FLAP

Leading Edge Area	26.1 Sq. Ft.
Trailing Edge Area	361.65 Sq. Ft.

AILERON

Inboard Area	39.0 Sq. Ft.
Outboard Area	80.6 Sq. Ft.

HORIZONTAL TAIL

Stabilizer Area	382.7 Sq. Ft.
Elevator Area	117.6 Sq. Ft.
Span	39 Ft. 8.4 In.

VERTICAL TAIL

Dorsal Area	8.7 Sq. Ft.
Fin Area	226.4 Sq. Ft.
Rudder Area	101.9 Sq. Ft.
Ventral Fin Area	25.5 Sq. Ft.

BODY

Length	138 Ft. 10 In.

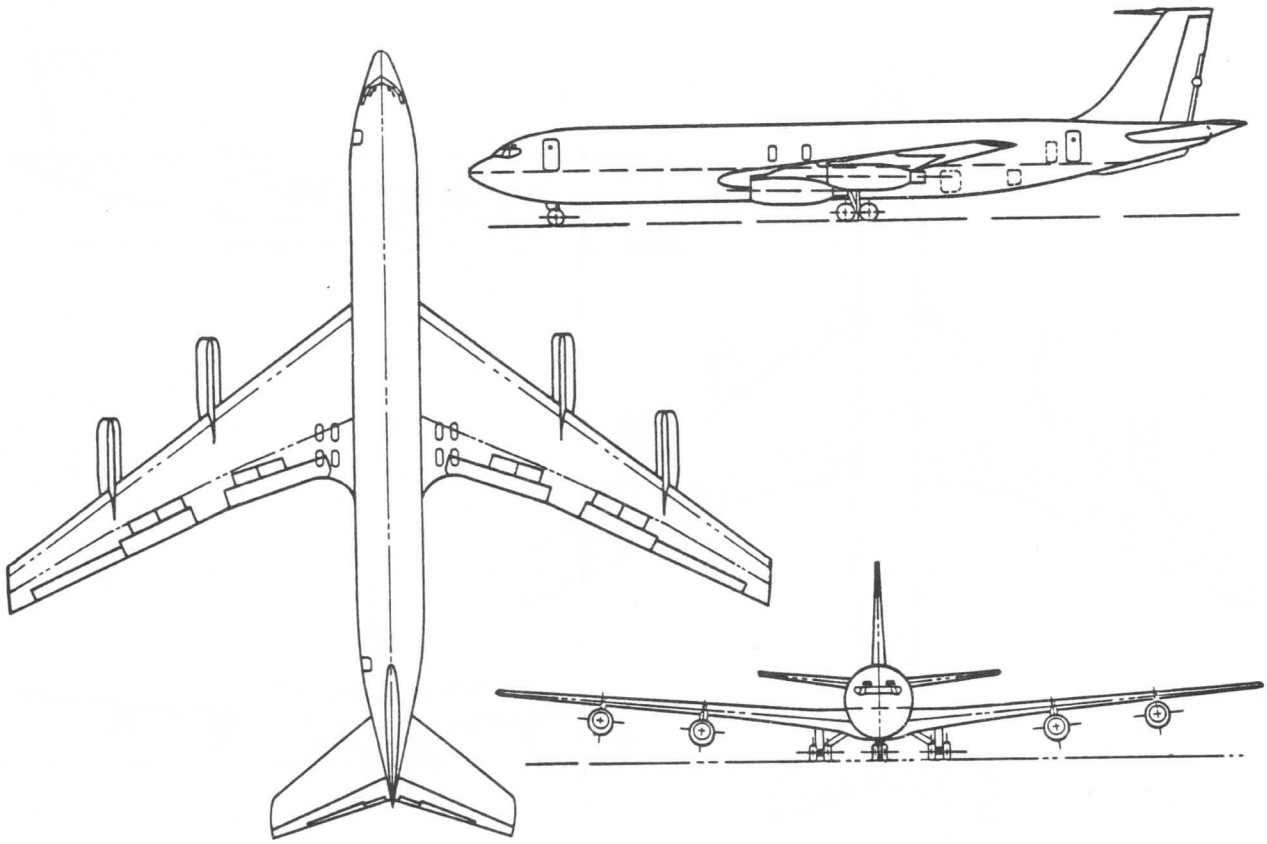

707-300 SERIES
PRINCIPAL DIMENSIONS

WING

Area	2892 Sq. Ft.
Span	142 Ft. 5 In
Basic Root Chord	406.7 In.
Reference Root Chord	347.1 In.
Tip Cord	112 In.
Taper Ratio	.275 (Basic) .323 (Ref.)
Incidence Root	+2°
Incidence Tip	+2°
Dihedral	7°
Sweepback C/4	35°
Aspect Ratio	7.056
M.A.C.	272.294 In.
M.A.C. LOC. (Sta)	762.97

FLAP

Leading Edge Area	26.1 Sq. Ft.
Trailing Edge Area	436.0 Sq. Ft.

AILERONS

Inboard Area	40.4 Sq. Ft.
Outboard Area	80.6 Sq. Ft.

HORIZONTAL TAIL

Stabilizer Area	474 Sq. Ft.
Elevator Area	151 Sq. Ft.
Span	45 Ft. 8 In.

VERTICAL TAIL

Dorsal Area	8.7 Sq. Ft.
Fin Area	226.4 Sq. Ft.
Rudder Area	101.9 Sq. Ft.
Ventral Fin Area	25.5 Sq. Ft.

BODY

Length	145 Ft. 6 In.

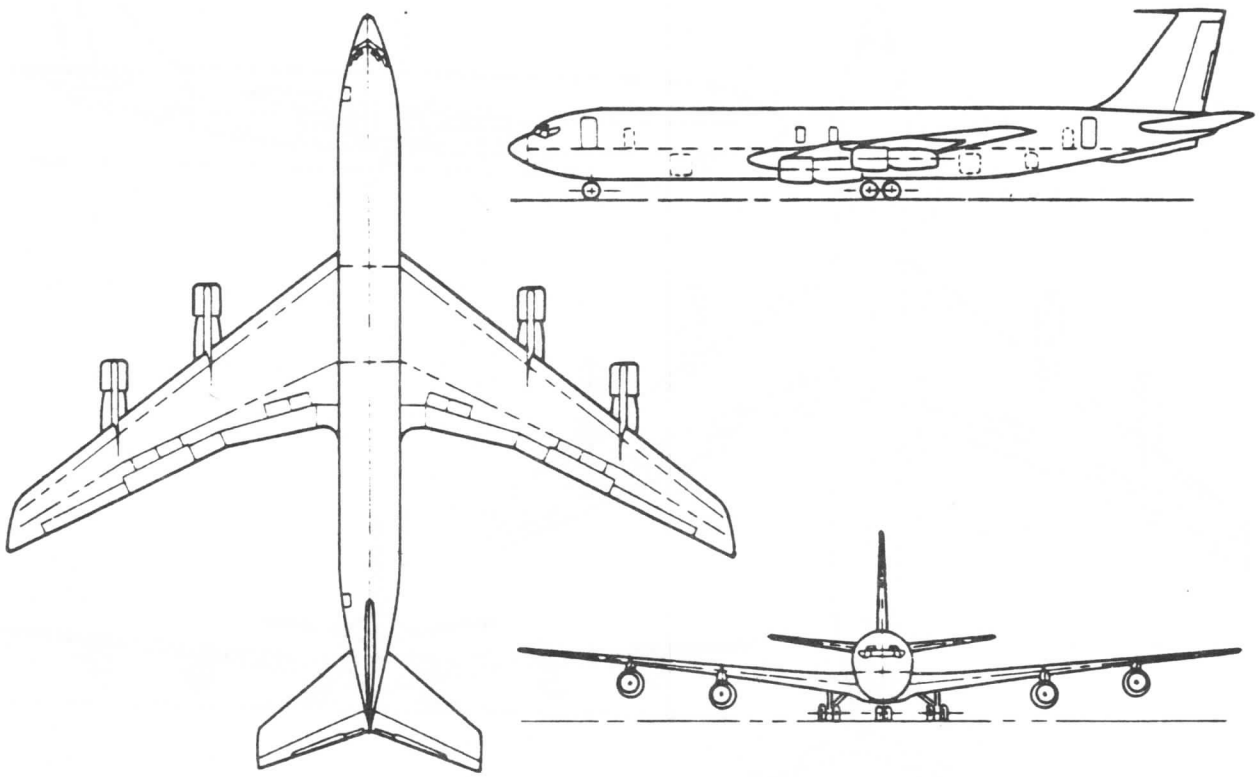

707-300B SERIES
PRINCIPAL DIMENSIONS

WING

Area	2892 Sq. Ft. *
Span	145 Ft. 9 In.
Basic Root Chord	406.682 In.
Ref. Root Chord	347.134 In.
Tip Chord	112 In.
Taper Ratio	.275 (Basic) .323 (Ref.)
Incidence at Root	+2°
Incidence at Tip	+2°
Dihedral	7°
Sweepback C/4	35°
Aspect Ratio	7.346
M.A.C.	272.294 In.
Leading Edge M.A.C.	Sta. 762.97

FLAP

Leading Edge Area	157.24 Sq. Ft.
Trailing Edge Area	491.72 Sq. Ft.

AILERON

Inboard Area	40.4 Sq. Ft.
Outboard Area	80.5 Sq. Ft.

HORIZONTAL TAIL

Stabilizer Area	474 Sq. Ft.
Elevator Area	151 Sq. Ft.
Span	45 Ft. 8 In.

VERTICAL TAIL

Dorsal Area	8.7 Sq. Ft.
Fin Area	226.4 Sq. Ft.
Rudder Area	101.9 Sq. Ft.
Ventral Fin Area	25.5 Sq. Ft.

BODY

Length	145 Ft. 6 In.

* (Excluding leading edge, trailing edge, and tip extensions.)

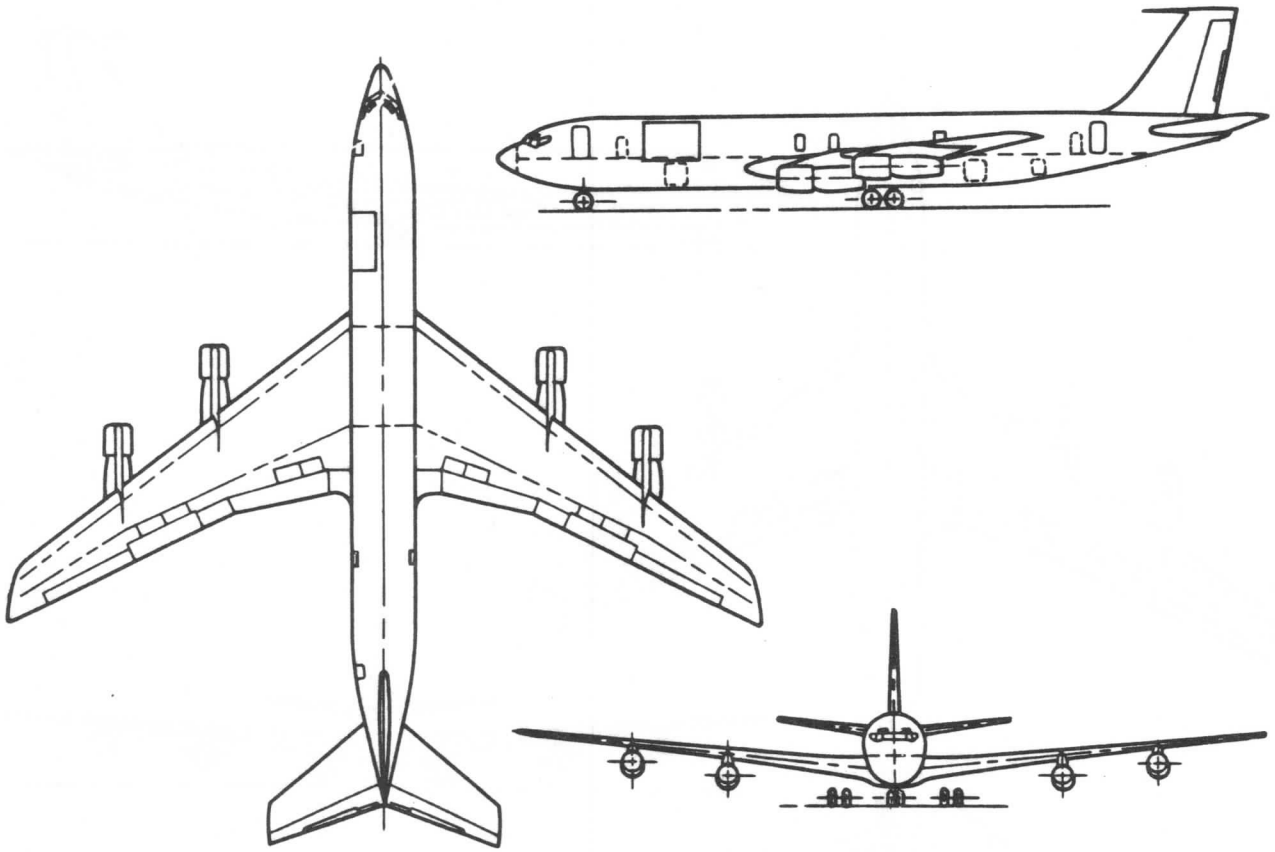

707-300ADV B and C SERIES
PRINCIPAL DIMENSIONS

WING

Area	2892 Sq. Ft. *
Span	145 Ft. 9 In.
Basic Root Chord	406.682 In.
Ref. Root Chord	347.134 In.
Tip Chord	112 In.
Taper Ratio	.275 (Basic)
	.323 (Ref.)
Incidence at Root	+2°
Incidence at Tip	+2°
Dihedral	7°
Sweepback C/4	35°
Aspect Ratio	7.346
M.A.C.	272.294 In.
Leading Edge M.A.C.	Sta. 762.97

FLAP

Leading Edge Area	197.88 Sq. Ft.
Trailing Edge Area	491.72 Sq. Ft.

AILERON

Inboard Area	40.4 Sq. Ft.
Outboard Area	80.5 Sq. Ft.

HORIZONTAL TAIL

Stabilizer Area	474 Sq. Ft.
Elevator Area	151 Sq. Ft.
Span	45 Ft. 8 In.

VERTICAL TAIL

Dorsal Area	8.7 Sq. Ft.
Fin Area	226.4 Sq. Ft.
Rudder Area	101.9 Sq. Ft.

BODY

Length	145 Ft. 6 In.

* (Excluding leading edge, trailing edge, and tip extensions.)

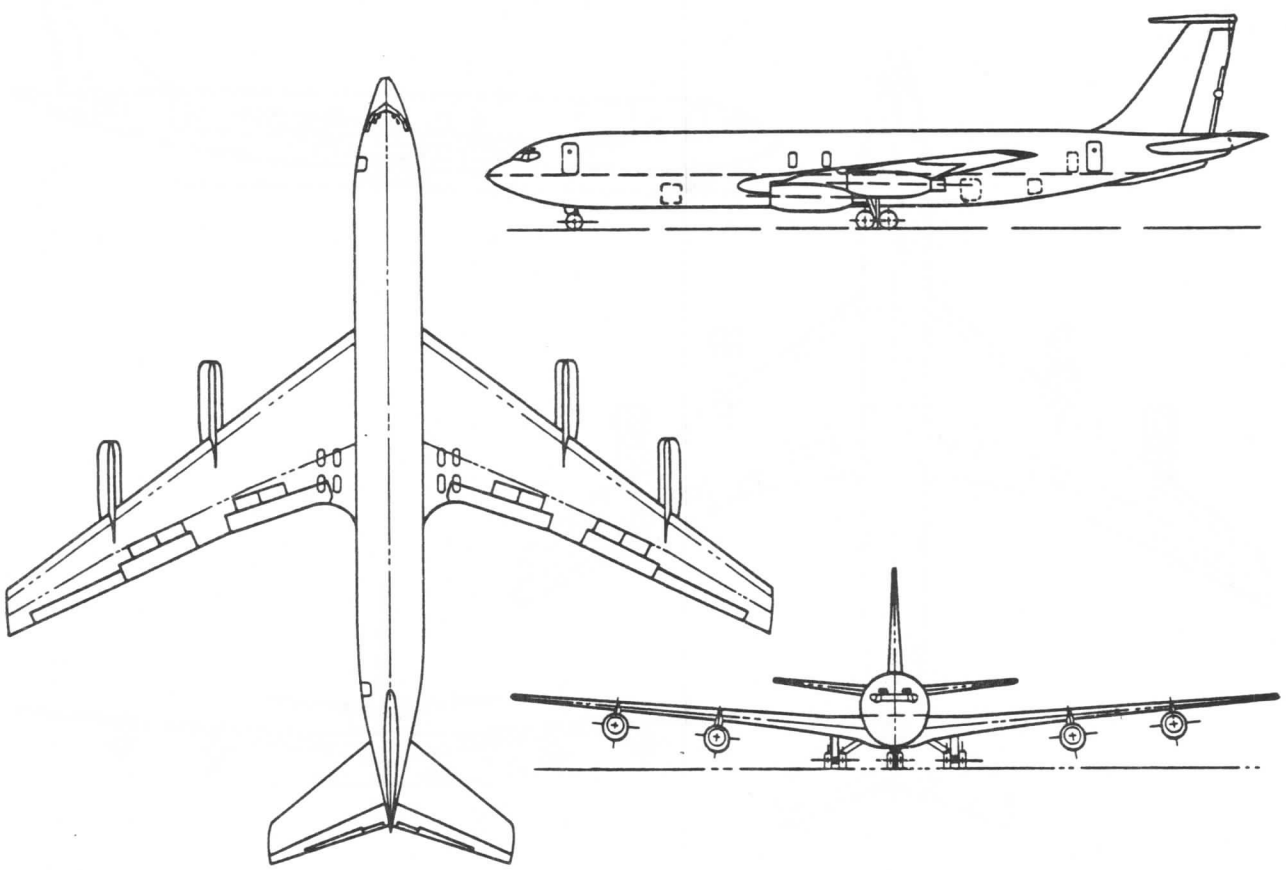

707-400 SERIES
PRINCIPAL DIMENSIONS

WING

Area	2892 Sq. Ft.
Span	142 Ft. 5 In.
Basic Root Chord	406.7 In.
Reference Root Chord	347.1 In.
Tip Chord	112 In.
Taper Ratio	.275 (Basic)
	.323 (Ref.)
Incidence Root	+2°
Incidence Tip	+2°
Dihedral	7°
Sweepback C/4	35°
Aspect Ratio	7.056
M.A.C.	272.294 In.
M.A.C. LOC. (Sta)	762.97

FLAP

Leading Edge Area	26.1 Sq. Ft.
Trailing Edge Area	436.0 Sq. Ft.

AILERON

Inboard Area	40.4 Sq. Ft.
Outboard Area	80.6 Sq. Ft.

HORIZONTAL TAIL

Stabilizer Area	474 Sq. Ft.
Elevator Area	151 Sq. Ft.
Span	45 Ft. 8 In.

VERTICAL TAIL

Dorsal Area	8.7 Sq. Ft.
Fin Area	226.4 Sq. Ft.
Rudder Area	101.9 Sq. Ft.
Ventral Fin Area	25.5 Sq. Ft.

BODY

Length	145 Ft. 6 In.

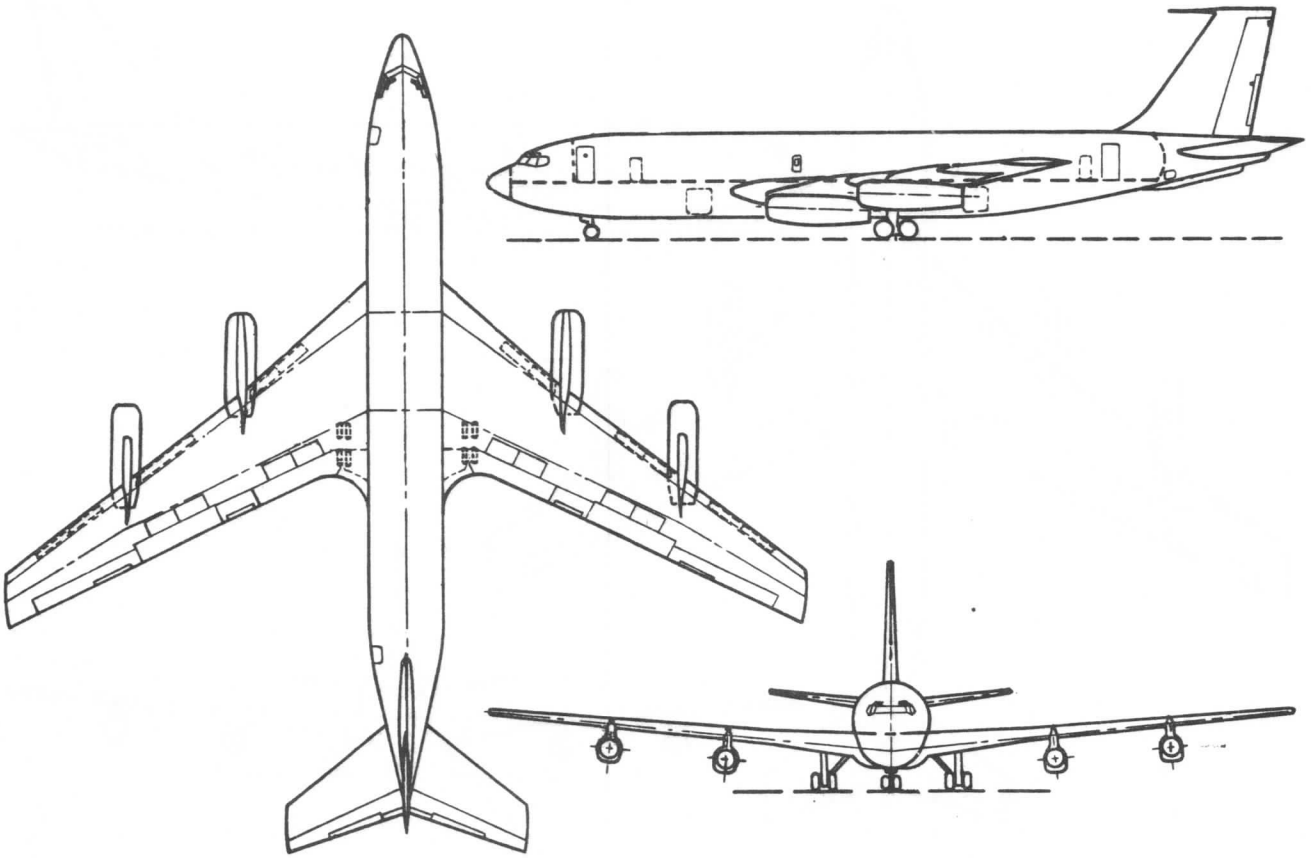

MODEL 720
PRINCIPAL DIMENSIONS

WING

Area	2433 Sq. Ft.*
Span	130 Ft. 10 In.
Root Chord	338 In.*
Tip Chord	112 In.
Taper Ratio	.342
Incidence Root	+2°
Incidence Tip	+2°
Dihedral	7°
Sweepback C/4	35°
Aspect Ratio	7.065 *
M.A.C.	241.88 In. *
M.A.C. LOC. (Sta)..	786.2

FLAP

Leading Edge Area	93.64 Sq. Ft.
Trailing Edge Area	362.2 Sq. Ft.

AILERON

Inboard Area	39.0 Sq. Ft.
Outboard Area	80.6 Sq. Ft.

HORIZONTAL TAIL

Stabilizer Area	382.7 Sq. Ft.
Elevator Area	117.6 Sq. Ft.
Span	39 Ft. 8.4 In.

VERTICAL TAIL

Dorsal Area	8.7 Sq. Ft.
Fin Area	226.4 Sq. Ft.
Rudder Area	101.9 Sq. Ft.
Ventral Fin Area	25.5 Sq. Ft.

BODY

Length	130 Ft. 6 In.

* (Excluding leading edge extension)

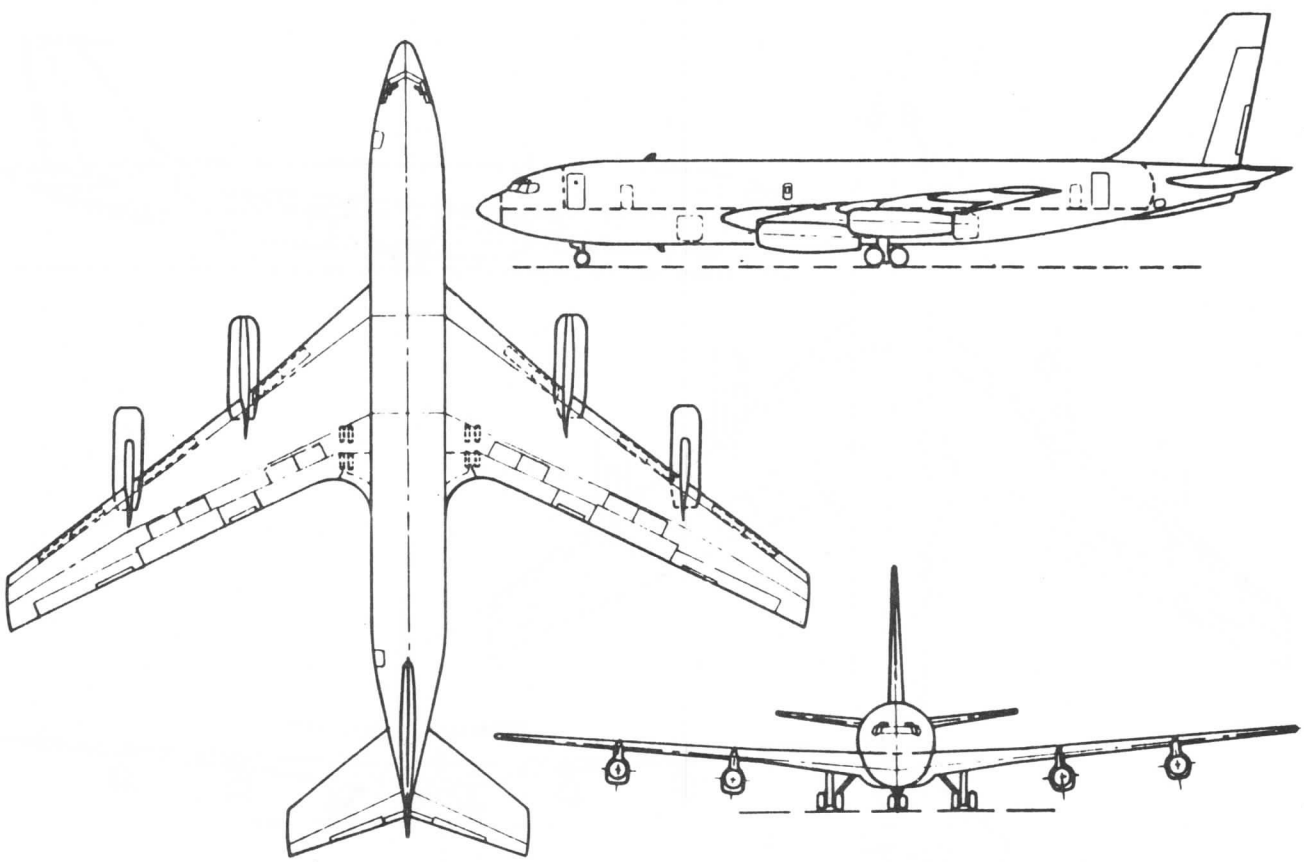

MODEL 720B
PRINCIPAL DIMENSIONS

WING

Area	2433 Sq. Ft. *
Span	130 Ft. 10 In.
Root Chord	338 In. *
Tip Chord	112 In.
Taper Ratio	.342
Incidence at Root	+2°
Incidence at Tip	+2°
Dihedral	7°
Sweepback C/4	35°
Aspect Ratio	7.065 *
M.A.C.	241.88 In. *
Leading Edge MAC	Sta. 786.2

FLAP

Leading Edge Area	93.64 Sq. Ft.
Trailing Edge Area	362.2 Sq. Ft.

* (Excluding leading edge extension)

AILERON

Inboard Area	39.0 Sq. Ft.
Outboard Area	80.6 Sq. Ft.

HORIZONTAL TAIL

Stabilizer Area	427.7 Sq. Ft.
Elevator Area	117.6 Sq. Ft.
Span	43 Ft.

VERTICAL TAIL

Dorsal Area	8.7 Sq. Ft.
Fin Area	226.4 Sq. Ft.
Rudder Area	101.9 Sq. Ft.
Ventral Fin Area	25.5 Sq. Ft.

BODY

Length	130 Ft. 6 In.

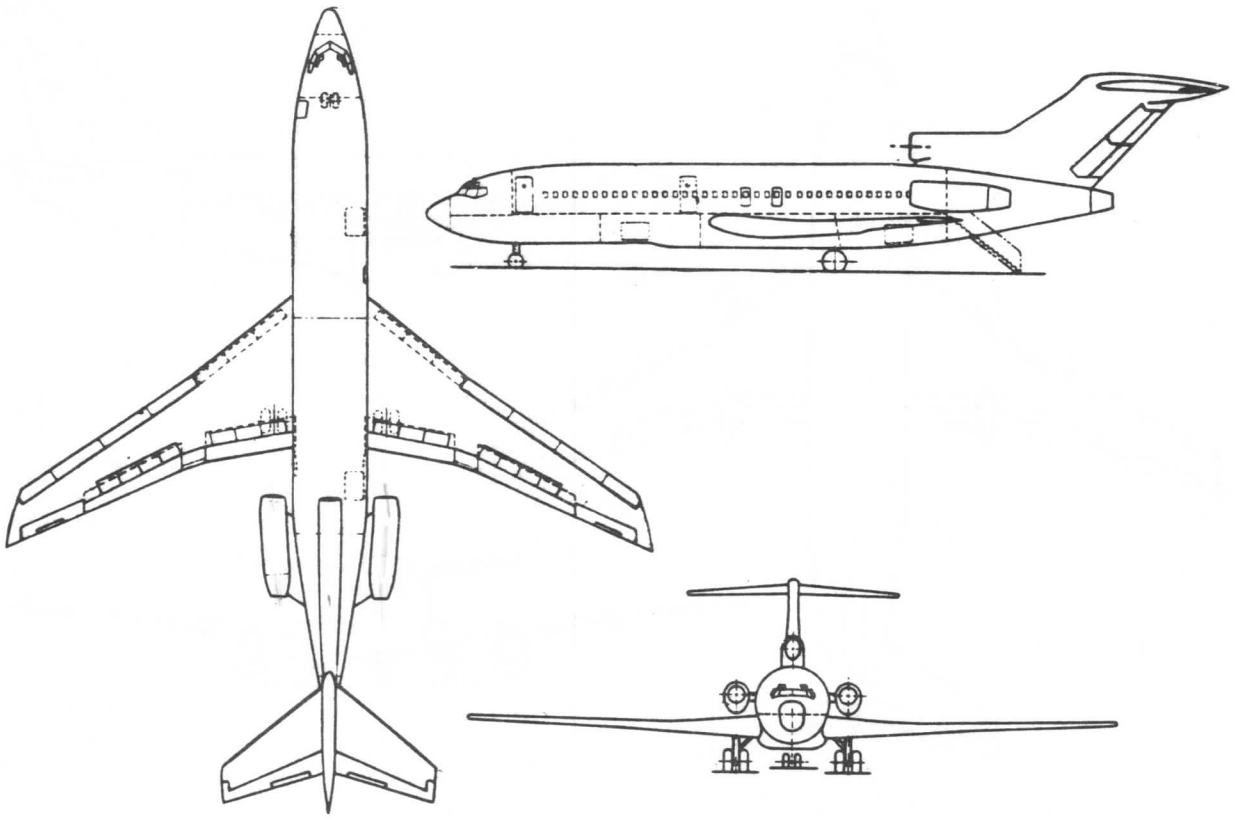

MODEL 727
PRINCIPAL DIMENSIONS

WING

Area	1560 Sq. Ft.
Span	106 Ft.
Root Chord (Basic)	246 In.
Tip Chord	91.6 In.
Taper Ratio (Basic)	0.372
Incidence at Root	+2°
Incidence at Tip	+2°
Dihedral	3°
Sweepback C/4	32°
Aspect Ratio	7.2
M.A.C.	180.0 In.
Leading Edge MAC	Sta. 860.2

FLAP

Leading Edge Area	54.8 Sq. Ft.
Trailing Edge Area	
(Retracted)	280 Sq. Ft.
(Extended)	388 Sq. Ft.

AILERON

Inboard Area	18.64 Sq. Ft.
Outboard Area	36.5 Sq. Ft.

HORIZONTAL TAIL

Anhedral	3°
Stabilizer Area	282.40 Sq. Ft.
Elevator Area	94.14 Sq. St.
Span	35 Ft. 9 In.

VERTICAL TAIL

Fin Area	283.37 Sq. Ft.
Rudder Area	72.63 Sq. Ft.

BODY

Length	
Short Body(727-100)	116 Ft. 2 In.
Long Body (727-200)	136 Ft. 2 In.

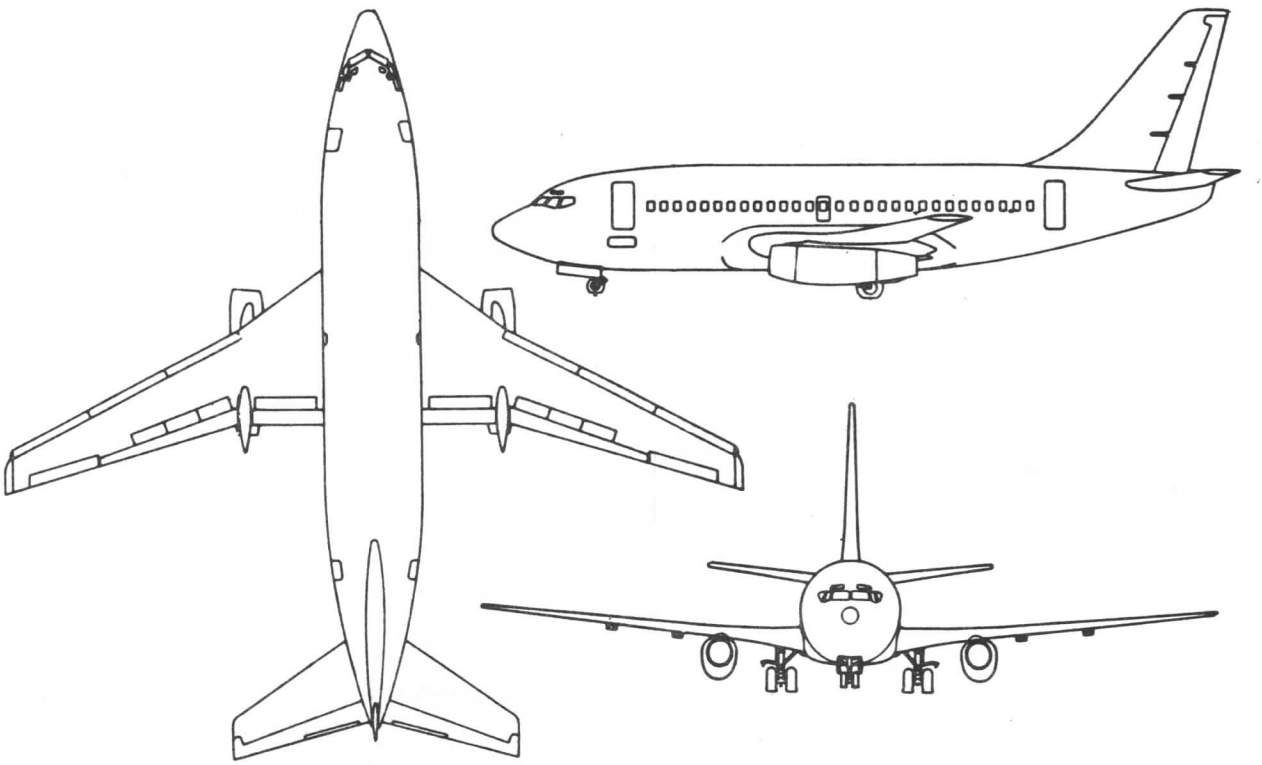

MODEL 737

PRINCIPAL DIMENSIONS

WING

Area	980 Sq. Ft.
Span	93 Ft.
Root Chord (Basic)	288.1 In.
Root Chord (Ref)	227.1 In.
Tip Chord	63.29 In.
Taper Ratio (Ref)	0.279
Incidence at Root	+1°
Incidence at Tip	+1°
Dihedral	6°
Sweepback c/4	25°
Aspect Ratio	8.83
M.A.C.	134.46 In.
Leading Edge MAC	Sta. 625.6

FLAP

Leading Edge Area	80 Sq. Ft.
Trailing Edge Area	
(Retracted)	171.5 Sq. Ft.
(Extended)	250.88 Sq. Ft.

AILERON

Aileron Area	13.4 Sq. Ft.

HORIZONTAL TAIL

Dihedral	7°
Stabilizer Area	241.54 Sq. Ft.
Elevator Area	70.46 Sq. Ft.
Total Area	312.00 Sq. Ft.
Span	36 Ft.

VERTICAL TAIL

Fin Area	167.80 Sq. Ft.
Rudder Area	56.20 Sq. Ft.
Total Area	224.00 Sq. Ft.

BODY

Length

Short Body (737-100)	90 Ft. 7 In.
Long Body (737-200)	96 Ft. 11 In.

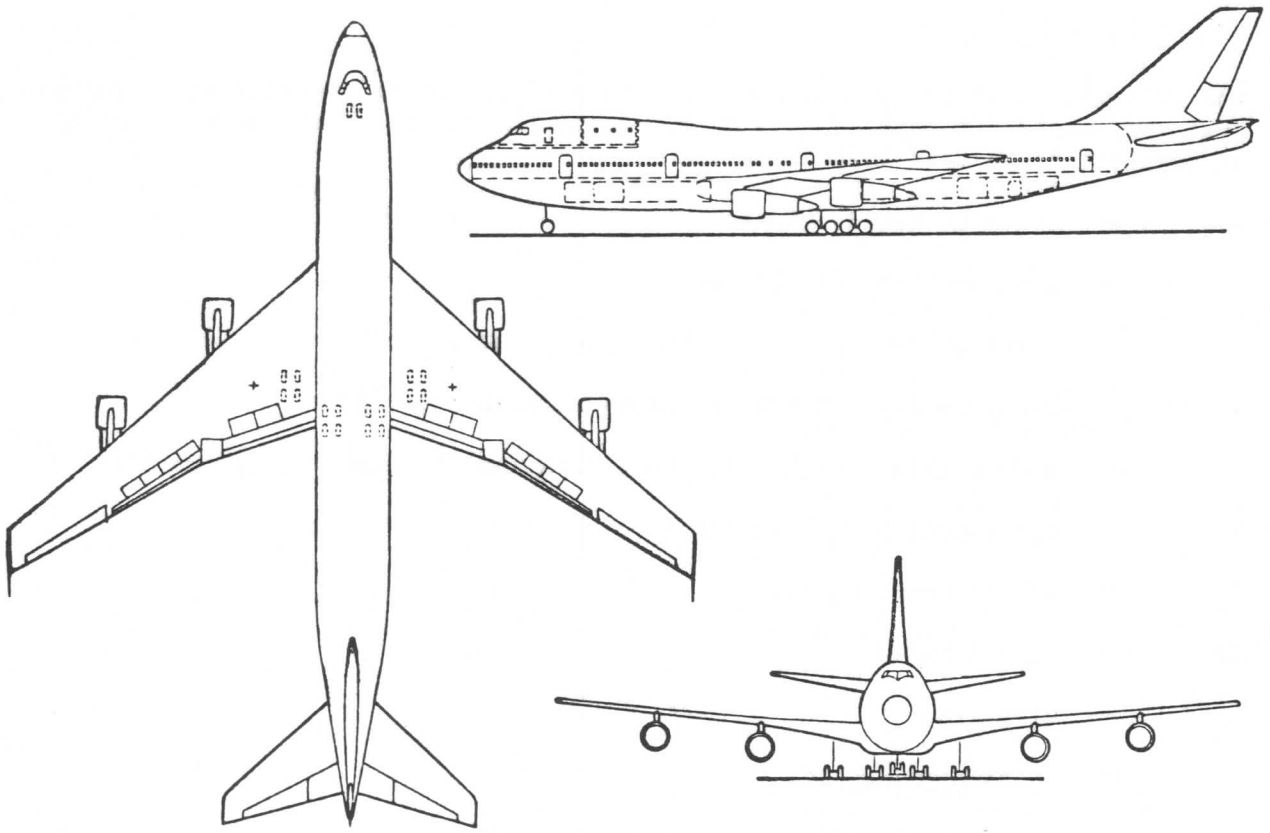

MODEL 747

PRINCIPAL DIMENSIONS

WING

Area	5500 Sq. Ft.
Span	195 Ft. 8 In.
Basic Root Chord	449.68 In.
Reference Root Chord	652.03 In.
Tip Chord	160.00 In.
Taper Ratio	.356 (Basic)
	.245 (Ref)
Incidence Root	+2°
Incidence Tip	-1.5°
Dihedral	7°
Sweepback c/4	37.5°
Aspect Ratio (Ref)	6.96
MAC (Basic only)	327.78 In.
MAC C/4 Location (Sta)	1339.91 In.

FLAP

Leading Edge Area (Retracted)	448 Sq. Ft.
Trailing Edge Area (Retracted)	847 Sq. Ft.

AILERON

Aileron Area (Inbd)	71.8 Sq. Ft.
(Outbd)	153.4 Sq. Ft.

HORIZONTAL TAIL

Area	1470 Sq. Ft.
Sweepback c/4	37.5°
Span	72 Ft. 9 In.
Root Chord	32 Ft. 4 In.
Tip Chord	8 Ft. 1 In.

VERTICAL TAIL

Area	830 Sq. Ft.
Sweepback c/4	45°
Span (Height)	32 Ft. 3 In.
Root Chord	38 Ft. 5 In.
Tip Chord	13 Ft. 1 In.

BODY

Length	225 Ft. 2 In.

0-3 NOMENCLATURE

The following list of symbols and their identification is included as a convenient reference. It represents a fairly complete listing of the more standard aerodynamic terms used in industry.

a	=	speed of sound, ft/sec.
a	=	acceleration, ft/sec/sec.
a	=	slope of the lift curve (C_L vs α), per degree
a	=	standard day temperature lapse rate, .003566 °F/ft.
a.c.	=	aerodynamic center, distance from leading edge, ft or fraction of c.
A	=	cross-sectional area, sq.ft.
A_w	=	wetted area, sq.ft.
AR	=	aspect ratio = b^2/S.
b	=	wing span, ft.
c	=	chord of wing, ft.
c_r	=	chord at the root of tapered wings, ft.
c_t	=	chord at the tip of tapered wings, ft.
C_D	=	drag coefficient, dimensionless.
C_{D_i}	=	induced drag coefficient, dimensionless.
C_{D_p}	=	parasite drag coefficient, dimensionless.
$C_{D_{pe}}$	=	equivalent parasite drag coefficient, dimensionless.
C_{D_π}	=	frontal area coefficient, dimensionless.
C_f	=	wetted area coefficient, dimensionless.
C_L	=	lift coefficient, dimensionless.
C_P	=	location of lift and drag forces, c.p./c.
C_p	=	pressure coefficient, dimensionless.
c.p.	=	center of pressure, distance from leading edge, ft.
c.g.	=	center of gravity.
c_v	=	specific heat at constant volume, Btu/lb/°F.

c_p = specific heat at constant pressure, Btu/lb/°F.

C_m = pitching moment coefficient = M/cqS.

$C_{ma.c.}$ = moment coefficient about aerodynamic center.

d = diameter, ft; length or distance, ft.

D = drag = C_D qS, lb.

D_i = induced drag, lb.

D_P = profile drag, lb.

E = bulk modulus, lb /sq. ft.

e = induced drag efficiency factor = $\frac{1/\pi AR}{dC_D/dC_L{}^2}$

f = equivalent parasite area, sq. ft.

F = force, lb.

g = acceleration due to gravity = 32.17 ft/sec/sec.

h = altitude, ft.

L = lift = C_LqS, lb.

l_t = wing C/4 to tail C/4, ft. "after tail length"

ln = natural logarithm.

log = common logarithm.

m = slope of the lift curve, per radian

M = mass in slugs, lb sec^2 per ft.

M = pitching moment = C_m cqS, ft lb.

M = Mach number.

M_o = free-stream Mach number.

n = load factor.

n = revolutions per second.

p_{am} = ambient pressure, lb/sq. ft.

p = static pressure, lb/sq.ft.

p_t = total pressure, lb/sq. ft.

p_o = free-stream static pressure, lb/sq. ft.

q = dynamic or impact pressure = $\rho V^2/2$, lb/sq. ft.

R = range, nautical air miles.

R = universal gas constant, ft lb/lb $^\circ F_{abs}$

R/C = rate of climb, ft/min.

R/D = rate of descent, ft/min.

RN = Reynolds number, dimensionless.

S_W = wing area, sq. ft.

S_G = ground run, ft.

S_π = proper area, plan or frontal, sq. ft.

S.L. = sea level

$()_s$ = stall condition

t = airfoil thickness, ft.

t = temperature, °F

t = time, sec.

T = thrust or other force, lb.

T = absolute temperature on Rankine scale = t + 460°F.

T.O. = takeoff condition

v = specific volume, cu ft/lb.

V_i = indicated airspeed, (uncorrected), kt.

V_I = indicated airspeed (corrected), kt.

V_c = calibrated airspeed, kt.

V_e = equivalent airspeed, kt.

V = true airspeed, kt.

V_A = maneuvering airspeed, kt.

V_B = maximum gust intensity airspeed, kt.

V_C = design cruising airspeed, kt.

V_D = diving airspeed, kt.

V_F = flap limit airspeed, kt.

V_{LE} = landing gear extended limit airspeed, kt.

V_{LO} = landing gear operating limit airspeed, kt.

V_{MC} = minimum control airspeed, kt.

V_{NE} = never-exceed (placard) airspeed, kt.

V_{NO} = normal operating limit airspeed, kt.

V_s = airplane stall airspeed, kt.

V_1 = critical engine failure speed, kt.

V_R = takeoff rotation speed, kt.

V_{LOF} = takeoff lift-off speed, kt.

V_2 = takeoff climb airspeed, kt.

W = airplane weight, lb.

w = specific weight, lb/cu ft.

α(alpha) = angle of attack of wing, degrees.

α_{LO} = angle of attack for zero lift, degrees.

γ(gamma) = glide angle, radians.

γ = ratio of specific heats, C_p/C_v.

Δ(delta) = increment notation.

δ (delta)= pressure ratio, p/p_o

θ (theta)= temperature ratio, T/T_o.

θ = turn angle or climb angle, degrees.

σ (sigma)= density ratio, ρ/ρ_o.

ρ (rho) = mass air density, slugs/cu ft.

ρ_o = mass air density at sea level, slugs/cu ft.

μ_B (mu) = coefficient of braking friction, dimensionless.

μ_R = coefficient of rolling friction, dimensionless

μ = dynamic viscosity, slugs/ft sec.

π (Pi) = 3.1416

ϵ = downwash angle, radians.

The following is a list of standard gas turbine symbols used by engine manufacturers.

C_f = fan nozzle gross thrust factor, dimensionless

C_g = gross thrust coefficient, dimensionless

EPR = engine pressure ratio.

F_g = gross thrust, lb.

F_g/δ_{am} = corrected gross thrust, lb.

F_n = net thrust, lb.

F_n/δ_{am} = corrected net thrust, lb.

ΔF_n = net thrust change, lb.

F_r = ram drag, lb.

F_r/δ_{am} = corrected ram drag, lb.

H_f = heat value of fuel, approx. 18,400 Btu/lb.

J = energy conversion factor, Joule's constant, 778 ft lb/Btu.

N_1 = low pressure rotor speed, rpm.

$N_1/\sqrt{\theta}_{t2}$ = corrected low pressure rotor speed, rpm.

N_2 = high pressure rotor speed, rpm.

$N_2/\sqrt{\theta}_{t3}$ = corrected high pressure rotor speed, rpm.

p_{t_2} = total pressure at compressor inlet, lb/sq ft.

p_{t_7} = turbine discharge total pressure, lb/sq ft.

p_{t_1}/p_{am} = ram pressure ratio.

p_{t_2}/p_{t_1} = inlet pressure recovery ratio.

p_{t_7}/p_{am} = jet nozzle expansion ratio.

p_{t_7}/p_{t_2} = engine pressure ratio, EPR.

T_{t_2} = engine inlet total temperature.

T_{t_7} = turbine discharge total temperature.

TSFC = thrust specific fuel consumption, lb/hr/lb thrust.

W_a = engine air flow, lb/sec.

W_g = total gas flow, lb/sec.

W_{ap} = primary engine airflow on fan engines, lb/sec.

W_{af} = fan airflow, lb/sec.

$\frac{W_a\sqrt{\theta}_{t_2}}{\delta_{t_2}}$ = corrected engine air flow, lb/sec.

W_f = engine fuel flow, lb/hr.

$\frac{W_f}{\delta_{t_2}\sqrt{\theta}_{t_2}}$ = corrected engine fuel flow, lb/hr.

θ_{am} = temperature ratio, T_{am}/T_o.

θ_{t_2} = ram temperature ratio, T_{t_2}/T_o.

δ_{am} = pressure ratio, p_{am}/p_o.

δ_{t_2} = ram pressure ratio, p_{t_2}/p_o.

γ = ratio of specific heats.

η(eta) = efficiency, per cent.

ψ = theoretical gross thrust function, dimensionless.

The following is a list of subscripts used throughout this manual.

a = air, (W_a)

am = ambient, (p_{am})

avg = average

c = compressible, (q_c)

cr = critical, (p_{cr})

f = fuel, (W_f)

g = gross, (F_g)

i = indicated, (V_i)

j = jet, (V_j)

n = net, (F_n)

o	=	standard sea level values, (p_o, t_o, etc.)
p	=	propulsion, (η_p)
p	=	constant pressure, (c_p)
r	=	ram, (F_r)
s	=	static, (T_s, p_s)
t	=	total, (T_t, p_t)
t	=	thermal, (η_t)
v	=	volume, (c_v)

The following list of symbols are used in Section 4 for stability and control analysis:

$\bar{c}$	=	mean aerodynamic chord, in.
C_h	=	hinge moment coefficient, dimensionless.
C_l	=	rolling moment coefficient, dimensionless.
C_n	=	yawing moment coefficient, dimensionless.
G	=	control gearing parameter, dimensionless.
HM	=	hinge moment, in lb.
i	=	incidence angle, degrees or radians.
l_t	=	tail length, wing .25$\bar{c}$ to tail .25$\bar{c}$, in.
$\mathscr{L}$	=	rolling moment, in lb.
N	=	yawing moment, in lb.
N_o	=	static neutral point, stick fixed, %$\bar{c}$
N_o'	=	static neutral point, stick free, %$\bar{c}$
N_m	=	maneuver point, stick fixed, %$\bar{c}$
N_m'	=	maneuver point, stick free, %$\bar{c}$
R	=	radius of turn, ft.
$\overline{V}$	=	tail volume coefficient, $S_t l_t / S\bar{c}$, dimensionless.
β	=	sideslip angle, plane to relative wind, degrees or radians.

γ = dihedral angle, degrees or radians.

δ = surface deflection angle, degrees or radians.

η_t = tail efficiency, q_t/q, dimensionless.

θ = pitch angle, degrees or radians.

Λ = sweep angle (.25c), degrees or radians.

ϕ = bank angle, degrees or radians.

Ψ = yaw angle, plane to fixed course, degrees or radians.

Ω = horizontal rotation angle in banked flight, degrees or radians.

For calculation purposes, the following values of the constants are used:

g = 32.17 ft/sec/sec.

R = 53.35 ft lb/lb $°F_{abs}$.

T_o = 518.688°F_{abs}.

a_o = 1116.44 ft/sec (661.5 knots)

p_o = 2116.2 lb/sq ft.

ρ_o = .002377 slugs/ft^3.

γ = 1.4 (for air)

SECTION 1

AERODYNAMICS

SECTION 1

AERODYNAMICS

1-1 GENERAL

It is the purpose of this section to discuss some of the fundamental physical relationships associated with the motion of bodies in air. In order to understand principles of flight and propulsion, it is necessary to review certain laws governing the behavior of fluids.

1-2 FLUIDS AT REST

There can be no shear on a liquid if the liquid is at rest. If any shear force exists, the liquid will deform. Forces acting on the fluid particles are normal to the surfaces and must be in equilibrium. Mathematically, the sum of the horizontal and vertical forces must be zero, and may be expressed:

$$\left.\begin{aligned} \Sigma F_H &= 0 \\ \Sigma F_V &= 0 \end{aligned}\right\} \qquad (1)$$

Force per unit of area is called "pressure." This statement may be written:

$$p = \frac{F}{A}$$

or,

$$F = pA \qquad (2)$$

The unit of pressure is "pound per square foot," since force is measured in pounds and area in square feet. An important principle was formulated by a French philosopher and mathematician, Pascal, in a statement that, if the gravitational effect is neglected, the pressures at any point in a fluid must be equal in magnitude in any direction. Any pressure increase in any part of the fluid, then, will result in an equal increase in pressure throughout the body of fluid. The effect of such pressure changes is familiar in its application in hydraulic systems of all types such as brakes, lifts, and presses.

When a finite difference in height exists, the weight of the fluid must be considered. In figure 1, a rectangular tank containing a fluid has a height, h, and cross-sectional area, A. The pressure on the lower surface of the tank is p_1, and on the upper surface is p_2. The weight of the fluid in the tank is the product of the specific weight of the liquid, w, the height of the liquid, h, and the area, A. Specific weight is defined as weight per unit volume.

Equation (1) may be written selecting the upward direction as positive:

$$\Sigma F_V = 0 = p_1A - p_2A - whA$$

$$p_1A - p_2A = whA$$

$$p_1 - p_2 = wh \qquad (3)$$

Equation (3) assumes that the fluid is incompressible; therefore w is constant. If the fluid is compressible, w varies and the difference of pressures, dp, depends on how w varies with a change in height, dh. Equation (3) for a compressible fluid is written:

$$dp = wdh \qquad (4)$$

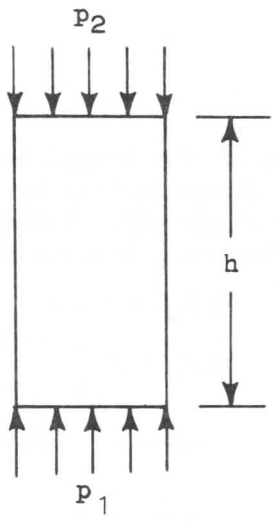

Figure 1.

A fluid may be either a liquid or a gas; the main difference between the two is in their resistance to compression. Gases are more easily compressed while liquids resist compression. Liquids are, in fact, generally considered incompressible. The fluid to be discussed in this section, primarily, will be air.

1-3 FLUIDS IN MOTION

Probably the most important physical laws governing the motion of solids and fluids are attributed to Sir Isaac Newton. These laws may be stated briefly as follows:

(1) Every body continues in a state of rest or of uniform motion in a straight line unless it is acted upon by an external force.

(2) An acceleration, proportional to the applied force, will be produced in the direction of the force.

(3) Every action results in an equal reaction, opposite in direction.

The first and third laws may be apparent from physical experience; however, the

second law is perhaps less evident. Mathematically, the law may be stated as:

$$F \propto a \qquad (5)$$

where, F is force, lb.
a is acceleration, ft/sec/sec

The property of a substance, whether solid or fluid, that is a measure of its quantity is called "mass." The mass of a body remains constant unless more matter is added or some is removed. The property of a body by virtue of which it tends to continue in the state of rest or motion in which it is placed is called "inertia." Mass, then, in addition to being the amount of matter in a body, is a measure of its inertia, or resistance to acceleration. The constant of proportionality, mass, enables equation (5) to be written in the form of an equality.

$$F = Ma \qquad (6)$$

When an object is allowed to fall freely in space (consider a vacuum exists), an acceleration is produced by the unbalanced force which is its own weight. This acceleration is commonly referred to as gravitational acceleration, g, since it is used extensively in analysis work in many fields. Equation (6) may be written for the freely falling body:

$$\left.\begin{aligned} W &= Mg \\ \text{or} \quad M &= \frac{W}{g} \end{aligned}\right\} \qquad (7)$$

The unit of mass is the "slug." One slug is the amount of mass which weighs 32.17405 pounds according to the international agreement as to the standard gravity condition. "Weight" of a body is the force with which the mass is being attracted, or pulled, toward the center of the earth. The unit of weight, and force, is the "pound". Acceleration bears the units of "feet per second per second," as does g. For the purposes of most calculations herein, the value of g used is 32.2 ft/sec/sec.

It is sometimes helpful to express mass in dimensions other than slugs. From equation (7):

$$M = \frac{\text{lb}}{\text{ft/sec}^2} = \frac{\text{lb sec}^2}{\text{ft}} \qquad (8)$$

"Mass density" is the mass per unit of volume and has the dimensions of "slugs per cubic foot." It bears the Greek letter Rho, ρ, and may be expressed more fundamentally using equation (8).

$$\rho = \frac{\text{slugs}}{\text{ft}^3} = \frac{\text{lb sec}^2}{\text{ft}^4} \qquad (9)$$

Mathematically, fluid mass density may be related to specific weight:

$$\rho = \frac{w}{g} \qquad (10)$$

1-4 STREAMLINES AND STREAMTUBES

A stream of air may be considered as consisting of many particles moving in the same general direction. The path of any one particle is called a "streamline." A collection of streamlines forming a closed curve or tube, as in Figure 2, is referred to as a "stream tube." Since the walls of the stream tube are streamlines, there can be no flow through the wall.

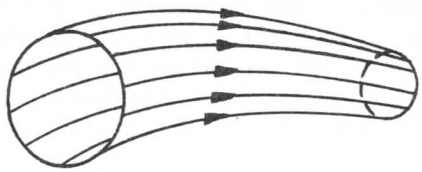

Figure 2.

1-5 CONTINUITY EQUATION

If a fluid is moving uniformly through a pipe or stream tube, as in Figure 3, the mass of fluid that leaves the tube every second must be the same as that entering the tube. This is continuity of flow. The law of continuity may be stated mathematically:

$$\left.\begin{aligned} \rho AV &= \text{constant} \\ \rho_1 A_1 V_1 &= \rho_2 A_2 V_2 \end{aligned}\right\} \qquad (11)$$

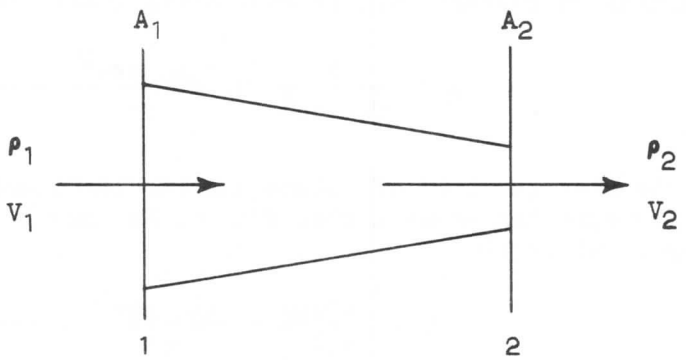

Figure 3.

The subscripts refer to particular stations of the tube.

The mass that is passing a section in one second is ρAV slugs, or

$$\frac{M}{t} = \rho AV \qquad (12)$$

where, M is mass, slugs
ρ is mass density, slugs/ft^3
A is cross-sectional area, ft^2
V is velocity, ft/sec
t is time, sec

In calculus, the formula for finding the differential of a product of three variables is:

$$d(xyz) = xy\ dz + xz\ dy + yz\ dx \qquad (13)$$

and the differential of a constant is 0:

$$d\ (c) = 0 \qquad (14)$$

Applying these formulae to equation (11):

$$\rho A\ dV + \rho V\ dA + AV\ d\rho = 0 \qquad (15)$$

Dividing both sides of equation (15) by ρAV results in another form of the continuity equation:

$$\frac{dV}{V} + \frac{dA}{A} + \frac{d\rho}{\rho} = 0 \qquad (16)$$

If the fluid is incompressible, that is, ρ remains constant, equation (11) becomes:

$$AV = \text{constant} \qquad (17)$$

Differentiating equation (17) and dividing by AV, a similar expression to equation (16) may be written for incompressible flow:

$$\frac{dA}{A} + \frac{dV}{V} = 0 \qquad (18)$$

or,

$$\frac{dA}{A} = \frac{-dV}{V} \qquad (19)$$

Although the fluid (air) is compressible, this is often ignored in some aerodynamic considerations for simplicity if the velocity is relatively low. Equation (19) shows that a positive change in area (dA) results in a negative change in velocity (dV).

1-6 INCOMPRESSIBLE BERNOULLI EQUATION

The Bernoulli equation, a mathematical method of showing variation of pressure and velocity within a streamtube, is of prime importance in fluid study and is based upon the principle that when fluid flows in the duct, such as shown in Figure 4, its total energy at all points along the duct is constant. If the interior is frictionless, the energy is of three forms; that due to height (potential energy), that due to pressure (pressure energy), and that due to movement (kinetic energy). In practically all fluid analysis work, horizontal flow is considered so that changes in height do not occur.

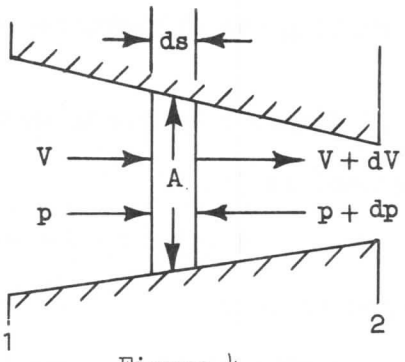

Figure 4.

Consider the tapering duct and an element with a cross-sectional area, A, as in Figure 4. If the air is considered incompressible, the continuity equation in the form of equation (17) will apply. It was shown that with a decreasing area, the flow velocity must increase so that in the nomenclature of calculus, the velocity, V, must increase after having travelled a short distance, ds, by the amount dV. Also the pressure, p, may be arbitrarily assumed to have increased by the amount dp. Assuming that the section or element of air under consideration is accelerating to the right, the net force acting in that direction causing the acceleration can be found.

Repeating equation (6) for convenience:

$$F = Ma$$

The force to the right from equation (2) is:

$$F = pA$$

The counteracting force to the left is:

$$F = (p+dp)A$$

The net force to the right is then:

$$\Delta F = pA - (p+dp)A = -dpA \qquad (20)$$

The mass of air involved is the mass density multiplied by the volume, or:

$$M = \rho A\, ds \qquad (21)$$

Also, acceleration is a change in velocity per change in time. In calculus, the expression may be written:

$$a = \frac{dV}{dt} \qquad (22)$$

Substituting equations (20), (21), and (22) into equation (6) results in:

$$-dp\ A = \rho A\ ds\ \frac{dV}{dt}$$

or,

$$dp = -\rho ds\ \frac{dV}{dt} \qquad (23)$$

By algebraic manipulation, certain terms may be rearranged:

$$ds\ \ \frac{dV}{dt} = \frac{ds}{dt}\ dV$$

A change in distance per change in time is simply velocity:

$$\frac{ds}{dt}\ dV = V\ dV$$

Thus equation (23) becomes:

$$dp = -\rho V\ dV \qquad (24)$$

Again in calculus, the formulae necessary to integrate this expression are:

$$\int dx = x + \text{constant} \qquad (25)$$

$$\int x dx = \frac{x^2}{2} + \text{constant} \qquad (26)$$

Applying these rules to equation (24), the equation becomes:

$$\int dp = -\rho \int V\ dV$$

The solution to the equation becomes:

$$p = -\rho \frac{V^2}{2} + \text{constant}$$

or in a more useful form:

$$p + \frac{1}{2}\rho V^2 = \text{constant} \qquad (27)$$

In the derivation of equation (27) it should be noted that the density, ρ, was considered constant. This is the incompressible flow equation.

Now since "p" is the "static" pressure of the fluid, the quantities $1/2\ \rho V^2$ and the constant must have the same dimensions of pressure. The quantity $1/2\ \rho V^2$ is known as the "dynamic" pressure since it embodies flow velocity. Dynamic and static pressures are the only pressures assumed to be in the system, so their sum is called the "total" pressure.

Thus equation (27) becomes, in its most familiar form:

$$p_s + \frac{1}{2}\rho V^2 = p_t \qquad (28)$$

Referring to Figure 4, the Bernoulli equation may be written in the form:

$$p_1 + \frac{1}{2}\rho V_1^2 = p_2 + \frac{1}{2}\rho V_2^2 \qquad (29)$$

The term $1/2\ \rho\ V^2$ appears so frequently in fluid analysis that it is given the symbol "q". Thus,

$$q = \frac{1}{2}\rho V^2 \qquad (30)$$

Equation (29) may also be written as:

$$p_1 + q_1 = p_2 + q_2 \qquad (31)$$

A direct application of the Bernoulli equation is the pitot tube, which is used to measure air speed. A schematic diagram of the instrument is shown in Figure 5.

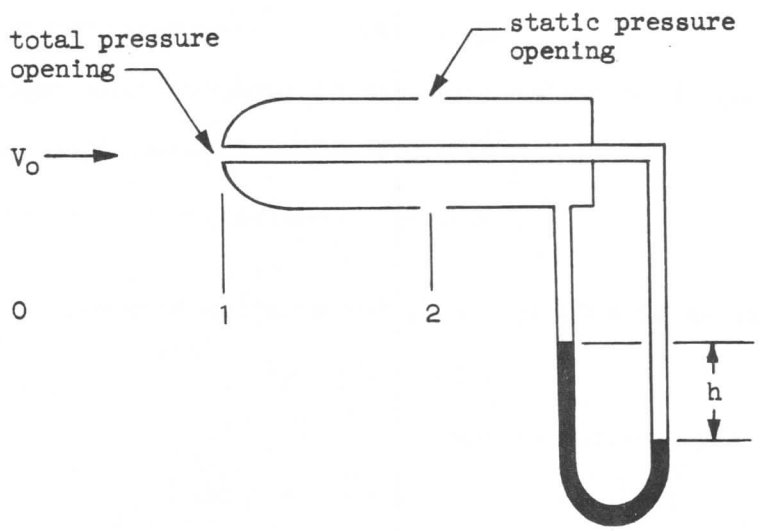

Figure 5.

The concentric tubes of the pitot are arranged so that the center tube is aligned in the direction of the approaching air. As the air directly in line with the hole in the center tube reaches the opening it must of necessity come to rest momentarily at point 1 before it turns and proceeds around the sides of the larger tube. As it passes along the outer tube it will finally attain essentially its original velocity, V_o, at some point, 2, where a hole is located. The subscript o here represents the remote or free stream condition.

The pressures acting at points 1 and 2 can be used to measure the velocity, V_o, by some pressure sensing device. The particular device depicted in Figure 5 is a manometer, which is merely a U-tube with some fluid in it. One side of the U is connected to point 1 and the other to point 2. If the pressure at point 1 is greater than at point 2 (as is the case) then the fluid will be forced to assume the position shown. The difference in the heights of the column, h, is a direct measure of the pressure difference between points 1 and 2. Equation (3) relates these quantities and is repeated here for convenience:

$$p_1 - p_2 = \Delta p = wh$$

where Δp is the pressure difference and w is the fluid density or specific weight.

Writing Bernoulli's equation for points 1 and 2 with relation to a remote point, o:

$$p_o + \frac{1}{2}\rho V_o^2 = p_1 + \frac{1}{2}\rho V_1^2$$

also,

$$p_o + \frac{1}{2}\rho V_o^2 = p_2 + \frac{1}{2}\rho V_2^2$$

From the previous explanations:

$$V_1 = 0$$

and,

$$V_2 = V_o$$

Thus:

$$p_1 = p_o + \frac{1}{2}\rho V_o^2$$

and,

$$p_2 = p_o$$

The manometer is set up to read the difference between p_1 and p_2, or Δp. Thus:

$$p_1 - p_2 = \Delta p = (p_o + \frac{1}{2}\rho V_o^2) - p_o$$

or,

$$\Delta p = \frac{1}{2}\rho V_o^2 \qquad \text{(32)}$$

Equating expressions (3) and (32) shows that the fluid height differential, h, is proportional to the dynamic pressure of the free stream $1/2\ \rho V_o^2$. Specifically, the fluid weight density relates the two:

$$wh = \frac{1}{2}\rho V_o^2$$

The pressure differential need not have been measured by a manometer. This device is confined solely to laboratory and wind tunnel work. The application in

airplanes would call for some form of mechanical pressure measuring device using a diaphragm, bellows, or bourdon tube arrangement.

The Bernoulli equation is fundamental to all aerodynamics problems, particularly those involving a discussion of pressure distributions on bodies immersed in a fluid. Additional applications of this important principle will be made in later sections as will the development of the compressible flow equation.

1-7 EQUATION OF STATE

The mass density of solids and liquids is essentially constant, but the mass density of gas depends upon the pressure and temperature. According to Physics, the relation between the pressure, density and temperature is:

$$p = \rho g R T \qquad (33)$$

where,

p is pressure, lb/ft^2
ρ is density, $slugs/ft^3$
g is in ft/sec^2
R is in ft/°F absolute
T is temperature, °F absolute

The absolute temperature, T, is the temperature in degrees Fahrenheit measured from absolute zero, -459.7. The expression for finding the absolute temperature is:

$$T = t + 459.7 \qquad (34)$$

The temperature, t, is the measured temperature in degrees Fahrenheit. R, in equation (33), is known as the gas constant and is different for different gases. For air, the value of the constant is 53.35 $ft/°F_{abs}$. (The universal gas constant for all gases is 1545.43 ft lb/$°F_{abs}$ lb mole. The molecular weight of air is 28.966 lb/lb mole, and the quotient of the two is 1545.43/28.966 = 53.35 $ft/°F_{abs}$). Equation (33) is sometimes written:

$$pv = RT \qquad (35)$$

where v is specific volume which is the reciprocal of specific weight, $v = \frac{1}{w}$.

The gas constant for air of 53.35 ft/°R, as given above, is only valid under sea level conditions where g equals 32.17 ft/sec^2. The equation of state, for a thermally perfect gas is:

$$p = \rho R' T \qquad (36)$$

where R', the thermal gas constant equal to 1716 $ft^2/sec^2 °R$, is valid at any altitude.

This relationship, (equation of state), would define the state of a gas in terms of three variables, p, v, and T. A "process" describes the relation between any two of the variables. Three such processes are readily apparent as a result of holding each variable constant. These are:

(1) constant pressure (isobaric)
(2) constant temperature (isothermal)
(3) constant volume (isochoric)

In each of the above processes, addition or release of heat is required. It is conceivable that in a fourth process, no heat energy is added or lost. Such a process is called "adiabatic."

Heat is a form of energy and can be transformed. A BTU (British thermal unit) is a measure of heat and is defined as the amount of heat energy required to raise a one pound mass of water through one degree Fahrenheit at standard conditions. One BTU is equivalent to 778 ft lb of mechanical work, usually assigned the letter J. It does not require as much additional heat energy to raise a pound of gas one degree Fahrenheit as it does water. The ratio of the number of BTU's required to raise one pound of gas through one degree Fahreheit to that of water is called "specific heat." When the operation is carried out at constant pressure, allowing volume to vary, it becomes the specific heat at constant pressure and has the symbol, C_p. For air $C_p = 0.240$ BTU/lb/°F. If carried out at constant volume, allowing pressure to vary, it becomes the specific heat at constant volume, having the symbol C_v. The value for air is $C_v = 0.172$ BTU/lb/°F. The ratio of specific heats occurs frequently in fluid analyses and is assigned the Greek letter Gamma, γ.

For air:
$$\gamma = \frac{C_p}{C_v} = \frac{.240}{.172} = 1.4 \qquad (37)$$

Of primary interest to the aerodynamicist are the isothermal and adiabatic processes. When the temperature is held constant in equation (35), the isothermal process is represented and the equation becomes:

$$pv = \text{constant} \qquad (38)$$

This is generally known as Boyle's Law. For the adiabatic processes encountered in aerodynamics, the relationship becomes:

$$\left.\begin{aligned} pv^{\gamma} &= \text{constant} \\ \text{or,}\quad \frac{p}{\rho^{\gamma}} &= \text{constant} \end{aligned}\right\} \qquad (39)$$

Various forms of equations (38) and (39) will be of interest in subsequent chapters.

1-8 FLUID VISCOSITY

In addition to the pressure, temperature, and density characteristics of a fluid, its compressibility and viscosity properties (that which offers resistance to motion) must be considered.

The viscous property of a fluid asserts itself when a fluid is in motion relative to some fixed surface. When a layer of fluid touches a surface, its velocity is reduced to zero by friction. Viscosity is the result of shear forces acting on the fluid, or the tendency of one layer of fluid to drag along the layer next to it. Next to a surface, there will be a finite thickness of fluid which will be retarded relative to the velocity farther away, or to the free stream velocity.

This retarded layer is known as a "boundary layer" and is shown diagrammatically in Figure 6.

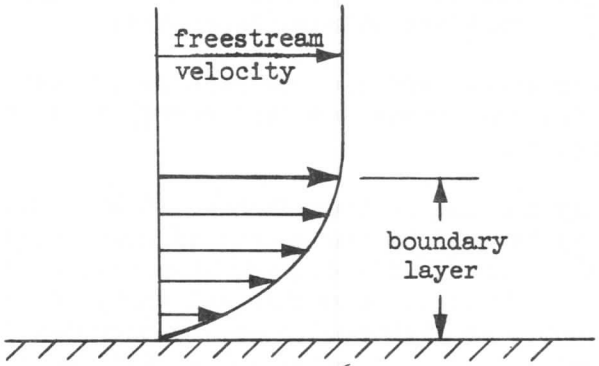

Figure 6.

The length of the arrows represents the magnitude of velocity at that distance from the surface. A measure of the viscosity of a fluid is represented in coefficient form by the Greek letter Mu, μ, and bears the dimensions of "slugs per foot second." The dynamic viscosity coefficient is assumed to vary with absolute temperature according to Sutherland's equation:

$$\mu = \frac{\beta T^{3/2}}{T+S} \qquad (40)$$

where,

μ = dynamic viscosity coefficient, $\frac{\text{lb-sec}}{\text{ft}^2}$

$\beta = \frac{\mu_o(T_o+S)}{T_o^{3/2}} = 0.3125059\ (10^{-7})$, $\frac{\text{lb-sec}}{\text{ft}^2\sqrt{^\circ\text{K}}}$

T = absolute temperature, $^\circ$K

S = Sutherland's constant, 120°K

The standard viscosity at sea level, μ_o, equals 3.745299 (10^{-7}) lb-sec/ft^2 at To equal to 288.16°K.

Fluids in liquid form are subject to viscous effects but may be considered incompressible.

1-9 SPEED OF SOUND

Gases, however, in addition to their viscous properties are highly compressible. When a disturbance producing a change in pressure occurs at a point in a fluid, this disturbance is propagated through the fluid in the form of a wave of the same type as a sound wave. Sound is the result of pressure waves, or compressions and rarefactions of the fluid of such frequencies as to be audible.

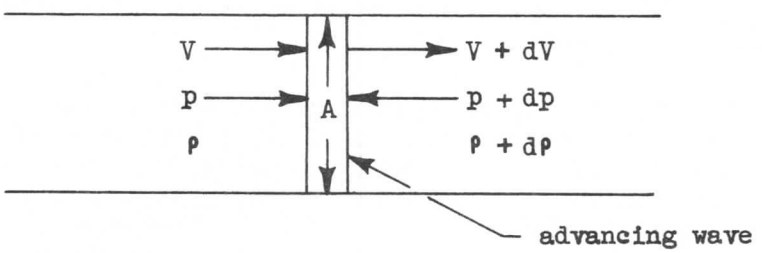

Figure 7.

Let us assume that there is a pressure wave moving to the right in the channel in Figure 7 at velocity V, pressure p and density ρ. The flow has acquired increments in velocity, pressure, and density downstream of the wave of dV, dp, and $d\rho$, respectively. The force due to fluid flow is:

$$F = Ma = M\frac{dV}{dt} \qquad (41)$$

Substituting equation (21) into equation (41) results in:

$$F = \rho A\ ds\frac{dV}{dt}$$

$$F = \rho A\frac{ds}{dt}\ dV$$

$$F = \rho AV\ dV \qquad (42)$$

The force due to pressure change is:

$$F = pA - (p + dp)A$$

$$F = -dpA \qquad (43)$$

Equating forces, equations (42) and (43), and simplifying:

$$-dpA = \rho A\ VdV$$

$$\frac{dp}{\rho} + VdV = 0 \qquad (44)$$

From the continuity equation (11):

$$\rho AV = (\rho + d\rho)A(V + dV)$$

$$\rho V = \rho V + \rho dV + Vd\rho + d\rho dV$$

or,

$$\frac{d\rho}{\rho} + \frac{dV}{V} = 0 \qquad (45)$$

Since the second order differential is very small, it can be neglected.

From equations (44) and (45):

$$dV = -\frac{dp}{\rho V} = -\frac{d\rho\ V}{\rho}$$

whereby,

$$V^2 = \frac{dp}{d\rho} \qquad (46)$$

Equation (46) shows that the speed of the pressure wave is related to the compressibility properties of the gas; that is, the rate of change of density with respect to that of pressure. Therefore, the greater the compressibility of a gas, the lower the speed of wave propagation. Since a sound wave is an example of a pressure wave in air, the quantity, a, is referred to as the local speed of sound and has the units of ft/sec.

$$a = \sqrt{\frac{dp}{d\rho}} \qquad (47)$$

The reciprocal of equation (46) is sometimes called the "compressibility factor."

It can be shown that the change of state across the pressure wave is adiabatic; therefore, the quantity $dp/d\rho$ may be determined from equation (39):

$$p = \text{const}\ \rho^{\gamma}$$

and,

$$\frac{dp}{d\rho} = \text{const}\ \gamma \rho^{\gamma - 1}$$

therefore,

$$\frac{dp}{d\rho} = \left(\frac{p}{\rho^{\gamma}}\right) \gamma \rho^{\gamma - 1} = \frac{\gamma p}{\rho} \qquad (48)$$

Substituting equation (48) into equation (47):

$$a = \sqrt{\frac{\gamma p}{\rho}} \qquad (49)$$

Using equation (33), another form of the speed of sound equation may be written:

$$a = \sqrt{\gamma g R T} \qquad (50)$$

Since γ, g, and R remain constant, it can be seen that the speed of sound varies directly with the square root of the absolute static temperature.

1-10 COMPRESSIBLE BERNOULLI EQUATION

Air moving at relatively low speeds, below 250 knots, may be treated as an incompressible fluid. At higher speeds, it is necessary to consider the variation of density as the airflow is compressed. At these speeds, another form of the Bernoulli equation must be used.

The compressible Bernoulli equation may be developed from equation (24), repeated here for convenience:

$$dp = -\rho V dV$$

Within the stream tube or duct, changes in density occur too rapidly for any appreciable heat flow to occur. Hence, the process is assumed ideally adiabatic. Equation (24) involves the variable ρ, which can be expressed in terms of pressure from equation (39):

$$\frac{p}{\rho^{\gamma}} = C$$

and,

$$\rho = \left(\frac{p}{C}\right)^{\frac{1}{\gamma}} \qquad (51)$$

Substituting for ρ in equation (24), rearranging, and integrating:

$$dp = -\left(\frac{p}{C}\right)^{\frac{1}{\gamma}} VdV$$

$$C^{\frac{1}{\gamma}} \frac{dp}{p^{\frac{1}{\gamma}}} = -VdV$$

$$C^{\frac{1}{\gamma}} \int p^{\frac{-1}{\gamma}} dp + \int VdV = \int 0$$

$$C^{\frac{1}{\gamma}} \frac{p^{\frac{-1}{\gamma}+1}}{\frac{-1}{\gamma}+1} + \frac{V^2}{2} = \text{constant}$$

Simplifying:

$$C^{\frac{1}{\gamma}} \frac{\gamma}{\gamma-1} p^{\frac{\gamma-1}{\gamma}} + \frac{V^2}{2} = \text{constant}$$

$$\frac{\gamma}{\gamma-1} p \left(\frac{C}{p}\right)^{\frac{1}{\gamma}} + \frac{V^2}{2} = \text{constant}$$

Substituting for $\left(\frac{C}{p}\right)^{\frac{1}{\gamma}}$, the Bernoulli equation for compressible fluids in horizontal flow becomes:

$$\frac{\gamma}{\gamma-1} \frac{p}{\rho} + \frac{V^2}{2} = \text{constant} \qquad (52)$$

As before, the flow equation may be written for any two points in the fluid:

$$\frac{\gamma}{\gamma-1} \frac{p_1}{\rho_1} + \frac{V_1^2}{2} = \frac{\gamma}{\gamma-1} \frac{p_2}{\rho_2} + \frac{V_2^2}{2} \qquad (53)$$

1-11 FLOW RELATIONS NEAR THE SPEED OF SOUND

A very useful and important relationship called "Mach number," after Ernst Mach, involves the velocity of sound. Mach number, M, is the ratio of the fluid velocity to the velocity of sound at the same point.

$$M = \frac{V}{a} \qquad (54)$$

Since V and a are velocities measured in feet per second, Mach number is dimensionless.

The behavior of fluid flow near the speed of sound is of primary importance. The relationship between temperature, pressure, mass density, and velocity may be predicted by the application of some of the fluid laws developed in the previous chapters.

There are five general classifications used to describe high speed flight. These are:

(1)	subsonic	($M < 1$)
(2)	sonic	($M = 1$)
(3)	supersonic	($M > 1$)
(4)	hypersonic	($M = 5$ to 10)
(5)	hypervelocity	($M = 10$ and up)

The term "transonic" is used often to describe the flow conditions through the sonic region. Mathematical treatment of the transonic region is rather difficult because of the mixed flow conditions; however, fairly accurate predictions of the aerodynamic characteristics of both subsonic and supersonic flow can be made.

Consider the flow of fluid in a frictionless channel, as in Figure 8, which has a

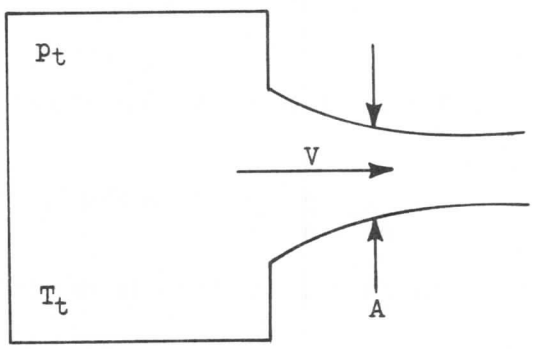

Figure 8.

varying cross-sectional area A, connected to a reservoir. The relationship between the velocity and pressure was developed earlier, equation (24).

$$dp = - \rho V dV$$

The continuity equation, equation (16), provides a relationship involving the

density.

$$\frac{dV}{V} + \frac{dA}{A} + \frac{d\rho}{\rho} = 0$$

Also from equation (47),

$$a = \sqrt{\frac{dp}{d\rho}}$$

or

$$a^2 = \frac{dp}{d\rho} \qquad (55)$$

Equation (24) may be written substituting the value of dp from equation (55).

$$a^2 d\rho = -\rho V dV$$

$$\frac{d\rho}{\rho} = -\frac{V dV}{a^2} \qquad (56)$$

Substitute for $\frac{d\rho}{\rho}$ in equation (16),

$$\frac{dA}{A} + \frac{dV}{V} - \frac{V dV}{a^2} = 0$$

By multiplying the third term by V/V, and expressing in terms of Mach number:

$$\frac{dV}{V}(1 - M^2) = -\frac{dA}{A} \qquad (57)$$

Inspection of equation (57) shows what happens to speed as the cross-sectional area is changed in a channel. At a fixed Mach number less than one, an increase in area produces a decrease in speed. When the Mach number is greater than unity, the equation states than an increase in area will cause further increase in speed. At these speeds, the density decreases so rapidly for a given speed increase that the channel must expand to continue this speed increase. This is supported by equation (56) rearranged.

$$\frac{d\rho}{\rho} = -M^2 \frac{dV}{V}$$

At the point in the channel, Figure 9b, where there is no change in area, that is, $dA/A = 0$, equation (57) indicates that two possibilities exist: $dV/V = 0$, or $M = 1$. The point where the cross-sectional area is a minimum is called the "throat," and is the point where $dA/A = 0$. At this point the speed is such that the Mach number reaches unity. Downstream of the throat the speed may continue to increase, and Mach numbers greater than unity may exist.

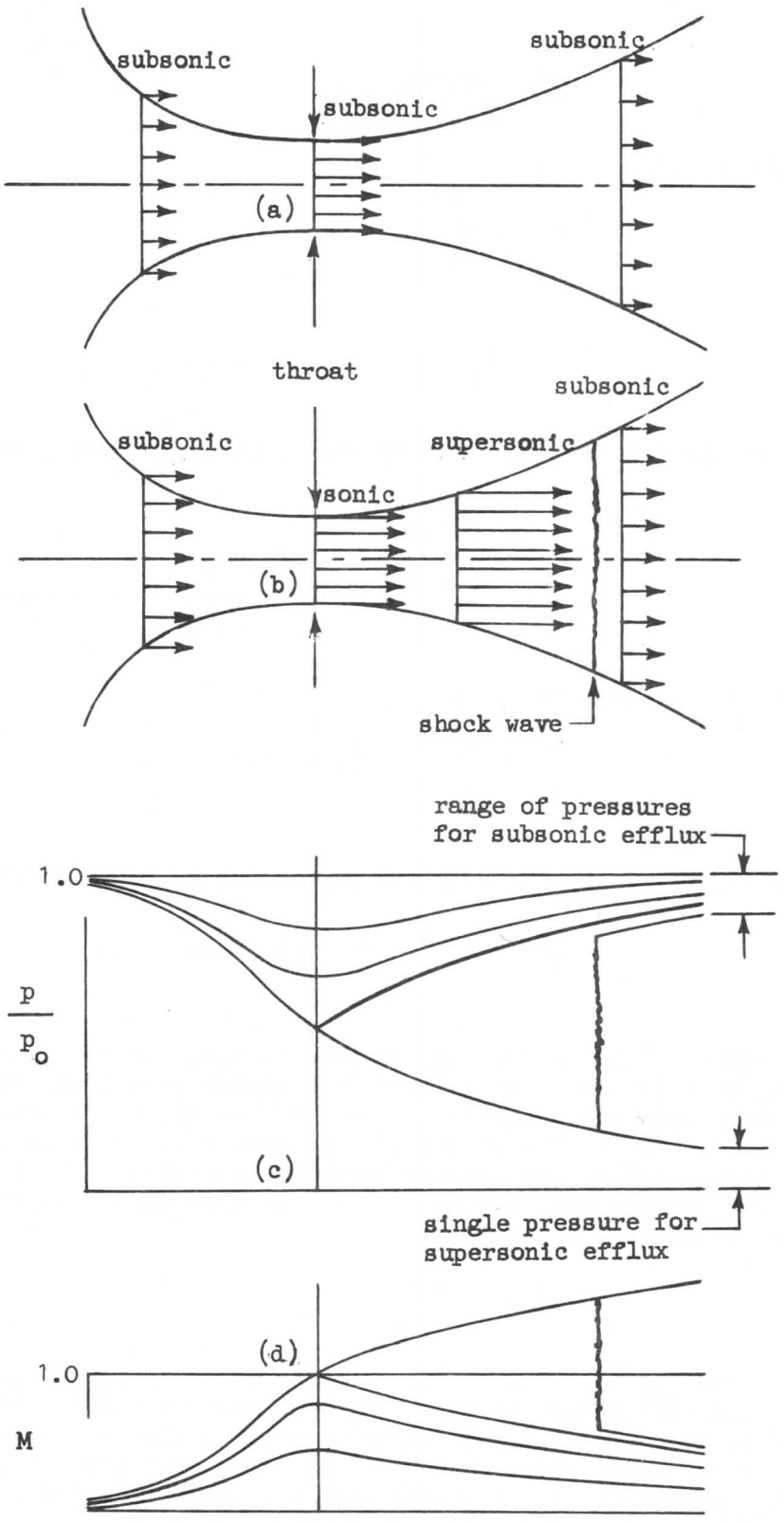
subsonic
subsonic
subsonic
(a)
throat
subsonic
supersonic
sonic
(b)
shock wave
range of pressures
for subsonic efflux
1.0
p
p_o
(c)
single pressure for
supersonic efflux
(d)
1.0
M

Figure 9.

Equation (57) shows the relationship between velocity and area as influenced by Mach number; a similar relationship may be developed showing how pressure varies with area. Equation (24) may be written:

$$\frac{dV}{V} = -\frac{dp}{\rho V^2} \qquad (58)$$

and equation (49) as:

$$\rho = \frac{\gamma p}{a^2} \qquad (59)$$

Substituting equation (59) into equation (58) and the result into equation (57), the following equation is obtained:

$$\frac{dp}{p} = \frac{\gamma M^2}{(1-M^2)} \frac{dA}{A} \qquad (60)$$

Equation (60) shows that, for a given Mach number, an increase in area requires a pressure rise for M less than one, and a pressure drop for M greater than one. From Figure 9a, it can be seen that if the flow through the tube is completely subsonic, the decrease in area before the throat results in an increase in velocity and a decrease in pressure; whereas, the increase in area downstream of the throat results in a decrease in velocity and an increase in pressure. Now with an increase in velocity ahead of the throat, there will be a corresponding increase in velocity at the throat. When the velocity at the throat just reaches the speed of sound, the flow has become "critical" (critical is defined only for M = 1 flow conditions). The pressure at the throat under this condition is known as the "critical pressure." As the pressure downstream of the throat is reduced below the "critical pressure" value, the flow upstream of the throat will be the same in all respects; i.e., no further increase in initial or throat velocity is possible, unless the stagnation state of the gas is changed. Downstream of the throat, however, the flow will be found to be supersonic. As a matter of fact, the lower the exit pressure the higher the value of supersonic flow and the further downstream the supersonic flow will go.

Figure 9b shows that the flow just downstream of the throat is supersonic, whereas further downstream the flow is subsonic. The physical process by which the change takes place (in the absence of special diffusing devices) is known as a "shock wave." The term "shock" is used because it is found that the transition from supersonic to subsonic flow occurs suddenly. Now, with a sudden change in velocity, the static pressure downstream in the subsonic region must be increased correspondingly (Bernoulli equation). This sudden increase in pressure will cause a compression in the air with a consequent increase in density and temperature. It will be found that in decreasing the downstream pressure to where the throat Mach number just reaches unity, the shock wave separating the supersonic and subsonic regimes will be very weak (small pressure change) and will occur at the throat. As the supersonic flow region becomes greater with lower exit pressures, the pressure rise after the shock will be greater. The curves for variation of pressure in the channel will be similar to the velocity curves and appear as in Figures 9c and 9d. Note that the pressure rise through the shock wave results in a pressure that does not equal the pressure for subsonic flow. There is a loss of pressure energy through the shock wave which results in an increase in free-stream temperature. However, the stagnation temperature remains constant.

There is a relationship between temperature and velocity that can be derived by

the following approach. The compressible Bernoulli equation, equation (52), may be written for the flow condition of Figure 8. The temperature, pressure and density conditions in the reservoir are all stagnation values, which are, in effect, the total temperature, pressure, and density existing; hence, the subscript, t.

$$\frac{1}{2}V_t^2 + \frac{\gamma}{\gamma - 1}\frac{p_t}{\rho_t} = \frac{1}{2}V^2 + \frac{\gamma}{\gamma - 1}\frac{p}{\rho}$$

Since in the reservoir, stagnation exists, $V_t = 0$,

$$\frac{\gamma}{\gamma - 1}\frac{p_t}{\rho_t} = \frac{1}{2}V^2 + \frac{\gamma}{\gamma - 1}\frac{p}{\rho}$$

From equation (49),

$$a^2 = \frac{\gamma p}{\rho}$$

and,

$$a_t^2 = \frac{\gamma p_t}{\rho_t}$$

Substituting,

$$\frac{1}{\gamma - 1}a_t^2 = \frac{1}{2}V^2 + \frac{1}{\gamma - 1}a^2$$

Dividing both sides of the equation by a^2:

$$\frac{1}{\gamma - 1}\frac{a_t^2}{a^2} = \frac{1}{2}\frac{V^2}{a^2} + \frac{1}{\gamma - 1}$$

From equation (50),

$$a^2 = \gamma g R T$$

or,

$$a_t^2 = \gamma g R T_t$$

Then,

$$\frac{a_t^2}{a^2} = \frac{T_t}{T}$$

Substituting $M^2 = \frac{V^2}{a^2}$:

$$\left(\frac{1}{\gamma - 1}\right)\frac{T_t}{T} = \frac{M^2}{2} + \frac{1}{\gamma - 1}$$

Rearranging,

$$\frac{T_t}{T} = 1 + \left(\frac{\gamma - 1}{2}\right)M^2 \qquad (61)$$

The temperature, T, is static temperature, and is sometimes written T_s to distinguish it from total temperature.

If the flow in the channel is considered ideally adiabatic, then the applicable pressure and density relationships may be developed. That is, applying equations (33) and (39) to equation (61), the following expressions may be derived:

$$\frac{\rho_t}{\rho} = \left[\left(1 + \frac{\gamma - 1}{2} M^2\right)\right]^{\frac{1}{\gamma - 1}} \qquad (62)$$

$$\frac{p_t}{p} = \left[\left(1 + \frac{\gamma - 1}{2} M^2\right)\right]^{\frac{\gamma}{\gamma - 1}} \qquad (63)$$

These relationships are very important and should be well understood.

The ratios of pressure, temperature, and density at the throat to those in the reservoir are of particular interest. These ratios are called "critical ratios" and are obtained from equations (61), (62), and (63); however shown here as the reciprocal of the above equations with $M = 1$ and $\gamma = 1.4$ for air substituted.

$$\frac{T}{T_t} = \frac{2}{\gamma + 1} = 0.833 \qquad (64)$$

$$\frac{p}{p_t} = \left(\frac{2}{\gamma + 1}\right)^{\frac{\gamma}{\gamma - 1}} = 0.528 \qquad (65)$$

$$\frac{\rho}{\rho_t} = \left(\frac{2}{\gamma + 1}\right)^{\frac{1}{\gamma - 1}} = 0.634 \qquad (66)$$

1-12 THE ATMOSPHERE

The ultimate performance of both the aircraft and the engine depends upon the generation of forces due to interactions between the aircraft or engine and the air mass through which it flies. So it is of importance to study the properties of the earth's atmosphere.

The atmosphere is a gaseous mixture composed of nitrogen, oxygen, and a small amount of other gases. Water vapor is always present, but in varying amounts, usually little more than one per cent on the surface of the earth.

The energy of the sun is responsible for heating the atmosphere, but little of this energy is transferred directly to the air. Most of it goes to heat the surface of the earth which in turn heats the air. The warm air near the surface rises and due to a decrease in pressure as altitude is increased, the air expands and is cooled.

Finally, an equilibrium is reached where there is no more reduction in temperature. This altitude is called the "tropopause" and it varies with latitude. The

region below, from the earth's surface to the tropopause, is called the "troposphere." That above the tropopause is called the "stratosphere." In the stratosphere, the temperature is essentially constant.

Seasonal changes, moving air masses and the like, have a pronounced effect on the temperature, pressure, and density of the air. In order to provide a basis for estimating and comparing airplane and engine performance, it is desirable to have a "standard." The standard as adopted in the United States by airplane manufacturers is that established by the International Civil Aviation Organization (ICAO). It is a condition established by averaging data studied over long periods of time. Since the studies were conducted in the mid latitudes of the northern hemisphere, the standard is most clearly representative of conditions in these regions. However, even though the expected deviations from this "standard" may be much larger in polar or equatorial regions, the same standard may be used as a reference. The International Standard Atmosphere establishes a sea level pressure, p_o, of 29.92 inches of mercury, or 2116 lb/ft^2 at a temperature, t_o, of 59°F. The mass density, ρ_o, of dry air under these conditions is 0.002377 $slugs/ft^3$. The subscript, $_o$, identifies these as standard, sea level values and will be used hereafter.

As indicated previously, the equation of state has several forms, and can be written in many ways. For example, equation (33), may be stated for the standard sea level condition:

$$p_o = \rho_o g R T_o \qquad (67)$$

Dividing equation (33) by equation (67) the constants g and R cancel:

$$\frac{p}{p_o} = \frac{\rho}{\rho_o}\frac{T}{T_o} \qquad (68)$$

The ratios appearing in equation (68) are used quite frequently and for this reason each has a special symbol:

(Delta) $$\delta = \frac{p}{p_o}, \quad \frac{\text{(pressure of air)}}{\text{(pressure of air at s.l. st'd day)}} \qquad (69)$$

(Sigma) $$\sigma = \frac{\rho}{\rho_o} \quad \frac{\text{(density of air)}}{\text{(density of air at s.l. st'd day)}} \qquad (70)$$

(Theta) $$\theta = \frac{T}{T_o}, \quad \frac{\text{(temperature of air)}}{\text{(temperature of air at s.l. st'd day)}} \qquad (71)$$

These symbols may be substituted in equation (68) to provide another useful equation:

$$\delta = \sigma\theta \qquad (72)$$

Variation of Temperature with Altitude

The International Standard Atmosphere assumes that there is a constant drop in temperature of 0.003566°F/ft from sea level to an altitude of 36,089 feet. The

standard temperature at any altitude below 36,089 feet may be found from the following:

$$T = T_o - ah \qquad (73)$$

Where "a" is the lapse rate, 0.003566°F/ft, and should not be confused here with any other use of the letter. The letter "h" represents altitude in feet. After substitution, equation (73) becomes:

or,

$$\left.\begin{aligned} T &= 518.7 - 0.003566\ h \\ t &= 59 - 0.003566\ h \end{aligned}\right\} \qquad (74)$$

Above 36,089 feet, a constant temperature of -69.7°F is assumed.

$$\left.\begin{aligned} T &= \text{constant} = 390.0°F_{abs} \\ t &= \text{constant} = -69.7°F \end{aligned}\right\} \qquad (75)$$

Figure 10 shows the standard temperature variation with altitude.

Variation of Pressure with Altitude

Unlike the temperature, the pressure continues to decrease above 36,089 feet as altitude is increased. The pressure variation with altitude below 36,089 feet is not the same as above the tropopause due to the influence of temperature. The relationship between the pressure and temperature is, of course, governed by the gas laws.

Below 36,089 feet, the pressure-temperature-density relationships may be developed in the following manner.

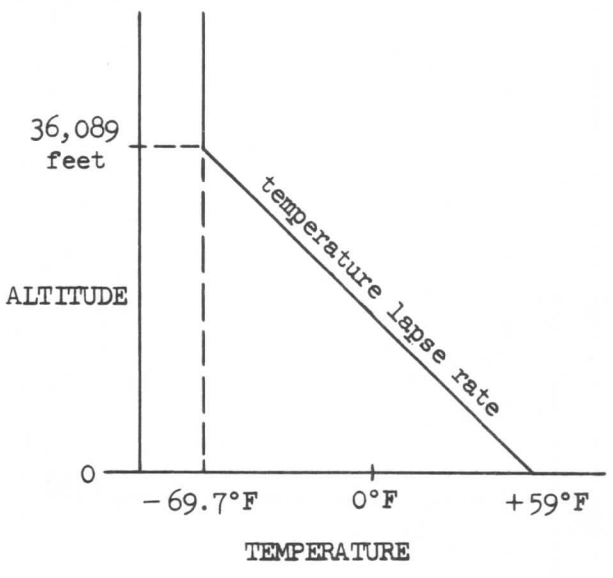

Figure 10

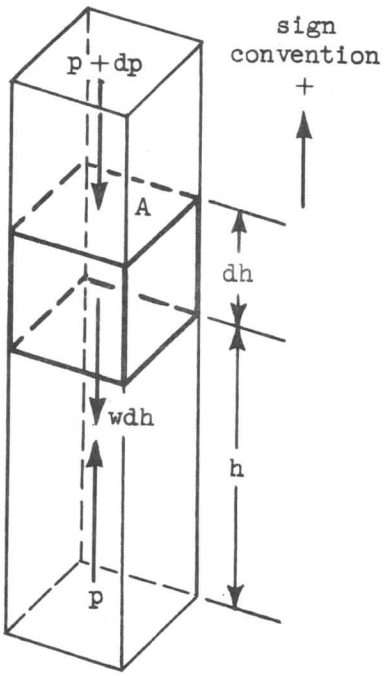

Figure 11

Consider the analysis of the pressure existing on an infinitesimal section of a column of air at altitude, h, as in Figure 11.

As in the section dealing with hydrostatics, the sum of the forces in a vertical direction is made:

From equation (1), $F_V = 0$

$$pA - (p+dp)A - wAdh = 0$$

From equation (4), $-dp = wdh$

From equation (10), $w = \rho g$

$$dp = -\rho g dh \qquad (76)$$

From equation (33), $p = \rho g R T$

$$\frac{dp}{p} = -\frac{1}{RT}\, dh \qquad (77)$$

From equation (73) $T = T_o - ah$

$$dT = -a\, dh$$

or, $$dh = \frac{-dT}{a}$$

Substituting in equation (77) for dh:

$$\frac{dp}{p} = \left(\frac{-1}{RT}\right)\left(\frac{-dT}{a}\right)$$

$$\int_{p_o}^{p} \frac{dp}{p} = \frac{1}{aR}\int_{T_o}^{T} \frac{dT}{T}$$

$$\ln p\Big]_{p_o}^{p} = \frac{1}{aR} \ln T\Big]_{T_o}^{T}$$

$$\left.\begin{aligned} \frac{p}{p_o} &= \left(\frac{T}{T_o}\right)^{\frac{1}{aR}} \\ \frac{p}{p_o} &= \left(\frac{T}{T_o}\right)^{5.256} \end{aligned}\right\} \qquad (78)$$

or, $$\delta = \theta^{5.256}$$

To find the density relationship, equation (68) may be combined with equation (78):

$$\frac{p}{p_o}=\left(\frac{T}{T_o}\right)^{\frac{1}{aR}}=\frac{\rho}{\rho_o}\quad\frac{T}{T_o}$$

$$\frac{\rho}{\rho_o}=\left(\frac{T}{T_o}\right)^{-1}\left(\frac{T}{T_o}\right)^{\frac{1}{aR}}$$

Therefore:

$$\left.\begin{aligned}\frac{\rho}{\rho_o}&=\left(\frac{T}{T_o}\right)^{\frac{1}{aR}-1}\\ \frac{\rho}{\rho_o}&=\left(\frac{T}{T_o}\right)^{4.256}\\ \sigma &= \theta^{4.256}\end{aligned}\right\}\qquad (79)$$

or,

Above 36,089 feet

The upper limit of the troposphere is the lower limit of the stratosphere; consequently, this will be reflected in the pressure-temperature-density relationships for the stratosphere. In the preceding section, a relation between pressure and altitude was derived:

Equation (77),
$$\frac{dp}{p}=-\frac{1}{RT}\,dh$$

With the temperature now a constant, the equation can be integrated:

$$\int_{p_{36}}^{p}\frac{dp}{p}=-\frac{1}{RT}\int_{36}^{h}dh$$

The subscript, 36, indicates the 36,089 foot condition.

$$\ln p\Big]_{p_{36}}^{p}=-\frac{1}{RT}\,h\Big]_{36}^{h}$$

$$\ln\frac{p}{p_{36}}=-\frac{1}{RT}\,(h-36{,}089)$$

or,

$$\frac{p}{p_{36}}=e^{-\left(\frac{h-36{,}089}{RT}\right)}$$

but,

$$p_{36} = p_o \left(\frac{T_{36}}{T_o} \right)^{5.256}$$

$$\left.\begin{aligned} \frac{p}{p_o} &= \left(\frac{T_{36}}{T_o} \right)^{5.256} e^{-\left(\frac{h - 36,089}{RT} \right)} \\ \frac{p}{p_o} &= (.2234)\ (2.718)^{-\left(\frac{h - 36,089}{20,806} \right)} \end{aligned}\right\} \qquad (80)$$

471

The letter "e" in the preceding equations, is the base of the natural logarithm.

To find the density relationship for the stratosphere, equation (68) may again be used.

$$\frac{p}{p_o} = (.2234)\ (2.718)^{-\left(\frac{h - 36,089}{20,806} \right)} = \frac{\rho}{\rho_o} \frac{T_{36}}{T_o}$$

$$\frac{\rho}{\rho_o} = \frac{T_o}{T_{36}} (.2234)\ (2.718)^{-\left(\frac{h - 36,089}{20,806} \right)}$$

but,

$$\frac{T_o}{T_{36}} = \frac{518.7}{390.0} = 1.330$$

Therefore,

$$\frac{\rho}{\rho_o} = (.2971)\ (2.718)^{-\left(\frac{h - 36,089}{20,806} \right)} \qquad (81)$$

From the equations developed in this section, a table can be made for all altitudes based on the international standard. Since this involves much tedious calculation, tables have been accurately calculated and published by various government agencies. These data are available in most engineering reference handbooks. A table is reproduced in this section for ready reference. See Figure 12. Specific information within the I.C.A.O. tables does not vary significantly with the former NACA data. The noticeable change is the isothermal condition which was 35,332 feet at -67°F. Airframe and engine manufacturers have adopted the international standard and are using it for all engineering and performance analyses.

AERODYNAMICS

INTERNATIONAL STANDARD ATMOSPHERE

h ft	t °F	t °C	$\frac{T}{T_o}=\theta$	$\sqrt{\frac{T}{T_o}}=\frac{a}{a_o}$	p in Hg	p $\frac{lb.}{ft^2}$	$\frac{P}{P_o}=\delta$	$\rho \times 10^6$ $\frac{lb-sec^2}{ft^4}$	$\frac{\rho}{\rho_o}=\sigma$	h ft
0	59.0	15.0	1.0000	1.0000	29.92	2116.2	1.0000	2377	1.0000	0
1,000	55.4	13.0	.9931	.9965	28.86	2041	.9644	2308	.9711	1,000
2,000	51.9	11.0	.9862	.9931	27.82	1968	.9298	2241	.9428	2,000
3,000	48.3	9.1	.9794	.9896	26.82	1897	.8962	2175	.9151	3,000
4,000	44.7	7.1	.9725	.9862	25.84	1828	.8637	2111	.8881	4,000
5,000	41.2	5.1	.9656	.9826	24.90	1761	.8320	2048	.8617	5,000
6,000	37.6	3.1	.9587	.9791	23.98	1696	.8014	1987	.8359	6,000
7,000	34.0	+1.1	.9519	.9757	23.09	1633	.7716	1927	.8106	7,000
8,000	30.5	-0.8	.9450	.9721	22.22	1572	.7428	1868	.7860	8,000
9,000	26.9	-2.8	.9381	.9686	21.39	1513	.7148	1811	.7620	9,000
10,000	23.3	-4.8	.9312	.9650	20.58	1455	.6877	1755	.7385	10,000
11,000	19.8	-6.8	.9244	.9615	19.79	1400	.6614	1701	.7156	11,000
12,000	16.2	-8.8	.9175	.9579	19.03	1346	.6360	1648	.6932	12,000
13,000	12.6	-10.8	.9106	.9543	18.29	1294	.6113	1596	.6713	13,000
14,000	9.1	-12.7	.9037	.9506	17.58	1243	.5875	1545	.6500	14,000
15,000	5.5	-14.7	.8969	.9470	16.89	1194	.5643	1496	.6292	15,000
16,000	+1.9	-16.7	.8900	.9434	16.22	1147	.5420	1447	.6090	16,000
17,000	-1.6	-18.7	.8831	.9397	15.57	1101	.5203	1401	.5892	17,000
18,000	-5.2	-20.7	.8762	.9361	14.94	1057	.4994	1355	.5699	18,000
19,000	-8.8	-22.6	.8694	.9324	14.34	1014	.4791	1310	.5511	19,000
20,000	-12.3	-24.6	.8625	.9287	13.75	972.5	.4595	1266	.5328	20,000
21,000	-15.9	-26.6	.8556	.9250	13.18	932.4	.4406	1224	.5150	21,000
22,000	-19.5	-28.6	.8487	.9212	12.64	893.7	.4223	1183	.4976	22,000
23,000	-23.0	-30.6	.8419	.9176	12.11	856.3	.4046	1143	.4806	23,000
24,000	-26.6	-32.5	.8350	.9138	11.60	820.2	.3876	1003	.4642	24,000
25,000	-30.2	-34.5	.8281	.9100	11.10	785.3	.3711	1065	.4481	25,000
26,000	-33.7	-36.5	.8212	.9062	10.63	751.6	.3552	1028	.4325	26,000
27,000	-37.3	-38.5	.8144	.9024	10.17	719.1	.3398	991.9	.4173	27,000
28,000	-40.9	-40.5	.8075	.8986	9.725	687.8	.3250	956.7	.4025	28,000
29,000	-44.4	-42.5	.8006	.8948	9.297	657.6	.3107	922.5	.3881	29,000
30,000	-48.0	-44.4	.7937	.8909	8.885	628.4	.2970	889.3	.3741	30,000
31,000	-51.6	-46.4	.7869	.8871	8.488	600.3	.2837	857.0	.3605	31,000
32,000	-55.1	-48.4	.7800	.8832	8.106	573.3	.2709	825.5	.3473	32,000
33,000	-58.7	-50.4	.7731	.8793	7.737	547.2	.2586	795.0	.3345	33,000
34,000	-62.2	-52.4	.7662	.8753	7.382	522.1	.2467	765.3	.3220	34,000
35,000	-65.8	-54.3	.7594	.8714	7.041	498.0	.2353	736.5	.3099	35,000
36,000	-69.4	-56.3	.7525	.8674	6.712	474.7	.2243	708.6	.2981	36,000
36,089	-69.7	-56.5	.7519	.8671	6.683	472.7	.2234	706.1	.2971	36,089
37,000	-69.7	-56.5	.7519	.8671	6.397	452.4	.2138	675.9	.2844	37,000
38,000	-69.7	-56.5	.7519	.8671	6.097	431.2	.2038	644.2	.2710	38,000
39,000	-69.7	-56.5	.7519	.8671	5.811	411.0	.1942	613.9	.2583	39,000
40,000	-69.7	-56.5	.7519	.8671	5.538	391.7	.1851	585.1	.2462	40,000
41,000	-69.7	-56.5	.7519	.8671	5.278	373.3	.1764	557.6	.2346	41,000
42,000	-69.7	-56.5	.7519	.8671	5.030	355.8	.1681	531.5	.2236	42,000
43,000	-69.7	-56.5	.7519	.8671	4.794	339.1	.1602	506.6	.2131	43,000
44,000	-69.7	-56.5	.7519	.8671	4.569	323.2	.1527	482.8	.2031	44,000
45,000	-69.7	-56.5	.7519	.8671	4.355	308.0	.1455	460.1	.1936	45,000

518.67

$T_o = 59.0 + 459.7 = 518.7\ ^\circ R$
$= 15.0 + 273.2 = 288.2\ ^\circ K$

$P_o = 2116.2\ LB/FT^2$

$\rho_o = .002377\ LB\ SEC^2/FT^4$

$a_o = 1116.4\ FT/SEC$
=661.475 kts,

$R = 53.35\ FT\ LB/LB\ ^\circ R$

$\gamma = C_p/C_v = 1.40$

Military max Temp = T_{STD} + 85°

Figure 12.

Non-Standard-Day Conditions

The major reason for establishing a standard or reference atmosphere is to permit performance and operation to be stated in such forms that they may be compared. All predictions and results are published on the basis of assumed standard day conditions; and actual data gathered under non-standard conditions are then transformed into equivalent standard day values by the use of the parameters, θ, δ, and σ. It is important to remember that the standard atmosphere is an arbitrary condition set up by definition.

At any geometric or "tapeline" altitude, the measured pressure may be other than the expected standard value. Thus, the altimeter, which measures pressure, will indicate an altitude corresponding to the measured pressure. This "pressure altitude" is the standard-day condition, the most natural and simple equivalence to use. (The altimeter used must be unbiased; it must be set for 29.92 inches or 1013 millibars of mercury reference.) The pressure ratio, δ, may be read from the standard table, Figure 12, by entering with the pressure altitude. But, temperature and density relations must be resolved on the basis of further measurements and calculations.

Since density may not be measured directly, it is common practice to measure static temperature and calculate θ. Then, with θ and δ, σ and density may be obtained from equation (72). For example, if the altimeter reads 4,000 feet and the OAT is 90°F, δ = .8637, θ = 1.0600, and σ = .8150.

1-13 PRESSURE DISTRIBUTIONS

The Bernoulli principle is fundamental to all aerodynamic problems, particularly those involving a discussion of pressure distributions on bodies immersed in a fluid. Explanations involving the fluid phenomena are frequently simplified by considering two dimensional flow, or flow of fluid in parallel planes over the body.

Let a blunt nosed object, a cylinder, be placed in a frictionless and incompressible moving fluid. The flow pattern or streamlines will have an appearance similar to Figure 13.

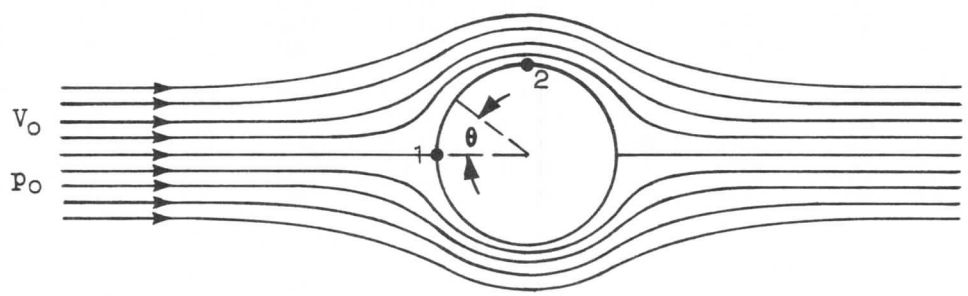

Figure 13.

In the flow around the body, some of the streamlines will be diverted to one side, some to the other. There will be one point at which the streamline will be normal to the body. This is called the "stagnation" point, point 1 on the figure.

The spacing of the streamlines about the cylinder indicates the magnitude of the velocity. That is, the closer together the streamlines are spaced, the higher the velocity. From the law of continuity, it has already been shown that the velocity is inversely proportional to the area. The streamlines are compressing the streamtubes, thereby decreasing the area and increasing the velocity.

The Bernoulli equation shows that along with changes in velocity, simultaneous changes in static pressure occur. Thus, whenever the velocity is different from the undisturbed, or free stream velocity, the static pressure will differ from that existing in the free stream. Examining Figure 13, air particles along the streamline striking point 1 will be brought to rest. The reduction of the velocity to zero at this point means that the static pressure will increase in value equal to the dynamic pressure, q.

Thus,

$$p_0 + q_0 = p_1 + q_1$$

but since,

$$q_1 = 0 \text{ because } V_1 = 0,$$

$$p_0 + q_0 = p_1$$

or,

$$p_1 - p_0 = q_0 \qquad (82)$$

This equation says that the difference between the static pressure of the free stream and that at point 1 is the dynamic pressure of the free stream. If both sides of equation (82) are divided by the quantity q_0, a more standard form results:

$$\frac{p_1 - p_0}{q_0} = 1 \qquad (83)$$

This manipulation non-dimensionalizes the equation since the units of the numerator and denominator are the same, and cancel.

The pressure difference $p_1 - p_0$, or Δp, when divided by the free stream q, is known as a "pressure coefficient" and is denoted by the symbol C_p. Thus, in general:

$$C_p = \frac{\Delta p}{q} \qquad (84)$$

Equation (83) states that the pressure coefficient at the stagnation point is equal to unity. Similar evaluations of C_p may be made at various points on the cylinder. For example, from theoretical flow considerations it has been found that the velocity at any point on a cylinder is subject to the relationship:

$$V = 2V_0 \sin \theta \qquad (85)$$

The angle, θ, is the angle shown on Figure 13.

At point 2, the velocity V_2, is equal to twice the free stream velocity, V_0, since the sin of 90° is unity. That is:

$$V_2 = 2V_0 \qquad (86)$$

The relationship can be written for point 2 as follows:

$$p_0 + q_0 = p_2 + q_2$$

$$p_0 + q_0 = p_2 + \frac{1}{2} \rho V_2^2$$

Substituting equation (86) into the above expression,

$$p_0 + q_0 = p_2 + \frac{1}{2} \rho (2V_0)^2$$

$$p_0 + q_0 = p_2 + 4\left(\frac{1}{2} \rho V_0^2\right)$$

Then,

$$p_2 - p_0 = -3q_0$$

or,

$$C_p = \frac{p_2 - p_0}{q_0} = -3 \qquad (87)$$

The negative value of C_p can exist only if p_2 is less than p_0. This must be the case, since V_2 is greater than V_0 which satisfies the Bernoulli equation.

A graphical representation of the static pressures existing on the surface of the cylinder is shown on Figure 14.

The arrows pointing toward the body are positive (greater than free stream) pressures; while arrows pointing away from the body indicate negative (less than free stream) pressures. The length of arrow is proportional to the value of C_p existing, and its magnitude may be found by scaling.

It should be noted that when an ideal fluid is considered, the static pressures are distributed symmetrically over the cylinder. Because the pressures acting over the area will neutralize, there can be no resulting force in any direction. Physically this is known to be untrue since there is a force in the downstream direction (called "drag"), due to the viscous characteristic of the fluid. The effect of the viscous force is to change the pressure distribution so that there is a drag force on the cylinder. A diagram of the static pressure distribution over a cylinder in a real fluid is shown on Figure 15.

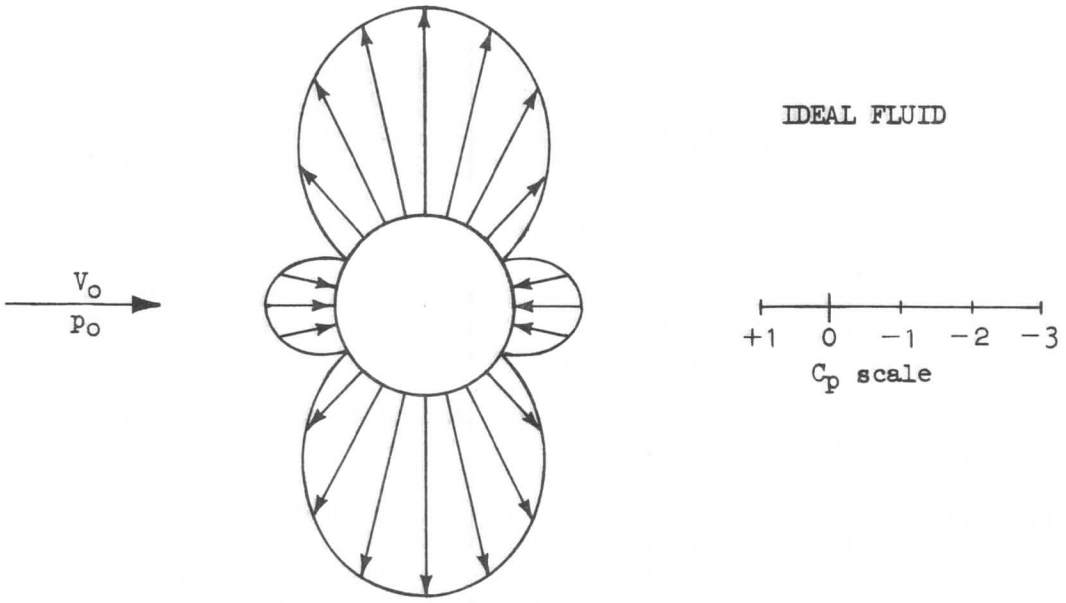

Figure 14.

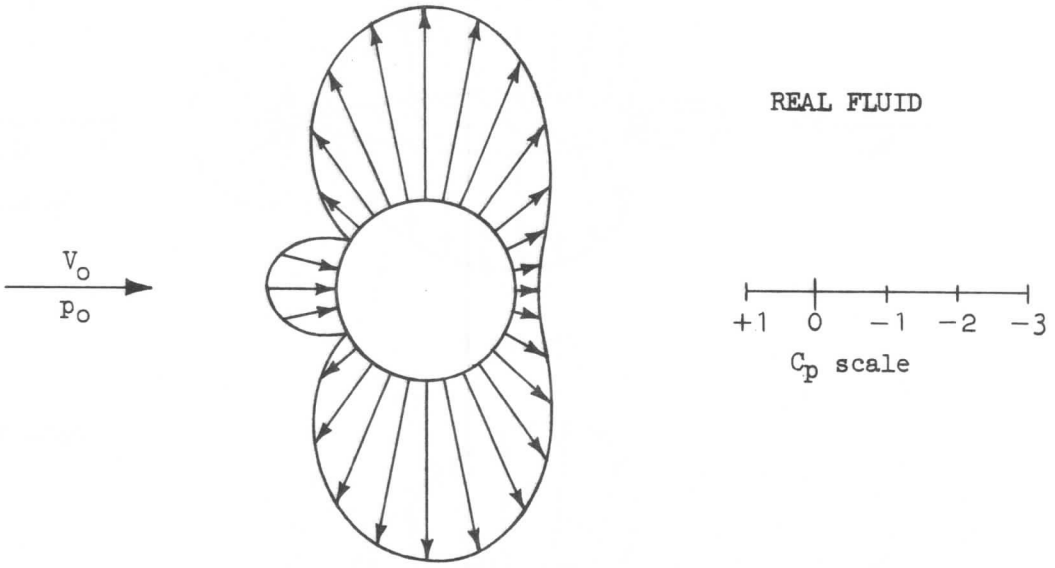

Figure 15.

The concept of pressure distribution over a geometrically simple object may be applied to a more practical aerodynamic shape. Figure 16 shows an airfoil section in an ideal fluid.

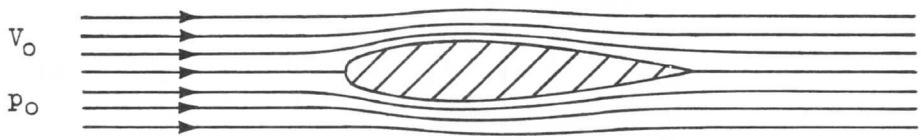

Figure 16.

The static pressure distribution may be shown graphically on this shape also. A symmetrical air foil section is shown, that is, the curvature is the same on top as it is on the bottom of the airfoil. See Figure 17.

Again, as with the cylinder, the net force acting on the body is zero, although it is not obvious from the figure.

In a real fluid the pressure distribution will be essentially as shown in Figure 17 except that at the trailing edge the pressure fails to rise to the stagnation value. See Figure 18. This difference will produce a drag in the direction of the flow. Drag is a force resisting forward motion. In practice it is tolerated only because it cannot be eliminated. The primary purpose of the airfoil shape is to generate a lifting force. The relationship of the lift and drag forces and their effect will be discussed in another chapter.

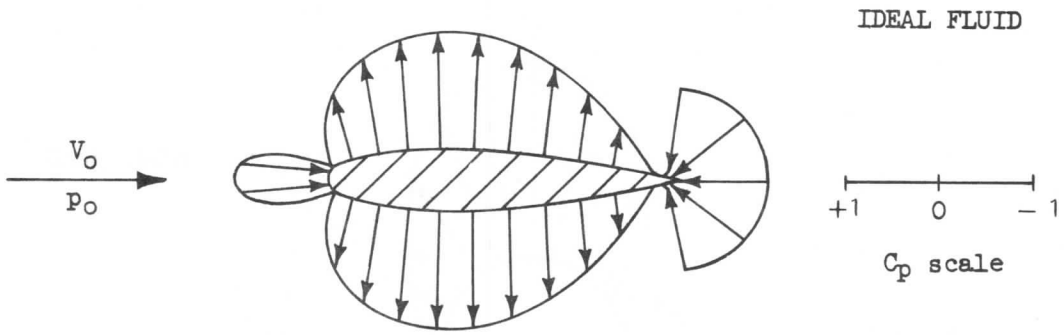

Figure 17.

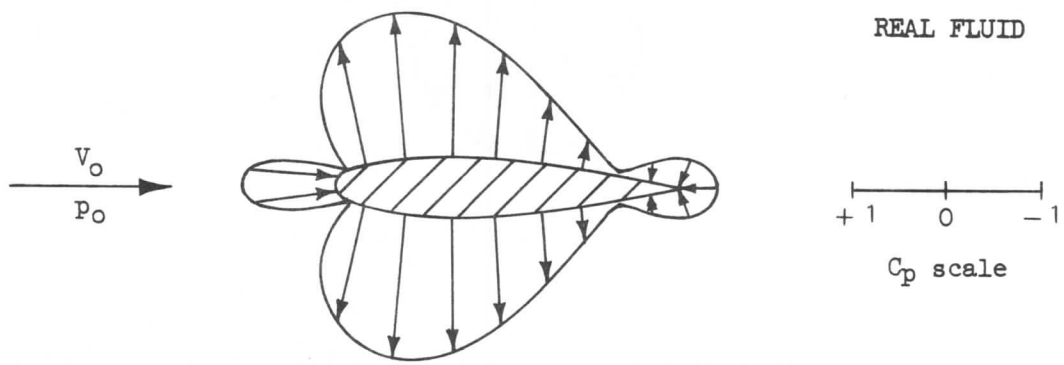

Figure 18.

1-14 FORCE EQUATIONS

The generalized equation for the force acting on any body immersed in a moving fluid is dependent on several variables. The basic force equation may be derived by a mathematical procedure known as "dimensional analysis."

Dimensional reasoning is based on the assumption that the most fundamental form in which variables may be related to form an equation is the exponential form. Also of major importance in this technique is the realization that the dimensions on both sides of the equation must be equal. For example, if the dimensions on one side of an equation reduce to the units of lb/ft^2, then the dimensions on the other side must also reduce to the same units. For most problems these dimensions may be expressed in terms of mass, length, and time symbolized by M, L, and T, respectively.

The first step in attempting to find the form of an equation is to consider all the variables that could affect the quantity being solved for. In this case, the force due to the fluid motion past a body is to be determined. The variables that are considered are:

(1) Velocity of fluid, V, in ft/sec.
(2) Fluid mass density, ρ, in $slugs/ft^3$
(3) Characteristic size, l, in ft
(4) Fluid coefficient of viscosity, μ, in slugs/ft.sec.
(5) Compressibility, Speed of sound, a, in ft/sec.

The latter two items manifest themselves since a real fluid is being considered.

A general relationship may be assumed for the fluid force, F:

$$F = C\rho^{\alpha}\, l^{\beta}\, V^{\gamma}\, \mu^{\delta}\, a^{\epsilon} \qquad (88)$$

Where C is a constant which depends on body shape and is dimensionless, and α, β, γ, δ, ϵ are as yet undetermined exponents.

The next step is to express all the variables in terms of the quantities M, L, and T. Writing Newton's second law of motion in terms of the fundamental units:

$$F = \frac{ML}{T^2} \qquad (89)$$

Equation (88) may now be written in terms of fundamental units:

$$\frac{ML}{T^2} = C\left(\frac{M^{\alpha}}{L^{3\alpha}}\right)\left(L^{\beta}\right)\left(\frac{L^{\gamma}}{T^{\gamma}}\right)\left(\frac{M^{\delta}}{L^{\delta}\, T^{\delta}}\right)\left(\frac{L^{\epsilon}}{T^{\epsilon}}\right) \qquad (90)$$

Powers of like variables are now equated:

$$\left.\begin{aligned} M:&\quad 1 = \alpha + \delta \\ L:&\quad 1 = -3\alpha + \beta + \gamma - \delta + \epsilon \\ T:&\quad 2 = \gamma + \delta + \epsilon \end{aligned}\right\} \qquad (91)$$

AERODYNAMICS

Since fluid forces are usually expressed in terms of ρ, V, and l, the exponents of these variables will be solved for absolutely. Therefore, equations (91) will be solved in terms of α, γ, and β.

$$\left.\begin{aligned} \alpha &= 1 - \delta \\ \gamma &= 2 - \delta - \epsilon \\ \beta &= 2 - \delta \end{aligned}\right\} \qquad (92)$$

Substituting the results of equations (92) into equation (88):

$$F = C\rho^{1-\delta} l^{2-\delta} V^{2-\delta-\epsilon} \mu^{\delta} a^{\epsilon}$$

or,

$$F = C\rho\, l^2 V^2 \left(\frac{\rho V l}{\mu}\right)^{-\delta} \left(\frac{V}{a}\right)^{-\epsilon} \qquad (93)$$

This expression shows that the fluid force is not only dependent on ρ, V^2, and l^2 as surmised, but is also dependent on two non-dimensional parameters raised to unknown exponents. The first combination of terms is called "Reynolds' number" after Osborne Reynolds, who first showed that the fluid flow pattern depends upon this number. The latter combination should be recognized as Mach number, which was discussed previously.

$$\text{Reynolds number, R.N.} = \frac{\rho V l}{\mu} \qquad (94)$$

$$\text{Mach number, M} = \frac{V}{a}$$

In order to simplify the notation, equation (93) is usually rewritten to envelope the fluid dynamic pressure, $1/2\ \rho V^2$, or q. It is noted that l^2 is the square of a representative length and is thus a representative area which may be called "A".

Thus,

$$F = 2CqA\ RN^{-\delta}\ M^{-\epsilon}$$

or,

$$F = C_f\ q\ A \qquad (95)$$

where C_f is now a new parameter which depends not only on body shape, but also on Reynolds number and Mach number.

Experience has shown that Reynolds number is the important criterion for lowspeed flight and Mach number is important for high-speed flight. More will be said later of these quantities. It may be mentioned in passing, however, that Mach number is by far the most important quantity with respect to large, high speed jet transports such as the Boeing 707 and 720.

Of considerable interest in aerodynamic work is the turning moment of the force of equation (95) about some arbitrary point. A "moment," as will be recalled, is the product of the force and the distance from its point of application to an arbitrary point. The usual dimensions for a moment are the "foot pound." Similar to the general force equation, the general moment equation can be developed by dimensional analysis. The expression will evolve in the form:

$$M = C\rho\, V^2\, l^3\, RN^{-\lambda} M^{-\Gamma} \qquad (96)$$

Where C is a different value, and λ and Γ are new exponents of Reynolds number and Mach number. The dimensionless quantities of equation (96) may be combined:

$$M = C_m\, qAl \qquad (97)$$

Where C_m is a non-dimensional moment coefficient like the force coefficient C_f in equation (95), and l is a representative length.

1-15 AIRFOIL PROPERTIES

An airfoil is a shape or contour which has aerodynamic properties. The more familiar examples of airfoils are airplane wings, propellers and compressor and turbine components of the jet engine. Before the aerodynamic properties of an airfoil are described, some physical definitions should be discussed. Primarily, these will be airplane particulars inasmuch as a separate discussion on the application of many of the principles presented herein follows in the turbojet engine section.

Physical Properties

Wingspan is the tip to tip dimension of the airplane wing, regardless of its geometric shape. The symbol for wingspan is b, and is illustrated on Figure 19.

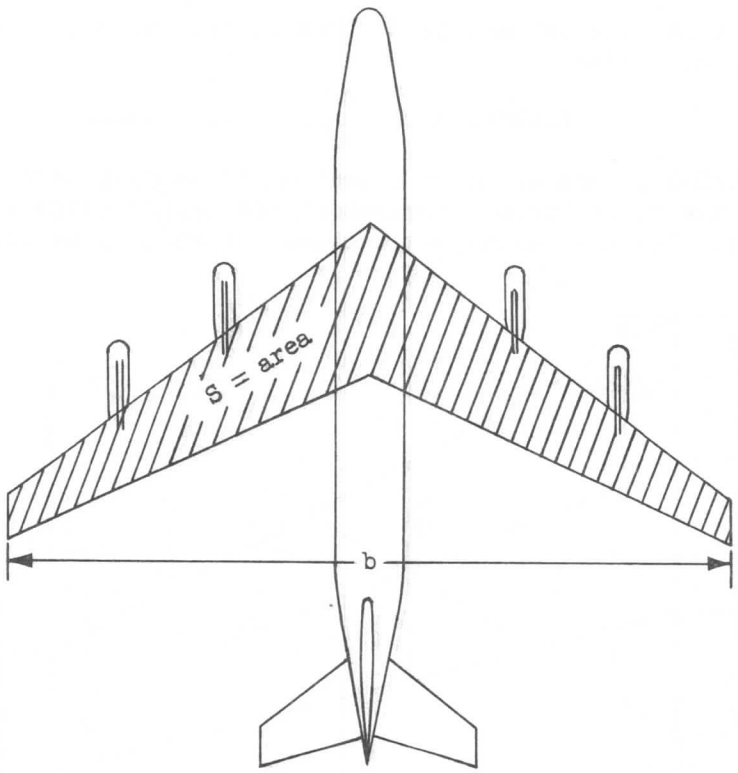

Figure 19.

Area of a wing is the projection of the outline on the plane of the chord. The wing is considered to extend without interruption through the fuselage and na-

celles. The shaded area on Figure 19 shows the area of a swept wing airplane. The area of a wing is usually symbolized by "S."

Chord is the distance from the wing leading edge to the trailing edge. The chord is seldom constant on a wing, due to tapering or curving boundaries, and so the chord used in calculations is then an average chord. The symbol for the chord is c.

A simple relationship may now be written involving area, span, and average chord.

$$S = b\,c \qquad (98)$$

Aspect ratio of a rectangular wing is the ratio of the span to the chord, and the notation is AR.

$$AR = \frac{b}{c} \qquad (99)$$

This holds for rectangular wings but for all other planforms another form may be derived from the basic relationship.

$$AR = \frac{b}{c}\frac{b}{b} = \frac{b^2}{bc}$$

$$AR = \frac{b^2}{S} \qquad (100)$$

Taper ratio is of some interest and is defined as the ratio of the tip chord, c_t, to the root chord, c_r. Thus,

$$\text{Lambda, } \lambda = \frac{c_t}{c_r} \qquad (101)$$

Mean aerodynamic chord is the chord of a section of an imaginary airfoil on the wing which would have force vectors throughout the flight range identical to those of the actual wing. The mean aerodynamic chord, or MAC, may be determined by

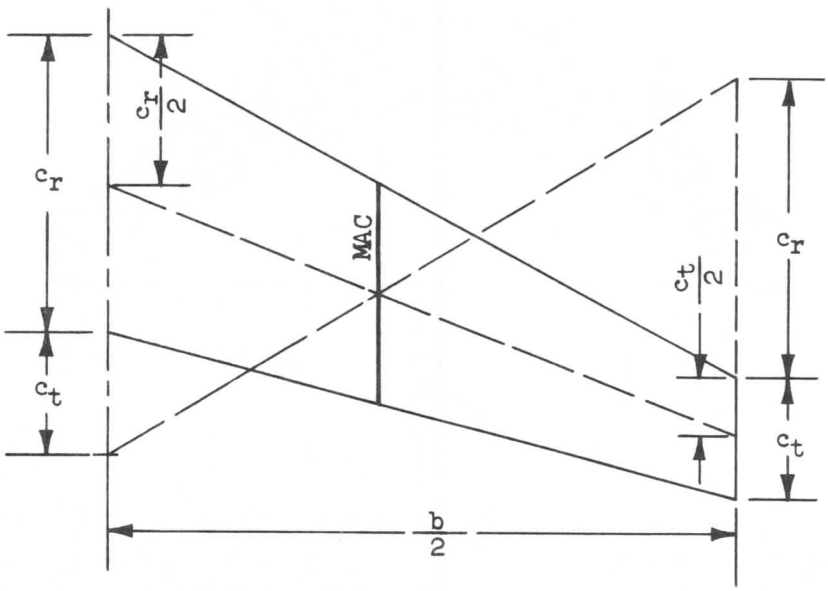

Figure 20.

calculation, as shown below. It has its usefulness as a reference for the location of the relative positions of the wing center of lift and the airplane center of gravity. Ultimately the load distribution determines the static balance and stability of the airplane.

Generally, the MAC can be closely approximated by the graphical method shown in Figure 20. This method introduces only a negligible error and is very simple to accomplish. c_r and c_t refer to the root chord and tip chord respectively.

The rigorous definition of the length of the MAC is given by the following calculus expression and by reference to Figure 21.

$$MAC = \frac{\int c^2 db}{\int c db}$$

$$MAC = \frac{\int c^2 db}{S} \qquad (102)$$

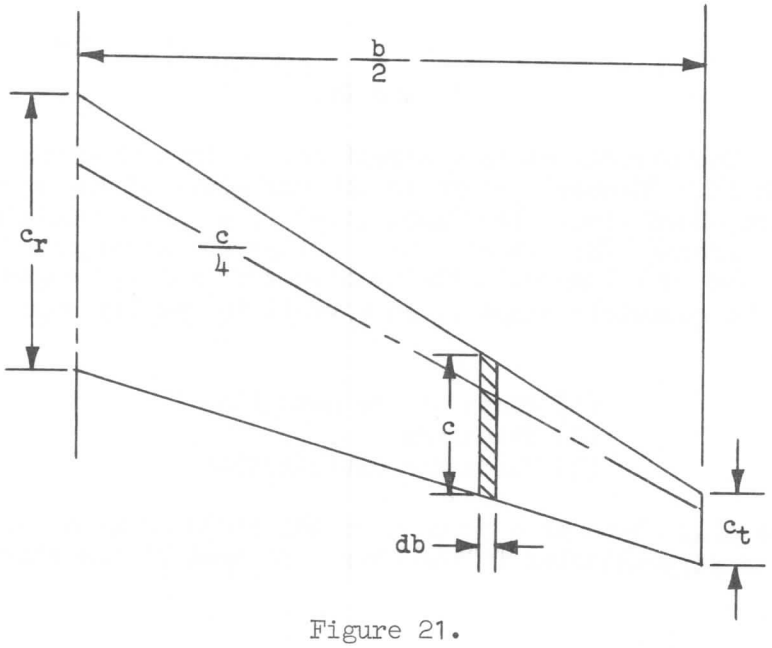

Figure 21.

Equation (102) will reduce to the following for a straight tapered wing as in Figure 21:

$$MAC = \frac{2}{3}\left(c_r + c_t - \frac{c_r c_t}{c_r + c_t} \right)$$

$$MAC = \frac{2}{3} c_r \left(\frac{\lambda^2 + \lambda + 1}{\lambda + 1} \right) \qquad (103)$$

Sweepback is the angle between a line perpendicular to the plane of symmetry of the airplane and the quarter chord, c/4, of each airfoil section. The symbol of the sweep angle is the Greek letter Lambda, Λ . See Figure 22.

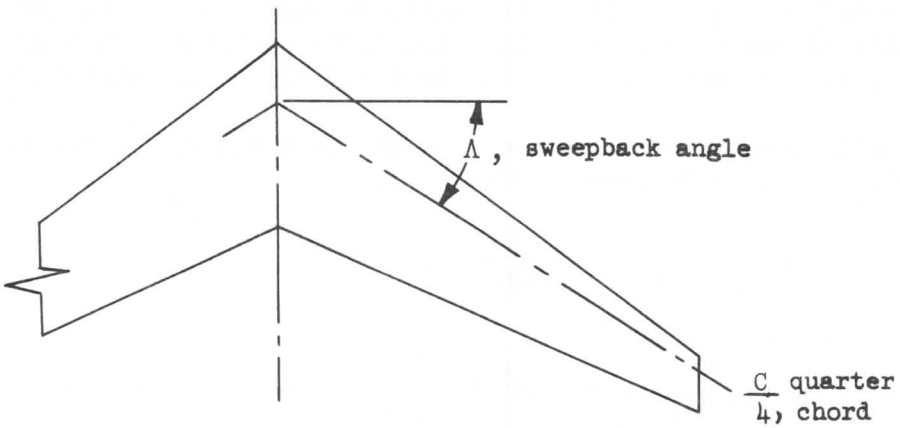

Figure 22.

Airfoil section. The airfoil section itself has certain physical characteristics which distinguish it. "Camber" refers to the curvature of the section, or the departure from the chord line. The "mean line" is a line equidistant from the upper and lower surfaces. The "chord line" is then the straight line joining the intersections of the mean line with the leading and trailing edges of the airfoil. See Figure 23. The geometric shape of an airfoil is usually expressed in terms of the following:

(1) Shape of the mean line
(2) Thickness
(3) Thickness distribution

Thickness is generally shown as a percent of the chord or as a ratio of the length of the line perpendicular to the chord to that of the chord; that is, t/c.

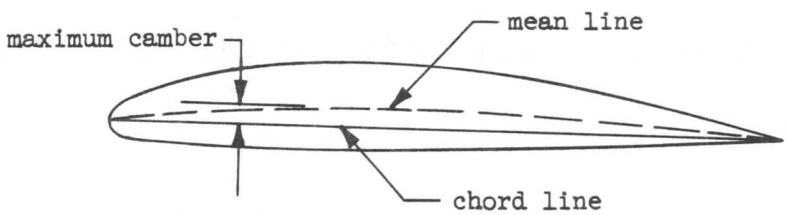

Figure 23.

AERODYNAMICS

The National Aeronautics and Space Administration, formerly National Advisory Committee for Aeronautics (NACA) has tested many airfoil shapes and has developed a systematic series of sections. The results of these tests are published and are available through the government printing agency. NACA Report No. 824, "Summary of Airfoil Data" explains the system of identifying the various series of airfoils in addition to the airfoil data presented. Of the various series airfoils, the NACA five-digit series will be described here. The numbering system for airfoils of the NACA five-digit series is based on a combination of theoretical and geometric characteristics. The first integer indicates that the amount of camber in terms of the relative magnitude of the design lift coefficient(in tenths)is thus three-halves of the first integer. The second and third integers together indicate the distance from the leading edge to the location of the maximum camber; this distance in percent of the chord is one-half the number represented by these integers. The last two integers indicate the airfoil thickness in percent of the chord. The NACA 23012 airfoil thus has a design lift coefficient of 0.3, has its maximum camber at 15 percent of the chord, and has a thickness ratio of 12 percent. Figure 24 shows the ordinates of this airfoil.

NACA 23012

(Stations and ordinates given in percent of airfoil chord).

UPPER SURFACE		LOWER SURFACE	
STATION	ORDINATE	STATION	ORDINATE
0	----	0	0
1.25	2.67	1.25	-1.23
2.5	3.61	2.5	-1.71
5.0	4.91	5.0	-2.26
7.5	5.80	7.5	-2.61
10	6.43	10	-2.92
15	7.19	15	-3.50
20	7.50	20	-3.97
25	7.60	25	-4.28
30	7.55	30	-4.46
40	7.14	40	-4.48
50	6.41	50	-4.17
60	5.47	60	-3.67
70	4.36	70	-3.00
80	3.08	80	-2.16
90	1.68	90	-1.23
95	.92	95	- .70
100	(.13)	100	(- .13)
100	----	100	0

Figure 24.

Aerodynamic Properties

When an airfoil experiences fluid motion, that is air moving over its surfaces, there exists a pressure pattern similar to that of Figure 18. If there is camber to the airfoil, there will be a difference in the pressure pattern of the

upper surface from that of the lower surface. Furthermore, if the airfoil is fixed at some angle to the airflow, the pressure distribution, hence, the velocities over the surface will be altered. The angle between the remote velocity, V_0, and the chord is called the "angle of attack" and is given the Greek symbol Alpha, α. See Figure 25.

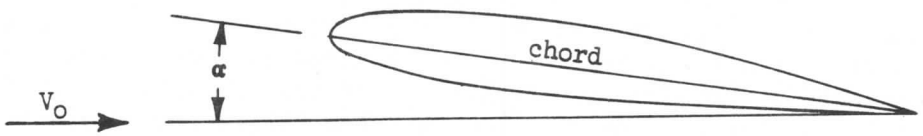

Figure 25.

The pressure distribution on the airfoil at some angle of attack might appear as shown on Figure 26.

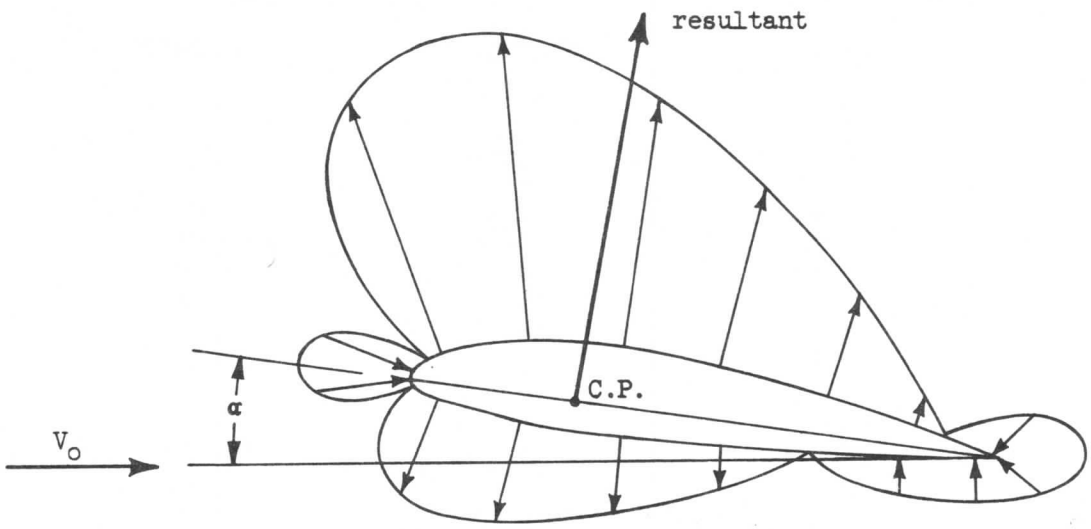

Figure 26.

The net result of the static pressure distribution over the surface is a lifting force. This resultant force is conveniently represented by a single force of some magnitude acting at a point on the chord called the "center of pressure," or CP.

The resultant force can now be resolved into two component forces, one component perpendicular to the relative or remote velocity and the other component parallel to it. The former force is called "lift" and the latter "drag." The resultant is thus replaced and is no longer considered. The forces on the airfoil now appear as in Figure 27.

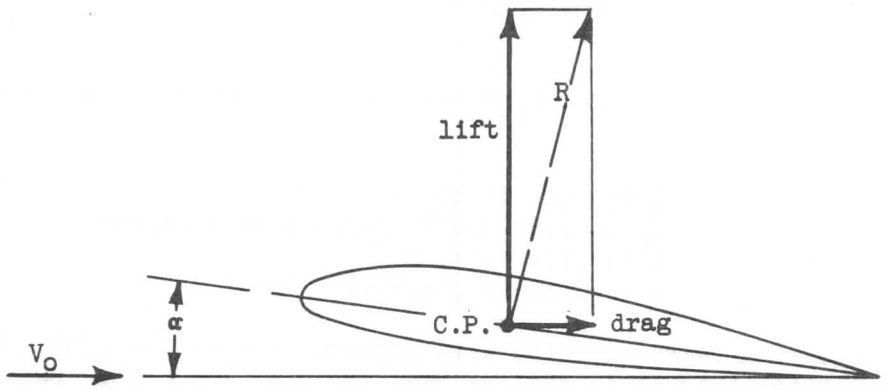

Figure 27.

It is known that the center of pressure will move with changes in angle of attack. At low angles of attack, the center of pressure is located near the trailing edge of the airfoil, and as the angle of attack is increased the center of pressure moves forward. Thus, it is desirable to have some fixed reference point to which the force system can be transferred. If this is done, compensation must be made on the airfoil for the change. A moment is introduced about the fixed reference point which will exactly compensate for the change in moment caused by moving the lift and drag vectors from the center of pressure. The quarter-chord point is commonly selected as the reference point since it has been found that the moment coefficient about the quarter-chord of most airfoils is nearly constant. (The point at which the moment is independent of angle of attack is called the aerodynamic center.) The magnitude of the moment obviously varies with camber and thickness as well as angle of attack. Figure 28 shows the transformation of forces.

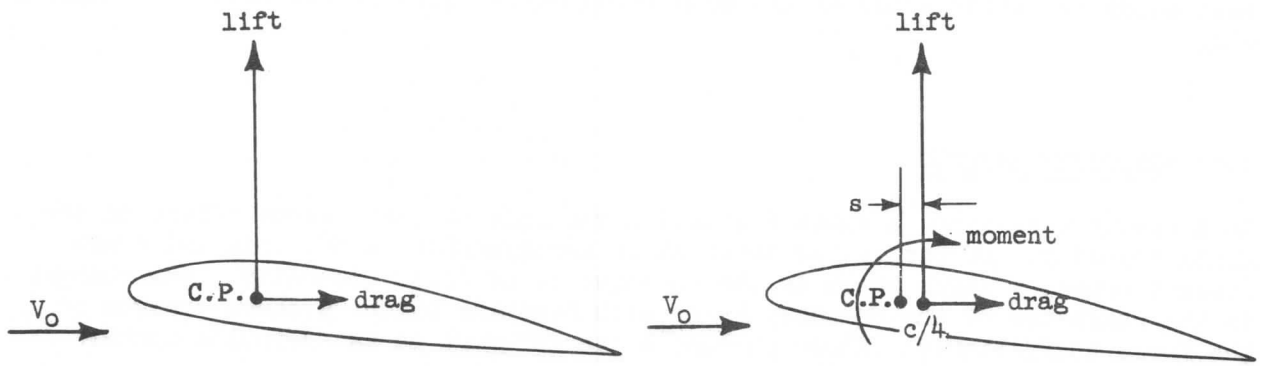

Figure 28.

From the application of equation (95) it is possible to evaluate the lift and drag forces; likewise, the moment from equation (97):

Equation (95),

$$F = C_f qA$$

For lift:

$$L = C_L qS \qquad (104)$$

where,

L is lift force, lb
C_L is lift coefficient, dimensionless
S is wing area, ft^2
q is dynamic pressure, lb/ft^2

It should be noted that a representative area appears in equation (95). With reference to a complete wing, it is obvious that the most reasonable representative area is the wing area. Similarly, the drag equation may be written:

$$D = C_D qS \qquad (105)$$

where,

D is drag force, lb
C_D is drag coefficient, dimensionless

Finally, the moment equation may be written:

Equation (97),

$$M = C_m qAl$$

For the wing,

$$M = C_m qSc \qquad (106)$$

where,

M is moment, ft-lb
C_m is moment coefficient, dimensionless
c is chord length, ft

The representative length, l, will be the chord length for pitching moments (moment about the pitch axis) or the mean aerodynamic chord in the case of a tapered wing.

1-16 VISCOSITY EFFECTS

In a previous section, a short discussion was made of the viscous effect on the fluid velocity. Of particular interest in aerodynamics is the thin and ever-present boundary layer which is the consequence of fluid viscosity. Any changes in the character of the boundary layer with Reynolds number produce changes in the force coefficients. These phenomena are referred to as "Reynolds-number effects" or "scale effects."

The type of flow in the boundary layer depends upon the smoothness of the fluid flow approaching the body, the shape of the body, the surface, the pressure gradient in the direction of flow, and the Reynolds number of the flow. There are found to be two basic types of boundary layers; the "laminar boundary layer," and the "turbulent boundary layer." Their distinguishing characteristics are shown in Figure 29.

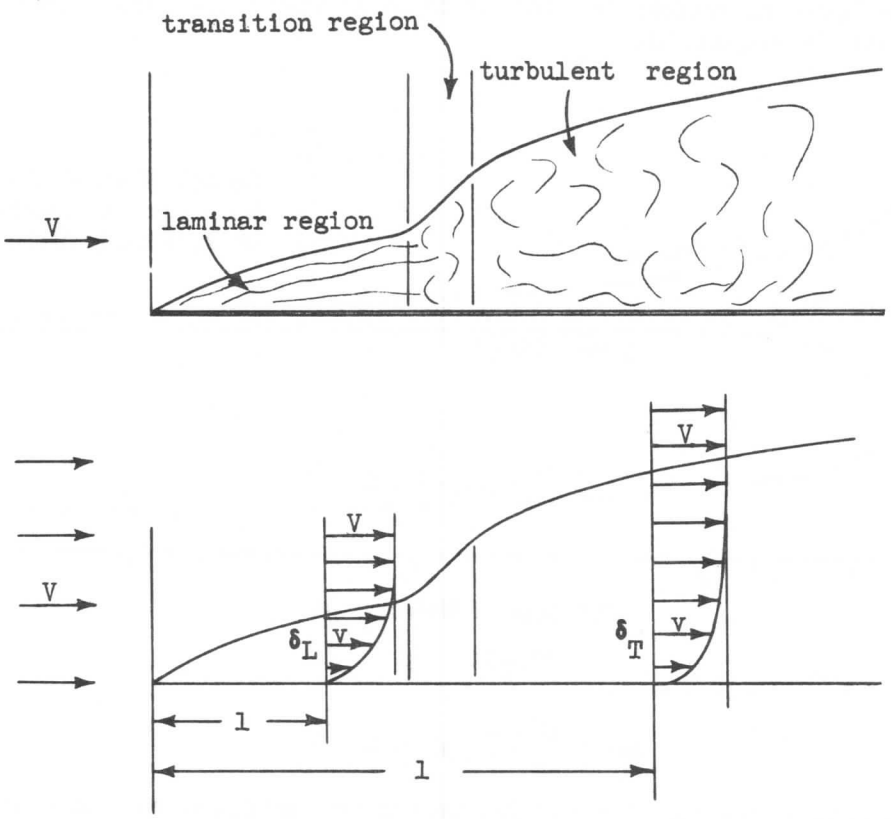

Figure 29.

Consider the frictional drag associated with the flow of fluid over one side of a smooth flat plate. The flow is parallel to the surface and is depicted in the figure. The flow of fluid immediately downstream of the leading edge is very smooth and is known as laminar flow. Further downstream it will be found that the thickness of the layer increases as more and more air next to the surface becomes affected. The thickness of this layer is usually expressed in terms of Reynolds number.

$$\delta_L = \frac{5.2(l)}{\sqrt{RN}} \qquad (107)$$

where,

δ_L is laminar thickness, ft
l is length from leading edge, ft
RN is Reynolds number $\left(\frac{\rho V l}{\mu}\right)$, dimensionless

As the air progresses downstream along the plate a point is reached where the laminar flow is found to break down and the flow tends to become unsteady and the thickness increases rather suddenly. This is a transition region and is found to vary considerably in character depending somewhat on the turbulence of the

remote airflow and the smoothness of the surface. It is found from experiments that the quantity which defines the transition is Reynolds number. Under ideal conditions, the Reynolds number for the transition region is approximately 530,000, as shown in Figure 30.

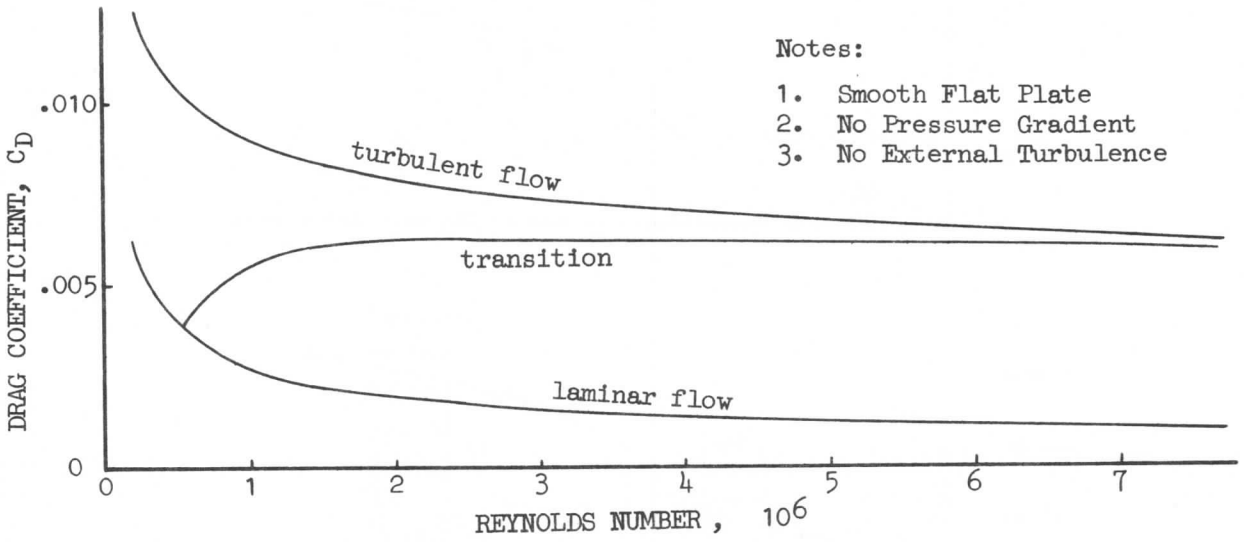

Figure 30.

Thus, $$RN = \frac{\rho V l}{\mu} \cong 530{,}000$$

Beyond the transition region, the air becomes more turbulent as there is considerable fluid particle motion. This region is the turbulent boundary layer and its thickness is expressed as:

$$\delta_T = \frac{.37(l)}{\sqrt[5]{RN}} \qquad (108)$$

The flow on a body other than a flat plate will be changed somewhat, primarily due to the shape. Because of the shape, the velocities over the surface become changed from the free stream velocity. This, in turn produces negative and positive "pressure gradients" on the forward and rearward sections of the body, respectively. A pressure gradient is the slope of the static pressure line on a surface, or the rate of change of static pressure with distance. On the forward portion of an airfoil the static pressure is growing more negative. This means that an air particle will feel a pressure gradient which is tending to assist the particle motion, or accelerate it. This is referred to as an "assisting" pressure gradient. However, over the rear portion of the airfoil, the opposite is true. The static pressure is becoming more positive with the result that the particle feels as though it were being resisted. This increasingly positive pressure gradient is thus called an "adverse" pressure gradient. See Figure 31.

An assisting pressure gradient is seeking to increase the velocities in the boundary layer. An adverse pressure gradient slows down the air in the boundary

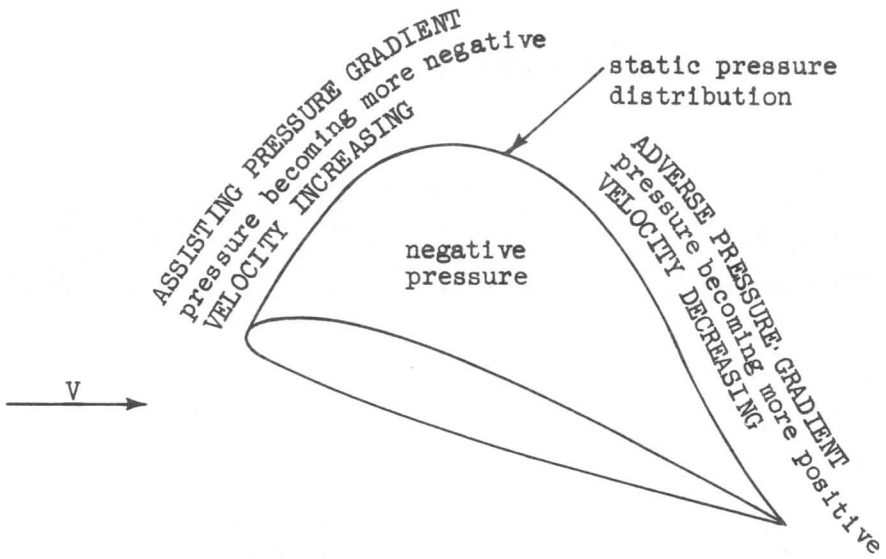

Figure 31.

layer, particularly the air immediately adjacent to the surface, where the velocity is initially the lowest. When the adverse pressure gradient becomes large enough, separation takes place. This means that a finite layer of air at the surface is actually stopped relative to the surface. This layer upsets the continuity of the airflow and an eddying condition is set up which results in air flow separation.

In Figure 32, two angle-of-attack conditions are shown. It will be noted in comparing the two pressure distributions that the adverse pressure gradient over the rear portion of the airfoil is much less at the low angle of attack than at the high angle. Thus, separation will occur more easily at high angles than at low angles of attack due to the boundary layer phenomenon just discussed. Thus, the high angle of attack separation may be said to be primarily instigated by the boundary layer characteristics.

In the application of the boundary layer phenomena to the modern airplane, much can be said. The flight Reynolds numbers on airplanes as large and as fast as the 707 and 720 are so large that transition from laminar to turbulent flow will occur almost immediately on the leading edges of all surfaces. Thus, all the flow is considered turbulent.

An important consideration in the control of boundary layer has to do with the layer thickness. As can be seen from Figure 29, the boundary layer grows in thickness as it proceeds rearward. This fact makes it more important to maintain surface smoothness near the leading edges of surfaces than farther aft. This is because a surface irregularity (rivets out of contour, or a poor skin joint) will cause a greater disruption to the normal flow when it is in a region of thin boundary layer than if it were farther aft and could be more easily buried in the thicker boundary layer. Thus, for maintenance of an airplane in a condition for minimum possible skin friction drag, its surface should be kept free from discontinuities, especially in the more forward regions of all surfaces.

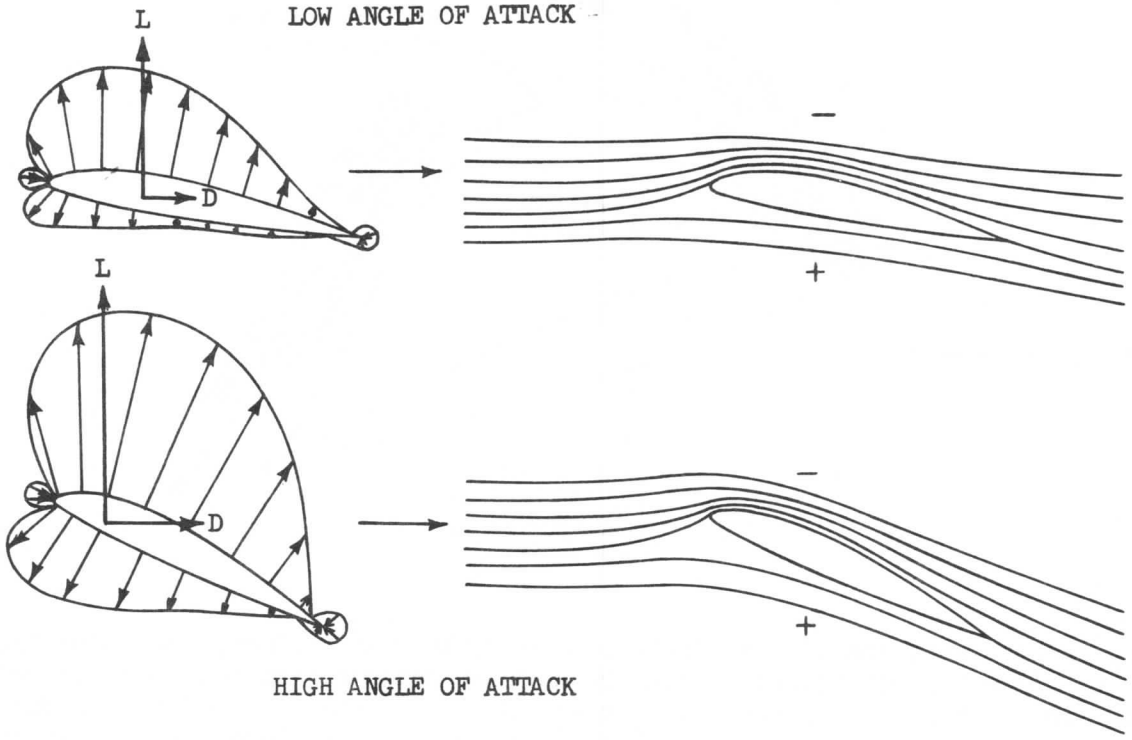

Figure 32

Another point which should be mentioned is that the boundary layer represents "dead air" which has had energy removed from it by internal friction within the layer. This means that air taken into the engine, for instance, will have this layer of dead air if there is an appreciable surface ahead of the air intake. On pod-mounted engines, the engine air intakes have essentially zero-length intakes, so that this problem is not encountered. On some fighter aircraft with fuselage-side intakes a boundary layer bleed system must be used to get rid of this air before it is taken into the engine where it would reduce efficiency.

1-17 LIFT AND DRAG

Obviously, if an airfoil section or wing is operating under fixed conditions of density and velocity, then the lift and drag will change if the angle of attack is changed. If the lift and drag change, then the coefficients of the lift and drag must also change in order for equation (104) and (105) to be valid.

If an airfoil section is considered which is first operating at a small, or low angle of attack, and then at a large, or high angle of attack, the lift and drag will both be smaller in the first instance than in the second. This has been borne out by countless experimental tests. Figure 32 shows the pressure distribution and flow pattern for these two conditions.

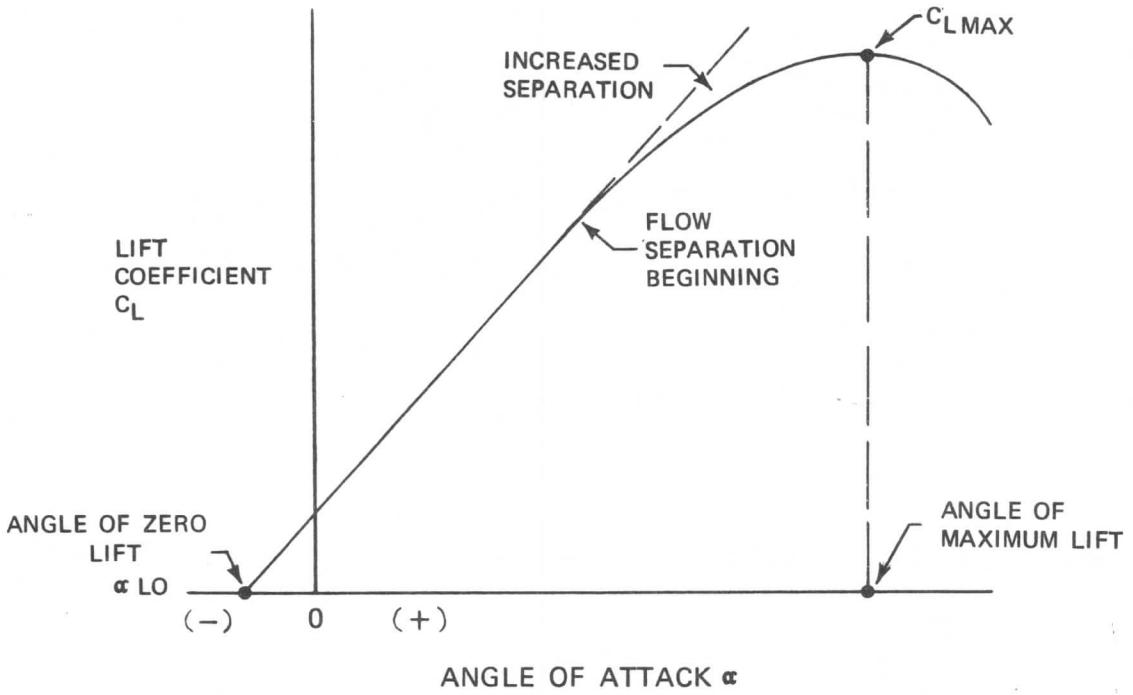

Figure 33.

From theoretical considerations it may be shown that the lift (or lift coefficient) at constant velocity will increase uniformly (or linearly) with increase in angle of attack. Test data on airfoils usually show a linear variation of lift coefficient, C_L, with angle of attack, α, through a considerable range of angles. Ultimately, however, the airfoil will reach such an angle that the air, in flowing over its top surface, will find it impossible to remain in contact with the surface. At this point airflow separation will begin and the lift curve will start to depart from linearity, see Figure 33. As the angle of attack is increased further the airflow separation increases until a maximum lift coefficient value is reached, $C_{L_{max}}$. Beyond this point C_L decreases, either abruptly or gradually, depending on the particular airfoil. This phenomenon is called "stalling", and the angle corresponding to $C_{L_{max}}$ is called the stall angle.

A diagram of the approximate flow condition at the stall angle is shown in Figure 34. This shows the turbulent eddying wake characteristic of separated airflow. It should be noted that at the other end of the lift curve (Figure 33) the point at which C_L is zero does not occur at "zero angle of attack," but at some small negative angle, α_{L_o}. This is characteristic of an air foil with camber; the more the camber the more negative is the angle of zero lift. For an uncambered, or symmetrical airfoil, the angle of zero lift is zero.

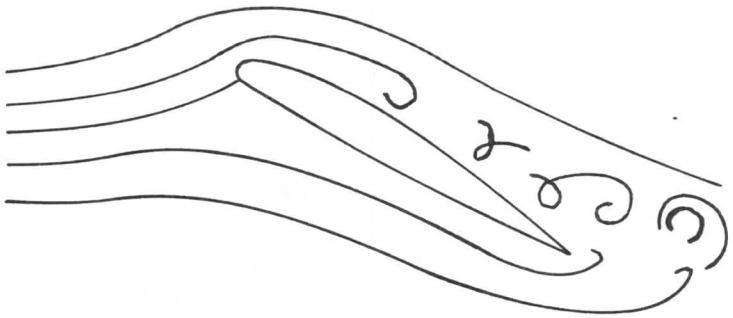

Figure 34.

The slope of the linear portion of the lift curve is of interest, mathematically.

$$C_L = m\alpha + b$$

When, $C_L = 0, \alpha = \alpha_{L_o}$

Thus, $0 = m\alpha_{L_o} + b$

or, $b = -m\alpha_{L_o}$

Therefore after substituting for b:

$$C_L = m\alpha - m\alpha_{L_o}$$

$$C_L = m(\alpha - \alpha_{L_o}) \qquad (109)$$

$$C_L = a(\alpha - \alpha_{L_o})$$

The letter "m" is usually written when the slope is measured per radian, and the letter "a" is written when the slope is measured per degree. The use of either letter here should not be confused with other definitions.

If the relationship between drag coefficient and angle of attack is shown, it will appear considerably different from the lift coefficient and angle of attack curve. Below the stall most airfoils produce the characteristic parabolic shape as shown on Figure 35.

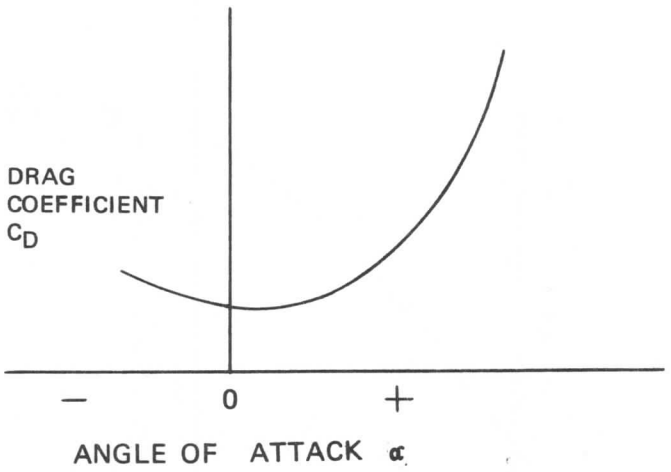

Figure 35.

During the accumulation of wind tunnel test data on an airfoil, lift and drag data are recorded for constant values of angle of attack. When applying this information to aerodynamic problems, particularly those concerned with performance, it is more useful in another form. Angle of attack, α, is eliminated and a curve showing the relationship of lift coefficient to drag coefficient is used. The curve is commonly called the "drag polar," and it is parabolic in shape. This curve is shown in Figure 36 for a wing, but the drag polar for the complete airplane will be found to have a similar shape.

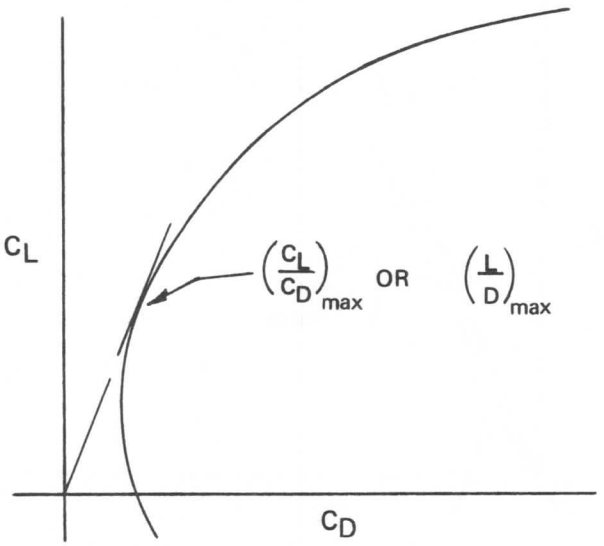

Figure 36.

There is still another curve of interest which can be derived from Figures 32 and 35. If C_L is divided by C_D at every angle of attack up to the stall, a new curve may be drawn as in Figure 37.

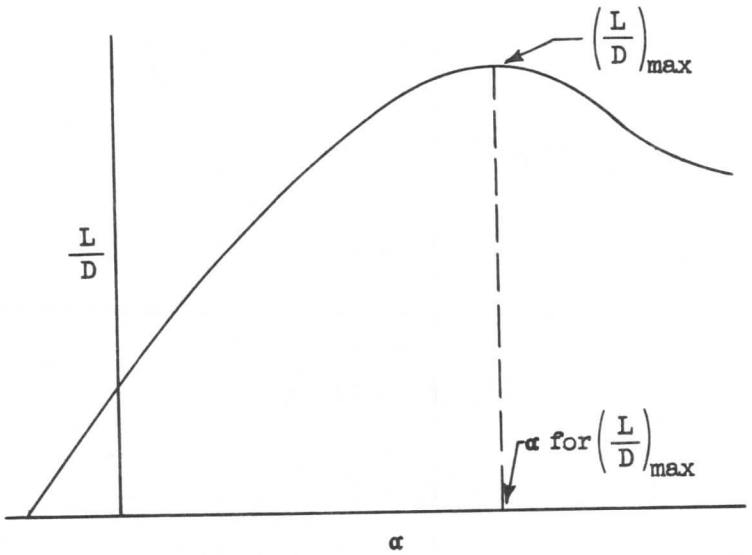

Figure 37.

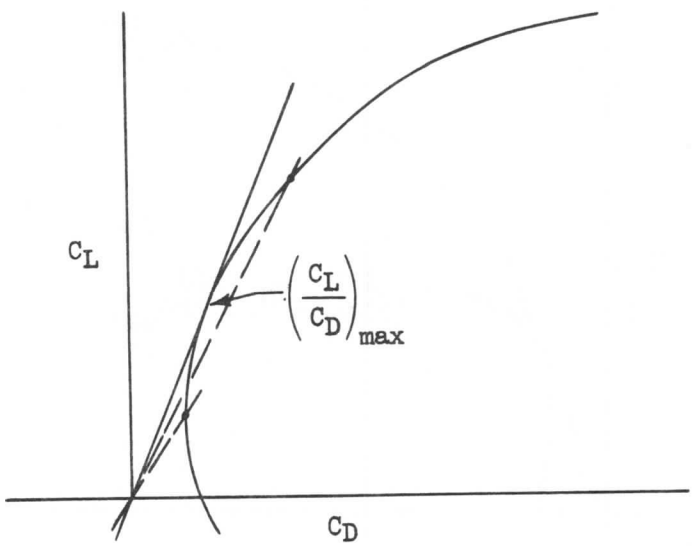

Figure 38.

From equations (104) and (105):

$$\frac{L}{D} = \frac{C_L qS}{C_D qS} = \frac{C_L}{C_D} \qquad (110)$$

It should be noted that at a certain angle of attack the L/D ratio becomes a maximum. The significance of this point is that it represents the most efficient operation of the airfoil. In effect, it is the point at which is obtained the most lift for the least drag. Another curve which will produce the same result, but from a slightly different approach to the determination of maximum L/D, is shown in Figure 38. At several points along the curve, there can easily be found the C_L/C_D ratio. If lines through the origin connect with these points, the slope of each line will define a C_L/C_D ratio. The maximum possible slope will obviously be defined by a line from the origin which is tangent to the curve. The point of contact with the curve will define the C_L and C_D values for $(L/D)_{max}$.

The reason for being concerned with $(L/D)_{max}$ will become more apparent in later discussions. However, a clue to the most efficient point of operation of an airplane may be found in the investigation of the maximum lift to drag ratio.

1-18 DRAG ANALYSIS

In the previous section, it was noted that the relationship between C_L and C_D is parabolic in shape. It is of interest to discover some of the reasons for this.

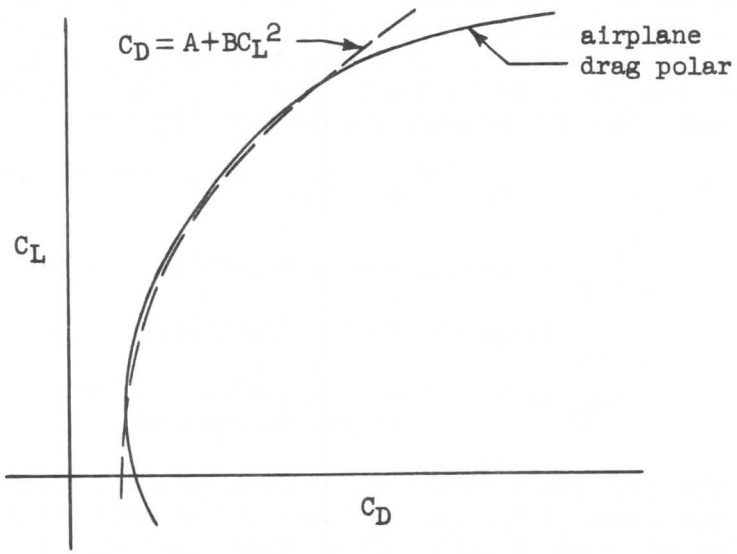

Figure 39.

The drag coefficient of the airplane may be expressed with sufficient accuracy by an equation of the form:

$$C_D = A + BC_L^2 \qquad (111)$$

The constants A and B are usually found by wind tunnel tests. The first, A, depends mostly on the airfoil section and its Mach number and Reynolds number; while B depends mostly on the aspect ratio of the wing. Figure 39 shows the close agreement of an airplane polar with the parabolic expression.

It is convenient to break the airplane drag down into components attributable to various causes. The basic drag equation (in coefficient form) is:

$$C_D = C_{D_P} + C_{D_i} + C_{D_M} \qquad (112)$$

where,

C_D is total airplane drag coefficient

C_{D_P} is parasite drag coefficient

C_{D_i} is induced drag coefficient

C_{D_M} is compressible drag coefficient

Parasite Drag

Parasite drag is the drag of any part on the airplane that does not contribute useful lift. The parasite drag of a wing is usually referred to as "profile" drag. It is composed of drag due to the pressure distribution and skin friction, and is denoted as C_{D_0}. It is to be distinguished from another kind of drag which is entirely a result of lift being derived from the wing. The parasite drag on the remaining components of the airplane (fuselage, tail, nacelles, etc.) is called "structural drag," and is denoted as C_{D_S}. This type of drag is attributed to several causes. Some is due to the pressure distribution on the body (sometimes called "form drag"); some is due to skin friction drag; and some to aerodynamic interference. The entire parasite drag of the airplane may be summed up as:

$$C_{D_P} = C_{D_0} + C_{D_S} \qquad (113)$$

where,

C_{D_P} is parasite drag coefficient of the airplane

C_{D_0} is parasite drag coefficient of the wing (profile)

C_{D_S} is parasite drag coefficient of the remaining components (structural)

On a given body, the relative proportions of form drag and skin friction drag will depend upon the shape of the body. Those bodies that have predominantly form drag are referred to as "bluff" bodies; those that have predominantly skin friction drag are called "streamlined" bodies. A typical variation of drag with body shape is shown in Figure 40. Here a body of revolution with a given diameter is progressively "stretched out" and the drag measured. Since the maximum cross sectional area is constant, the reference area for computing the drag

coefficient is chosen at this cross-sectional area. It can be seen that the minimum drag coefficient occurs at an l/d ratio (length to maximum diameter) of about 2.5. The l/d ratio is commonly referred to as "fineness ratio." For the lower fineness ratios, separation takes place, giving a relatively large form drag, hence a relatively large drag coefficient. For the larger fineness ratios the large exposed skin surface area of the body causes relatively large skin friction, hence a relatively large coefficient. The drag characteristics of a body of revolution are of interest because of their application to fuselages and nacelles.

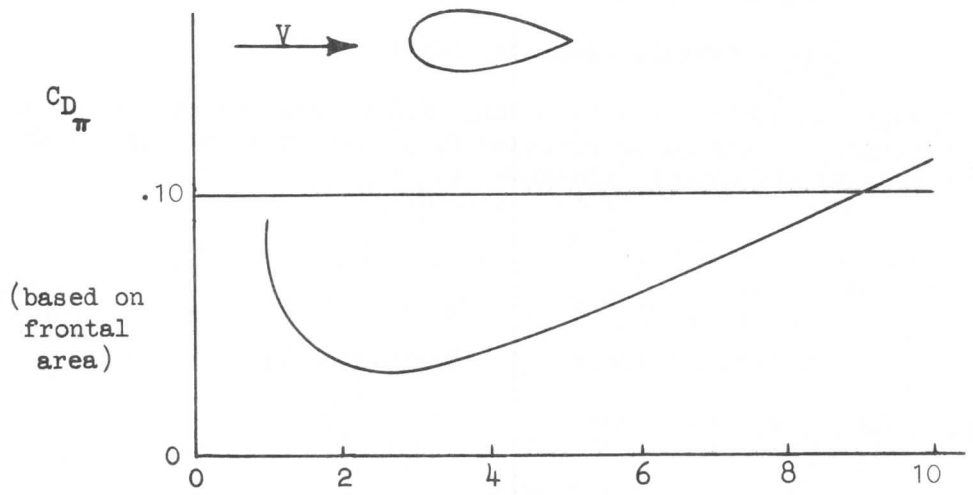

Figure 40.

Another factor that contributes to drag force is called interference drag. Interference drag exists from the change in flow pattern that accompanies the placing of two bodies in close proximity. Thus, the total drag of the two bodies placed close together is generally different from the sum of the individual drags. Quite often this interference is unfavorable, causing an increase in drag over that experienced by the separate bodies. It thus becomes necessary for the designer to find the appropriate geometric layout of the airplane components which will result in a minimum of interference drag. The intersection of the wing with the body is usually troublesome in this respect. It is found that a high wing airplane produces little or no interference. For a low wing airplane, however, there is a marked tendency for separation at the root at high angles of attack. This is because the intersection requires an expansion of the streamlines near the trailing edge on the top surface, which means a deceleration of the air and a tendency toward separation. A common method of alleviating this condition on the low-wing airplane is the use of a "fillet" at the intersection. The determination of the location and amount of interference is most easily made in the wind tunnel through the analysis of force data and airflow "tuft" observations.

There are other ways of denoting drag. In Figure 40, the drag coefficient was based on the frontal area. Since an aerodynamic coefficient is completely arbitrary, it may be based on any convenient area. The use of the frontal area as a

basis of the drag coefficient is quite common for a body such as a fuselage or nacelle. In this case, it is called the "proper" drag coefficient, denoted by the subscript, π.

Thus,
$$D = C_{D_\pi} S_\pi q \qquad (114)$$

where, D is drag of the body, lb

C_{D_π} is proper drag coefficient, dimensionless

S_π is frontal area, ft^2

q is dynamic pressure, lb/ft^2

The procedure of using an arbitrary area to base a drag coefficient on may be extended still further. It should be realized first that the drag of a body is directly proportional to the dynamic pressure, q, or:

$$D \propto q$$

Thus,
$$D = f\, q$$

where, f is the constant of proportionality.

From former equations, it is known that:

$$D = C_D S q$$

$$D = C_{D_\pi} S_\pi q$$

Then,
$$\left.\begin{aligned} f &= C_D S \\ f &= C_{D_\pi} S_\pi \end{aligned}\right\} \qquad (115)$$

The constant, f, is called the "equivalent parasite area" and is particularly convenient since it embodies no characteristic area. The usefulness of this nomenclature is that a body, such as a nacelle of given dimensions, will have one value of "f" regardless of the airplane to which it is considered to be applied, assuming no change in interference drag.

Another method of denoting drag is by the skin friction drag coefficient. As was mentioned previously, after a body is lengthened past a certain point its drag coefficient based on frontal area increases. As a matter of fact this increase will be found to be proportional to the increase in skin surface area. In other words, the drag characteristics of a long slender body will be essentially those of a flat plate with the same surface area as the body set parallel to the remote velocity. Thus, instead of using the frontal area as a reference for the drag coefficient, the surface area could be used instead. A plot showing drag based on "wetted" or skin surface area appears in Figure 41. This shows that the drag coefficient approaches a value of about .003, which is the value found to exist on a flat plate. The drag equation may be written:

$$D = C_f A_w q \qquad (116)$$

where, C_f is the coefficient based on wetted area

A_w is wetted area, ft^2

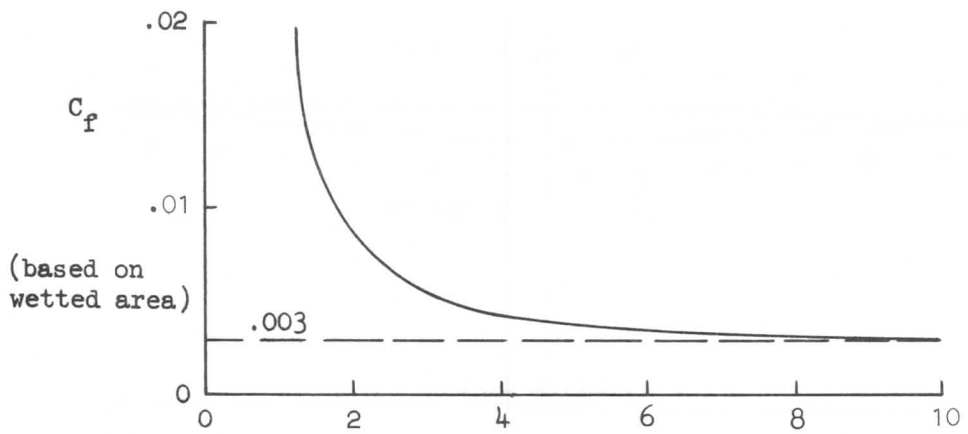

Figure 41.

Induced Drag

The drag which is induced by the wing is called "induced drag," C_{D_i}. The total wing drag may be considered as that made up of profile and induced drag. Written in coefficient form:

$$C_{D_w} = C_{D_o} + C_{D_i} \qquad (117)$$

where, C_{D_w} is total wing drag coefficient

C_{D_o} is profile drag coefficient

C_{D_i} is induced drag coefficient

Induced drag may be approached by considering the flow over a wing at such an angle of attack that it has positive lift. For this condition, the air pressure on the upper surface is less than the air pressure on the lower surface. There is thus a pressure differential existing with a natural tendency for the air to flow toward an area of lower pressure to alleviate the differential. This occurs at the wing tips. Air flowing backward over the upper and lower surfaces of the wing is influenced by the action at the wing tips. The action is rearward and inward on the upper surface, and rearward and outward on the lower surface. This is shown in Figure 42.

The transverse flow is logically most predominant at the tips, decreasing inboard until nullified at the wing centerline by an equal and opposite transverse flow generated by the other tip. The wing is shown (in Figure 42) as viewed from the top, with the solid lines denoting flow on the upper surface and dashed lines denoting flow on the lower surface. With such a condition, the air immediately behind the wing will have a swirling or "vortex" motion, most predominant at the tips, and less intense inboard. The net effect of these vortex systems, or trail-

ing vortices, is to give an average downward inclination to the air leaving the wing. The average angle through which the velocity vector is rotated is called "downwash angle," denoted by the Greek letter Epsilon, ϵ. The air flow pattern about a section airfoil appears as in Figure 43.

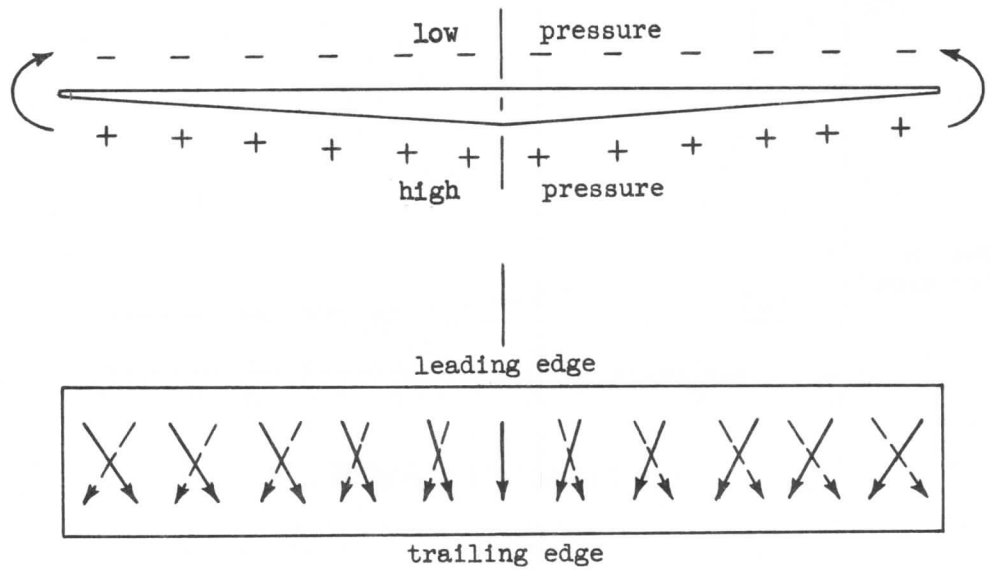

Figure 42.

If an airplane had an infinite span the transverse flow at the tips would influence only a very small portion of the wing. The gradual decrease of the cross flow effect toward the center results in a zero downwash angle at the wing centerline. It can thus be seen that the influence of the transverse flow at the tips (tip vortices) on the rest of the wing will depend primarily upon the aspect ratio of the wing.

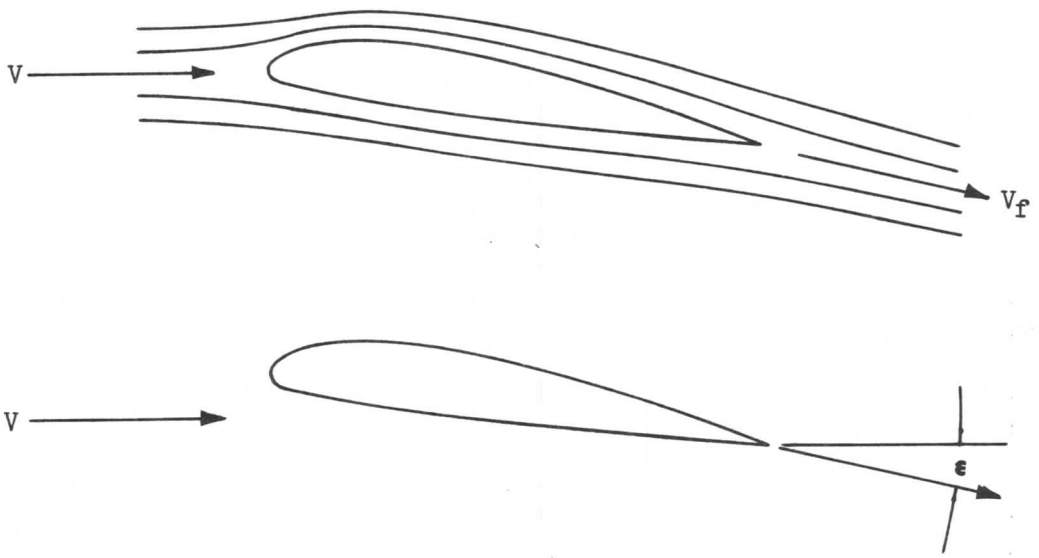

Figure 43.

For a finite aspect ratio, the downwash angle is of definite measurable magnitude; and for an infinite aspect ratio (finite chord but infinite span) the downwash angle may be assumed zero.

It is assumed, now, that there exists an average constant downwash angle across the span of a (finite) wing. The actual spanwise distribution of downwash may be shown to be a function of the planform of the wing considered. A rectangular wing, for example, would be expected to have a much higher concentration of vortex action at the tip where the chord is large, than a tapered wing whose tip chord is relatively small.

Consider a stream of fluid moving over an airfoil section, being deflected some average angle, ϵ. Newton's law may be applied to the deflected stream of fluid to determine the forces exerted on the airfoil.

From equation (6), $F = Ma$

and equation (22), $a = \frac{dV}{dt}$

$$a = \frac{\Delta V}{\Delta t}$$

Then, $$F = \frac{M}{\Delta t} \Delta V \qquad (118)$$

Consider now that this stream of some arbitrary but as yet undefined cross-sectional area is moving with an average velocity, V, past the wing. The mass per second, (M /t), passing any given point is equal to ρAV.

$$\frac{M}{t} = \rho AV$$

The change in velocity of the stream may be seen in Figure 44. Assuming that the stream is deflected through an angle ϵ (by the action of the wing) the vector diagram may be drawn.

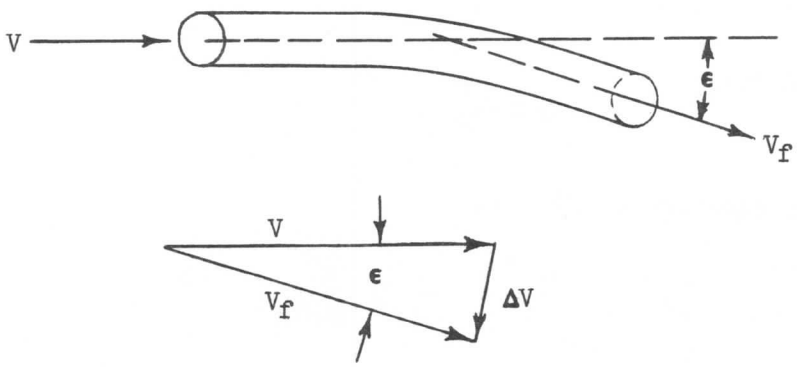

Figure 44.

There has been a change in the velocity, an acceleration, due to changing the direction of the velocity vector. The magnitude of the velocity change is:

$$\Delta V = V \sin \epsilon$$

For small angles, the sin is equal to the angle itself, measured in radians. Since ϵ is small, sin ϵ is equal to ϵ. Thus,

$$\Delta V = V\epsilon$$

Equation (118) may now be written:

$$F = \rho A V \cdot V\epsilon$$

In this particular instance, the force under consideration is lift; therefore:

$$L = \rho A V^2 \epsilon$$

Also from equation (104);

$$L = C_L \frac{1}{2} \rho V^2 S$$

Equating the two, results in:

$$\rho A V^2 \epsilon = C_L \frac{1}{2} \rho V^2 S$$

or,

$$A\epsilon = \frac{1}{2} C_L S \qquad \text{(119)}$$

It can be shown that the area, A, in the equation, is the cross-section of the stream of fluid affected by the wing enclosed by a circle whose diameter is the span of the wing. This does not mean that only this area is deflected, but rather that it is an equivalent area which may be considered deflected through a constant angle of downwash ϵ.

Therefore,

$$A = \frac{\pi b^2}{4}$$

From equation (100),

$$S = \frac{b^2}{(AR)}$$

Substituting in equation (119) gives:

$$\frac{\pi b^2}{4} \epsilon = \frac{1}{2} C_L \frac{b^2}{(AR)}$$

or,

$$\epsilon = \frac{2C_L}{\pi(AR)} \qquad (120)$$

This equation shows that the downwash is a function of both lift coefficient and aspect ratio.

Consider now a wing of infinite aspect ratio set at a geometric angle of attack, α_0, as in Figure 45. For convenience, let the lift and drag coefficients be denoted as C_{L_0} and C_{D_0} for this condition.

From previous assumptions it is known that there will be no downwash, thus the velocity vector behind the wing will have the same direction as that in front.

Now let the wing be subjected to exactly the same geometric angle of attack, but with some finite aspect ratio instead of infinite aspect ratio. The velocity field in the region of the wing now consists of a curved flow, with the velocity vector behind the wing deflected through an angle ϵ. This curved flow may be represented by an effective linear velocity which bisects the downwash angle and denoted as V_{EFF} in Figure 46. It is important to recognize that the effective angle of attack is now less than the geometric angle of attack, α, by half the downwash angle. Since this angular reduction is induced by the lift on the wing, it is called induced angle of attack, α_i.

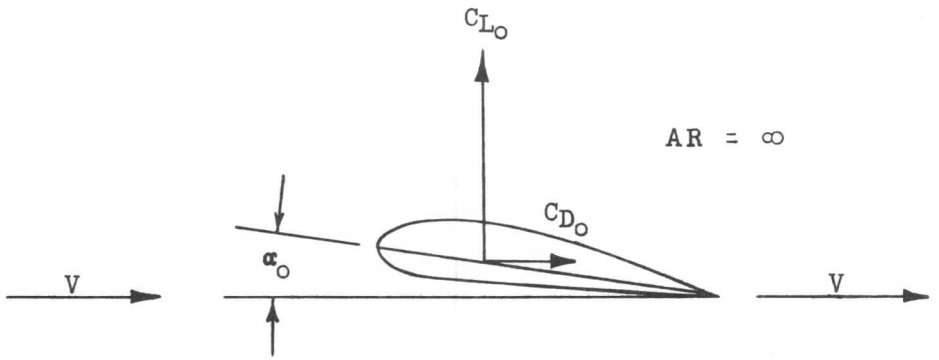

Figure 45.

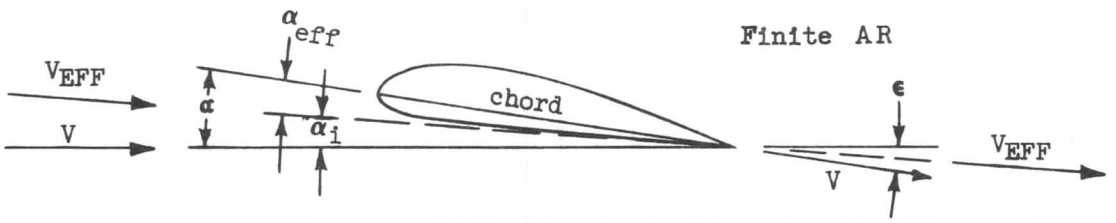

Figure 46.

Thus,

$$\alpha_i = \frac{\epsilon}{2} \qquad (121)$$

Now let the geometric angle of attack of the finite aspect ratio wing be increased until its effective angle of attack is the same as the angle of attack of the infinite aspect ratio wing. See Figure 47.

Thus,

$$\alpha = \alpha_0 + \alpha_i \qquad (122)$$

where,

α_0 is effective angle of attack

α_i is induced angle of attack

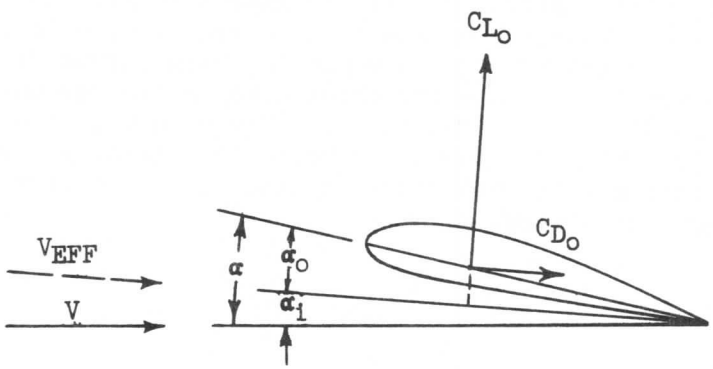

Figure 47.

Effectively, the only difference between Figure 45 and Figure 47 is that Figure 45 has been rotated through an angle α_i; thus C_{L_O} and C_{D_O} may be made perpendicular and parallel respectively, to V_{EFF}. In order to conform to the standard practice of resolving the lift and drag coefficients perpendicular and parallel, respectively, to the remote velocity, the coefficients C_{L_O} and C_{D_O} must be resolved into components in those directions. This is done in Figure 48.

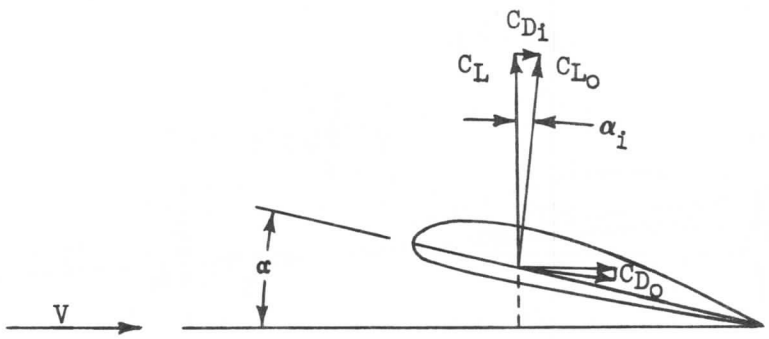

Figure 48.

The resolution of C_{D_O} into its two components results in a horizontal component that is essentially equal to C_{D_O}, and a vertical component that may be ignored due to its small size relative to the magnitude of C_L and C_{L_O}. The resolution of C_{L_O} into its two components results in a vertical component that is essentially equal to C_{L_O}, and a horizontal component that may be of such large proportions as to be greater than the profile drag of the wing. To this horizontal component is given the name "induced drag coefficient," and it may be seen to be related to the induced angle of attack according to the following. A portion of Figure 48 is enlarged in Figure 49 to show the mathematical relationship that exists.

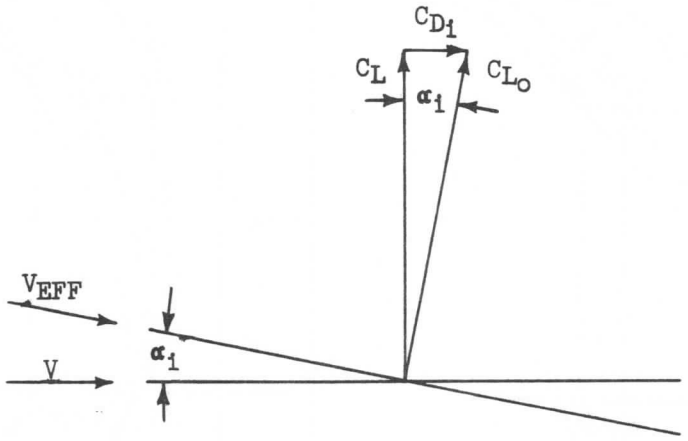

Figure 49.

From Figure 49:

$$\tan \alpha_i = \frac{C_{D_i}}{C_L}$$

$$C_{D_i} = C_L \tan \alpha_i$$

If α_i is small, tan α_i will equal the angle α_i if expressed in radians.

Therefore:

$$C_{D_i} = C_L \alpha_i \qquad (123)$$

where, C_{D_i} is induced drag coefficient

C_L is lift coefficient

α_i is induced angle of attack, radians

Equations (120) and (121) may be combined to give another relationship for α_i:

$$\alpha_i = \frac{C_L}{\pi(AR)} \qquad (124)$$

This equation may now be used with equation (123) to give another relationship for C_{D_i}.

$$C_{D_i} = \frac{C_L^2}{\pi(AR)} \qquad (125)$$

Figure 50 shows the effect of aspect ratio on the lift curve and the polar curve of an airfoil. These curves show the magnitude of the effect of aspect ratio on the lift and drag characteristics.

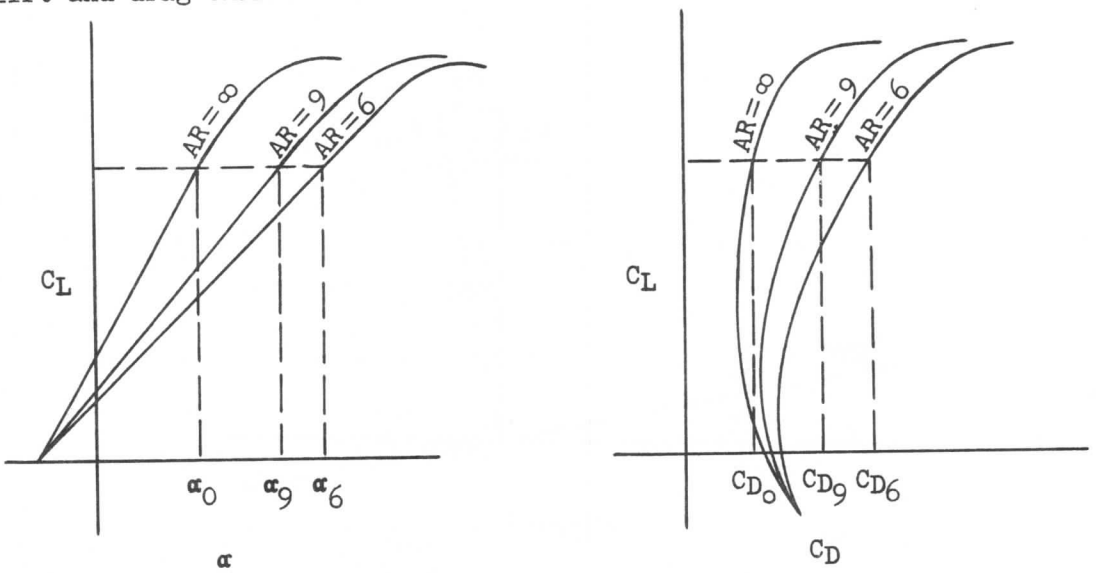

Figure 50.

Some general statements may be made about the effects of aspect ratio. As can be seen in Figure 50, the infinite aspect ratio characteristics are optimum for a given airfoil section since the least drag occurs for a given lift coefficient. The aspect ratio chosen by the airplane designer will be governed by a compromise between structural and aerodynamic considerations and by the purpose for which the airplane was designed.

Compressibility Drag

Compressibility drag is that part of the total drag due to the compressibility effects coexistent with high speed. In order to show the effects of compressibility it is convenient to associate the flow of fluid at high velocities around an airfoil section with that flowing through a channel. In an earlier section, a discussion was made involving shock wave phenomena and the accompanying pressure and velocity changes. The same phenomena can be expected to occur in the flow over an airfoil.

Air flowing over an airfoil surface may attain locally sonic velocity. Local speeds greater than that of sound may, and frequently do, exist on the airfoil surface because the rear portion of the airfoil, by its geometry, requires an expansion of the stream tube. The conversion of this very high speed air to the lower speed necessary at the trailing edge produces a shock similar to that in a

channel. Unfortunately, the sudden rise in pressure through the shock wave frequently causes separation of flow, and the effect leads to a general decay of the aerodynamic characteristics of the airfoil.

Figure 51 shows a view of the boundary layer ahead of and behind the shock wave. It is found that there is an interaction between the shock wave and the boundary layer such that the layer thickens rather abruptly on passing through the shock wave. This thickening, plus the fact that an adverse pressure gradient exists across the shock wave, is sufficient to cause the boundary layer to separate just as it does in the case of a high angle of attack stall. This separation affects both the lift and the drag characteristics of the airfoil.

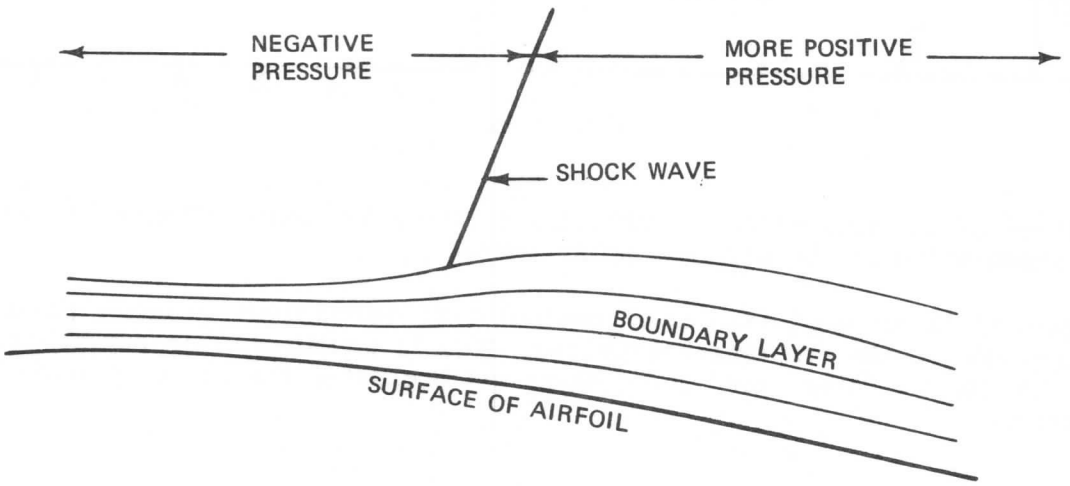

Figure 51.

The lift under given conditions of angle of attack will increase with Mach number according to the following expression which will not be derived here.

$$C_L = \frac{C_{L_{inc}}}{\sqrt{1 - M_o^2}} \qquad (126)$$

Where $C_{L_{inc}}$ is the lift coefficient for incompressible flow and M_o is the remote Mach number.

This relationship is shown, in Figure 52, to be reliable up to the point where separation begins to take effect. Assuming now that separation induced by shock wave formation is taking place. Figure 52 will be modified as indicated by the dashed lines. The reason the lift decreases at the high Mach numbers is that the shock wave causes flow separation with the resultant loss in lift.

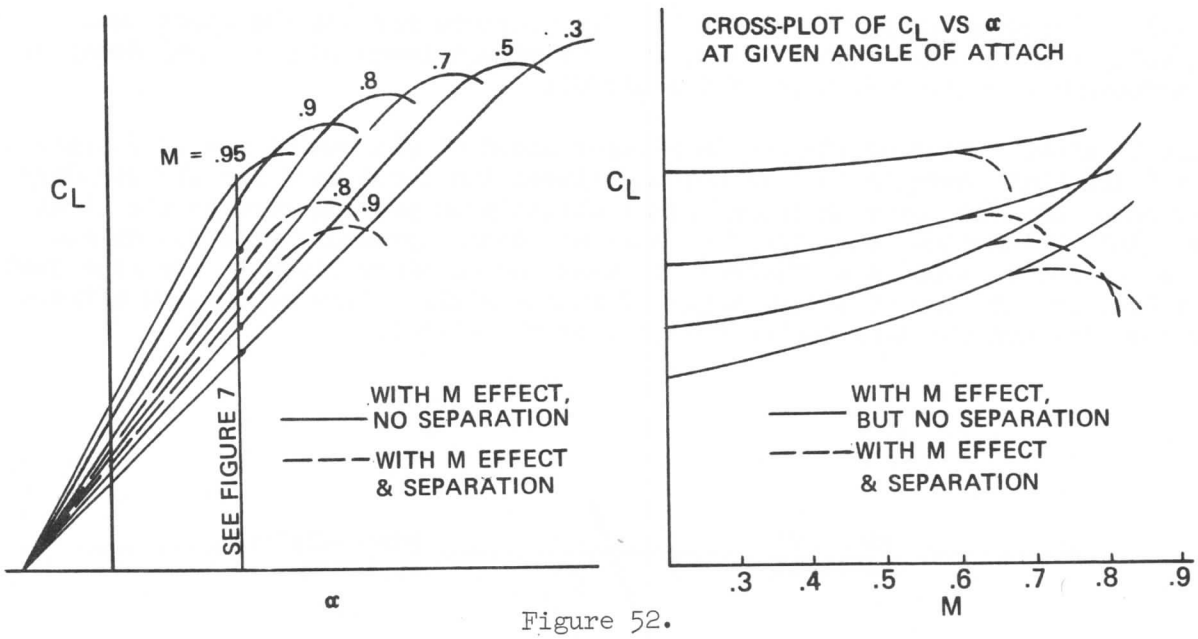

Figure 52.

The effect of the separation is reflected in the polar curve, Figure 53, which is representative of the airplane polar curve.

If Figure 53 is cross-plotted at a constant lift coefficient, a curve showing the magnitude of the compressibility drag, C_{D_M}, is obtained. This curve, Figure 54, shows the typical "drag rise" curve shape which denotes the onset of shock wave separation.

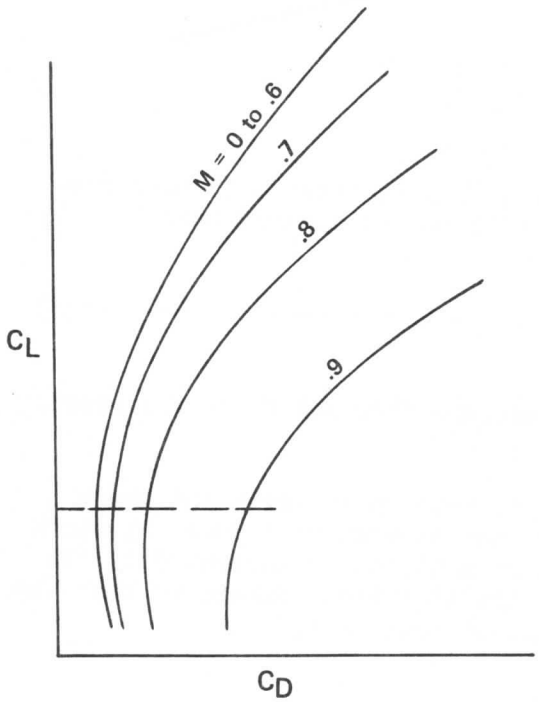

Figure 53.

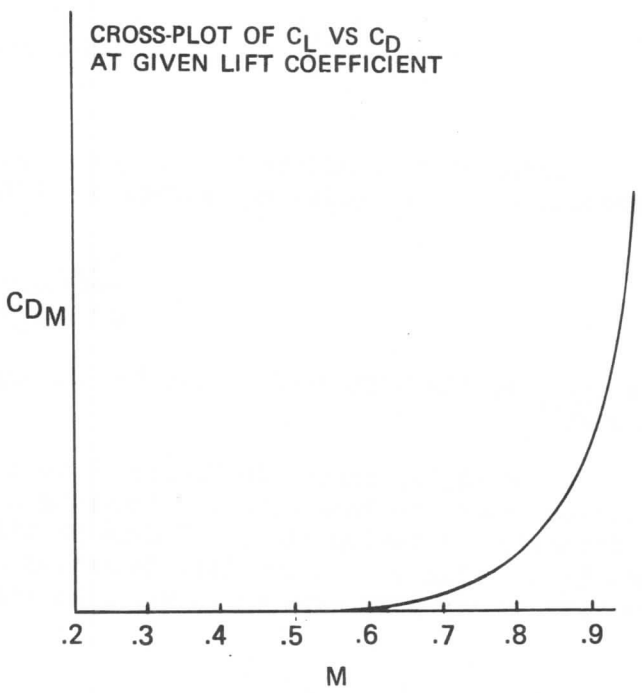

Figure 54.

The lowest remote velocity at which sonic velocity (M = 1) is attained on any part of an airfoil is called "critical Mach number." This does not mean that a dangerous condition exists on the airfoil, but rather that it represents a limit below which no shock waves can occur. The pressure coefficient associated with the critical Mach number is called "critical pressure coefficient." It is possible to predict what pressure coefficient must exist to produce a local Mach number of unity. Consider the airfoil in Figure 55.

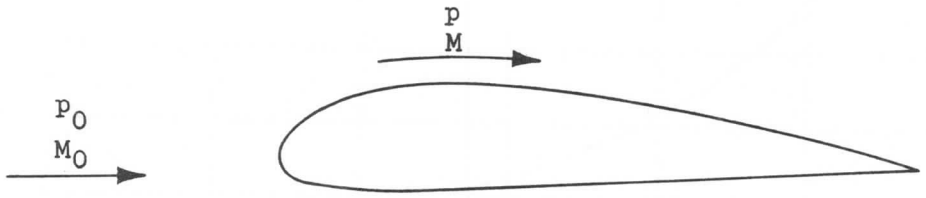

Figure 55.

The pressure coefficient, developed in a previous chapter as equation (84), remains:

$$C_p = \frac{p - p_0}{q_0}$$

From compressible flow theory, it may be shown that for M = 1 on the airfoil, the critical pressure coefficient is:

$$C_{p_{CR}} = \frac{2}{\gamma M^2_0}\left[\left(\frac{2}{\gamma+1} + \frac{\gamma-1}{\gamma+1} M_0^2\right)^{\frac{\gamma}{\gamma-1}} - 1\right] \qquad (127)$$

This equation, when plotted, appears as in Figure 56.

The changes in density accompanying changes in static pressure produce a pressure distribution which is different from that predicted for incompressible fluid. The development of equations to show modifications to the incompressible pressure distribution is, in general, a rather elaborate procedure and will not be discussed here. The results, however, are shown.

For an incompressible fluid, the pressure at the stagnation point is greater than the remote static pressure by the amount of the dynamic pressure q.

Thus,
$$C_{p_s} = \frac{\Delta P_s}{q_0} = 1$$

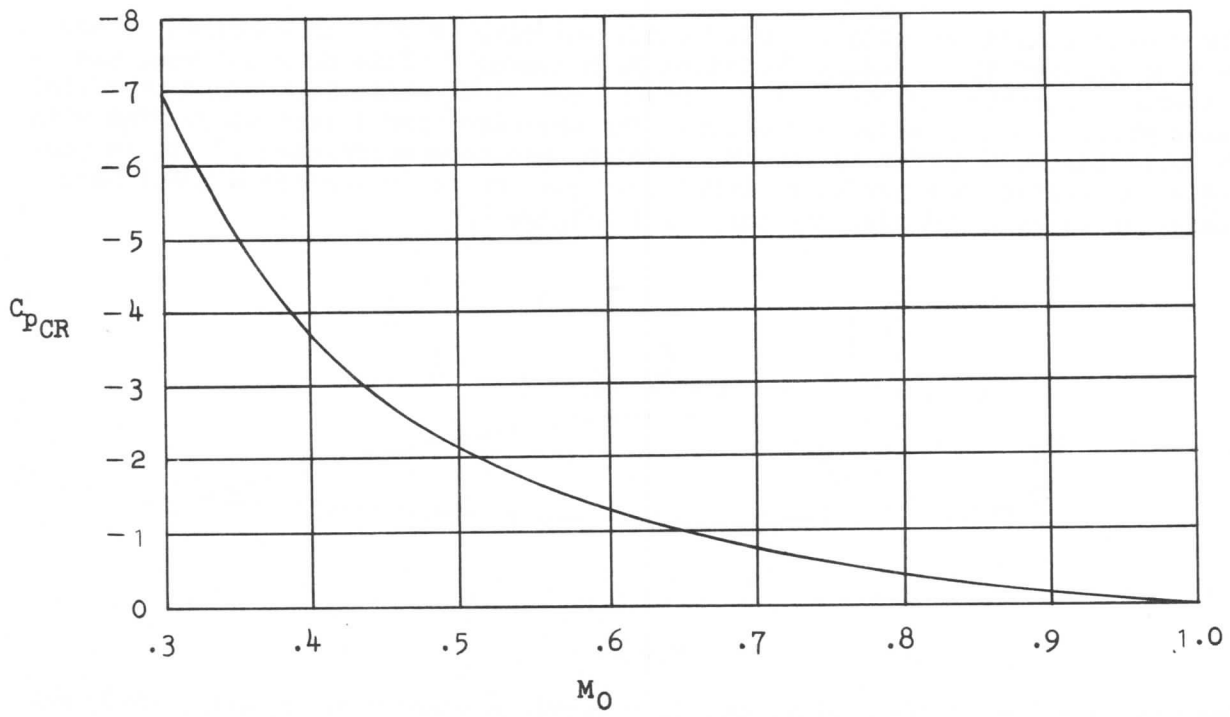

Figure 56.

where, C_{p_s} is the pressure coefficient at the stagnation point

ΔP_s is the change in static pressure at stagnation point from remote value

q_0 is remote dynamic pressure

For a compressible fluid, the pressure at the stagnation point is increased, due to compressibility, according to the following equation:

$$C_{p_s} = 1 + \frac{1}{4} M_0^2 + \frac{2-\gamma}{24} M_0^4 + \ldots\ldots\ldots\ldots$$

For most practical applications, this may be expressed simply as:

$$C_{p_s} = 1 + \frac{M_0^2}{4} \qquad \text{(128)}$$

For the remaining pressure on the airfoil, a commonly used equation is employed. It does not apply accurately where the local velocity on the airfoil is considerably different from the remote velocity; hence, it does not apply at the stagnation point or on the upper and lower surfaces of an airfoil at high angles of attack. The equation is:

$$C_p = \frac{C_{p_{inc}}}{\sqrt{1 - M_0^2}} \qquad \text{(129)}$$

Also, since the lift coefficient depends upon pressure coefficients, equation (126) may be applied directly for a similar prediction of lift coefficient, C_L, and slope, m, of the lift curve. The lift equation appeared as equation (126) in this chapter, but the slope of the lift equation is shown as follows:

$$m = \frac{m_{inc}}{\sqrt{1 - M_0^2}} \qquad (130)$$

Figure 57 shows the effect of compressibility on the pressure distribution at low and high Mach numbers. The difference between the two pressure distributions is noticeable, especially on the upper surface. It will be noted that for the high Mach number diagram, the flow is supersonic for a considerable portion of the upper surface and finally becomes subsonic by means of passing through a shock wave. The same angle of attack is considered in both cases.

In designing a new airplane it is highly important to estimate as accurately as possible what the lift and drag characteristics under all conditions will be. The aerodynamicist depends largely on three sources for this information. Initially, data obtained on other airplanes or previous NACA test results may be used. Wind tunnel models are built and tested to verify previously estimated data, and also to investigate certain design features for which there has been no previous data available. The basic drag polar is obtained for the complete airplane from wind tunnel tests. The polar describes the lift and drag characteristics of the model which is geometrically similar to the full scale airplane, however, it is not generally used to represent the actual airplane directly. The shape and spacing of the curves relative to each other are used directly, but the intersection of the low Mach number (incompressible) polar with the C_D axis is obtained by other means. The reason for this is that past experience has shown that wind tunnel data will accurately predict the polar shape and drag rise characteristics but will not predict the basic "drag level." One reason for this is that it is difficult to accurately separate out the drag and interference effects of the model suspension system.

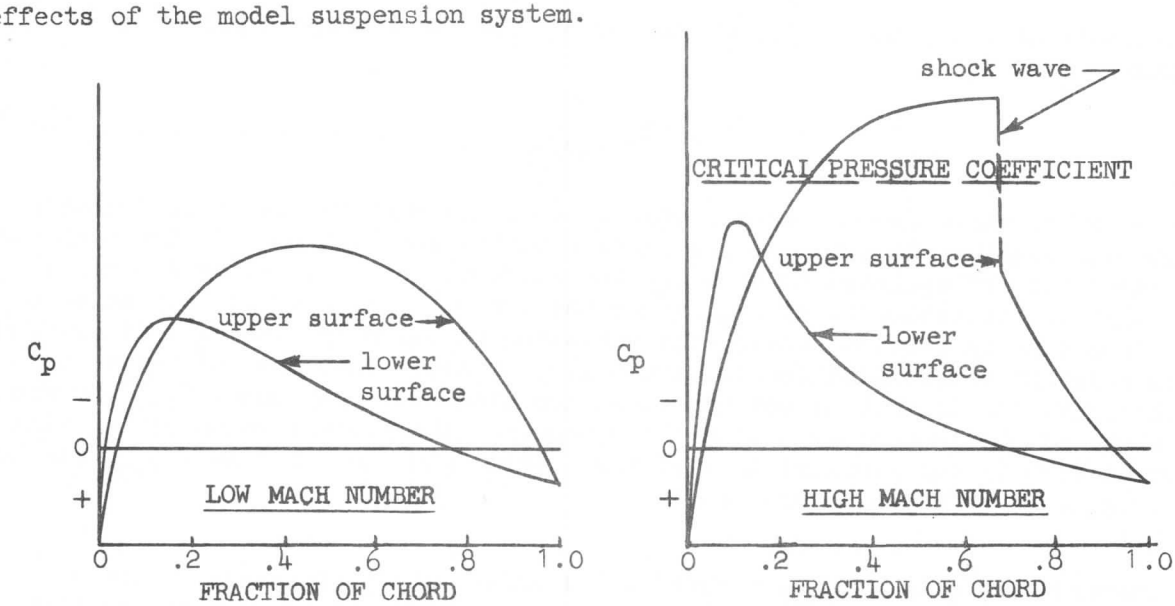

Figure 57.

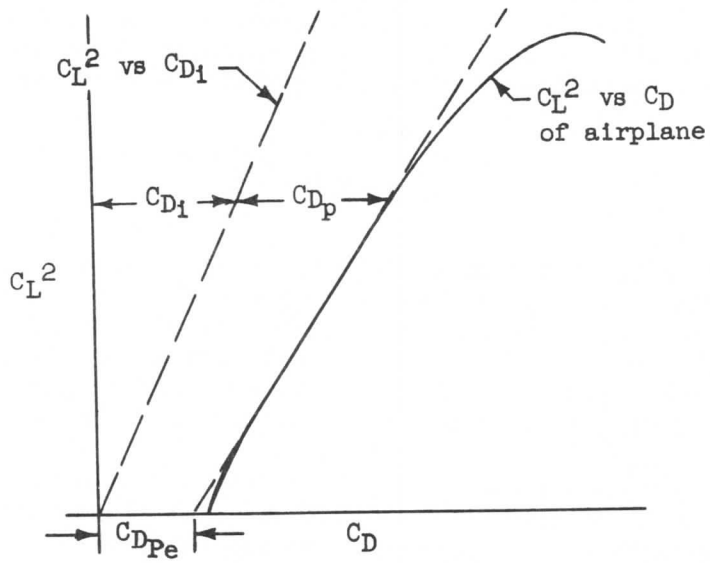

Figure 58.

The concept of drag level may be seen best by reference to Figure 58 in which a low-speed polar is plotted on axes of C_L^2 vs C_D. It is readily apparent that the curve becomes practically a straight line. This happens because, as was mentioned previously, the parabolic shape of the drag curve is primarily caused by the induced drag of the wing. Equation (111) suggests this presentation:

$$C_D = A + BC_L^2.$$

From equations (112) and (125), an expression for the low-speed polar may be written.

$$C_D = C_{D_P} + \frac{C_L^2}{\pi(AR)} \qquad (131)$$

In Figure 58, there appears some deviation from the mathematical representation at low and high coefficients. If a representative straight line is drawn through the curve and extrapolated to zero C_L, the intersection will define a minimum C_D, which is composed only of C_{D_P}, since the induced drag becomes zero at zero C_L. If a line is plotted showing the variation of C_{D_i} only with C_L^2, it is found to be straight and, in addition, to have a slope steeper than that of C_D vs C_L^2. Graphically, the difference between these two lines will represent C_{D_P}, and since the slope of the induced drag line is steeper, the minimum value of C_{D_P} will occur at zero C_L for symmetrical airfoils. This value is known as $C_{D_{P_{MIN}}}$ and is the drag level referred to previously.

For cambered airfoils, $C_{D_{P_{MIN}}}$ occurs at low values of C_L depending on the amount of camber, but not at zero C_L. A transport airplane is so designed that $C_{D_{P_{MIN}}}$ occurs at a C_L approaching optimum cruise condition. To illustrate this,

Figure 59 shows a low-speed polar and in addition a curve of the parasite drag. The difference between the two curves represents the induced drag. It is obvious now that the minimum C_{D_P} occurs at a finite value of C_L and very close to the optimum L/D.

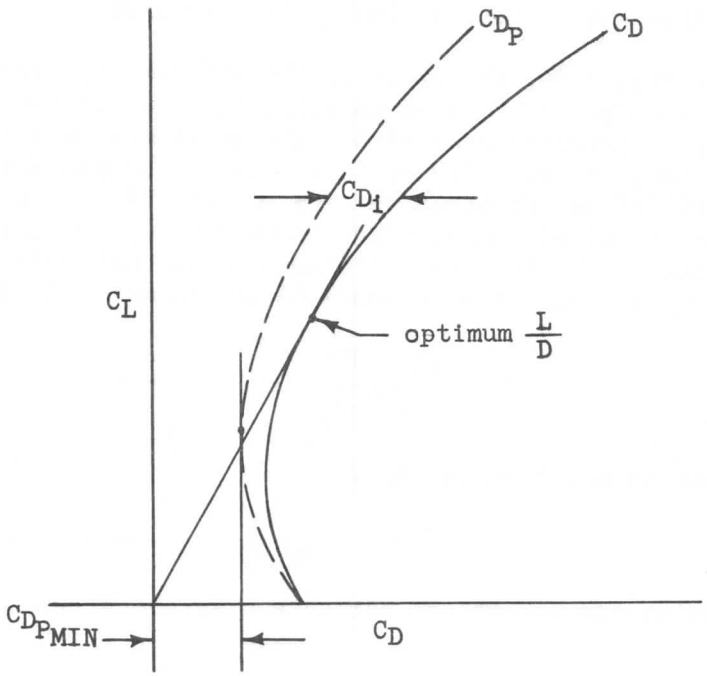

Figure 59.

The determination of $C_{D_{P_{MIN}}}$ is usually made by noting first that pure parasite drag is a function of form and skin friction drag. From experience it has been found convenient to compute the C_{D_P} of various parts of the airplane by assuming the C_{D_P} is a function of skin friction only. By analyzing past flight data from similar airplanes, various values of skin friction drag coefficient, C_f, are assigned to each part of the airplane. Various values are required due to shape and fineness ratio differences. In general it will be found that these values average out to about .003, as was indicated in Figure 41. Thus, in order to compute $C_{D_{P_{MIN}}}$ it is necessary to select the proper C_f, and since the skin wetted area is known, the f for any section of the airplane can be computed. The f_{MIN} of the total airplane is obviously equal to the sum of the various equivalent parasite areas (f's) of the components. Thus, $C_{D_{P_{MIN}}}$ can be computed. In the above calculations it should be noted that the following relationships are assumed to hold:

$$f_{MIN} = C_f A_w$$

or,

$$f_{MIN} = C_{D_{P_{MIN}}} S \qquad (132)$$

Thus, having computed the minimum f of the airplane, the wind tunnel polar can be shifted to agree with this value, and the full scale polar will be obtained. Verification of all previous estimations and of wind tunnel tests is, of course, made in the construction and flight testing of the airplane.

It was noted that, in Figure 58, the slope of the C_L^2 vs C_{D_i} curve was greater than that of the C_L^2 vs C_D. If it were possible to so shape the airplane that there be no increase in parasite drag with angle of attack (and thus C_L) then the two curves would be parallel. The ratio of the two slopes would then be unity, or the slope of C_L^2 vs. C_D would be 100% of that of C_L^2 vs C_{D_i}. The ratio of these slopes is called the airplane "induced drag efficiency factor" and is denoted by the symbol "e". For most airplanes it is difficult to approach a 100% efficiency factor, and values of around 80% are common. In terms of calculus nomenclature:

$$e = \frac{dC_L^2/dC_D}{dC_L^2/dC_{D_i}} \qquad (133)$$

Equation (131) may now be modified to read:

$$C_D = C_{D_{Pe}} + \frac{C_L^2}{\pi(AR)e} \qquad (134)$$

where $C_{D_{Pe}}$, defined as the equivalent parasite drag coefficient, is shown in Figure 58.

1-19 PLANFORM EFFECTS

As was mentioned previously, the wing planform has an effect on the strength of the vortex pattern at any point on the wing with a resultant effect on the downwash behind the wing. The downwash has the effect on the lift distribution over the wing such as to approach an elliptic shape. For the theoretical infinite aspect ratio wing, the lift distribution is constant across the wing as there is no downwash, as in Figure 60.

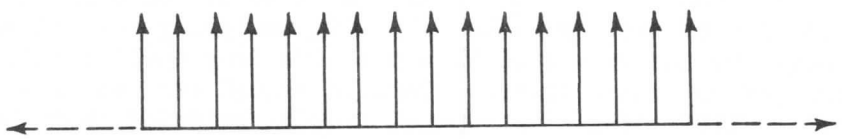

INFINITE ASPECT RATIO WING

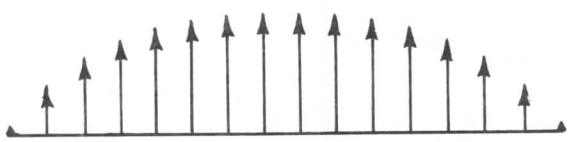

FINITE ASPECT RATIO WING

Figure 60.

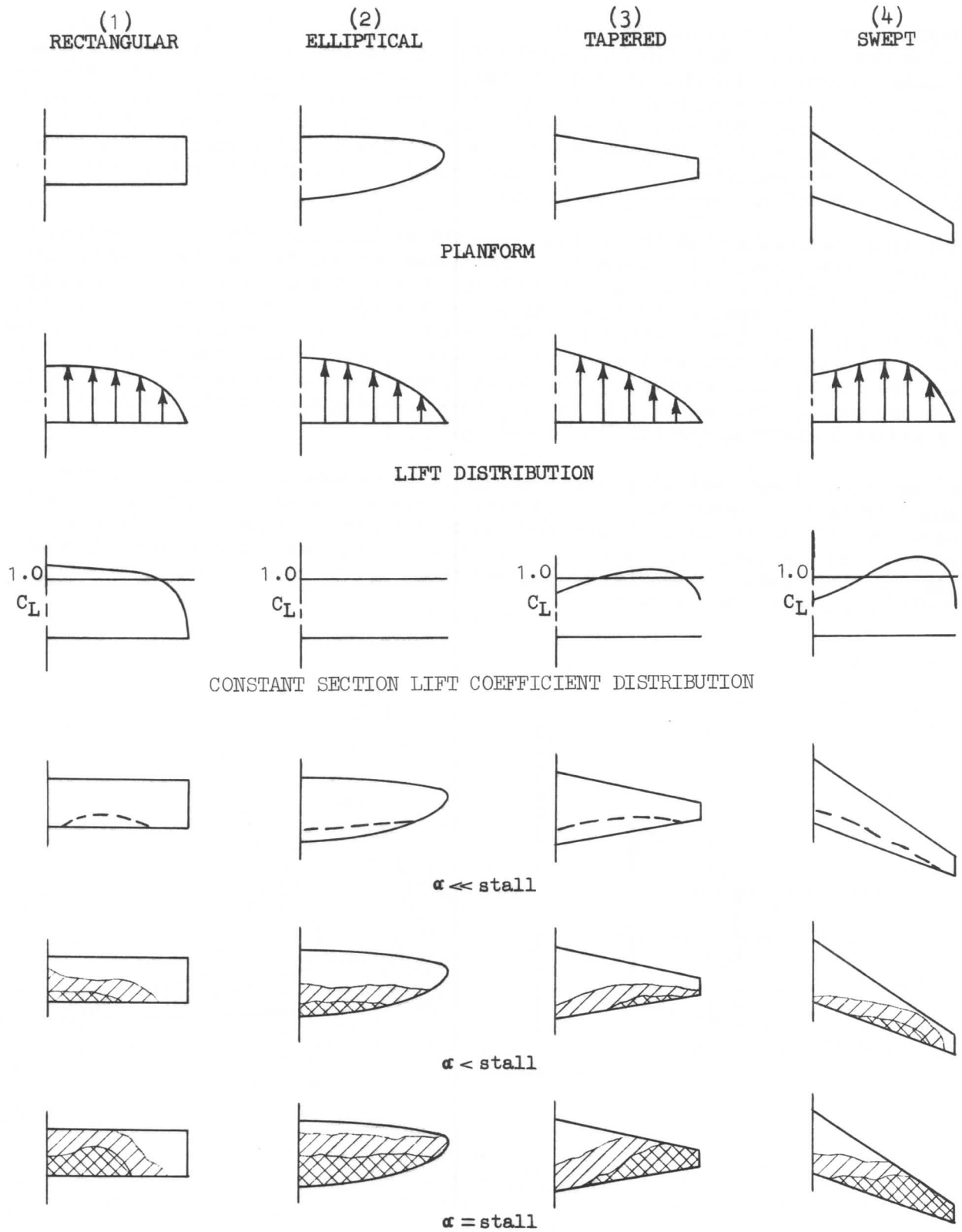
(1)
RECTANGULAR
(2)
ELLIPTICAL
(3)
TAPERED
(4)
SWEPT
PLANFORM
LIFT DISTRIBUTION
1.0
C_L
1.0
C_L
1.0
C_L
1.0
C_L
CONSTANT SECTION LIFT COEFFICIENT DISTRIBUTION
$\alpha \ll$ stall
$\alpha <$ stall
$\alpha =$ stall

Figure 61.

AERODYNAMICS

Variations in the planform of a finite wing produce spanwise load distributions which are varied. An elliptical shaped wing is unique in that it incurs essentially a constant downwash behind the wing: hence, an elliptical lift distribution. The entire wing tends to stall at the same time. Because a rectangular wing has a larger downwash angle at the tip, the effective angle of attack is reduced, hence the tip sections are the last to stall. On a tapered wing, the downwash decreases toward the tip section and the tip section tends to stall first. The effects are shown in Figure 61.

The wing that has a tendency to stall the tip section first is very undesirable from a lateral stability standpoint. There are various devices employed to prevent or delay the stalling characteristics. One method of alleviating an early tip stall is to physically reduce the angle of attack of the tip relative to the root by geometrically twisting or "washing out" the tip. Another method employed is to make the airfoil section at the tip more cambered than those inboard. This enables the airfoil to attain a higher C_L toward the tip before stalling. Still another method that may be used is to install leading edge "slats" near the tip to assist in keeping the tip from stalling.

A feature of swept back wings which should be mentioned at this point is the characteristic of spanwise flow. Consider a swept back wing with a fairly high positive lift on it, as in Figure 62. In particular, consider two chordwise sections on the wing. If these sections were viewed from a point near the wing tip and their respective pressure distributions drawn, the picture in Figure 62 would approximate the situation.

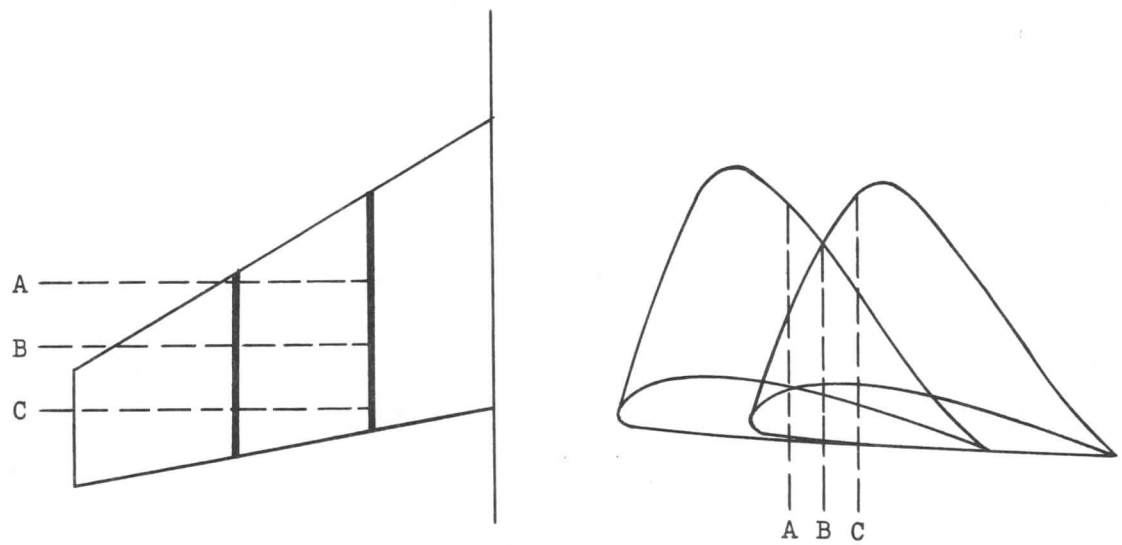

Figure 62.

Considering a spanwise section at Point A, it will be noted that the static pressure distributions are such that a greater negative pressure (lower static pressure) will exist inboard than outboard. This will create a tendency for an air

particle when moving over the upper surface in the vicinity of the leading edge to move inboard due to the lower static pressure inboard. When point B is reached, however, the static pressures are equal at the two stations, so the air particle will merely travel aft. At point C, the situation is reversed over point A; that is, the particle will tend to move outboard. An overall picture of particle motion may be gained from Figure 63. The condition described is apparent at fairly high lift coefficients, but less obvious at lower lift coefficients since the pressure differentials are less. As the stall is approached, however, it will be found that the flow near the wing tip at the trailing edge will be almost parallel to the trailing edge. One method of eliminating this flow effect is to add wing fences at several locations on the wing. This tends to keep the air flow going in a straight line direction.

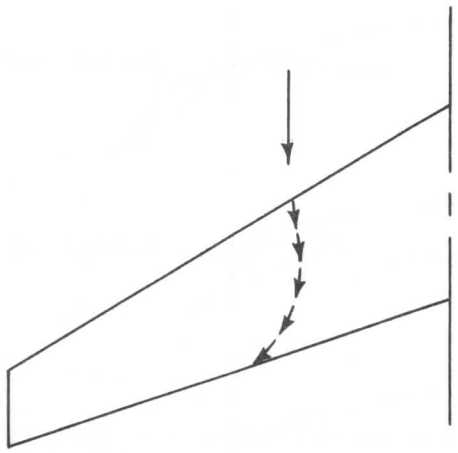

Figure 63.

Simple constant-section wings such as used to obtain the effects shown in Figure 61 are seldom used. In practical applications, section changes, variations in incidence, and other devices are used to tailor the wing to fit the requirements.

1-20 HIGH-LIFT DEVICES

There are several devices employed to increase $C_{L_{MAX}}$ of a wing. This is done to delay the stall, thus lowering the stalling speed. Initially, the choice of the airfoil determines the $C_{L_{MAX}}$. Increasing the camber increases the $C_{L_{MAX}}$ and simultaneously changes the angle of zero lift.

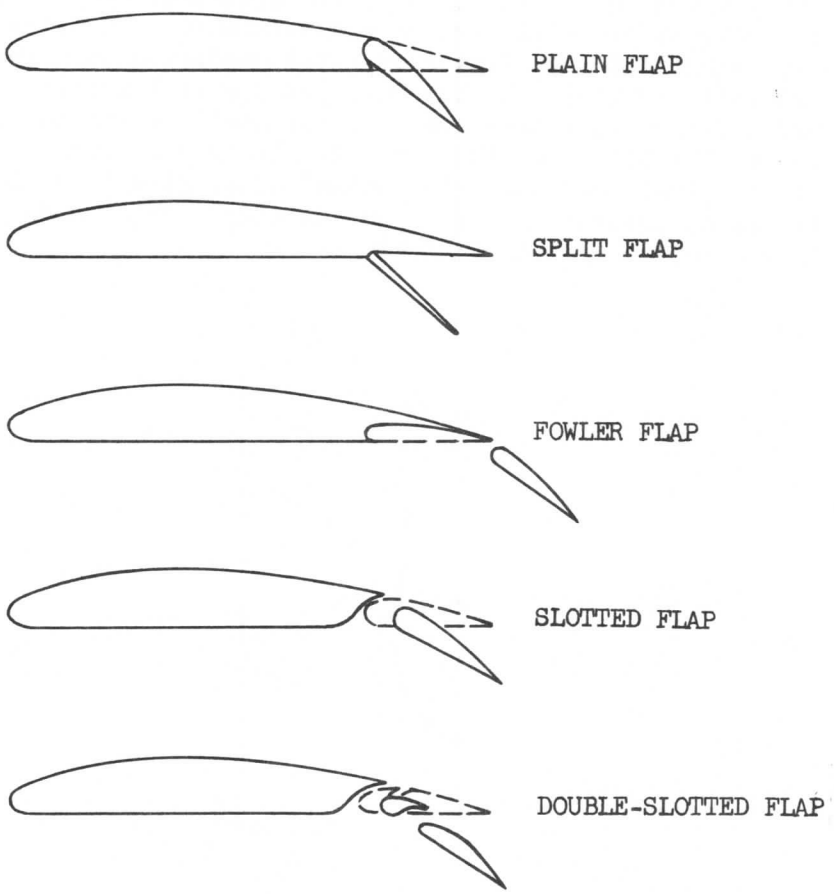

FLAP CONFIGURATIONS

Figure 64.

Having established the airfoil design, the most common method of increasing the lift potential is in the use of flaps. There are, of course, many types, some of which are shown on Figure 64. The selection of the size and type is determined as a result of compromise. The effect of flaps is similar to increasing the camber of the airfoil. While the maximum lift coefficient is increased due to the flaps, the drag is also increased. The effect of the increased drag is to decrease the speed; this is desirable during landing. The use of flaps produces certain changes in the characteristics curves for the wing as shown on Figure 65. There may be slight variations from those shown due to the various flap configurations.

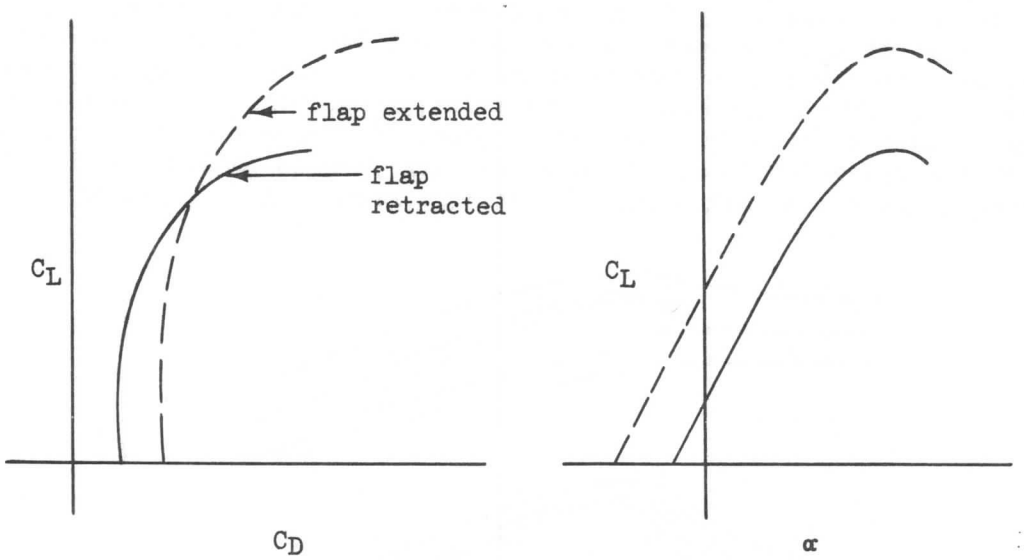

Figure 65.

In order to further increase lift, and also to help balance the pitching effects of large trailing edge flaps, it may be necessary to add flaps or similar devices to the leading edges of the wing. Such devices can increase capability in either of two ways: they may increase camber and they may provide smoother flow or boundary layer control to suppress flow-separation tendencies. Adjusting the leading edge or putting on a flap as in Figure 66 allows the wing to be rotated to a high angle without as much tendency for the flow to separate. The flap leads the air over the edge in a smooth manner without asking it to flow backward from a stagnation point under the chin. Without such help, the streamlines over the edge, as shown in the dotted lines, lose so much energy that they tend to separate.

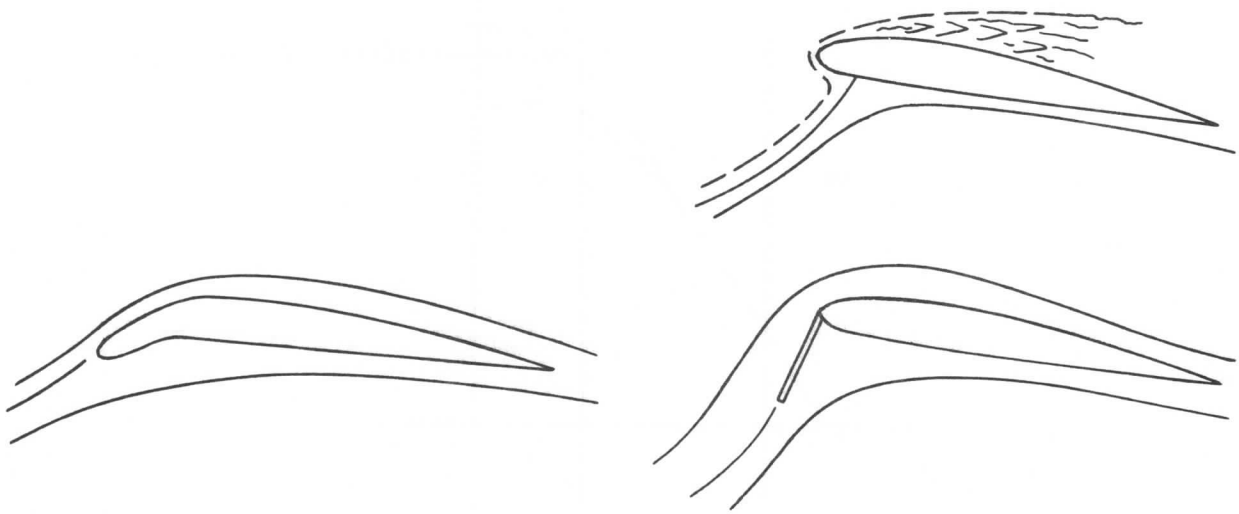

Figure 66.

Further help may be obtained by introducing energy into the airstream just behind the leading edge where the separation tendency is felt. This might be done by using a separate energy source such as a suction or blowing device, or it may utilize the energy of the airstream by taking high pressure air from under the wing through a slot to the upper surface as shown in Figure 67. The structure in front of the wing which forms the slot with the wing is called a slat. It may be fixed, or movable to allow the slot to be closed at low angles of attack.

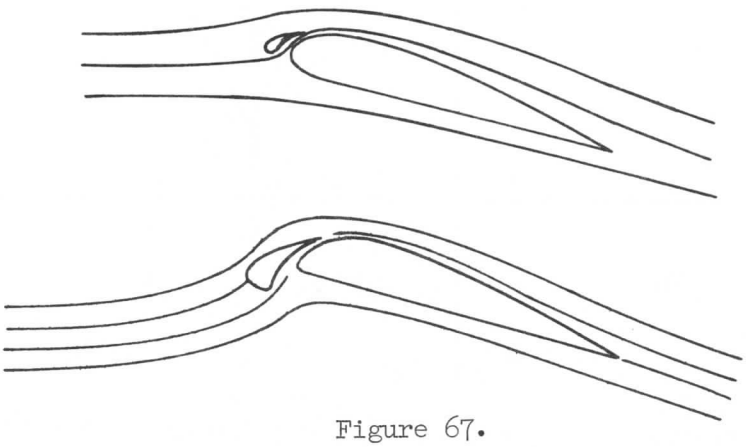

Figure 67.

Of particular interest is the improvement in the behavior of the airplane near the stall. Ideally, the maximum lift coefficient is increased, providing a reduction in the stalling speed. This effect is shown in Figure 68.

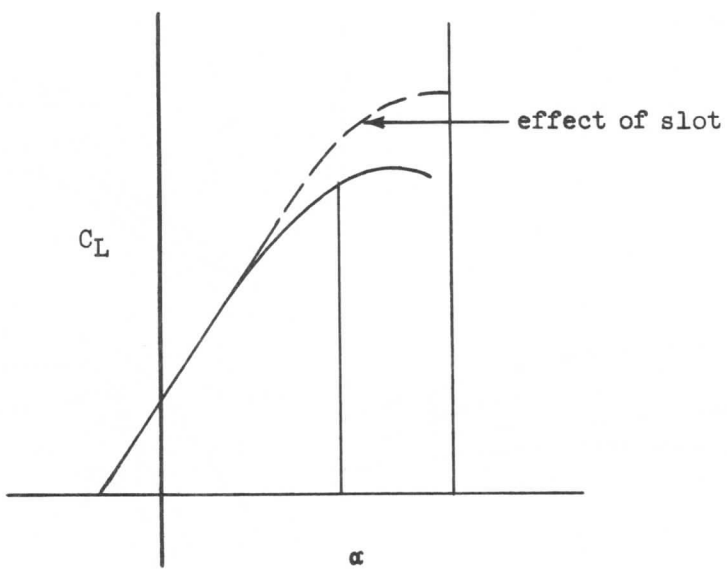

Figure 68.

There are other devices which are similar to the trailing edge flap, but differ in that they do not contribute to the lift. In fact, the purpose of these devices is to do just the opposite; either destroy lift, or add drag to the airplane. These devices are spoilers, dive brakes, and speed brakes.

Sometimes it is advantageous to employ spoilers on the wings. These may be used either separately or in conjunction with ailerons to produce roll. On very clean airplanes it is sometimes necessary to provide dive flaps or speed brakes to either limit or reduce the speed of the airplane, or increase the glide angle. Typical examples of these devices are shown in Figure 69.

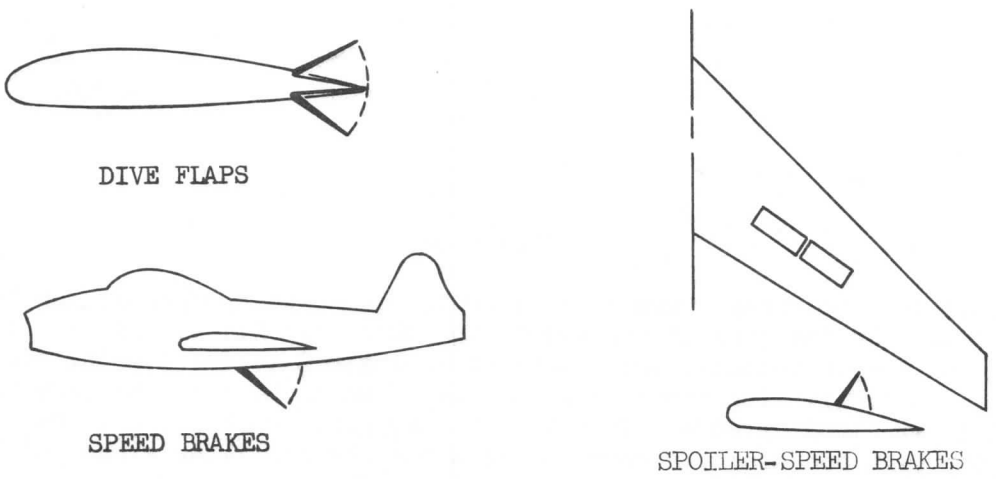

Figure 69.

1-21 HIGH-SPEED FLIGHT

It is obvious that the adverse effects of compressibility must be minimized for successful flight at high speeds. The means for doing this has been evolved from countless wind tunnel tests over a period of years.

It is reasonable to expect that compressibility difficulties will be minimized if the local velocities over the airfoil surface are kept as low as possible. In other words, the air passing over the airfoil surface should be accelerated a minimum possible amount, since the compressibility problems are a function of the local Mach number. If the airfoil is very thin and does not have any abrupt changes in contour, the above result will be obtained.

Another variable at the disposal of designers is the amount and type of camber used in the airfoil section. Still another tool available for alleviating the adverse effects of compressibility is the use of sweepback. Consider first two identical wings; one with no sweep and the other with some arbitrary sweep angle, Λ, as in Figure 70.

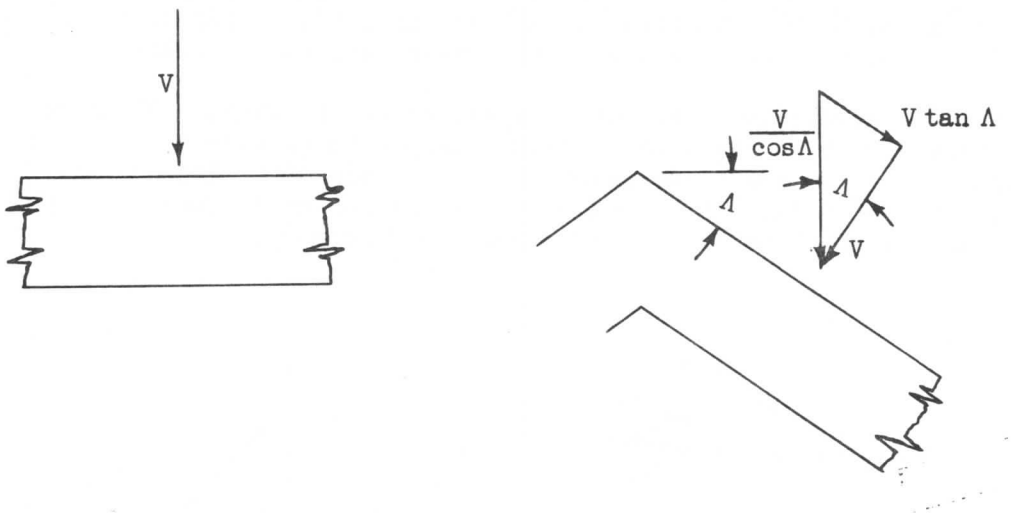

Figure 70.

Assume that in both cases there is a velocity, V, acting perpendicular to the leading edge. In the case of the swept wing this velocity is one of the components of the remote velocity which acts at an angle Λ to the leading edge, and of magnitude $V/\cos \Lambda$. The other component is V tan Λ which can be made to act parallel to the leading edge. This latter component can be seen to have no effect on the lift and drag pressure forces since the air flows along parallel lines of constant elevation. The pressure distribution is effected only by the flow perpendicular to the leading edge. It is apparent that the free stream velocity can be increased by a factor $1/\cos \Lambda$ over that of the straight wing for equal aerodynamic forces. This implies that the critical Mach number of a wing with sweepback is increased over one without sweep by the factor of $1/\cos \Lambda$. Although sweepback is beneficial for increasing critical Mach number, the above factor is too optimistic for predicting the effect in three-dimensional flows. Such things as spanwise flow, boundary layer thickening near the wing tips, and spanwise load distribution make it impossible for such a simple relationship to be valid.

The effect of sweep on the drag rise curve of an airfoil may be seen on Figure 71. At the same lift coefficient; one wing unswept, and the other with sweep, both having the same thickness streamwise, there is a noticeable difference in the drag critical Mach number. The definition of drag critical Mach number from the drag rise curves is somewhat arbitrary but is usually defined as the Mach number at which a .0020 increase in C_D has occurred over the incompressible C_D.

Another device used to alleviate the effects of compressibility is the vortex generator. When airflow separation due to compressibility occurs, it is always associated with the formation of a shock wave resulting in an adverse effect upon the boundary layer and the airflow characteristics downstream of the shock wave. To relieve this adverse effect, energy must be given to the air in the boundary layer to accelerate the slow moving particles, thereby preventing separation. The vortex generator is designed to do this job.

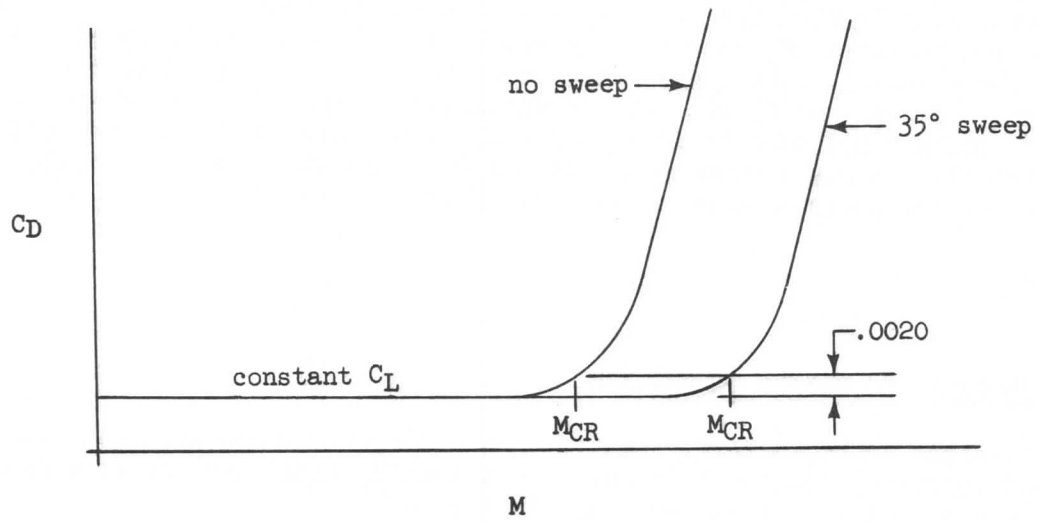

Figure 71.

The vortex generator is actually a small low aspect ratio wing placed vertically at some angle of attack on the surface of the large wing. The generator will produce lift under these conditions, and it will also have an associated tip vortex. This vortex will be large relative to the generator since the aspect ratio is small. The characteristic cork-screw shape of the vortex results in considerable vertical height. An illustration of the generator action is shown in Figure 72.

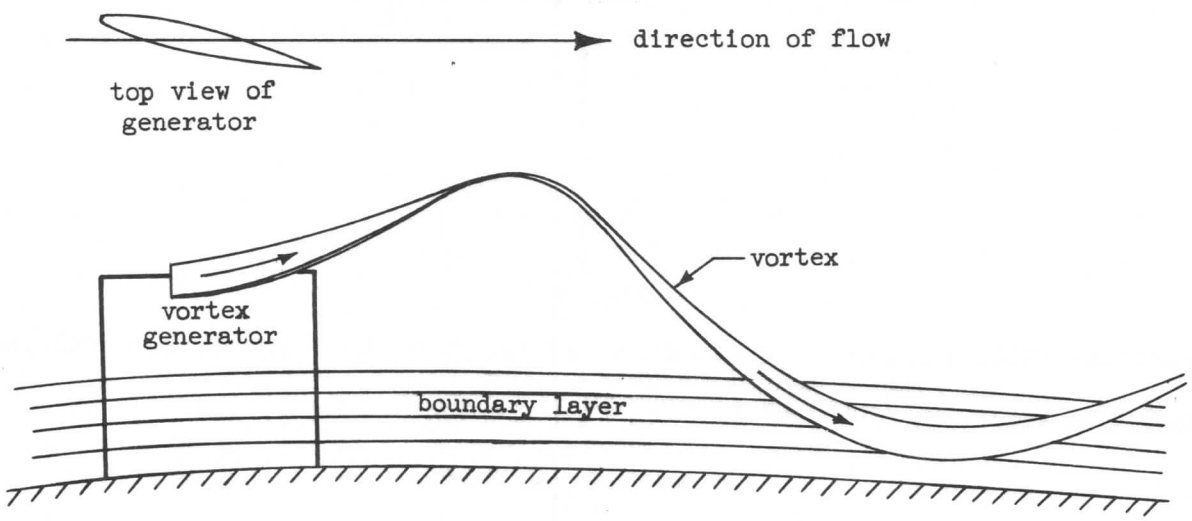

Figure 72.

The generator is taking relatively high energy air from outside the boundary layer and mixing it with the low energy air in the boundary layer. Obviously, the size and location of the vortex generator must be such as to penetrate through the boundary. The number of generators and the orientation on the wing has largely depended on flight test investigation. The addition of vortex generators, while beneficial in some respects, is not made without some cost. The small airfoils obviously produce additional drag, so the overall estimate of the worth of the generators must take this fact into account.

1-22 AIRPLANE AND ENGINE PARAMETERS

For an airplane to be in level, unaccelerated flight, thrust and drag must be equal and opposite, and the lift and weight must be equal and opposite according to the laws of motion. Thus, as shown in Figure 73:

$$T = D \qquad (135)$$

$$L = W \qquad (136)$$

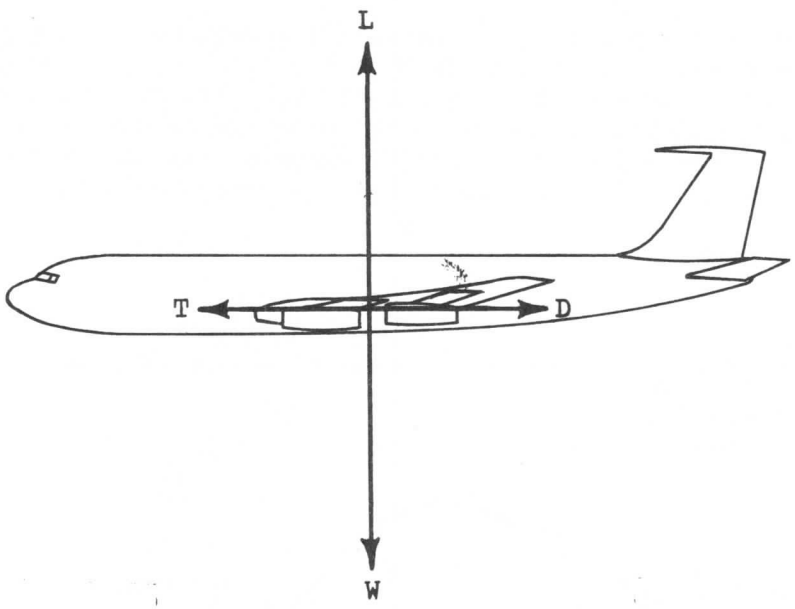

Figure 73.

Equations (104) and (105) are useful in another form which may now be developed.

Rewriting equations (104) and (105):

$$L = C_L S \frac{1}{2} \rho V^2$$

$$D = C_D S \frac{1}{2} \rho V^2$$

It should be remembered that:

$$M = \frac{V}{a}$$

or,

$$V = Ma$$

Writing the speed of sound, equation (50), for the general and sea level standard conditions, it is convenient to divide the former by the latter, thus:

$$a = \sqrt{\gamma g R T}$$

At sea level,

$$a_o \sqrt{\gamma g R T_o}$$

Therefore,

$$\frac{a}{a_o} = \sqrt{\frac{T}{T_o}}$$

or,

$$a = a_o \sqrt{\theta} \qquad \text{(137)}$$

Substituting for V^2 in equation (104) results in:

$$L = C_L S \frac{1}{2} \rho M^2 a_o{}^2 \theta \qquad \text{(138)}$$

Also remembering that:

$$\delta = \sigma \theta$$

$$\sigma = \frac{\rho}{\rho_o}$$

equation (138) may be rewritten thus:

$$L = C_L S \frac{1}{2} \rho_o \delta M^2 a_o{}^2 \qquad \text{(139)}$$

Since ρ_o and a_o are both standard values for air, and are:

$$\rho_o = .002377 \text{ slugs/ft}^3$$

$$a_o = 1116.4 \text{ ft/sec}$$

equation (139) may now be written with the above values substituted.

$$L = 1481.4 C_L M^2 S \delta$$

or,

$$\frac{L}{\delta} = 1481.4 C_L M^2 S \qquad \text{(140)}$$

In effect, $1481.4 M^2 \delta$ was substituted for $1/2\ \rho\ V^2$ in equation (104). The same reasoning may be applied to equations (105, (135), and (136), producing:

$$\frac{D}{\delta} = 1481.4 C_D M^2 S \qquad \text{(141)}$$

$$\frac{W}{\delta} = 1481.4 C_L M^2 S \qquad \text{(142)}$$

$$\frac{T}{\delta} = 1481.4 C_D M^2 S \qquad \text{(143)}$$

These equations form the basis of many performance calculations and, although they are merely the lift and drag equations modified, may appear somewhat strange. It should be noted that Mach number instead of true airspeed is used as the velocity parameter. This is logical since Mach number is the more signigicant parameter when considering high speed aircraft. The use of Mach number, however, introduces the pressure ratio, δ, into the equations. This quantity is placed on the left side of the equation to make the new parameters, W/δ and T/δ.

Since δ is a function of altitude, for a given weight and thrust, W/δ and T/δ will vary with altitude. The turbojet engine responds basically to pressure and temperature, as will be shown in the following section. Above 36,089 feet altitude, the temperature is constant in the standard atmosphere. This means that thrust under any specific condition of engine RPM and airplane speed will vary directly with the ambient atmospheric pressure. The thrust, then, will decrease in proportion to the pressure ratio, δ, as altitude is increased above 36,089 feet. In other words, T/δ will remain constant under these conditions. Thus, T/δ is a logical parameter on the basis of the engine characteristics, since it will be found that much of the jet operation will be above 36,089 feet. Since T/δ is to be used as a parameter, then W/δ must be used to be consistent.

The application of equations (142) and (143) to performance computations is made in the following manner. The value of C_L at a given W/δ and Mach number may be computed from equation (142). Knowing C_L and Mach number, the corresponding C_D may be found from an airplane polar such as shown in Figure 53. This will enable one to calculate T/δ from equation (143). Selecting a range of Mach numbers for the given W/δ as before will result in a series of points defining a curve which may be plotted on axes of T/δ and Mach number. By selecting several values of W/δ, more curves may be obtained, resulting in a "family" of curves as in Figure 74. These curves now define the T/δ required by the engines to fly in level unaccelerated flight.

On this same plot may be superimposed lines of T/δ available from the engines at various altitudes. On Figure 74 the available thrust is shown for 36,089 feet and up, and for two altitudes below 36,089 feet. This plot is the basic jet airplane performance plot and is the source of much performance information. As will be shown later it can be used to determine rate of climb, and with the appropriate engine fuel consumption data superimposed, range and holding performance. For the present it will be sufficient to note that the intersections of the thrust available and thrust required curves will determine the maximum level flight speeds attainable at each altitude.

It will be noticed that the thrust parameter, T/δ, will be notated frequently

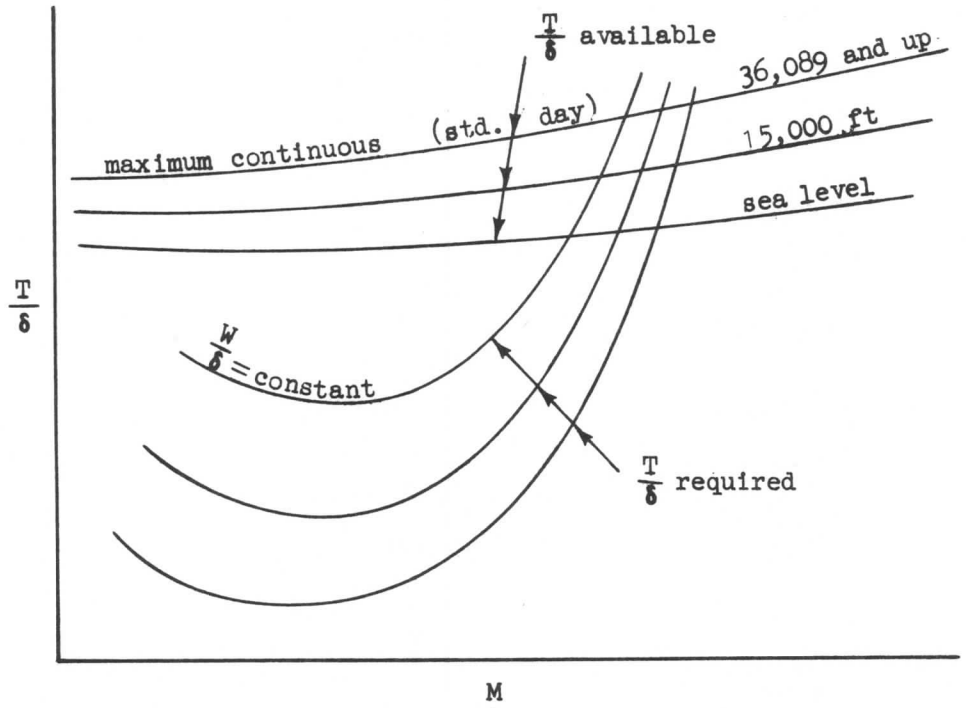

Figure 74.

as F_n/δ in succeeding chapters; however, the two terms are identical. In engine analysis work, it is helpful to use the term net thrust, F_n, as distinguished from gross thrust, F_g. The significance of the latter terms will be discussed in Section 2.

SECTION 2

TURBOJET ENGINE PRINCIPLES

SECTION 2

JET ENGINES

2-1 GENERAL TURBOJET DEVELOPMENT

Probably the first demonstration of the principle of jet propulsion was made by Hero, an Alexandrian philosopher, near the beginning of the Christian era. Hero's apparatus consisted of a hollow sphere mounted so as to rotate between two supports. Through one of the supports was piped steam generated in a closed vessel over a fire. Two nozzles were attached at right angles on opposite sides of the sphere through which the steam was ejected, causing the sphere to revolve. The mechanism, called an aeoliphile was not intended as a device to do useful work, but to be a showpiece of the inventor's ingenuity.

In 1629, an Italian engineer, Giovanni Branca, proposed the first turbine. The device made use of principles already established by previous experimenters. Branca's idea was to direct a powerful stream jet tangentially against open vanes formed on the circumference of a wheel mounted on a vertical spindle. From this wheel other mechanisms were to be driven at reduced speed through crude reduction gearing.

Later in 1687, Sir Isaac Newton realized the possibilities of jet propulsion by the formulation of his third law of motion: that action and reaction are equal in magnitude and opposite in direction. His suggestion was to propel a carriage by the reaction of a steam jet through a nozzle. The carriage was a four-wheeled vehicle supporting a spherical boiler with the nozzle on top directed toward the rear. The speed was to be regulated by the driver controlling a steam cock in the nozzle.

The first patent for a gas turbine was taken out by John Barber, an Englishman, in 1791. The power-producing plant consisted of a gas producer and receiver, air and gas compressors, a combustion chamber, a turbine wheel and speed-reduction gearing. In 1849, Charles Golightly obtained a patent for an aircraft operated by jet propulsion. The power unit consisted of a steam boiler and exhaust jet. This idea, as was true of most others in those days, never passed the design stage.

The first jet-propelled flight was made in Germany on June 20, 1939 in a Heinkel HE-176. The power plant was a Heinkel-Hurt HE-S3 gas turbine unit. The maximum speed was approximately 150 miles per hour. In 1940 in Italy, a jet flight was made from Milan to Rome, a distance of 170 miles, by Colonel Bernardi. The airplane was a Campini design built by the Caproni Aircraft Company designated the CC-2, and powered by an Isotta-Fraschini engine. The 900 horsepowered liquid-cooled piston engine drove a three stage compressor and ducted fan with "afterburning" equipment. The maximum speed was 205 miles per hour but could be increased, with the afterburner on, to 230 miles per hour.

Air Commodore Frank Whittle of the Royal Air Force in England was highly interested in the potential of jet propulsion. In January 1930, Whittle filed application for his first patent. The engine was designed around a centrifugal compressor employing a new principle, that of using a turbine driven by the expansion of heated compressed air instead of a reciprocating engine. The first successful test run was made in 1937 and the first successful flight was made in 1941. This engine, the Whittle W1, was the prototype for all British and American developments in the succeeding years.

The Whittle unit was sent to the United States in 1941 for further development and manufacture. Within one year, an airplane equipped with two of the American units was built and test flown. The aircraft was a Bell P-59 and the engines were designated I-16 (J-31).

Early progress in the development of jet propulsion was comparatively slow. Recent rapid progress has been due to the combined efforts of many persons engaged in continuous research in high-temperature metallurgy, development of new fuels, and the designing and testing of jet power units.

Improvements in the centrifugal flow engine and the development of an axial-flow type compressor proved successful. Due to the smaller diameter and higher compression ratios available, the axial flow engine has become more attractive to the designer in recent years.

World War II brought about a number of other propulsion devices previously thought unattractive economically. The need for higher speeds, altitudes, and larger and heavier bombing platforms gave rise to developments in other than the gas turbine or turbojet engine. Included in this category are the rocket, ram jet, pulse jet, and turbo-propeller engines.

2-2 JET-REACTION ENGINES

The primary purpose of all aircraft power plants is to impart a change in momentum to a mass of fluid. The fluid may be air, air and combustion products, or combustion products only. As will be shown subsequently, a change in momentum is equivalent to an acceleration of a working mass producing a force, or thrust.

The propeller-equipped engine generates thrust by imparting acceleration to a quantity, or mass of air. The jet engine accomplishes the same result. The propulsive force reacts on the engine internal structure to give forward motion to the aircraft.

The Basic Jet Powerplant

Gas turbines, or jet power plants, are of the type shown in Figure 1. The engine has several jobs to perform and utilizes several different parts to do these jobs. Conveniently enough, these parts can be designed into a small housing with each member compatible with another. The atmospheric air enters the intake duct, or diffuser, which serves to reduce the velocity somewhat and increase the static pressure. A rotating mechanical compressor further increases the pressure and delivers the compressed air to the combustion chamber. Here fuel is injected and the mixture ignited and burned. The combustion product is then directed against a turbine wheel where the mass is expanded to produce shaft power and discharged through the exit nozzle to the atmosphere. The energy removed by the turbine wheel is used to turn the compressor and power accessory units.

Unlike a piston-type engine which operates on a four-stroke cycle, intake, compression, power and exhaust, all of which intermittantly occur in the same chamber; the jet engine is designed for continuous operation, and each operation occurs in a separate chamber.

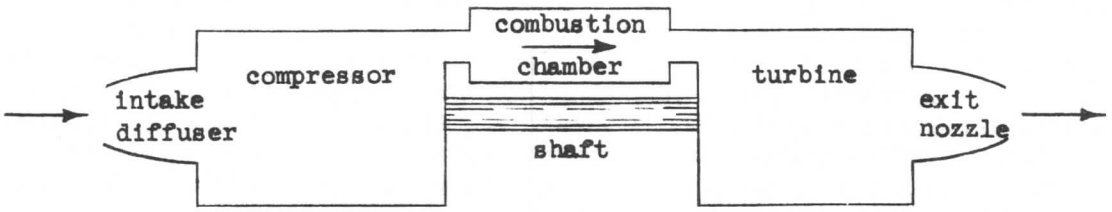

Figure 1.

In addition to the components already named, a typical jet engine usually incorporates also an accessory section, cooling system, starting system, lubrication system, fuel system, and often, a water injection system.

There are two widely used types of turbojet engines: centrifugal-flow and axial-flow. The characteristics of each are pronounced; the primary difference is in the compressor appearance. Although combinations of the two types are possible, the axial flow type has appealed to engine and airframe manufacturer alike to produce a most compatible arrangement for aircraft use.

Turboprop Engine

The turboprop is essentially a turbojet designed to drive a propeller. The propeller operates from the same shaft as the compressor and turbine through reduction gearing. The thrust is derived through the propeller for the most part although as much as 20% may be obtained from jet action. This engine retains the advantage of having a light weight and low frontal area, together with the ease of installation that goes with turbojet engine design. In addition, it has a high efficiency at relatively low speeds. However, present propeller design limits the use of this type of powerplant to speeds below 450 knots.

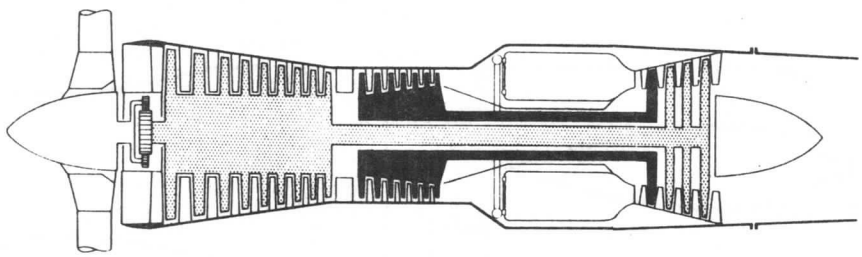

Figure 2.

SECTION 2

JET ENGINES

Turbofan Engine

The turbofan version of an aircraft gas turbine is the same as the turboprop; the geared propeller being replaced by a duct-enclosed fan driven at engine speed. One fundamental operational difference between the turbofan and the turboprop is that the airflow through the fan of the turbofan is unaffected by airspeed of the aircraft. This eliminates the loss in operational efficiency at high airspeeds, which limits the airspeed capability of a turboprop engine. Also, the total airflow through the turbofan engine is much less than that through the propeller of a turboprop. In the turbofan engine, 30 to 60 percent of the propulsive force is produced by the fan.

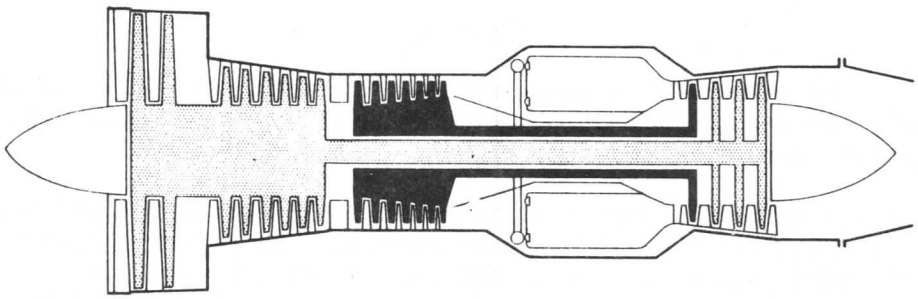

Figure 3.

Ramjet Engine

The ramjet is perhaps the simplest of engines in principle. Air is compressed through a diffuser into a combustion chamber by the relative motion of the engine and air. Fuel is introduced in the combustion chamber and burned. The hot products of combustion are expanded out of the nozzle, producing an exit velocity in excess of that of the free stream. The resulting increase in the momentum of the combustion product determines the thrust produced by the engine. Since the combustion chamber pressure must be greater than ambient, the engine cannot produce thrust unless there exists relative movement between it and the air. As speed is increased, pressures in the engine increase and fuel economy is improved. The potential of the ramjet lies in the transonic and supersonic speed ranges. The main advantages of this type of engine are its simplicity, lack of moving parts and tremendous potential power at high speeds.

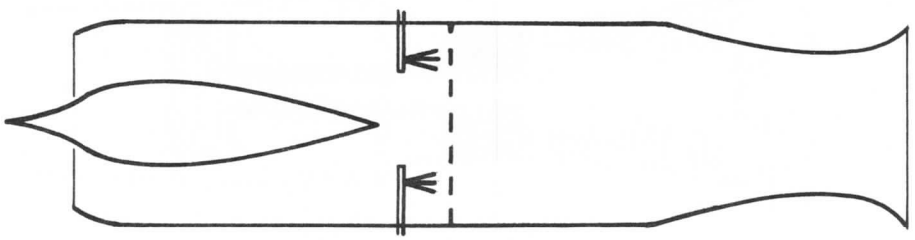

Figure 4.

Pulse Jet Engine

A modification of the ramjet is the pulse jet. It incorporates a disc in the inlet duct with valves which alternately open and close as a function of the intake pressure and back pressure from combustion. This type of engine can be started from a static condition. It has the disadvantage, however, of being extremely noisy and in addition vibrates badly. Fuel consumption at lower speeds is high; and at high speeds, the ramjet appears more promising. Its usefulness is somewhat limited to pilotless aircraft.

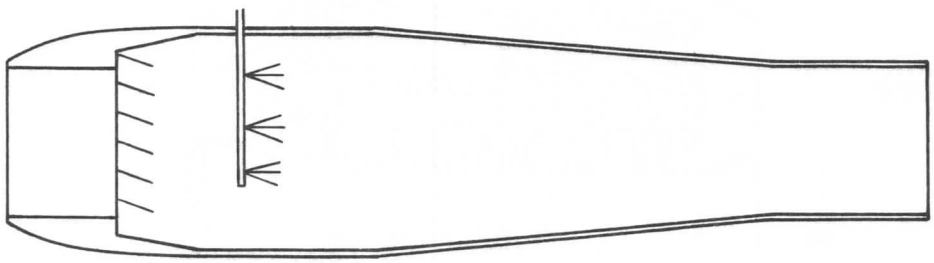

Figure 5.

Rocket Engine

The rocket engine is a self-contained powerplant which does not depend on atmospheric air for operation. The fuel used in the rocket is either solid or liquid depending on the type of rocket. An oxidizer is carried along with the fuel, and an ignition system is installed if such is necessary. Most rockets burn fuel and oxidizer at a constant rate; therefore, a constant thrust is produced. The burning gases expand out of a nozzle and produce mechanical energy; hence, thrust. The static pressure at the nozzle exit influences the thrust; since expansion to low pressure aids in converting thermal energy into mechanical energy, thrust is increased with altitude. The rocket engine has the greatest potential of all since it does not depend upon the atmosphere for combustion. There are few moving parts and maintenance problems are minimized, but consumption of the propellant is high at the present time.

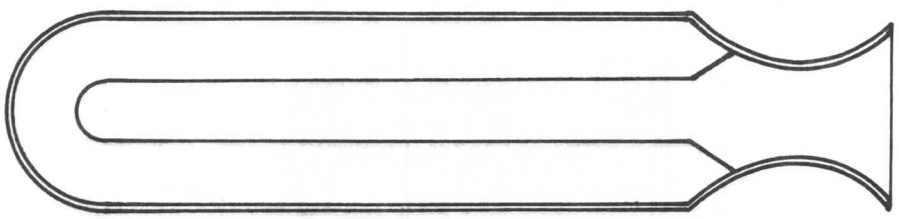

Figure 6.

2-3 ENGINE STATION IDENTIFICATION

It is convenient to assign numbers to the stations separating the major components of the engine. The station numbers may vary somewhat between manufacturers and types of engines, however. For example, the Rolls Royce Company refers to the low pressure compressor inlet as station 1, while the Pratt and Whitney and General Electric Companies refer to this position as station 2. Figure 7 shows the station identification for single and dual rotor systems including the turbofan and by-pass engines.

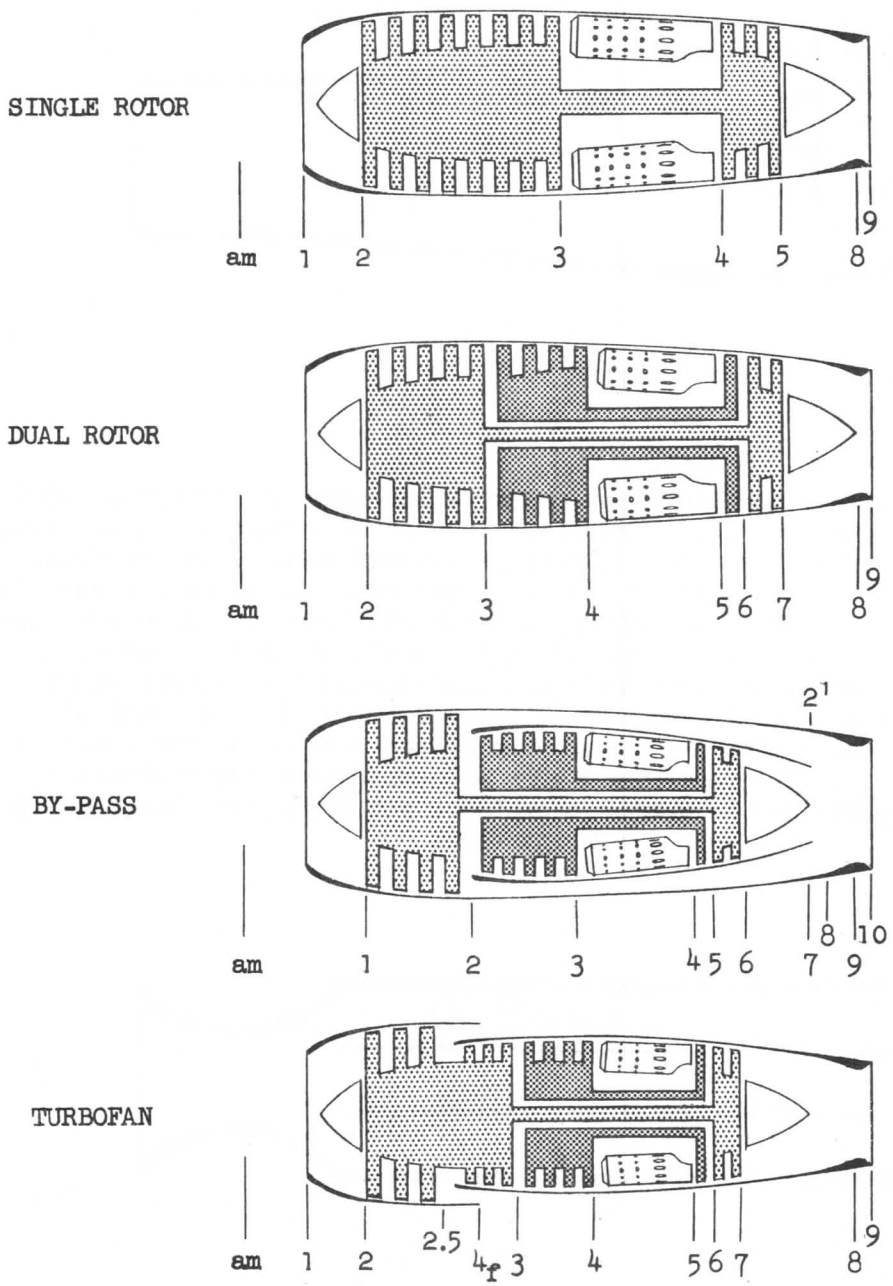

Figure 7.

2-4 ENGINE PARAMETERS

The performance characteristics of the turbojet engine can be obtained from non-dimensional plots of engine data. The basic performance curves of gross thrust F_g, airflow, W_a, and fuel flow, W_f, are derived in terms of the following (for a single rotor engine):

Compressor inlet total pressure, p_{t_2}
Ambient static pressure, p_{am}
Turbine RPM, N
Compressor inlet total temperature, T_{t_2}
Linear dimension, D

Following the procedure used in the preceding section, a general (although arbitrary) relation may now be written for the fluid force, F_g.

$$F_g = C\,(p_{t_2})^{\alpha}\ (p_{am})^{\beta}\ (N)^{\gamma}\ (T_{t_2})^{\delta}\ (D)^{\epsilon} \qquad (1)$$

Newton's second law of motion written in terms of the fundamental units of M, L, T is:

$$F = \frac{ML}{T^2} \qquad (2)$$

Equation (1) is now written in terms of the fundamental units:

$$\frac{ML}{T^2} = C\left(\frac{M}{LT^2}\right)^{\alpha}\left(\frac{M}{LT^2}\right)^{\beta}\left(\frac{1}{T}\right)^{\gamma}\left(\frac{L^2}{T^2}\right)^{\delta}(L)^{\epsilon} \qquad (3)$$

With regard to the temperature factor, it will be noted that temperature is a measure of thermal energy per unit mass and has the fundamental dimensions of velocity squared:

$$T_{t_2} = \frac{\frac{1}{2}MV^2}{M}$$

Therefore, the fundamental units of temperature are L^2/T^2.

Powers of like variables are now equated:

$$\left.\begin{aligned} &M: \quad 1 = \alpha + \beta \\ &L: \quad 1 = -\alpha - \beta + 2\delta + \epsilon \\ &T: \quad 2 = 2\alpha + 2\beta + \gamma + 2\delta \end{aligned}\right\} \qquad (4)$$

Since the above three equations contain five unknowns, it is necessary to express any three equations in terms of two unknowns. Assuming p_{am} and T_{t_2} to be of least importance, α, γ, and ϵ are found in terms of β and δ :

$$\left.\begin{aligned} \alpha &= 1 - \beta \\ \varepsilon &= 1 + (1-\beta) + \beta - 2\delta \\ \varepsilon &= 2 - 2\delta \\ \gamma &= 2 - 2(1-\beta) - 2\beta - 2\delta \\ \gamma &= -2\delta \end{aligned}\right\} \qquad (5)$$

Substituting these values in equation (1), the following is obtained:

$$F_g = C\ (p_{t_2})^{1-\beta}\ (p_{am})^{\beta}\ (N)^{-2\delta}\ (T_{t_2})^{\delta}\ (D)^{2-2\delta} \qquad (6)$$

or,

$$F_g = C\ p_{t_2}\ D^2 \left(\frac{p_{am}}{p_{t_2}}\right)^{\beta} \left(\frac{T_{t_2}}{N^2 D^2}\right)^{\delta} \qquad (7)$$

The dimension, D, may be eliminated for a particular power plant for presentation of performance data. Equation (7) may be shown simply as:

$$\frac{F_g}{p_{t_2}} = C \left(\frac{p_{t_2}}{p_{am}}\right)^{-\beta} \left(\frac{N^2}{T_{t_2}}\right)^{-\delta} \qquad (8)$$

or, F_g/p_{t_2} stated as a function of two parameters:

$$\frac{F_g}{p_{t_2}} = f\left(\frac{p_{t_2}}{p_{am}}, \frac{N}{\sqrt{T_{t_2}}}\right) \qquad (9)$$

The numerical values of F_g/p_{t_2} and $N/\sqrt{T_{t_2}}$ are not easily recognized as thrust and RPM, therefore, it is more convenient to use a multiplying constant such that the nondimensional groups are equal to gross thrust and actual RPM at standard sea level conditions. These parameters, referenced to standard sea level conditions, are called "referred paramters."

Thus,

$$\frac{F_g\ p_o}{p_{t_2}} \quad \text{and} \quad \frac{N\sqrt{T_o}}{\sqrt{T_{t_2}}}$$

may become:

$$\frac{F_g}{p_{t_2}/p_o} \quad \text{and} \quad \frac{N}{\sqrt{T_{t_2}/T_o}}$$

By defining:

$$\delta_{t_2} = \frac{p_{t_2}}{p_o}$$

and,

$$\theta_{t_2} = \frac{T_{t_2}}{T_o}$$

equation (9) becomes:

$$\frac{F_g}{\delta_{t_2}} = f\left(\frac{p_{t_2}}{p_{am}}, \frac{N}{\sqrt{\theta_{t_2}}}\right) \qquad (10)$$

To develop an equation for air flow, consider the mass flow rate,

$$\frac{W_a}{g} = C\,(p_{t_2})^{\alpha}\,(p_{am})^{\beta}\,(N)^{\gamma}\,(T_{t_2})^{\delta}\,(D)^{\varepsilon}$$

and in terms of fundamental units

$$\frac{M}{T} = C\left(\frac{M}{LT^2}\right)^{\alpha}\left(\frac{M}{LT^2}\right)^{\beta}\left(\frac{1}{T}\right)^{\gamma}\left(\frac{L^2}{T^2}\right)^{\delta}(L)^{\varepsilon}$$

Equating powers of like variables

$$M:\ 1 = \alpha + \beta$$

$$L:\ 0 = -\alpha - \beta + 2\delta + \varepsilon$$

$$T:\ -1 = -2\alpha - 2\beta - \gamma - 2\delta$$

Therefore,

$$\alpha = 1 - \beta$$

$$\delta = -\tfrac{1}{2} - \frac{\gamma}{2}$$

$$\varepsilon = 2 + \gamma$$

and,

$$\frac{W_a}{g} = C\,(p_{t_2})^{1-\beta}(p_{am})^{\beta}\,(N)^{\gamma}\,(T_{t_2})^{-\frac{1}{2}-\frac{\gamma}{2}}(D)^{2+\gamma}$$

$$\frac{W_a}{g} = C\,\frac{p_{t_2}\,D^2}{\sqrt{T_{t_2}}}\left(\frac{p_{t_2}}{p_{am}}\right)^{-\beta}\left(\frac{ND}{\sqrt{T_{t_2}}}\right)^{\gamma}$$

This, for a particular powerplant, can be written as

$$\frac{W_a\sqrt{\theta_{t_2}}}{\delta_{t_2}} = f\left(\frac{p_{t_2}}{p_{am}}, \frac{N}{\sqrt{\theta_{t_2}}}\right) \qquad (11)$$

In a similar way, to develop an equation for fuel flow, it is necessary to think of fuel flow as potential energy flow; therefore

$$W_f = \text{Energy/Time}, \frac{\text{ft lb}}{\text{sec}}$$

$$W_f = C\ (p_{t_2})^{\alpha}\ (p_{am})^{\beta}\ (N)^{\gamma}\ (T_{t_2})^{\delta}\ (D)^{\epsilon}$$

In terms of fundamental units

$$\frac{ML^2}{T^3} = C \left(\frac{M}{LT^2}\right)^{\alpha+\beta} \left(\frac{1}{T}\right)^{\gamma} \left(\frac{L^2}{T^2}\right)^{\delta} (L)^{\epsilon}$$

and equating powers of like variables

$$M: \quad 1 = \alpha + \beta$$

$$L: \quad 2 = -(\alpha + \beta) + 2\delta + \epsilon$$

$$T: \quad -3 = -2(\alpha + \beta) - \gamma - 2\delta$$

Therefore,

$$\alpha = 1 - \beta$$

$$\delta = \tfrac{1}{2} - \frac{\gamma}{2}$$

$$\epsilon = 2 + \gamma$$

and,

$$W_f = C\ (p_{t_2})^{1-\beta} (p_{am})^{\beta}\ (N)^{\gamma}\ (T_{t_2})^{\frac{1}{2}-\frac{\gamma}{2}}\ (D)^{2+\gamma}$$

$$W_f = C\ p_{t_2}\ \sqrt{T_{t_2}}\ D^2 \left(\frac{p_{t_2}}{p_{am}}\right)^{-\beta} \left(\frac{ND}{\sqrt{T_{t_2}}}\right)^{\gamma}$$

This, for a particular powerplant, can be written as

$$\frac{W_f}{\delta_{t_2}\sqrt{\theta_{t_2}}} = f\left(\frac{p_{t_2}}{p_{am}}, \frac{N}{\sqrt{\theta_{t_2}}}\right) \qquad (12)$$

Typical non-dimensional engine characteristics are shown in Figures 8, 9, and 10. Data from charts such as these furnish the information for thrust - fuel flow - airflow curves throughout the range of operation.

Performance curves published by the engine manufacturers showing the thrust - fuel flow - air flow relationships may appear as in Figure 11 where the information for this curve is obtained from Figures 8, 9, and 10. These curves are available for various altitudes throughout the range of airspeeds from idle

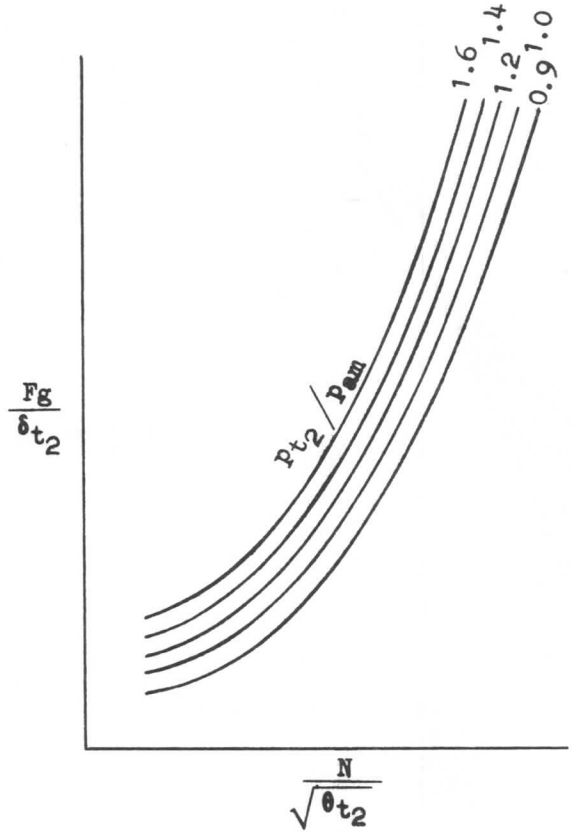

Figure 8.

Figure 9.

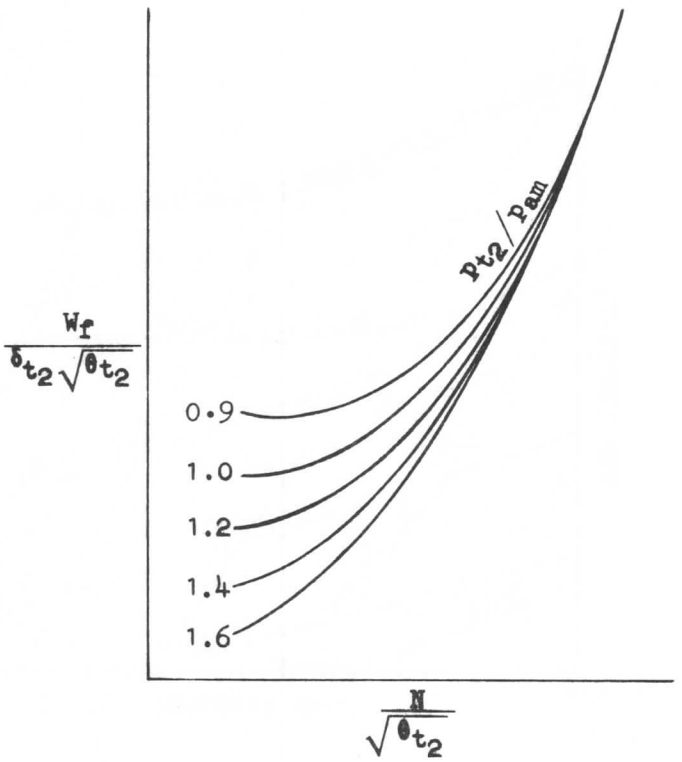

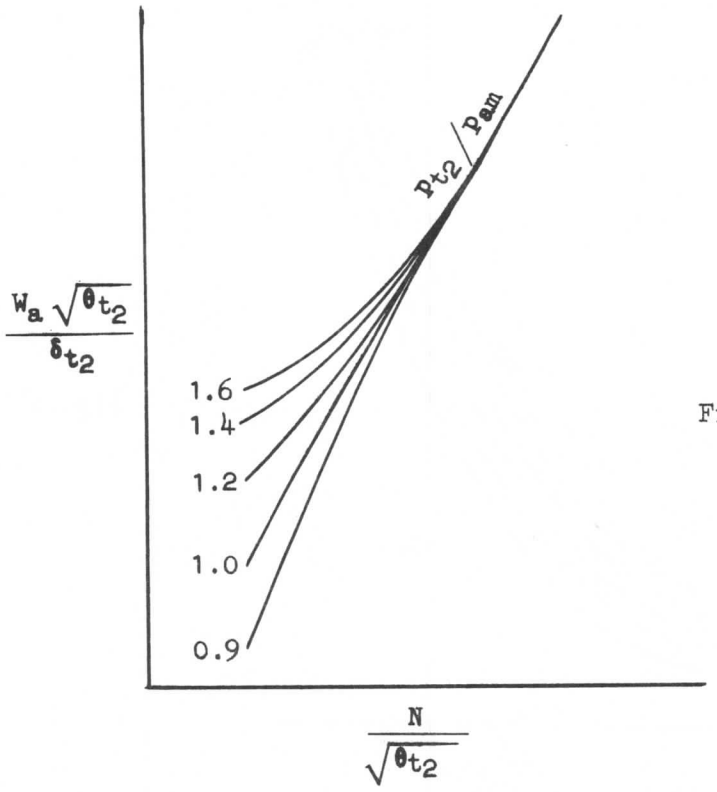

Figure 10.

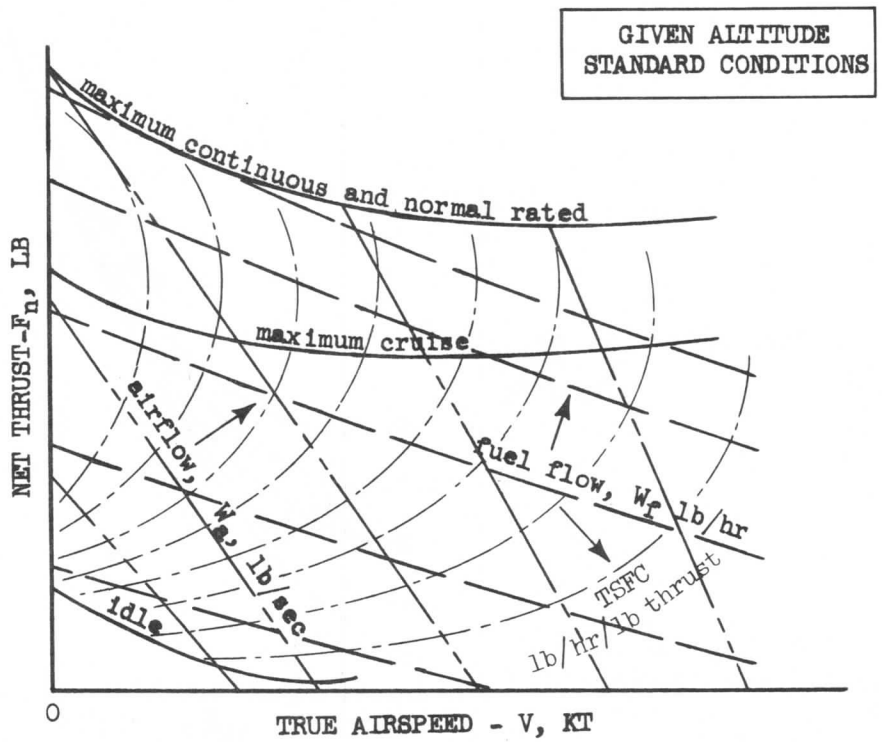

Figure 11.

thrust to takeoff thrust. Sometimes the fuel consumption data are presented in terms of "thrust specific fuel consumption," TSFC, which is fuel flow divided by net thrust. In this form, the data are more easily used for airplane performance calculation.

It should be noted that the term, net thrust, F_n, has been used. Net thrust is the total usable force derived from the engine by accelerating the air mass.

$$F_n = Ma$$

$$F_n = M \frac{\Delta V}{\Delta t}$$

$$F_n = \frac{M}{\Delta t} \Delta V \qquad (13)$$

But,

$$\frac{M}{\Delta t} = \frac{W_a}{g}$$

and,

$$\Delta V = V_j - V_a ,$$

where V_a is the freestream (or airplane) velocity; therefore,

$$F_n = \frac{W_a}{g} (V_j - V_a) \qquad (14)$$

Thus, the net thrust is the difference between the force of the airstream at the tailpipe and the force of the airstream at the inlet. Since the first term is the total force output of the engine, it is known as the gross thrust,

$$F_g = \frac{W_a}{g} V_j \qquad (15)$$

Since the force at the inlet tends to reduce the usable thrust, it is called ram drag,

$$F_r = \frac{W_a}{g} V_a \qquad (16)$$

By adding the weight of fuel and its acceleration from a relative velocity of zero to jet velocity, the equation for net thrust may be rewritten:

$$F_n = \frac{W_a}{g} (V_j - V_a) + \frac{W_f}{g} (V_j - 0) \qquad (17)$$

Since the last term of equation (17) is small in comparison, it is often neglected.

It is noteworthy that Newton's third law of motion explains why thrust (a force) is obtained from the ejection of mass from the nozzle of a jet engine. The second law indicates the magnitude of thrust as shown by equation (14). This equation or variations will be amplified in subsequent chapters.

JET ENGINES

To see that discharge total pressure, p_{t_7} and pressure ratio, p_{t_7}/p_{t_2} are valid indexes of thrust output of the engine, consider ram drag as a function of velocity as shown in equation (14). Therefore, at a fixed speed, net thrust will vary as gross thrust. Airflow rate in the above equations may be considered in terms of the continuity equation:

$$\frac{W_a}{g} = \rho AV \qquad (18)$$

where A and V are the jet nozzle throat area and velocity. Thus equation (15) becomes,

$$F_g = \rho AV(V)$$

$$F_g = \rho AV^2 \qquad (19)$$

Substituting Mach number for velocity,

$$F_g = \rho AM^2 a2 \qquad (20)$$

By use of the basic relationships:

$$a = \sqrt{\gamma gRT}$$

$$\rho = \frac{p}{gRT}$$

equation (20) can be written as

$$F_g = \frac{pAM^2 \gamma gRT}{gRT}$$

$$F_g = pAM^2 \gamma \qquad (21)$$

It should be noted that the pressure, p, used in equation (21) is the static pressure. Thus, gross thrust varies with static pressure and Mach number, since A and γ are constant. But static pressure is related to total pressure, p_t, as shown in section 1:

$$\frac{p_t}{p} = \left(1 + \frac{\gamma-1}{2} M^2\right)^{\frac{\gamma}{\gamma-1}}$$

By substituting this relationship into equation (21),

$$F_g = \frac{p_{t_7} A_7 M_7^2 \gamma}{\left(1 + \frac{\gamma-1}{2} M_7^2\right)^{\gamma/\gamma-1}} \qquad (22)$$

It may be seen from this equation that gross thrust, and therefore net thrust, is a function of total pressure in the exhaust nozzle, p_{t_7}.

$$F_n = f\,(p_{t_7}) \qquad (23)$$

In the same way, applying the same analysis to flow into the engine inlet yields,

$$F_r = \frac{p_{t_2} A_2 M_2^2 \gamma}{(1 + \frac{\gamma-1}{2} M_2^2)^{\gamma/\gamma-1}} \qquad (24)$$

Since

$$F_n = F_g - F_r$$

$$F_n = \frac{p_{t_7} A_7 M_7^2 \gamma_7}{(1 + \frac{\gamma-1}{2} M_7^2)^{\gamma/\gamma-1}} - \frac{p_{t_2} A_2 M_2^2 \gamma_2}{(1 + \frac{\gamma-1}{2} M_2^2)^{\gamma/\gamma-1}}$$

$$\frac{F_n}{p_{t_2}} = \frac{p_{t_7}}{p_{t_2}} \frac{A_7 M_7^2 \gamma_7}{(1 + \frac{\gamma-1}{2} M_7^2)^{\gamma/\gamma-1}} - \frac{A_2 M_2^2 \gamma_2}{(1 + \frac{\gamma-1}{2} M_2^2)^{\gamma/\gamma-1}}$$

$$\frac{F_n}{\delta_{t_2}} = \frac{p_{t_7}}{p_{t_2}} f(A,V,T)_{exhaust} - f(A,V,T)_{inlet}$$

This analysis shows that net thrust is a direct function of geometric design, inlet airflow conditions, exhaust flow conditions, and engine pressure ratio. The exhaust flow conditions are determined by inlet conditions, compression ratio and fuel flow (throttle position). Therefore, an engine of given design will yield net thrust proportional to EPR, p_{t_7}/p_{t_2}, when operating at a given airplane speed, altitude, temperature, and thrust lever position.

$$F_n = f(EPR) \qquad (25)$$

Since P_{t_7} is really an index of gross thrust whereas EPR is an index of net thrust, if P_{t_7} is used as the basic thrust index in an application, it should be corrected for changes in inlet ram conditions. Therefore, on aircraft, where inlet conditions vary over wide extremes, EPR is preferred and recommended as the thrust setting variable. Thrust is not measured directly in engine installations on airplanes.

Although RPM is sometimes considered to be an adequate thrust index for setting power on centrifugal-flow engines, it is not often used with axial-flow machines. Its use is usually limited to that of a secondary index employed to check the thrust-power set by means of EPR or as an emergency index in case of failure of the pressure instrumentation. Several reasons for not using RPM as the primary index are these:

(1) Since high-pressure RPM, N_2, on dual-spool engines, or compressor RPM on single-spool engines, is governed by the fuel control unit, RPM does not provide an accurate means of determining what the rest of the engine is doing. In fact, the control unit may change the N_2 RPM to compensate for problems in other parts of the engine.

(2) Since most engines are "trimmed" by a fuel control adjustment to produce rated thrust at a fixed thrust lever position under standard operating conditions, RPM will vary slightly from engine to engine due to manufacturing tolerances compensated for by changes in trim speed. Accounting for such small differences makes operation of multi-engine airplanes difficult.

(3) The net thrust output of the engine does not vary in direct proportion to the RPM over the entire thrust range.

(4) On dual-spool engines a one percent change in low-pressure RPM, N_1, results in about four percent change in thrust in the flight portion of the operating speed range. A one percent change in high-pressure RPM, N_2, or in RPM of the single-spool engine, results in a five percent change in thrust.

Thrust output is much less sensitive to changes in p_{t_7} or EPR. As shown in Figure 12, a one percent variation in exhaust pressure results in only one and one-half percent change in net thrust.

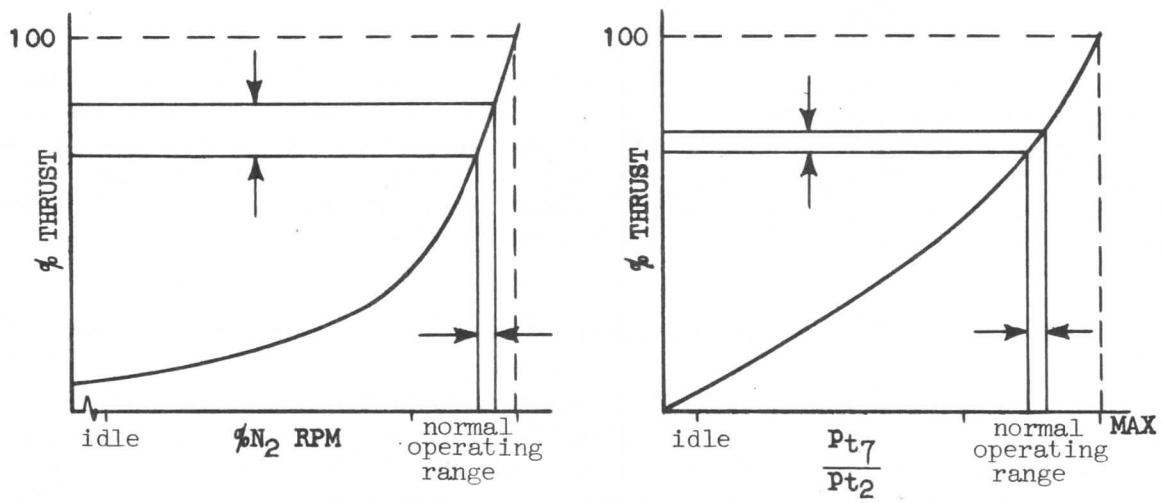

Figure 12.

The relationship of p_{t_7} to p_{t_2} may be shown for dual rotor engines to be:

$$\frac{p_{t_4}}{p_{t_2}} \times \frac{p_{t_5}}{p_{t_4}} \times \frac{p_{t_7}}{p_{t_5}} = \frac{p_{t_7}}{p_{t_2}} \qquad (26)$$

The ratio P_{t4}/P_{t2} is compression ratio, which varies with RPM changes. The ratio P_{t5}/P_{t4} is the burner pressure loss and is considered constant. P_{t7}/P_{t5} is the turbine expansion ratio which is a function of jet nozzle and turbine areas, which are usually constant.

2-5 ENGINE EFFICIENCY

One of the first laws of thermodynamics states that heat and work are two forms of energy, and that they are interchangeable. This means then, that work can be converted into heat, and heat converted to work. The first process is, of course, possible, but the exchange of heat to work is not possible without losses. The ratio of work produced to the heat energy supplied represents the efficiency of a process. The most efficient engine, for example, would be a type that would receive heat at the highest temperature conceivable and exhaust its gas at the lowest temperature possible.

All propulsion devices are heat engines that convert fuel energy (heat energy) into mechanical energy in combination with a system for converting the mechanical energy into useful thrust. The efficiency of a propulsion unit can be expressed as the percent of total heat energy of the fuel that is converted to work. This is sometimes referred to as over-all efficiency, η_o, to distinguish it from thermal efficiency, η_t, or propulsive efficiency, η_p.

$$\eta_o = \frac{\text{Useful work done on airplane}}{\text{Heat energy of fuel}} \qquad (27)$$

Over-all efficiency is the product of thermal and propulsive efficiencies, or:

$$\eta_o = \eta_t \ \eta_p \qquad (28)$$

where,

$$\eta_t = \frac{\text{Mechanical work produced in system}}{\text{heat energy of fuel}} \qquad (29)$$

and,

$$\eta_p = \frac{\text{Useful work done on airplane}}{\text{Mechanical work produced in system}} \qquad (30)$$

The numerator of equation (29) may be developed by observing that work is measured by the product of a force and the distance through which it moves in the direction of the force.

$$\text{Work} = F\ s$$

where,

$$F = \frac{W_a}{g}\ (V_j - V_a)$$

and,

$$s = \frac{(V_j + V_a)}{2}\ t$$

Therefore,

$$\frac{\text{work}}{\text{unit time}} = \frac{W_a}{g}\ (V_j - V_a)\ \frac{(V_j + V_a)}{2}$$

or,

$$\frac{\text{work}}{\text{unit time}} = \frac{W_a}{2g}\ (V_j^2 - V_a^2)\ , \text{ ft lb/unit time}$$

The denominator of equation (29) may be determined by evaluating the energy of the fuel. The constants J and H_f are

$$J = 778 \text{ ft lb/BTU}$$

$$H_f = 18{,}400 \text{ BTU/lb}$$

$$\frac{\text{Energy}}{\text{unit time}} = J\, H_f\, W_f \text{ , ft lb/unit time}$$

Mathematically, thermal efficiency of a turbojet may be expressed as

$$\eta_t = \frac{\frac{W_a}{2g}(V_j^2 - V_a^2)}{J\, H_f\, W_f} \qquad (31)$$

In the gas-turbine type engines, the greatest portion of heat energy input is utilized in driving the compressor rotor. Anything which will cause an increase in the air mass and air pressure head available to the combustion chamber (compression ratio) with no further increase in heat energy input will naturally tend to improve the thermal efficiency.

Two outstanding methods in obtaining such an increase in thermal efficiency would be improvement in compressor efficiency or increase in combustion chamber temperature. If a compressor's ability to pump air with less losses could be increased, then the same mass airflow and compressor ratio could be obtained with less energy input to the compressor, which would result in less fuel flow (heat energy input) for the same thrust output. The increase in combustion temperature results in an increase in tailpipe velocity. This, in turn, results in a higher thermal efficiency as seen by equation (31).

A jet engine's thermal efficiency will tend to improve with air speed due to the ram effect. Ram pressure, when multiplied across the compressor by the compressor ratio could mean an improvement in W_a and combustion chamber pressure head, and thus increased thrust output, with little or no change in shaft energy input to the compressor. Such an increase in useful output with no appreciable change in heat energy input would result in raising the engine's thermal efficiency with airspeed.

A piston engine's thermal efficiency does not increase with airspeed because it cannot take full advantage of the ram effect. Both factors affecting its output are limited; RPM limited by bearing loading, and manifold pressure by detonation. A gas turbine engine operates on a low pressure cycle and, therefore, is not limited by detonation. It is, however, limited by a maximum allowable internal operating temperature dictated by the structural strength and materials of the gas turbine's component parts.

The numerator of equation (30) may be developed by determining the work done on the airplane (per unit of time) as the product of thrust and velocity, (power).

$$\text{power} = T\,V$$

$$\text{thrust} = \frac{W_a}{g}\,(V_j - V_a)$$

$$\text{velocity} = V_a$$

$$\frac{\text{work}}{\text{unit time}} = \frac{W_a}{g}\,(V_j - V_a)\,V_a$$

Mathematically, propulsive efficiency of a turbojet may be expressed as:

$$\eta_p = \frac{\frac{W_a}{g}\,(V_j - V_a)\,V_a}{\frac{W_a}{2g}\,(V_j^2 - V_a^2)}$$

$$\eta_p = \frac{2\,V_a}{V_j + V_a} \qquad (32)$$

The effect of fuel flow is negligible in the above equations.

By inspection of equations (31) and (32), the variables influencing the thermal and propulsive efficiencies may be recognized. How these variables affect the operation of the engine is discussed later. The average jet engine has a overall efficiency under static sea level conditions of 20 to 25 percent, while aircraft piston engines have efficiencies of 25 to 30 percent.

2-6 PRESSURE - VOLUME CYCLES

Engine cycles can be described most easily by the use of pressure - volume diagrams. The diagrams depict the process to which the gases are subjected beginning with atmospheric pressure, through the complete compression and expansion processes, and back to atmospheric pressure again. The area inside the curve in the diagrams represents the work done in the process.

The Otto or constant volume cycle of the piston engine is perhaps the most common, and is shown in Figure 13. The diagram shows the suction and exhaust strokes of the cycle as a dashed line representing a condition where the mass in the cylinder is changing. At the start of compression, the pressure is atmospheric

or nearly so. The pressure is increasing from 1 to 2 as the piston moves to decrease the volume. From 2 to 3 the volume is essentially constant, giving rise to the descriptive name of the cycle. During this time, ignition occurs and the pressure increases. During the expansion or power stroke, 3 to 4, the pressure is relieved and the volume increases due to piston movement. The exhaust begins at point 4 and the pressure reduces to atmospheric again.

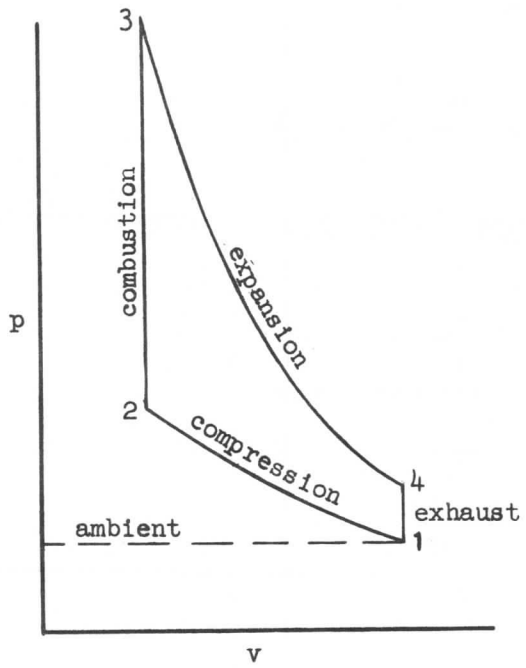

Figure 13.

The turbine jet cycle is known as the Brayton or constant pressure cycle. It operates at much lower pressures than does the Otto cycle to obtain maximum efficiencies and lower fuel consumption rates in addition to compressor design considerations. This cycle is shown in Figure 14. From 1 to 2 the air is entering the inlet and is being compressed from 2 to 3. For cycle analysis it is immaterial that the work of compression is done partly by the intake diffuser and partly by the rotary compressor. Point 3 represents the pressure achieved by the compressor and is essentially maintained throughout the combustion process. From 4 to 1 expansion takes place through the turbine and exhaust nozzles, returning the pressure to its initial ambient condition. The total air mass in the jet cycle represents not only air for combustion (the primary air), but also cooling air, often referred to as dilution air.

In the Otto cycle, combustion occurs at constant volume with the result that the pressure rise is of great magnitude. In the Brayton cycle, however, combustion takes place at a constant pressure, resulting in an increase in volume. It should be noted that in the turbine engine each operation in the cycle is performed continuously and by a separate component designed for the particular function. In the reciprocating engine, the cycle is repeated intermittently in one section of the engine designed to accomplish more than one function.

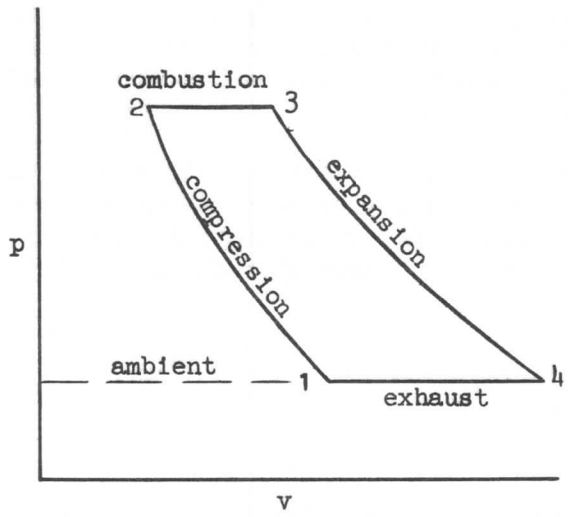

Figure 14.

Superimposing the jet constant pressure cycle over the piston constant volume cycle, as in Figure 15, a comparison of the two may be made.

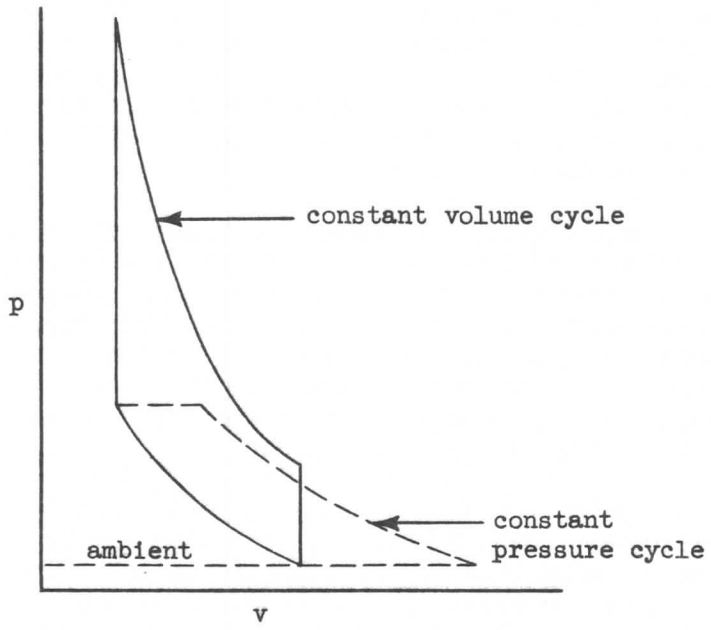

Figure 15.

The area bounded by the lines on the p-v diagram represents the useful work output. The work output of the reciprocating engine is derived by means of its high pressures. It is possible to develop pressures over 1200 psi in the cylinder of a piston engine during the combustion. With further increases in volumetric compression ratio, a greater amount of work may be harnessed from a given

quantity of fuel. This, of course, improves thermal efficiency which in turn results in improved economy. Present jet engines develop pressures in the combustion chamber over 150 psi. When ways are found to increase compressor efficiencies, the useful work output will increase, and, in addition, the thermal efficiency will improve.

Further comparison of the two basic engine cycles shows that the jet engine gains useful work by expanding the gases down to atmospheric pressure where expansion outside the jet nozzle occurs. In the reciprocating engine, the expansion takes place across the exhaust valve and exhaust duct and is therefore lost to the cycle as useful work.

2-7 COMPONENT DESIGN

A study of engine components and their design will serve to increase the understanding of the operation of the engine and its performance. This study is meant to be general in nature; if design details are needed, the reader should go to the basic engine - manufacturer's literature for the engine in which he is interested.

Air Inlet Duct and Diffuser Design

The air inlet duct is usually designed by the airframe manufacturer and not by the engine manufacturer. However, the design of the duct is so important to engine performance that it must be considered in any analytical discussion of the complete engine. Since a gas turbine engine is consuming large quantities of air and is operating at high airspeeds, any inefficiencies of the duct result in large losses throughout the engine.

The inlet duct has to accomplish three functions; first, it must be able to recover as much of the total pressure of the airflow as possible (known as "ram recovery") and deliver this pressure to the engine compressor with a minimum loss; second, the duct must deliver the air to the compressor inlet with as little turbulence as possible; and last, the duct must accomplish items one and two above holding to a minimum the drag effect it creates. In other words, the air inlet duct is so designed as to reduce energy losses in the form of aerodynamic drag or through ram pressure drop.

The shape of the inlet duct and diffuser depends largely on the Mach number for which it is designed. Duct design for airplanes flying supersonic speeds is different than for airplanes flying subsonic speeds. The following write-up will be for subsonic Mach numbers. From Figures 8, 9, and 10, it can be seen that a high ram pressure ratio, P_{t2}/P_{am}, ahead of the compressor will result in high corrected thrust, F/δ_{t2}; high corrected airflow, $W_a\sqrt{\theta_{t2}}/\delta_{t2}$; and low corrected fuel flow, $W_f/\delta_{t2}\sqrt{\theta_{t2}}$. A high ram pressure ratio gives a high ram efficiency,

$$\text{Ram efficiency, } \eta_r = \frac{P_{t2} - P_{am}}{q_c} \qquad (33)$$

where q_c is the free-stream dynamic pressure including compressibility effects.

A high ram efficiency can be obtained in the inlet duct if the friction loss and separated flow are kept to a minimum. For pod type engine installations, friction losses are insignificant and flow separation is of prime importance. In order to reduce internal duct separation for pod type engines, a low inlet velocity ratio, V_1/V_o, is desired. To accomplish this, a good portion of the deceleration may be designed to occur before station 1 since compression in this region is isentropic and compression aft of station 1 involves duct losses. This process of converting directed kinetic energy into pressure is called diffusion. From an engine standpoint, the more diffusion that occurs ahead of station 1 the better. See Figure 16.

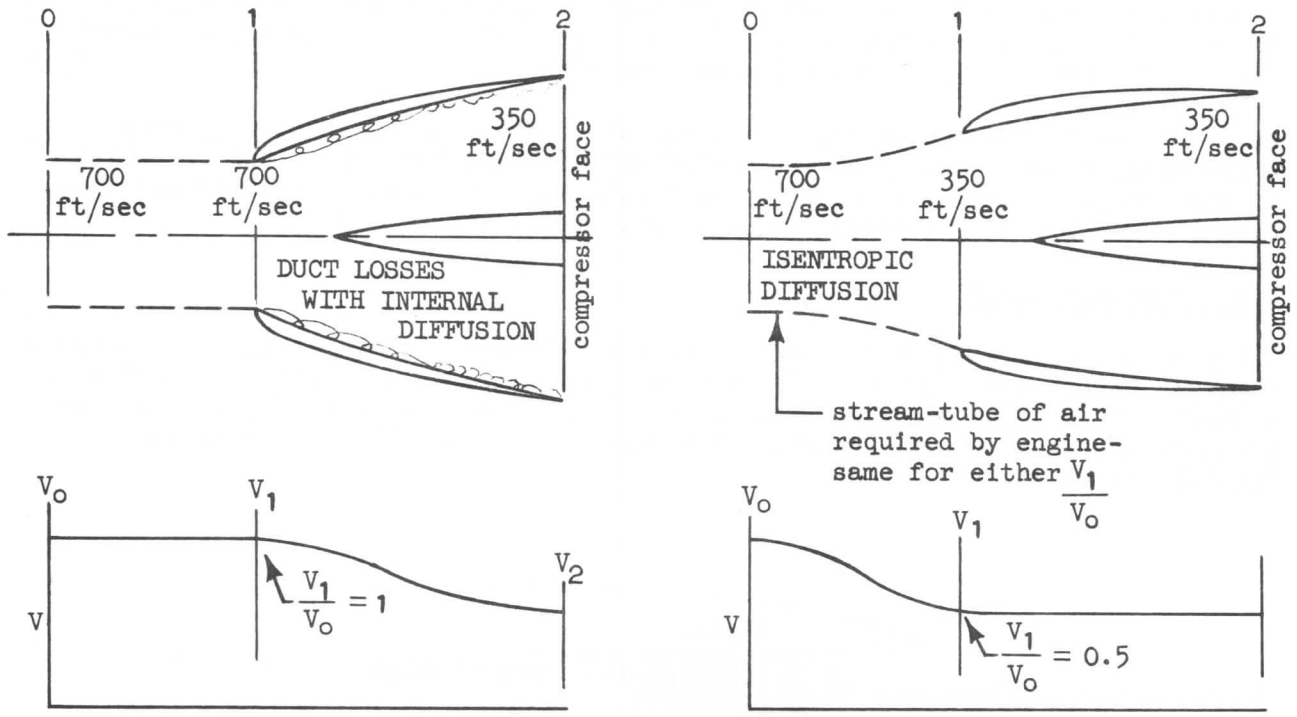

Figure 16.

A high inlet velocity ratio (V_1/V_o near 1) is undesirable since the large deceleration of the air inside may cause flow separation from the walls of the inlet duct. This separation inside the duct takes place because of the high adverse static pressure gradient, resulting in a reduction in ram efficiency.

Actually, a more serious consideration is the fact that the inlet may not pass the required airflow for take-off. For many engines, if the inlet is designed for cruise with $V_1/V_o = 0.8$ or higher, the inlet will actually choke at take-off conditions and thrust is seriously affected. In practice, the upper limit of V_1/V_o is usually determined by the inlet size required for good take-off pressure recovery.

So far, it appears that the pod type inlet duct should be designed for low V_1/V_o (.4 to .5 maximum), but this relates only to the engine performance. Aerodynamically, it is desirable to operate at high V_1/V_o in order to achieve a high-critical-Mach-number design. For high V_1/V_o the air does not have to accelerate nearly so much in going around the inlet cowl lip as it does for the lower V_1/V_o.

This reduces ram drag resulting from external diffusion. This problem becomes more and more difficult as the desired maximum flight speed is increased.

Two considerations limit the length of the diffuser. First, the length must be adequate to turn the external flow to the axial direction without incurring large drag penalties. To avoid internal separation of the flow, the angle of the containing wall and the mean flow path should be less than 3° for best results. Second, the diffuser must be long enough and have a lip shape such that the flow within the diffuser will be insensitive to angle of attack. The diffuser must not be so long that excessive friction losses will occur. The design of the duct then becomes a compromise between a long duct with large viscous friction losses and low turbulence, and a short duct with low friction losses and a high order of flow separation and turbulence.

At the inlet to the compressor, it is desired to provide the most uniform possible velocity and total pressure distribution. Variations in either of these factors result in deterioration in the performance by engine stalls or excessive fuel consumption during normal steady-state operation.

Air Compressor Design

The purpose of the compressor is to increase the energy level of the air received from the intake duct, compress it, and discharge it into a combustion chamber in a desirable quantity and pressure. Most gas turbine engines employ rotary compressors of either straight-through (axial) flow, Figure 17, or centrifugal (radial) flow, Figure 18.

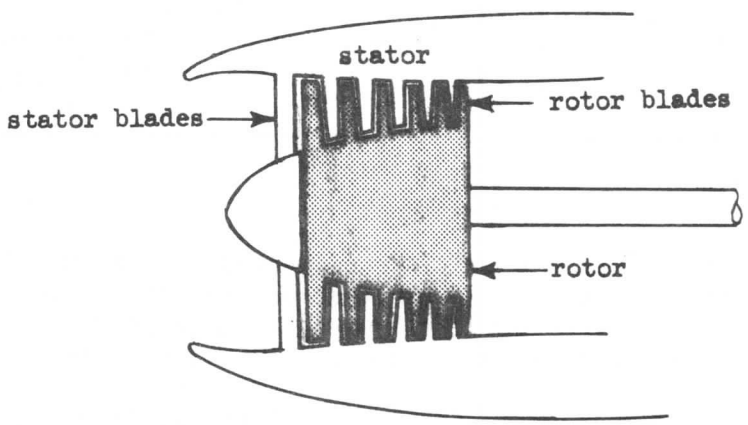

Figure 17.

The axial flow engine consumes about two to three times as much airflow per square foot of frontal area as the centrifugal type. Since thrust is proportional to airflow, the axial type enjoys a similar advantage in thrust per square foot of frontal area. The axial flow engine also has a higher fineness ratio than the centrifugal type. High fineness ratio (length to maximum diameter) and low frontal area are both important considerations for minimizing drag in high speed flight.

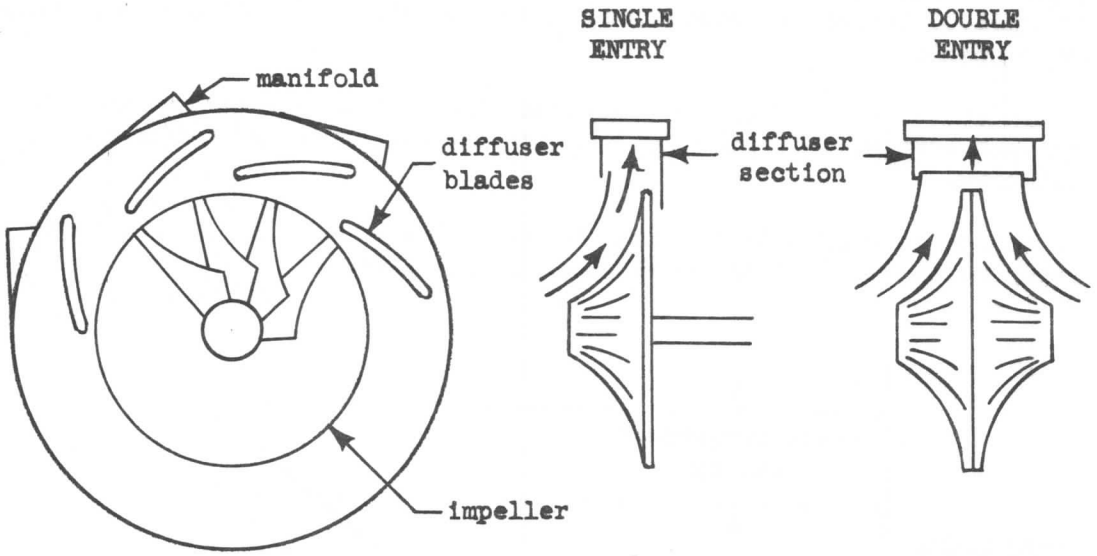

Figure 18.

Higher compression ratios can be obtained with good efficiencies in the axial flow compressor. The centrifugal compressor may reach an efficiency of 75% to 80% up to pressure ratios as high as four. Above this range, the efficiency drops off at a rapid rate. The axial flow compressor may have an efficiency of 80% to 90% over a wide range of compression ratios. Since the efficiency of the compressor directly affects the fuel consumption and since high compression ratios themselves induce good economy, the centrifugal engine is ruled out as a high economy type. Satisfactory combustion at extremely high altitudes and high efficiency combustion at intermediate altitudes may be practical only with the high compression ratios attainable with the axial flow engine.

One highly important characteristic is the compressor efficiency. Compressor efficiency is the ratio of the work that would be required to compress the air if there were no losses involved (therefore purely theoretical), to the work actually done including the losses. Since some losses will always exist, this ratio, or efficiency, will always be less than 100%.

If calculations showed that, to compress the specified mass airflow to the designed compression ratio, it would require 25,500 shaft horsepower energy rate; yet under actual test, the compressor required 30,000 shaft horsepower energy rate, then:

$$\text{Compressor efficiency} = \frac{\text{ideal energy required}}{\text{actual energy required}}$$

$$\text{Compressor efficiency} = \frac{25,500}{30,000} \times 100 = 85\%$$

Any reduction in the existing losses would tend to reduce the actual energy required to compress the air and, therefore, increase the compressor efficiency.

Figure 19 shows the effect of compressor efficiency on compressor power requirement. If the compressor's efficiency could be raised, a sizeable reduction in

the compressor shaft horsepower requirement would be effected. Now the turbine would not have to harness as much energy from the gas flow. From this, two results are possible:

(1) Increased thrust. With the same fuel flow, more heat energy is left in the gas stream, thus resulting in greater expansion and increased jet velocity.

(2) Increased economy with the same thrust. Less fuel flow is needed since less energy input to the compressor is required.

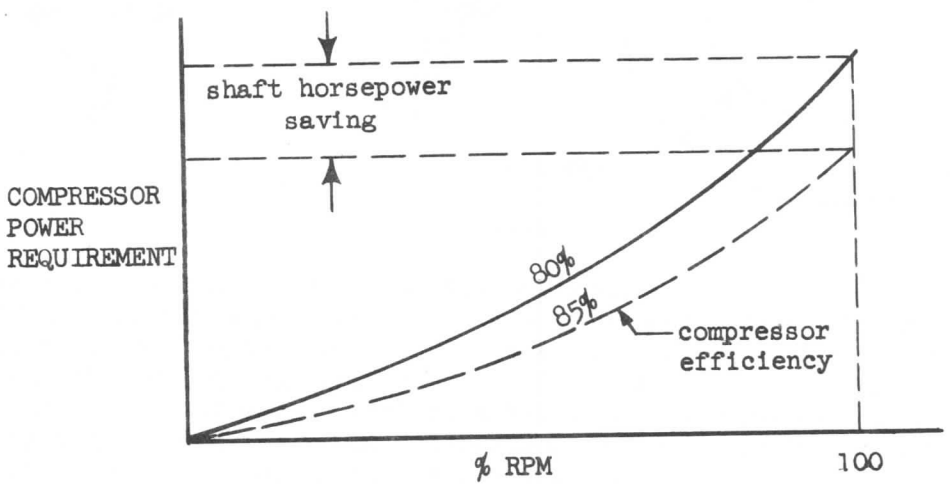

Figure 19.

Some disadvantages are encountered with the use of axial flow type compressors. Since top performance can be obtained only when the compressor and turbine are operating simultaneously at their peak efficiencies, it sometimes becomes difficult to match the sharp peaked characteristics of the axial flow compressor with those of the gas turbine and still maintain stability through the full operating range. The axial compressor is more sensitive to erosion and fouling of blading due to dust and oil and experiences vibrations of a complex nature. In addition, the air bleed is rather critical.

The compression ratio selection for an engine design is an extremely important consideration. Compression ratio in conjunction with turbine inlet temperature determines the thrust specific fuel consumption of the engine and the thrust output per pound of airflow. Higher pressure ratios provide for a higher altitude limit.

The compression ratio of a given compressor is basically a function of the Mach number of the rotor tip (first stage) which is usually expressed as $N/\sqrt{\theta}$. (Note that $M = V/a_o\sqrt{\theta} = N/k\sqrt{\theta}$). This may be observed from a curve which describes the compressor performance very conveniently, as in Figure 20.

This compressor performance curve is obtained by driving the compressor under constant rotational speed corrected to standard conditions and measuring the pressure and temperature relations as the air flow rate is varied. Curves of

constant $N/\sqrt{\theta}$ are defined for each corrected speed. The upper end of each curve defines the flow or axial velocity condition under which the corresponding blade speed combines to give blade stall. The locus of all such values is called the stall or surge line, the stability limit. Operation in the region to the left of this line is impractical, if possible, for the blade is stalled and no longer working properly.

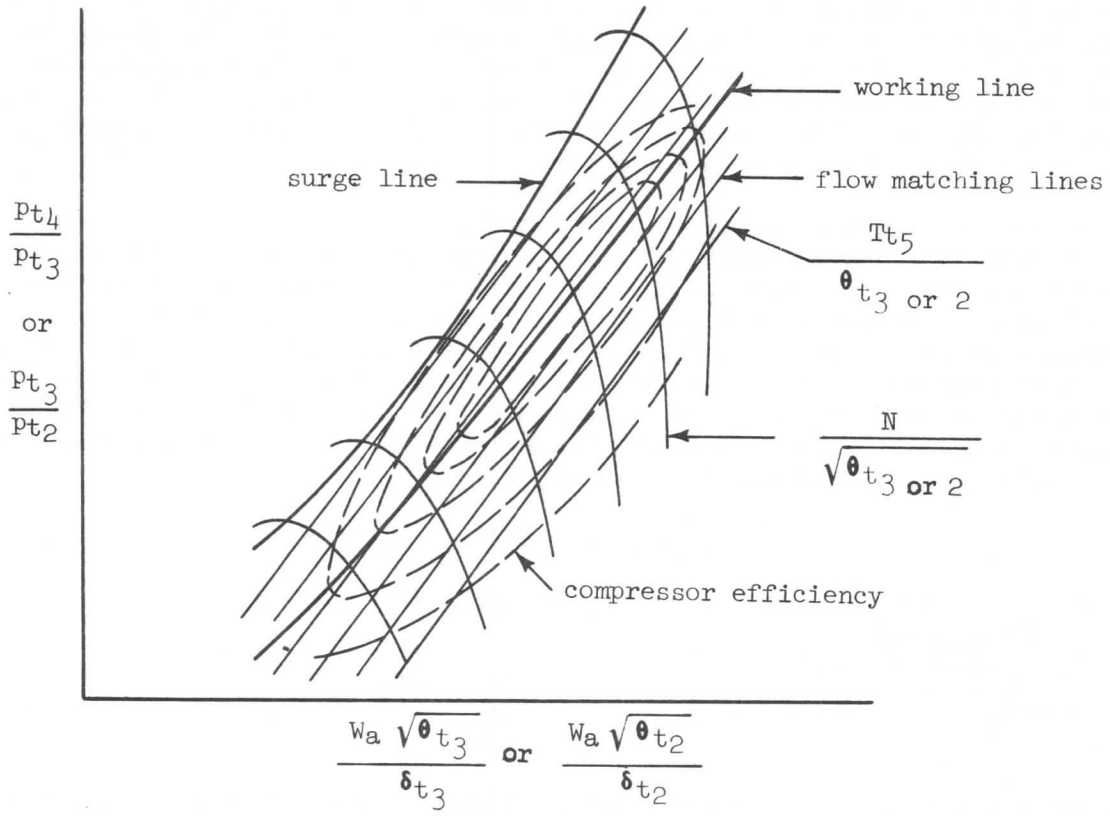

Figure 20.

The other curves on Figure 20 are obtained to show additional restrictive conditions of operation. It must be recognized that the compressor is physically connected to the turbine and must be matched to it. The first consideration is that the air flow through the two must be the same (except for off-design operational bleed).

$$(W_a)_{compressor} = (W_a)_{turbine} = W_a$$

Corrected flow rate may be written as

$$\frac{W_a\sqrt{\theta_{t_3}}}{\delta_{t_3}} = \frac{W_a\sqrt{T_{t_5}}}{P_{t_5}} \frac{P_{t_5}}{P_{t_4}} \frac{P_{t_4}}{P_{t_3}} \frac{\sqrt{\theta_{t_3}}}{\sqrt{T_{t_5}}} P_o$$

Therefore, the pressure ratio can be found:

$$\frac{P_{t_4}}{P_{t_3}} = \frac{W_a\sqrt{\theta_{t_3}}}{\delta_{t_3}} \frac{\sqrt{T_{t_5}}}{\sqrt{\theta_{t_3}}} \frac{P_{t_4}}{P_{t_5}} \frac{P_{t_5}}{P_o} \frac{1}{W_a\sqrt{T_{t_5}}}$$

$$\frac{P_{t_4}}{P_{t_3}} = \frac{W_a\sqrt{\theta_{t_3}}}{\delta_{t_3}} \sqrt{\frac{T_{t_5}}{\theta_{t_3}}} \frac{P_{t_4}}{P_{t_5}} \frac{1}{\frac{W_a\sqrt{T_{t_5}}}{\delta_{t_5}}} \qquad (34)$$

Equation (34) shows that when the turbine is considered, the pressure performance of the compressor is dependent upon not only air flow rate but also three other factors which control the rotational speed. The three relate to temperature, pressure and area at the turbine inlet. Thus when the turbine area is fixed and the burner pressure loss, P_{t_4}/P_{t_5}, is determined, curves of constant corrected turbine inlet temperature plotted on Figure 20 represent matched compressor-turbine flow and are called flow-matching lines.

It is obvious that each steady-state operating condition must be such as to satisfy both the pressure-flow-RPM and the matched-flow conditions simultaneously. So when the compressor and turbine are combined, a steady-state operating or "work" line is defined. Therefore, it is important to consider the turbine area relations which affect the turbine pressure drop and efficiency, and the operating temperatures which contribute to fuel consumption as well as compressor efficiency before the final design is fixed. A consideration of the equality of power consumed by the compressor and power delivered by the turbine sheds more light upon the parameters to be chosen:

$$\text{Work}_{\text{compressor}} = \text{Work}_{\text{turbine}}$$

It can be shown that these work terms can be stated in the form,

$$\frac{C_p\, T_{t_3}\left[\left(\frac{P_{t_4}}{P_{t_3}}\right)^{\frac{\gamma-1}{\gamma}} - 1\right]}{\eta_c} = C_p\, T_{t_5}\left[1 - \left(\frac{P_{t_6}}{P_{t_5}}\right)^{\frac{\gamma-1}{\gamma}}\right] \eta_t \qquad (35)$$

The easiest way to adjust these relationships is through change in the turbine pressure ratio, P_{t_5}/P_{t_6}, by variation in the inlet and exit areas of the turbine.

Compressor efficiency, η_c, is plotted on Figure 20. It is the objective to design such that the work line runs through the peaks of the efficiency contour.

The thrust output per pound of airflow increases with compression ratio at a fixed turbine inlet temperature, reaching a maximum after which it decreases with an increase in pressure ratio. Figure 21 shows this condition. As higher compression ratios are reached, the compressor discharge temperature becomes so high that very little heating of the air may be done before a fixed turbine inlet temperature is reached. This inability to supply as much heat energy in combustion as might be desired is the cause of the downward trend discussed above.

At a given turbine inlet temperature, thrust specific fuel consumption decreases with increasing compression ratio. This trend continues until the addition of the desired amount of energy is restricted by the high compressor discharge temperature. This is shown in Figure 22.

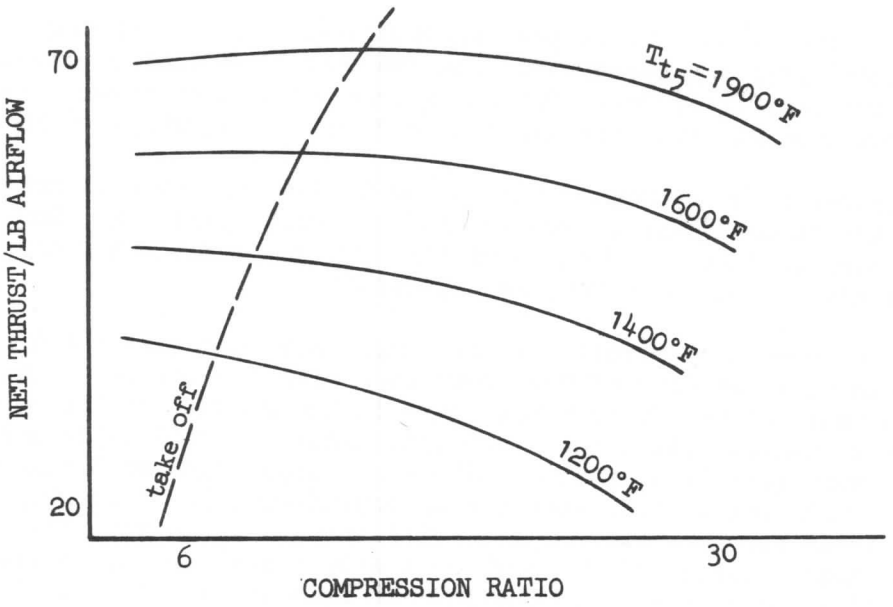

Figure 21.

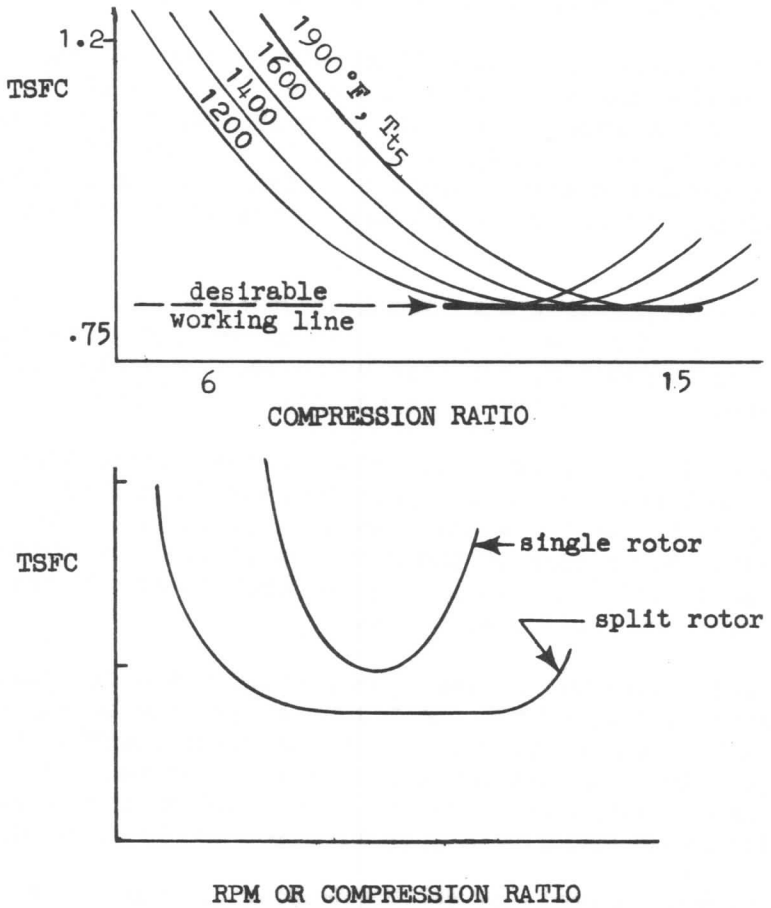

Figure 22.

Engine weight increases with increasing compression ratio not only due to the weight of added stages necessary for the increase, but also to accommodate safely the higher internal pressures. Obviously some compromise between compression ratio, thrust specific fuel consumption, and increasing weight must be reached.

The compressor-turbine system of the engine is designed to give optimum performance under design conditions, usually cruise thrust operation. However, since the engine must satisfy the demands of the airplane under other conditions also, it is necessary to look at off-design operation.

Increasing the compression ratio of the compressor increases the difficulty of the part-load flow matching of the compressor with the turbine. The compressor compression ratio at any given rotor speed is the product of the compression ratios of all stages. Thus, the compression ratio at full rotor speed will increase much more rapidly with the addition of stages than will compression ratio at a lower rotor speed. This exponential characteristic of compression ratio with rotor speed becomes more and more difficult to match with the linear pressure flow characteristics of the turbine nozzle. The turbine nozzle flow characteristics are linear since the flow at this station is usually sonic. The two diagrams, Figure 23 and 24, pictorialize the difficulty encountered with higher pressure ratios.

These difficulties may be overcome by one of the following methods.

(1) Bleeding to overcome matching difficulties. Since at part-load the compressor is delivering too much airflow for the size of the turbine, some of this air may be removed from the flow system, the remaining airflow being in quantity and quality such that it will satisfactorily pass through the turbine nozzle. Since bleeding is a wasteful process, it is not desirable to employ this means in the useful output range of the engine.

(2) Variable turbine nozzle area. It may be possible to alter the effective flow area of the turbine nozzle to accommodate the part-load characteristics of the compressor, but this would require a high order of mechanical complexity at a station where the heat is intense.

(3) Split rotor. A very satisfactory means for obtaining high compression ratios and avoiding much of the part-load matching difficulty is to make the compressor in two parts which have no mechanical relationship between their speeds. Since each of the compressors is of relatively low compression ratio by itself, no particular problem is offered in matching them with their respective turbines.

(4) Variable stator blades. At part-load, where mismatch usually occurs, the stator blades of part of the compressor stages may be adjusted such that the airflow from the compressor is of the right quantity to be handled by the turbine. In this type of design there is no wasteful loss of air by bleeding, and the efficiency can be maintained at higher levels. However, this solution also introduces a problem in mechanical design and control.

Increasing the compression ratio of any compressor increases the range of operation the blading of each stage must accommodate. Splitting the compressor into two rotors alleviates this problem to a marked degree.

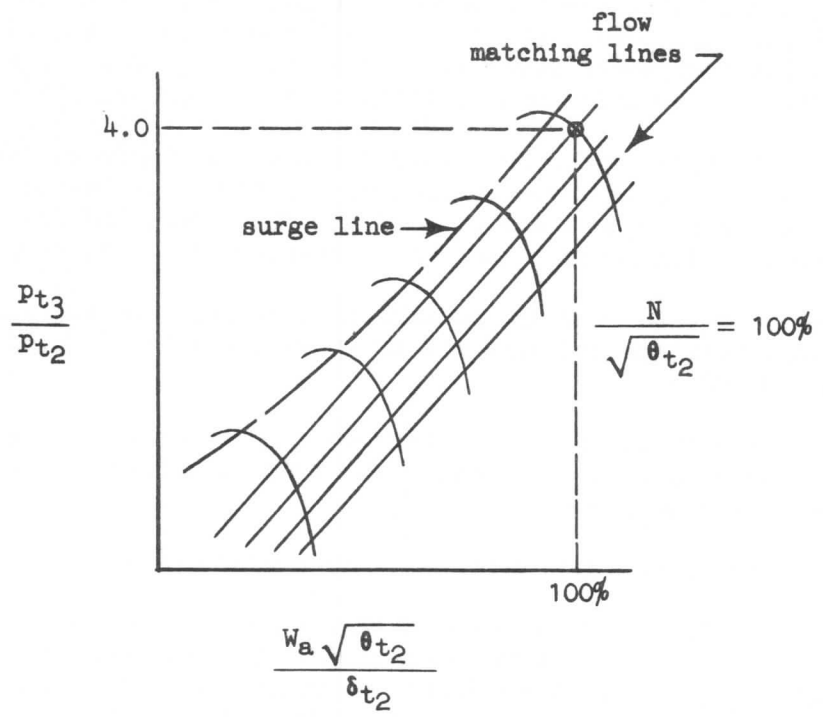

Figure 23.

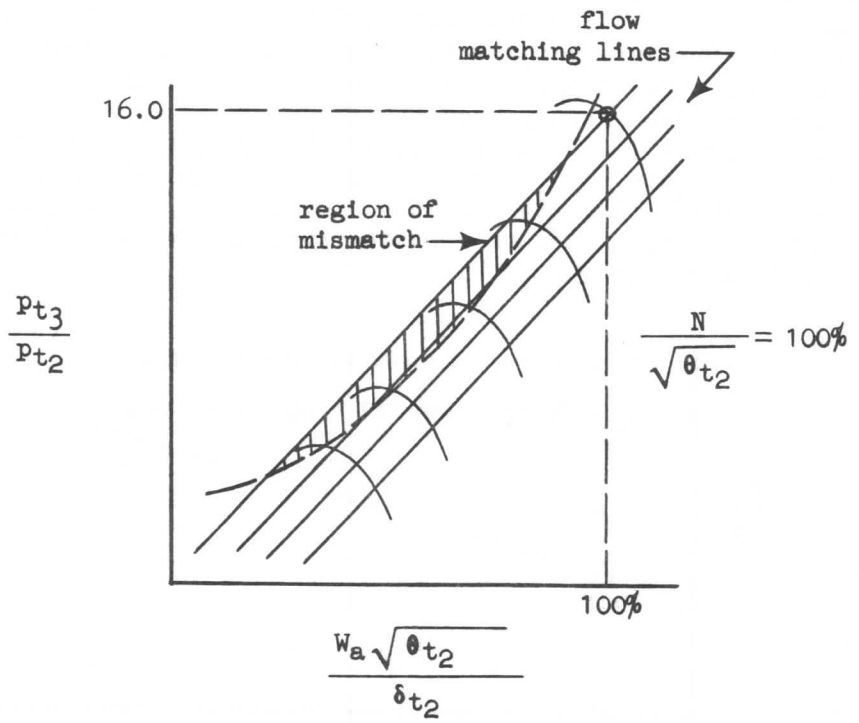

Figure 24.

The problem of matching a given compressor with the other components for a given engine design is complex. Consideration must be given to the compression ratio,

RPM, and efficiency at which the compressor is to operate at cruise and high output conditions of operation. All operation must be in a region sufficiently removed from the compressor surge line to allow for good acceleration. The consideration of idle operation and starting is also important.

Advantages of the split rotor configuration are low starting power, good acceleration characteristics, improved compressor performance, greater flexibility in matching, easier development due to smaller components, and the opportunity to use higher compression ratios than can be obtained by other means.

Disadvantages of split rotor are mechanical complications and added weight of extra shafting, bearings and supports and possible extra turbine stages for a given expansion ratio.

In the split rotor engine the high pressure compressor rotor, N_2, is normally composed of less stages of compression and runs at a higher RPM than does the low pressure compressor, N_1.

Under design conditions, each compressor runs near or at its peak efficiency.

As rotor speed is increased, the low pressure rotor speed increases at a faster rate than does the high pressure rotor speed. The compressor airflow parameter may be thought of as being proportional to volume flow which would be the case if compressor inlet temperature were held constant. Increasing rotor speed along the work line as shown in Figure 20 reveals that volume at the inlet of any compressor increases with increasing rotor speed. For this discussion it may be assumed that the volume increases linearly with speed, which describes the relation at the low pressure compressor inlet. As speed increases, however, the pressure ratio also increases. This causes the volume at the compressor discharge to increase less rapidly than the inlet volume. The low pressure discharge is the inlet to the high pressure compressor, which indicates that the high pressure inlet volume flow does not increase as rapidly as the low pressure inlet volume. The high pressure rotor speed, being proportional to its inlet volume, then, will increase less rapidly than low pressure rotor speed. This relation is shown in Figure 25.

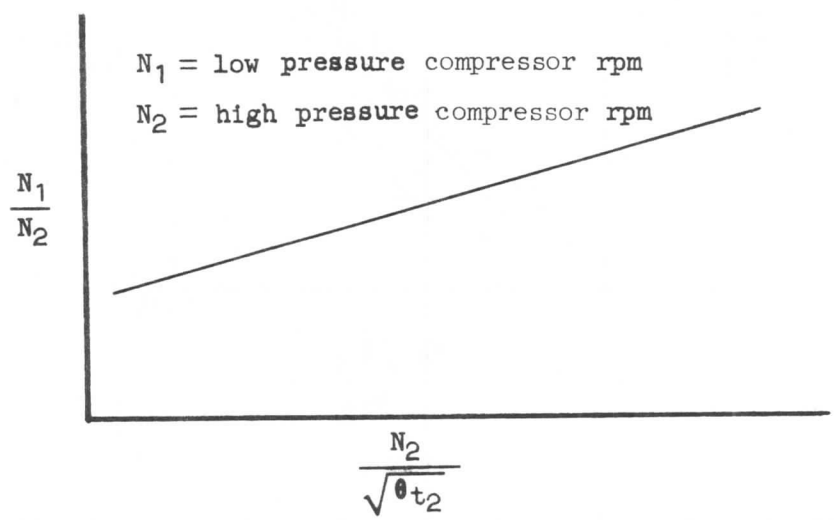

Figure 25.

With a fixed jet nozzle area and constant high pressure rotor speed control, the low pressure rotor speed increases with decreasing compressor inlet temperature. Figure 25 reveals how this takes place. With constant N_2, decreasing compressor inlet temperature causes $N_2/\sqrt{\theta_{t2}}$ to increase. This increases the ratio N_1/N_2. N_2 was held constant, which indicates an increase in N_1.

This increase in N_1, as compressor inlet temperature decreases, causes the low pressure compressor, and hence the engine, to handle a larger volume of air. This effect produces a more gradual decrease in thrust output with increasing altitude than would be experienced with a single-rotor engine. The comparison to a single-rotor engine may be seen in Figure 26. This speed effect may be altered by changing N_2 speed with temperature. Sometimes N_2 may be altered by having an inlet temperature sensing bulb for the fuel regulator. If the N_2 compressor speed increases with increasing temperature or decreases with decreasing temperature, this temperature bias may be used to gain additional thrust for hot-day take-offs provided the turbine inlet temperature limit is not exceeded.

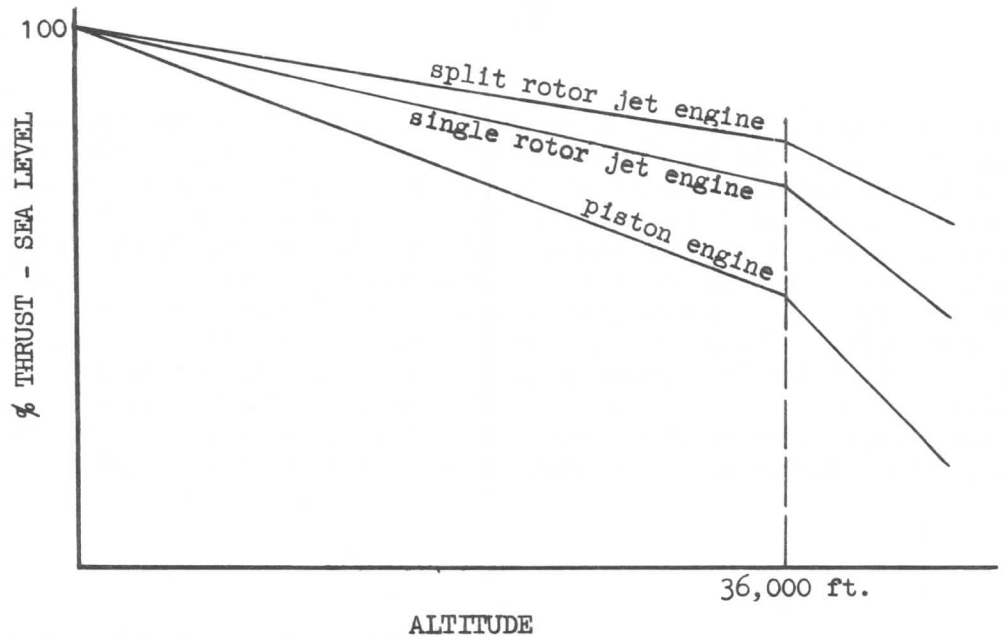

Figure 26.

With constant N_2 control, change in tailpipe nozzle area varies only the speed of the low pressure rotor, because the first stage turbines are in critical flow, as shown in Figure 27, and no pressure disturbance downstream caused by a change of tailpipe area could be reflected upstream to the high pressure rotor. With an increase in tailpipe discharge area the expansion ratio across the low pressure turbine would be increased due to the reduced back pressure, and the low pressure rotor would accelerate and reach equilibrium operation at a higher rotor speed. Since the low pressure compressor speed would be increased, the airflow handled by the engine would be increased and a lesser lapse rate of thrust with increased altitude would result, as indicated in Figure 26. The working line (see Figure 20) on the low pressure compressor would lie further from the surge line. The working line on the high pressure compressor is determined by the

high pressure turbine inlet guide vane area and the low pressure turbine inlet nozzle area. These areas, being unchanged, would not effect the relation between the working and surge lines of the high pressure rotor.

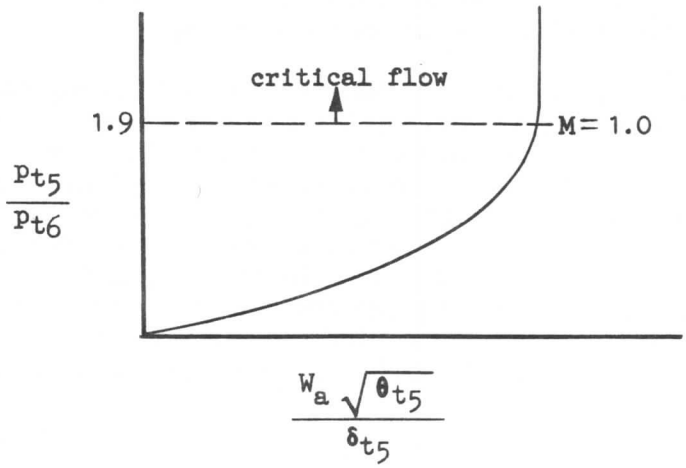

Figure 27.

As mentioned previously in this section, air bleed and split rotor can be used on engines (may be seen in Figure 28) to aid the stability, and thus aid the efficiency. The higher the compression ratio and the more stages added to an axial flow compressor, the greater the instability. The blade angles of the two compressors are designed for the airflow and RPM to match in the flight range only. The mismatch in the lower RPM range may be corrected by bleeding off air, which normally will be from the forward stages or from the forward compressor in case of split rotor engine. Figure 28 also shows that in the case of a split rotor engine, by the RPM of the N_1 compressor being less than N_2, the amount of airbleed required to match the compressor is decreased. This relationship also increases the flight range of RPM. Airbleed is not necessary for some by-pass type engines since the by-pass duct tends to take care of any mismatch.

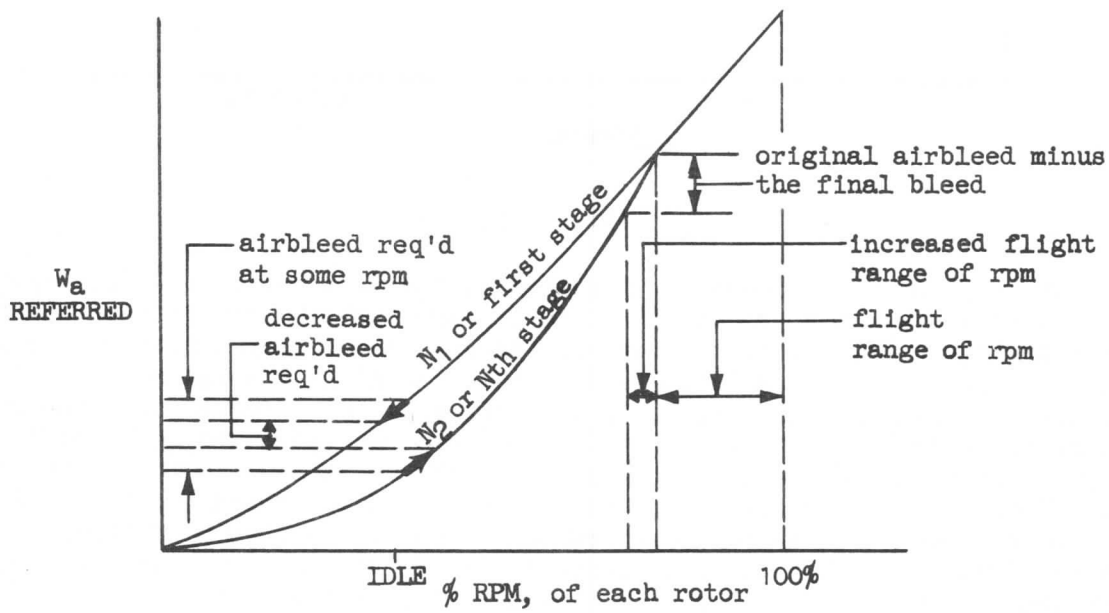

Figure 28.

The effects of air bleed on the low pressure and high pressure rotor stall limits are shown schematically on typical compressor flow charts on Figures 29 and 30, respectively. These figures show the compressor pressure ratio on the ordinate and the referred airflow on the abscissa. Superimposed are the steady state operating line and typical engine acceleration and deceleration schedules. On a low pressure rotor, the acceleration schedule would be below the steady state operating line. During acceleration, the high pressure rotor, normally being lighter in weight, accelerates at a more rapid rate than the low pressure rotor causing the pressure at the exit of the low pressure rotor to reduce and operate further away from surge than its steady state condition. Upon deceleration the opposite would occur and operate the low pressure rotor closer to surge. From this consideration it may be seen that surge would occur in the high pressure rotor on acceleration and the low pressure rotor on deceleration. It can be seen that without the low pressure compressor having bleed valves open in the low RPM region the low pressure compressor (Figure 29) would be in the surge region at steady state (operating line) and also on the deceleration schedule. This condition does not exist on the high pressure compressor. (Figure 30)

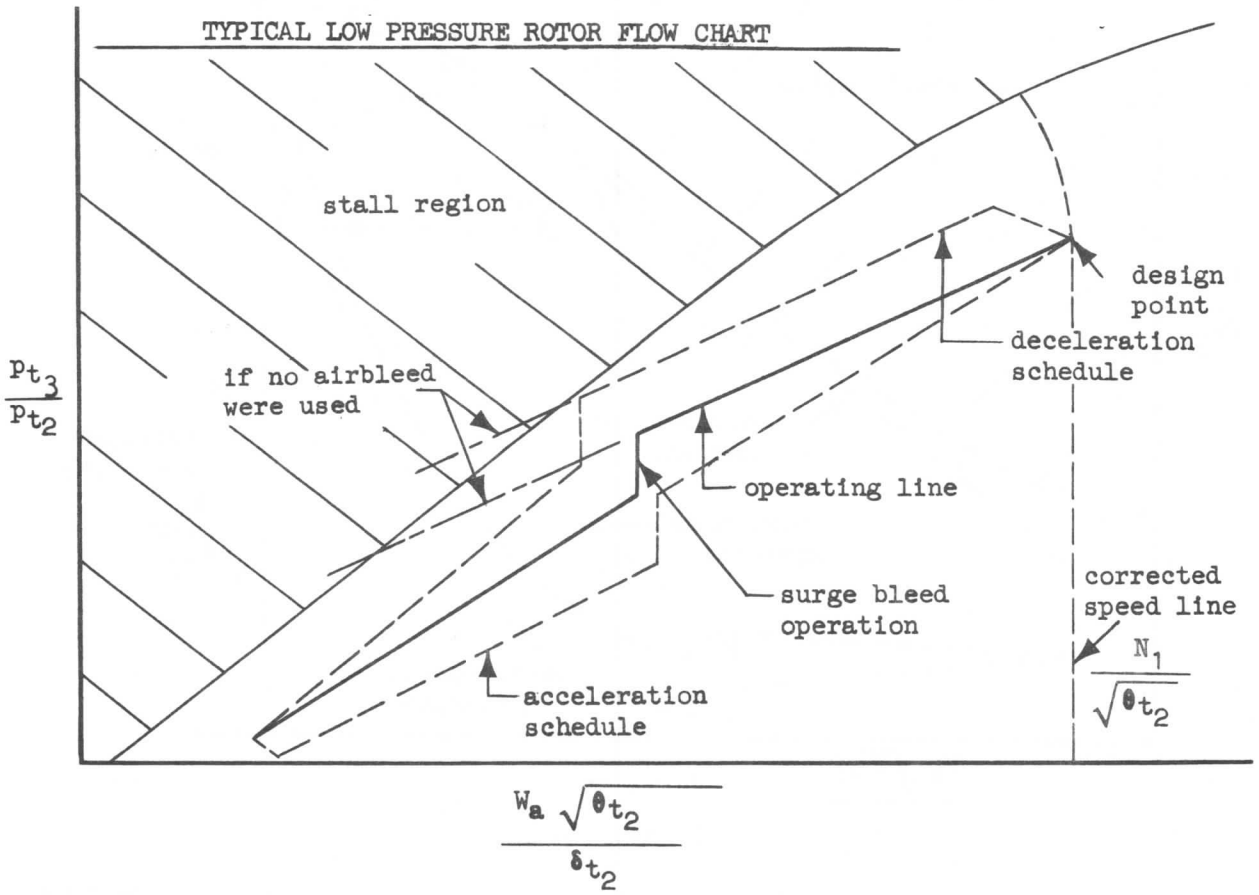

Figure 29.

In order for an engine to accelerate, the fuel rate into the engine must be higher than its steady state operating condition. This causes higher temperature and pressure conditions at the inlet of the turbine which drives the rotor. In the case of the split rotor, as shown in Figures 29 and 30, the acceleration of the engine is limited by the high pressure rotor surge limits, and consequently the

control system is designed to operate as close to surge as possible in order to achieve maximum acceleration performance of the engine. Any malfunction of the engine fuel control system or reduction in surge margin will cause the high pressure rotor to surge during acceleration. Engine deceleration increases the surge margin of the high pressure rotor.

Figures 29 and 30 also show that decreasing the compressor inlet total temperature and density while operating at high power increases the surge margin on the low pressure rotor and decreases the surge margin on the high pressure rotor. Operation at extreme altitudes also introduces Reynolds number effects which tend to lower the surge line for both compressors in the same way that lowering Reynolds number decreases $C_{L_{max}}$ for any other airfoil. Commercial operation at or below 40,000 feet should be free of this effect. An indication of surge is variation of EPR or P_{t_7}, variation of fuel flow and variation of EGT.

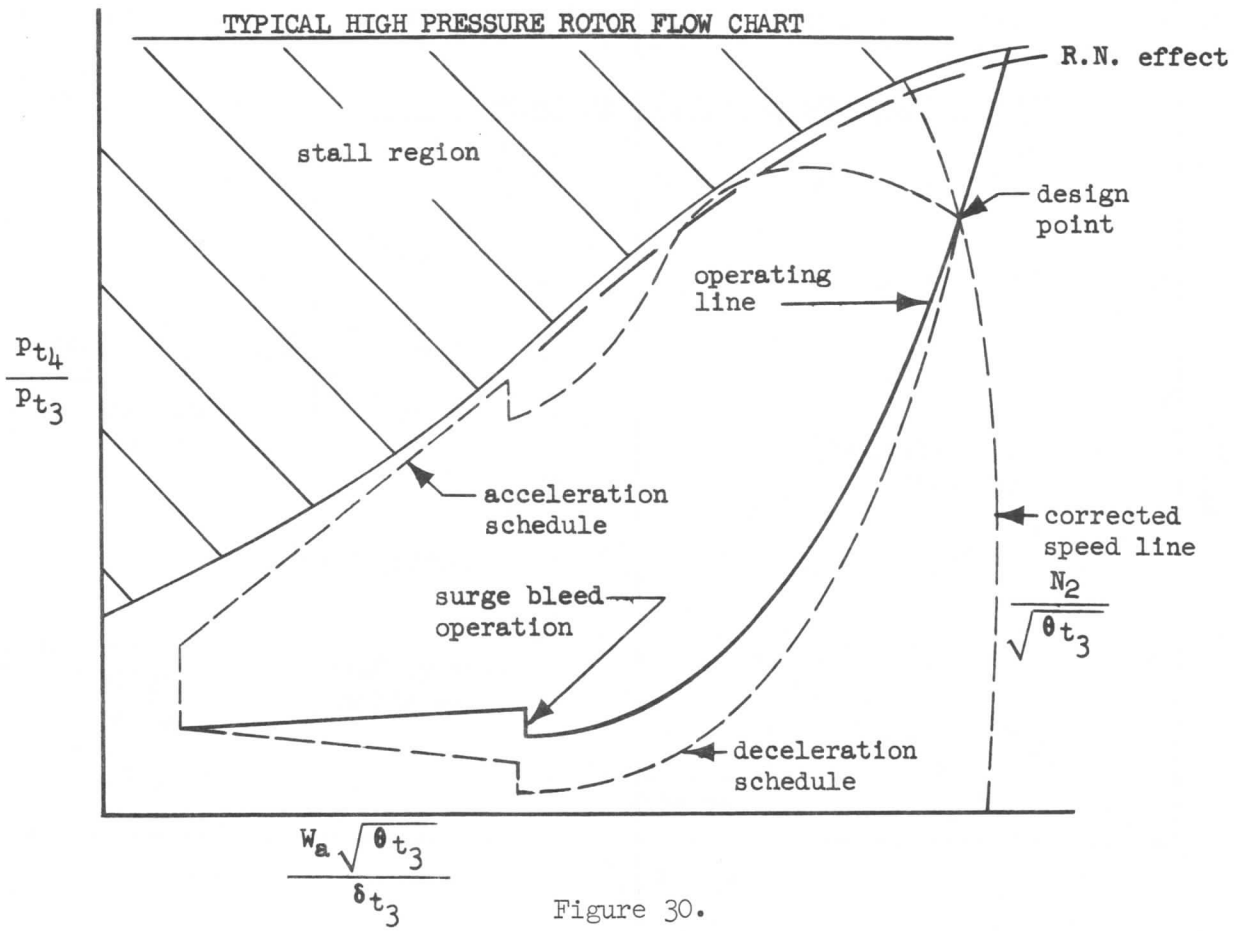

Figure 30.

The effect of poor pressure distribution in the compressor is to change the compressor flow relationship with respect to speed and also decrease the surge margin. This can be shown by comparing the compressor blades to miniature wings as shown in Figure 31.

It can be seen that anything which causes a decrease in airflow (decrease in velocity) would move the compressor blades to a higher effective angle of attack and closer to stall. Two of the most common factors that might cause this airflow decrease are high back pressure and poor compressor inlet distribution.

There are a number of things that might cause high back pressure. The most common is too much fuel during acceleration. Compressor inlet distribution is determined by inlet cowl design and may be varied by airplane attitude and speed. The Reynolds number effect may be added to either of the above effects, because it changes primarily with altitude.

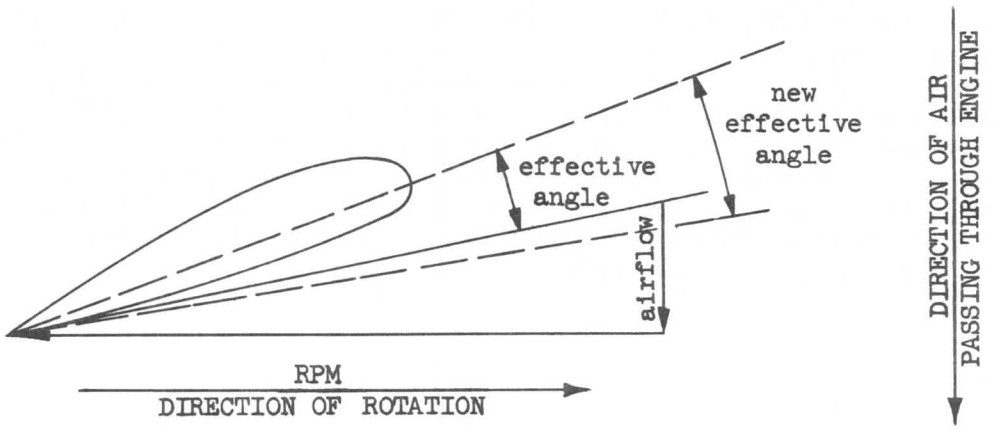

Figure 31.

Combustion Chamber Design

The main purpose of the combustion chamber section is to bring the fuel and air together, and to introduce heat energy into the mass air by means of combustion. To effectively accomplish this purpose, three basic steps are to be followed:

(1) Injection of fuel. The fuel nozzle must take the fuel from the fuel regulator, deliver it into the combustion portion of the chamber, and in so doing, break the fuel up into fine particles which can then readily mix with the combustion air.

(2) Meter out combustion and cooling air. Contrary to general belief, all the air passing through a jet engine is not utilized to support combustion. If all the air and fuel were mixed, we would have a non-combustible charge. A typical present day engine might have a total air - fuel ratio of about 73 to 1. Since hydrocarbon fuels prefer an ideal A/F ratio near 15/1, the combustion chamber must, therefore, separate approximately 20% of the total air from the compressor and divert it into the burner section where it will mix with the fuel and burn. The remaining 80% of airflow, known as cooling or dilution air, must be temporarily withheld from the burner section until the process of combustion has taken place.

The combustion air is metered out by means of angled orifices which introduce the air around the fuel nozzles in a centrifugal manner. Introduction of the air in this method allows the combustion air to be at high centrifugal velocity but relatively low linear velocity. This allows more time for mixing and burning of the fuel in the forward portion of the combustion chamber and allows better mixing of the cooling air in the latter half of the combustion chamber. The centrifugal introduction of the

combustion air with its lower linear combustion chamber velocity increases the air speed and altitude at which inflight engine starts may be accomplished. A typical plot of an inflight start envelope is shown on Figure 32. A certain head of combustion chamber pressure must be maintained in order to have sufficient air for initiating combustion and for cooling when an inflight start is made, because of the constant fuel flow that is used during start on jet engines. The constant head of pressure can be obtained only by increasing the air speed with altitude as shown in Figure 32. If an inflight start is attempted at too low a speed, ignition is not accomplished or the combustion is not completed in the burner section and continues into the turbine and exhaust sections, overheating them. The maximum constant air speed on the inflight envelope is a speed which represents the maximum linear combustion chamber velocity for inflight starts. Above this speed the combustion chamber velocity would be too high for an initial light.

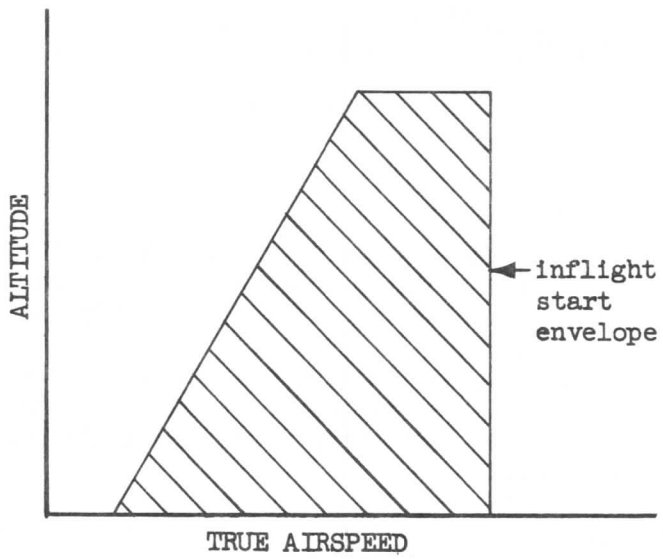

Figure 32.

(3) Dilution of combustion gases. After combustion, the remaining 80% of the airflow must be rapidly introduced into the burner section to dilute the hot combustion gas before it has an opportunity of coming in contact with the turbine nozzle guide vanes. The combustion gas may be as hot as 3500°F. To insure longer life of the turbine nozzle guide vanes, cooling air dilutes the combustion gases, reducing the gas temperature to within the present allowable maximum limit of 1600°F (for uncooled - turbine engines) to 1800°F (for engines with air-cooled turbine blades).

Although combustion chambers today have a thousand and one different configurations, they all simplify down to three basic types, namely: Multiple Chamber, Annular Chamber, and Can-Annular Chamber. See Figure 33.

(1) Multiple Chamber. This type of combustion system lends itself readily

to the centrifugal flow engine since the air must be divided to give equal proportions to each can or chamber. Variations in the can are adaptable to the axial flow engine. One advantage of the can type is that the liner surface has a large degree of curvature which results in high strength and resistance to warping. Some disadvantages are: (1) the available space is not utilized efficiently and, (2) the large amount of metal required to enclose the desired volume of gas flow results in a heavier combustion chamber.

(2) The annular type has some desirable advantages over and above efficient air and gas handling. There is little doubt that this type gives the most efficient usage of the available space. For this reason, the annular type will require only about half the diameter for the same mass airflow. The sheet metal surface to enclose the required volume is low resulting in lighter weight. While the annular type is basically simpler in construction, the lower degree of curvature makes it more susceptible to warping which distorts the temperature pattern at the turbine section. This problem tends to complicate the construction, because intricate reinforcing is required.

(3) Can-Annular Chamber. The can-annular is a combustion chamber with characteristics of both annular and can types, the advantages of both types being retained. This type of combustion chamber is composed of combustion chamber liners located circumferentially at equal distances within an annular combustion chamber case. Greater ease in development is still possible, thereby encouraging the use of this type. Each liner has its own fuel nozzle or nozzles. Individual liners also tend to even out the air velocity distribution into the combustion chamber. The can-annular combustion chamber operates at a high pressure level aiding efficient combustion at reduced powers and high altitudes. Each liner having multiple nozzle arrangements has the added advantage of minimizing temperature variation caused by the clogging of any one element.

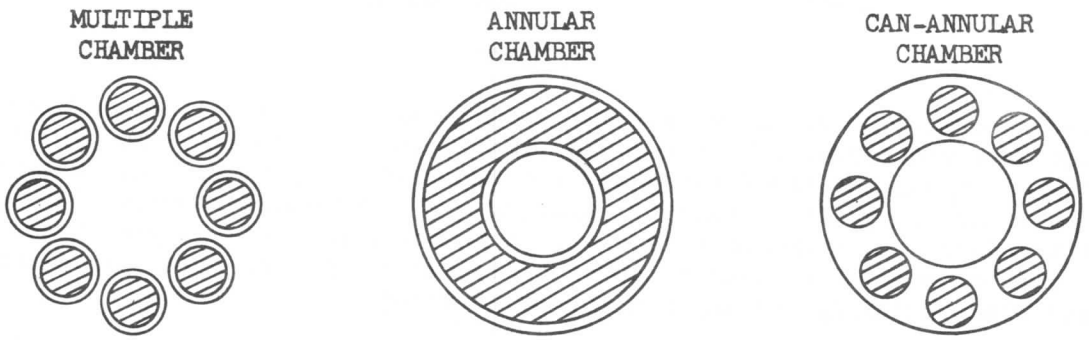

Figure 33.

It is highly desirable to maintain a uniform temperature of the gases at the discharge cross section of the liner so that the turbine nozzle and blading will

expand uniformly and not set up high localized blade stresses and thermal shock which are apt to result in warpage or cracking. A poor temperature distribution decreases life of the engine as well as efficiency.

Figure 34 is used to illustrate this temperature distribution. If a plot is drawn of gas temperature versus the cross section of the liner at its discharge end, the dotted line would indicate the theoretical or desired distribution of temperature while the solid line shows a normal acceptable distribution and the dashed line depicts an undesirable over-heating condition caused by faulty, uneven flow distribution. Normally, the temperature at each side of the liner walls should run relatively cool due to the cooling air blown longitudinally along the liner wall. The temperature should then rise rapidly to the allowable maximum and remain at that value across the liner until it approaches the opposite liner wall where the action of the liner wall cooling air again reduces the temperature to a safe value within the limits of the liner material.

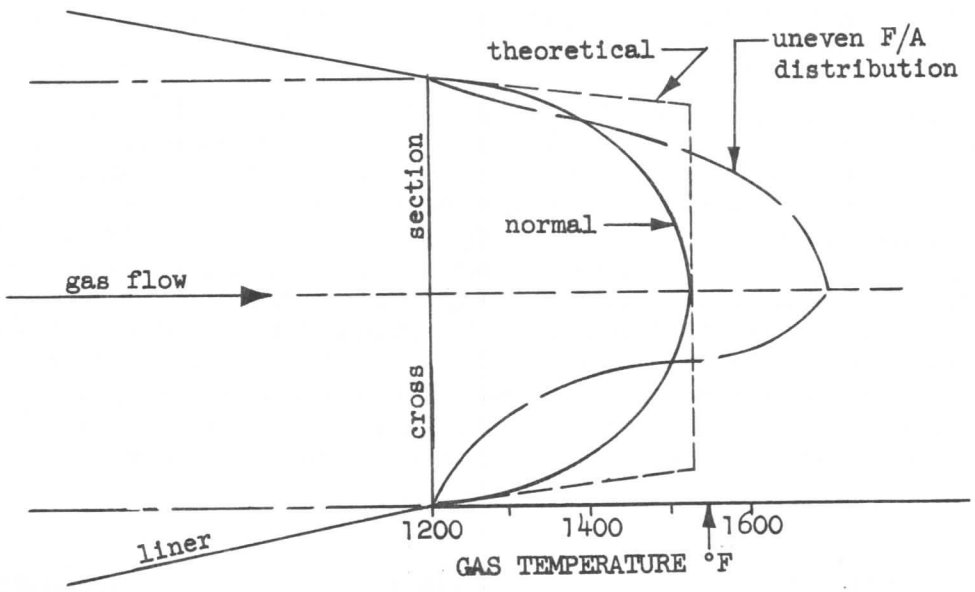

Figure 34.

Since the practical rarely equals the theoretical, the actual temperature distribution would appear like the solid line, indicating less of the liner's cross section remaining at the desired maximum temperature. Uneven flow distribution resulting in lower flame velocity might give a temperature distribution too low near the liner walls and excessively high in the center of the gas stream. Such exceeding of maximum allowable temperatures, when existing more than momentarily, causes blade burning, warpage and stress cracking.

In order to control this temperature pattern, sufficient distance of travel must be provided for the introduction of the main cooling air and its dilution of the hot combustion gas, thus resulting in an acceptable degree of evenness of temperature distribution. If this distance is limited, then the liner must be designed to accomplish this job. A typical pattern for this might be as shown in Figure 35. Presently-used values of maximum turbine inlet temperature are in the order of 1500°F to 1600°F. A top value for turbine inlet temperature without cooled turbine blades would probably be 1700°F. With cooled blades, a

temperature in the order of 1900°F seems possible and would provide an output increase about proportional to the temperature increase. Cooled blades, however, reduce the turbine efficiency, increase the cooling air drag, and are more difficult to fabricate.

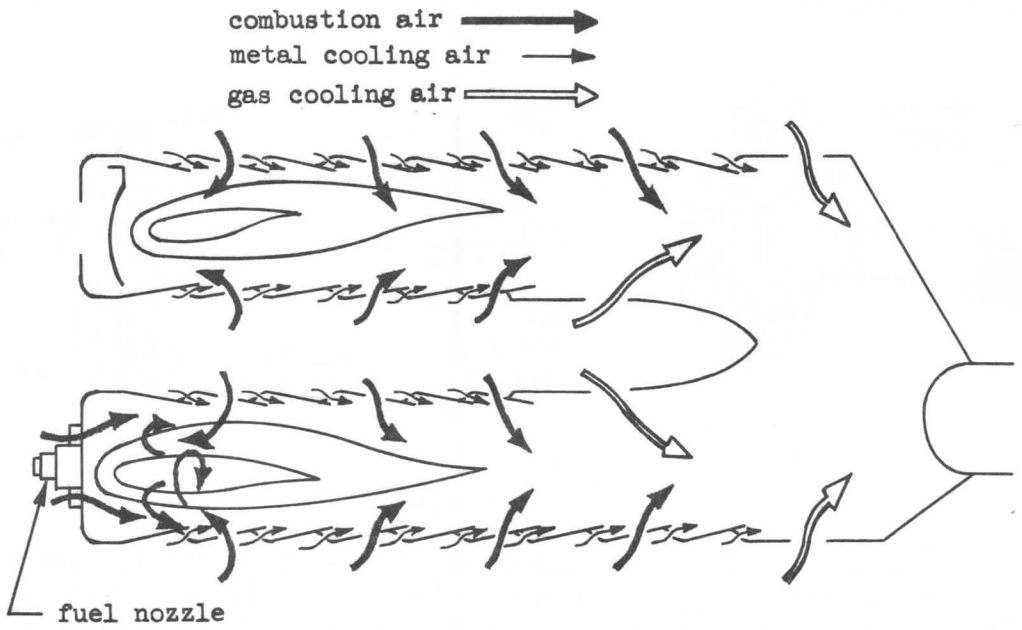

Figure 35.

With other factors remaining constant, increasing turbine inlet temperature at low compression ratios increases the thrust specific fuel consumption (See Figure 22). Despite the fact or even though increasing turbine inlet temperature improves the thermal efficiency, it lowers the propulsive efficiency of the jet such that the net result is a decrease in economy (Figure 21). This might lead one to suspect that a very low turbine inlet temperature would be desirable for cruising economy. At high compression ratios, however, a turbine inlet temperature in the order of 1300°F seems to be about optimum for long range operation.

Turbine Design

The purpose of the turbine is to transform some of the heat and pressure energy of the exhaust gases into shaft horsepower to drive the compressor and accessories. The remaining kinetic energy and pressure energy of the gases produce engine thrust.

The turbine is comprised of two main elements, the nozzle vanes and turbine wheel. See Figure 36.

(1) Turbine Nozzle Vanes. There are stationary blades attached radially to the turbine case at the entrance to the unit as well as between the rotor stages. These blades are contoured and set at such an angle that they form small nozzles discharging the gas as jets. The jets are directed against the rotating turbine blades in a direction so as to efficiently transfer the kinetic energy into mechanical energy.

(2) Turbine Wheel. The turbine wheel consists of contoured blades attached to a disc. This in turn is attached to the power transmitting shaft of the engine. The jet gases leaving the stationary blades act upon the turbine wheel, turning it at very high speeds. This places high centrifugal loads upon the wheel.

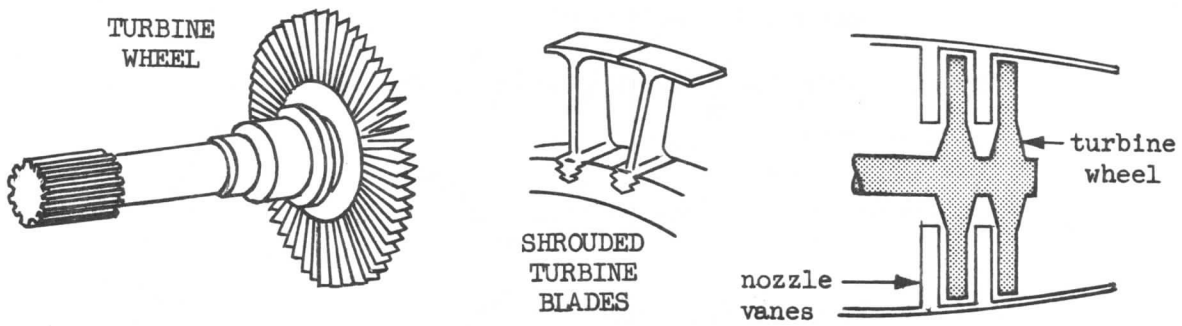

Figure 36.

The turbines in use on axial flow engines are of two major types, impulse and reaction. In the impulse type of turbine, there is no change in pressure between the rotor inlet gas and the rotor exit gas, but there is a large deflection of the gases. The nozzle guide vanes are shaped to form passages which increase the velocity and reduce the pressure of escaping gases. The high velocity generated in the turbine nozzle guide vanes impinges on the moving rotor blades as shown in Figure 39. In the reaction type of turbine a pressure change takes place as the gases flow through the rotor blades resulting in an equal and opposite reactive force. The reduction in pressure and the increase in velocity of the gases are accomplished by the shape of the passage between the rotor blades. In most practical designs, the turbine is a combination of both of these two types and is known as a reaction-impulse turbine. However, all turbine designs have one important principle in common; that of expanding a high-pressure and high-temperature gas to lower pressures and temperatures.

The mass airflow from the combustion chamber is delivered evenly to the turbine nozzles. The nozzles serve to accomplish two functions; that of accelerating the gases, and of deflecting the gases to a specific angle in the direction of turbine wheel rotation. See Figure 37.

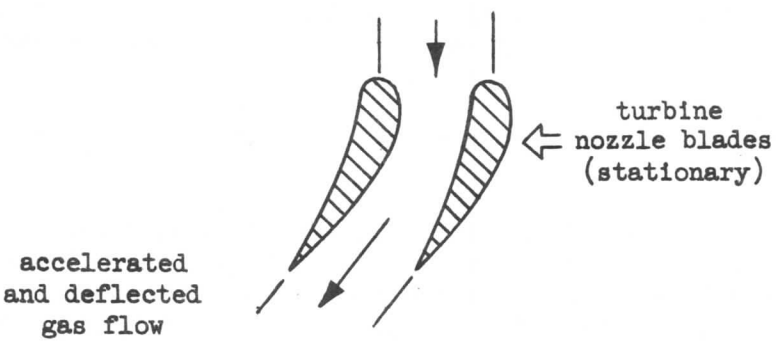

Figure 37.

The design of the stator nozzles may be converging-diverging (high pressure ratios), or they may be wholly converging (low pressure ratios), as shown in Figure 38.

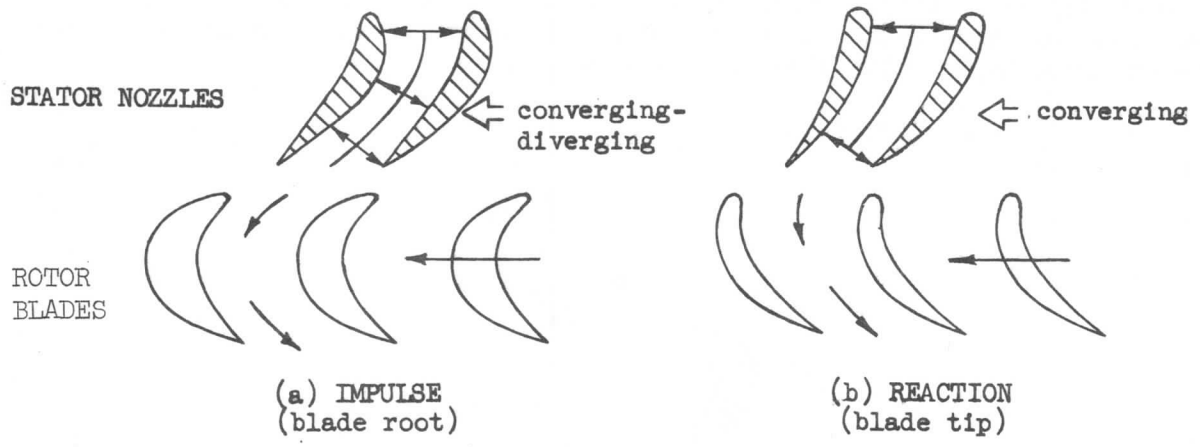

Figure 38.

The effective area of the nozzle passages is measured at right angles to the direction of flow. The shapes, lengths, numbers of nozzles (and turbine blades), and size of the nozzle area may vary considerably between designs.

To understand the effect of the combination impulse-reaction turbine design, it is convenient to discuss the properties of each type separately.

In a pure impulse turbine, the entire pressure drop occurs in the stator nozzles; the pressure in the rotor buckets (often called blades or vanes) is the same as the pressure of the discharge region. The density of the fluid remains approximately constant in the rotor passages, and the area of the passages is essentially constant from the entrance to the exit, as in Figure 39.

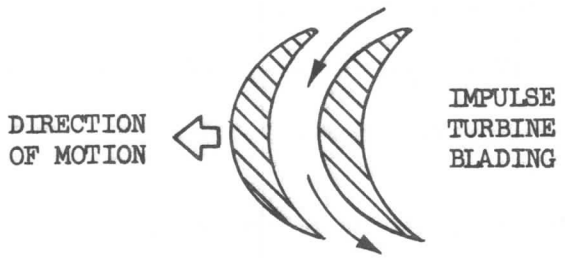

Figure 39.

The function of the rotor blades is to deflect the fluid, lose velocity in the rotational direction and perhaps acquire some in the opposite direction. In doing so the blades exert a force on the fluid to change its momentum, and the fluid exerts a corresponding reactive force on the blades. This reactive force acts about the axis of rotation (moment) equalizing the resisting moment of the load, and the rotor turns continuously.

Analytically, the change in momentum can be demonstrated by referring to the diagram of Figure 40. The entrance velocity V_1, is the resultant of the axial velocity V_a, and the turbine rotor tangential velocity V_t. As the fluid leaves the turbine blades, the direction of the relative velocity has been changed, but the magnitude is essentially the same. Figure 40 shows the exit angle the same as the entrance angle which simplifies the analysis.

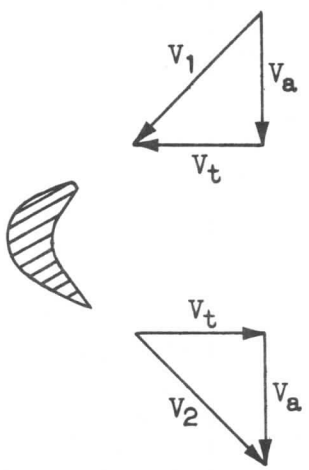

Figure 40.

The product of mass and velocity is called "momentum" and may be expressed

$$\text{momentum} = MV \qquad (36)$$

A moving body is characterized by its momentum. The product of M times ΔV expresses a change in momentum. Since a change in momentum is equal to impulse, the product of an average value of a force and the time during which it acts, an equation relating the two may be written:

$$M\ \Delta V = F\ \Delta t \qquad (37)$$

Referring to Figure 40, an expression for obtaining the momentum change may be written from equation (37).

$$\text{momentum change} = \frac{W}{g} 2V_t$$

The force imparted to the wheel is proportional to the rate of momentum change and may be determined as follows:

$$\text{Force} = 2\ \frac{W}{g}\frac{V_t}{\Delta t}$$

In pure reaction turbines, all the pressure drop occurs in the rotor blades. The velocity in the nozzles is increased; the momentum of the fluid delivered to the rotor blades is increased. The area of the stator passages is approximately constant, whereas the area of the rotor passages decreases from entrance to exit. See Figure 41.

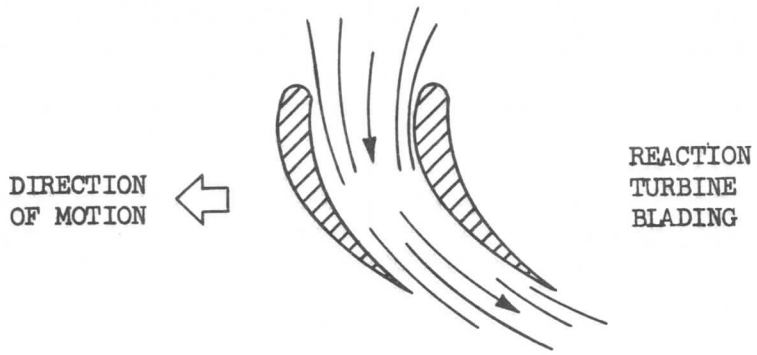

Figure 41.

As a result of the pressure drop, the velocity increases in the blades, becoming a maximum at the exit. The immediate accelerating force is the pressure gradient (exactly as in the nozzles of an impulse turbine). This force is transmitted to the blades so that the momentum of the fluid is really changed by a force exerted on the blades just as in the impulse turbine. In both types, the effective force acting on a blade is physically the difference of pressure on the two sides times the blade area.

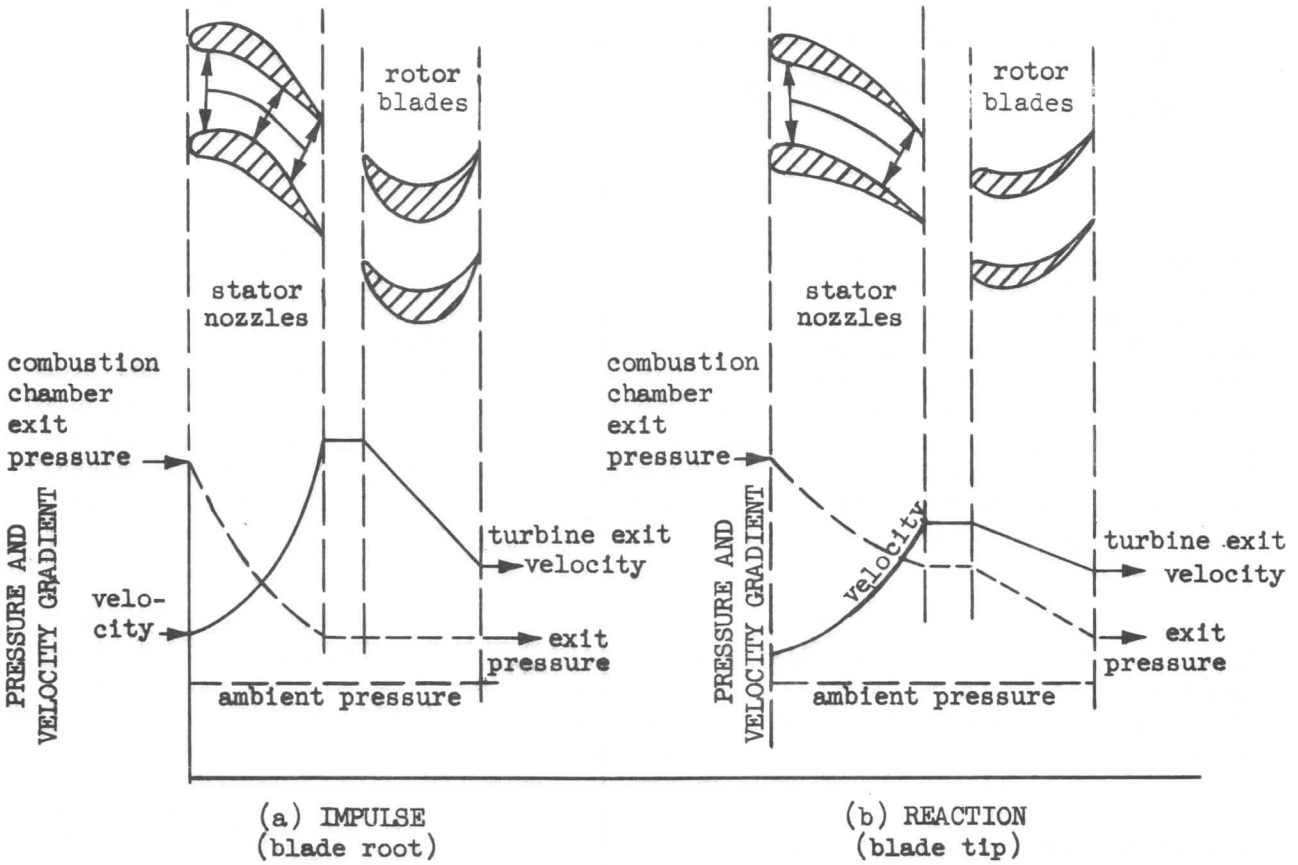

Figure 42.

The two types of turbines can be successfully combined by designing the blade tips for reaction, and the blade roots for impulse, and blending one into the other so that the characteristics are approximately half reaction and half impulse. Under these conditions, the pressure and velocity characteristics, through the turbine with respect to the stationary engine components, may be seen in Figure 42.

In Figure 43 a turbine blade is shown with a pressure gradient indicating the amount of pressure drop across the turbine blade. The higher tip pressure helps to reduce outward flow and tip loss due to centrifugal effects, thus making the blade more efficient.

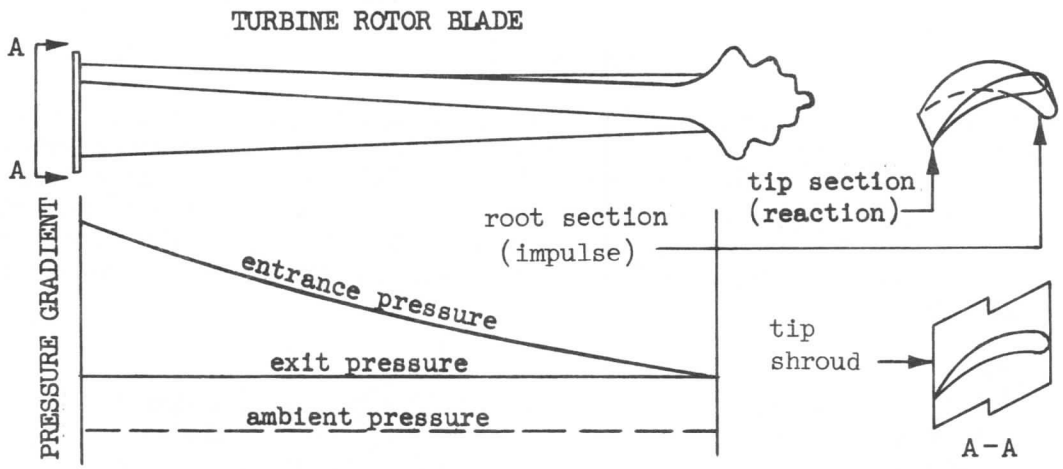

Figure 43.

The advantage of tip shrouding as shown in Figure 43 is that the gap between the tips of the turbine blades and turbine case can be more easily sealed, since the shroud reduces the problem to that of sealing between two flat surfaces. This seal reduces the gas leakage around the tip of the turbine blade and increases the turbine efficiency. Another advantage is that shrouding dampens the blade vibrations permitting the use of reduced blade chords, and this results in a shorter and lighter engine. Shrouding, however, reduces the maximum allowable turbine inlet temperature since the effect of centrifugal action on the mass of the shroud must be resisted by the blades. Some of the latest engine designs which are operating at high turbine inlet temperatures have non-shrouded first stage turbines.

The characteristics of gas flow through the turbine may be shown conventionally by means of a gas flow diagram. The diagram, Figure 44, graphically represents the blade and passage contour. The direction of gas flow and the magnitude of the velocity is indicated by the length of the arrow. Velocities relative to the rotating blade are shown by dashed-line vectors.

The gas flow enters the nozzle blade tip at a moderate velocity V_1, and is accelerated through the nozzle to an exit velocity V_2. Note the deflection from the axis by the nozzle. Since the rotor blades are rotating, the tip speed and direction can be indicated by vector V_3. With the rotor blade moving in the same general direction but at an angle to the nozzle exit velocity V_2, the direction

and magnitude of the gas velocity V_4, entering the rotor blade, will be the vectorial difference between V_2 and V_3. This is a relative velocity and represents the angle of gas entrance relative to the rotor blades. If there should be insufficient deflection angle from the nozzle, the rotor speed would be limited to a lower value than desired. At any design RPM, the gas deflection out of the nozzle must be such as to provide a gas flow into the rotor blade at the optimum angle of attack. Thus the blade angles of both rotors and stators relative to the case must be determined together and for some design condition. The distance between blades must be held to a minimum to reduce engine length and weight, but it must provide running clearance and enough space to attenuate wake affects which might induce vibration.

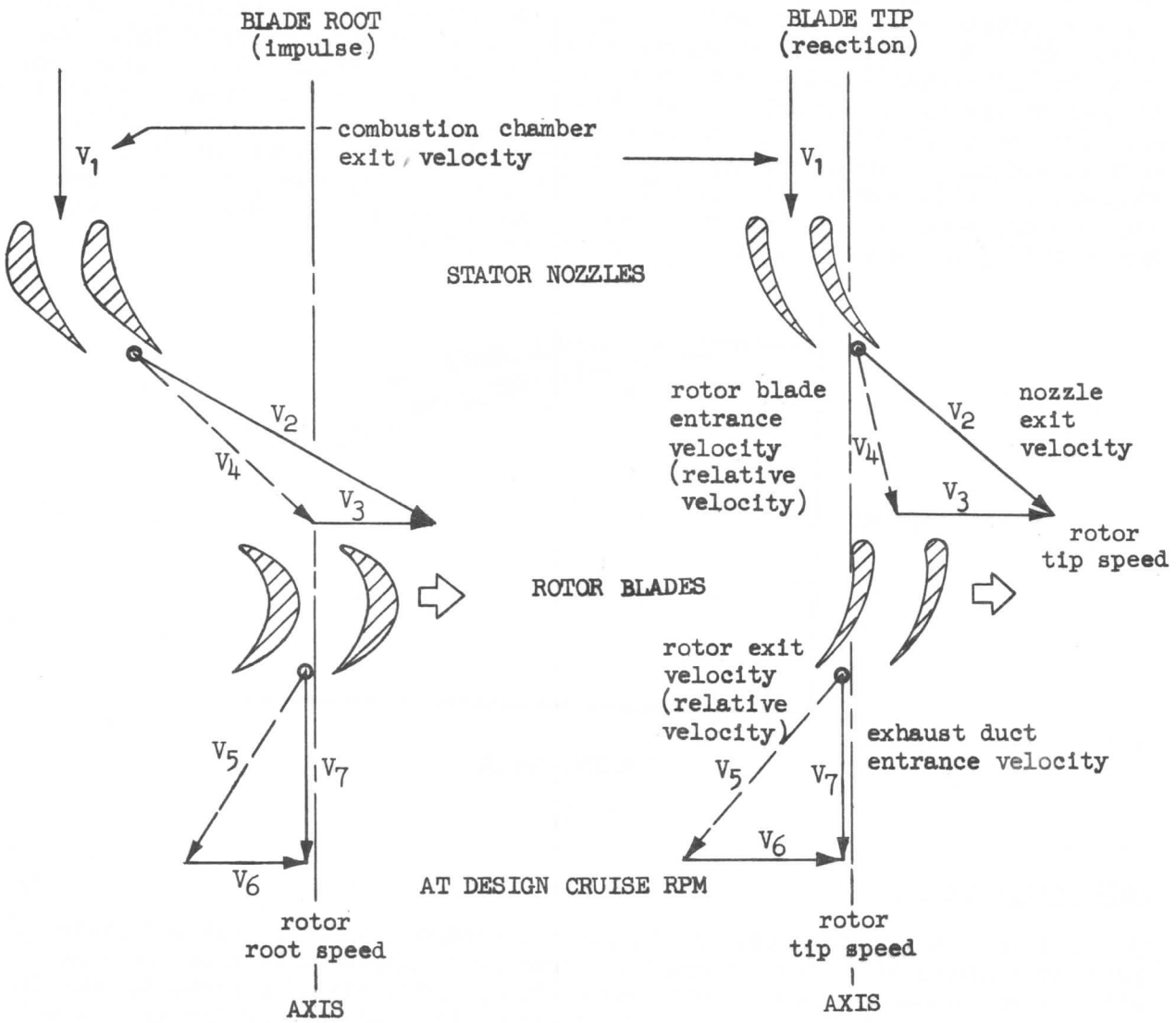

Figure 44.

Assuming flow to be axial at the root as well as at the tip, the flow angles must be altered to compensate for the lower speed, V_6, of the blade root. To obtain the greatest rate of momentum change for impulse, a high degree of

direction change of the gas flow through the rotor blade must be maintained. To accomplish this, a greater deflection through the nozzle is provided. With the lower root speed, V_3, the rotor blade entrance velocity, V_4, will be greater than at the tip and its angle of attack will be increased.

A similar situation exists with the gas flow out of the rotor blades and through the exhaust duct. In order to obtain approximately axial flow down the duct, the rotor blades must deflect the exit gas flow, V_5, sufficiently to compensate for desired rotor RPM. If the angle of exit flow does not properly match the desired rotor speed, the exhaust duct flow, V_7, would be deflected off the axis and result in a swirl flow instead of axial flow down the duct. The presence of swirl means a loss in gas energy during transmission to the jet nozzle. Any turbine could eliminate exhaust duct swirl at only one specific rotor speed; the engine design RPM. As the turbine is operated above or below this specified RPM, swirl in either direction would be anticipated. For example, Figure 44 indicates conditions at one specified RPM. If the RPM should change, the diagram would be altered; the blade contour and blade angles can not change, but the gas flow vectors and angles would change, resulting in duct swirl. Therefore, the gas flow diagram will change with each RPM. For this reason, straightening vanes are commonly used in jet engines of today. The effects of straightening vanes for operating at an unspecified RPM may be seen in Figure 45.

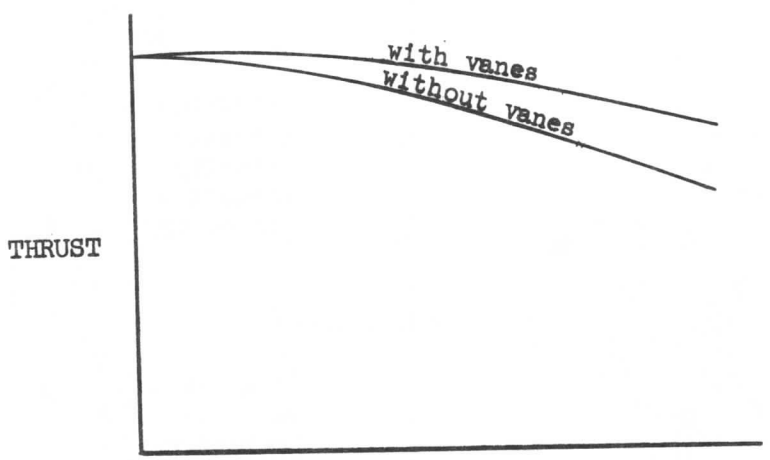

Figure 45.

Exit Nozzle Design

The exit nozzle, or tailpipe, is designed to expand the hot combustion gases from the turbine discharge pressure to atmospheric pressure in a manner that will produce a maximum amount of thrust. The performance of a turbojet unit is quite sensitive to tailpipe and nozzle design. The majority of installations employ a single direct exhaust to obtain the advantages of low weight and simplicity with a minimum of duct losses. Mechanical devices designed to alter the orifice area or direction of jet exhaust gases are used for after-burning, thrust-reversing and noise-suppression.

Varying requirements make it impractical for the powerplant manufacturer to include the duct in its entirety as part of the powerplant. The airplane manufacturer is obliged to complete the exhaust system by designing to the particular airplane.

The chief function of the exhaust nozzle is to straighten the gas flow as it comes off the last turbine stage, and to accelerate the exhausting gas stream. A tailcone is installed in the duct to provide a path for the gas to the exit without abrupt changes in cross section. The struts supporting the tailcone may be streamlined and of such length as to serve as straightening vanes. As discussed previously, the straightening vanes aid in maintaining a straight flow through the exit. The area of exhaust is usually fixed; however, in some installations the nozzle area can be varied by varying the position of the tailcone. While the variable type nozzle configuration presents many mechanical difficulties and requires a more complicated analysis, it offers some advantages; it is possible to extract additional thrust at higher temperature for short periods of time, useful for takeoffs and emergencies.

The fixed nozzle area design is such that the selection of exit area results in either the maximum thrust at allowable gas temperature for takeoff or continuous operation, or in some maximum allowable specific fuel consumption. As was seen by the relationship,

$$F_n = \frac{W_a}{g} (V_j - V_a)$$

the effect of increasing the exhaust velocity is such as to increase the thrust. Note that the expression has been simplified by neglecting the fuel. It is normal to increase the exhaust velocity to produce sonic velocity at the orifice; that is, M = 1. When the static pressure at the exhaust nozzle is equal to the ambient static pressure, there will be no further increase in exhaust velocity. If, however, conditions are such that the static pressure is greater than ambient and M = 1 at the throat of the exhaust nozzle, the flow must expand to ambient pressure and additional thrust is made available by velocity increase to supersonic speeds. If the expansion takes place behind the physical confines of the nozzle, some of the energy is lost into the airstream; but if the nozzle is designed with a divergent section to allow for the expansion, the maximum energy transfer to thrust can be achieved. Thus, it is not unusual to find a convergent-divergent exhaust nozzle on engines of this type. See figure 46.

Thrust calculations made up to this point have been based on the assumption of subsonic or sonic flow at the exhaust. No allowance has been made for the added reaction to any supersonic expansion. Therefore, a term to account for this additional thrust must be added. It can be calculated in terms of the pressure difference times the throat area. And the net thrust equation becomes:

$$F_n = \frac{W_a}{g} (V_j - V_a) + A_j (p_{s8} - p_{am}) \qquad (38)$$

In equation (38), A_j is the throat nozzle area, V_j is the exhaust velocity at the throat, and the pressure term is the result of the expansion from the nozzle throat to atmosphere.

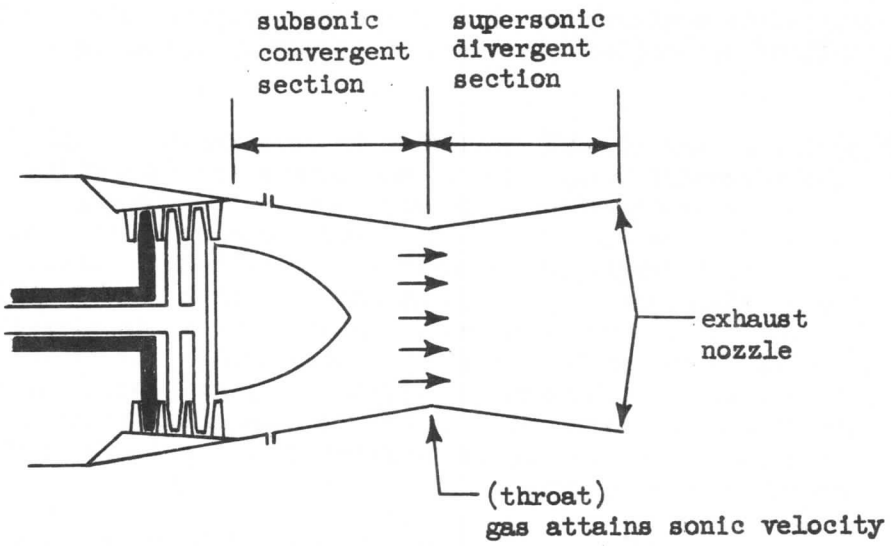

Figure 46.

2-8 RATINGS

The turbine inlet temperature is a function of the amount of fuel introduced into the combustion chamber. There is a practical maximum allowable temperature which the turbine wheel can withstand under the high stress of rotation. This allowable temperature constitutes a "rating." The maximum temperature that the turbine can withstand over limited time periods is the TAKEOFF RATING.

TAKEOFF (WET) - This is the maximum thrust available for takeoff. The rating is obtained by actuating the water injection system and setting the computed (wet) thrust with the thrust lever. The rating is restricted to takeoff, may have an altitude limitation, and is normally time-limited.

TAKEOFF (DRY) - This is the maximum thrust available without the use of water injection. The rating is obtained by either placing the thrust lever in the full forward position or adjusting the thrust lever to obtain the computed takeoff (dry) thrust for the existing ambient conditions, whichever is obtained first. It is time-limited and to be used for takeoff only.

The design temperature is approximately 1600°F for this rating and is normally limited to 5 minutes, of which about one-half may be with water injection if desired.

A lower turbine inlet temperature, approximately 200°F lower than the maximum, is called MAXIMUM CONTINUOUS RATING.

MAXIMUM CONTINUOUS - This rating is the maximum thrust which may be used continuously and is intended only for emergency use at the discretion of the pilot. The rating is obtained by adjusting the thrust lever to obtain a predetermined turbine discharge pressure or N_2 RPM, depending on type of engine.

The next lower rating is the NORMAL RATING or MAXIMUM CLIMB RATING which is a turbine inlet temperature slightly lower than the maximum continuous rating.

NORMAL - This rating is the maximum approved for normal climb. The rating is obtained in the same manner as maximum continuous. For some engines, maximum continuous and normal rated thrust are the same.

An arbitrary lower rating, approximately 100°F lower than the normal rating, is the MAXIMUM CRUISE RATING.

MAXIMUM CRUISE RATING - This is the maximum thrust approved for cruising. It is obtained in the same manner as maximum continuous.

IDLE - This is not an engine rating but, rather, a thrust lever position suitable for minimum thrust operation on the ground or in flight. It is obtained by placing the thrust lever in the idle detent on the thrust lever quadrant.

The various ratings for an engine are specified by the engine manufacturer and published for ICAO standard, sea level, static conditions, assuming no losses. The effect of altitude, off-standard temperature, and airspeed on thrust will be discussed later.

2-9 TEMPERATURE AND VELOCITY VARIATIONS

So far nothing has been said about the magnitude of the temperatures and velocities existing throughout the cycle. The temperature reaches its maximum in the combustion chamber; however, it is limited by the highest temperature that the turbine wheel can withstand. At the present time this temperature becomes critical at approximately 1600°F for the JT3 and JT4 engines and 1800°F for the Conway engine. Some temperature rise results from heat generated in the compression process, but a drop in temperature occurs across the turbine section.

The velocity is carefully controlled through the jet engine, both in magnitude and direction. The direction is kept generally in a straight-through manner to avoid unnecessary losses in energy. The magnitude of the velocity profile varies from a relatively low speed at the entrance to sonic or supersonic speeds through the turbine nozzles and tail pipe or exhaust nozzle.

A profile showing the manner in which the air is processed as it passes through the engine appears on Figure 47. The compressor adds energy to the air which results in changes in pressure, temperature and velocity. The reaction to this action is the largest portion of thrust produced by the engine. This forward force is imposed on the various compressor elements and is transmitted to the airframe through the engine structure.

Outside energy is supplied to the cycle in the combustion chamber by the addition and burning of fuel. The large increase in temperature causes a large velocity increase with virtually little change in pressure due to design of the passageways. The thrust reaction to the acceleration is transferred to the engine through the structure of the combustion chamber.

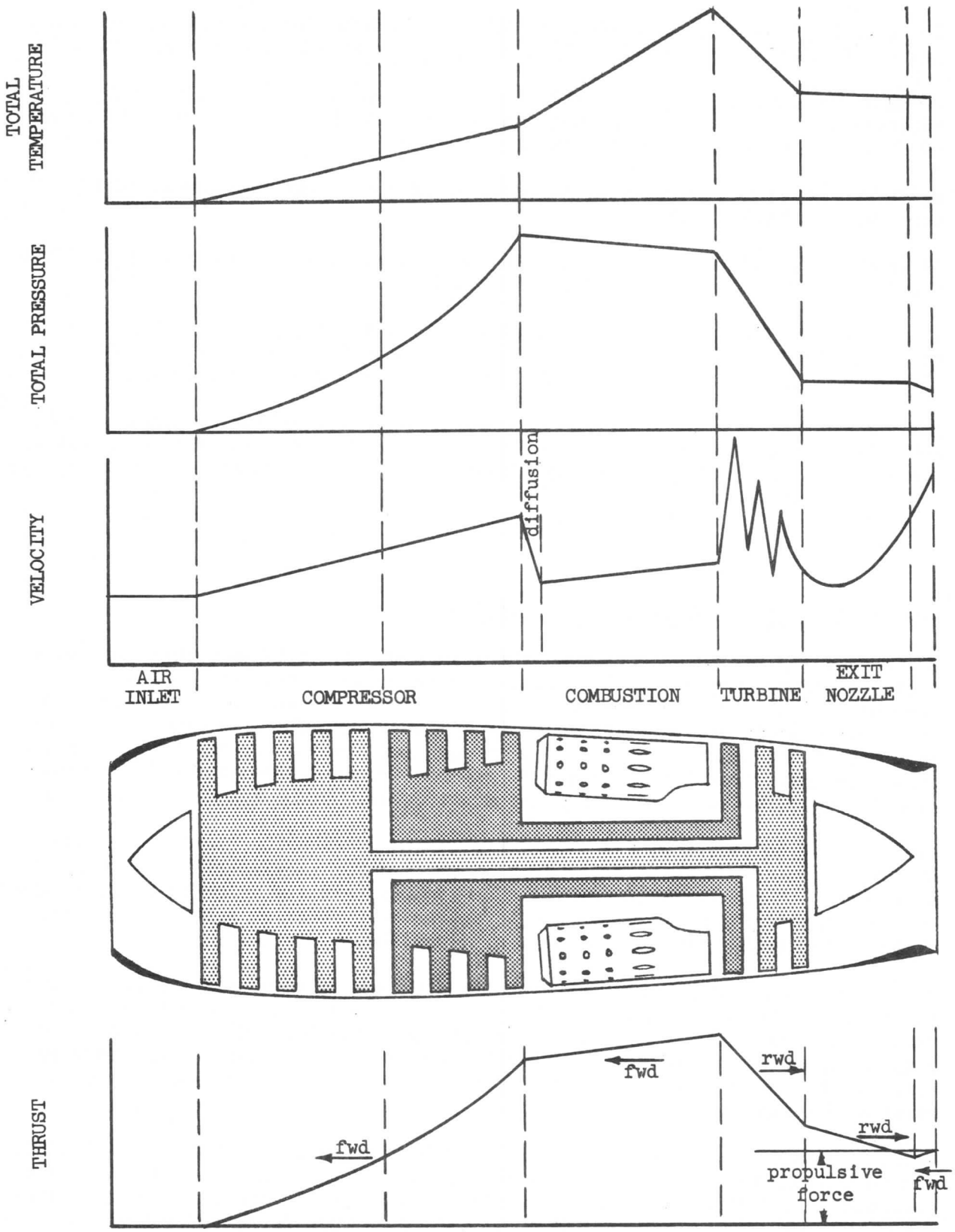
TOTAL TEMPERATURE
TOTAL PRESSURE
VELOCITY
diffusion
AIR INLET
COMPRESSOR
COMBUSTION
TURBINE
EXIT NOZZLE
THRUST
fwd
fwd
rwd
rwd
propulsive force
fwd

Figure 47

Due to the shape of the turbine section, the velocity is increased in the nozzle; but since no heat is added, the pressure, temperature, and velocity are reduced at the rotor exit due to the extraction of work by the turbine.

The design of the tailpipe is such that the effect on overall air flow is highly favorable to engine performance. Generally this is an expanding passage resulting in decreased velocity with very little pressure or temperature change. Various engine models may employ devices at the exhaust nozzle to further improve the performance.

Note that from the turbine entry to the tailpipe exit, Figure 47, there exists a loss in thrust cancelling roughly two-thirds of the forward force built up in the compressor and combustion sections. The diagrams are only representative, as variations occur with individual engines.

2-10 BY-PASS AND TURBOFAN ENGINES

In addition to the turbojet engine, the by-pass and turbofan engines are becoming more important. The question may be asked as to why we should have engines of this type. The answer is simply that the addition of a by-pass or turbofan duct improves the propulsive efficiency, at the cruising speeds under consideration, by producing a lower jet velocity than that of a simple jet without reducing the thermal or cycle efficiency of the engine. This effect increases the overall efficiency, the product of thermal efficiency and propulsive efficiency, as seen by equation (28). Equation (31) shows that the thermal efficiency, the conversion of heat energy into power, continually increases with increase in turbine inlet temperature. This increase in turbine inlet temperature increases the jet velocity and engine thrust. Unfortunately however, equation (32) shows that this increase in jet velocity reduces the propulsive efficiency which reduces the overall efficiency. The increase in engine thrust at these high jet velocities is obtained at the expense of higher fuel consumption. The general principle of the fan engine is to convert more of the fuel energy into pressure energy which results in more thrust without an increase in fuel flow.

It is not generally known how low the turbine inlet temperature can be taken for the best fuel consumption of a modern high-pressure-ratio jet engine. Figure 48 shows the propulsive efficiency, thermal efficiency, specific fuel consumption, and turbine inlet temperature plotted against thrust per lb. of air flow for a typical high-pressure-ratio jet engine. The condition shown is at 475 knots in the stratosphere. It will be seen that the propulsive efficiency falls with increase in thrust per lb. of air flow or increase in turbine inlet temperature. It shows the increase in thermal efficiency with increase in turbine inlet temperature, due to the compressor and turbine having efficiencies less than 100%. If the components had no losses, the thermal efficiency would depend on the compression ratio alone.

Another item of interest is the opposing influence of thermal and propulsive efficiency on fuel consumption. The specific consumption curve is the inverse of the product of the thermal and propulsive efficiency curves. It may be noticed that the turbine inlet temperature for the best fuel consumption is about 800 degrees Kelvin (approximately 1000° Fahrenheit).

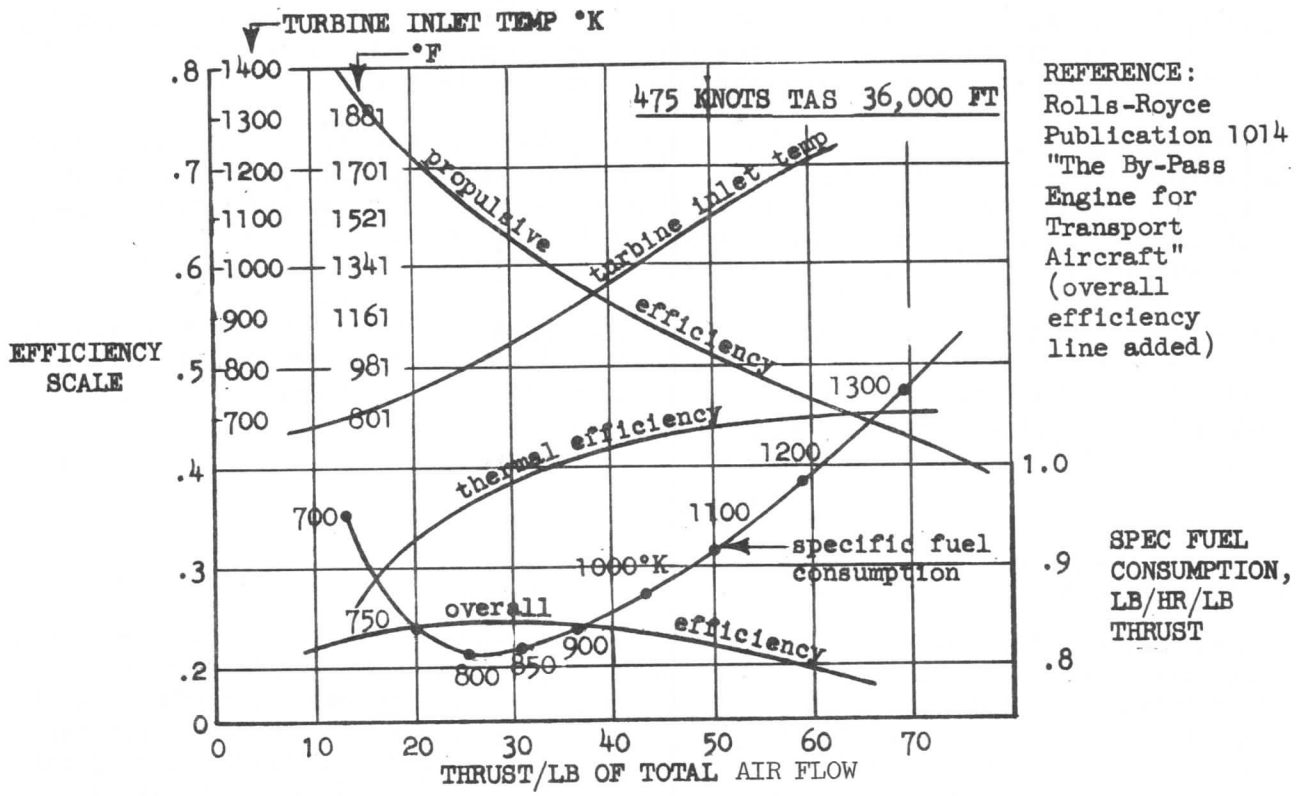

Figure 48.

In practice, a higher temperature is selected to increase thrust with only a small penalty in fuel consumption and without increase in size and weight.

One method of increasing the thrust output without further increasing the fuel consumption is by taking the power from the jet gases through a turbine to drive a propeller. This is a turboprop engine. The mass airflow through the propeller is very high and its jet velocity is low; therefore, under these conditions this will give very high propulsive efficiencies at static conditions and low flight speeds. However, the propulsive efficiency is very much influenced by changes in airspeed. The turboprop has very good thrust and fuel flow capabilities at low speeds but loses much of this advantage as airspeed increases. It suffers serious losses at high subsonic flight speeds, due largely to high Mach numbers of the air relative to the blade tips. A method suggested a few years ago to avoid these tip speed losses was to surround the propeller with a duct. The effect is to cause compression of the air ahead of the blades, and to keep the blade Mach number substantially the same as at low speeds, i.e., constant over a wide range of speeds. This is the ducted fan. Since the propeller is a heavy form of fan, it is possible to consider a smaller, higher speed fan of such size that it may be directly driven at turbine shaft speeds and can supercharge the rest of the engine, becoming an integral part of the overall compression system.

Since the size of this fan is restricted, the amount of air it can handle is restricted; but the pressure rise of the air may be quite large. It therefore seems sensible to use part of the air from the fan to feed the rest of the engine

and so increase the pressure ratio. Figure 49 shows a by-pass jet engine in which the engine consists of a low pressure compressor feeding part of its air to the high pressure compressor and the rest ducted around the engine. The high pressure compressor discharge passes through the combustion chamber, the high pressure turbine, and then through a second low pressure turbine which drives the low pressure compressor. Finally the jet expands through a nozzle either before or after mixing with the by-pass air.

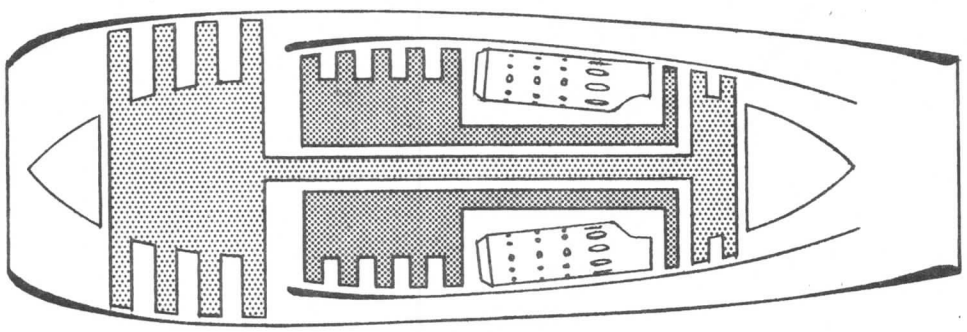

BY-PASS ENGINE

Figure 49.

The advantage of this arrangement, when compared with the same system in which the low pressure compressor is just large enough to feed the high pressure compressor only, is that most of the energy is removed by the low pressure turbine so that the exhaust velocity is reduced to a velocity at which the propulsive efficiency is quite high. The energy removed will be conveyed through the turbine and low pressure compressor to a stream of relatively cold "by-pass" air whose velocity is again such that the propulsive efficiency is high. In this way a good overall efficiency can be obtained by operating at a high turbine inlet temperature where the thermal efficiency is high. The pure jet engine can also be made to operate at a low turbine inlet temperature to give the same order of jet velocity as that of a by-pass engine, but only by compromising its thermal or cycle efficiency. This may be seen in Figure 50 which shows the comparison between a pure jet engine and a by-pass engine with a by-pass ratio of one.

The disadvantages are that this transfer of energy from the gas exhaust to the ducted air is not done without losses. There are losses in the turbine, the low pressure compressor and the by-pass duct. For given airflow and turbine inlet temperature, the thrust will always be less than can be obtained from a simple jet engine. This is shown in Figure 51 for two engines having the same compression ratio, similar component efficiencies, and the same airflow.

It now remains to consider the weight. For a given total airflow, the by-pass engine is lighter than a pure jet engine. Also, in this case, the thrust is lower for the by-pass engine since the thrust per unit of airflow is lower. If both engines were scaled to give the same thrust, it would appear that the weight

COMPARISON OF PURE JET AND BY-PASS ENGINE

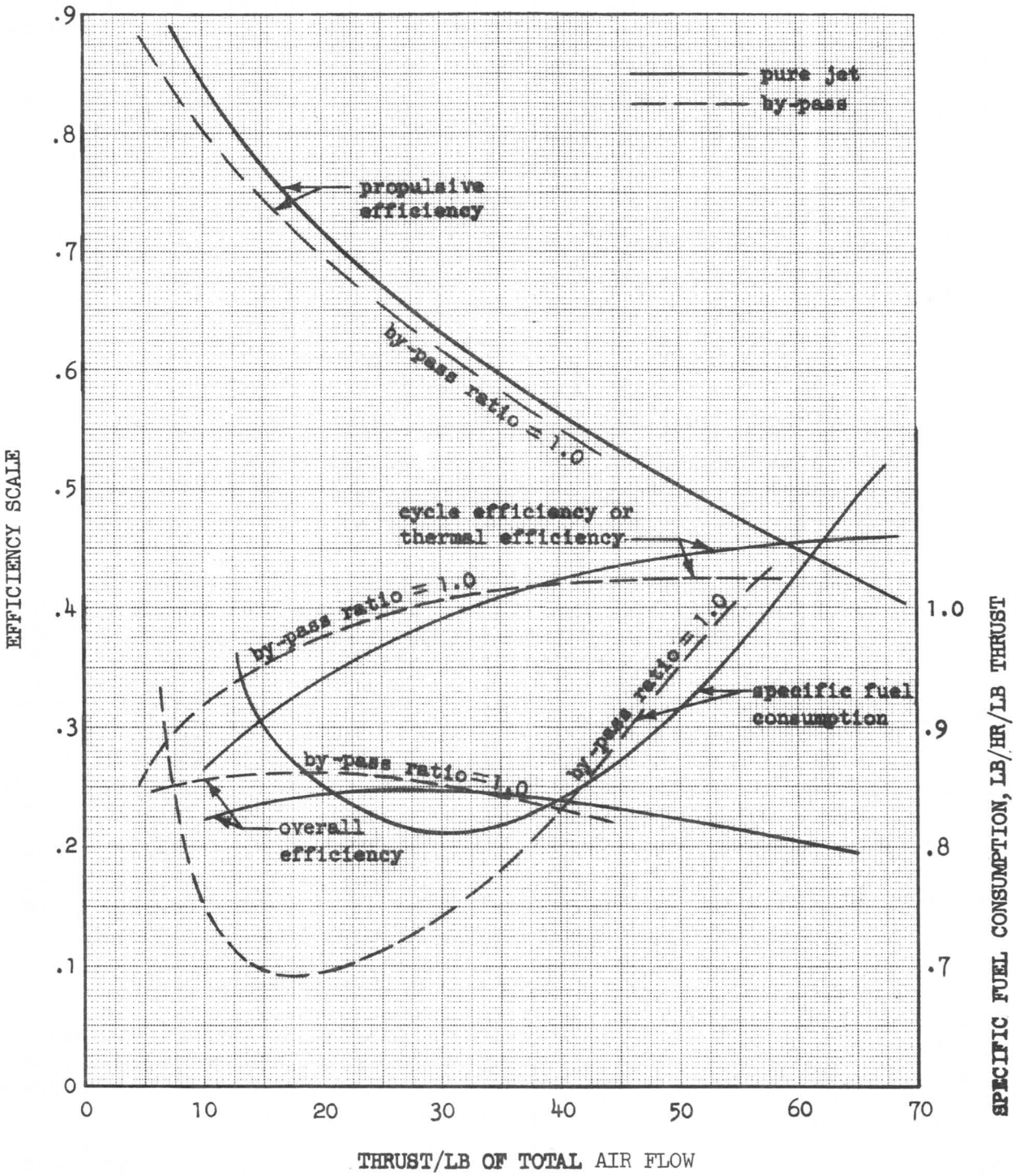

Figure 50.

of the by-pass engine would approach that of the simple jet. This is not the case, however. The weight of the pure jet engine still exceeds that of the by-pass engine. It has been stated that this increased weight would be equivalent to an increased fuel consumption of about 5%, and so the range of the airplane may be approximately 5% better when fitted with by-pass engines.

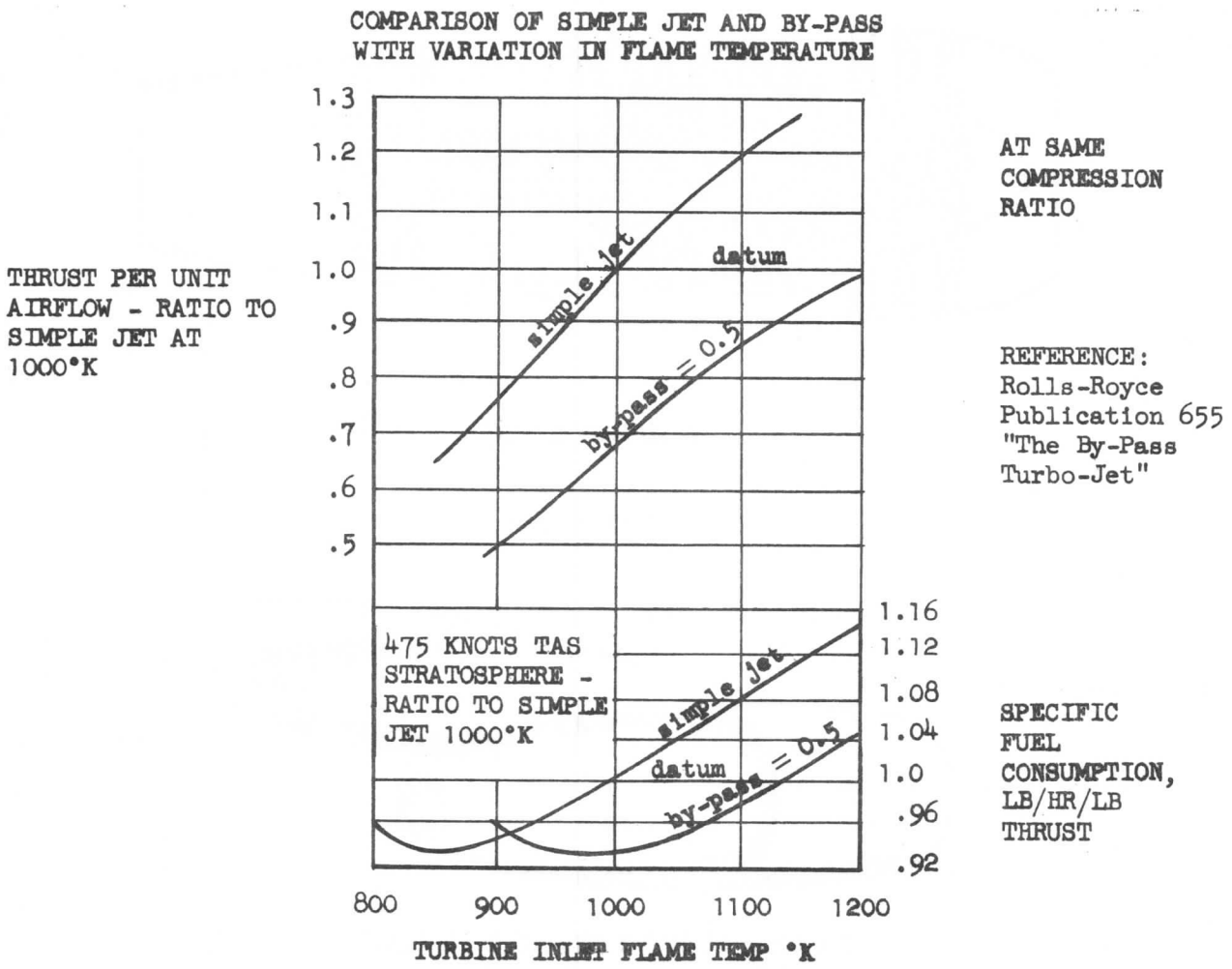

Figure 51.

The turbofan engine is essentially a by-pass engine. The most significant differences between the two types of engines are the amount of air that is by-passed and the general construction. There can be a number of designs of fan engines.

One of these designs is the forward fan engine. In this configuration, the fan consists of one or more stages of extra large compressor-type blades that are a part of the forward end of the low pressure compressor of a dual axial compressor engine as shown in Figure 52.

Air passing through the central portion of the fan feeds into the engine through the compressors in the normal manner. After going through the fan stages of the low pressure compressor, part of the air is exhausted overboard and the rest goes

through the remaining stages of the low-pressure compressor and then into the high speed compressor. The fan serves to provide extra thrust by accelerating a large mass of air in much the same manner as a propeller encased in a shroud. The exhaust from the outer perimeter of this large forward fan is exhausted overboard through a duct along the outside of the engine nacelle as shown in Figure 53.

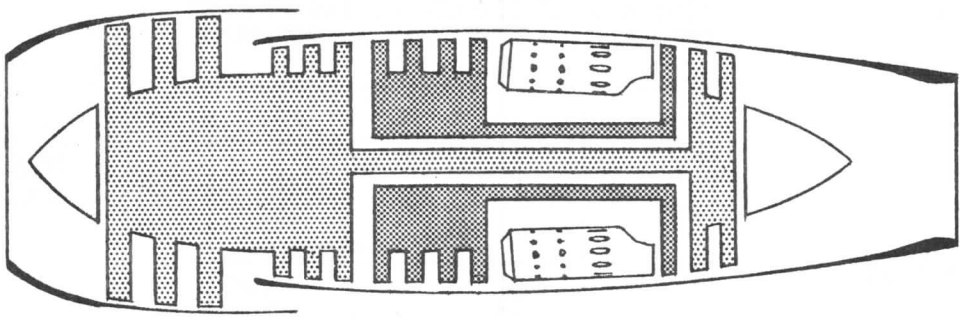

TURBOFAN ENGINE

Figure 52.

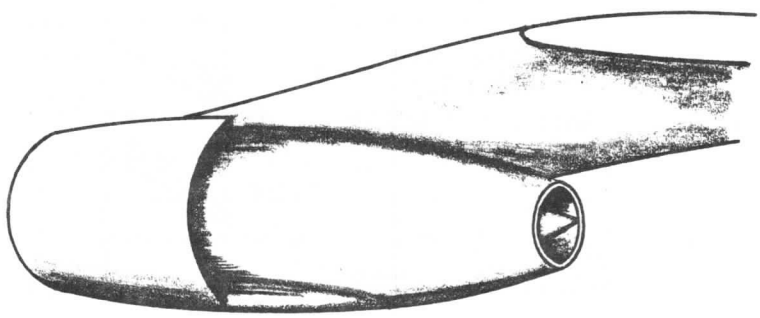

TYPICAL TURBOFAN ENGINE INSTALLATION

Figure 53.

Another of these designs is the aft fan engine. In this configuration there is an aft fan assembly attached to the engine in place of the rear turbine assembly. It has two concentric annular flow passages. The inner passage conveys the gas flow from the turbines that drive the compressor through a single-stage free floating turbine and discharges it through the jet nozzle. The part that makes up the free floating turbine is also the part comprizing the fan airflow compressor, making up a combination turbine and compressor blading unit as seen in Figure 54. This blading unit has a seal midway along each blade to prevent mixing of the primary flow and by-pass flow at this point. The fan airflow is furnished to the aft fan front flange by airframe ducting.

In operating characteristics, the turbofan engine lies between the turboprop engine and the turbojet engine. A turbojet is basically a low-mass-rate, high-

jet-velocity unit. The conversion of a turbojet engine to a turbofan engine provides us with an engine having a higher mass rate and lower jet velocities. The resulting performance improvement is largely due to the resulting increase in propulsive efficiency (Equation 32) and to the increase in the mass rate handled for a given amount of fuel consumed (lower specific fuel consumption). The efficiency of the fan engine remains high since the air is taken in through the inlet and duct providing about the same Mach number at the face of the fan regardless of forward speed (even at high airspeeds).

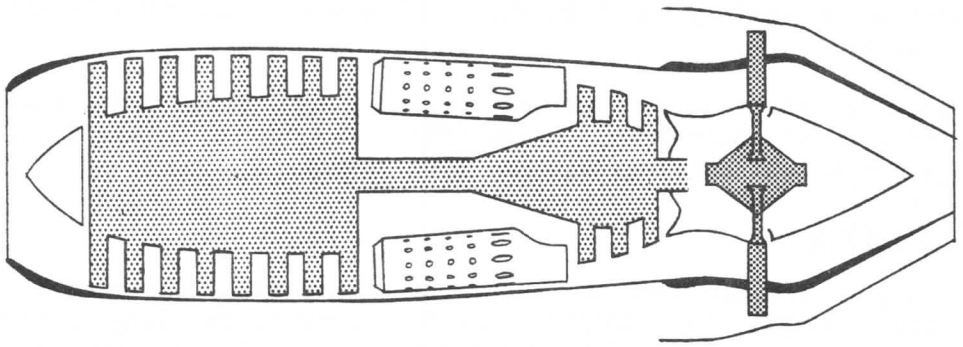

AFT TURBOFAN ENGINE

Figure 54.

Converting a turbojet engine to a fan version of the same engine will give more static takeoff thrust, more thrust for climb and cruise for the same fuel flow resulting in lower thrust specific fuel consumption, and quieter operation during takeoff and cruise conditions because of the lower tailpipe velocities.

When computing thrust for a turbofan engine having two exhausts, equation (17) has to be modified to account for both the fan exhaust and the primary exhaust. Since the fan exhaust velocity and airflow are different from the primary exhaust velocity and airflow, equation (17) now reads:

$$F_n = \frac{W_{ap}}{g}(V_j - V_a) + \frac{W_{af}}{g}(V_f - V_a) + \frac{W_f}{g}(V_j - 0) \qquad (39)$$

for a turbofan engine, where W_{ap} is the primary airflow that goes through the complete engine and W_{af} is the fan airflow.

2-11 FACTORS AFFECTING THRUST

As previously illustrated, the development of thrust is a relatively straight forward process requiring only the knowledge of specific quantities of mass airflow and velocity changes. What is not so straight forward is the resulting effect of the multitude of variables, always present during any form of jet engine operation, on the specific quantities of mass airflow and velocity changes. Since these variable factors affect the components from which the thrust is derived, they will affect the thrust output.

Effect of Pressure

From previous discussions of thrust and the constant pressure jet engine cycle, it was seen that the greater the combustion chamber inlet pressure the greater would be the area within the cycle diagram and thus the greater would be the thrust output. Therefore, any cause for a change in pressure within a jet engine will also be a cause for a change in thrust output, whether it be a low barometric pressure, a reduced inlet pressure due to altitude, or increased inlet pressure due to ram. Such pressure variations will cause a variation in the air density within the engine, which in turn will cause a variation in airflow and velocity change.

Since airflow is weight of air per unit of time, and, since under constant RPM the compressor volume discharge remains fixed, any change in air density will also change the weight airflow (W_a) and thus thrust.

Effect of Airspeed

Theoretically, as the airspeed of the airplane increases, the engine's maximum or rated thrust output would decrease due to increased ram drag of engine inlet air. This fact, under actual flight conditions, is only half true due to increased inlet air density produced by the ram effect in the inlet duct system. However, before discussing the effect of ram, we should first investigate this theoretical falling off of thrust with airspeed.

Applying the simplified thrust equation from above,

$$\text{Thrust} = \frac{W_a}{g} \quad (V_j - V_a)$$

it becomes apparent that, as the airplane speed (V_a) increases without an appreciable change in jet velocity (V_j), the term ($V_j - V_a$) decreases and therefore the thrust output decreases. The dotted line in Figure 55 graphically illustrates this theoretical decrease in thrust with increased airspeed. Additional effects under static conditions and low airspeeds will be discussed under engine calibration.

It will also be noted that, eventually, the thrust output approaches zero. This would occur at a point where V_j and V_a are equal. Such performance is altered in actual practice by the forward motion of the airplane, causing the air to be pressurized at the front face of the compressor. The rise in pressure above existing outside atmospheric pressure is, as mentioned previously, referred to as ram.

Effect of Ram

In Figure 55 the solid line will represent more closely what is actually experienced in flight. Since any ram effect will cause an increase in compressor entrance pressure over atmospheric, the resulting pressure rise will cause an increase in the airflow (W_a) and jet velocity, V_j, both of which tend to increase thrust.

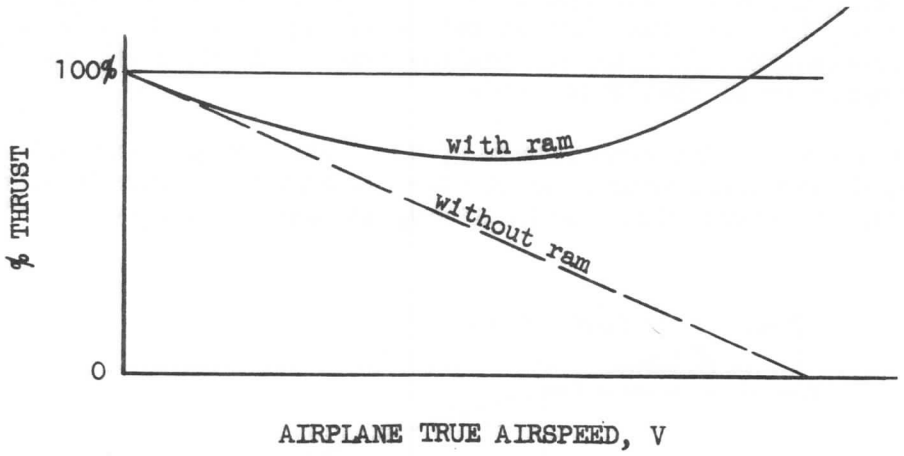

Figure 55.

It will be noted that, with ram, the available thrust output temporarily falls off as the airplane speed increases, but at higher speeds it begins to increase again. This effect is caused primarily by the fact that ram pressure recovery varies with airplane speed and altitude as shown in Figure 56.

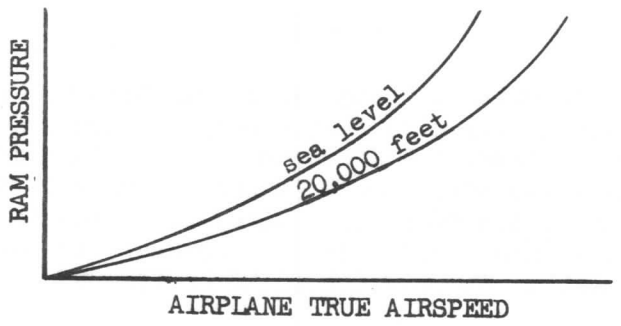

Figure 56.

At low speeds, there is not sufficient ram pressure build-up to fully compensate for the engine's natural tendency to lose thrust with airspeed. However, as air speed increases into the middle range, usually around 450 MPH (dependent upon the aircraft inlet ducting), the ram pressure increases to a point where it fully compensates for engine thrust loss, and net thrust output ceases to fall off. At high speeds, ram pressure becomes sufficient to more than compensate for the engine's tendency to lose thrust; an increase in net thrust results. Recovery to 100% thrust is not possible on present day aircraft because of aircraft speed limitations.

Effect of Temperature

The gas turbine engine has proved to be very sensitive to variations in temperature of the air. Its thrust output might vary as much as 20%, plus or minus,

from the specified rating with operation on a cold day or hot day, respectively. For this reason, the specified thrust rating of any engine must be made at a specified temperature. So that all engines can be rated on the same basis, a standard temperature of 59.0°F is used.

At air temperatures colder than standard, the thrust output increases; conversly, it decreases at air temperatures hotter than standard. Figure 57 shows the typical variation of thrust with inlet air temperature variation.

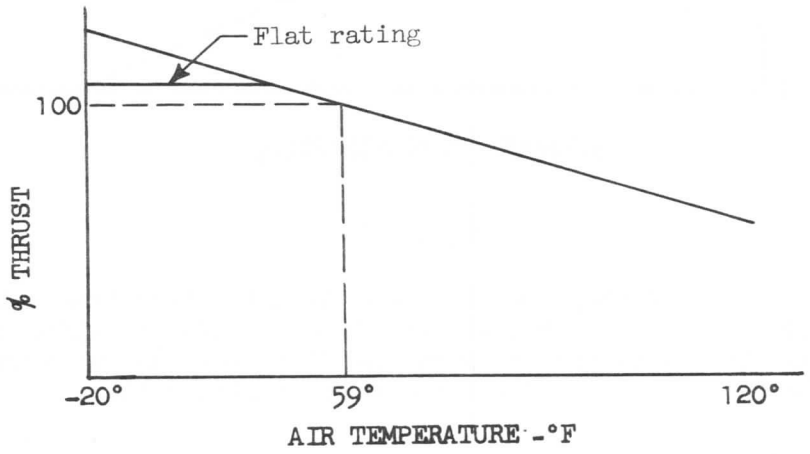

Figure 57.

Cause for thrust variation with air temperature can best be explained by again referring back to the previously discussed theory of thrust development. If the air temperature should decrease, the air density would increase, meaning that each unit volume of air would weigh more. Since at constant RPM the volume capacity of the compressor, and thus the engine, would remain constant, the increased weight per unit volume would result in greater airflow (W_a), and therefore, greater thrust output. The reverse would be true when the temperature is higher than standard.

For some engines, thrust may be limited at low temperatures which correspond to ambient densities above a specified value. Such engines are said to be "flat-rated." The thrust restriction is an internal pressure limitation necessary to insure structural integrity of the light engine wall. At fixed RPM, the higher the density of the air at the inlet, the higher the internal pressure level behind the compressors. Typical flat-rated performance might be as shown in Figure 57. Many engines are flat-rated at 100% takeoff thrust.

Effect of Humidity

It is interesting to note the different effect of humidity upon the jet engine's output over that of the piston-type engine.

In a piston engine, increasing the humidity decreases the weight per unit volume of air. Also, an increase in humidity at high air temperatures increases the vapor pressure of the gas. Since power is set by measuring intake manifold pressure and the carburetor meters fuel to manifold pressure, the fuel-air ratio will

rise since the carburetor does not compensate fuel flow for the pressure change due to humidity. This enrichment of the fuel-air ratio and the falling-off of airflow available for combustion under constant RPM results in a decrease in horsepower.

The increased humidity causes a decrease in weight per unit volume of air within the jet engine also. Its reducing effect on output is almost negligible (see Figure 58). Because the jet engine operates with an excess of air needed for complete combustion of all fuel, any air weight lacking in the combustion air supply to give the proper fuel-air ratio, will be made up by air weight from the cooling air supply. The engine will not be penalized by loss of heat energy from improper fuel-air combustion ratio as in the case of the piston engine. Therefore, its output will not be reduced as much.

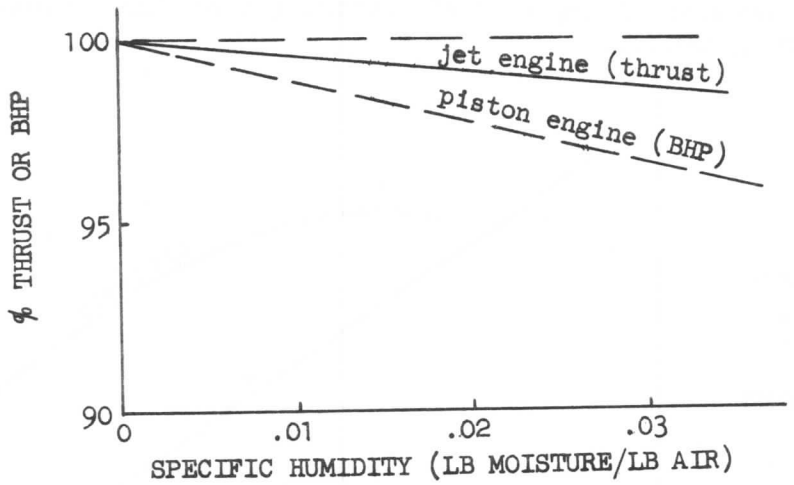

Figure 58.

Effect of Water Injection

As with the piston engine, it is sometimes desirable to momentarily raise the output of the gas turbine engine beyond its 100% rating. A method of thrust augmentation commonly used on multi-engine aircraft is the use of water injection. The principle of water injection in a turbine engine is different from that for a piston engine. In the latter, water and alcohol are injected into the cylinders to suppress detonation during high BMEP operation. Water injected into turbine engines is used to increase the mass flow or velocity of the exhaust gas, thereby increasing the thrust.

There are three common methods of injecting water into turbine engines. One is to inject into the compressor inlet, another is to inject into the diffuser section just ahead of the combustion section, and the third is to inject directly into the combustion zone within the combustion chamber.

Water injected into the compressor inlet evaporates as it goes through the engine, absorbing heat from the air stream. The compressor pumps more mass since the air density is greater. Since the fuel control maintains the proper balance of fuel to air to maintain a given burner temperature for a given thrust lever position, the operating temperatures and pressures within the engine are similar to what they would be on a colder day.

Water injection ahead of the combustion section of the engine utilizes a different principle. The water evaporation draws a large amount of heat energy out of the air stream and lowers the temperature. The fuel flow may be increased to bring the turbine inlet temperature up to rated value. The additional heat energy gives thrust augmentation by increased jet velocity. The mass of the water and added fuel contribute to added thrust, but the amount is small with respect to the total thrust output.

Water injected directly into the combustion chamber is usually mixed with a combustible fuel. A typical coolant consists of 40% methyl alcohol and 60% water. Vaporization of this fluid reduces the temperature, but the combustion of the alcohol increases it again. The added fuel energy raises the RPM and jet velocity and increases the thrust output. Injection of the fuel-water mixture allows the engine to use a much simpler fuel control system than is needed to operate with pure water injection.

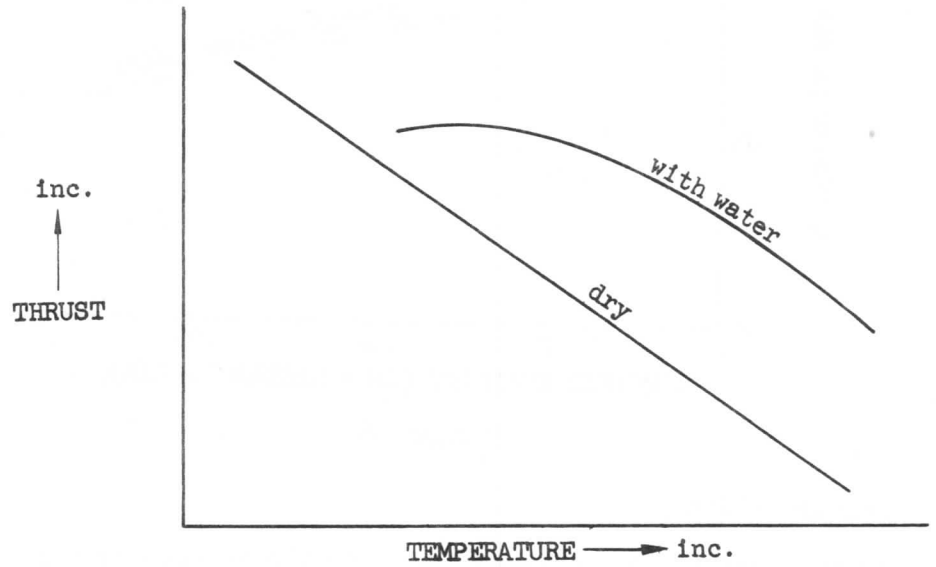

Figure 59.

Figure 59 shows the typical effect of water injection on thrust for varying temperatures.

Effect of Altitude

A gas turbine engine, like the basic piston-type engine, develops its maximum output at high inlet pressure or lowest pressure altitude. With any increase in altitude, the jet engine's thrust output, for any constant RPM schedule, decreases as shown in Figure 60. In both engine types, the gradual reduction of atmospheric pressure reduces the airflow (W_a), and with it, the output. However, Figure 60 indicates the falloff of output of the jet engine to be less rapid than that of the piston type. This effect is caused by the jet engine reacting more favorably to the gradual reduction in air temperature with increasing altitude, tending to slow up its rate of thrust fall-off by giving an improvement in the cycle efficiency.

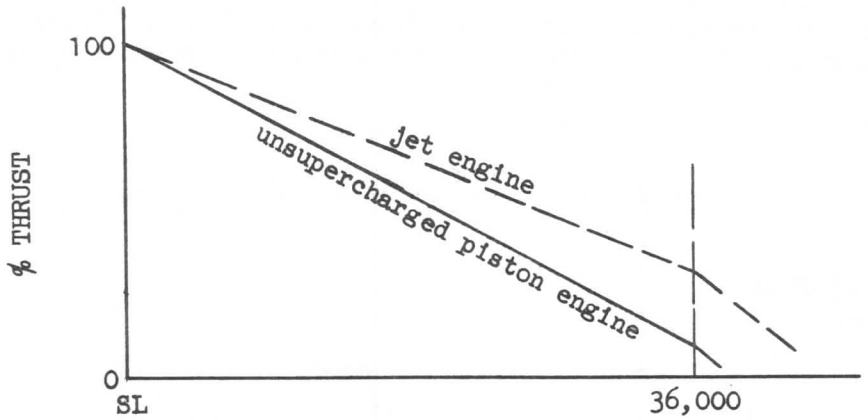

Figure 60.

Notice in Figure 60 the sudden change in rate of fall-off in both engine types at approximately 36,000 feet. This is caused by entry into the stratosphere, the region where atmospheric temperature remains constant with further increase in altitude. From here up, both engine types are deprived of any favorable action the gradually reducing temperature might have given.

The decrease in temperature experienced with increasing altitude at constant rotor RPM increases the compression ratio (see Figure 20) which in turn raises the jet velocity slightly. However, there is a decrease in airflow (W_a) even though the referred airflow has increased. The airflow effect is greater than the velocity effect; therefore, the result is a decrease in thrust with increase in altitude. On a split rotor jet engine, the thrust decrease is less because of the low pressure rotor speed increase due to the resulting decrease in back-pressure.

Effect of RPM

Up to this point these factors affecting thrust have dealt only with the varying physical properties of air and their respective effects on thrust output. Rotor speed or RPM is a mechanical factor, but its variation has the greatest effect of all on thrust.

The input of heat energy to accomplish the required amount of work upon the air mass is controlled by the fuel control system. The variation in airflow upon which the work is to be done is controlled by the engine's RPM. Since the thrust variation will be a function of both fuel flow and airflow variation, it becomes the job of the fuel control system to control both fuel flow and RPM. As a result, in order to increase thrust, the fuel control system must increase both fuel flow and RPM in such proportions as to neither overheat nor overspeed the engine.

The variation of airflow and thrust with change in RPM is shown in Figure 61. Except for small compressibility effects, W_a varies linearly with RPM in the same way as C_L varies with α, since each compressor blade is just a lifting

airfoil. However, thrust is influenced by pressure level, temperature, fuel flow, and RPM. Through the fuel control unit, these variables are inter-related. Therefore, the variation of thrust with RPM is a complex functional relationship.

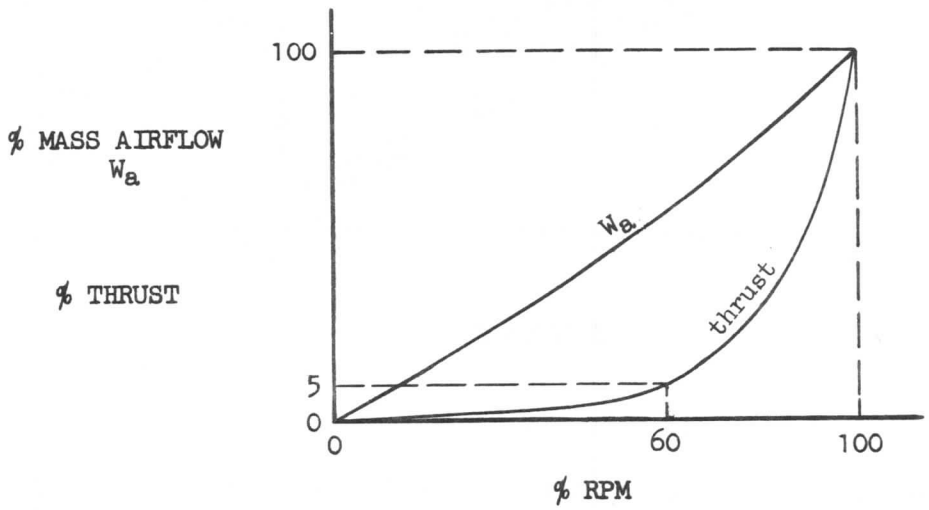

Figure 61

2-12 ENGINE CALIBRATION

In order to establish the thrust output of any turbojet or turbofan engine in flight and on the ground when installed on a jet airplane, it is essential to know the engine gross thrust. The engine manufacturer calibrates the bare engine for performance and furnishes this information to the airplane manufacturer. The airplane manufacturer assumes responsibility for developing the incremental performance loss caused by the production installation hardware on the engine. In the case of a turbojet engine, the thrust is produced by flow through a single primary nozzle. In the case of a turbofan engine, the thrust is produced by exhaust flow through both a fan nozzle and a primary (hot) nozzle. Thrust is calculated from the measured nozzle exit areas, the nozzle pressure ratios, and the nozzle gross thrust coefficients, as given by the following formula:

$$F_g = Cg\ \psi\ A\ p_{am} \qquad (40)$$

where,

Cg = gross thrust coefficient, dimensionless

ψ = theoretical gross thrust function, dimensionless

A = discharge area of nozzle, $ft.^2$

p_{am} = ambient pressure, $lbs/ft.^2$

The gross thrust coefficients of the production nozzles may be developed on the basis of full-scale ground-test-rig engine data and scale-model-test data.

Development of Theoretical Gross Thrust Function, ψ, for a Convergent Nozzle

In the development of the theoretical gross thrust function for a convergent nozzle, assume gas flow from a nozzle into a discharge section as shown in Figure 62.

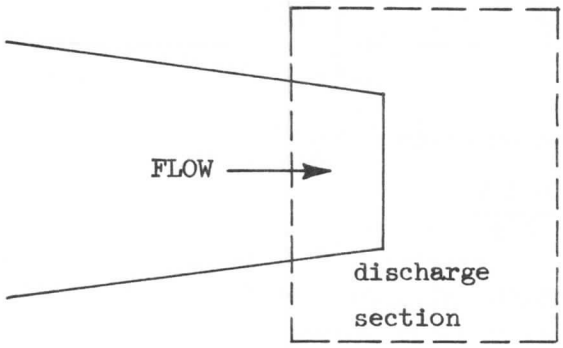

Figure 62.

Let

A = discharge area of nozzle, ft^2

p_t = total pressure at discharge area, lbs/ft^2

p = static pressure at discharge area, lbs/ft^2

p_{am} = ambient pressure, lbs/ft^2

W_g = gas flow, lbs/sec

V = discharge velocity, ft/sec

T_t = total temperature at discharge area, °R

T = static temperature at discharge area, °R

M = Mach number of gas at discharge

From the basic momentum relationship, the gross thrust,

$$F_g = \frac{W_g V}{g} + A (p - p_{am}) \qquad (41)$$

From the continuity relationship,

$$W_g = g \rho A V \qquad (42)$$

From the perfect gas law,

$$p = \rho g R T \qquad (43)$$

From the definition of Mach number,

$$M = \frac{V}{\sqrt{\gamma g R T}} \qquad (44)$$

From the isentropic relationship,

$$\frac{p_t}{p} = \left(1 + \frac{\gamma - 1}{2} M^2\right)^{\frac{\gamma}{\gamma - 1}} \qquad (45)$$

Combining equation (42) and equation (43),

$$W_g = \frac{p A V}{R T}$$

and substituting into equation (41), results in

$$F_g = \frac{p A V^2}{g R T} + A(p - p_{am}) \qquad (46)$$

Combining equations (44) and (45),

$$M^2 = \frac{V^2}{\gamma g R T} = \left[\left(\frac{p_t}{p}\right)^{\frac{\gamma - 1}{\gamma}} - 1\right] \frac{2}{\gamma - 1}$$

Substituting V^2 from the resulting equation into equation (46) gives

$$F_g = \frac{p A \gamma g R T}{g R T}\left[\left(\frac{p_t}{p}\right)^{\frac{\gamma - 1}{\gamma}} - 1\right] \frac{2}{\gamma - 1} + A(p - p_{am})$$

which when multiplied by p_{am}/p_{am} results in

$$F_g = p_{am} \frac{p}{p_{am}} A \gamma \left[\left(\frac{p_t}{p}\right)^{\frac{\gamma - 1}{\gamma}} - 1\right] \frac{2}{\gamma - 1} + p_{am} A \left(\frac{p}{p_{am}} - 1\right)$$

Factoring out $p_{am} A$

$$F_g = p_{am} A \left\{ \frac{p}{p_{am}} \left[\left(\frac{p_t}{p}\right)^{\frac{\gamma - 1}{\gamma}} - 1\right] \frac{2\gamma}{\gamma - 1} + \frac{p}{p_{am}} - 1 \right\}$$

Substituting $\frac{p_t/p_{am}}{p_t/p}$ for p/p_{am} and factoring,

$$F_g = p_{am} A \left[\frac{p_t/p_{am}}{p_t/p} \left\{ \frac{2\gamma}{\gamma - 1} \left[\left(\frac{p_t}{p}\right)^{\frac{\gamma - 1}{\gamma}} - 1\right] + 1 \right\} - 1 \right]$$

Therefore,

$$F_g = p_{am} A \psi \qquad (47)$$

where,

$$\psi = \frac{p_t/p_{am}}{p_t/p}\left\{\frac{2\gamma}{\gamma-1}\left[\left(\frac{p_t}{p}\right)^{\frac{\gamma-1}{\gamma}} - 1\right] + 1\right\}^{-1} \quad \text{(48)}$$

This gross thrust function, ψ, is shown in Figure 63.

If p_t/p_{am} is below the critical pressure ratio, i.e., the nozzle is unchoked, it is assumed that

$$p_t/p = p_t/p_{am}$$

Therefore,

$$\psi_{unchoked} = \frac{2\gamma}{\gamma-1}\left[\left(\frac{p_t}{p_{am}}\right)^{\frac{\gamma-1}{\gamma}} - 1\right]$$

If p_t/p_{am} is above the critical pressure ratio, the jet velocity at the nozzle throat is sonic (M = 1.0) and p_t/p equals the critical pressure ratio.

$$\frac{p_t}{p} = \left[1 + \frac{\gamma-1}{2} M^2\right]^{\frac{\gamma}{\gamma-1}} = \left(\frac{\gamma+1}{2}\right)^{\frac{\gamma}{\gamma-1}}$$

and,

$$\psi_{choked} = 2\,\frac{p_t}{p_{am}}\left(\frac{2}{\gamma+1}\right)^{\frac{1}{\gamma-1}} - 1$$

Note that since the pressure-area term is included in the definition from which ψ is derived, gross thrust calculated with ψ choked includes expansion to supersonic speed behind the exhaust nozzle throat.

Equation (47) shows that the engine manufacturer's method of thrust determination is based on determining the theoretical gross thrust of the jet nozzle from nozzle throat area, A, and nozzle throat pressure ratio, p_t/p_{am}, measurement. This theoretical gross thrust is then corrected to an actual gross thrust value by applying a gross thrust correction factor, C_g. This factor therefore represents the ratio of F_g (measured)/F_g (theoretical) at any given nozzle pressure ratio for a particular nozzle configuration. C_g corrects the theoretical thrust for such errors as the assumption that the flow is completely isentropic, that p is equal to p_{am} for the unchoked case, and nozzle losses.

Since ψ is a function of p_t/p_{am}, p_t/p and γ only, and since p_{am} is independent of a particular nozzle configuration, the only two parameters that influence the gross thrust of a nozzle are C_g, and A, the area of the nozzle throat at a particular exhaust gas temperature.

The area term, A, in equation (47) will vary for changes in exhaust gas temperatures; therefore, it is necessary to evaluate the effect of temperature on the nozzle metal. The exhaust gas temperatures which influence metal temperatures, and the thermal coefficient of expansion of the nozzle metal are used to develop a relationship of A_{hot}/A_{cold} versus exhaust gas temperature. This relationship is shown in Figure 64.

The ratio of specific heats, γ, also varies with temperature. The laws of thermodynamics show that the difference between the specific heats at constant pressure,

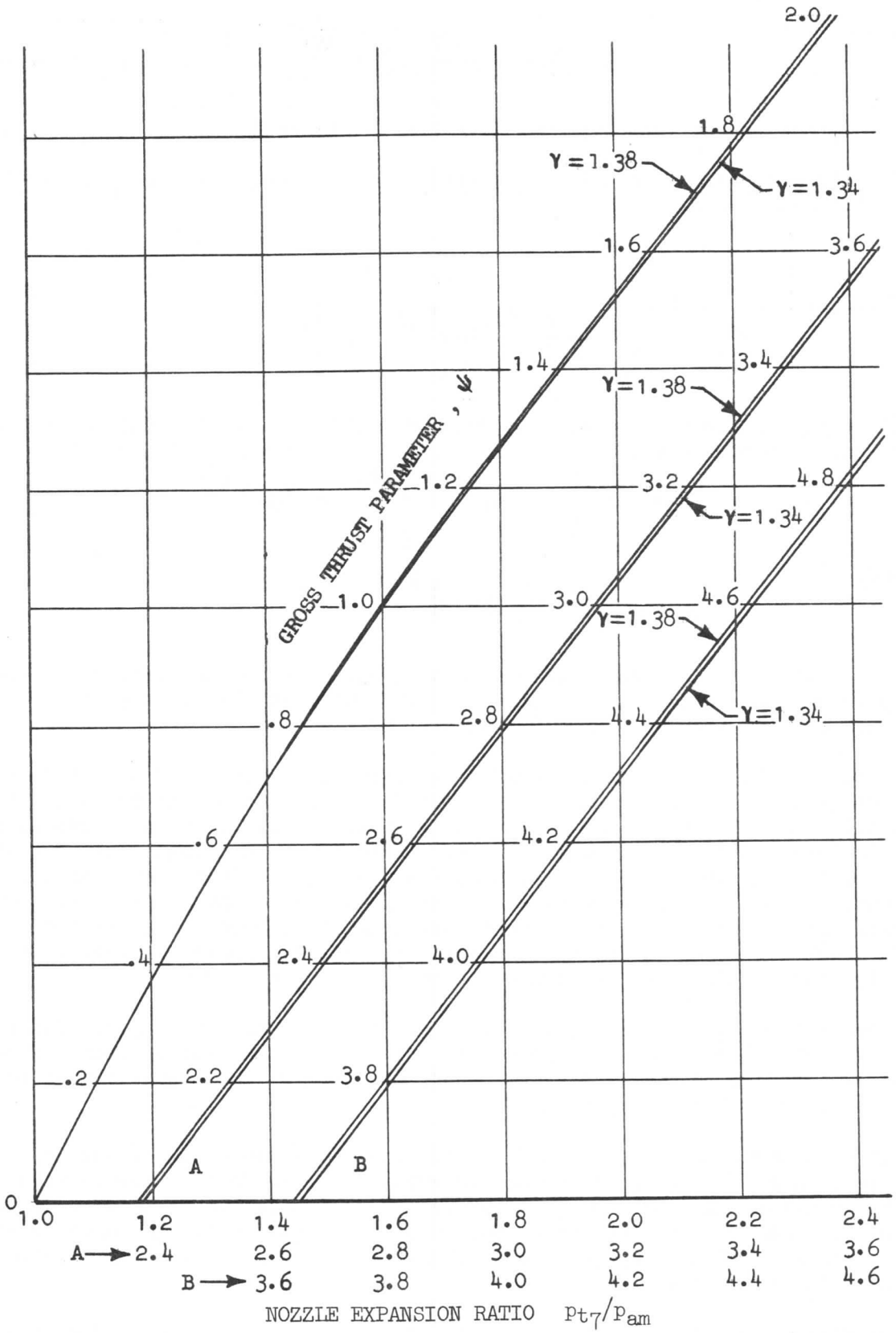
GROSS THRUST PARAMETER, $\frac{F_g}{P_{am}}$
2.0
1.8
1.6
1.4
1.2
1.0
.8
.6
.4
.2
0
Y = 1.38
Y = 1.34
3.6
3.4
3.2
3.0
2.8
2.6
2.4
2.2
4.8
4.6
4.4
4.2
4.0
3.8
A
B
1.0
1.2
1.4
1.6
1.8
2.0
2.2
2.4
A → 2.4
2.6
2.8
3.0
3.2
3.4
3.6
B → 3.6
3.8
4.0
4.2
4.4
4.6
NOZZLE EXPANSION RATIO P_{t_7}/P_{am}

Figure 63.

C_p, and constant volume, C_v, remains constant. Since this is so, it is evident that their ratio, γ , must change, decreasing in magnitude as temperature increases. This variation in γ is shown in Figure 65.

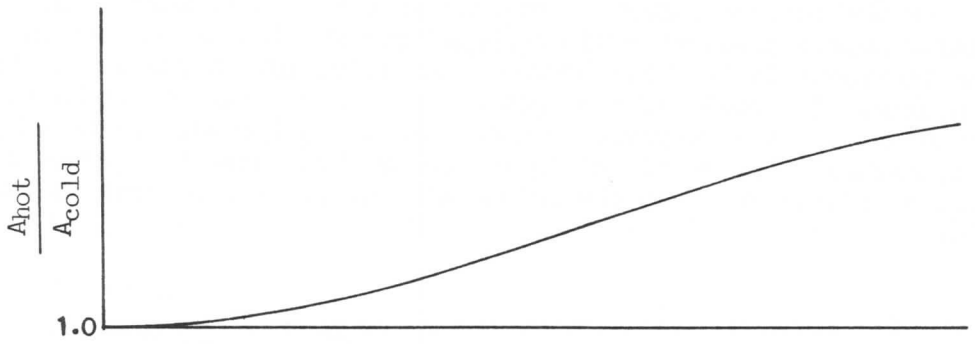

Figure 64.

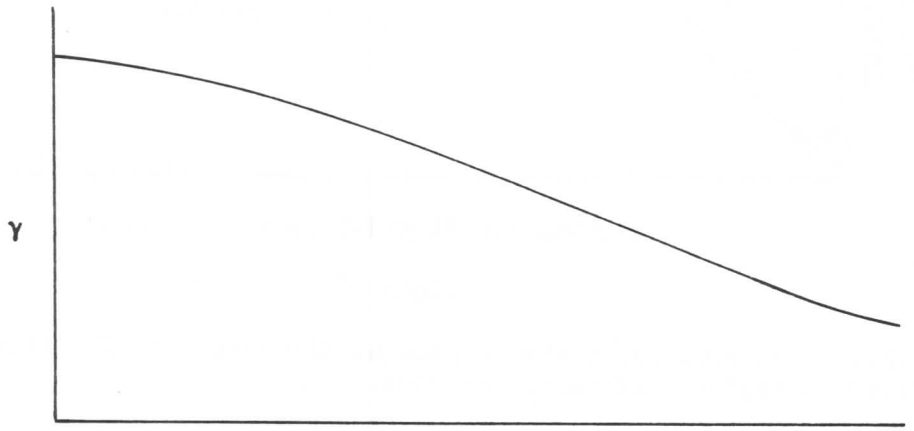

Figure 65.

Method of Analysis for Turbojet Engines

To develop the gross thrust coefficient for the production nozzles used by the airplane manufacturer on the turbojet engines, the procedure is as follows:

(1) A calibration run is made with bellmouth inlet and standard exhaust nozzle, as designed by the engine manufacturer for reference purposes, to serve as a base run.

(2) A second run is made with the bellmouth inlet and with the production nozzle (thrust reverser/noise suppressor) exhaust configuration. Comparison of data from this run with that from run (1) gives the effect of the production nozzle on engine performance.

(3) A third run is made with a production flight inlet and production exhaust nozzle. Comparison of data from this run with run (2) gives the effect of the production flight inlet.

For run (1) C_g is calculated as the ratio of the measured thrust on the test stand to the theoretical thrust as calculated from the standard nozzle area and the measured nozzle pressure ratio p_t/p_{am}. For run (2) the method used is to obtain an increment in C_g value between the production nozzle and the standard exhaust nozzle. The ratio of the production nozzle actual C_g value to the reference standard C_g value represents the ratio of C_g (production nozzle)/ C_g (standard nozzle). The ratios of C_g values are then used to correct the reference standard nozzle curve to the production configuration curve as shown in Figure 66.

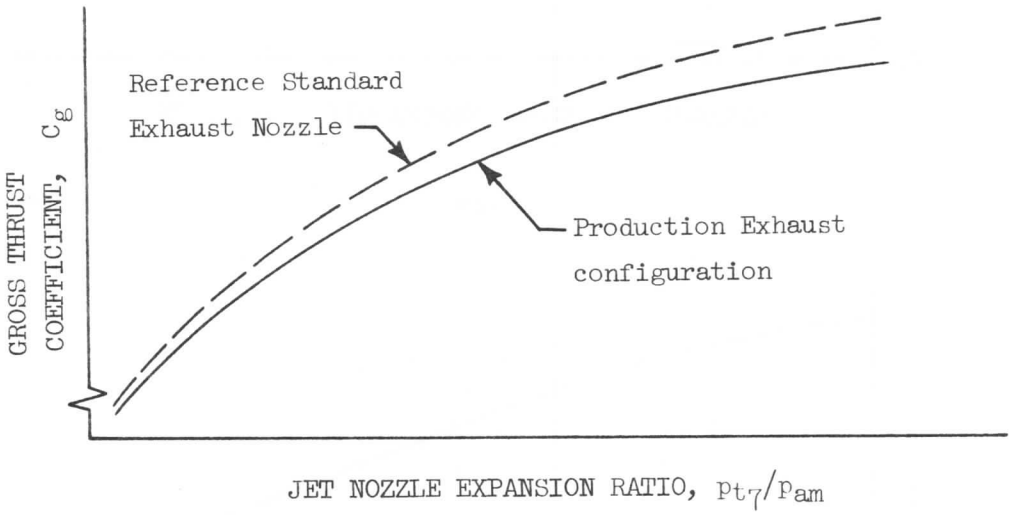

Figure 66.

Run (3) will be covered later when a general discussion of flight inlet installation effects on engine performance is made.

Method of Analysis for Turbofan Engines (Dual Exhaust)

In order to develop the gross thrust coefficients for the production nozzles used by the airplane manufacturer on the turbofan engines, it is necessary to determine the following:

(1) A method of isolating the individual gross thrusts of the fan and primary nozzles, so that one reference primary nozzle and the thrust-measuring test rig can define both fan and primary exhaust flows.

(2) A method of correlating the airplane manufacturer's measured test-rig thrust with the engine manufacturer's test-rig thrust, since it is necessary to establish absolute thrust level as well as thrust increment.

To solve item 1, the engine manufacturer designs a duct system which isolates the fan thrust from the primary, and then he develops a gross thrust coefficient for a standard primary nozzle. This is plotted against nozzle pressure ratio. The thrust of such a nozzle is defined and calculable when the nozzle pressure

ratio is known. The airplane manufacturer constructs the standard nozzle according to engine manufacturer's specifications, and this nozzle becomes the primary reference nozzle for measuring primary flow.

To solve item 2, it becomes necessary for the airplane manufacturer to run engine manufacturer's hardware on an engine which has also been calibrated on the engine manufacturer's test rig. A comparison of the two thrust readings produces a calibration curve for the airplane manufacturer's test rig.

With the ability to separate thrust developed, the airplane manufacturer runs an engine with both reference fan and primary exhaust nozzles. Since the primary thrust is calculable from the calibrated reference primary nozzle and total thrust can be corrected by the rig calibration, subtracting this primary thrust from the total thrust produces the fan reference duct thrust. With the fan reference thrust defined, the primary standard nozzle is now replaced by various airplane manufacturer's production exhaust nozzle systems. Subtraction of the reference-duct thrust from the total gross thrust produces the primary gross thrust and makes the primary gross thrust coefficient calculable. The fan reference-duct is now replaced by the production fan exhaust configuration and the total thrust measured. Since the primary thrust is known, production fan thrust can be obtained by subtraction.

A plot of primary gross thrust coefficient, C_g, versus primary nozzle pressure ratio, P_{t7}/P_{am}, can now be made for the production nozzles. See Figure 66.

The fan gross thrust coefficient is handled in a slightly different manner. Since the engine side cowling and primary reverser sleeve produce the surface over which the fan exhaust air flows, they may be considered a part of the fan nozzle flow path and as a result produce a "scrubbing" drag which reduces the fan gross thrust. Since the drag produced by the "scrubbing" is primarily a function of fan nozzle pressure ratio rather than airplane Mach number, this loss can be included in the fan nozzle performance as a power-package installation loss. Therefore, when considering fan nozzle performance with the scrubbing drag included as an installation loss, a new fan nozzle gross thrust coefficient will be introduced. This coefficient is called "fan nozzle gross thrust factor, C_f" and will indicate fan nozzle installed performance to distinguish it from the engine-manufacturer's coefficient, which does not include the scrubbing loss. The fan nozzle gross thrust factor appears as Figure 67 when plotted versus fan nozzle pressure ratio, $P_{t2.5}/P_{am}$.

Method of Analysis for Ducted-Fan or By-Pass Engines (Single Exhaust)

The method of computing in-flight thrust for long-ducted turbofan engines, where the primary gas flow and the by-pass airstream exhaust through a common exhaust nozzle, will be somewhat different than that for a turbojet engine. The main difference is not in the basic thrust equation, equation (40), nor in the testing procedure, but in the method of expressing the parameters used in the thrust equation.

Since the primary and by-pass streams are mixed before exhausting through the nozzle, it is necessary to define a "mixed-flow" parameter to use in determining the gross thrust. It is not practical to instrument the nozzle far enough aft to secure true mixed-flow conditions, so total pressure is measured at station 7 in both primary and by-pass ducts. Then a mixed total pressure value is

determined empirically in terms of the two readings:

$$p_{t_{M7}} = \frac{p_{t_7} + 0.8\, p_{t_{f7}}}{1.8} \qquad (49)$$

Inserting this value into equation (48) yields,

$$\psi = \frac{p_{t_{M7}}/p_{am}}{p_{t_{M7}}/p_{s_{M7}}} \left\{ \frac{2\gamma}{\gamma - 1} \left[\left(\frac{p_{t_{M7}}}{p_{s_{M7}}} \right)^{\frac{\gamma - 1}{\gamma}} - 1 \right] + 1 \right\} - 1 \qquad (50)$$

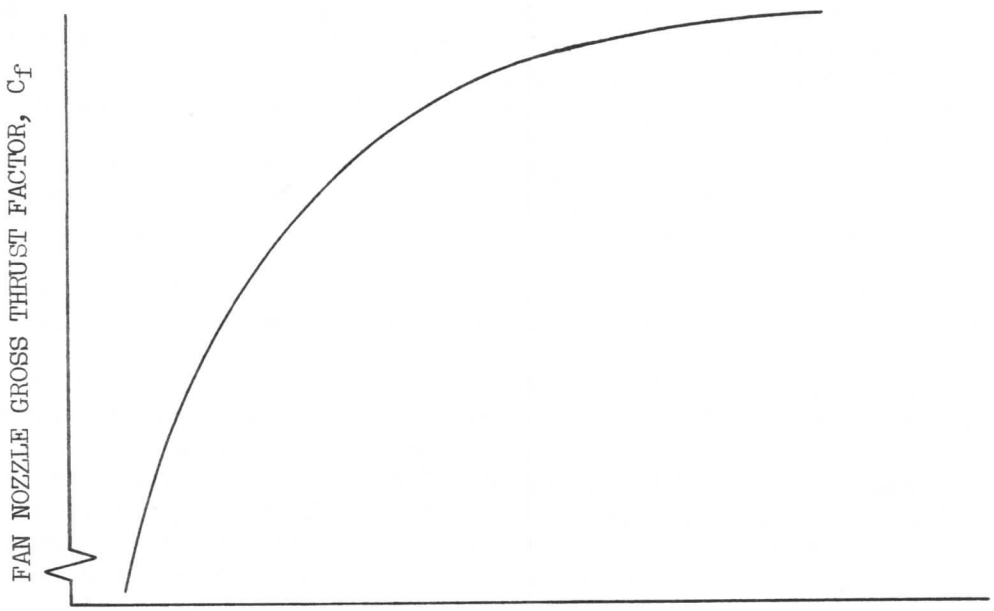

Figure 67.

The determination of γ is handled differently for engines with mixed exhaust gas flow. Since it is difficult to measure total pressure under mixed flow conditions, it is equally hard to measure total temperature under mixed flow conditions. The total temperature at the exhaust nozzle will be a function of the ram air temperature at the flight inlet, the total airflow, and the amount of fuel burned. The total airflow and fuel flow determine an overall fuel-air ratio; therefore, a plot of γ versus fuel-air ratio for constant ram air temperatures can be drawn. See Figure 68.

C_g may now be determined from the measured thrust and plotted as shown in Figure 69.

Effect of Flight Inlet Installation on Performance

The effect of the flight inlet on engine performance is to reduce the total pressure at the engine face, p_{t_2}, thereby reducing the absolute pressure level throughout the engine. This brings about a reduced p_{t_7}, so that while the engine feels

the same power level of operation or engine pressure ratio, P_{t7}/P_{t2}, there is a reduction in thrust due to a lower nozzle pressure ratio, P_{t7}/P_{am}.

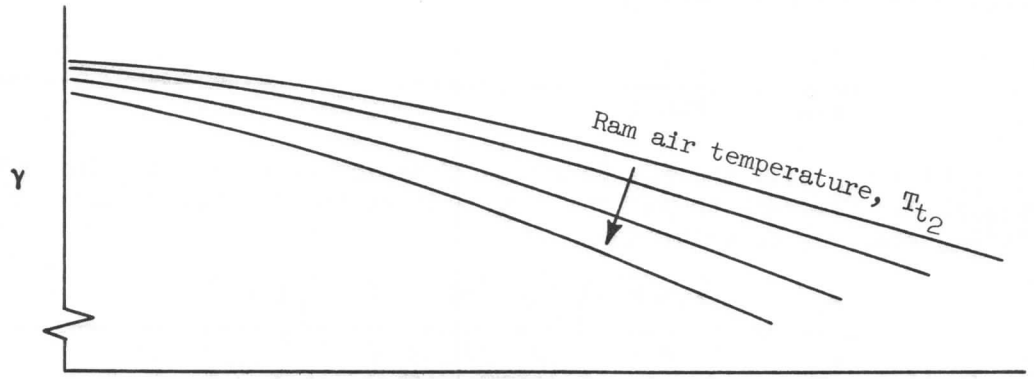

Figure 68.

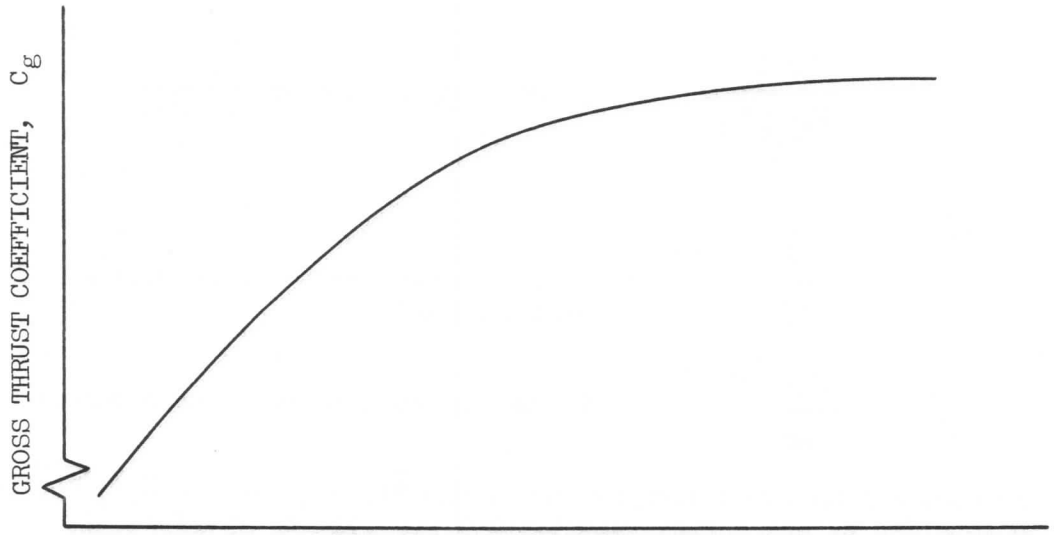

Figure 69.

This portion of the engine calibration test is conducted after the effects of the production exhaust nozzle have been established with the bellmouth inlet. It is run with the engine in production configuration, with production flight inlet and production exhaust nozzle.

The flight inlet affects the ram drag, F_r, of the engine and is a factor in determining the internal power level necessary to produce the desired net thrust output. It was learned from equation (16) that the ram drag is the free stream momentum of air entering the compressor inlet per second.

$$F_r = \frac{W_a V}{g}$$

It was also learned that for comparison purposes, it is convenient to refer thrust or drag parameters to sea level standard day conditions by correcting for prevailing conditions; therefore, ram drag may be written as

$$\frac{F_r}{\delta_{am}} = \frac{W_a\, V}{\delta_{am}\, g} \qquad (51)$$

Equation (51) shows that the ram drag is a function of engine airflow and airplane velocity. However, to put ram drag into convenient parameters for measurement, F_r/δ_{am} also can be written as

$$\frac{F_r}{\delta_{am}} = \left(\frac{W_a\sqrt{\theta_{t2}}}{\delta_{t2}}\right)\left(\frac{F_r/\delta_{t2}}{\frac{W_a\sqrt{\theta_{t2}}}{\delta_{t2}}}\right)\left(\frac{p_{t2}}{p_{t1}}\right)\left(\frac{p_{t1}}{p_{am}}\right) \qquad (52)$$

where,

$\frac{W_a\sqrt{\theta_{t2}}}{\delta_{t2}}$ is corrected engine airflow, lbs/sec

$\frac{F_r/\delta_{t2}}{\frac{W_a\sqrt{\theta_{t2}}}{\delta_{t2}}}$ is ram drag parameter, $\frac{\text{lbs}}{\text{lbs/sec}}$

$\frac{p_{t_2}}{p_{t_1}}$ is inlet pressure recovery ratio, dimensionless

$\frac{p_{t_1}}{p_{am}}$ is ram pressure ratio, dimensionless

The corrected engine total airflow curve, $W_a\sqrt{\theta_{t2}}/\delta_{t2}$ versus $N_1/\sqrt{\theta_{t2}}$ (Figure 10), is supplied by the engine manufacturer and can be used for flight conditions since it is assumed that the inlet distribution is equivalent to static bellmouth distribution.

The inlet pressure recovery information used to correct for this assumption is obtained from flight test data and appears as shown in Figure 70.

The ram drag parameter is a function of Mach number which can be derived as follows:

From the definition of Mach number,

$$M = \frac{V}{\sqrt{\gamma\, g\, R\, T}}$$

The ram drag parameter can be written as,

$$\frac{F_r/\delta_{t2}}{\frac{W_a\sqrt{\theta_{t2}}}{\delta_{t2}}} = \frac{F_r}{W_a\sqrt{\theta_{t2}}} = \frac{W_a\, V}{g\, W_a\sqrt{\frac{T_{t2}}{T_o}}}$$

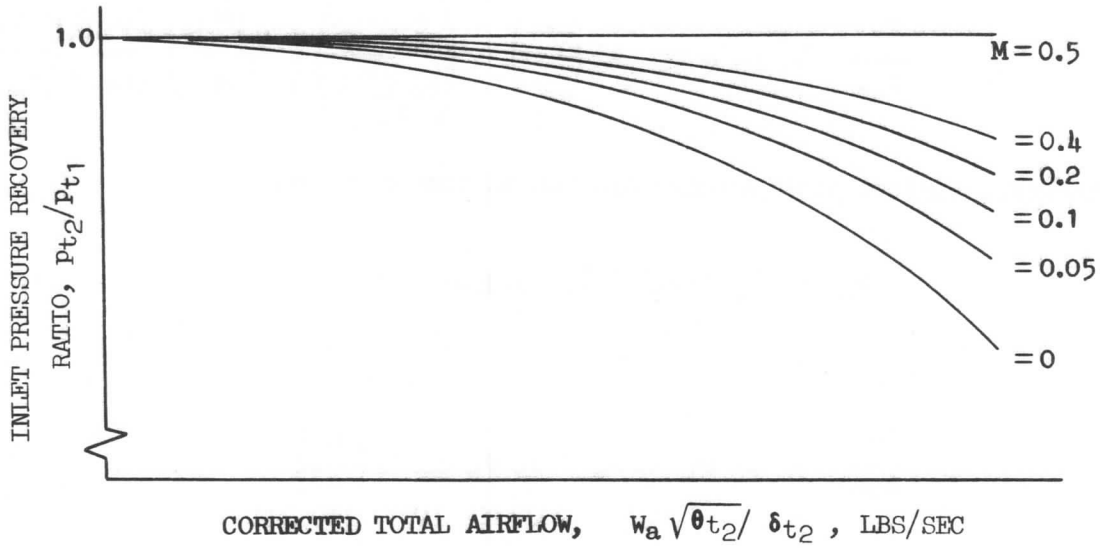

Figure 70.

$$\frac{F_r/\delta_{t_2}}{\frac{W_a\sqrt{\theta_{t_2}}}{\delta_{t_2}}} = \frac{M\sqrt{\gamma g R T}}{g\sqrt{\frac{T_{t_2}}{T_o}}}$$

$$= \sqrt{\frac{T_o \gamma R}{g}} \; \frac{M}{\sqrt{\frac{T_{t_2}}{T}}}$$

$$\frac{F_r/\delta_{t_2}}{\frac{W_a\sqrt{\theta_{t_2}}}{\delta_{t_2}}} = \frac{a_o}{g} \; \frac{M}{\sqrt{1 + \frac{\gamma - 1}{2} M^2}} \qquad (53)$$

Equation (53) may be plotted as shown in Figure 71.

The ram pressure recovery, P_{t_1}/P_{am}, is also a function of Mach number and can be determined from equation (45).

$$\frac{P_{t_1}}{P_{am}} = \left(1 + \frac{\gamma - 1}{2} M^2\right)^{\frac{\gamma}{\gamma - 1}}$$

Since the net thrust equals the gross thrust minus the ram drag, the net thrust equations for the various engines can be determined by combining equation (52) and equation (40). For single exhaust turbojet, ducted-fan, and by-pass engines,

$$F_n = F_g - F_r$$

or,

$$\frac{F_n}{\delta_{am}} = p_o \psi C_g A_c \left(\frac{A_h}{A_c}\right) - \left(\frac{F_r/\delta_{t2}}{\frac{W_a\sqrt{\theta_{t2}}}{\delta_{t2}}}\right)\left(\frac{W_a\sqrt{\theta_{t2}}}{\delta_{t2}}\right)\left(\frac{p_{t2}}{p_{t1}}\right)\left(\frac{p_{t1}}{p_{am}}\right) \quad (54)$$

For turbofan engines with primary and fan exhaust nozzles,

$$F_n = F_g\,(\text{fan}) + F_g\,(\text{primary}) - F_r$$

or,

$$\frac{F_n}{\delta_{am}} = p_o \psi_f C_f A_f + p_o \psi_p C_g A_c \left(\frac{A_h}{A_c}\right) - \left(\frac{F_r/\delta_{t2}}{\frac{W_a\sqrt{\theta_{t2}}}{\delta_{t2}}}\right)\left(\frac{W_a\sqrt{\theta_{t2}}}{\delta_{t2}}\right)\left(\frac{p_{t2}}{p_{t1}}\right)\left(\frac{p_{t1}}{p_{am}}\right) \quad (55)$$

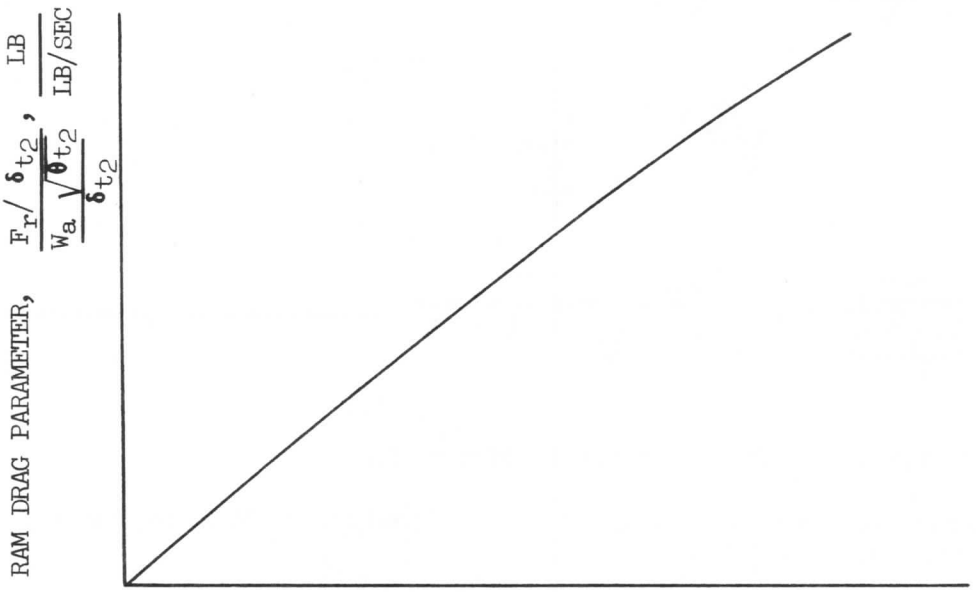

Figure 71.

Note in equation (55) that there is no A_h/A_c ratio for the fan nozzle. It is usually established by testing that the effect of fan nozzle exhaust air temperature and pressure on the exit area is negligible; therefore, only the cold measured fan area is used in the calculations.

The above engine calibration analysis results in the installed engine performance data shown in Figure 72.

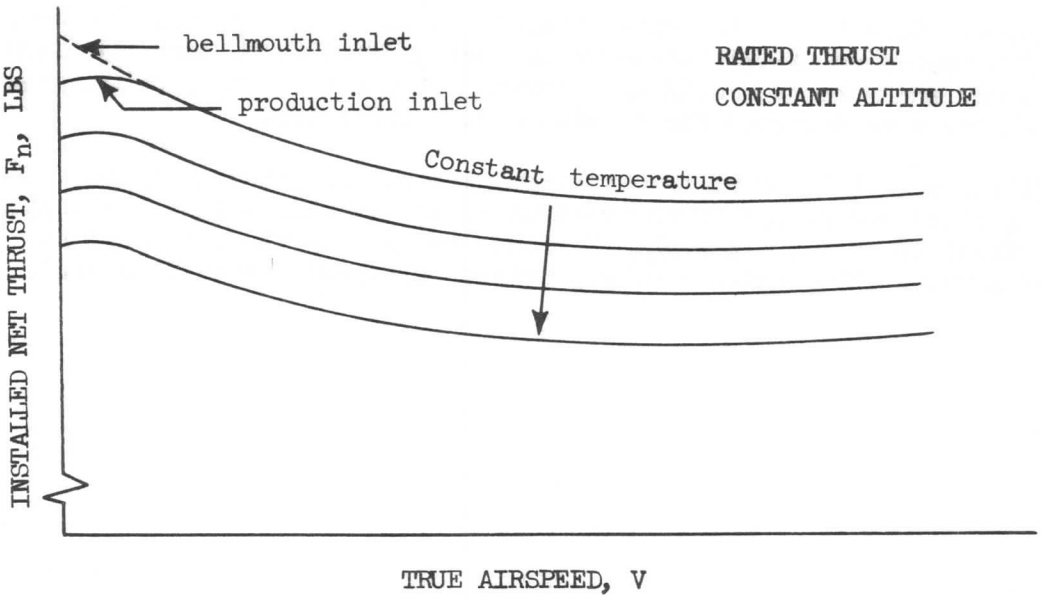

Figure 72.

2-13 ENGINE TRIM AND SPEED BIAS

The decision to rate an engine in terms of thrust introduces a necessity to allow for differences in RPM to compensate for slight thrust differences between engines due to manufacturing tolerances. The fuel control unit can be adjusted within specified limits to vary the RPM and thrust. The RPM which gives the specified rated thrust output under standard-day sea-level static operation is known as "engine trim speed." This speed is determined for each engine by actual operation in the manufacturer's test stand and is stamped on the engine data plate in both RPM and % RPM. The process of adjusting the fuel control is called "engine trimming."

Although some engines are trimmed at full throttle, most commercial engines are trimmed at "part-power" or part-throttle for field adjustment to compensate for deterioration with age or change in control components. A removable stop is inserted or attached to the fuel-control throttle and the fuel flow adjusted to the rated thrust output as indicated by the EPR or p_{t7} corrected to standard day conditions. The trim operation must be very carefully carried out to avoid any error in adjustment made necessary by other than true trim requirements.

Since thrust is to be measured in terms of exhaust total pressure, the engine is designed with a fixed-area exhaust duct so that every engine will operate at the same p_{t7}- or EPR-thrust relation. Since this is true, the trim relations are usually specified in terms of a trim curve of p_{t7} or EPR variation with compressor inlet temperature, T_{t2} (for various barometric pressures if P_{t7} is used) at the trim throttle setting.

The logical decision to use turbine-inlet temperature as the basic engine-operation limit permits operation to maximum available thrust for any ambient operating temperature without exceeding safe limits. However, if the turbine-inlet temperature is to be a direct function of throttle or thrust lever position, there must be provision for speed or RPM variation with engine inlet

temperature. This is called "speed bias." It is built into the fuel control unit. Constant-turbine-inlet-temperature design results in less than rated thrust on a hot day and more on a cold day; however, the variation is not as great as if the engine were designed for constant-speed operation.

Thus a fixed thrust lever or throttle position will maintain only an approximation of a fixed percentage of the maximum thrust available from the engine. Neither throttle position nor N_2 RPM should be used as the parameter for setting up rated thrust. EPR, being a direct measure of thrust, should be used.

SECTION 3

AIRPLANE PERFORMANCE

AIRPLANE PERFORMANCE

3-1 AIRSPEED MEASUREMENT

Terminology

Before undertaking the study of specialized performance problems, it will be advantageous to review velocity parameters used in aerodynamic work.

V_i is the instrument indicated airspeed which is uncorrected for position error, or equal to the pitot static airspeed indicator reading. It includes the sea level standard adiabatic compressible flow correction in the calibration of the airspeed instrument dials.

V_I is the instrument indicated airspeed corrected for instrument error only. It is abbreviated as IAS and is related to V_i by the following expression:

$$V_I = V_i + \Delta V_i \qquad (1)$$

Where ΔV_i is the instrument error correction.

V_c is calibrated airspeed and is equal to the airspeed indicator reading corrected for position and instrument error. The abbreviation for this airspeed is CAS and the equation relating V_c and V_I is:

$$V_c = V_I + \Delta V_p \qquad (2)$$

Where ΔV_p is the position error correction.

V_e is the equivalent airspeed and is equal to the airspeed indicator reading corrected for position error, instrument error, and for adiabatic compressible flow for the particular altitude. The abbreviation for this airspeed is EAS and the relationship between V_c and V_e is:

$$V_e = V_c - \Delta V_c \qquad (3)$$

Where ΔV_c is the compressibility correction.

V is true airspeed. It is related to V_e by the following:

$$V = V_e \quad 1/\sqrt{\sigma} \qquad (4)$$

Where σ is the density ratio ρ/ρ_o.

Remembering that the dynamic pressure, q, is a function of velocity:

$$q = \frac{1}{2}\rho V^2 \quad (V, \text{ in ft/sec})$$

It is permissible to manipulate the expression by multiplying the right hand member by ρ_o/ρ_o, thus:

$$q = \frac{1}{2}\rho_o \sigma V^2$$

It is found when measuring velocity in knots, the equation reduces to:

$$q = \frac{V^2\sigma}{295.37} \qquad (V, \text{ in knots}) \qquad (5)$$

Substituting equation (4) into equation (5) results in:

$$q = \frac{V_e^2}{295.37} \qquad (V_e, \text{ in knots}) \qquad (6)$$

Therefore, it can be seen that the dynamic pressure is a function of equivalent airspeed.

Pitot Static Systems

A brief discussion of the basic theory of the pitot tube in incompressible flow was made in Section 1. As was seen, the pitot tube is a direct application of the Bernoulli Equation and actually measures the difference between total air pressure and ambient, or static pressure, which is the indicated dynamic pressure, q. Equation (6) says that for incompressible flow, assuming no errors in either total or ambient pressure measurement, the pitot tube will record a pressure differential which is proportional to the square of equivalent airspeed. By a suitably calibrated instrument, equivalent airspeed may be read directly. The way in which actual airspeed instruments are calibrated is somewhat different. They are calibrated to read true airspeed at all Mach numbers under standard sea level conditions if no instrument or pressure source errors are assumed.

Obtaining airspeed from a non-perfect airspeed system and for non-standard conditions involves establishing the corrections for each potential error source and the relationship between non-standard and standard atmospheric conditions. Errors can exist in instruments, total pressure recovery, and static pressure. Instrument error can be determined in laboratory tests. Total pressure errors can result from the location of the pitot tube in a reduced energy region such as a boundary layer. For this reason pitot tubes are always supported away from the skin on short struts. Another source of total pressure error is that due to large inclinations of the pitot head relative to the stream direction.

Assuming that the above errors are known (in the case of instrument error) or can be made negligible (in the case of total head error) then the only other error source is that due to the location of the static source at a point of non-ambient static pressure. In general, it is neither possible nor practical to locate the static source at a singular point that remains at ambient static pressure for all flight conditions. The reason for this is that the ambient pressure is altered in the proximity of the airplane by the influence of the airplane. The particular part of the airplane which is most responsible for this effect is the wing. Without the wing it would be relatively easy to select a location on the fuselage somewhere aft of the nose, on a constant diameter section, similar to the static location on the pitot-static tube, discussed in Section 1. But with the wing, static pressures both ahead of and behind the wing will affect the pressures experienced on the fuselage.

To see why the static pressures near the wing will be different from remote static pressures, refer to the theory of Section 1. When considering airflow around an airfoil section, the streamlines will be found to be affected not only at the

wing but in the immediate vicinity of the wing as shown in Figure 1.

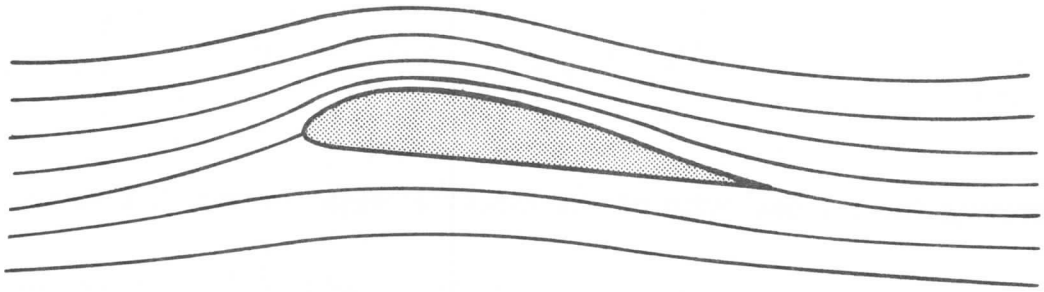

Figure 1.

Whenever the streamlines are disturbed, the static pressures will also be disturbed. Thus, the wing influence on static pressure will be extensive and difficult to escape. What must be done, then, is to find a static pressure location which not only reads close to ambient static, but also minimizes the effects of angle of attack changes, which will obviously vary the static pressure field around the wing.

In the past it was customary to locate the static source by means of extensive airspeed calibrations in flight. On the B-47 bomber, however, it was proved that considerable flight time could be saved by using wind tunnel tests to discover where the best location for the static source would be. This practice was extended to subsequent Boeing-manufactured airplanes.

An explanation of the relationship between indicated airspeed, Mach number, and true airspeed is necessary to show the effect of a static source, or "position" error. Indicated airspeed can be considered a measurement of total pressure less static pressure. As mentioned previously, if no errors or compressibility existed, then equivalent airspeed, V_e, would be measured. With position error and compressibility effects considered, however, indicated airspeed, V_I, would be measured. Thus, a given value of V_I corresponds to a given value of $p_t - p$. The altimeter is connected to the airspeed static source and its reading corresponds to the static pressure, p. Mach number is directly related to the ratio of total pressure to static pressure; therefore, a given Mach number corresponds to a singular value of p_t/p. True airspeed is obtained from Mach number and air temperature.

The expression relating the pressures to Mach number is given by equation (63) of Section I, shown below:

$$\frac{p_t}{p} = \left(1 + \frac{\gamma - 1}{2} M^2\right)^{\frac{\gamma}{\gamma - 1}}$$

Subtracting 1 from each side of the equation does not change the equality; thus:

$$\frac{p_t - p}{p} = \left[\left(1 + \frac{\gamma - 1}{2} M^2 \right)^{\frac{\gamma}{\gamma - 1}} - 1 \right] \qquad (7)$$

Substituting for γ, the ratio of the specific heats for air, the value 1.4:

$$p_t - p = p \left[\left(1 + .2M^2 \right)^{3.5} - 1 \right] \qquad (8)$$

The quantity $(1 + .2M^2)$ is the expression for the so-called "adiabatic temperature rise" due to compressibility. Under standard sea level conditions the airspeed indicator is calibrated such that:

$$V = V_e = V_c$$

The relationship between V_c and $p_t - p$ for standard sea level conditions is:

$$p_t - p = p_o \left\{ \left[1 + .2 \left(\frac{V_c}{661.5} \right)^2 \right]^{3.5} - 1 \right\} \qquad (9)$$

where p_o is the standard sea level ambient pressure. By equating equations (8) and (9), Mach number may be solved as a function of altitude and calibrated airspeed. The resulting equation is as follows:

$$M^2 = 5 \left[\left(\frac{1}{\delta} \left\{ \left[1 + .2 \left(\frac{V_c}{661.5} \right)^2 \right]^{3.5} - 1 \right\} + 1 \right)^{\frac{1}{3.5}} - 1 \right] \qquad (10)$$

This equation may be plotted as true Mach number vs calibrated airspeed for constant pressure altitudes. If indicated airspeed, V_I, and indicated pressure altitude ratio, δ_I, are used in equation (10) instead of V_c and δ, then indicated Mach number will result. A plot of equation (10) is shown in Chart 1.

High Speed Position Error - Mach Number

The procedure by which the errors in the pitot-static system are discovered is called airspeed calibration. The technique involves simply flying an airplane under all speed and altitude conditions in company with an accurately calibrated "pacer" airplane. By flying both airplanes together under stabilized speed conditions, the indicated readings of Mach number, airspeed, and altitude are recorded for both airplanes. The indicated readings from the pacer airplane are first reduced to true values, since the calibrations for the pacer are known. The difference between the true Mach number values and the test airplane indicated values represents the Mach position error, ΔM_p. The expression for true

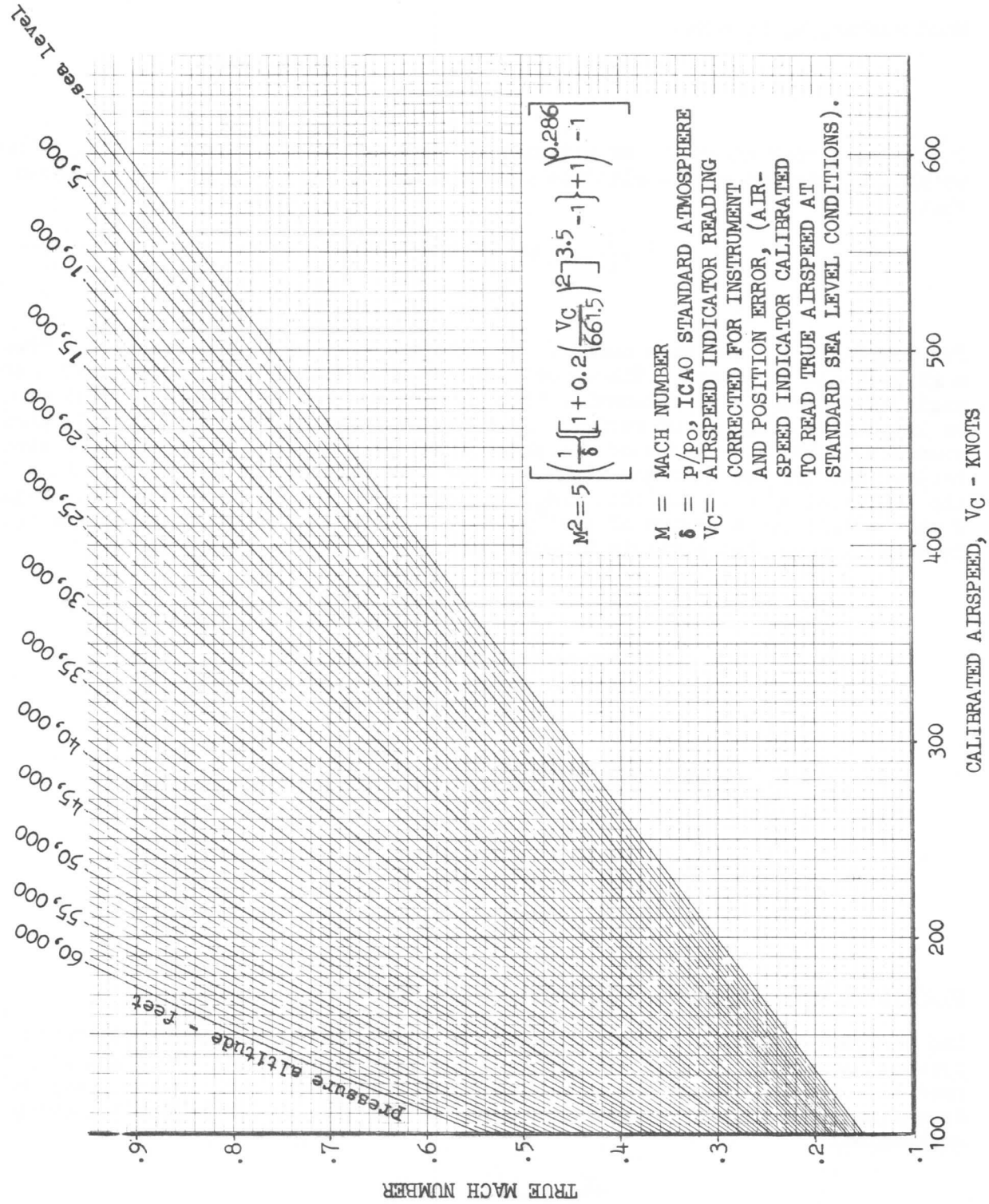
Sea Level
5,000
10,000
15,000
20,000
25,000
30,000
35,000
40,000
45,000
50,000
55,000
60,000
Pressure altitude - Feet
.6
.7
.8
.9
TRUE MACH NUMBER
.1
.2
.3
.4
.5
100
200
300
400
500
600
CALIBRATED AIRSPEED, Vc - KNOTS
$M^2 = 5\left[\left(\frac{1}{\delta}\left[1+0.2\left(\frac{Vc}{661.5}\right)^2\right]^{3.5}-1\right)+1\right)^{0.286}-1\right]$
M = MACH NUMBER
δ = P/Po, ICAO STANDARD ATMOSPHERE
Vc = AIRSPEED INDICATOR READING CORRECTED FOR INSTRUMENT AND POSITION ERROR, (AIR-SPEED INDICATOR CALIBRATED TO READ TRUE AIRSPEED AT STANDARD SEA LEVEL CONDITIONS).

Chart 1.

Mach number, M, is thus:

$$M = M_I + \Delta M_p \qquad (11)$$

It is found convenient in jet performance work to use the parameter of airplane weight, W, divided by the altitude pressure ratio, δ. It will be remembered that:

$$\frac{W}{\delta} = 1481.4 C_L M^2 S \qquad (12)$$

For a given W/δ and Mach number, the airplane will be at a given C_L and thus at a given angle of attack. Since position error is basically associated with wing angle of attack, it is reasonable that the parameter W/δ should be used since it is indicative of angle of attack. From the observation in flight of indicated pressure altitude, a value of indicated δ can be obtained from a standard altitude table. Knowing the airplane weight at the time will enable one to determine W/δ_I the indicated W/δ. Now that ΔM_p, M_I, and W/δ_I are known, the plot in Figure 2 can be made for a series of test points. However, in many instances the spread in data is such that a single line for all W/δ's may be drawn.

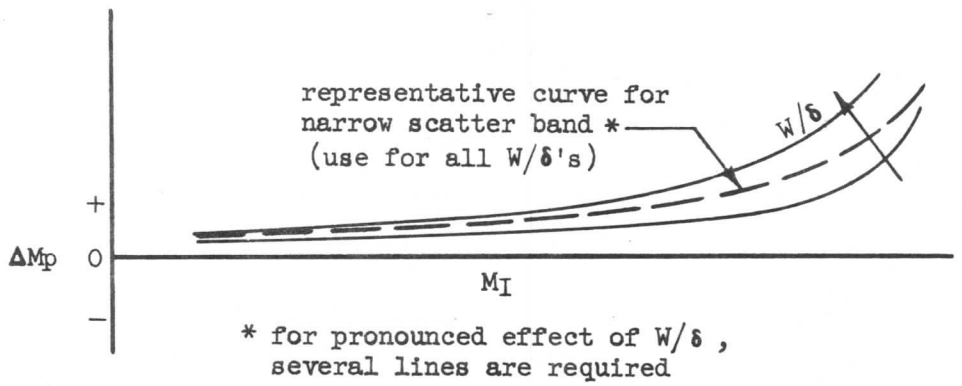

Figure 2.

High Speed Position Error - Airspeed (Flaps Up)

The airspeed indicator is connected to the static source of the pitot-static system; therefore, it will also pick up any existing position error and will thus read incorrectly. Since the Mach number position error, ΔM_p, has already been determined, the high speed position error can be evaluated from the following expression:

$$\Delta V_p = \frac{dV_c}{dM} \quad \Delta M_p$$

or:

$$\Delta V_p = \Delta M_p \Big/ \frac{dM}{dV_c} \qquad (13)$$

where dM/dV_c is the change in true Mach number divided by the corresponding change in calibrated airspeed at a constant altitude. By introducing the multiplying factor, dp/dp, the differential term dM/dV_c is the product of two other differential terms as shown:

$$\frac{dM}{dV_c} = \frac{dM}{dp}\,\frac{dp}{dV_c} \qquad (14)$$

dM/dp is evaluated from equation (63) of Section 1 and the result is:

$$\frac{dM}{dp} = -\frac{1 + .2M^2}{\gamma M p} \qquad (15)$$

The expression for dp/dV_c is derived from equation (9) and is found to be:

$$\frac{dp}{dV_c} = -\frac{\gamma p_o V_c \left[1 + .2\left(\frac{V_c}{661.5}\right)^2\right]^{2.5}}{a_o^2} \qquad (16)$$

Substituting equations (15) and (16) into equation (14), the expression for dM/dV_c can now be obtained:

$$\frac{dM}{dV_c} = \frac{(1 + .2M^2)\left[1 + .2\left(\frac{V_c}{a_o}\right)^2\right]^{2.5} V_c}{\delta\, a_o^2 M} \qquad (17)$$

A chart showing the solution of equation (17) for constant values of δ or pressure altitude and for various values of V_c can now be made, see Chart 2.

Low Speed Position Error - Airspeed

At low airspeeds, below about M = .4, where Mach number effects are small, it is convenient to modify the calculations in the following manner. The airspeed position error, ΔV_p, is determined from equation (2), repeated below.

$$V_c = V_I + \Delta V_p$$

As in the case of the Mach number position error this error could be simply plotted as ΔV_p vs V_I. However, at various airplane weights at a given V_I, different corrections would be obtained since the static pressure error is a function of angle of attack C_L, as stated before. It will then be necessary to convert V_I to some index of C_L. Consider the lift equation, assuming here that $V_I = V_e$.

$$W \approx \frac{C_L S V_I^2}{295.37}$$

$$C_L \approx \frac{295.37\,W}{S V_I^2} \qquad (18)$$

Now, for the airplane to be at the same C_L at another weight, W_S:

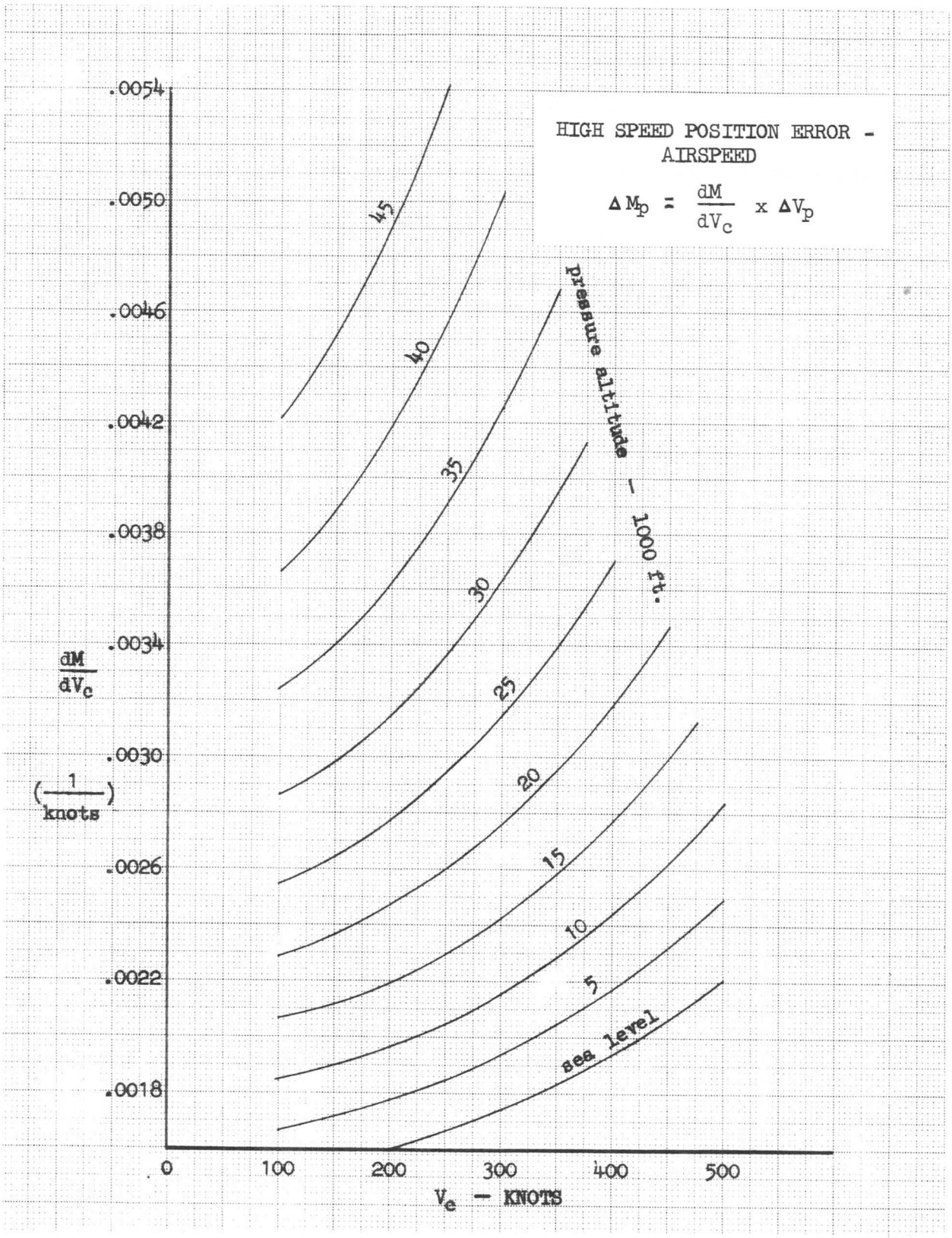
HIGH SPEED POSITION ERROR - AIRSPEED
$\Delta M_p = \frac{dM}{dV_c} \times \Delta V_p$
.0054
.0050
.0046
.0042
.0038
.0034
.0030
.0026
.0022
.0018
$\frac{dM}{dV_c}$
$(\frac{1}{knots})$
45
40
35
30
25
20
15
10
5
sea level
pressure altitude - 1000 ft.
0
100
200
300
400
500
V_e — KNOTS

Chart 2.

$$\frac{295.37\,W}{SV_I^2} = \frac{295.37\,W_S}{SV_{I_W}^2}$$

where V_{I_W} is the indicated airspeed corresponding to the weight, W_S. Solving for V_{I_W}:

$$V_{I_W} = V_I \sqrt{\frac{W_S}{W}} \qquad (19)$$

This equation is made use of in the following manner. A value is arbitrarily assigned to W_S which is within the weight range of the airplane being considered. For the Model 707 this weight is 100,000 pounds. Thus, equation (19) is:

$$V_{I_W} = V_I \sqrt{\frac{100,000}{W}} \qquad (20)$$

Equation (20) now says that for an airplane weighing W pounds, and flying at V_I knots, the 100,000 pound airplane at the same C_L will be flying at V_{I_W} knots. If the airplane were assumed to be at another weight and speed, a corresponding V_{I_W} could be calculated which would be at the same C_L as the airplane flying at the new flight condition. Therefore, V_{I_W} can be thought of as an index of C_L since it effectively changes the actual airspeed into one which corresponds to an arbitrary fixed weight.

So far V_I has been generalized into the form of V_{I_W} which is proportional to C_L. Let us now discuss the airspeed position error, ΔV_p. Since the static pressure error, Δp, is basically a function of angle of attack, or C_L, it would be logical to plot $\Delta p/q$ vs C_L ($\Delta p/q$ being non-dimensional) for constant values of W/δ. But, since the static pressure error determines the airspeed position error, the airspeed position error must be generalized into the form of $\Delta p/q$ so as to make a plot comparable to $\Delta p/q$ vs C_L. To develop the alternate form of $\Delta p/q$, consider that the pressure error, Δp, is caused by the local velocity at the static port, V_I, being different from the remote velocity, V_c. This difference is of course the position error, ΔV_p.

$$\Delta p = \frac{1}{2}\rho_o V_c^2 - \frac{1}{2}\rho_o V_I^2$$

$$q = \frac{1}{2}\rho_o V_c^2$$

Thus,

$$\frac{\Delta p}{q} = \frac{\frac{1}{2}\rho_o V_c^2 - \frac{1}{2}\rho_o V_I^2}{\frac{1}{2}\rho_o V_c^2}$$

$$\frac{\Delta p}{q} = \frac{V_c^2 - V_I^2}{V_c^2}$$

Substituting for V_c in the above equation from equation (2), results in:

$$\frac{\Delta p}{q} = \frac{V_I^2 + 2V_I\,\Delta V_p + \Delta V_p^2 - V_I^2}{V_I^2 + 2V_I\,\Delta V_p + \Delta V_p^2}$$

Since ΔV_p is small, ΔV_p^2 is very small and may be considered negligible. Thus:

$$\frac{\Delta p}{q} = \frac{2V_I \ \Delta V_p}{V_I^2 + 2V_I \ \Delta V_p}$$

or,

$$\frac{\Delta p}{q} = \frac{2 \ \Delta \ V_p}{V_I + 2 \ \Delta \ V_p} \qquad (21)$$

If ΔV_p is small compared to V_I, which it should be, then it can be said that $\Delta p/q$ will vary approximately as $\Delta V_p/V_I$. This reasoning justifies the use of the parameter, $\Delta V_p/V_I$, for generalizing the low speed airspeed position error. A plot of $\Delta V_p/V_I$ vs V_{I_W} is made, Figure 3, and is faired from results of flight tests aided by previous wind tunnel tests. **Flight test data is usually obtained from "trailing" bomb instrumentation, a technique which permits the use of a known static source.**

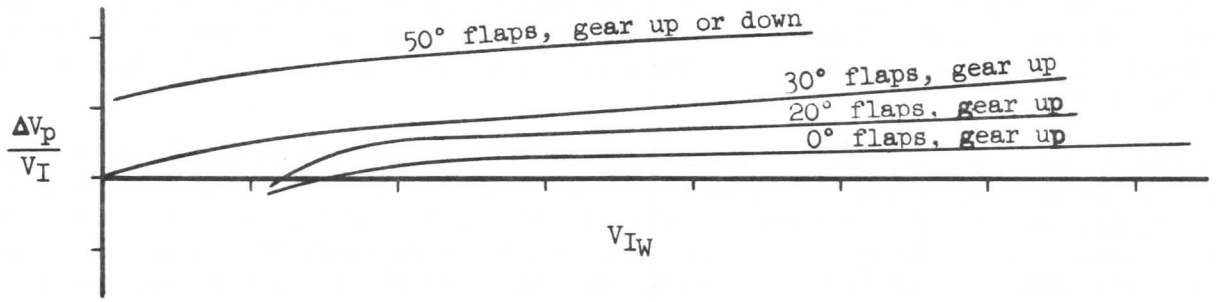

Figure 3.

When the flaps are lowered, the airplane will be found to be at a different angle of attack at a given indicated airspeed. Thus, position error will be affected by flap extension, also shown in Figure 3. Figure 3 is now valid for all gross weights when used with equation (20).

It was previously stated that the position error could be simply plotted as ΔV_p vs V_I at various airplane gross weights. Plotting this relationship yields the family of curves in Figure 4. In some instances the plot of Figure 4 can be simplified with only a small loss in accuracy by fairing a single line through the family of weight curves.

Compressibility Correction

The airspeed indicator is, as was mentioned previously, incapable of perfect velocity measurement. While it may be made to read differential pressures existing across the orifices of the pitot and static sources, it would require a different airspeed scale graduation at every pressure altitude. Consider again the compressible flow relationship, equation (7), shown here for convenience.

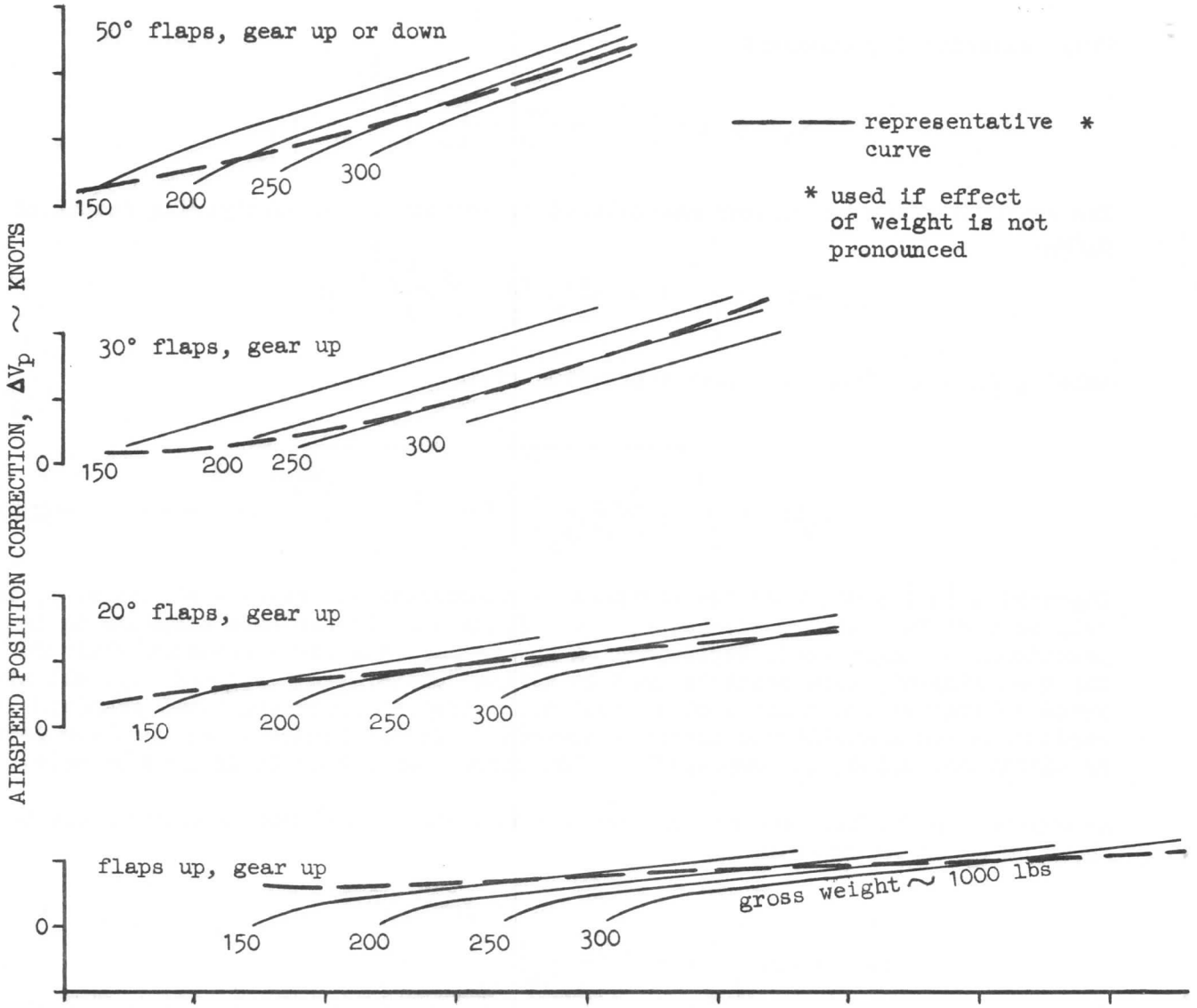

Figure 4.

$$p_t - p = p\left[\left(1 + \frac{\gamma-1}{2} M^2\right)^{\frac{\gamma}{\gamma-1}} - 1\right]$$

A substitution is made for Mach number by remembering that:

$$M = \frac{V}{a}$$

and,

$$a = \sqrt{\frac{\gamma p}{\rho}}$$

Thus, equation (7) becomes:

$$p_t - p = p\left[\left(1+\frac{\gamma-1}{2}\frac{\rho V^2}{\gamma p}\right)^{\frac{\gamma}{\gamma-1}} -1\right]$$

The expression may be further manipulated by introducing a multiplying factor of ρ_o/ρ_o:

$$p_t - p = p\left[\left(1+\frac{\gamma-1}{2\gamma}\frac{\rho_o}{p}V^2\sigma\right)^{\frac{\gamma}{\gamma-1}} -1\right]$$

Solving for $V\sqrt{\sigma}$ from the above expression gives:

$$V\sqrt{\sigma} = \sqrt{\frac{2\gamma p}{(\gamma-1)\rho_o}\left[\left(\frac{p_t - p}{p}+1\right)^{\frac{\gamma-1}{\gamma}} -1\right]} \qquad (22)$$

Expression (22) shows that the airspeed is a function of pressure altitude, p, as well as a differential pressure, $p_t - p$. Since a scale for each altitude is impractical, a single scale corresponding to standard sea level pressure altitude has been adopted; this scale is used to define "calibrated" airspeed, V_c. All airspeed indicators are calibrated to read true airspeed under sea level standard day conditions (no installation errors); therefore, for altitudes other than sea level an additional adiabatic compressible flow correction for altitude must be made.

In evaluating the Mach number position error, equation (9) was developed, and is shown here for convenience.

$$p_t - p = p_o\left\{\left[1+.2\left(\frac{V_c}{661.5}\right)^2\right]^{3.5} -1\right\}$$

This expression involves V_c which may be resolved in a similar manner; however, it is more convenient to equate expressions (7) and (9):

$$p\left\{\left[1+\frac{\gamma-1}{2\gamma}\frac{\rho_o}{p}\left(V\sqrt{\sigma}\right)^2\right]^{\frac{\gamma}{\gamma-1}} -1\right\} = p_o\left\{\left[1+.2\left(\frac{V_c}{661.5}\right)^2\right]^{3.5} -1\right\}$$

From this, $V\sqrt{\sigma}$ may be resolved and the expression reduced to:

$$V\sqrt{\sigma} = 1479\sqrt{\frac{p}{p_o}\left\{\left(\frac{\left[1+.2\,(V_c/661.5)^2\right]^{3.5}-1}{p/p_o}+1\right)^{1/3.5} -1\right\}} \qquad (23)$$

when V_c is measured in knots.

The parameter $V\sqrt{\sigma}$ is a measure of the kinetic energy of the air and is defined as "equivalent" airspeed, V_e. Also $V\sqrt{\sigma}$ appears in the force and moment coefficients as constants, except for Mach number effects.

Equation (23) may be evaluated for various values of V_c and pressure altitude. The difference between V_e and V_c is, of course, ΔV_c, as expressed in equation (3). Results of the evaluation have been plotted and are shown in Chart 3.

3-2 ALTITUDE AND TEMPERATURE MEASUREMENT

High Speed Position Error - Altimeter

Since the altimeter is connected to the static source, it will also pick up any existing position error and will therefore read incorrectly. The altitude calibration for flaps up is based on the high-speed Mach number calibration. The calibration curve as it is presented in the flight manual is this reference calibration curve with the Mach number correction converted to an altitude correction and the Mach number converted to airspeed. This involves the following relationship:

$$\Delta h_p = \frac{dh}{dM} \Delta Mp \qquad (24)$$

By introducing the multiplying factor, dp/dp, the differential term dh/dM is the product of two other differential terms as shown:

$$\frac{dh}{dM} = \frac{dh}{dp} \frac{dp}{dM} \qquad (25)$$

Since pressure, p, is a function of altitude, h, dh/dp is obtained from equation (76) of Section 1:

$$\frac{dh}{dp} = -\frac{1}{\rho g} \qquad (26)$$

Substituting equations (26) and (15) into equation (25), the expression for dh/dM becomes:

$$\begin{aligned} \frac{dh}{dM} &= \frac{\gamma p}{\rho} \frac{M}{g} \frac{1}{(1 + .2M^2)} \\ &= \frac{a^2}{g} \frac{M}{(1 + .2M^2)} \\ &= \frac{a_o^2 \theta M}{g (1 + .2M^2)} \\ &= 38,749 \frac{\delta}{\sigma} \frac{M}{(1 + .2M^2)} \end{aligned} \qquad (27)$$

A chart showing the solution of equation (27) for standard day conditions can now be made, see Chart 4.

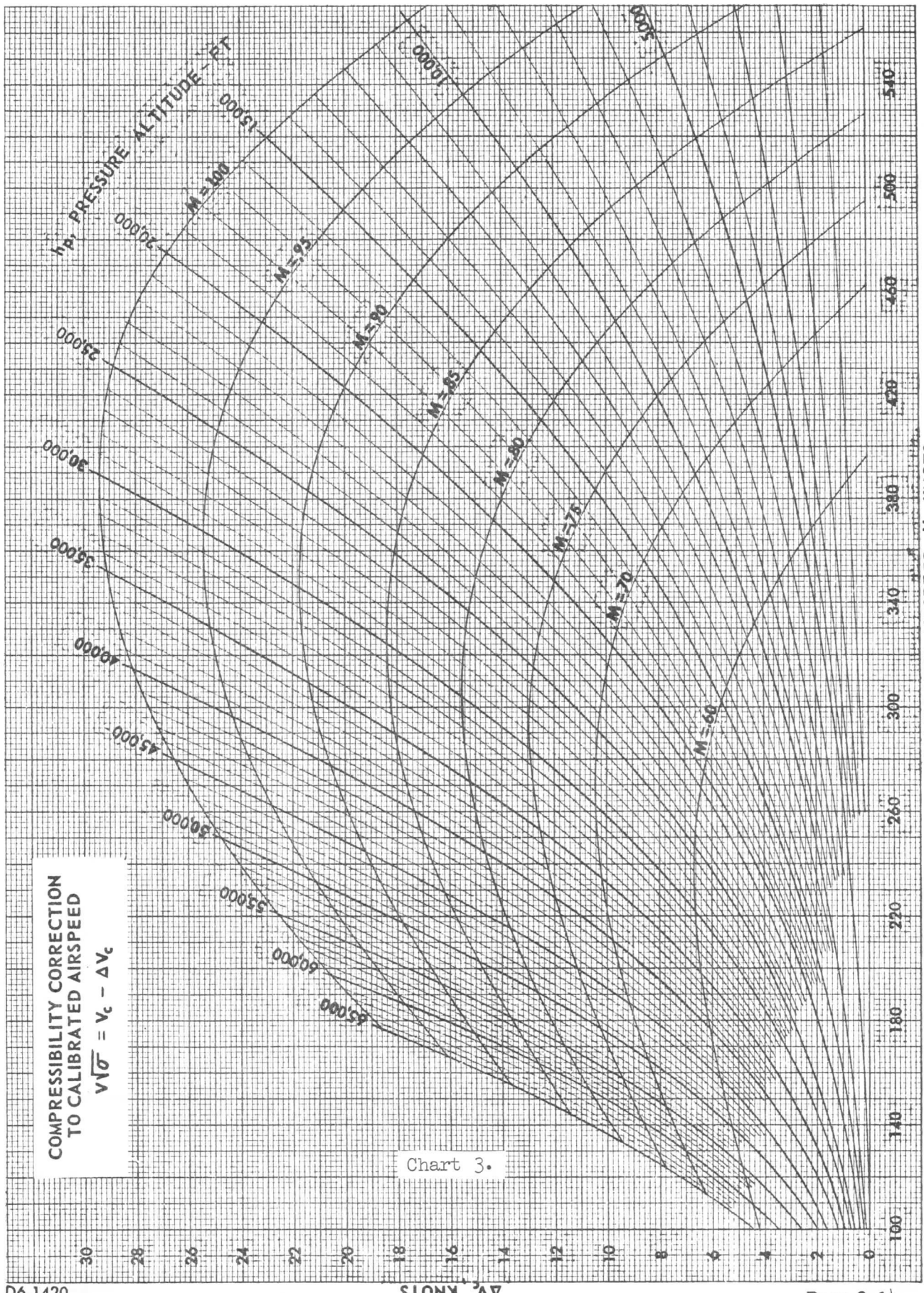
COMPRESSIBILITY CORRECTION TO CALIBRATED AIRSPEED
$V\sqrt{\sigma} = V_c - \Delta V_c$
h_p, PRESSURE ALTITUDE - FT
5000
10,000
15,000
20,000
25,000
30,000
35,000
40,000
45,000
50,000
55,000
60,000
65,000
M=100
M=95
M=90
M=85
M=80
M=75
M=70
M=60
CALIBRATED AIRSPEED, V_c, KNOTS
540
500
460
420
380
340
300
260
220
180
140
100
30
28
26
24
22
20
18
16
14
12
10
8
6
4
2
0
ΔV_c, KNOTS

Chart 3.

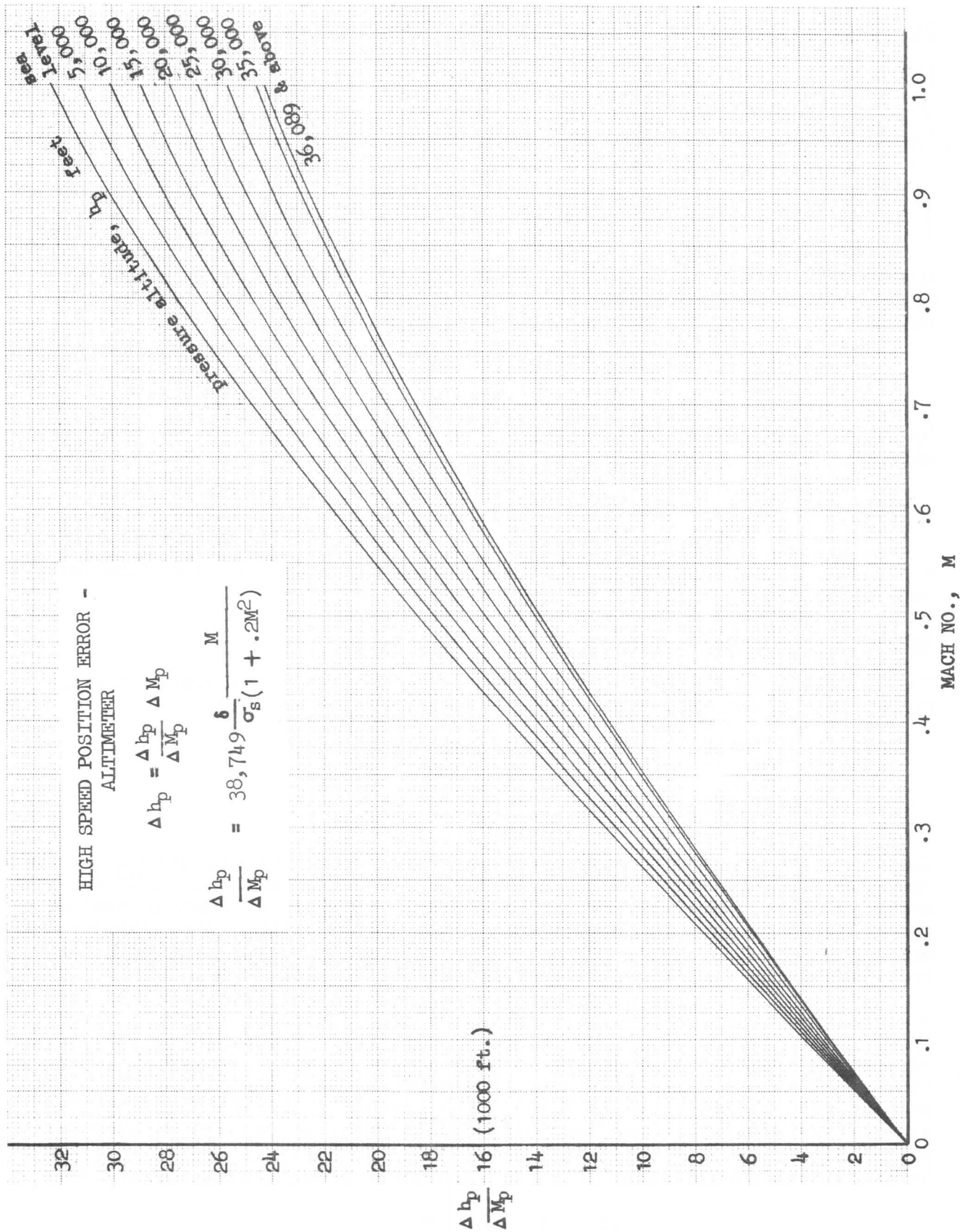
HIGH SPEED POSITION ERROR - ALTIMETER
$\Delta h_p = \frac{\Delta h_p}{\Delta M_p} \Delta M_p$
$\frac{\Delta h_p}{\Delta M_p} = 38,749 \frac{\delta}{\sigma_s} \frac{M}{(1 + .2M^2)}$
Pressure altitude, h_p
Sea level
5,000 feet
10,000
15,000
20,000
25,000
30,000
35,000
36,089 & above
$\frac{\Delta h_p}{\Delta M_p}$ (1000 ft.)
MACH NO., M

Chart 4.

AIRPLANE PERFORMANCE

Low Speed Position Error - Altimeter

The altimeter position error at low speeds is obtained more accurately by utilizing the ΔV_p that is measured from the "trailing" bomb instrumentation. Rather than go through a procedure similar to that for velocity position error of generalizing the altimeter position error, Δh_p on a plot of $\Delta h_p/h_I$ vs V_{I_W} (similar to Figure 3), it is convenient to recognize that:

$$\Delta h_p = \frac{dh}{dV_c} \Delta V_p \qquad (28)$$

Having found ΔV_p from the previous theory, it is necessary only to evaluate dh/dV_c so that Δh_p may be resolved. The differential term dh/dV_c may be manipulated by introducing a multiplying factor, dp/dp, thus:

$$\frac{dh}{dV_c} = \frac{dh}{dp} \frac{dp}{dV_c} \qquad (29)$$

By multiplying equation (26) by equation (16), the expression for dh/dV_c can be obtained.

$$\frac{dh}{dV_c} = 0.08865 \left[1 + .2\left(\frac{V_c}{661.5}\right)^2 \right]^{2.5} \frac{V_c}{\delta/\theta}, \frac{ft}{kt} \qquad (30)$$

A plot showing the solution of equation (30) under standard day conditions for various values of V_c can be made, see Chart 5.

Temperature Correction

The primary variables which must be most accurately known or determined during flight to obtain the optimum performance for a jet aircraft are:

(1) Mach number
(2) Gross weight
(3) Altitude
(4) Free air temperature

Therefore, the instruments which are considered to be of prime importance are the Machmeter, fuel quantity indicators, altimeter, free air temperature indicator and engine pressure ratio indicator (or tachometer). Of those instruments itemized above, the Machmeter and altimeter errors have been discussed. Fuel quantity and engine pressure ratio indicators operate satisfactorily and deviation from the true reading can usually be corrected in installation alterations.

The free air temperature indicator is very important since the indicated temperature has two specific uses associated with performance: the determination of true airspeed and fuel flow and the determination of engine pressure ratio (or RPM) for the required thrust settings. Free air temperature gages are usually operated by an electrical resistance thermometer bulb located flush with the body skin. Because of the "adiabatic temperature rise," due to compressibility, the thermometer bulb picks up a temperature reading higher than the static temperature of the air. Total temperature is related to the static by an expression developed in Section 1:

$$\frac{T_t}{T} = 1 + \frac{\gamma - 1}{2} M^2$$

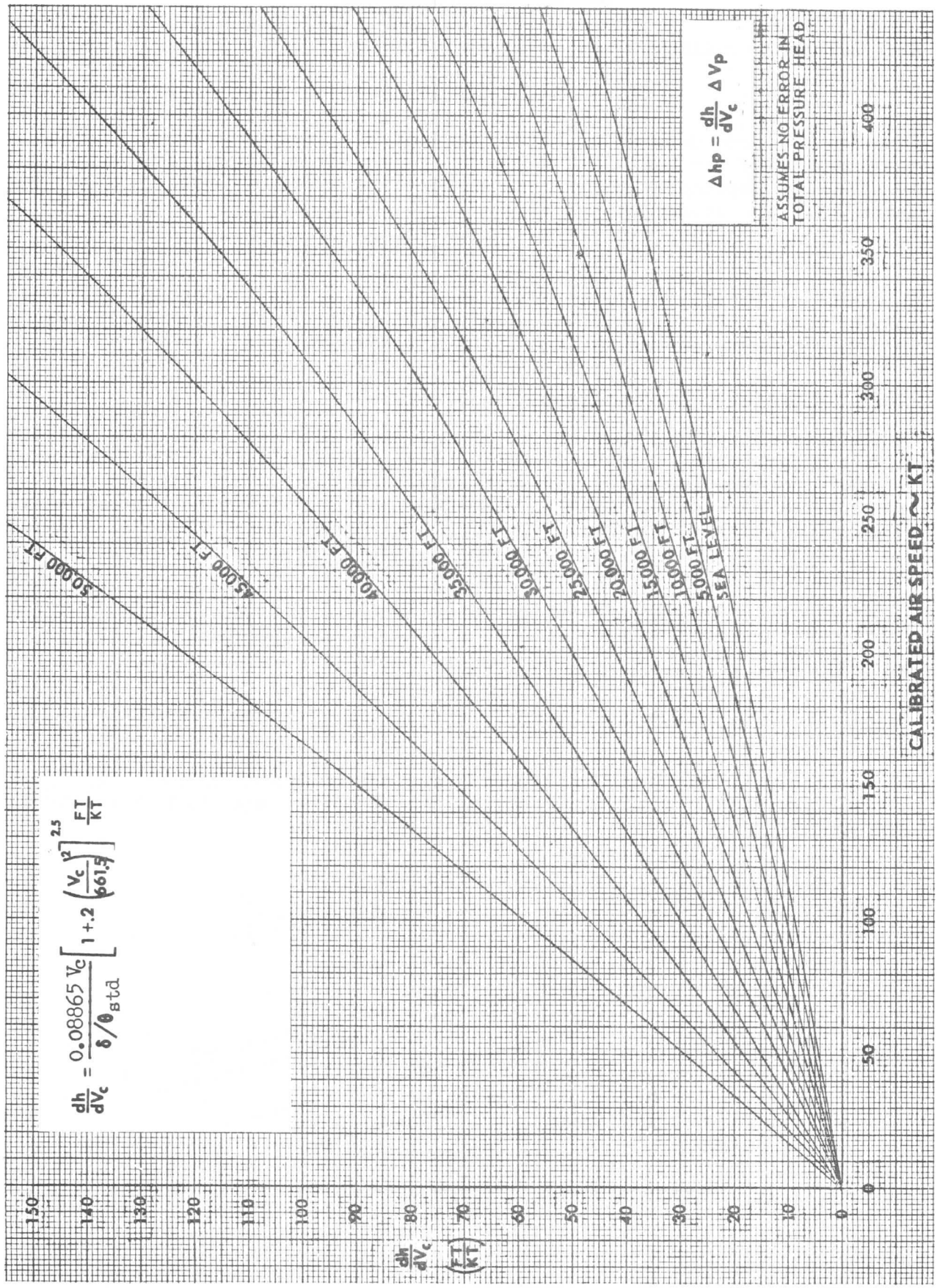
$\frac{dh}{dV_c} = \frac{0.08865\ V_c}{\delta/\theta_{std}}\left[1+.2\left(\frac{V_c}{661.5}\right)^2\right]^{2.5}\ \frac{FT}{KT}$
$\Delta hp = \frac{dh}{dV_c}\ \Delta V_p$
ASSUMES NO ERROR IN TOTAL PRESSURE HEAD
CALIBRATED AIR SPEED ~ KT
0
50
100
150
200
250
300
350
400
SEA LEVEL
5000 FT.
10000 FT.
15000 FT.
20,000 FT.
25,000 FT.
30000 FT.
35000 FT.
40000 FT.
45,000 FT.
50000 FT.
$\frac{dh}{dV_c}\ \left(\frac{FT}{KT}\right)$
0
10
20
30
40
50
60
70
80
90
100
110
120
130
140
150

Chart 5.

This now may be modified by substituting the value of $\gamma = 1.4$ for air, thus:

$$T_t = T(1 + .2M^2) \qquad (31)$$

Equation (31) must be modified further to include a "recovery factor," K, due to the inability of the instrument system to recover the full temperature rise due to adiabatic compressible flow of air as picked up by the thermometer bulb. Equation (31) now becomes:

$$T_{t_i} = T_{am}\ (1 + .2\ K\ M^2) \qquad (32)$$

The value of "K" will be known for an installation and is usually of the magnitude of 0.8 to 1.0. The calculation of true O.A.T. is easily made keeping in mind that the temperatures T_{t_i} and T_{am} are absolute values.

Temperature Indicator Calibration

The calibration of a temperature indicator is very difficult unless one has a reference instrument to be flown with the one to be calibrated. Bench calibration or wind tunnel comparison are not satisfactory because of the large wind tunnel effects and the influence of installation and environment. Therefore, a method of calibrating the first instrument must be developed. Then the second and succeeding systems may be calibrated by the same method or by comparison to the first when flown with or in parallel to it.

Total Temperature (Reference) Indicator

Consider equation (32) in the form

$$\frac{1}{T_{t_i}} = \frac{1}{T_{am}} - \frac{K}{5}\,\frac{M^2}{T_{t_i}} \qquad (33)$$

If a calibration run is made at constant altitude in relatively calm air, T_{am} may be considered to be constant, and T_{t_i} can be plotted against M in the form of Figure 5.

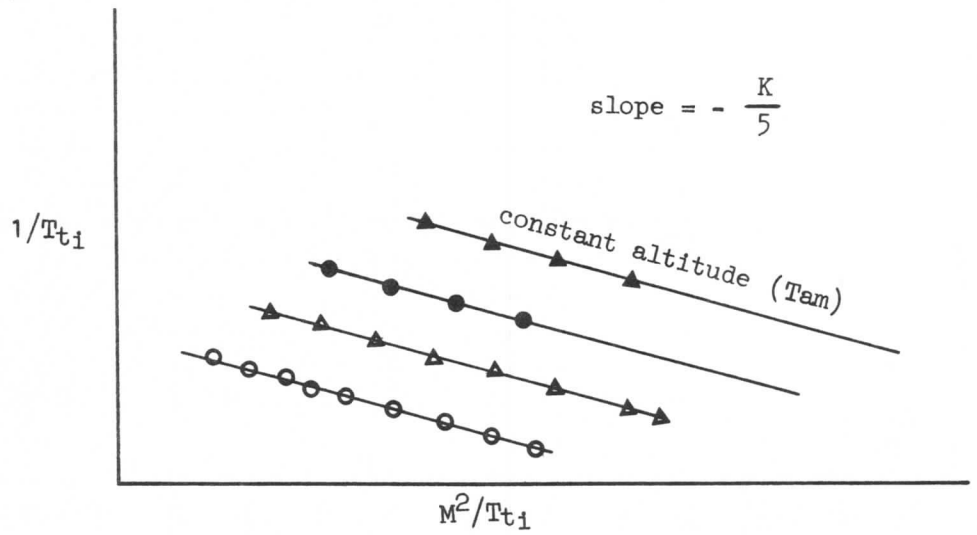

Figure 5.

Equation (33) shows that the slope of this family is -K/5 and the recovery factor is determined. Note that the value of K and its determination are independent of T_{am} so long as it is constant for each run. This is the method used to calibrate the reference system for Boeing airplanes. This calibrated instrument can then be used to determine T_{am} at any time through T_{t_i} and M only.

Ram Air Temperature (RAT) Indicator

Calibration of the ram temperature indicator consists of determining a calibration factor, C, which takes care of instrument installation effects and the recovery factor, K, in the equation:

$$T_{RAM} = T_{am} \left[(1 + C) + .2KM^2 \right] \qquad (34)$$

Solving this equation for K yields

$$K = \frac{\frac{T_{RAM}}{T_{am}} - (1 + C)}{M^2/5} \qquad (35)$$

Therefore, when the flight data is plotted as in Figure 6, the slope of the linear array gives K and the intercept defines C. The values of T_{am} are obtained from the reference instrument flown with this one.

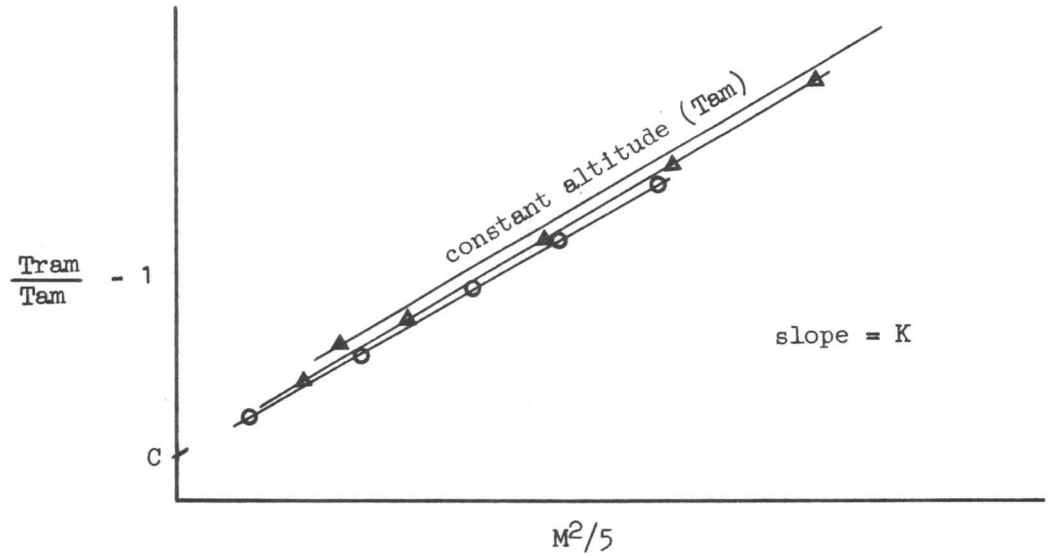

Figure 6.

Static Air Temperature Indicator

Static air temperature indication is referenced directly to the T_{am} or t_{am} calculated from the reference indicator reading:

$$\Delta t = t_i - t_{am} \qquad (36)$$

where t_i is the static air temperature indicator reading. Calibrations are run at a series of altitudes (t_{am}) and plotted as in Figure 7.

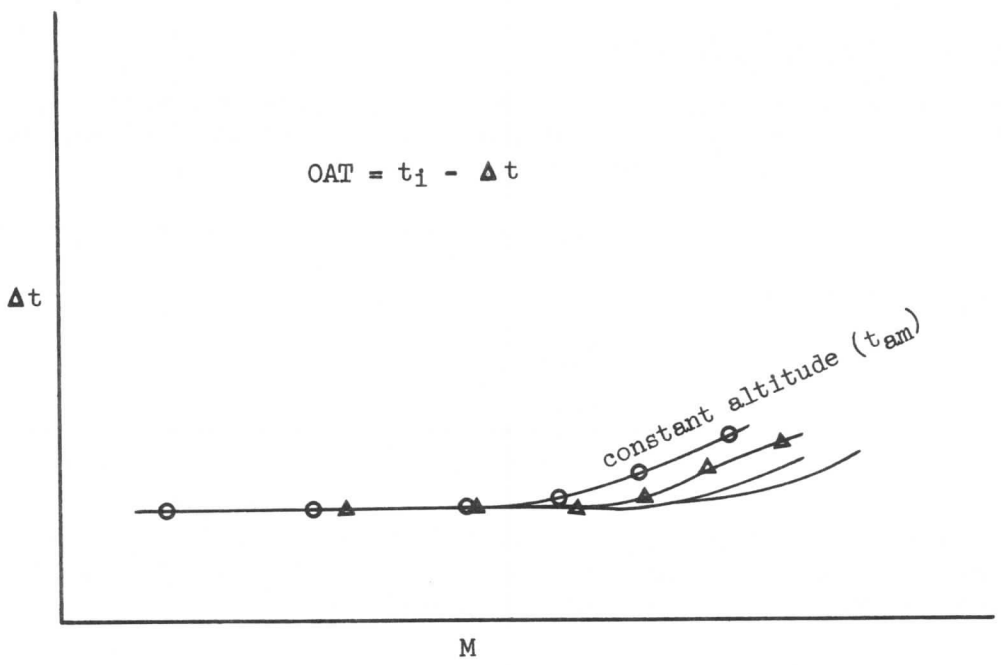

Figure 7

Ground Effect Position Error

When an airplane is flown near the ground it will be found that the ground will affect the airflow pattern around the wings. It does this by actually preventing the downwash from developing to the extent that it would in free air. Consider Figure 8, which shows two wings at the same angle of attack, one in free air, and the other near the ground. It will be noted that the flow patterns around the wings are different, for the reason that the ground forces the airflow to conform to it. This will result in a changed static pressure field around the wing which, therefore, will be felt by the static pressure pickup on the fuselage. This will cause an additional error that must be accounted for.

The approach for landing of an airplane is usually considered at a fixed lift coefficient (fixed angle of attack) regardless of airplane weight. In addition, during the flare, the airplane is rotated to a higher lift coefficient determined as either the maximum or near-maximum C_L condition. When the airplane is on the ground it will be at a fixed lift coefficient. It may be said that since all flight near the ground will be at a fixed lift coefficient, no generalization to account for C_L is necessary in presenting the data. As a result, the curves of airspeed and altimeter correction may be shown independent of weight.

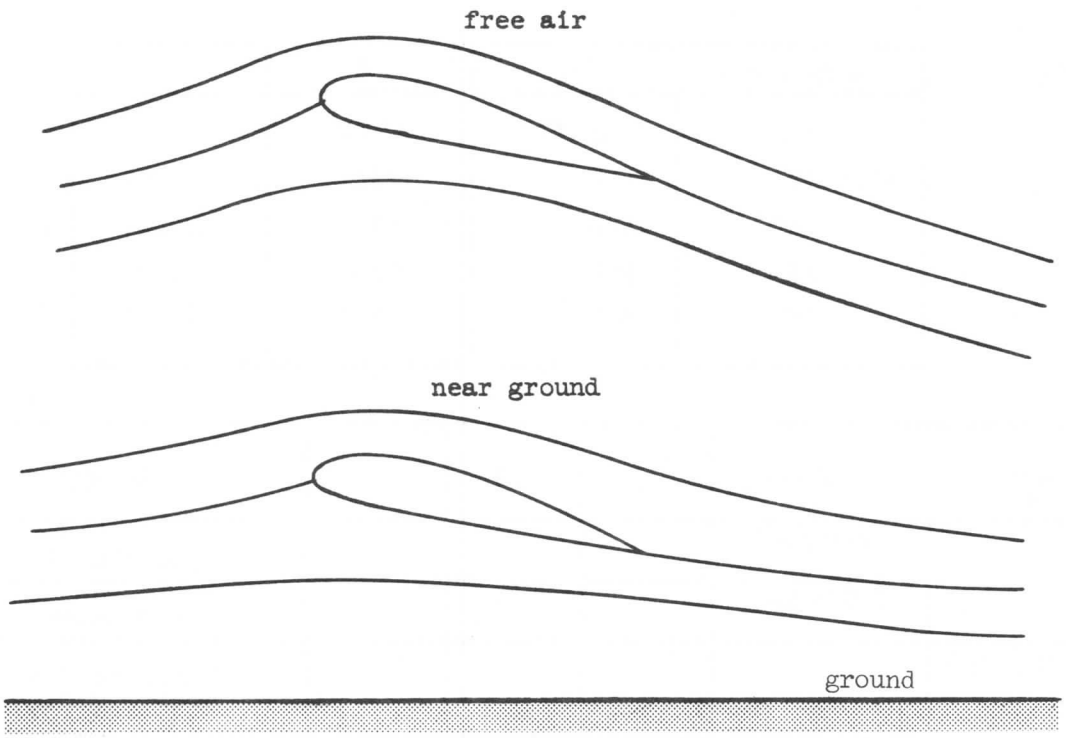

Figure 8.

3-3 AIRPLANE AND ENGINE GRID

Thrust Required

Previously, in Section 1, a short discussion of thrust required for level flight was made, and the following equations were developed:

$$\frac{W}{\delta} = 1481.4 C_L M^2 S \qquad (37)$$

$$\frac{T}{\delta} = 1481.4 C_D M^2 S \qquad (38)$$

In order to calculate the T/δ required for an airplane, a table similar to that shown in Figure 9 may be used to facilitate the calculations. If the various Boeing commercial airplanes with their respective wing areas are now considered, equations (37) and (38) can be arranged as follows:

$$C_L = A \times 10^{-6} \frac{W/\delta}{M^2} \qquad (39)$$

$$\frac{T}{\delta} = B \times 10^{6} \; C_D M^2 \qquad (40)$$

where,

Airplane	S_W	A	B
707	2433 ft^2	.27745	3.604
Inter 707	2892	.23341	4.284
727	1560	.4327	2.311
737	980	.6888	1.452
747	5500	.1227	8.1477

W/δ	M ⟶	.3	.5	.7	REMARKS
	$.2775/M^2$				Calculated
	$3.604\ M^2$				Calculated
1.0×10^6	C_L				Calculate from Equation (39)
	C_D				Obtain from C_L - C_D polar
	T/δ				Calculate from Equation (40)
1.2×10^6	C_L				
	C_D				
	T/δ				
1.4×10^6					

REPEAT FOR OTHER W/δ's

Figure 9.

This tabulation, when filled out for desired values of W/δ , will enable one to plot T/δ versus M, as in Figure 10. It should be pointed out that sufficient Mach number points must be calculated to obtain a well defined curve.

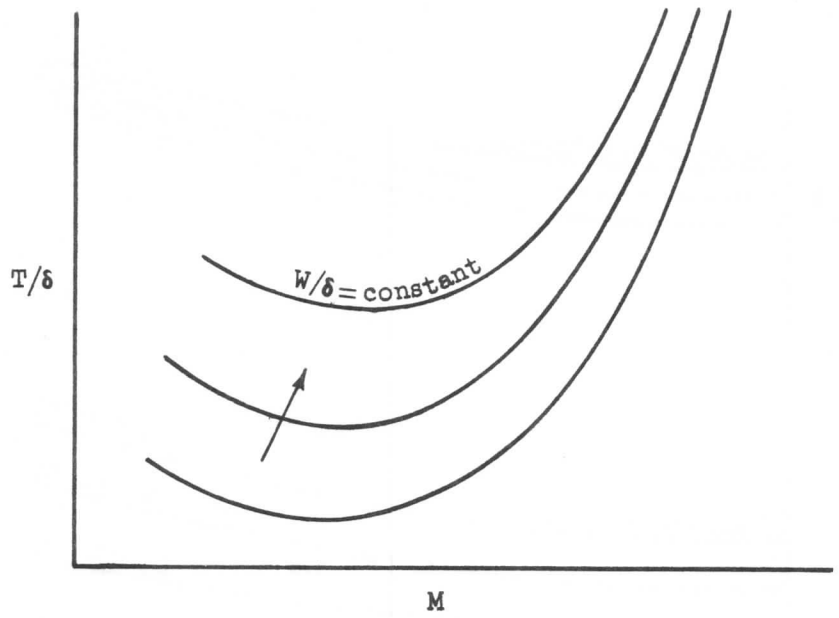

Figure 10.

Thrust Available

As was explained in Section 1, the logical parameter for expressing available engine thrust above 36,000 foot altitude is T/δ . This is because the maximum thrust available diminishes in proportion to δ at a given true airspeed and engine RPM; thus, the ratio T/δ will remain constant, theoretically. However, engine tests above 36,000 feet have indicated an additional deterioration in thrust available with increase in altitude above 36,000 feet which is due to Reynolds number effects and additional turbocompressor bleed requirements causing a reduced airflow over that anticipated. The net result of this is that a series of lines of maximum T/δ above 36,000 feet will be obtained. This is shown in Figure 11. At altitudes below 36,000 feet there is a reduction in maximum T/δ available. This is because below 36,000 feet not only will pressure increase but temperature will also, resulting in a further change in thrust.

The thrusts considered so far are the maximum thrusts available (called "maximum continuous" thrust) under given conditions of altitude and airplane velocity, assuming standard atmospheric conditions. If now at a given altitude a hotter than standard day is considered, the maximum T/δ will be reduced, and conversely it will be increased for a colder than standard day. Considering less than maximum thrusts, the temperature effects will be the same as indicated above for a given thrust lever setting. The thrust rating below the maximum continuous thrust that is of particular interest in performance work is "normal" thrust, since it is that rating which is used for normal climb.

It was seen in Section 1 how Figures 10 and 11 may be superimposed to form a single plot for all altitudes, as shown in Figure 12. Data to construct the thrust available lines are furnished by the engine manufacturer in the form of

thrust vs velocity for various altitudes. This information is then calibrated for installation effects and replotted introducing δ and changing true airspeed to Mach number.

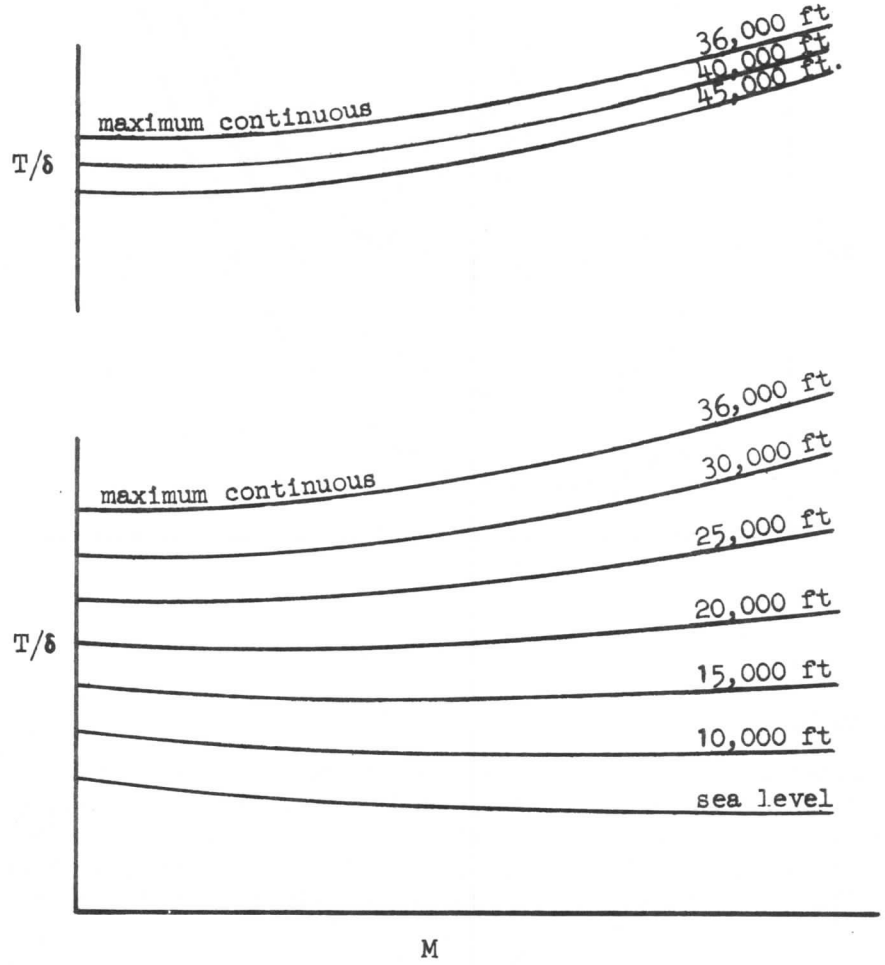

Figure 11.

Engine Fuel Flow Grid

The complete engine data as presented by the engine manufacturer consist of a series of plots from sea level to the altitude limits of the airplane in increments of usually 5,000 feet as shown roughly for one altitude in Figure 13. This plot shows the complete picture of thrust and fuel flow variation with speed at a given altitude. However, it is not in the form which is useful in performance calculations. In the first place, thrust and true airspeed would have to be converted into terms of T/δ and Mach number as was done for the thrust available curves. The fuel flow data, however, must be given special treatment to put it into usable form. The units of fuel flow are "lb/hr" and will be unchanged if the numerator and denominator are multiplied by the units of nautical air miles.

Thus:
$$W_f = \frac{\text{lb}}{\text{hr}} = \frac{\text{lb}}{\text{hr}} \quad \frac{\text{nam}}{\text{nam}}$$

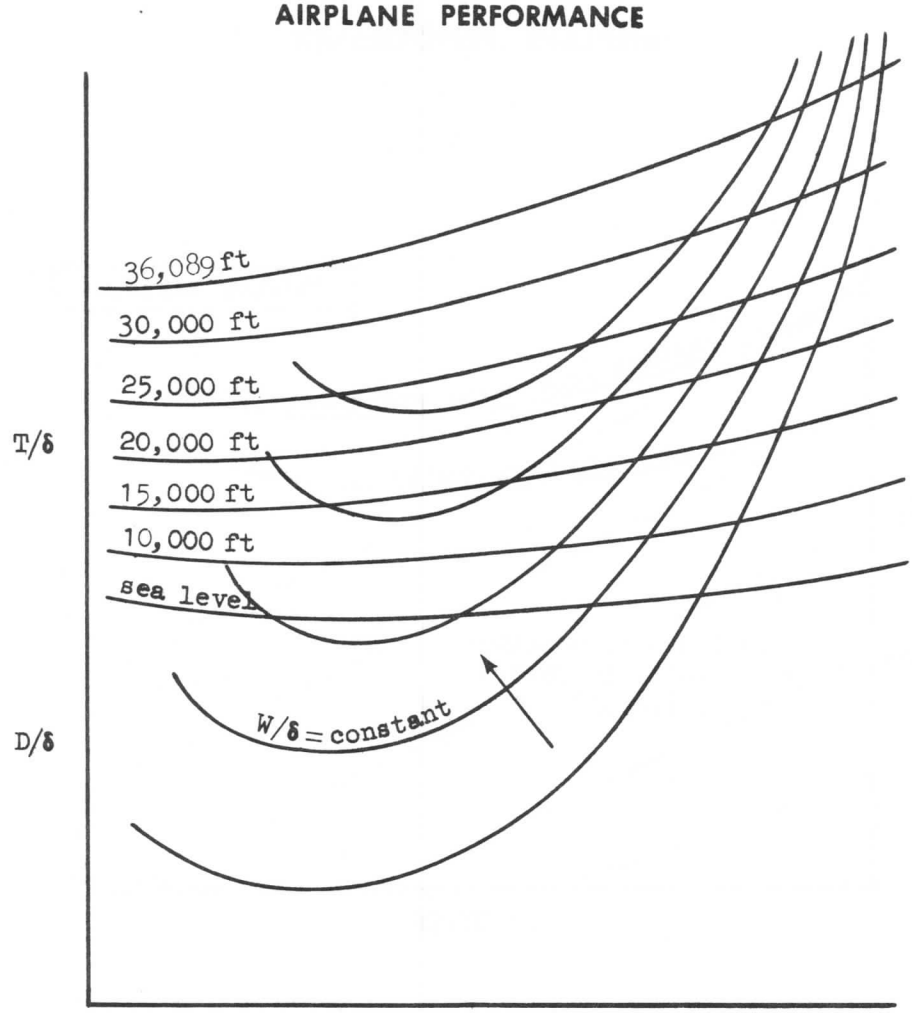

Figure 12.

This equation can be rearranged in the form:

$$W_f = \frac{\text{nam}}{\text{hr}} \quad \frac{\text{lb}}{\text{nam}} = \frac{V}{\text{nam/lb}} \qquad (41)$$

It should be noted that fuel mileage, nam/lb, is simply related to velocity and fuel flow by this equation. Equation (41) is still not in generalized form, however, and must be manipulated further to make it useful for performance work.

The specific fuel consumption, lb of fuel per hr per lb thrust, is essentially constant at a given value of Mach number and T/δ regardless of altitude. Thus:

$$W_f = \text{TSFC} \quad T \qquad (42)$$

where TSFC is specific fuel consumption, lb-fuel/hr/lb-thrust, and T is thrust in lb. However, since it is desired to use the parameter T/δ , equation (42) may be written:

$$\frac{W_f}{\delta} = \text{TSFC} \quad \frac{T}{\delta} \qquad (43)$$

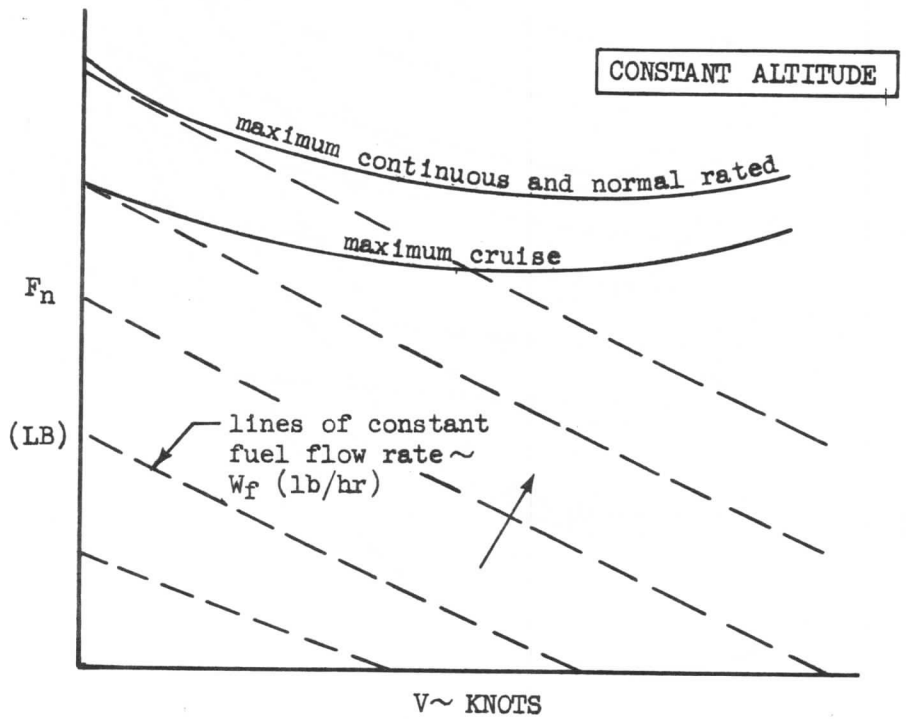

Figure 13.

This equation states that at a given T/δ (and speed) there will exist a constant W_f/δ since TSFC is constant. Returning to equation (41), and dividing by δ :

$$(TSFC)\frac{T}{\delta} = \frac{W_f}{\delta} = \frac{V}{(NAM/LB)\,\delta} \qquad (44)$$

In addition to using the parameter T/δ, Mach number is also used in plotting the thrust required and available curves as shown in Figure 12. It will be remembered that

$$M = \frac{V}{a_o\sqrt{\theta}}$$

Thus to convert from units of velocity, appearing in equation (44), to Mach number, the quantity $\sqrt{\theta}$ must be introduced. Dividing equation (44) by $\sqrt{\theta}$:

$$\frac{TSFC}{\sqrt{\theta}}\,\frac{T}{\delta} = \frac{W_f}{\delta\sqrt{\theta}} = \frac{V/\sqrt{\theta}}{\frac{nam\,\delta}{lb}} = \frac{Ma_o}{\frac{nam\,\delta}{lb}} \qquad (45)$$

The result has accomplished two purposes. First it generalizes the fuel flow information and removes the variable of altitude. Second, it converts from units of true airspeed to Mach number. Thus, instead of having a plot like Figure 13 for every altitude, a new plot which is independent of altitude can be drawn, as in Figure 14.

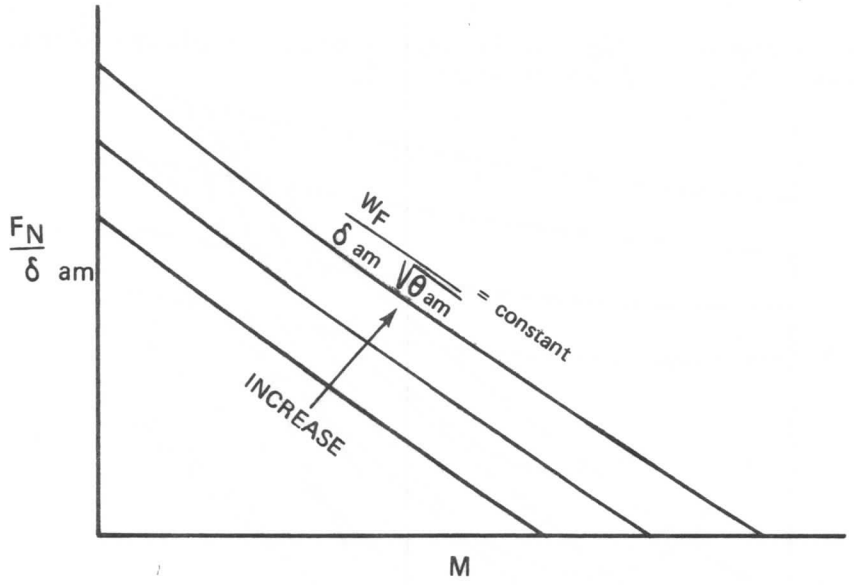

Figure 14.

This plot is still not in the form which is most useful for performance work. Referring to equation (45), the terms may be rearranged into the form:

$$\frac{nam\ \delta}{lb} = \frac{Ma_o}{W_f/\delta\sqrt{\theta}} \qquad (46)$$

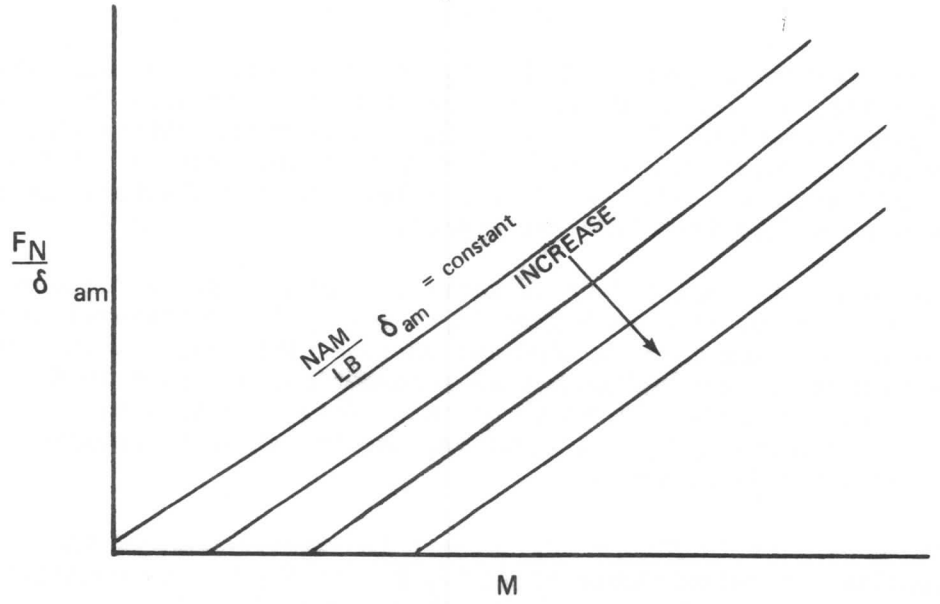

Figure 15.

Using this equation, the lines of constant $W_f/\delta\sqrt{\theta}$ in Figure 14 can be converted into lines of constant nam δ/lb. When plotted on the axes of T/δ vs. M. these lines will look similar to those in Figure 15.

This plot represents the form which may be used in performance calculations.

The information on Figure 15 may now be superimposed on Figure 12 and is useful for all altitudes. This is shown on Figure 16.

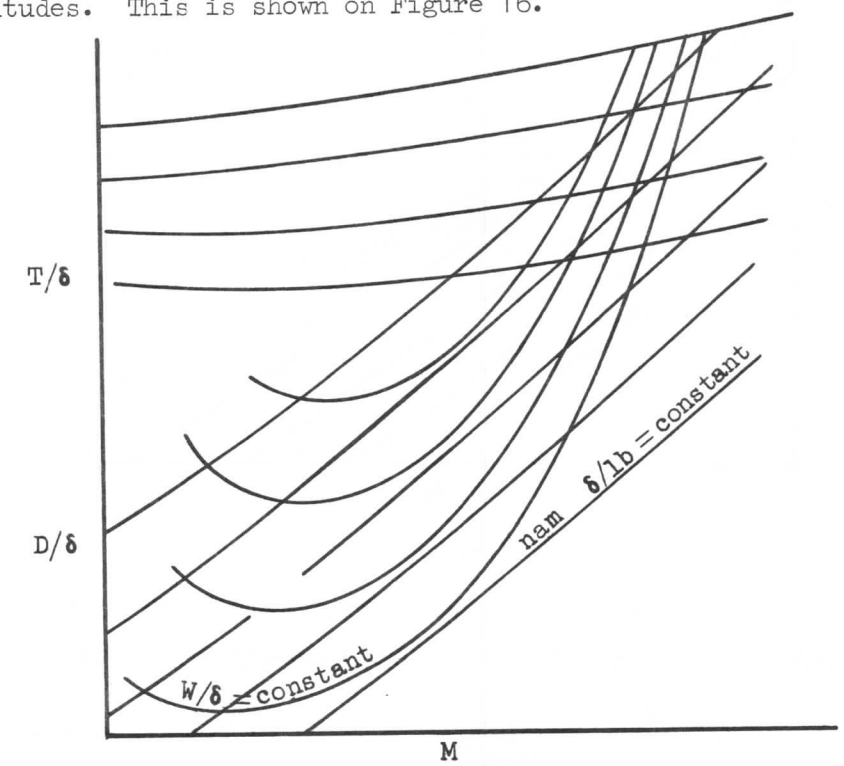

Figure 16.

The type of information as presented in Figure 16 is typical of some types of engines, depending on design. Other engines have peculiarities which do not permit such generalization. The specific fuel consumption varies slightly with altitude, requiring either a plot such as Figure 15 for various altitudes (usually in increments of 5000 feet from sea level to the altitude limits of the airplane), or a slightly different approach.

The manner in which the engine data is usually presented is as follows. From the basic chart, such as that in Figure 13, values of F_n for several W_f values are tabulated at constant Mach numbers and various altitudes. From this tabulation, another chart is made relating this information, as shown in Figure 17, for the altitudes selected. The value of this cross-plot is that it permits a selection of even values of F_n. A table may now be set up to facilitate further calculations as shown in Figure 18.

From the tabulated data in Figure 18, a chart is constructed for the various altitudes showing the relationship of $TSFC/\sqrt{\theta}$ to F_n/δ for constant Mach numbers. See Figure 19. This plot shows that for a given T/δ (or F_n/δ) and

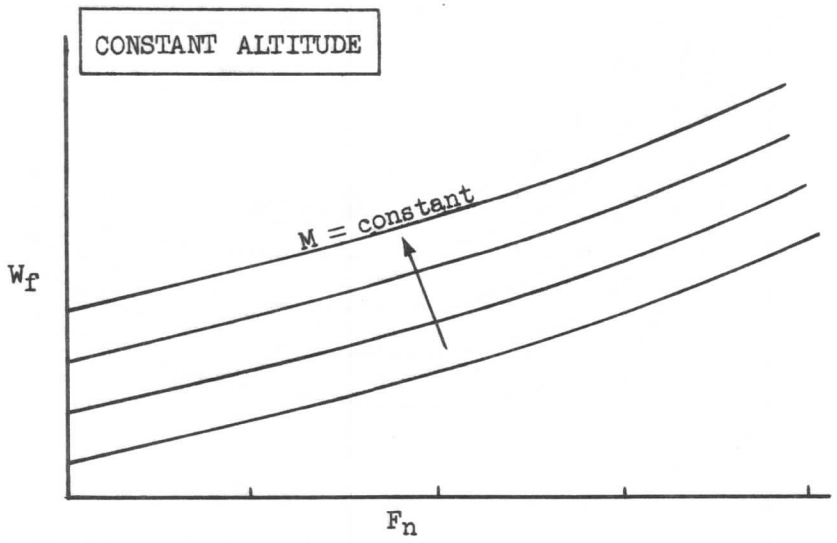

Figure 17.

ALTITUDE = CONSTANT					
M	W_f (LB/HR)	F_n (LB)	TSFC (LB/HR/LB)	TSFC/$\sqrt{\theta}$ (LB/HR/LB)	F_n/δ (LB)
(1)	(2)	(3)	(4)	(5)	(6)
Select	Select	Engine Data	$\frac{(2)}{(3)}$	Calculate	Calculate

Figure 18.

M, a value of TSFC/$\sqrt{\theta}$ is defined for a particular altitude. The parameter nam δ/lb (or nam/lb) is obtainable from equation (45).

$$\text{nam } \delta/\text{lb} = \frac{Ma_o}{\frac{\text{TSFC}}{\sqrt{\theta}}\frac{F_n}{\delta}} \qquad (47)$$

Note that F_n is used for the thrust term instead of T in equation (47).

Recently, engine data from the Pratt and Whitney Company has been presented in a slightly different manner than that shown in Figure 13. Instead of showing lines of constant fuel flow, lines of constant TSFC are shown as in Figure 20.

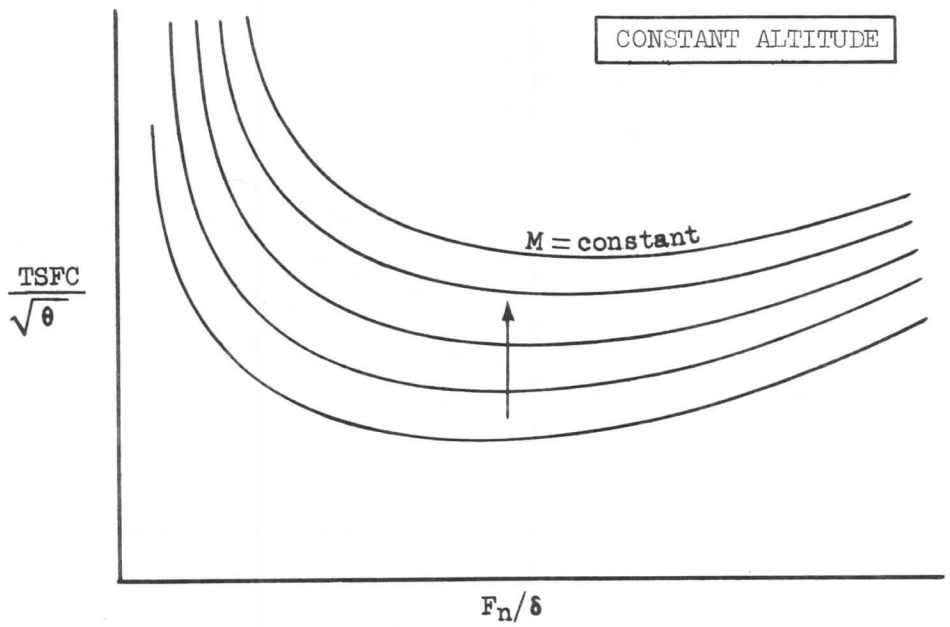

Figure 19.

Lines of constant airflow, W_a, that appear on the actual engine data, have not been shown on either Figure 13 or Figure 20 in the interest of clarity. The slight change in data presentation simplifies the calculations required to produce the same end results as before.

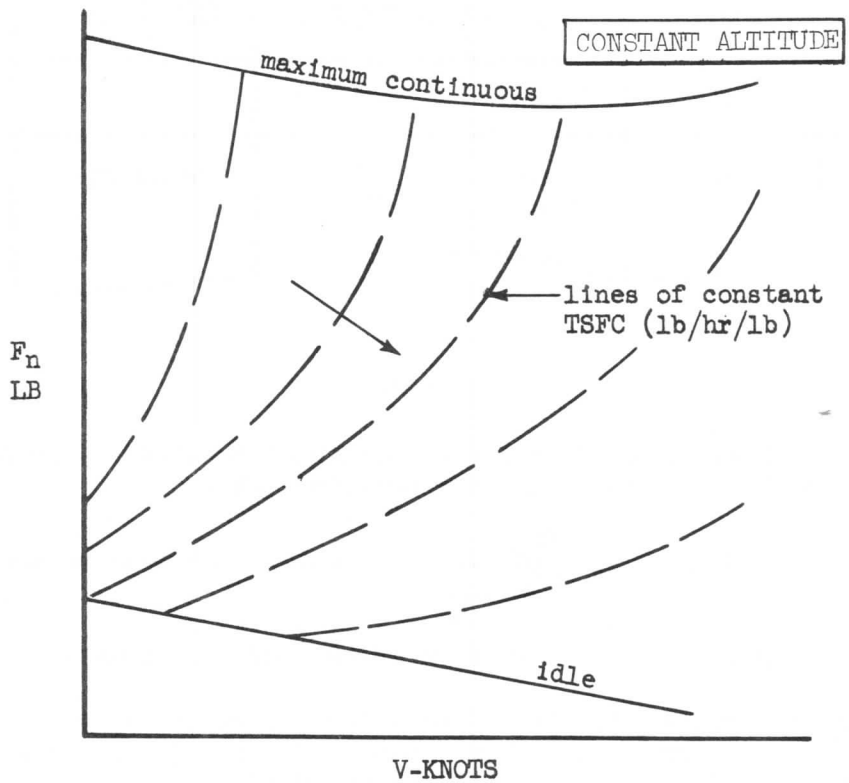

Figure 20.

3-4 FLIGHT LIMITATIONS

The flight limits of any airplane may be defined as the speed, altitude, and acceleration limits within which it must fly. The factors which apply these restrictions are its aerodynamic, powerplant, and structural limits. The aerodynamic and powerplant limits will be discussed at the same time since in some instances the airplane limitations are a result of both acting at once.

Minimum Speeds

The minimum speed that an airplane can fly is of greatest importance in handling an airplane near the ground during takeoff, approach, and landing. This speed is that associated with the maximum lift produced by the wing. Assuming an airplane of given weight, from the relationship:

$$W = C_L S \frac{V_e^2}{295.37}$$

$$V_e = \sqrt{\frac{295.37\,W}{C_L\,S}} \qquad (48)$$

It can be seen that with W and S constant, by making C_L a maximum, V_e will be made a minimum. By referring to the lift curve of the airplane, Figure 21, it is seen that $C_{L_{MAX}}$ occurs on the curved portion of the curve. As was explained in Section 1, the departure of the lift curve from linear represents an increasing airflow separation which finally results in complete airflow breakdown, or stall, at or near $C_{L_{MAX}}$. A pilot, when approaching the stall, will become aware of airflow separation through the phenomenon of "buffeting." Buffeting is caused by the turbulence of the airflow separation shaking some part of the airplane (usually the wing or horizontal tail). Between the two points of initial separation and maximum lift, there is a varying degree of buffeting. An arbitrary point along this curve where the shaking becomes objectionable to the pilot is the basis for the buffet limit chart.

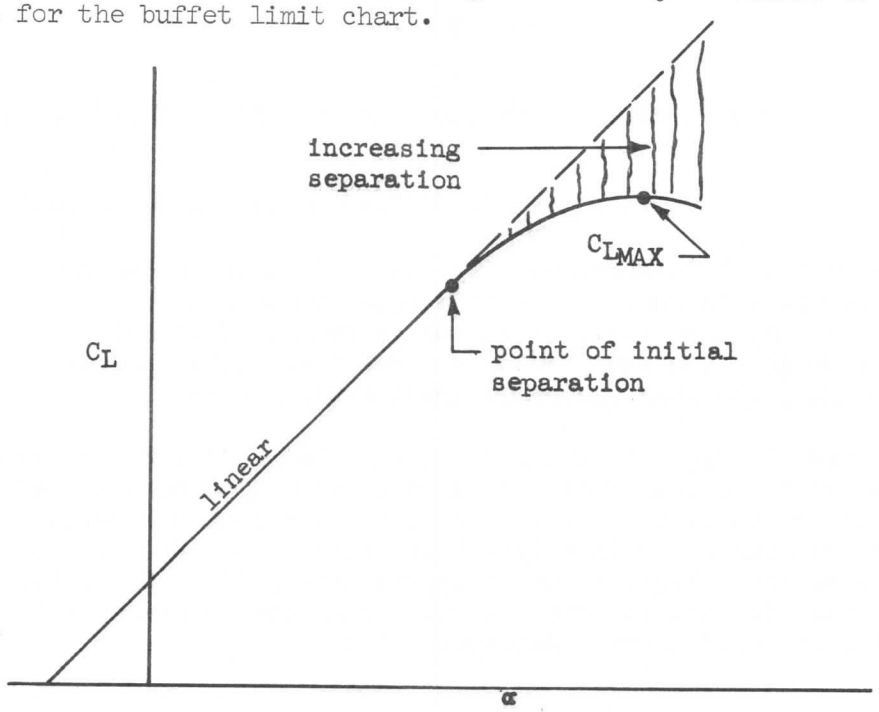

Figure 21.

AIRPLANE PERFORMANCE

The effect of flaps on the airplane was discussed briefly in Section 1. It was seen that the flaps altered the C_L vs α plot so as to increase the lift coefficient at a given angle of attack. See Figure 22. This means that ultimately a higher maximum lift coefficient is possible and usually occurs at a lower angle of attack. The reason for the increase in lift is that the wing with the flap now has a much greater camber, producing more lift. The increased lift, hence lift coefficient, afforded by the flaps will obviously allow lower flight speeds, which is their chief purpose. This is supported by equation (48).

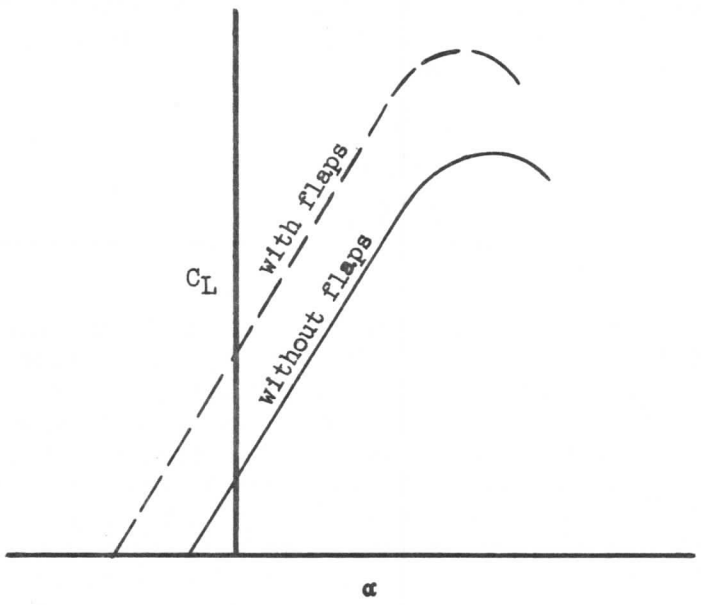

Figure 22.

At this point, it is convenient to introduce the concept of "load factor." By definition:

$$n = \frac{L}{W} \qquad \text{(49)}$$

where n is load factor, L is airplane lift, and W is airplane weight. Thus, when an airplane is flying such that the lift is equal to the weight, a condition existing in level flight, then the load factor is unity. Obviously, when the lift is less than the weight, the load factor is less than unity, and when the lift is more than the weight, the load factor is greater than unity.

Returning to Figure 21, $C_{L_{MAX}}$ is the maximum C_L obtainable for a given condition which is determined for a load factor of unity, $(n = 1)$, as established in wind tunnel tests. At the stall in actual flight, the airplane has begun to fall through and the load factor becomes less than unity. The value of the load factor, as established from flight tests, is approximately 0.9. There is, then, an effective $C_{L_{MAX}}$ that is used in computing the stall speeds associated with the effective stall lift coefficient. Mathematically:

$$C_{L'_{MAX}} = \frac{C_{L_{MAX}} \ (n = 1)}{n(stall)} \qquad \text{(50)}$$

where $C_{L'_{MAX}}$ is the effective $C_{L_{MAX}}$ during the stall. Using the C_L vs α curve for the airplane and equation (50), the effective $C_{L_{MAX}}$ may be obtained to substitute in equation (48) to obtain the airplane stall speeds. By selecting various weights for each flap position, a stall speed chart for the various flap positions throughout the weight range of the airplane may be constructed. This technique is used when estimating $C_{L_{MAX}}$ from wind tunnel data; however, actual values of $C_{L_{MAX}}$ based on flight test stall speeds are used when available. A minimum stall speed is defined which in turn defines an effective $C_{L_{MAX}}$ for $n < 1$.

Stall Speed Determination

Normally, all low-speed testing is done with "trailing bomb" instrumentation. The "bomb" is an instrumented body of revolution extended below the airplane by cables. The objective is to obtain data far from the influence of the airplane and thus approximate free stream conditions as closely as possible. Since the instrument leads are long, it is important that the indications, especially pressure indications, be lag checked to find out how long a stabilized condition must be flown before reading data. It must also be dynamically balanced such that the pitot and static leads have equivalent lag to eliminate pressure oscillations in the instrumentation.

The regulations, 25.103, define the power-off stall speed as the minimum controlled flight speed at most adverse C.G. position and specify the rate at which the demonstration flight is to be decelerated to stall. So the test flight must yield both stall speed and entry rate. The speed must be specified in equivalent airspeed, so indicated airspeeds from trailing-bomb readings are converted to V_e values and correction is made to find the values at the most critical C.G. position.

The speeds to be determined are defined thus:

V_S -- calibrated stalling speed, or the minimum steady flight speed, in knots, at which the airplane is controllable, with the airplane in the specified configuration, at zero thrust or idle thrust if it is shown that the resultant thrust has no appreciable effect on the stalling speed, and center of gravity in the most unfavorable position.

When obtaining stalling speeds, the airplane must be trimmed for straight flight at any speed not less than 1.2 V_S or more than 1.4 V_S. At a speed sufficiently above the stall speed to ensure steady conditions, the elevator control is applied at a rate so that the airplane speed reduction does not exceed one knot per second. The airplane must also meet the stall characteristics provisions of 25.203.

The tests are made by flying with trailing-bomb from a speed between 1.2 and 1.4 V_S through full stall demonstration, recording indicated airspeed vs. time. V_I is converted to V_e and plotted as in Figure 23.

Entry rate is defined as the slope of the line connecting V_e min and 1.1 V_e min:

$$\text{entry rate} = \frac{dV_e}{dt} = \frac{V_e \text{ min} - 1.1 \ V_e \text{ min}}{\Delta t} \qquad \text{(51)}$$

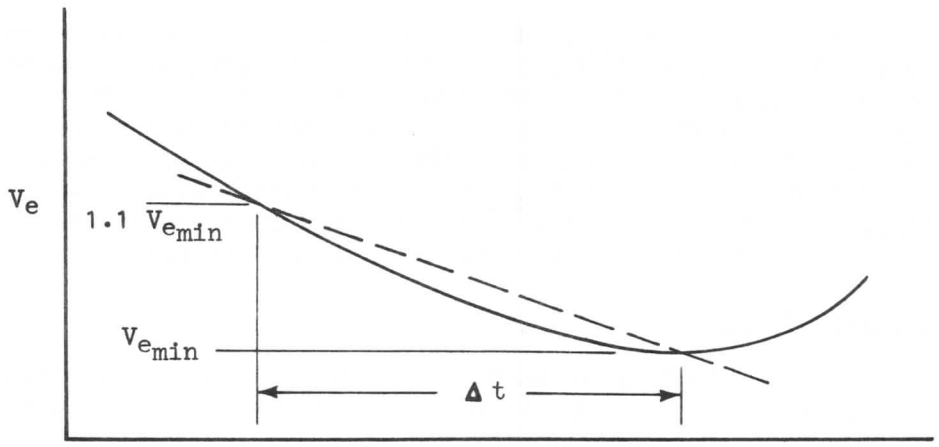

Figure 23.

The C_L at each $V_{e_{min}}$ is calculated by use of the standard lift equation,

$$C_L = \frac{295.37\ W}{V_e^{\,2}\ S}$$

and corrected to the most unfavorable (forward) CG position by the equation,

$$C_{L_{cg(fwd)}} = C_{L_{test}} \left\{ 1 + \frac{MAC}{l_t} \left(CG_{std} - CG_{test} \right) \right\} \qquad (52)$$

where l_t is tail length from the quarter-chord of the wing MAC to the quarter-chord of the horizontal stabilizer MAC and CG_{std} is equal to the forward limit CG for each flap setting.

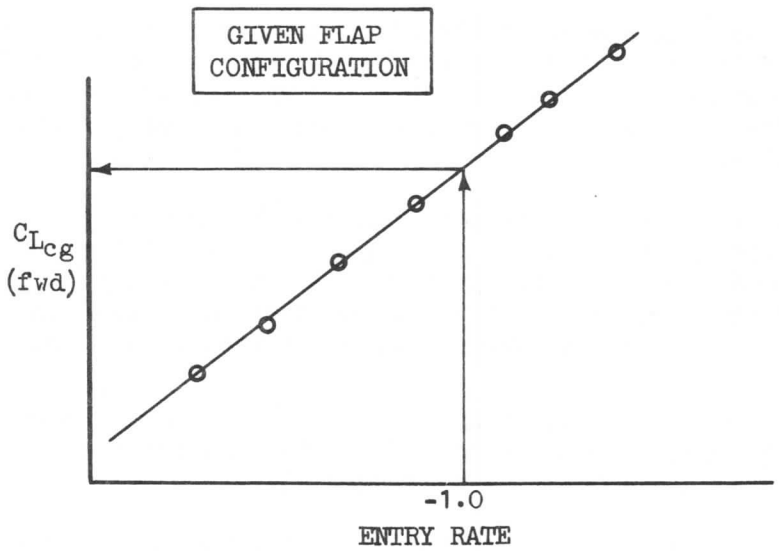

Figure 24.

For each flap configuration tested, a plot of $C_{L_{cg}}$ vs. stall entry rate is constructed as in Figure 24.

The final $C_{L_{stall}}$ is chosen as the value corresponding to the entry rate of -1.0 kt/sec. on an average fairing of these data. Under some conditions, there may be a $C_{L_{stall}}$ variation with gross weight for each flap configuration.

Although certification test flights are run with engines at idle thrust settings, the regulations require that the data be presented for zero thrust operation. It is not always necessary to make a correction, but if the data is to be corrected, it is done in this manner: Stall tests are run not only at idle thrust but also at a low power setting for each configuration. These power-on stall C_L's at -1.0 kt/sec. entry rates are calculated and C_{L_s} vs. net thrust is plotted as in Figure 25.

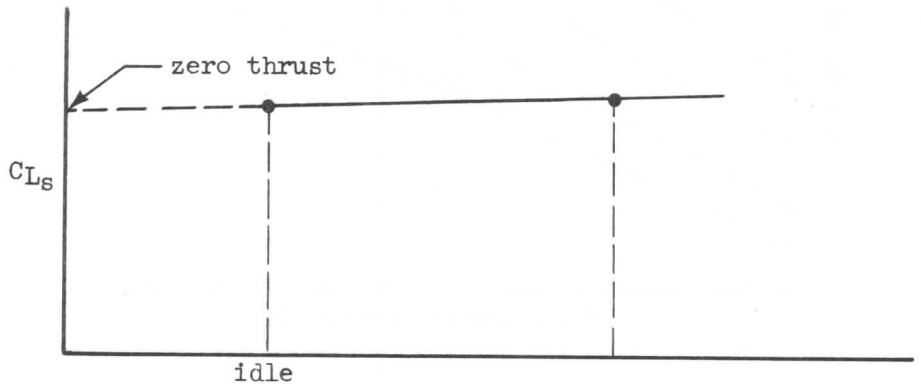

Figure 25.

An extrapolation of these data to zero thrust is used to define the regulation-required-zero-thrust stall data.

Finally, a plot of C_{L_s} vs. δ flap can be drawn and stall speeds plotted as in Figure 26 by calculating V_{e_s} using equation (48).

Not only is it necessary to determine stall speeds for publication; it is mandatory also that the operating characteristics of the airplane in flight close to and through stall be demonstrated according to FAR 25.201 and 25.205. These flight demonstrations must satisfy the regulations and the certification pilots, both in straight flight and in banked turns power-off and power-on. The thrust used for power-on demonstration is that necessary for level, straight flight at $1.6V_s$ (approach configuration, gear retracted, and maximum landing weight). Power-on straight flight demonstrations must be run with one engine inoperative also. The power used to determine the power-on point in Figure 25 is often $1.6V_s$ in order that both the determination of that curve and the demonstration may be accomplished at the same time.

Buffet Limits

The previous discussion dealt with buffet limits as concerned specifically with low speed flight. Actually it is found that airflow separation, which causes buffeting, can be experienced at all flight speeds under certain conditions. This introduces the subject of high speed airflow separation. As the flight

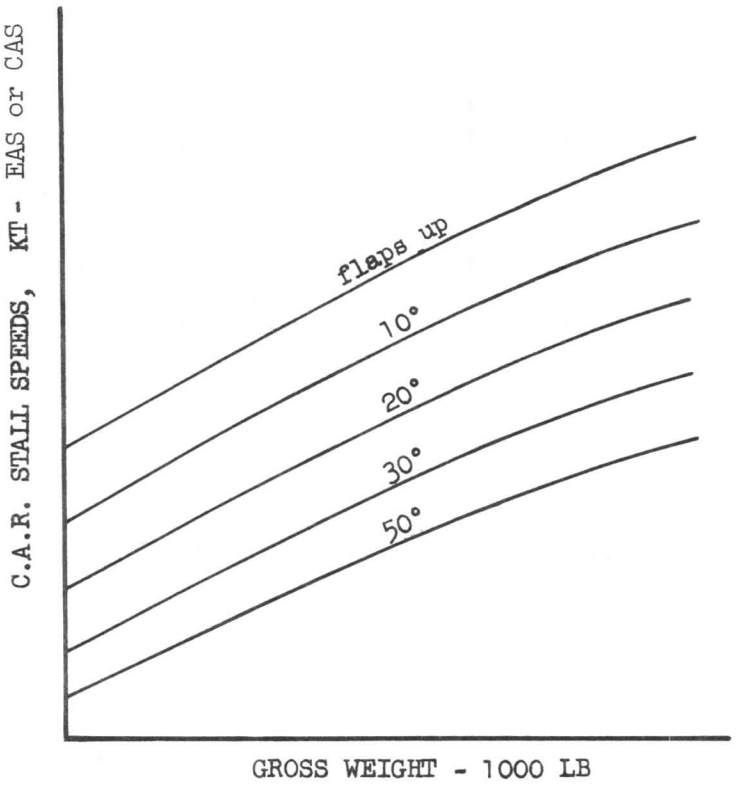

Figure 26.

velocity is increased there is reached a condition where the velocity over some part of the wing becomes supersonic. As was discussed in Section 1, it is found that the deceleration of the supersonic air to subsonic velocity before the air leaves the wing causes a shock wave, which in turn precipitates airflow separation. This separation is capable of causing buffeting just as in the low speed region. The only difference will be that as speed is increased the high speed separation will be aggravated, causing greater buffeting. (The low speed buffeting was aggravated by lowering the speed.)

The buffet limits for the complete speed range of the airplane are defined from the results of flight tests. In these tests the airplane is flown to maximum level flight speed at various altitudes and if buffet is not encountered before maximum speed is reached, then the airplane is dived until it is. At the low speeds the airplane must be accelerated in a banked turn or pull-up to reach buffet. The result of these tests can be conveniently plotted on a single graph as illustrated in Figure 27.

Lines of constant W/δ may also be plotted on Figure 27 by the application of equation (37).

$$\frac{W}{\delta} = 1481.4\ C_L\ M^2\ S$$

By choosing values of W/δ and by knowing the wing area, a relationship between

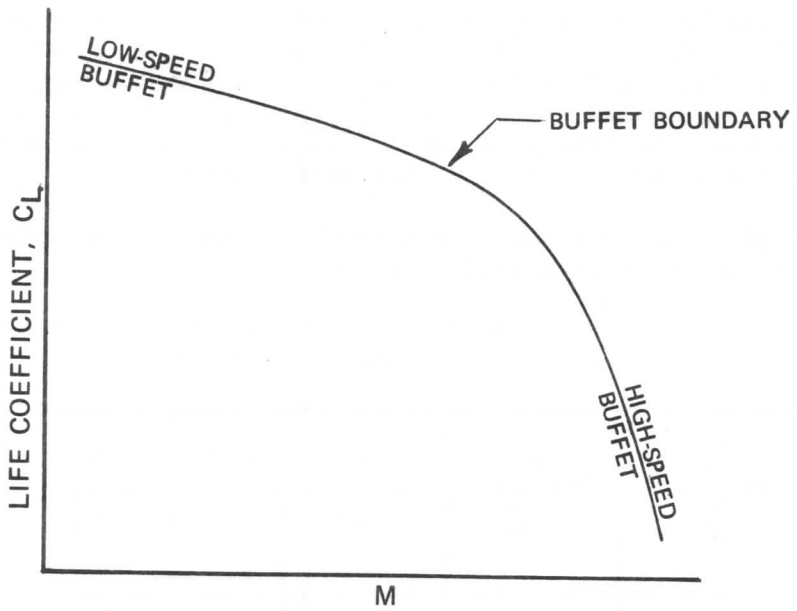

Figure 27.

C_L and Mach number can be obtained. These lines of constant W/δ have particular significance and merit further discussion. Assume that an airplane is initially flying in level flight at a given altitude, weight, and speed. The condition can be shown on the buffet C_L vs Mach number plot as shown in Figure 28.

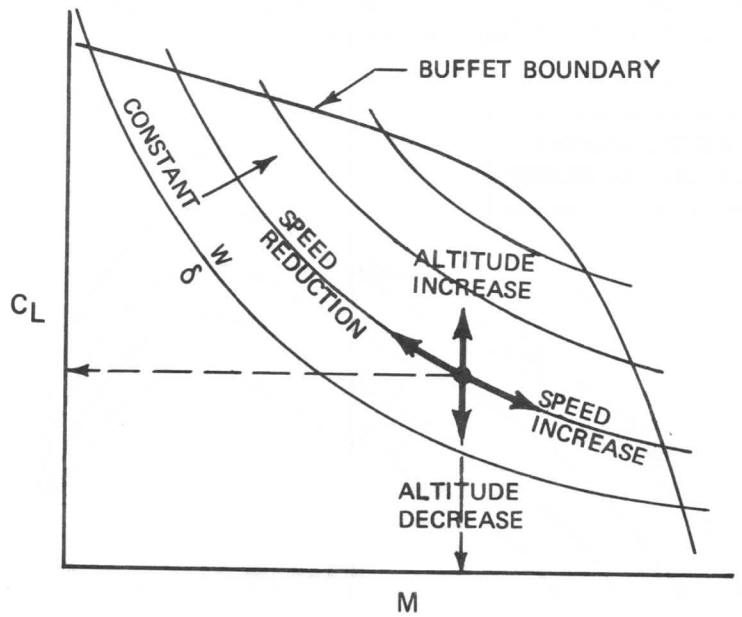

Figure 28.

If the airplane is now speeded up or slowed down it will do so along the line of constant W/δ, assuming that the altitude is maintained constant. But, if the altitude is increased, then at the same gross weight, a higher value of W/δ will result. This means that at the same Mach number as before the lift coefficient will be greater. Conversely, a lower altitude at the same weight will result in a lower W/δ and a lower C_L at the same Mach number.

From such a plot, another chart more useful to the flight crew may be made. Equation (37) may be manipulated to give:

$$\delta = \frac{W}{1481.4\ M^2\ SC_L} \qquad (53)$$

M (Select) (1)	C_L (Fig. 27) (2)	W (Select) (3)	δ (Eq. 53) (4)	ALT (5)	W (Select) (6)	δ (Eq. 53) (7)	ALT (8)

Figure 29.

A table such as shown in Figure 29 may be constructed, selecting a range of Mach numbers for a given weight. By repeating the procedure for several weights, and performing the indicated computations with the use of equation (53), a chart such as that shown in Figure 30 may be made.

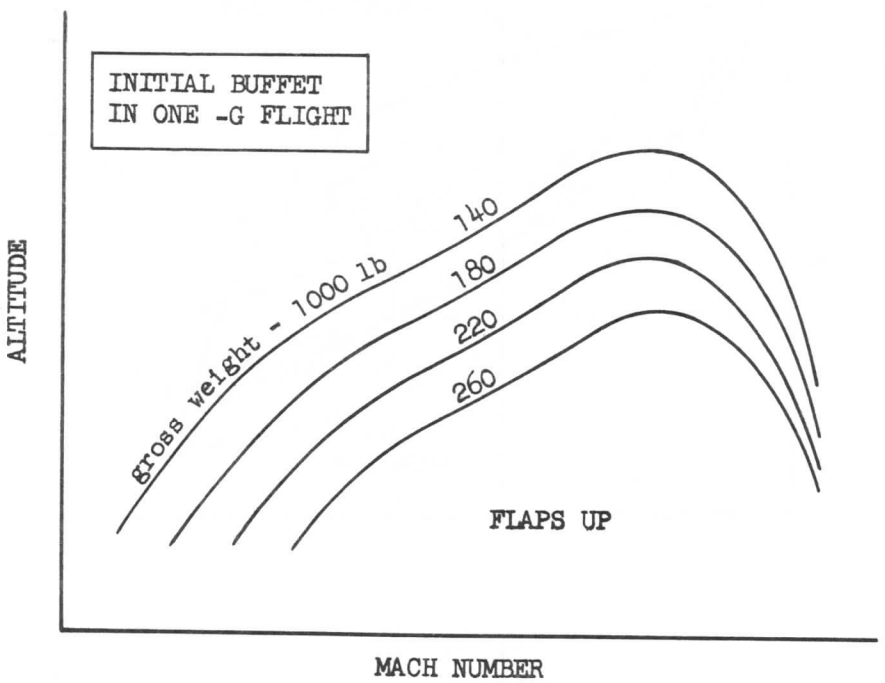

Figure 30.

Having introduced the concept of load factor earlier, another application may now be explored in the area of maneuvering flight.

Consider an airplane in a coordinated banked turn such that no loss of altitude is sustained. Refer to Figure 31. Resolve the lift, L, into its components and note that

$$L \cos \phi = W \qquad (54)$$

where ϕ is the bank angle. Thus the airplane is in equilibrium vertically, but not laterally. There is an unbalanced lateral component of lift, $L \sin \phi$, which will give it a lateral acceleration. In other words, the airplane is in its turn by virtue of the lateral acceleration imparted to it by the lateral component of lift. The situation may be analysed by thinking of the center of gravity of the airplane rotating in a circle as shown in Figure 32. The acceleration may be shown to be $V\, d\theta/dt$, where V is the linear velocity in ft/sec and $d\theta/dt$, the angular velocity, in radians/sec.

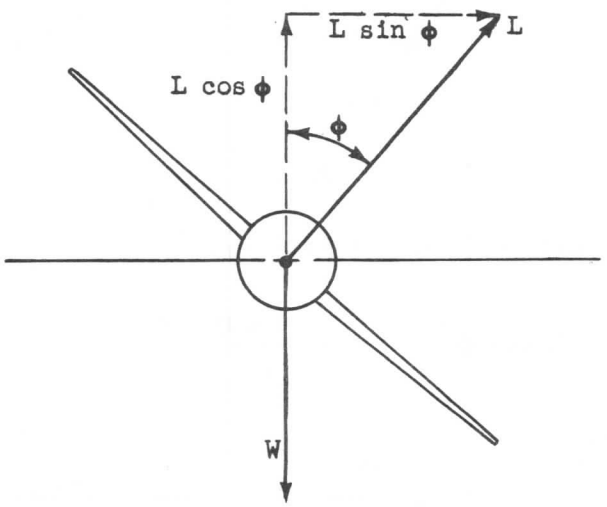

Figure 31.

The accelerating force, (F = Ma), necessary to hold the weight, W, in the circular path is,

$$F = \frac{W}{g} V \frac{d\theta}{dt} \qquad (55)$$

Thus,

$$L \sin \phi = \frac{W}{g} V \frac{d\theta}{dt} \qquad (56)$$

The linear velocity is related to the circular motion:

$$V = R \frac{d\theta}{dt}$$

or,

$$\frac{d\theta}{dt} = \frac{V}{R} \qquad (57)$$

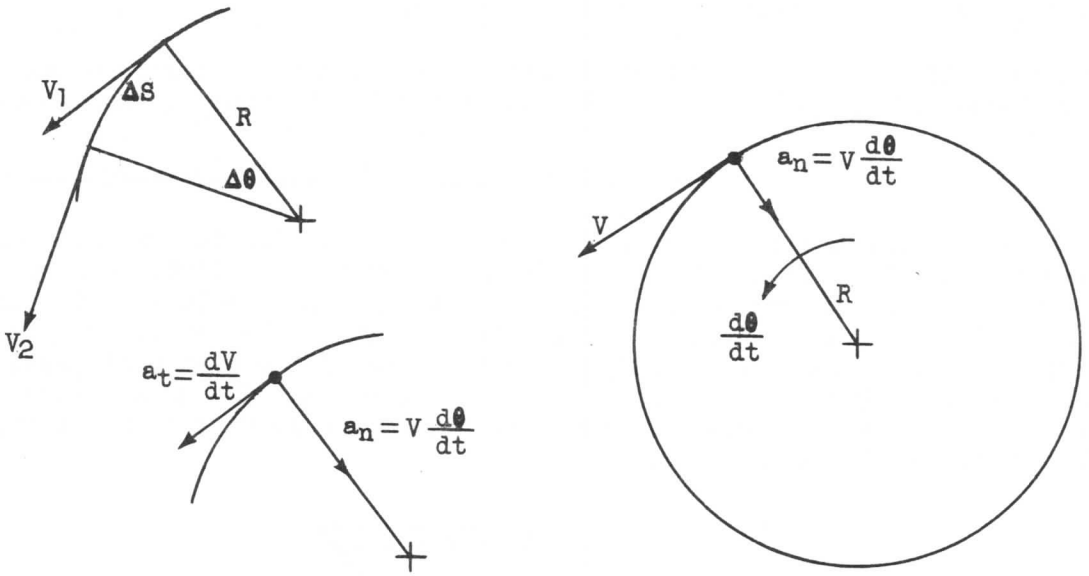

Figure 32.

Substitution of equations (55) and (57) into equation (56) yields

$$L \sin \phi = \frac{L \cos \phi}{g} \frac{V^2}{R}$$

which simplifies into

$$R = \frac{V^2}{g \tan \phi} \qquad (58)$$

This is an expression for the turn radius of an airplane in terms of its true velocity and bank angle. Returning to Figure 31 and equation (49), solving for the load factor, n, in terms of the bank angle:

$$n = \frac{L}{W}$$

$$n = \frac{L}{L \cos \phi}$$

Therefore,

$$n = \frac{1}{\cos \phi} \qquad (59)$$

In a turn, then, the load factor (or number of "g's") experienced is equal to the inverse of the cosine of the bank angle, assuming no loss or gain of altitude during the maneuver. Note also, that if the level maneuver is assumed, then engine thrust must be increased since the lift must be increased over straight and level flight, which in general will cause an increase in drag. Figure 33 shows the solution to equation (58).

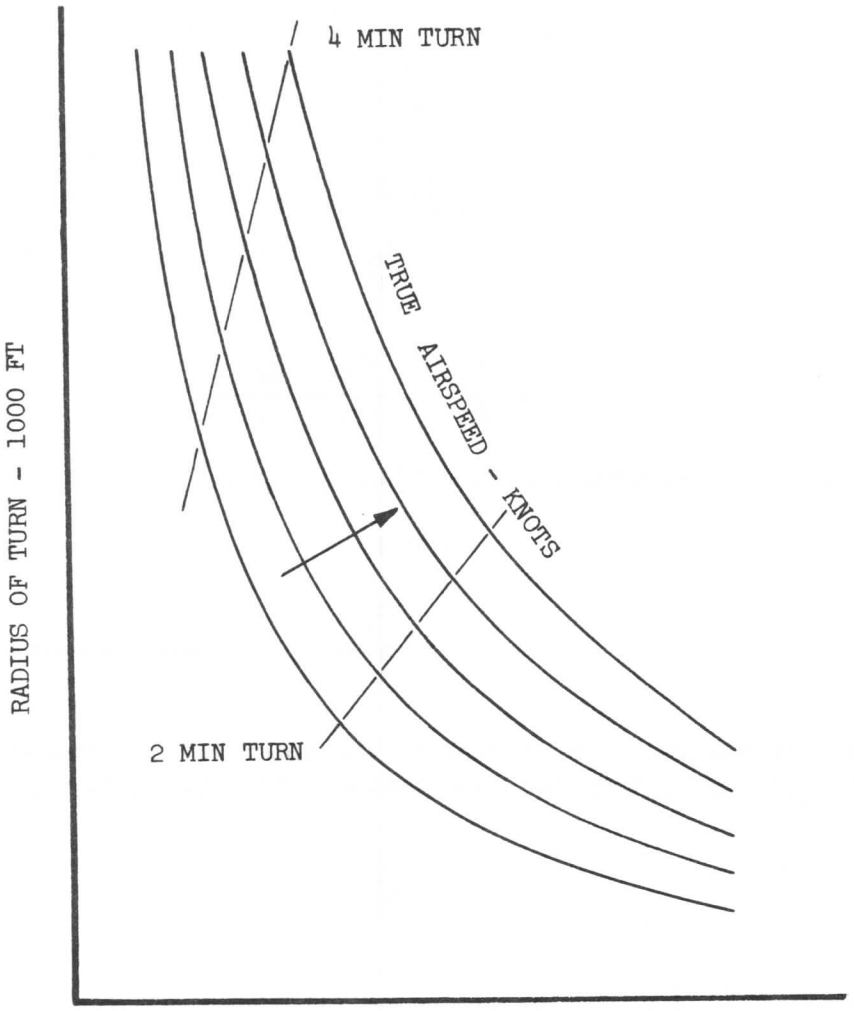

Figure 33.

The preceding discussion of load factor has dealt exclusively with banked turns as the method for producing accelerations on the airplane. Another method, of course, is the "pull-up," or "push-over", which is of interest in the design criteria.

The application of load factor to the present subject of buffet limits is made by referring again to the C_L vs Mach number plot of Figure 28, which is redrawn for convenience in Figure 34. Again, a level flight point is located for a given weight, altitude, and speed. This will define a C_L (denoted as C_{L_1}) and Mach number. Assume now that at the same Mach number the airplane is put into a level flight turn such that the lift now increases to the point corresponding to a new C_L (denoted as C_{L_2}). Once again from equation (49),

$$n = \frac{L}{W}$$

and at C_{L_1},

$$L_1 = W$$

Thus,

$$n = \frac{L_1}{W} = 1$$

But at C_{L_2},

$$L_2 \neq W$$

$$n = \frac{L_2}{W}$$

$$n = \frac{L_2}{L_1} = \frac{C_{L_2}}{C_{L_1}} \frac{q_2}{q_1} \frac{S}{S}$$

If the same speeds are assumed for conditions 1 and 2:

$$q_1 = q_2$$

Thus,

$$n = \frac{C_{L_2}}{C_{L_1}} \qquad \text{(60)}$$

If the airplane is assumed to be banked to the point that it reaches the buffet limit (C_{L_3} in Figure 34), then the load factor developed at this point will be:

$$n = \frac{C_{L_3}}{C_{L_1}}$$

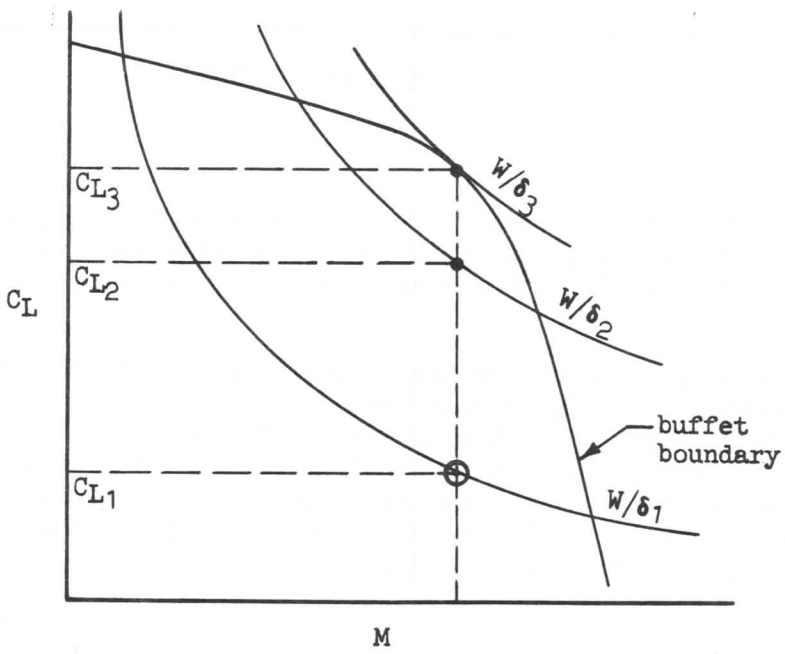

Figure 34.

Thus, in general, considering accelerated flight conditions:

$$L = nW$$

or,

$$\frac{L}{\delta} = \frac{nW}{\delta} \qquad (61)$$

In plotting Figure 34, it was assumed that L = W (level flight) in computing W/δ curves. Actually the calculations were more general since what was really done was to calculate lines of constant L/δ . The curves can thus be labeled as lines of constant nW/δ. as indicated by equation (61). It should also be noted that from equation (60):

$$n = \frac{(L/\delta)_2}{(L/\delta)_1}$$

or,

$$n = \frac{\left(n\frac{W}{\delta}\right)_2}{\left(n\frac{W}{\delta}\right)_1} \qquad (62)$$

With the preceding theory and with the C_L vs Mach number plot, Figure 34, a new plot of the initial buffet boundary on axes of nW/δ and M can be made. See Figure 35. Figure 35 finds its usefulness in defining the acceleration characteristics of the airplane. With this curve as a basis, and assuming equivalent 1-g airplane gross weights a useful chart for any maneuver condition can now be drawn as shown in Figure 36. For a given equivalent 1-g gross weight value, an infinite number of gross weight-load factor combinations may apply.

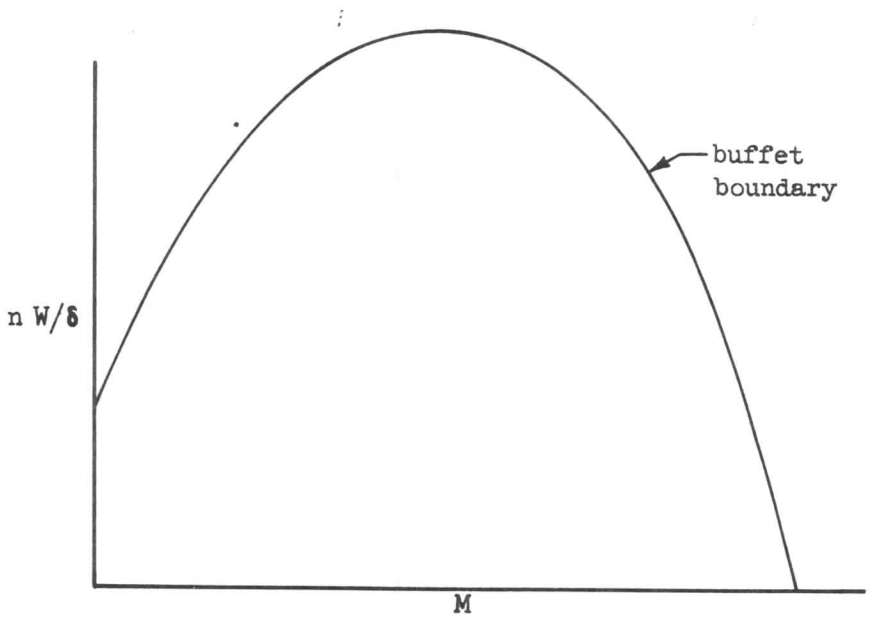

Figure 35.

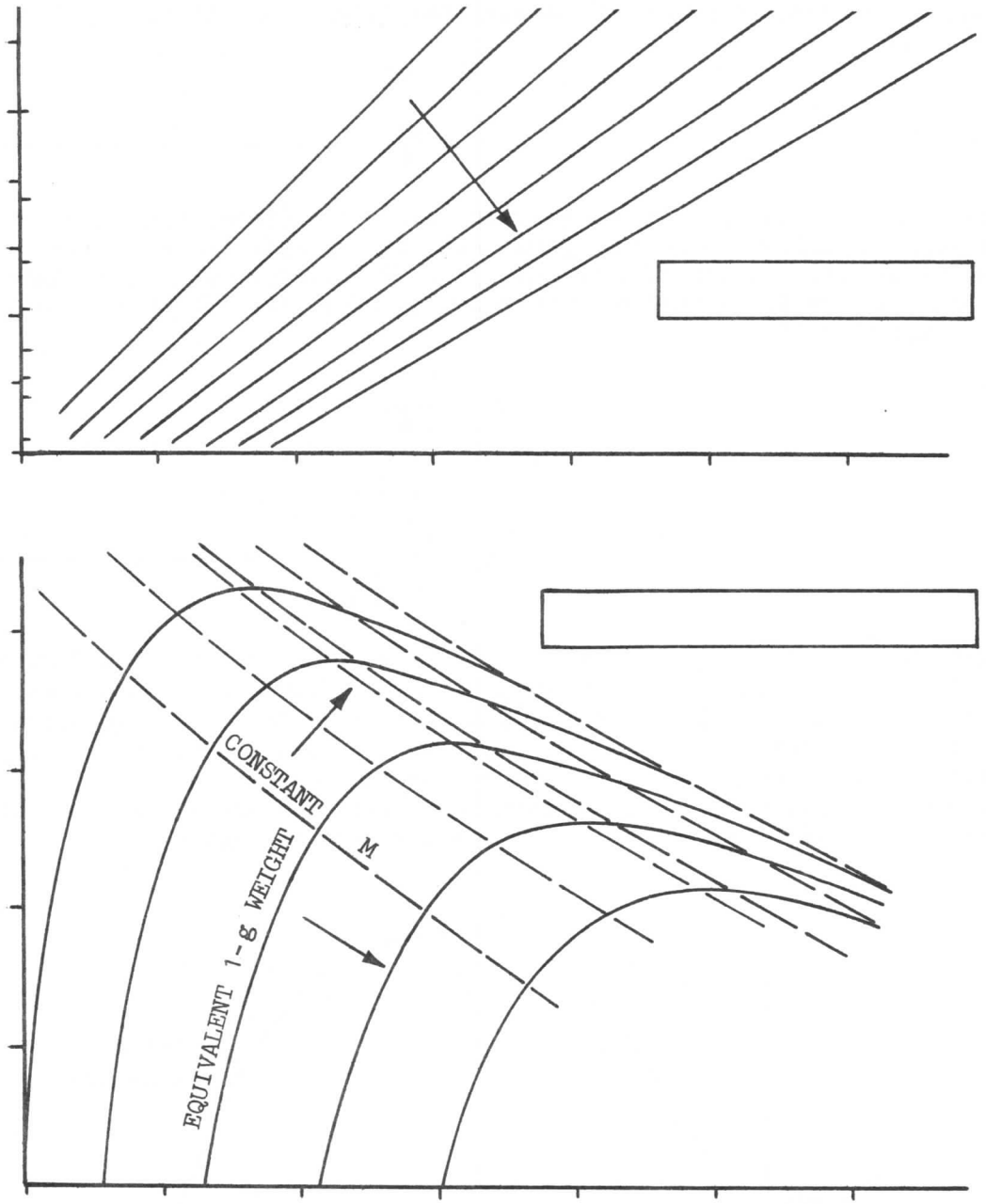

INDICATED AIRSPEED - KNOTS

Figure 36.

Stall Warning

As the airplane is decelerating toward low speed stall, it will encounter initial stall buffet speed at some margin above the stall speed. FAR 25.207 requires that clear and distinctive stall warning shall be apparent to the pilot with sufficient margin to prevent inadvertent stalling of the airplane in all possible landing gear and flap configurations.

It shall be acceptable for the warning to be furnished either through the inherent buffeting characteristics of the airplane or through a device which will give adequate stall warning. A stall warning beginning at a speed 7 percent above the

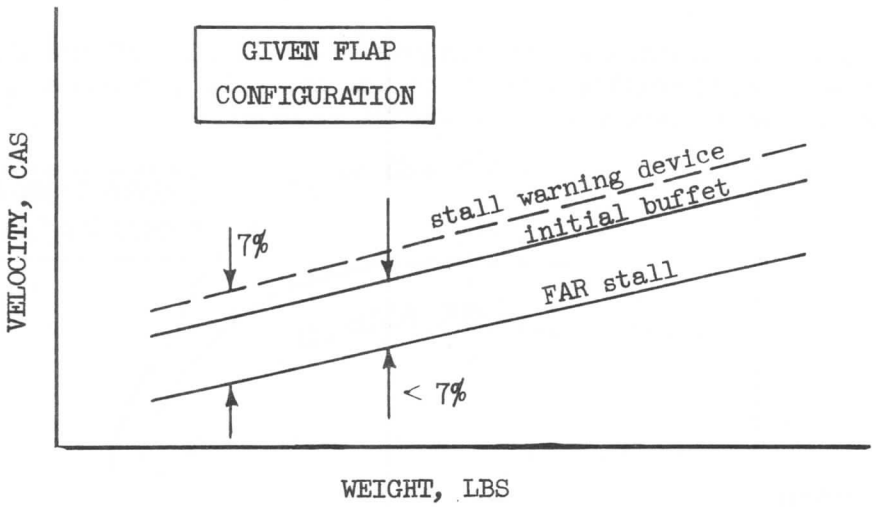

Figure 37.

stalling speed is normally considered sufficient margin. For some flap configurations, where the margin between initial buffet and stall is less than the required 7 percent as shown in Figure 37, a stall warning device is required.

Maximum Speeds

Another flight limit is maximum speed limit under given conditions of weight, altitude, and thrust setting. The determination of maximum speeds can be made from speed - thrust charts similar to Figure 12. This is done by realizing that under all stabilized flight conditions the thrust must equal the drag. Thus, the intersection of any T/δ available line with a T/δ required line will define a maximum speed point for those particular conditions. Of interest are the maximum speeds at all altitudes under conditions of maximum cruise thrust. The intersections, when taken from a plot such as Figure 12, can be plotted on axes of W/δ vs M as in Figure 38. Also, the buffet boundary can be drawn on Figure 38. The appearance of the buffet line on Figure 38 indicates the ability of the airplane to approach buffet in level flight conditions. From such a plot as Figure 38 another useful and more easily understood plot can be made.

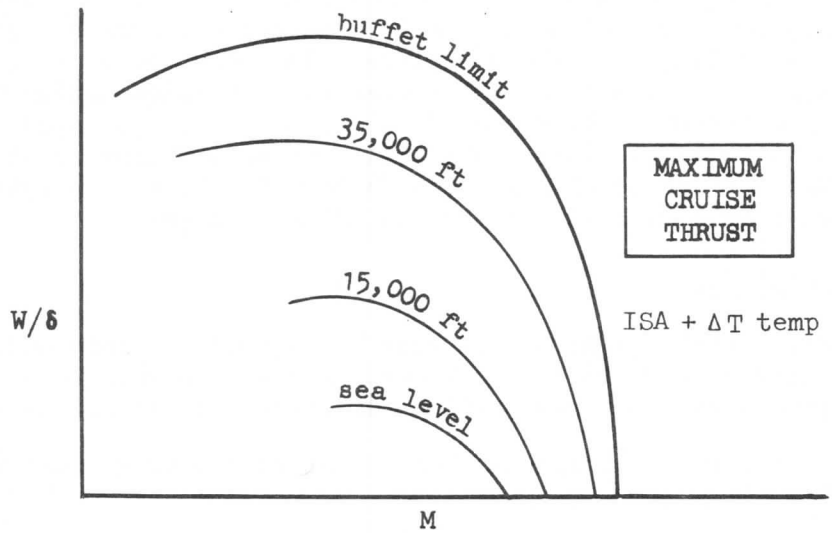

Figure 38

Figure 39 shows the altitude - true airspeed capabilities of the airplane at various weights when operating with rated thrust. The structural placard speed limit, to be discussed later, is also shown.

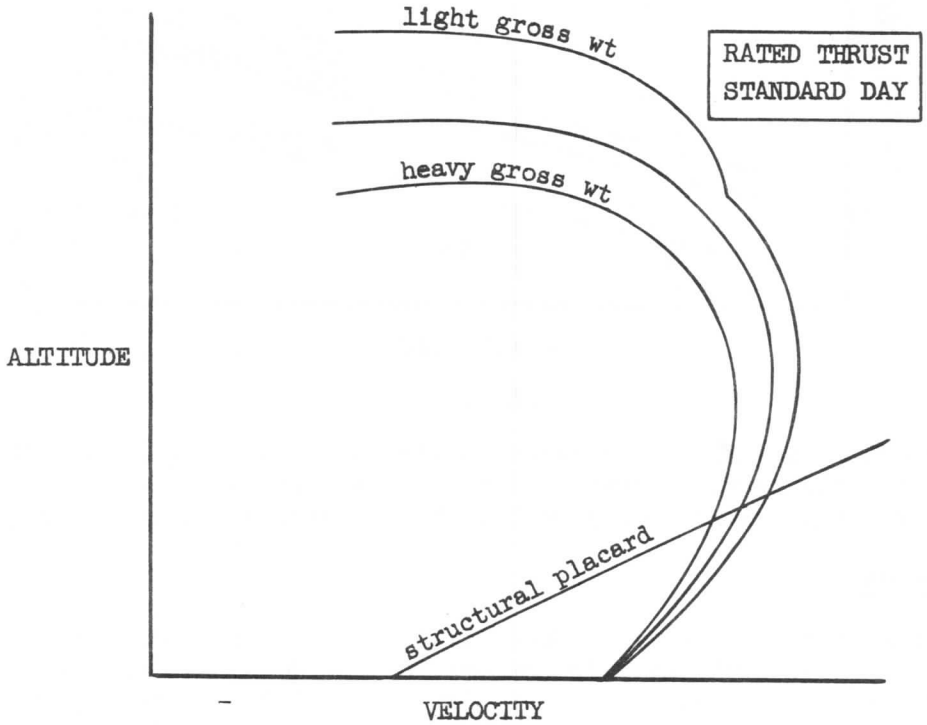

Figure 39.

Ceilings

The maximum altitude obtainable under given conditions of thrust and weight is defined as the absolute ceiling of the airplane. Although the altitude capability of the jet transport is not approached, it is desirable to discuss this condition briefly. Referring to Figure 38, it can be seen that the highest points on each curve of constant altitude represent the maximum W/δ attainable at that altitude and thus define the maximum weight attainable. These altitudes are the absolute ceilings for those weights. The same may be seen from Figure 39 in which, again, the peaks of the constant-weight lines define the absolute ceilings at those weights. Note that in all cases, a unique speed is associated with the absolute ceiling. This means that when an airplane is at its absolute ceiling (a practical impossibility) it will have to fly at one speed only. To fly either faster or slower will result in altitude loss.

Structural Limitations

Since structural airspeed limitations must be considered, some additional terminology, as defined in Part 25 of the Federal Aviation Regulations, is required. Some of the speed limits and explanations of their determinations are given below.

V_A -- design maneuvering airspeed. The design maneuvering speed V_A shall not (per FAR 25.335(c)) be less than:

$$V_A = V_S \sqrt{n} \qquad (63)$$

where n is the limit maneuvering load factor at V_c (n = 2.5 for 707 airp.) and V_s is the FAR stall speed for clean configuration at maximum flight gross weight. (As determined by FAA flight test of the airplane.) V_A is the maximum speed at which application of full available rudder or elevator will not overstress the airplane. In the flaps up configuration, full aileron can be applied at any speed. Aileron, rudder or angle-of-attack controls must be designed for full deflection at V_A (FAR 25.1583(a)(3)).

Example:

From equation (37), $$\frac{L}{\delta} = \frac{nW}{\delta} = 1481.4\ C_L M^2 S$$

and for the 707/720 with a wing area of 2433 square feet,

$$C_L M^2 = .27745 \times 10^{-6} \frac{nW}{\delta} \qquad (64)$$

From equation (64), a value of $C_L M^2$ may be found for the condition specified; that is, the flaps up stalling speed at the maximum weight. Evaluating equation (64) for W = 243,000 pounds, n = 1, and at sea level (δ = 1.000), $C_L M^2$ = .067. From a curve showing the variation of $C_L M^2$ with M, the stall Mach number, hence the stall speed, V_S, may be determined. Figure 40 shows the variation of Mach with $C_L M^2$, and is constructed from $C_{L_{MAX}}$ vs Mach number relationships as shown in Figure 41. Figure 40 shows the stall Mach number, M_S, to be .244. At sea level, this corresponds to V_{eS} = 161 knots.

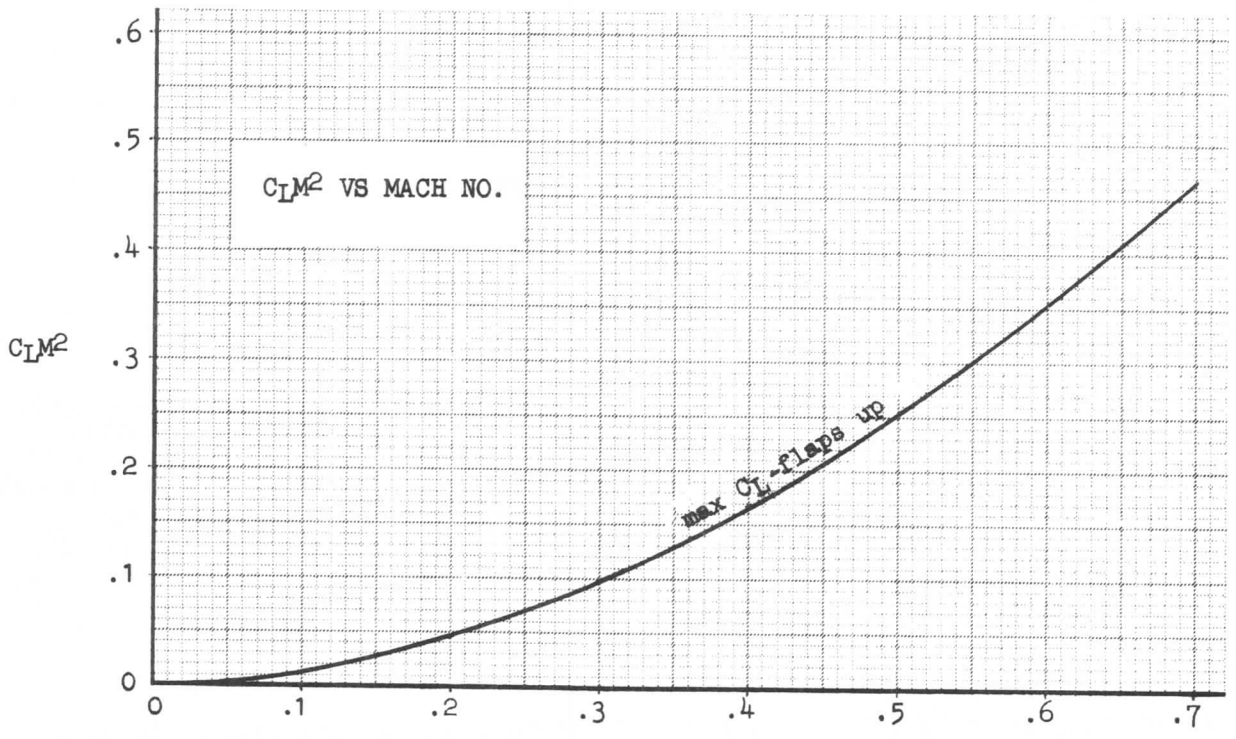

Figure 40.

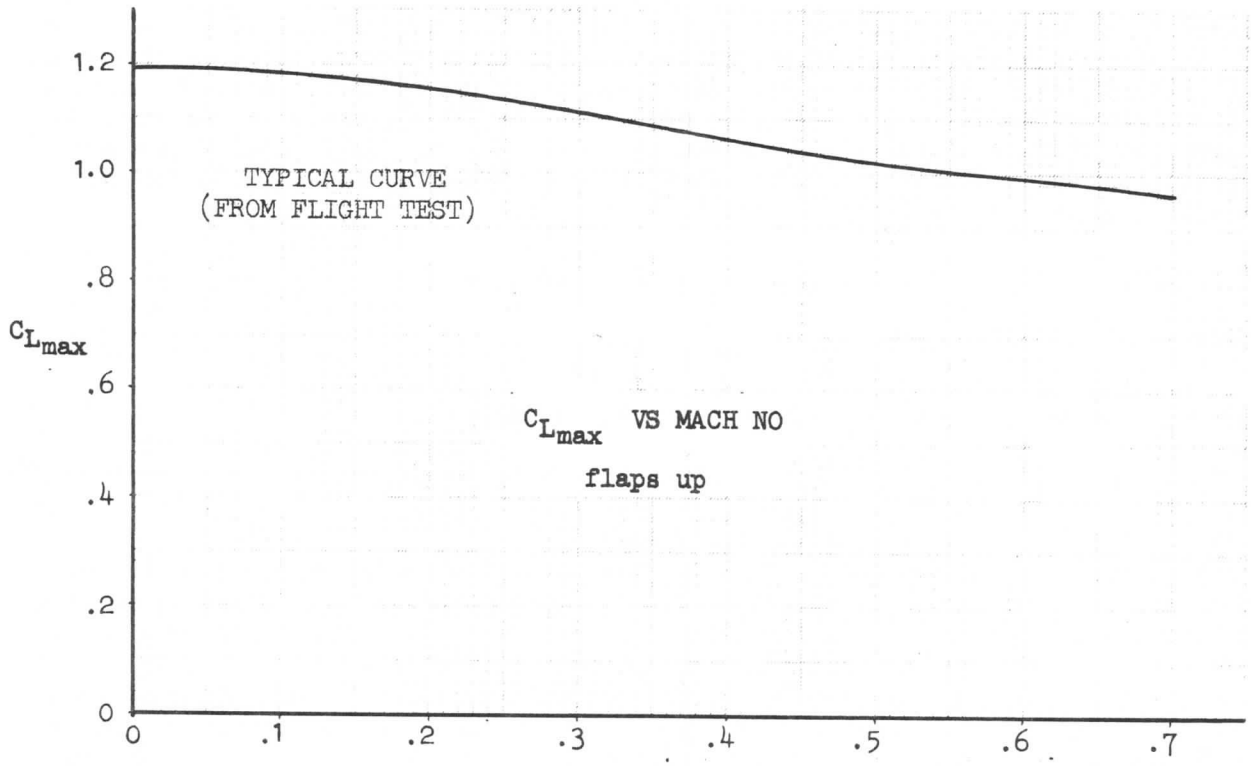

Figure 41.

Evaluating V_A at sea level,

$$V_A = 161 \sqrt{2.5} = 255 \text{ knots, EAS.}$$

where limit load factor n = 2.5.

V_B -- design speed for maximum gust intensity. This speed shall be selected not to be lower than:

$$V_B = V_S \sqrt{n_{gust} @ V_C} \qquad \text{(WHEN BELOW 20,000 FT)} \quad (65)$$

or as determined by the intersection of the 66 fps gust line and $C_{L_{MAX}}$ line on the V-n diagram as shown in Figure 42. V_S is the flaps-retracted stalling speed at the particular weight under consideration. V_B need not be greater than V_C. per FAR 25.335 (d).

For Boeing airplanes, a V_B speed greater than FAR requirements is used for structural analysis.

The V-n Diagram

The V-n diagram, Figure 42, is a very convenient means of indicating the loading conditions on the airplane due to a sudden pull-up, push-over, maneuver or gust penetration which the airplane must be designed to withstand. In trimmed level flight through still air, the airplane is subjected to loads normal to its

longitudinal axis of only such magnitude as to counteract the gravitational force of its weight. The condition is called 1 "g" or n = 1 flight. In order to pull up, push over, or maneuver, additional forces must be applied and additional loads are imposed upon the structure. Also, vertical gusts or the vertical components of other gusts impose the same type of loading by changing the relative angles of attack. These loading conditions must be taken into consideration in the design of the structure. The commercial transport is not expected to be subjected to violent maneuvers such as might be expected to be the case with fighter aircraft, missiles, or even large bombardment airplanes. Figure 42 shows that operating close to the FAR V_B speed (as determined by the intersection of the maximum gust line and the $C_{L_{MAX}}$ line) in gusty weather results in the least increase in load factor, and increasing the gust penetration speed for design and operational purposes increases the load factor for a given gust intensity. Since an airplane is limited to its design load factor it will be limited to some maximum rough air gust speed. The above analysis is for vertical gusts and the maximum V_B speed may be limited by horizontal gusts on the vertical fin and rudder. On 707 airplanes, the horizontal gusts are usually most limiting. Therefore, the recommended gust penetration speed under gusty conditions can be any speed between the minimum speed as defined by FAR, and the maximum V_B speed used for structural analysis.

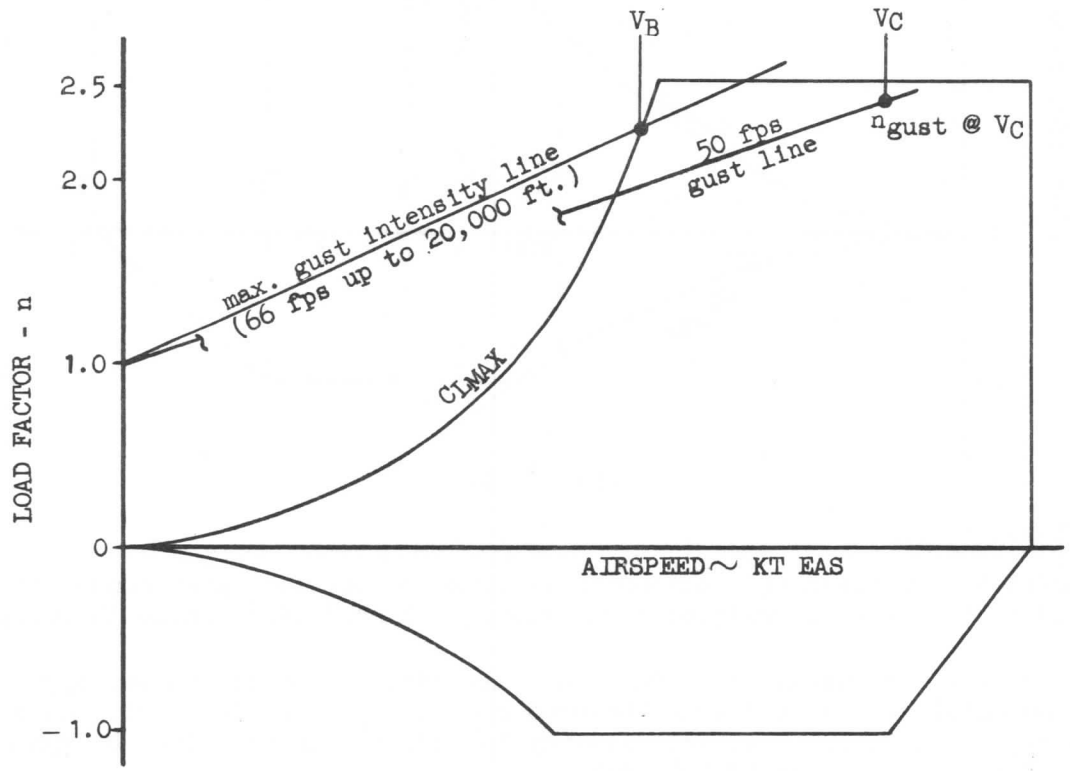

Figure 42.

Maneuvering Envelope

Maximum maneuvering acceleration limits have been imposed to comply with Federal Aviation Regulations.

"The positive maneuvering load factor n for any flight speed up to V_D shall be selected by the applicant, except that it shall not be less than 2.5.

The negative maneuvering load factor shall have a minimum value of -1.0 at all speeds up to V_C, and it shall vary linearly with speed from the value at V_C to zero at V_D." (per FAR 25.337 (b) and 25.337 (c).)

The maneuvering envelope can now be drawn using the pull up and push-over values up to V_A and the design maneuver factors defined previously. The envelope is shown on Figure 43.

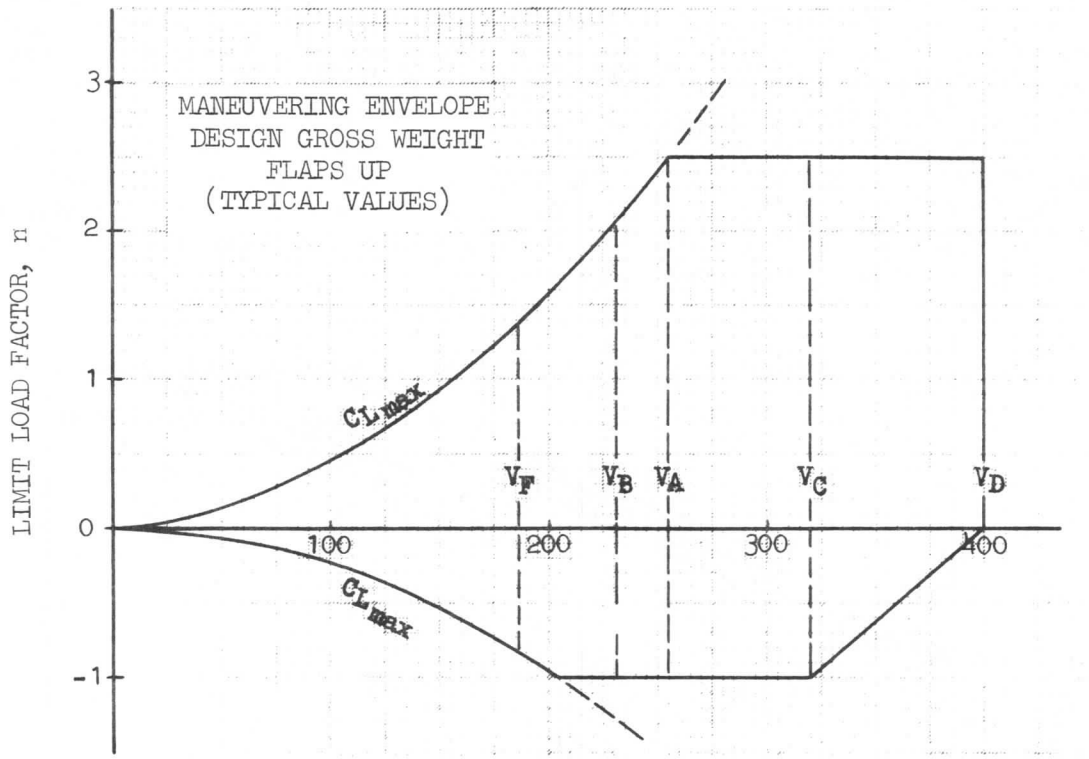

Figure 43.

Gust Envelope

Gust effects are based upon encountering standard vertical gust components as defined in the Federal Aviation Regulations, FAR 25.341(a), while in level flight:

"Positive (up) and negative (down) rough air gusts of 66 fps at the speed V_B shall be considered at altitudes between sea level and 20,000 feet. At altitudes above 20,000 feet, the gust velocity may be reduced linearly from 66 fps at 20,000 feet to 38 fps at 50,000 feet.

Positive and negative gusts of 50 fps at speed V_C shall be considered at altitudes between sea level and 20,000 feet. At altitudes above 20,000 feet, the gust velocity may be reduced linearly from 50 fps at 20,000 feet to 25 fps at 50,000 feet.

Positive and negative gusts of 25 fps at the speed V_D shall be considered at altitudes between sea level and 20,000 feet. At altitudes above 20,000 feet, the gust velocity may be reduced linearly from 25 fps at 20,000 feet to 12.5 fps at 50,000 feet.

Gust load factors shall be assumed to vary linearly between the specified conditions. See Figure 44.

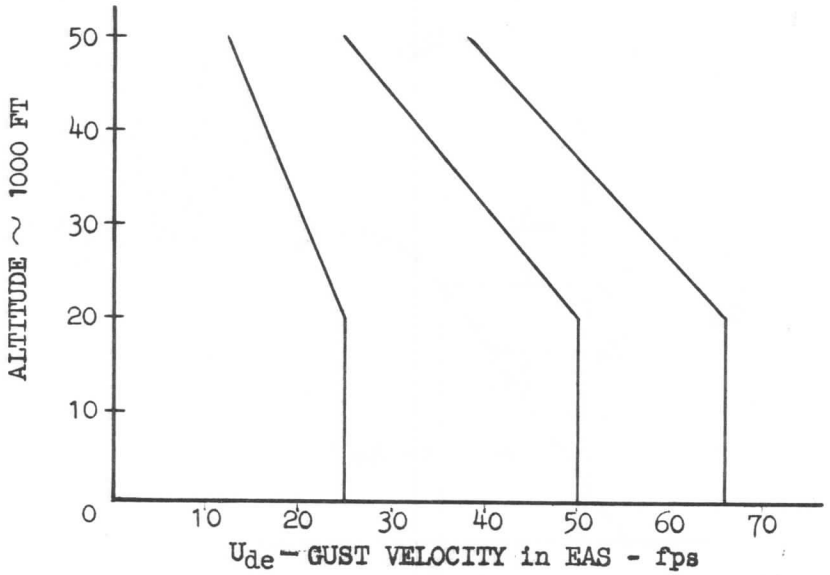

Figure 44.

"In the absence of a more rational analysis, the gust load factors shall be computed in accordance with the following formula:

$$n = 1 + \frac{K_g \, U_{de} \, V_e \, m}{498 \, (W/S)} \qquad \text{(66)}$$

where:

m = slope of airplane normal force coefficient curve C_{N_A} per radian if the gust loads are applied to the wings and the horizontal tail surface simultaneously by a rational method. It shall be acceptable to use the wing lift curve slope C_L per radian when the gust load is applied to the wings only and the horizontal tail loads are treated as a separate condition."

per FAR 25.341 (c)

The load factor equation prescribed above can be derived in this manner:

Consider the velocity vector diagram in Figure 45:

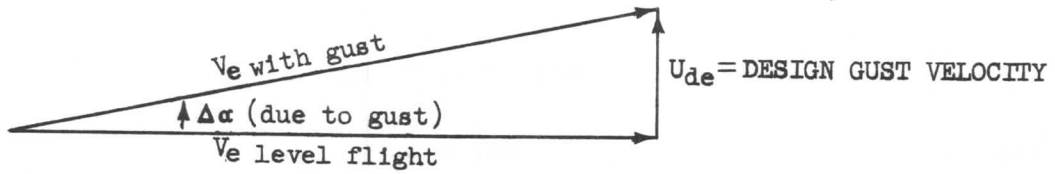

Figure 45.

As a result of the gust whose vertical velocity component is U_{de}, the angle of attack is changed by the increment $\Delta\alpha$ and the C_L is increased suddenly by the increment ΔC_L in Figure 46.

Since the change is sudden, the velocity has not had time to change appreciably, so,

$$L_2 \sim C_{L_2}$$

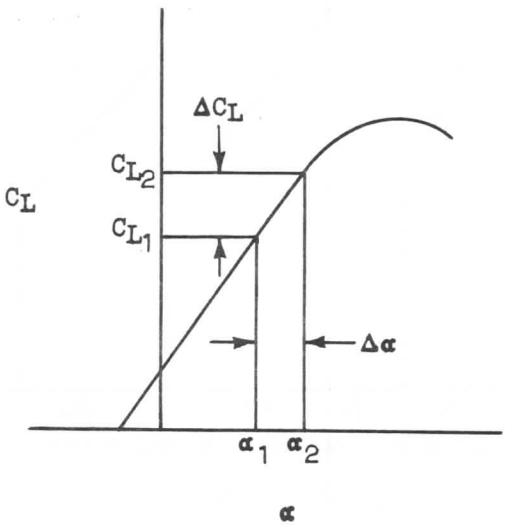

Figure 46.

and,

$$n = \frac{C_{L_2}}{C_{L_1}}$$

But,

$$C_{L_2} = C_{L_1} \pm \Delta C_L,$$

so,

$$n = \frac{C_{L_1} \pm \Delta C_L}{C_{L_1}}$$

$$n = 1 \pm \frac{\Delta C_L}{C_{L_1}}$$

$$\Delta C_L = \frac{dC_L}{d\alpha} \Delta\alpha$$

or,

$$\Delta C_L = m \Delta\alpha$$

where m is the slope of the lift curve per radian. If $\Delta\alpha$ is given in degrees, it must be changed to radians or m replaced by a, the slope per degree.

Since design gust velocity, U_{de}, is specified in fps and velocity is in knots,

$$\Delta\alpha = \frac{U_{de}}{1.688\ V_e}$$

The angle $\Delta\alpha$ is assumed to be small.

$$\Delta C_L = \frac{m\ U_{de}}{1.688\ V_e}$$

Also,

$$C_{L_1} = \frac{295.37\ W}{V_e{}^2 S}$$

Since,

$$n = 1 \pm \frac{\Delta C_L}{C_{L_1}}$$

$$n = 1 \pm \frac{m\ U_{de}}{1.688\ V_e} \quad \frac{V_e{}^2 S}{295.37\ W}$$

$$n = 1 \pm \frac{m\ U_{de}\ V_e}{498\ (W/S)} \qquad (67)$$

This is a "sharp edge gust formula" based on an assumption of instantaneous gust penetration. That is, the gust is assumed to act on the entire airplane at the same time. However, as an airplane penetrates an actual gust, the gust does not act on the entire airplane at the same time. This condition tends to alleviate the acceleration loading and decreases the value of the load factor determined by equation (67) by a factor, K_g. The value of K_g, known as the "gust alleviation factor", has been determined empirically to yield the formula:

$$K_g = \frac{.88\ \mu_g}{5.3 + \mu_g} \qquad (68)$$

where, μ_g, the "airplane mass ratio" equals,

$$\mu_g = \frac{2(W/S)}{\rho\ \bar{c}\ m\ g}$$

and $\bar{c}$ is the mean geometric chord.

Thus, including the "Kussner-Wagner" effect, the equivalent sharp edge gust formula is:

$$n = 1 \pm \frac{K_g\ m\ U_{de}\ V_e}{498\ (W/S)} \qquad (69)$$

Equation (69) assumes that the lift curve slope, m, has incorporated the compressible and aeroelastic effects of the wing. The data for the 707 airplane are based on a lift curve determined by a steady-state aeroelastic analysis of the wing which includes the Mach number effects and the flexibility characteristics.

The gust envelope calculated at the critical altitudes and with the CG at 33.5% MAC for a typical 707 is shown in Figure 47.

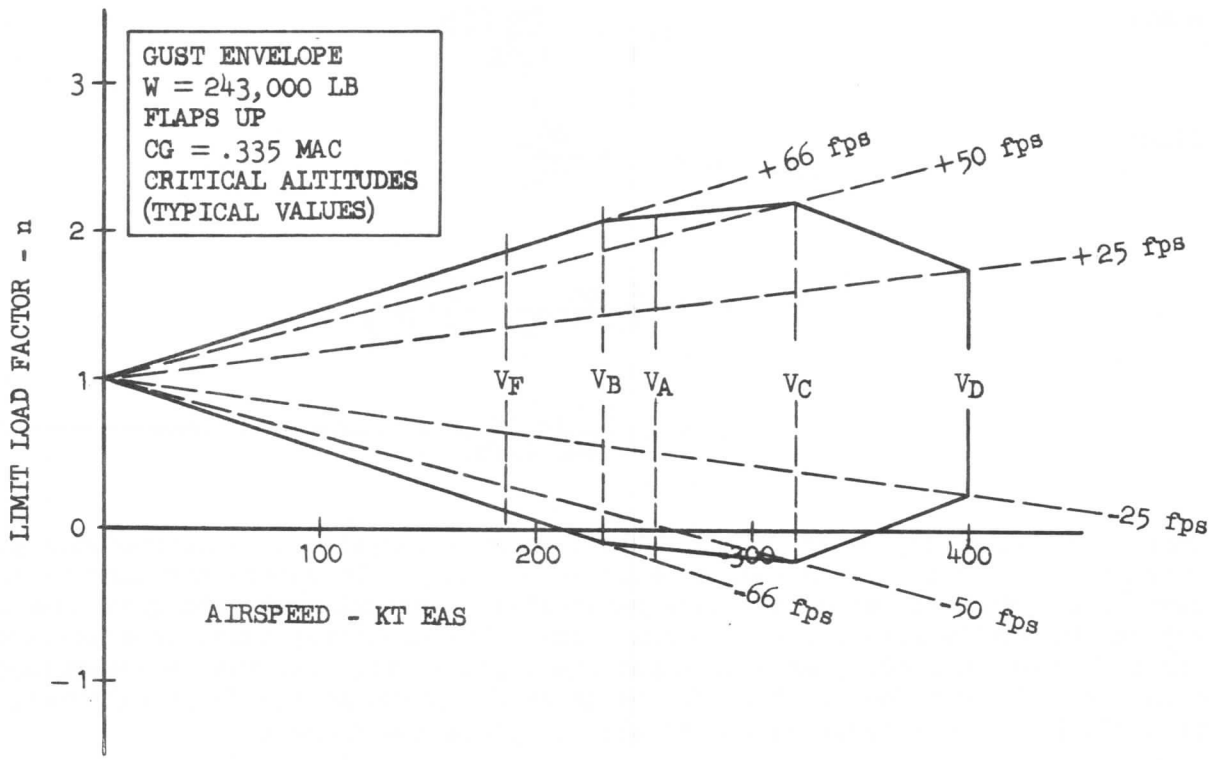

Figure 47.

Composite V-n Diagram

The airplane must be structurally able to withstand all load factors included on or within the two envelopes presented above. Thus all the design load factors can be given on and within a composite envelope which includes all regions enclosed by the two envelopes. This design V-n diagram for the critical altitudes with CG at .335 MAC is shown on Figure 48.

The diagram has been limited to speeds above stall since it is impossible to fly at lower speeds. It will be noted that the envelope does not include the line for the 66 fps gust at velocities near V_S even though the load factor is greater than that for the pull-up condition. The reason for this is that the pull-up line was drawn to reflect a high angle of attack for which lift was maximum. Therefore, the pull-up line represents the maximum loading condition in this region. Although the gust line indicates higher values, they cannot be attained and are of academic interest only.

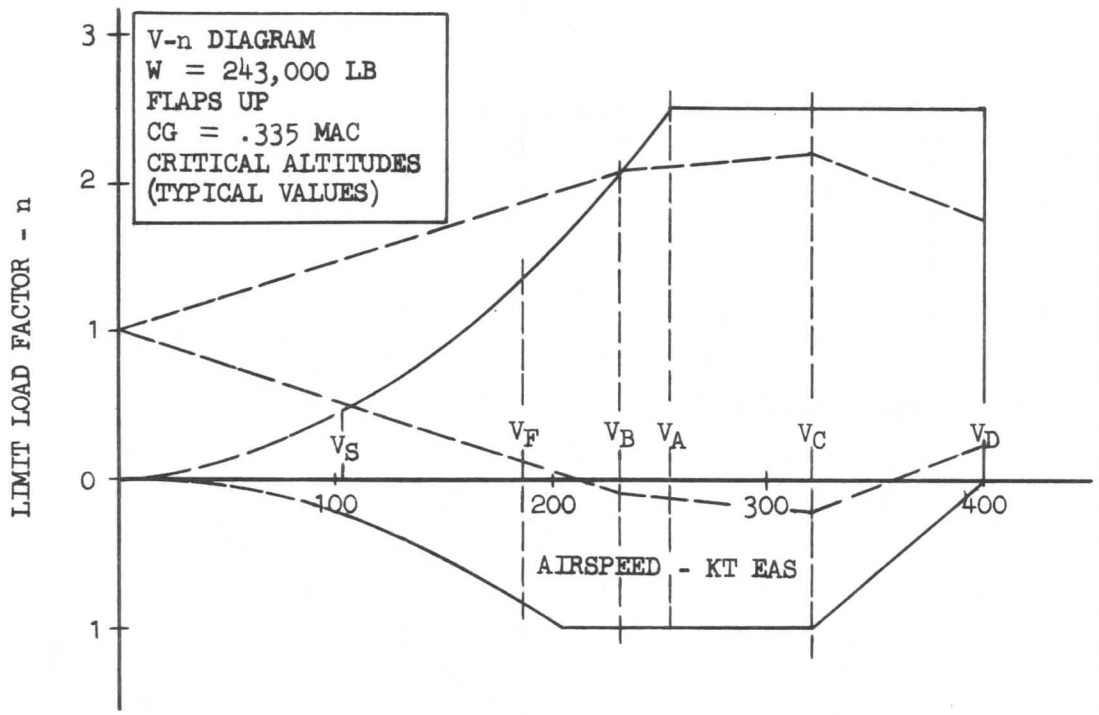

Figure 48.

V_C -- design cruising speed. "The minimum design cruising speed, V_C, shall be sufficiently greater than V_B to provide for inadvertent speed increases likely to occur as a result of severe atmospheric turbulence. In the absence of a rational investigation substantiating the use of other values:

$$V_C \geq V_B + 43 \text{ knots} \qquad (70)$$

except that it need not exceed the maximum speed in level flight at maximum continuous power for the corresponding altitude. At altitudes where V_D (design dive speed) is limited by Mach number or compressibility, it shall be acceptable to limit V_C to a Mach number selected by the applicant."

per FAR 25.335 (a)

V_C and M_C values for 707 airplane are arbitrarily selected by Boeing, meeting FAR requirements.

V_D -- design dive speed. The design dive speed chosen by the applicant shall be used in determining the maximum operating limit speed for the airplane in accordance with FAR 25.1505 ;" which section insures that this speed shall not be exceeded if the airplane is upset from flight at normal maximum operating speed."

per FAR 25.335 (b)

For 707 type airplanes, V_D and M_D are selected as required for certification.

The structural design speeds for a typical 707 airplane are shown in Figure 49.

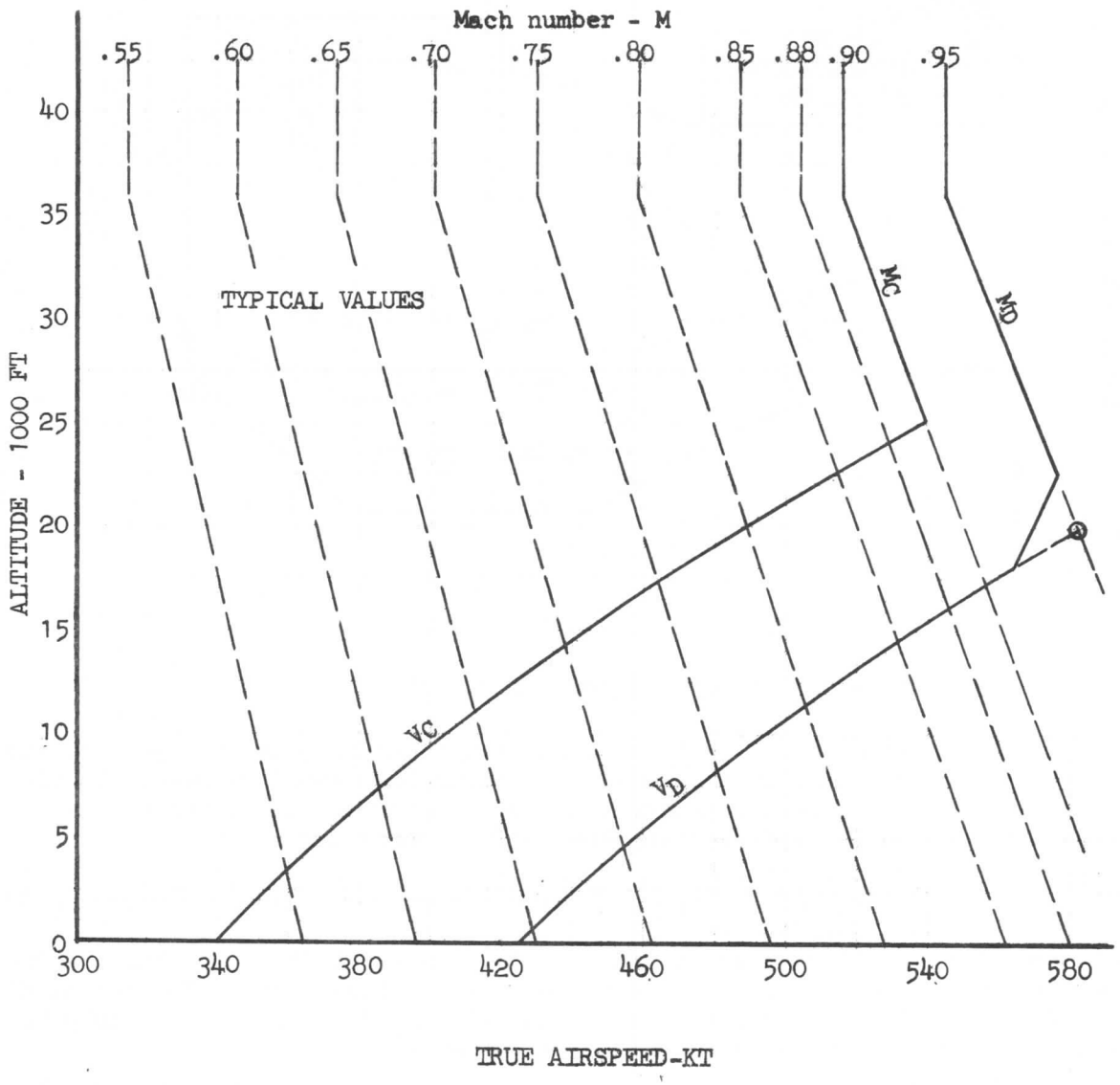

Figure 49.

V_F -- design flap speeds. The flap placard speeds are determined to meet design criteria per FAR 25.335 (e)(3):

"V_F shall not be less than:

1.6 V_S with flaps in takeoff position at maximum takeoff weight;

1.8 V_S with flaps in approach position at maximum landing weight; and

1.8 V_S with flaps in landing position at maximum landing weight."

"Wing flaps and their supporting structure and operating mechanism **must** be designed for the critical loads resulting from the conditions prescribed in **FAR** 25.345 taking into account the loads occurring during transition from one flap position and airspeed to another."

per FAR 25.457

"The wing flap control shall be designed to retract the flaps from the fully extended position during steady flight at maximum continuous engine power at any speed below V_F + 8.5 (kts)."

per FAR 25.697 (d)

The stall speed for the maximum takeoff and landing weights may be obtained from Figure 26.

A typical set of flap placard speeds are tabulated in Figure 50. For convenience, a plot of the flap placard speeds is shown in Figure 51. Also, for some airplanes, there may be an altitude placard for flaps-down operation since it may be possible to exceed limit loads when applying maximum roll capability.

DEGREES	PLACARD SPEEDS, **KTS EAS**
50	185
30	210
20	220
10	230

Figure 50.

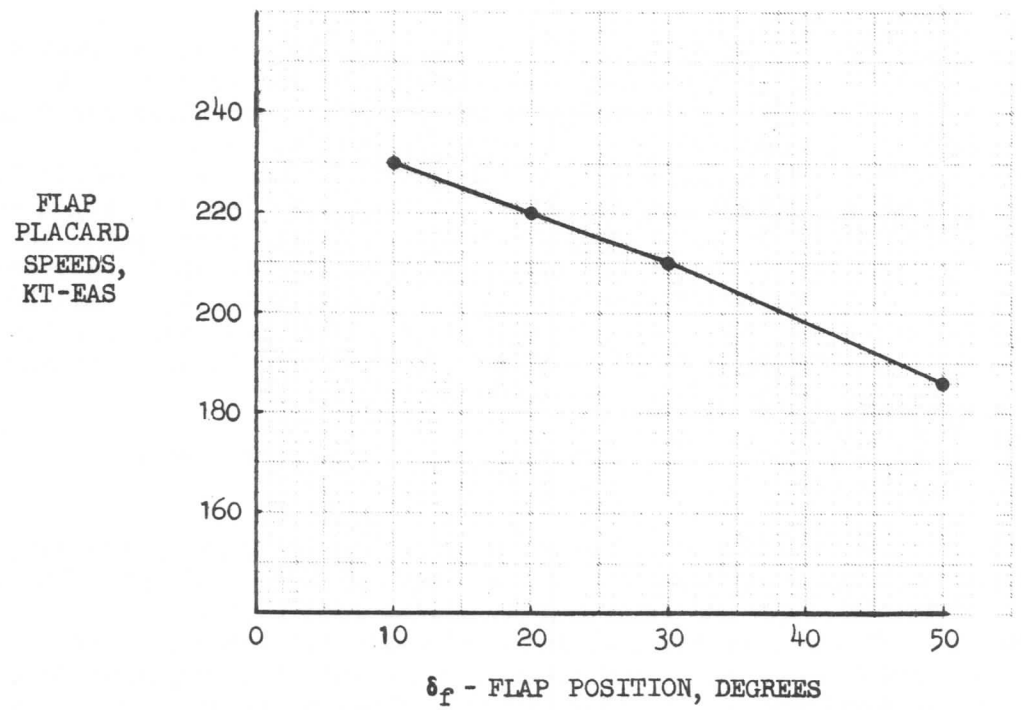

Figure 51.

There are no speed limitations imposed on the spoilers. The spoiler angle, for a given input signal will decrease with an increase in airspeed. As the "q" force on the spoilers increases it will overcome the hydraulic pressure in the actuator, and the spoiler will "blow down." Figure 52 shows the design blowdown speeds. It should be understood that the spoiler angle decreases with altitude for any given equivalent airspeed because of compressibility effects. However, deviations are small enough that they are usually neglected.

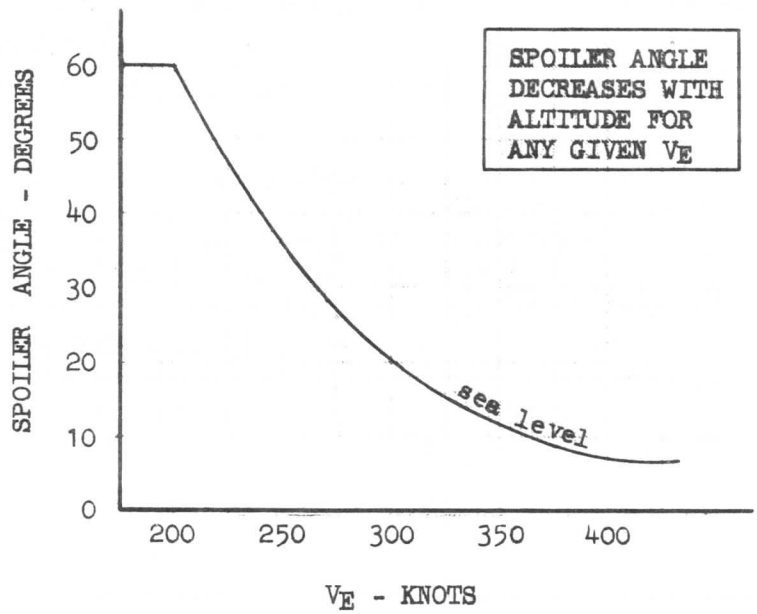

Figure 52.

V_{MO}/M_{MO} -- maximum operating limit speed. "(a) The maximum operating limit speed is a speed which shall not be deliberately exceeded in any regime of flight (climb, cruise, or descent), except where a higher speed is authorized for flight test or pilot training operations. This operating limitation, denoted by the symbols V_{MO}/M_{MO} (airspeed or Mach number, whichever is critical at a particular altitude), shall be established to be not greater than the design cruising speed V_C and sufficiently below V_D/M_D or V_{DF}/M_{DF} (demonstrated flight dive speed) to make it highly improbable that the latter speeds will be inadvertently exceeded in operations. The speed margin between V_{MO}/M_{MO} and V_D/M_D or V_{DF}/M_{DF} shall be determined in accordance with either paragraph (b) or (c) of this section, but shall not be less than the margin found necessary in flight tests in accordance with 25.253.

(b) The minimum margin shall be the greater of the values determined in accordance with subparagraphs (1) and (2) of this paragraph:

(1) From an initial condition of stabilized flight at V_{MO}/M_{MO}, the airplane shall be assumed to be upset, flown for 20 seconds along a flight path 7.5 degrees below the initial path and pulled up at a load factor of 1.5 (.5g acceleration increment). It shall be acceptable to calculate the speed increase occurring in this maneuver, provided reliable or conservative aerodynamic data are used. Power, as specified in 25.175(b)(1)(iv), shall be assumed until the pullup is initiated, at which time power reduction and the use of pilot controlled drag devices may be assumed.

(2) The margin shall be sufficient to provide for atmospheric variations, such as horizontal gusts, penetration of jet stream or cold front, and for instrument errors and airframe production variations. It shall be acceptable to consider these factors on a probability basis but the margin at altitudes where M_{M_O} is limited by compressibility effects shall not be less than .05M.

(c) V_{M_O}/M_{M_O} shall not be greater than 0.8 V_D/M_D or 0.8 V_{DF}/M_{DF}."

per FAR 25.1505

V_{LO} -- landing gear operating speed. "The landing gear operating speed, V_{LO}, shall be established not to exceed a speed at which it is safe to extend or retract the landing gear as limited by design in accordance with FAR 25.729 or by flight characteristics."

per FAR 25.1515 (a)

"(1) The landing gear retracting mechanism, wheel well doors, and supporting structure shall be designed for loads occurring in the flight conditions when the gear is in the retracted position, and for the combination of friction, inertia, brake torque, and air loads occurring during retraction and extension at any speed up to 1.6 V_S, (flaps in the approach position at design landing weight), and any load factor up to those specified per FAR 25.345 for the flaps extended condition."

per FAR 25.729 (a)(1)

Example:

V_{S_1} = 103.5 knots, EAS

1.6 V_{S_1} = 1.6 (103.5) = 166 knots EAS

V_{LO} is selected at 270 knots EAS

M_{L_O} is selected at .83

The speed limitation is a structural placard on the landing gear doors which are down during gear operation. Upon completion of the operation, the wheel well doors are automatically closed and the airplane may operate at increased speed with the landing gear in the extended position.

V_{LE} -- landing gear extended speed. "The landing gear extended speed, V_{LE}, shall be established not to exceed a speed at which it has been shown that the airplane can be safely flown with the landing gear secured in the fully extended position, and for which the structure has been proven in accordance with FAR 25.729 "

per FAR 25.1515 (b)

"(2) The landing gear, the retracting mechanism, and the airplane structure (including wheel well doors) shall be designed to withstand the flight loads occurring with the landing gear in the extended position at any speed up to 0.67 V_C, unless other means are provided to decelerate the airplane in flight at this speed."

per FAR 25.729(a)(2)

In the example, it was found that V_C could be as much as 360 knots, EAS.

0.67 V_C = 0.67 (360) = 241 knots EAS

V_{LE} is selected at 320 knots EAS

M_{LE} is selected at .83

3-5 TAKEOFF

Takeoffs may be considered as consisting of three parts: the ground run, transition, and flare to 35 foot height. The attitude of the airplane, relative to the ground, during the taxi condition and the ground run is fixed by geometry. The takeoff transition for commercial airliners is determined from flight test from the taxi attitude on the ground to the first takeoff segment attitude. Climbout after takeoff also has to be considered. The takeoff climbout requirements, as given in the regulations, are referred to certain segments of the flight path from lift-off to enroute climb. The first takeoff climb segment refers to flight conditions immediately after the airplane leaves the ground; landing gear down and flaps in take-off position. The second takeoff climb segment, is that portion of the climbout which is made after the landing gear is retracted, with the flaps still in the takeoff position. The final takeoff climb segment is that portion of the takeoff which is made with the landing gear and flaps up prior to the transition to enroute climb.

Although the takeoff climbout segments following the point at which the airplane leaves the ground are considered a part of the takeoff, analysis of these parts will not be made until the climb is discussed.

General Takeoff Distance Equation

In developing the equation for ground distance under any acceleration condition, it should be noted that

$$\left.\begin{aligned} V &= \frac{ds}{dt} \\ a &= \frac{dV}{dt} \end{aligned}\right\} \qquad (71)$$

From equation (71),

$$ds = V\,dt$$

and,

$$dt = \frac{dV}{a}$$

thus,

$$ds = \frac{V\,dV}{a} \qquad (72)$$

Integrating equation (72) between any two arbitrary speeds and distances, the following equation results:

$$s_y - s_x = \int_{V_x}^{V_y} \frac{V\,dV}{a} \qquad (73)$$

If the takeoff ground run situation is considered, $s_y - s_x$ can be replaced by S_G (ground distance), V_x by V_w (airplane starting from rest where V_w is the wind velocity), and VdV by $(V - V_w)\,dV$ since the acceleration, a, in the integrand is a function of the ground velocity $(V - V_w)$. V_y is replaced by V_{LOF}, lift-off speed, as defined below. The acceleration, a, in the integrand is related to velocity change and is therefore independent of the velocity reference point.

$$S_G = \int_{V_w}^{V_{LOF}} \frac{(V - V_w)}{a}\, dV \qquad (74)$$

The acceleration of an airplane during the ground run may be found by considering the forces existing on the airplane, as in Figure 5 . The airplane is seen to be under the influence of lift, drag, thrust, weight, and ground friction forces.

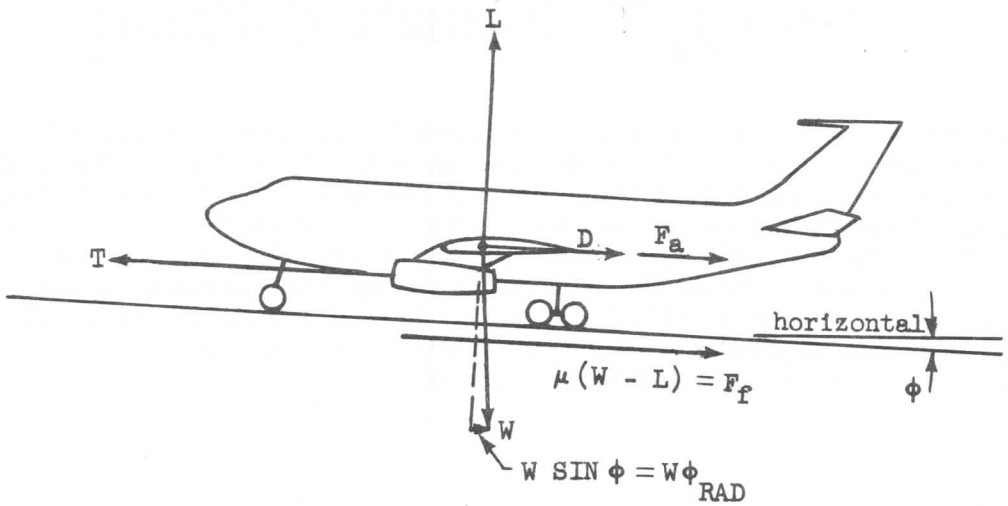

Figure 53.

Since the tangential force tending to retard the motion of a moving body is found to be proportional to the perpendicular, or normal force existing, a general relationship may be written letting the Greek letter Mu, μ , represent the constant of proportionality.

$$F_f = \mu F_n \qquad (75)$$

where,

F_f is frictional force, lb.

F_n is normal force, lb.

The constant, μ , is usually referred to as a "coefficient of friction." The friction forces shown to exist on the airplane of Figure 53 may be determined from the application of equation (75), as the product of the coefficient, μ , and the weight on the wheels, which at any given instant is equal to (W-L). The value of the coefficient is found to be approximately .020 under rolling conditions on dry concrete which means that the retarding force will be equal to 2 percent of the weight on the wheels. This value can be used in all estimated calculations involving the coefficient of rolling friction. If flight test information is available showing μ to be slightly different than .020, then the actual results are used.

$$F_a = Ma = \frac{W}{g} a$$

Thus,

$$T - D - \mu (W - L) - W\phi = \frac{W}{g} a$$

or,

$$a = \frac{g}{W} \left[(T - \mu W) - (D - \mu L) - W\phi \right]$$

$$a = \frac{g}{W} \left[(T - \mu W) - (C_D - \mu C_L) Sq - W\phi \right] \qquad (76)$$

$$S_G = \int_{V_W}^{V_{LOF}} \frac{W}{g} \frac{(V - V_W)\, dV}{\left[(T - \mu W) - (C_D - \mu C_L) Sq - W\phi \right]} \qquad (77)$$

This is the general expression for the takeoff distance. In order to be able to carry out the integration, however, the variation of thrust, weight, drag, and lift with velocity must be determined. In general, thrust is a function of velocity, air temperature and pressure; weight will be very nearly constant for the ground run; drag and lift will be functions of velocity and air density. With a tricycle gear, the airplane attitude will be assumed constant during the taxi condition, thus C_L and C_D will be constant during the ground run. If a plot is made to show the approximate order of magnitude of the forces acting during a takeoff run, it will look similar to Figure 54.

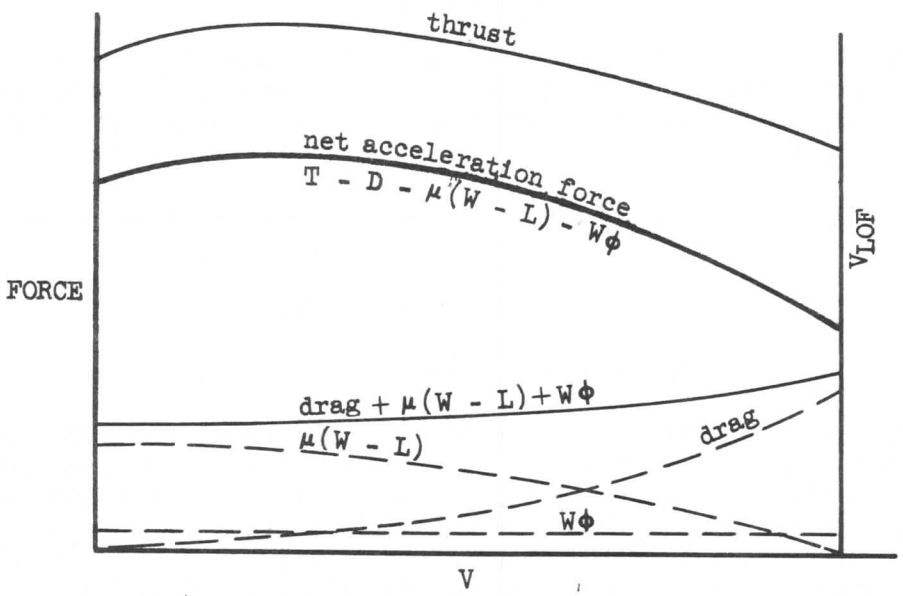

Figure 54.

Winds close to the ground are subjected to considerable shear effects, so for accurate calculation of ground distances, tower-reported winds must be corrected. The tower reports wind at 50-foot height, but the wing MAC of the Boeing commercial airplanes is at 8 or 10 feet. Experimental values of wind shear seem to follow the law:

$$\frac{\text{wind}_1}{\text{wind}_2} = \left(\frac{\text{height}_1}{\text{height}_2}\right)^{1/7} \qquad \text{per CAM 4b, Appendix A} \qquad (78)$$

So the factor 0.795 is applied to the wind value at 50 feet to obtain the actual wind at 10 feet. For 8 feet, the factor is 0.770; used on the 737 airplanes.

The FAA requires a conservative view of wind correction on calculations of ground performance. FAR 25.105 (d)(1) states that the takeoff and landing distance data must be calculated on the basis of 50% of headwind components measured at 50 feet and corrected to the height of the center of aerodynamic drag, and 150% of tailwind components. The intent is to use only half of any wind which improves performance, but 150% of any which hinders.

The ARB rules which correspond are drawn upon a wind prediction at 10 meters (32.8 feet) and define the correction at wing-tip height (12.5 feet). This wind shear equation gives a factor of .8712.

Normal Takeoff Ground Run, Distance and Time

Returning to equation (74), it will be seen that to be able to find the ground run requires knowing the relationship between a, the acceleration, and V, the velocity. From such a plot as Figure 54, and from equation (76), the quantity 1/a can be computed for any velocity, and a plot of 1/a vs V and $(V-V_W)/a$ vs V as in Figure 55 may be made. It will be noted that equation (74) specifies that to obtain the ground run, it is necessary to integrate the expression $(V-V_W)$ dV/a. Referring to Figure 55 it is seen that the area of the shaded element is also $(V-V_W)$ dV/a. Thus, the total ground run will be equal to the summation of all such elemental areas between the limits of zero velocity (adjusted for wind) and the lift-off speed. This is another way of stating that the ground run is equal to the total area under the curve.

The integration of a plot such as in Figure 55 may be accomplished in several different ways. The rigorous manner would be to solve the basic equation using the IBM electronic computer to yield the exact answers. Lacking this means, the same results could be accomplished by mechanical integration utilizing a planimeter to obtain the area under the curve in Figure 55. Also, highly accurate results may be obtained by careful step-by-step integration using small velocity increments and assuming constant values of $(V-V_W)/a$ for each increment.

Equation (74) may be modified as follows:

$$\Delta S_G = \frac{1}{\bar{a}} \int_{V_X}^{V_y} (V - V_W)\, dV \qquad (79)$$

where ΔS_G is the incremental ground distance traveled between velocities V_X and V_y, and $\bar{a}$ is the average acceleration between V_X and V_y.

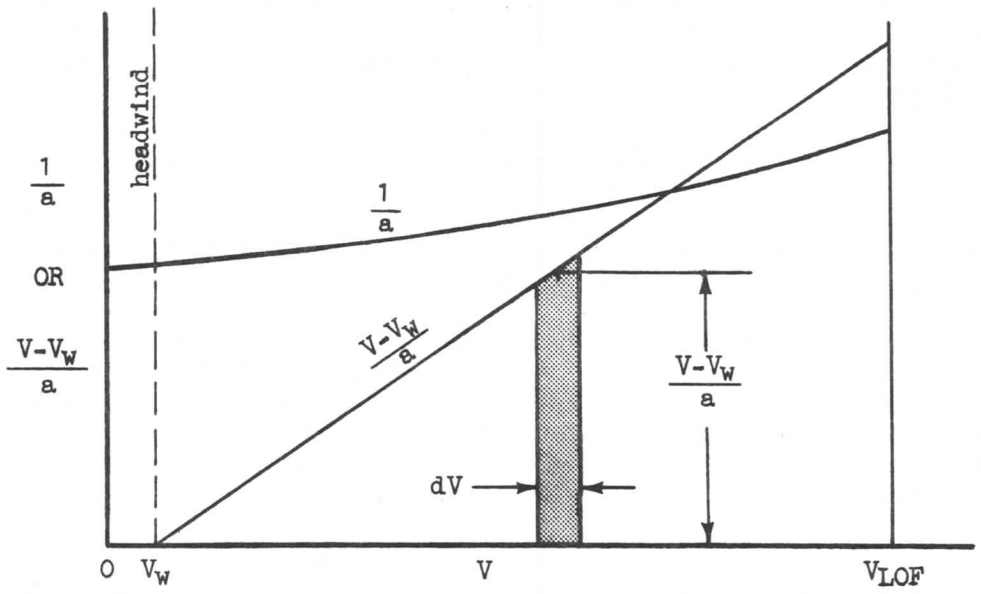

Figure 55.

Integrating results in:

$$\Delta S_G = \frac{1}{2\bar{a}} \left[V^2 - 2V V_w \right]_{V_x}^{V_y}$$

$$= \frac{1}{2\bar{a}} \left[(V_y^2 - 2V_y V_w) - (V_x^2 - 2V_x V_w) \right]$$

$$= \frac{1}{2\bar{a}} \left[(V_y^2 - V_x^2) - 2V_w (V_y - V_x) \right]$$

$$= \frac{1}{2\bar{a}} \left[(V_y - V_x)(V_y + V_x) - 2V_w (V_y - V_x) \right]$$

$$= \frac{1}{2\bar{a}} \left[(V_y + V_x) - 2V_w \right] (V_y - V_x)$$

$$= \frac{1}{\bar{a}} \left[\frac{V_y + V_x}{2} - V_w \right] (V_y - V_x)$$

The term $(V_y + V_x)/2$ equals the average velocity between V_x and V_y and ΔV is the velocity change from V_x to V_y; therefore, the above equation will read:

$$\Delta S_G = \frac{1}{\bar{a}} \left[V_{avg} - V_w \right] \Delta V \qquad \text{(80)}$$

The total ground distance is the sum of the incremental distances, determined from equation (79), integrating between V_W and V_{LOF}.

Then, $$S_G = \Sigma \Delta S_G \qquad (81)$$

A table may be set up to systematically handle the calculations involved. Such a table is shown in Figure 56, but may be expanded to provide greater detail.

V	ΔV	T	T - μW	q	$(C_D - \mu C_L)S_q$	a	$\bar{a}$	$(V_{avg}-V_W)$	ΔS_G	$\Sigma\Delta S_G$	Δt	$\Sigma\Delta t$
0		---	----	---	----	--				0		0
	20						--	----	---		---	
20		---	----	---	----	--				---		---
	20						--	----	---		---	
40		---	----	---	----	--				---		---
	20						--	----	---		---	
60		---	----	---	----	--				---		---

Figure 56.

A simplified means of integrating equation (77) is to assume an average acceleration during the ground roll. Since ground roll is a function of V^2 and acceleration, the average acceleration for calculating ground roll will occur at some average V^2. If a plot of acceleration versus velocity squared is made for jet-powered aircraft, it appears as in Figure 57. Since this plots out nearly as a straight line, the average acceleration occurs at $V_{LOF}^2/2$; thus $V_{avg} = .707V_{LOF}$. This simplified approach is very convenient to use for preliminary design work or other situations where the degree of accuracy obtainable from the more rigorous presentation is not necessary.

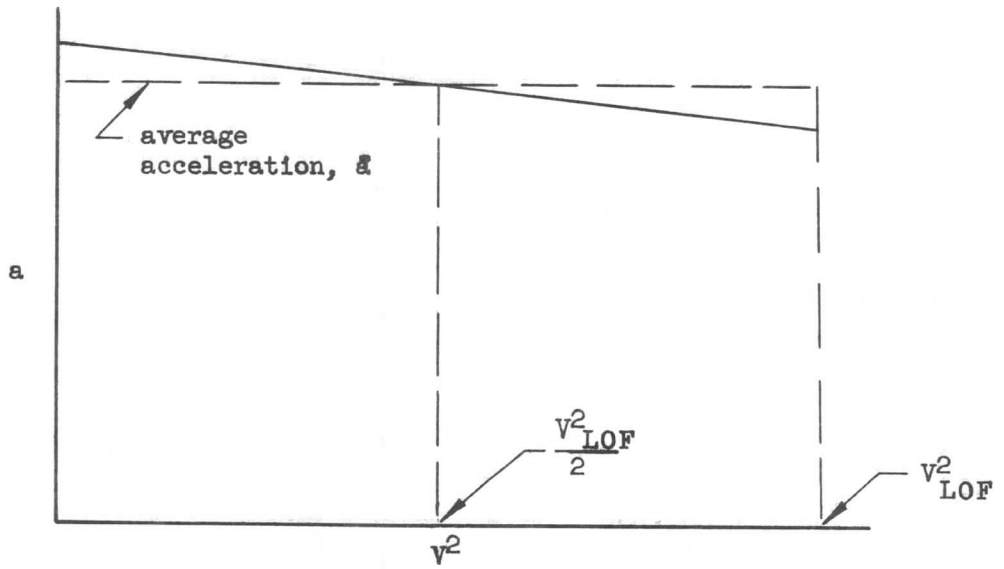

Figure 57

Calculating the acceleration at this speed and declaring it constant for the complete ground run modifies equation (77) as follows:

$$S_G = \frac{1}{\bar{a}} \int_{V_W}^{V_{LOF}} (V - V_W)\, dV$$

where V is in fps, and S_G is in feet.

Integrating,

$$S_G = \frac{1}{2\bar{a}} \left[V^2 - 2V_W V \right]_{V_W}^{V_{LOF}}$$

$$= \frac{1}{2\bar{a}} \left[(V_{LOF}^2 - 2V_W V_{LOF}) - (V_W^2 - 2V_W^2) \right]$$

$$= \frac{(V_{LOF} - V_W)^2}{2\bar{a}}$$

or,

$$S_G = \frac{(V_{LOF} - V_W)^2}{\frac{2g}{W} \left[(T - \mu W) - (C_D - \mu C_L)\, qS - W\phi \right]_{\text{at } .7V_{LOF}}} \qquad (82)$$

For V in knots:

$$S_G = 2.849 \left[\text{equation (82)} \right] \qquad (83)$$

Takeoff Time

Time-to-accelerate data for acceleration charts are based on relationships similar to those used in computing the takeoff distances. In developing the equations for takeoff, an analysis was made of the forces acting on an airplane as shown in Figure 53. Similarly, from equation (71),

$$a = \frac{dV}{dt}$$

or,

$$dt = \frac{dV}{a}$$

From equation (76):

$$a = \frac{g}{W} \left[(T - \mu W) - (C_D - \mu C_L)\, Sq - W\phi \right]$$

Thus,

$$dt = \frac{dV}{\frac{g}{W} \left[(T - \mu W) - (C_D - \mu C_L)\, Sq - W\phi \right]}$$

Integrating,

$$t = \int_{V_W}^{V_{LOF}} \frac{W}{g} \frac{dV}{(T - \mu W) - (C_D - \mu C_L)\, Sq - W\phi} \qquad (84)$$

This is the general expression for the time to lift-off speed. The resolution of this equation is conducted simultaneously with, and in the same manner as the distance calculation. The solution to equation (84) may be found, using any of the following methods:

(1) Rigorous computation using a computer.

(2) Careful step-by-step integration of the curve of 1/a vs V, as shown on Figure 55, using small velocity increments and assuming constant values of 1/a for each increment.

(3) Mechanical integration of the $\frac{1}{a}$ curve in Figure 55 utilizing a planimeter.

(4) Simplified form of equation (84) where the average acceleration for calculating time will be found to occur at $.5V_{LOF}$ or slightly higher since time is approximately linear with respect to velocity.

When using the second method, an incremental time, Δt, is determined from a modified form of equation (84):

$$\Delta t = \frac{1}{\bar{a}} \int_{V_x}^{V_y} d(V-V_w)$$

where Δt is the incremental time elapsed between velocities V_x and V_y.

$$\Delta t = \frac{1}{\bar{a}} \left[V - V_w \right]_{V_x}^{V_y}$$

or,

$$\Delta t = \frac{1}{\bar{a}} \left[(V_y - V_w) - (V_x - V_w) \right]$$

$$\Delta t = \frac{1}{\bar{a}} \left[V_y - V_x \right]$$

$$\Delta t = \frac{\Delta V}{\bar{a}} \qquad (85)$$

As indicated previously, the time data may be added to the data already shown in Figure 56.

When using the last method, equation (84) is modified as follows:

$$t = \frac{1}{\bar{a}} \int_{V_w}^{V_{LOF}} d(V-V_w)$$

Where V is in fps and t is in seconds.

Therefore,

$$t = \frac{1}{\bar{a}} \left[V-V_w \right]_{V_w}^{V_{LOF}}$$

$$= \frac{V_{LOF} - V_w}{\bar{a}}$$

$$t = \frac{(V_{LOF} - V_w)}{\frac{g}{W}\left[(T - \mu W) - (C_D - \mu C_L)Sq - W\phi\right]_{.5V_{LOF}}} \qquad (86)$$

For V in knots:

$$t = 1.688 \ [\text{equation (86)}] \qquad (87)$$

Takeoff Speeds

Before discussing takeoff further, let us define the various speeds which will be involved.

V_1 - critical engine failure speed. V_1 is the critical engine failure speed in terms of calibrated airspeed. It shall not be less than the minimum speed at which controllability by aerodynamic controls alone is demonstrated during the takeoff run to be adequate to permit proceeding safely with the takeoff using average piloting skill, when the critical engine is suddenly made inoperative.

per FAR 25.107 (a)

V_{mc} - minimum control speed. V_{mc} is the minimum control speed with the critical engine inoperative. When the critical engine is suddenly made inoperative at this speed, it shall be possible to recover control of the airplane with the engine still inoperative, and maintain it in straight flight at that speed, either with zero yaw or with an angle of bank not in excess of 5°. Rudder forces may not exceed 180 lbs.

per FAR 25.149

V_R - takeoff rotation speed. V_R is defined as the speed at which rotation is initiated during the takeoff to attain the V_2 climb speed at the 35 foot height. V_R must not be less than 1.05 times the minimum control speed (air) nor less than V_1.

per FAR 25.107 (e)

V_{mu} - minimum unstick speed. V_{mu}, in terms of calibrated airspeed, shall be the speed at and above which the airplane can be made to lift off the ground and to continue the takeoff without displaying any hazardous characteristics. V_{mu} speeds shall be selected by the applicant for the all-engines-operating and the one-engine-in-operative condition.

per FAR 25.107 (d)

V_{LOF} - airplane lift-off speed during takeoff. The lift-off speed is closely associated to the V_R speed and will be dictated by that speed. The all-engines-operating lift-off speed must not be less than 110% of V_{mu}. The one-engine-inoperative lift-off speed must not be less than 105% of V_{mu}. If the airplane incorporates an attitude warning system, the V_{LOF} requirements may be reduced without jeopardizing takeoff operation.

per FAR 25.107 (e)(1)(iv)

V_2 - takeoff climb speed. V_2 is equal to the actual speed at the 35 foot height as demonstrated in flight and must be equal to or greater than both 120% stall speed in the takeoff configuration and 110% minimum control speed (in the air).

per FAR 25.107 (c)

Lift-off speed is determined as a function of thrust to weight ratio (T/W) from flight test data so as to satisfy the certification rules governing the airplane concerned. For new airplanes, such a curve is established by using data from similar airplanes previously flight tested. For example, the 707-120 series of airplanes certified to SR-422 had as a criterion the requirements of V_2 speed (120% V_s) "on or near the ground," which was interpreted as a height of 2 feet above the ground. The rotation is started at such a speed as to give lift-off at the desired speed.

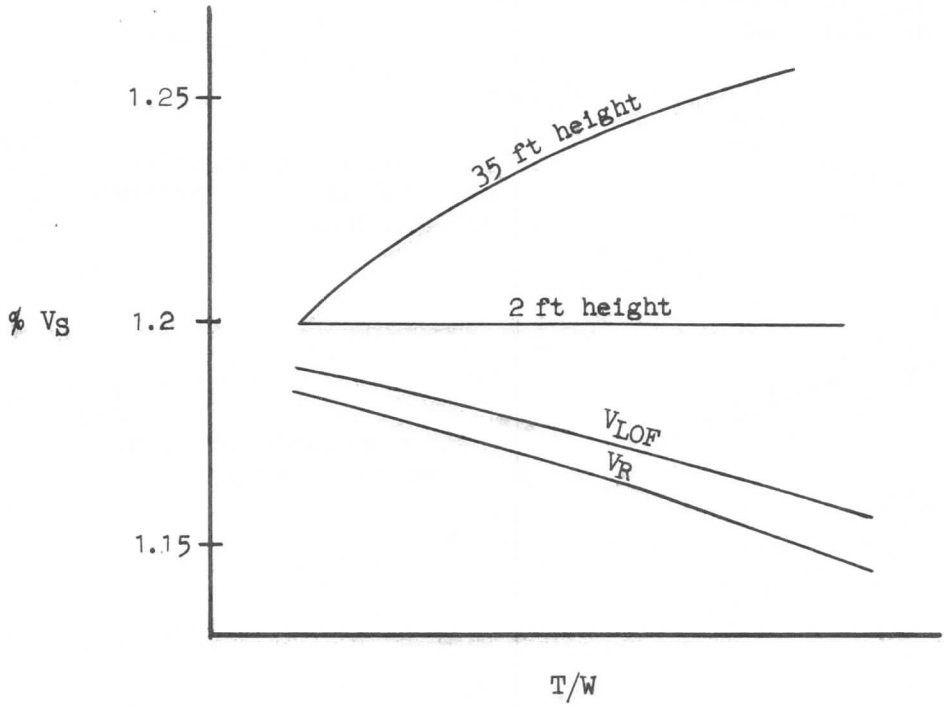

Figure 58.

Under the SR-422B and the FAR part 25 rules, the emphasis is on rotation speed. The criteria for establishing rotation speed are functions of several variables. The rotation speed, V_R, shall not be less than a speed where, if the airplane is rotated at its maximum practicable rate, there will result a lift-off speed not less than 110% (108% may be used for geometry limited airplanes with an operating attitude warning system) of V_{mu} in the all-engines-operating condition and when rotated at its normal rate, not less than 105% of V_{mu} in the one-engine-inoperative condition. Another limiting condition is that one specifying a V_2 climb speed ($\geq$ 120% V_S) at a height of 35 feet above the ground. Such other limitations as body contact may be limiting. Assuming V_R as defined by V_{mu} is limiting, rotation speed as a function of T/W ratio will appear as in Figure 59. The apparent discrepancy shown is due to the same rotation speed being required for either all-engine-operating or one-engine-inoperative conditions.

Rotation and Flare to 35-foot Height

The total takeoff distance to a 35-foot height is the sum of the ground-run distance previously calculated and the distance to flare from lift-off to a 35-foot height. The flare distance is determined from flight test by establishing the time to flare and multiplying by the average speed during the flare. For a given T/W ratio, the average speed may be obtained from Figure 58 or 59 as applicable.

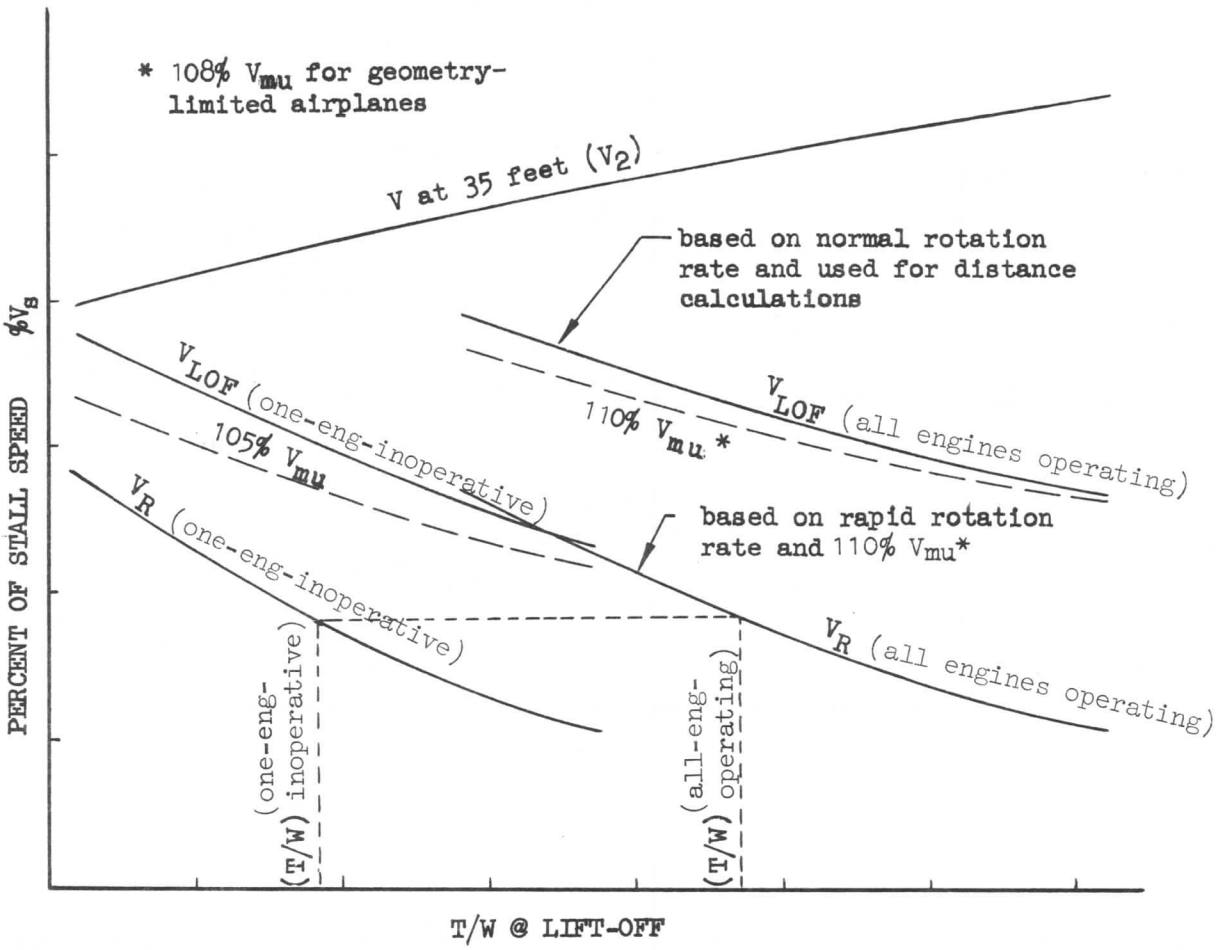

Figure 59.

Time to rotate and time from lift-off to 35 feet show good generalization with T/W, as shown in Figure 60. Since the times are influenced by "pilot technique", the data is averaged-out by fairing the test points. Figure 60 is required to compute the distance from V_R to V_{LOF} (Segment B_2) and V_{LOF} to V_2 (Segment C). Figure 61 illustrates takeoff distance for all-engines-operating and one-engine-inoperative.

$$\text{Segment } B_2 = 1.688 \left(\frac{V_R + V_{LOF}}{2} - V_W\right) \Delta t \qquad (88)$$

where,

$$\Delta t = t_{(V_R - V_2)} - t_{(V_{LOF} - V_2)}$$

and,

$$\text{Segment } C = 1.688 \left(\frac{V_{LOF} + V_2}{2} - V_W\right) \Delta t_{(V_{LOF} - V_2)} \qquad (89)$$

where the velocity is in knots.

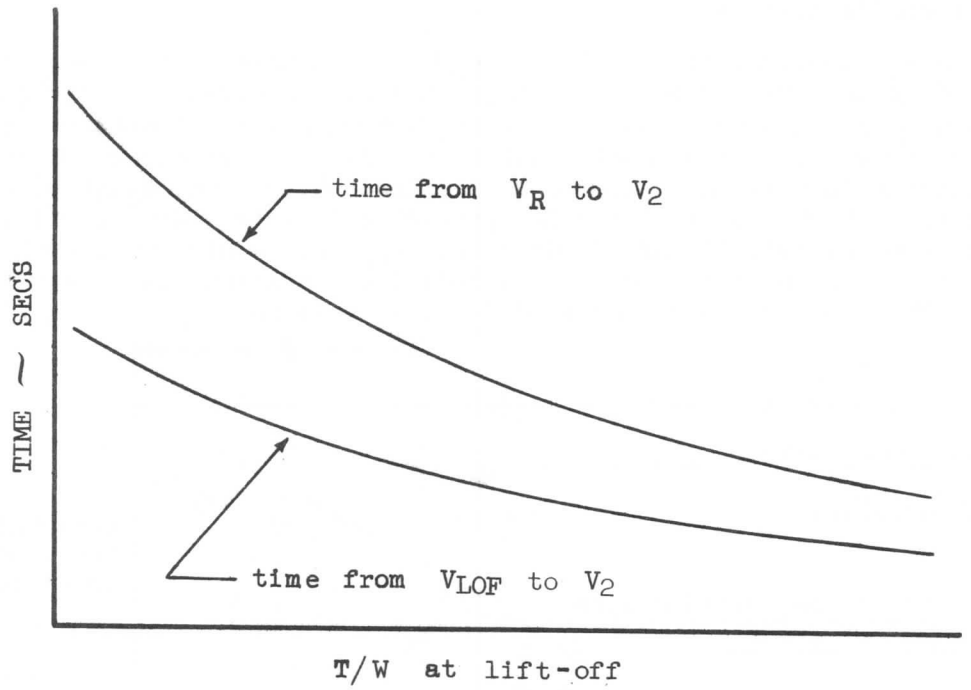

Figure 60.

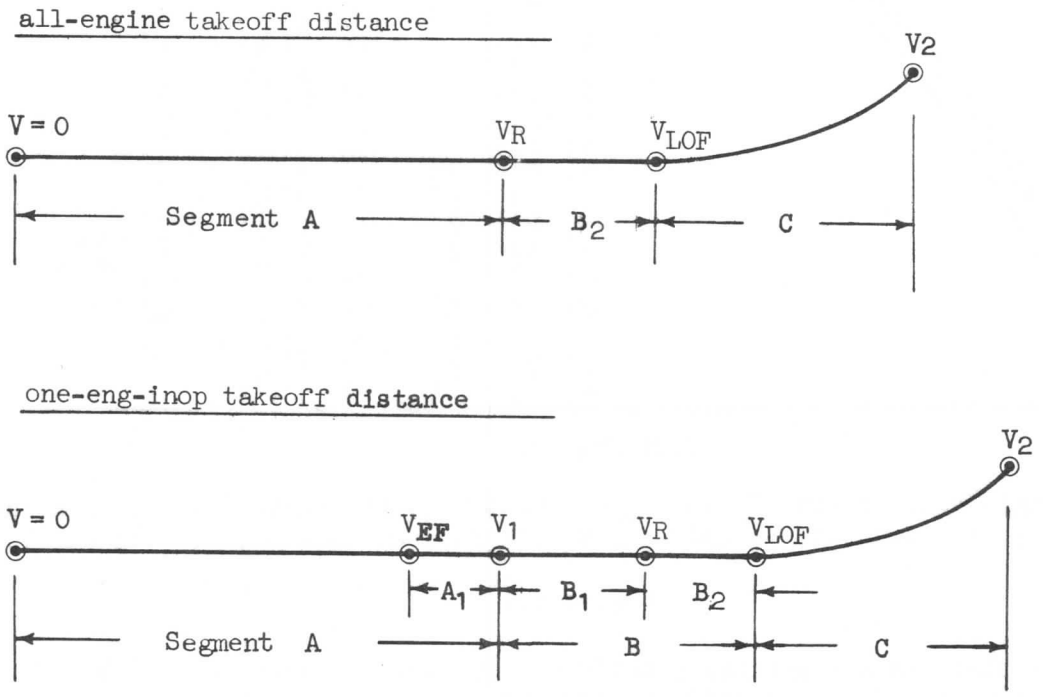

Figure 61.

One-Engine-Inoperative Takeoff

A takeoff calculated according to Civil Air Regulations, SR-422, provided for a single field length that satisfied both the takeoff and accelerate-stop requirements. The minimum field length under these requirements was a "balanced" field length. That is an engine failure was assumed to occur at a speed such that the distance to continue takeoff and climb to a stipulated height was equal to the distance required to stop. SR-422B and FAR part 25 stipulates using a field length which is the greatest of either the accelerate and go distance, the accelerate and stop distance, or 115% times the all-engine-operating distance to a 35-ft. height. The stop and go portions need not be balanced.

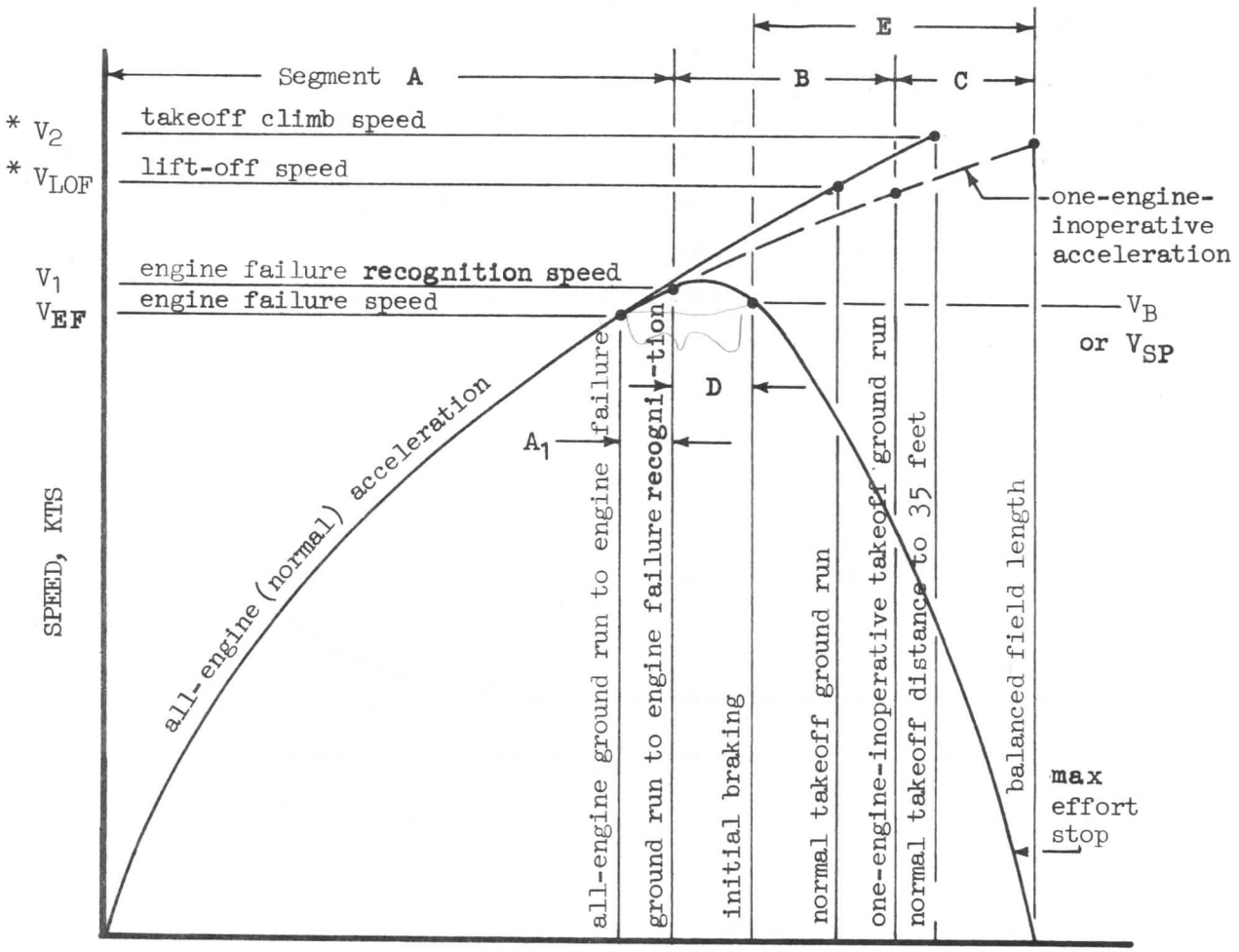

*one-engine-inoperative V_2 and V_{LOF} speeds will be slightly lower than the all-engines-operating V_2 and V_{LOF} speeds for the same rotation speed, V_R.

Figure 62.

Takeoff calculations are generally performed in discrete segments which define the distinct parts of the takeoff as shown in Figure 62. Each segment for the one-engine-inoperative condition is defined and its length calculated as follows:

Segment A

Segment A is the acceleration distance to the engine failure recognition speed, V_1 (see Figure 61). Equation (77) may be used, integrating between V_W and V_1. The thrust term will consist of the thrust of all engines operating at the takeoff rating.

Segment A_1

Segment A_1 is the one-engine inoperative acceleration distance from the engine failure speed, V_{EF}, to the engine-failure-recognition speed, V_1. Segment A_1 is a time period allowing for engine failure recognition for those airplanes producing little or no yaw at engine failure. An appropriate time delay period is added to allow the pilot to detect engine failure from the engine instruments. Also, engine spin down for the inoperative engine is taken into consideration. This defines $\bar{\eta}$ which is a ratio of the average thrust for this segment based on the all-engine thrust at V_1. Since the velocity change between engine failure, V_{EF}, and V_1, is,

$$\Delta V = \frac{\Delta t \times \bar{a}}{1.688}$$

and,

$$V_{EF} = V_1 - \Delta V$$

where the average acceleration is,

$$\bar{a} = \frac{g}{W}\left((T\bar{\eta} - \mu W) - (C_D - \mu C_L)\, S \frac{V^2 \sigma}{295.37} - W\phi\right)$$

and,

$$T\bar{\eta} = T_{V_1}\bar{\eta}$$

then the distance for segment A_1 is,

$$S_{A_1} = 1.688\,(V_{avg} - V_W)\,\Delta t$$

Simplification, with little loss in accuracy, is obtained by finding "a" at V_1 speed. Therefore, the equations for segment A_1 become:

$$V_{EF} = V_{1_T} - \frac{\Delta t\, g}{1.688}\left(\bar{\eta}\left(\frac{T}{W}\right)_{V_1} - \mu - (C_D - \mu C_L)\frac{S\, V_{1_T}^2\, \sigma}{295.37W} - \phi\right) \qquad (90)$$

$$S_{A_1} = 1.688\,(V_1 - \frac{\Delta V}{2} - V_W)\,\Delta t \qquad (91)$$

Segment B

Segment B is the one-engine-inoperative acceleration distance from V_1 to V_{LOF}. Segment B is the sum of segment B_1, equation (73) integrated between V_1 and V_R, and segment B_2 which is obtained from equation (88). See Figure 61. For this segment, all but one engine are performing at the takeoff thrust rating. The thrust for the engine-inoperative condition for segment B_1 is found by multiplying the all-engine thrust at V_1 by the average spindown factor, $\bar{\eta}_{avg}$. $\bar{\eta}_{avg}$ is a function of the time from V_{EF} to V_R. Since the engine windmilling drag and the aerodynamic drag due to controlling the asymmetric thrust must be added to the basic airplane drag, this defines an engine-inoperative value of $(C_D - \mu C_L)$ to be used in equation (73) for determining the average acceleration in segment B_1.

Segment C

Segment C is the flare distance between lift-off and a 35 ft. height with one-engine-inoperative. The equation used is the same as for the all-engine flare to a 35 ft. height, equation (89). This distance is independent of V_1 speed.

Segment D

Segment D, sometimes known as the transition distance, is defined as the distance traveled between recognition of an engine failure and the establishment of the full braking configuration. The procedural steps for anti-skid operating are: 1) engine failure recognition; 2) brake application; 3) thrust levers to idle position; and 4) speed brake actuation. During certification tests, time increments for the above steps are determined:

a. Time between engine failure recognition and brake application, t_{BA}.

b. Brake application to thrust reduction (engine chop) on remaining engines, $t_{EC} - t_{BA}$.

c. Thrust reduction on remaining engines to spoiler (speed brake) action, $t_{SP} - t_{EC}$.

For certification, one-second time delay is added to b and to c to account for differences in pilot reaction.

During transition, speed increases as much as one knot due to acceleration during the recognition time, then reduces during brake application, especially after thrust is reduced, so that initial braking speeds are a few knots lower than V_1. Using an IBM program, Segment D is rigorously calculated in the time increments as indicated above and the exact horizontal distance determined using equation (81) with appropriate limits and parameters for each increment. This also enables the exact initial speed for Segment E to be determined.

The latest method of calculating segment D with the same accuracy as above is to calculate it in one step where the total transition time is utilized. This method is similar to that used for calculating segment A_1. Since the velocity change between V_1 and V_{SP} (the initial braking velocity for segment E) can be approximated by the following equation,

$$\Delta V = \frac{\Delta t \times \bar{a}}{1.688}$$

and,

$$V_{SP} = V_1 + \Delta V$$

then the distance for segment D is,

$$S_D = 1.688\ (V_{avg} - V_W)\ \Delta t$$

$$S_D = 1.688\ \left(V_1 + \frac{\Delta V}{2} - V_W\right)\ \Delta t \qquad (92)$$

With little loss in accuracy, $\bar{a}$ is determined at the V_1 speed.

$$\bar{a} = \frac{g}{W}\left(T_{\bar{\eta}} - \mu_{avg} W - (C_D - \mu C_L)\frac{S V_{1_T}^2 \sigma}{295.37} - W\phi\right)$$

where,

$$T_{\bar{\eta}} = T_{V_1}\bar{\eta}$$

and μ_{avg} is the average transition brake coefficient from engine failure to spoiler (speed brake) actuation. Since the brake coefficient is assumed to vary linearly between brake application and flight test spoiler application, and to account for the additional transition time required for certification, the average transition brake coefficient is:

$$\mu_{avg} = \mu_E + \frac{(t_{BA} + t_{SP})\ F.T.}{2\ t_{SP_{F.M.}}}(\mu_R - \mu_E) \qquad (93)$$

where,

μ_E = braking coefficient of friction from anti-skid limited region of μ versus $W V_{Bg}^2$ plot.

μ_R = rolling coefficient of friction.

t_{BA} = flight test time between engine failure recognition and brake application, sec.

t_{SP} = flight test time between engine failure recognition and spoiler action, sec.

$t_{SP_{F.M.}}$ = Flight Manual time between engine failure recognition and spoiler action for certification, sec.

The initial braking velocity is,

$$V_{SP} \text{ or } V_B = V_{1_T} + \frac{\Delta t\ g}{1.688}\left(\bar{\eta}\left(\frac{T}{W}\right)_{V_1} - \phi - \mu_{avg} - (C_D - \mu C_L)\frac{S V_{1_T}^2 \sigma}{295.37W}\right) \qquad (94)$$

When calculating the transition distance for anti-skid inoperative, the procedural steps are: 1) engine failure recognition; 2) thrust levers to idle position; 3) speed brake actuation; and 4) brake application. The braking coefficient of friction will be the rolling coefficient of friction, μ_R.

Segment E

A final requirement in handling problems involving takeoff is the calculation of stopping distance. The theory used to set up the takeoff ground-run calculations

may also be used in the treatment of stopping distances. Realizing that under stopping conditions the airplane is decelerating, equation (77) may be rewritten in the form:

$$S_G = \int_{V_B}^{V_W} \frac{W}{g} \frac{(V - V_W)\, dV}{\left[(T - \mu W) - (C_D - \mu C_L) S_q - W\phi\right]} \qquad (95)$$

where V_B is initial braking velocity calculated from equation (94).

When stopping, the terms in equation (95) differ from those in equation (77) in that thrust is reduced to idle, drag is increased by means of auxiliary drag devices such as spoilers, lift is reduced by the use of spoilers, and the coefficient of friction is increased because of wheel braking. During the stopping phase, the coefficient of braking friction is a function of the energy parameter WV_{Bg}^2, where W is the gross weight of the airplane at V_{Bg}, the ground speed at the start of braking. In equation (95), the acceleration term to be integrated becomes negative, indicating a deceleration. However, since the limits of integration go from a large number to a small number, which is in a negative direction, the algebraic sign for the stopping distance comes out positive. Segment E is the braking distance for a refused takeoff and is calculated using equation (95), integrating between the limits V_B and V_W.

Balanced Field Length

When it is necessary to define a "balanced" field length, the engine failure speed, V_1, must be determined such that segments

$$B + C = D + E$$

The method used is to assume several V_1 values and solve for segments B, D and E to correspond. Segment C, independent of V_1, also is calculated. By comparing B + C and D + E, V_1 may be obtained; this relation may be plotted as in Figure 63 or numerically compared. Then Segment A is calculated and the balanced field length defined.

Unbalanced Field Length

At low weights and altitudes, and consequently low engine failure speeds, it is possible to calculate a value for V_1 below ground minimum control speed with one engine inoperative. This means that the value of V_1 defined for a balanced field length must be increased to the value of the ground minimum control speed. This will result in an unbalanced field length, since segment B + C is less than segment D + E. In this event, the field length will be identified by segments A + D + E with V_1 defined by ground minimum control speed.

It is also possible that the calculated V_2 speed could occur at less than 110% of the air minimum control speed at low weights and altitudes. In this event, V_2 must be increased to 110% of air minimum control speed, and the unbalanced field length is then defined by segments A + B + C.

A third possibility for unbalanced field lengths has to do with the amount of heat energy the airplane brakes will accept without incurring brake failure. This is known as a brake energy limit and is most likely to occur at high gross weights and at high altitudes. If the V_1 speed for a balanced field length is above the brake energy limit speed, V_1 must be reduced. In this case, the FAR field length under one-engine-inoperative requirements is defined by segments A+B+C.

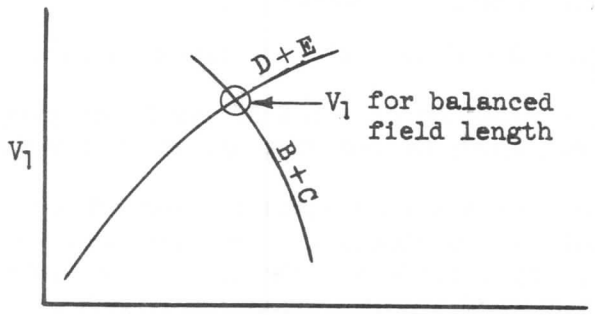

Figure 63.

A fourth possibility for unbalanced field lengths occurs when the calculated V_1 speed for a balanced field length is greater than the takeoff rotation speed, V_R. This occurs for airplanes having good stopping capabilities. This means that the airplane could experience an engine failure during takeoff rotation at a speed equal to or greater than the V_R speed and still be stopped on the remaining runway. However, damage to the aircraft may occur when the nose of the airplane is lowered to the runway for stopping; therefore, the policy has been to reduce the V_1 speed to equal the takeoff rotation speed, V_R. For this situation, the FAR field length under one-engine-inoperative requirements is defined by segments A+B+C.

A brief discussion of the determination of minimum control speed may be helpful at this point. The minimum speed at which the airplane may be controlled in its most adverse engine-inoperative condition and at a maximum bank angle of 5° is determined through either flight tests or wind tunnel tests. Test data may then be presented for a series of altitudes and for given temperature conditions. Ground minimum control speeds, V_{MCG}, have been established for the 707 airplane from flight test and were determined without nose-wheel steering. A more detailed analysis of this presentation is made in Section 4.

Clearways and Stopways (SR-422B and FAR Part 25)

Clearway - A clearway is an area beyond the runway, not less than 500 feet wide, centrally located about the extended center line of the runway, and under the control of the airport authorities. The clearway is expressed in terms of a clearway plane, extending from the end of the runway with an upward slope not exceeding 1.25 percent, above which no object nor any portion of the terrain protrudes, except that threshold lights may protrude above the plane if their height above the end of the runway is not greater than 26 inches and if they are located to each side of the runway.

defined per FAR Part 1.1

Stopway - A stopway is an area beyond the runway, not less in width than the width of the runway, centrally located about the extended center line of the run-

way, and designated by the airport authorities for use in decelerating the airplane during a refused takeoff. To be considered as such, a stopway must be capable of supporting the airplane during a refused takeoff without inducing structural damage.

defined per FAR Part 1.1

By using the advantages of clearways and stopways, higher takeoff weights are possible for a given runway length. However:

(1) The takeoff run (A + B + C/2) shall not exceed the length of runway.

(2) The accelerate-stop distance (A + D + E) shall not exceed the length of the runway plus the length of the stopway, where present.

(3) The takeoff distance (A + B + C) shall not exceed the length of the runway plus the length of the clearway, where present, except that the takeoff distance shall not include a clearway distance greater than one-half of the runway or one-half segment C.

per FAR 91.37 (c)

These definitions are illustrated in Figure 64. It should be noted that when clearways are being considered, a reduction in V_1 speed may have to be made.

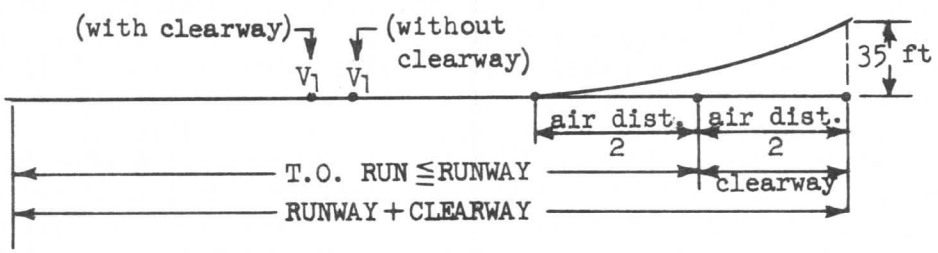

Figure 64.

From the definitions, it can be seen that a stopway may also be a clearway, but the reverse is not true.

Takeoff Presentation

A form of takeoff presentation showing field length as a function of weight is shown in Figure 65. Such a plot shows the effects of altitude and various flap deflections for a given temperature condition. Current civil regulations require a constant clearance height of 35 feet be considered for all temperature conditions. However, certain foreign operators may desire other clearance heights to be considered.

In establishing Figure 65, the optimum flap deflections are selected as follows: For a given altitude and flap setting, a relationship may be shown between field length and gross weight. A different flap setting produces different field lengths. On a single chart, it is possible to show for a given altitude and OAT the field lengths associated with the various flap configurations throughout the weight range of the airplane. Figure 66 shows that the field length requirements are least at the 30° flap setting for all weights up to W_1. Beyond W_1, a 20° flap setting produces lower FAR field lengths. In some instances, it is the lower FAR field lengths that establish the takeoff weight and flap settings.

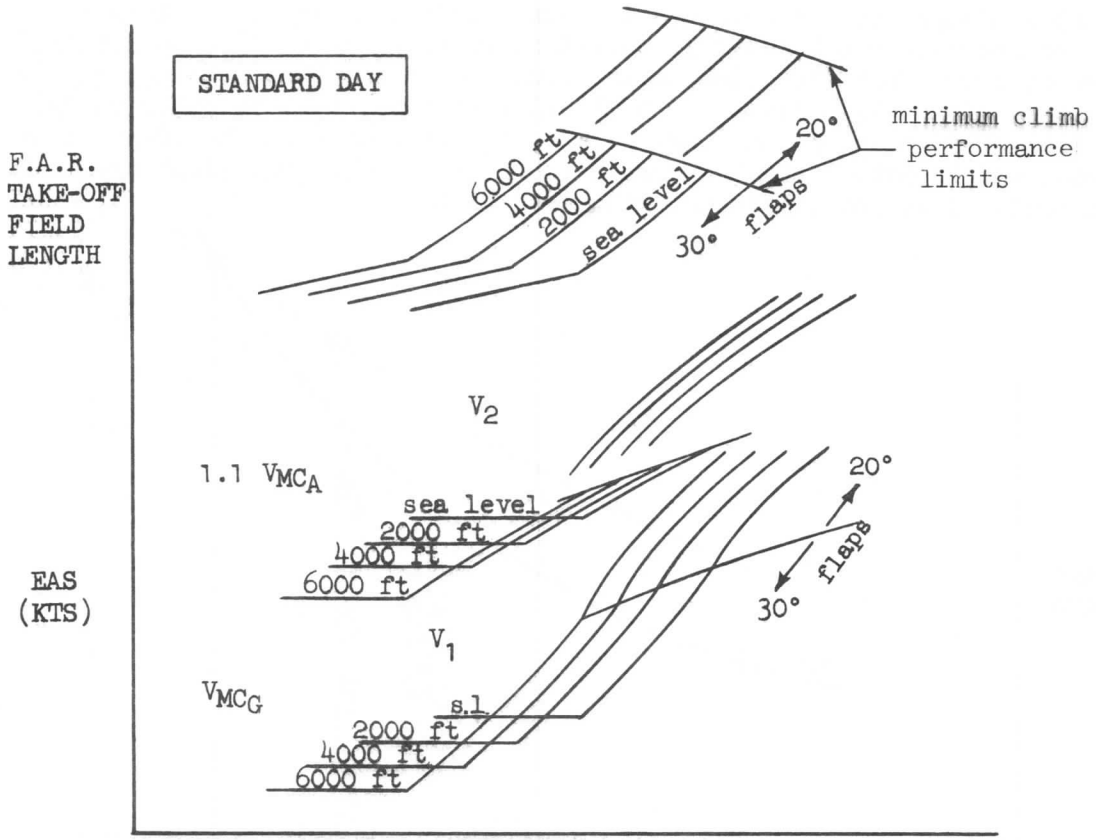

Figure 65.

However, it is possible that either the second segment or final segment climb gradient requirements may establish the weight above which a lower flap setting is required. For example, in Figure 67, if W_2 (the second segment or final climb weight limit) is greater than W_1 (determined by field length), the minimum field length determines the flap angle. If, however, the second segment or final weight limit occurs at a lower weight than W_1, then it is the climb weight limit that determines the flap setting.

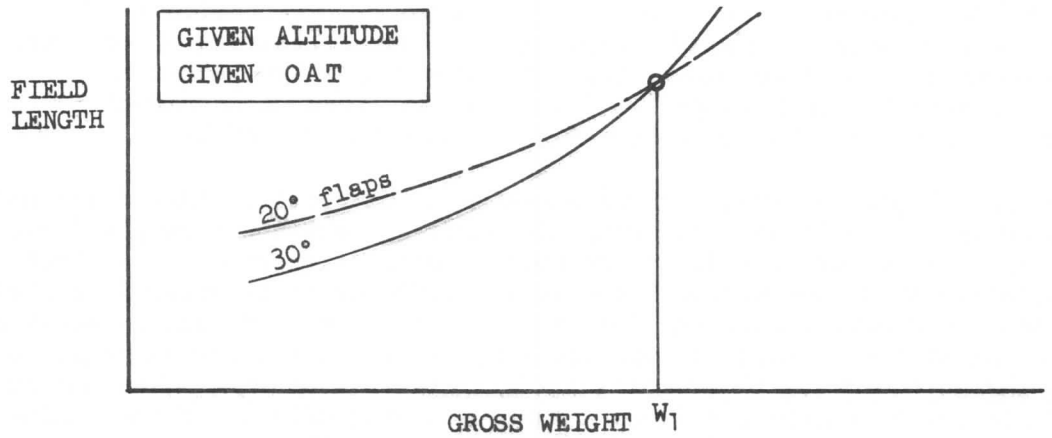

Figure 66.

If the FAR field length thus determined is less than the actual field length, it is possible to increase the takeoff gross weight by going to a 20° flap setting, since Figure 67 shows that the climb weight limit for a 20° flap setting, W_3, is higher than the climb weight limit for a 30° flap setting, W_2. In other words, with a 20° flap configuration, the same climb-out performance can be obtained at a higher gross weight with a small increase in field length. The climb gradients and associated weight limits are discussed below.

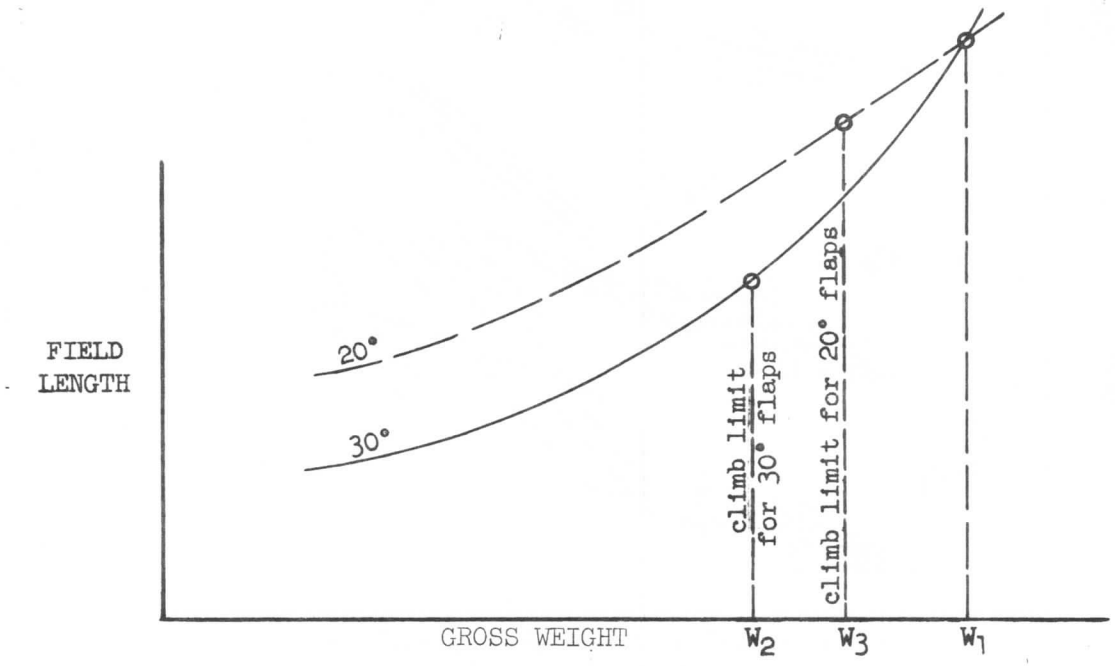

Figure 67.

Under certain conditions, both ground and air minimum control speeds may define the field length. This is the unbalanced field length condition mentioned previously. The mechanics of this effect is shown in Figure 68 for one altitude.

Data such as shown in Figure 65 shows the general takeoff performance characteristics for the airplane, and can be used for preliminary analysis work. A more detailed presentation is made for flight operations and flight crew use and is contained in the FAA Approved Flight Manual. One form of presentation is as shown in Figure 69. Complete temperature, wind, and runway gradient effects are shown for a selection of pressure altitudes throughout the weight range of the airplane. The information is arranged in "chase-around" fashion to reduce the number of charts and to show the data in a form as simple as possible.

Under SR-422B and FAR part 25 rules, where one-engine-inoperative takeoff distance must be compared with all-engines-operating distance, and where clearway and stopway benefits may be considered, a different form of chart presentation has been made. The engine-failure (one-engine-inoperative) performance is shown in Figure 70. Accelerate-go distance including clearway considerations and accelerate-stop distance including stopway considerations are compared in such a way as to yield an effective one-engine inoperative distance and V_1 speed information. Wind and runway slope effects are considered, and the adverse stopping effects of anti-skid-inoperative takeoff refusals are shown. There is also a method for defining the maximum allowable clearway, a function of runway slope. From this chart is read

V_1/V_{1B} where V_{1B} is the V_1 speed under equivalent balanced field length conditions: no wind, no slope, and no airbleed. The intercept of the accelerate-go and accelerate-stop trace lines must be transferred to a reference line to obtain the "corrected one-engine-inoperative distance" based upon balanced field from the unbalanced field situation. Figure 70 is often called the one-engine-inoperative "web" chart. The all-engines-operating performance chart, Figure 71, accounting for clearway, wind and slope, yields a "corrected all-engines-operating distance." From these data it would be possible to convert distance to corresponding all-engines and engine-inoperative limiting weights, the lesser being used for dispatch. However, to reduce the number of charts, only the corrected all-engines-operating distance versus weight chart, Figure 72, is prepared; the corrected one-engine-inoperative distance is converted on Figure 70 to an equivalent all-engines-operating distance usually called "corrected takeoff distance." The lesser of the two all-engines-operating distances defines the limiting takeoff weight on Figure 72.

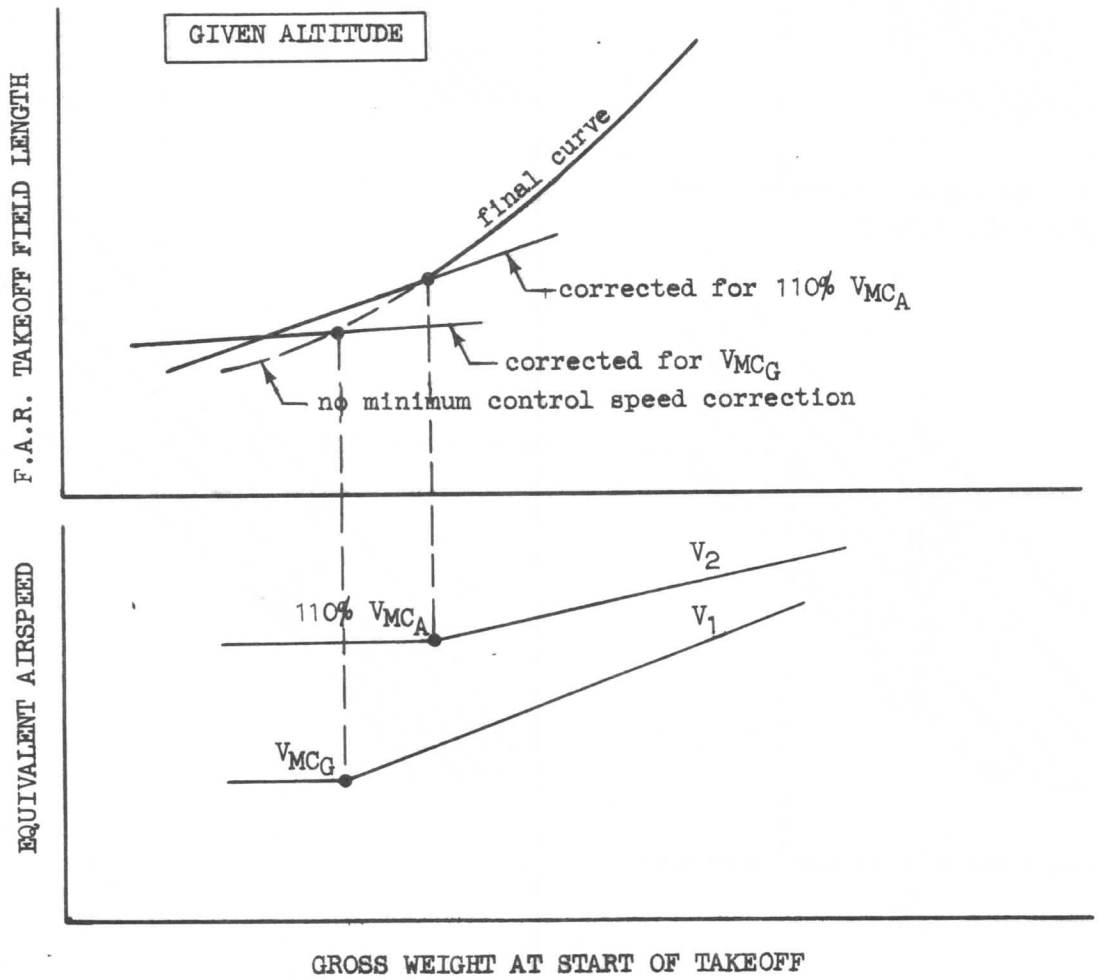

Figure 68.

It should be noted that to obtain the increase in takeoff weight to be gained by applying credit for a geometry-limited airplane with an operative attitude warning system, it is necessary to change the basic speed requirements. A completely

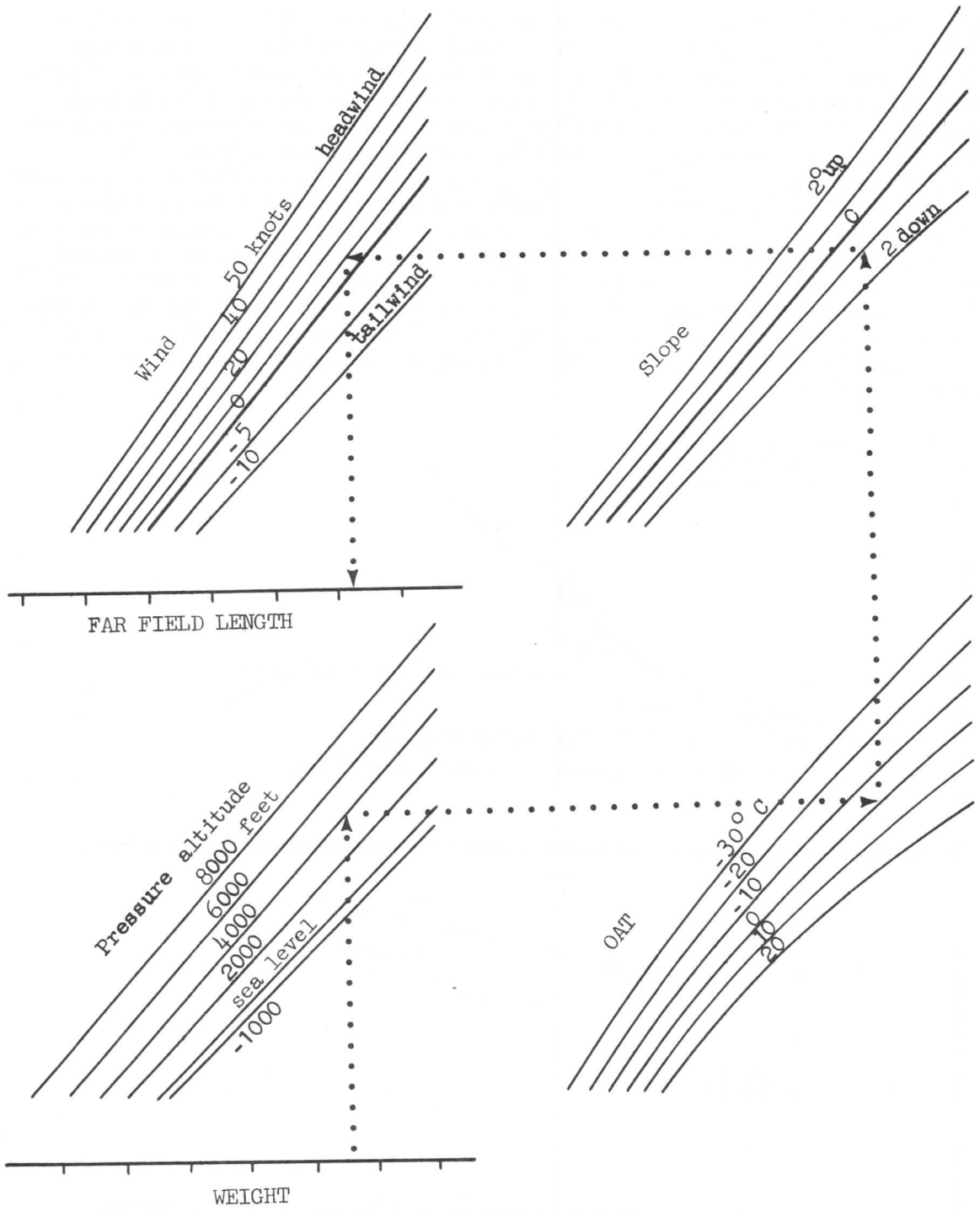

Figure 69.

different system of takeoff and climb-out charts or chart correction factors must be applied. Figure 72, for instance, shows an increase in weight for the same corrected takeoff distance; however, the actual takeoff distances will be different.

runway length available
up
dn
max. clearway limits defined by slope
clearway length
(downhill) (uphill) slope
t.w. wind
h.w.
engine failure speed ratio V1/V1B
ref. line
corrected one-eng.- inop. distance
equiv. all-eng.- oper. distance
corrected takeoff distance
(used to obtain one-engine-inoperative weight allowable from all-engines-operating weight chart)
anti-skid inoperative
anti-skid on
h.w.
wind t.w.
(uphill) slope (downhill)
stopping distance available
GIVEN FLAP SETTING
ONE-ENGINE-INOPERATIVE CHART

Figure 70

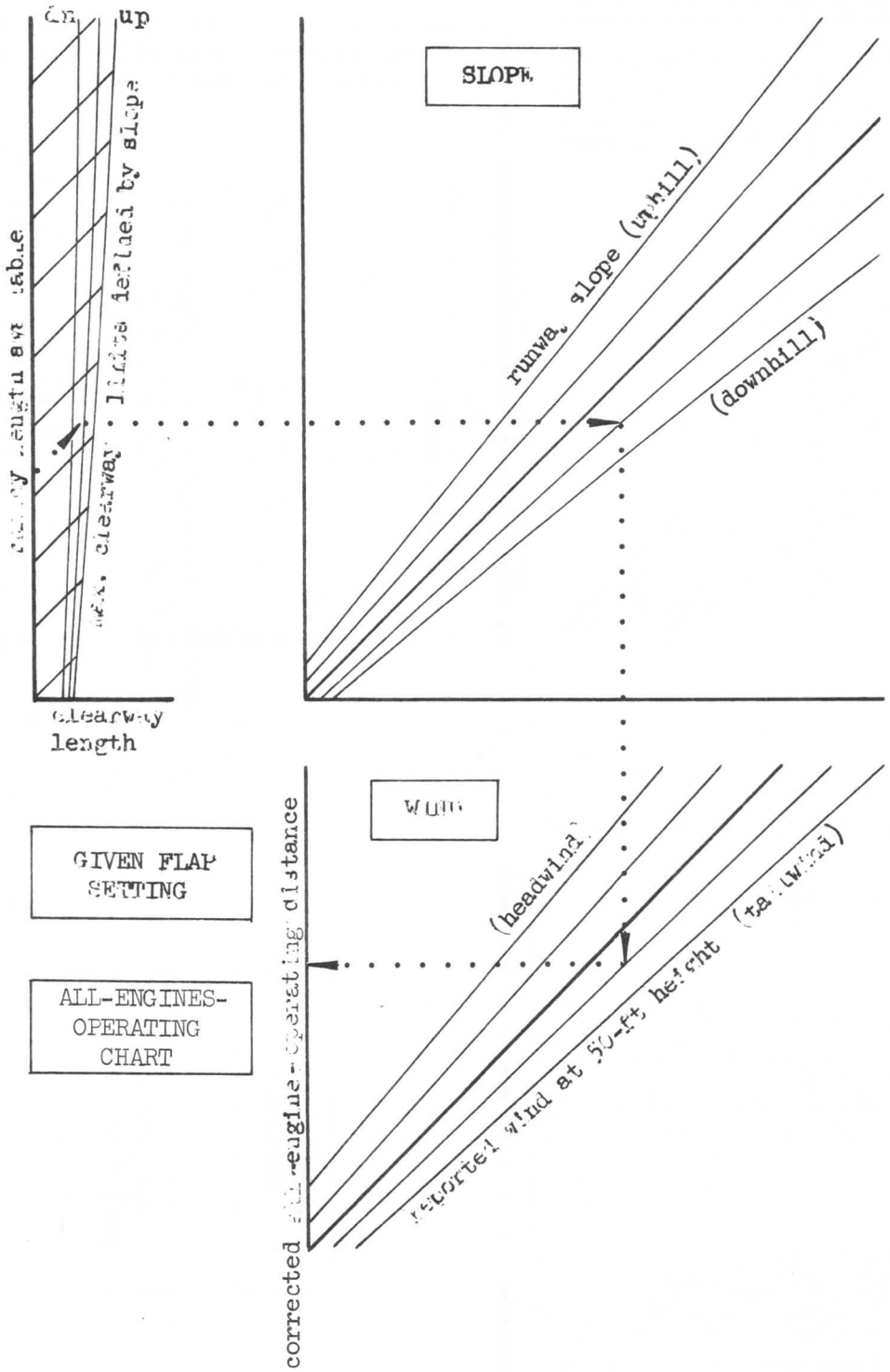
SLOPE
runway slope (uphill)
(downhill)
clearway length
GIVEN FLAP SETTING
ALL-ENGINES-OPERATING CHART
(headwind)
reported wind at 50-ft height

Figure 71.

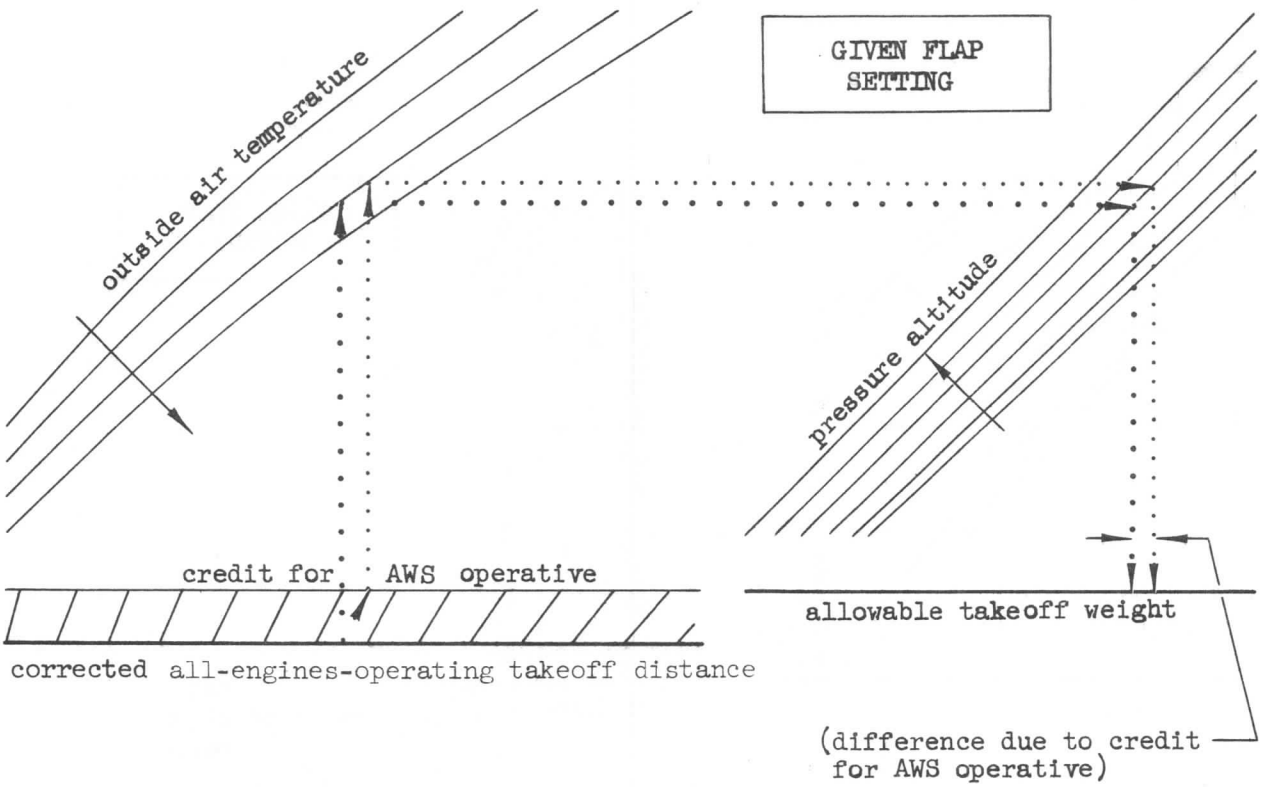

Figure 72.

V_1 is obtained by using the V_1/V_{1B} ratio from the "web" chart and entering Figure 73. The value obtained has to be checked against the minimum V_1, (V_{MCG}). V_R and V_2 are presented in a form similar to Figure 74. The attitude-warning-system rotation speed schedule must be observed to obtain credit for an operative attitude warning system. Minimum V_R (1.05 V_{MCA}) must still be observed and credit for an operative attitude warning system is not available when V_R is limited by minimum V_R.

Multiple V_1

Another feature of the "web" chart, Figure 70, is that a complete range of V_1 speeds can be determined as shown in Figure 75 if either excess all-engines-operating distance is available or weights are limited by other criteria and excess runway exists.

A range of V_1 exists only for takeoffs that are not one-engine-inoperative field length limited and will allow selection of the single operating value from this range of a V_1 as desired on the basis of runway conditions, thus providing more operational flexibility. Stopping performance for calculating field length requirements is based on maximum braking effort on a smooth, dry, hard surfaced runway, but without credit for the stopping margin provided by reverse thrust. Ice, snow or water can lengthen the stopping distance required and reduce the stopping margin now being provided by reverse thrust. When a range of V_1 exists, minimum V_1 will put the airplane in a "go" position earlier in the takeoff run. At the same time, if an engine failure occurred at minimum V_1, more stopping distance would be available than would be if V_1 were calculated by the standard method.

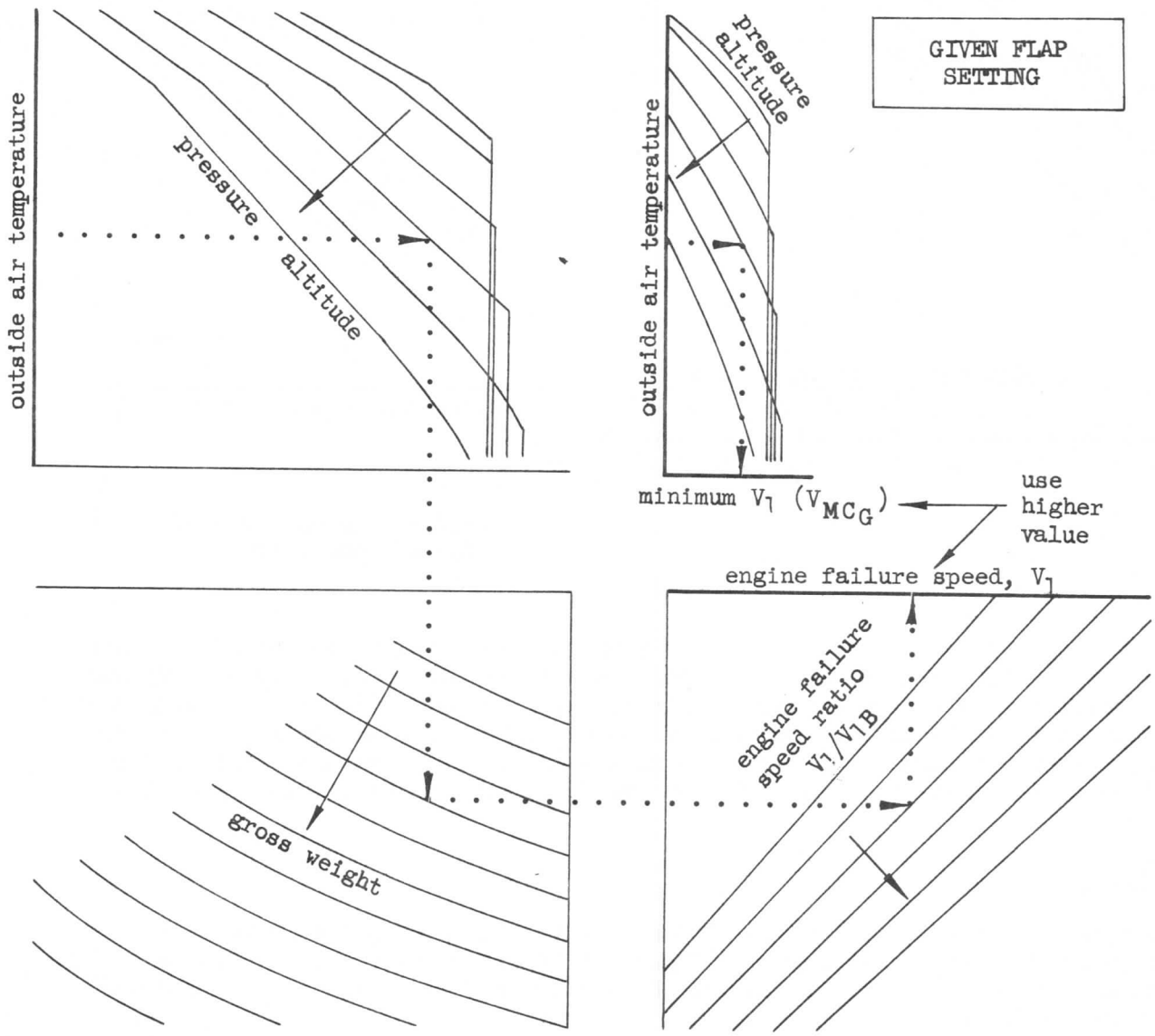
outside air temperature
pressure altitude
GIVEN FLAP SETTING
pressure altitude
outside air temperature
minimum V_1 (V_{MC_G})
use higher value
engine failure speed, V_1
engine failure speed ratio V_1/V_{1B}
gross weight

Figure 73.

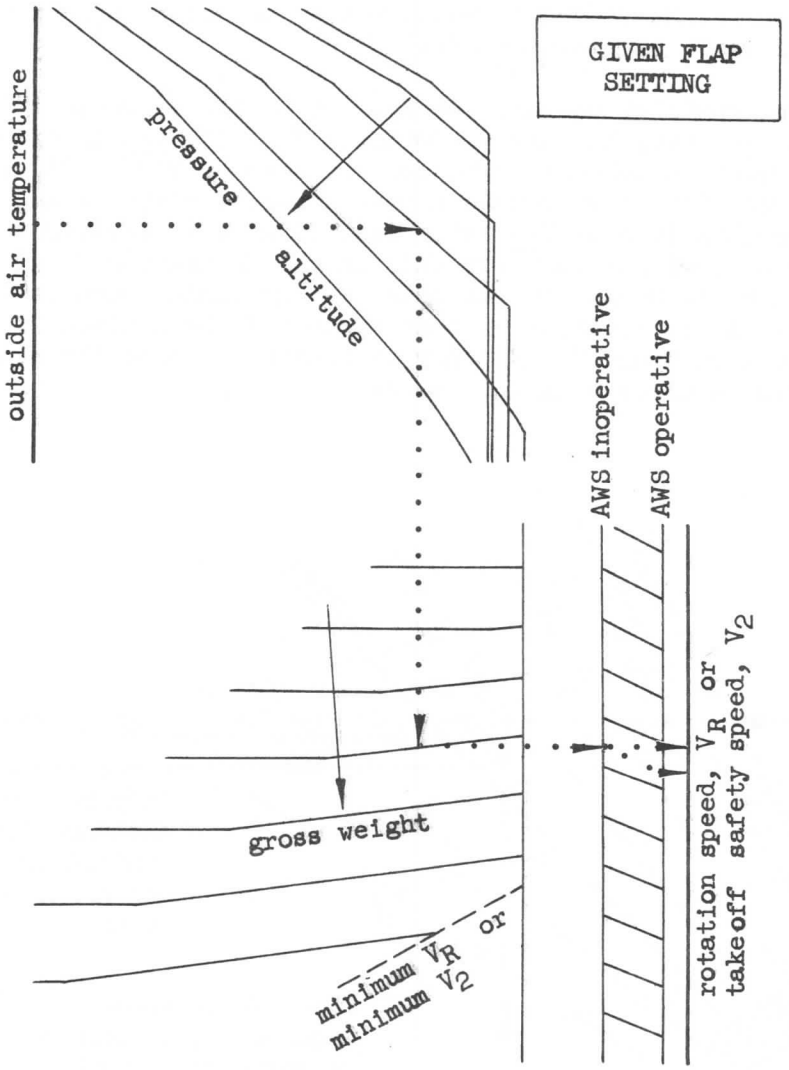
GIVEN FLAP SETTING
outside air temperature
pressure altitude
AWS inoperative
AWS operative
gross weight
minimum V_R or minimum V_2
rotation speed, V_R or takeoff safety speed, V_2

Figure 74.

Another advantage of multiple V_1 is that V_1 may be chosen to avoid the gross weight reduction that is sometimes necessary in brake limited takeoffs, usually at high altitude airports. Under former rules for determining V_1, a gross weight reduction was required until the resulting V_1 did not exceed the corresponding brake energy limit speed. If the brake energy limit speed lies within the allowable V_1 range, the brake energy limit speed becomes maximum V_1 and off-loading is not necessary. Gross weight reduction would not be necessary unless the brake energy limit speed were lower than minimum V_1.

The following additional restrictions must be applied to the V_1 range. If V_{MC_G} is greater than minimum V_1, V_{MC_G} becomes the minimum V_1. If V_{MC_G} is greater than than maximum V_1, the corrected takeoff distance, as shown on Figure 75, must be reduced until the intersection of corrected accelerate-stop distance and corrected takeoff distance results in a V_1/V_{1B} ratio that gives a V_1 greater than or equal to V_{MC_G}. Only one V_1 will result for this case. If maximum V_1 exceeds the brake energy limit or V_R, the lesser of brake energy limit speed or V_R must be used for maximum V_1. It is recommended that maximum V_1 be limited to values less than or equal to the standard V_1 in order to assure at least the same amount of stopping margin as was available in that case.

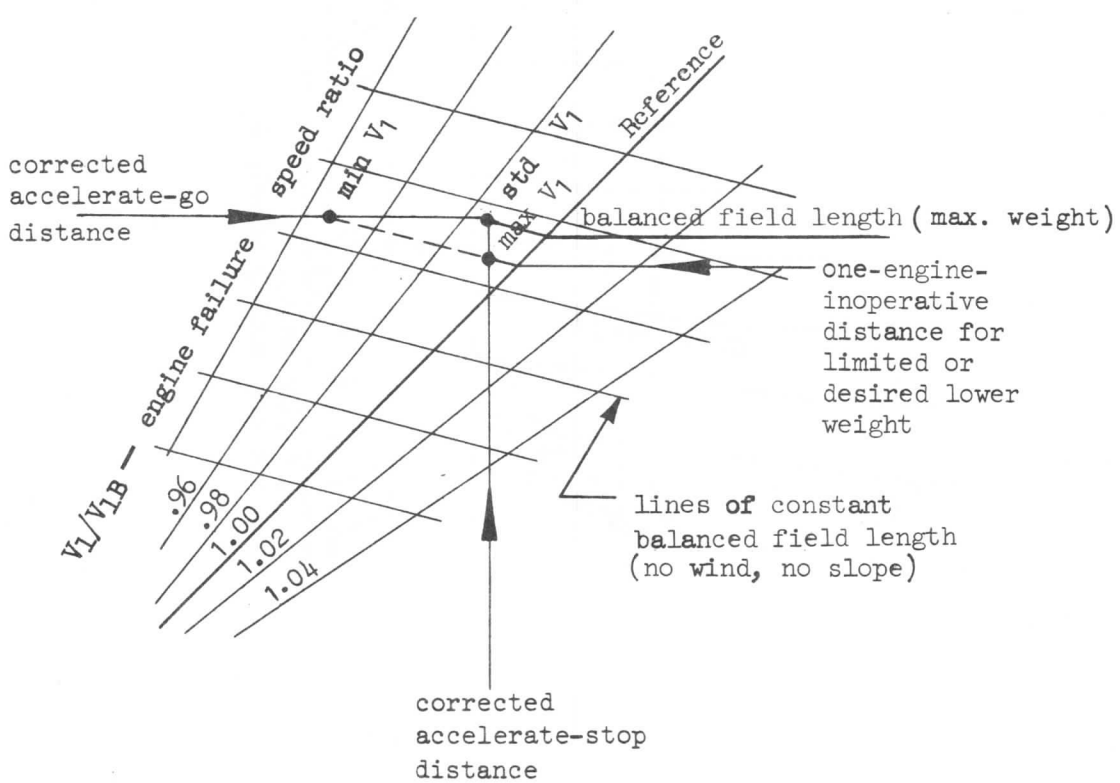

Figure 75.

Figure 75 may also be drawn as shown in Figure 76, which offers some advantages in determining the maximum take-off gross weight over that of Figure 70.

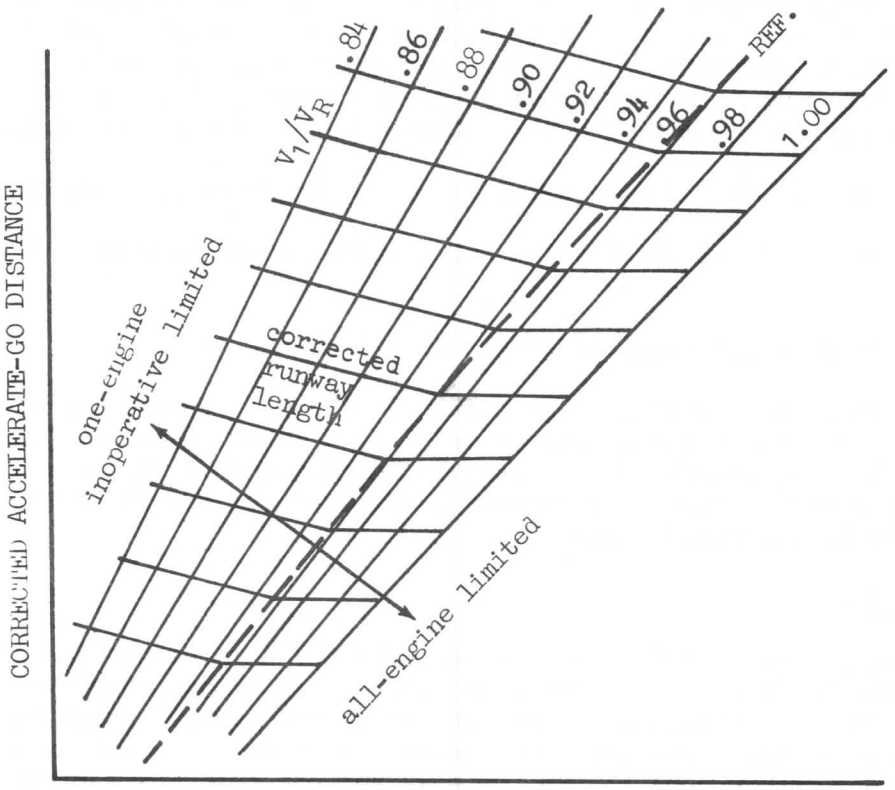

Figure 76.

As stated previously, for any combination of unbalanced distances, slope and wind effect, there is a reference or equivalent field length which will support the same take-off weight with zero slope and zero wind. The reference distance chosen may be for either the all-engine or the one-engine-inoperative condition. In Figure 76 the all-engine distance has been chosen as the reference, so the reference distance guide lines have cardinal (turning point) values at the boundary between all-engine and one-engine-inoperative conditions. These guide lines are labeled with the reference distances, so corrected runway lengths may be obtained by direct interpolation between guide lines instead of sliding to the reference line as on Figure 70. Since no improvement in corrected runway length is possible with increased accelerate-stop distance in the all-engine limited area, the guide lines are horizontal to the right of the boundary line.

Another difference in this format is in showing the speed ratio in terms of V_1/V_R instead of V_1/V_{1B}. This establishes a positive upper limit to V_1, and reduces the number of charts in the flight manual since V_1, V_R and V_2 can be combined on a single chart. Also, the takeoff distance corrections for clearway, runway slope and wind are based on the more conservative of all-engine or one-engine-inoperative conditions; therefore, a separate all-engine operating chart, Figure 71, is not necessary.

Water Injection Requirements

A chart is furnished for airplanes requiring water injection to show the water requirements from brake release to 35 foot height, and another to show the water requirements from a 35 foot height to the flaps-up point. Water weights include water for an all-engines-operating run-up prior to brake release, usually 10 seconds. The water-required charts are based on regulated water flow rates which are constant for a particular engine model. These rates for the JT3C engine are:

(1) 39,700 lb/hr/eng. or 44.1 lb/sec total for 4 engines, OAT above 40°F.

(2) 21,900 lb/hr/eng or 24.5 lb/sec total for 4 engines, OAT between 11° and 48°F.

(3) 0 flow below 11°F, since water injection is not used.

The controlling factor in determining the quantity of water required is time. For the water required from brake release to a 35 foot height, the time histories computed for the time vs velocity or time vs distance charts may be used. The charts showing water requirements for various conditions are presented in "chase-around" form in the FAA Approved Manual.

Thrust Presentation

Takeoff thrust data in terms of EPR, or P_{t7}, are presented for altitudes of sea level, 2,000, 4,000, 6,000 and 8,000 feet, and for ambient temperatures as shown in Figures 77 and 78. The horizontal lines represent the maximum (flat-rated) thrust allowed under static conditions for commercial operation. This means that the thrust levers may not be advanced to the full forward position. Figures 77 and 78 are representative curves for engines operating without water injection.

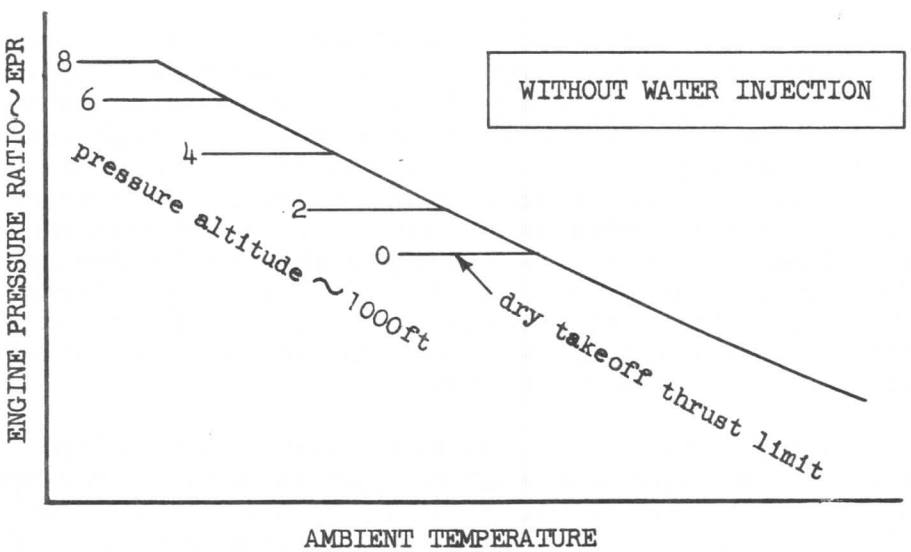

Figure 77.

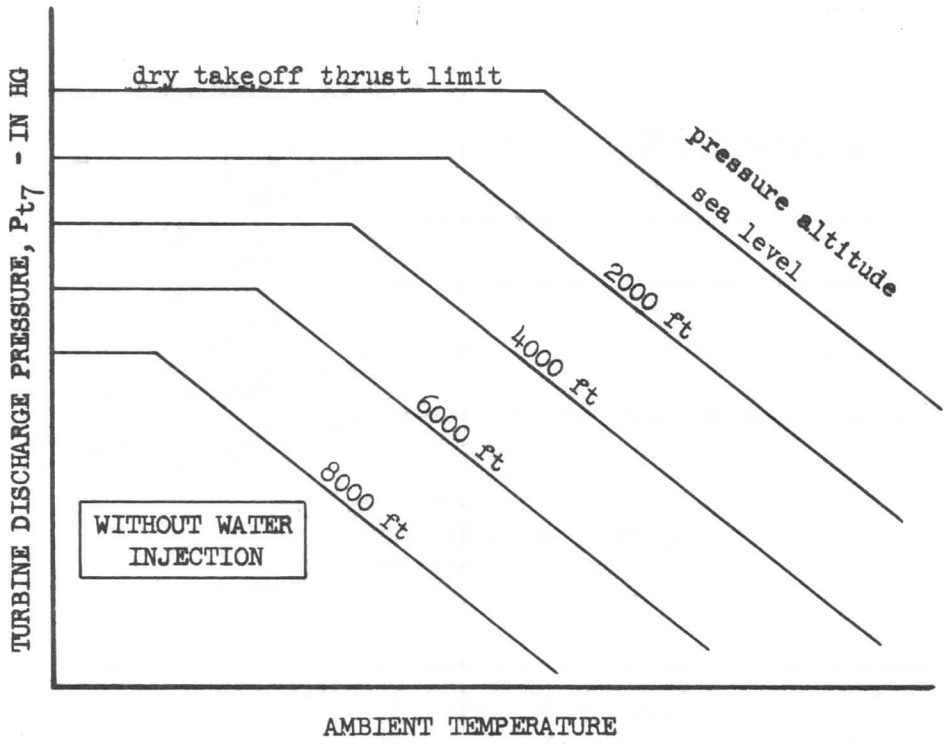

Figure 78.

For those engines using water injection during takeoff, the takeoff thrust data will appear as shown in Figures 79 and 80.

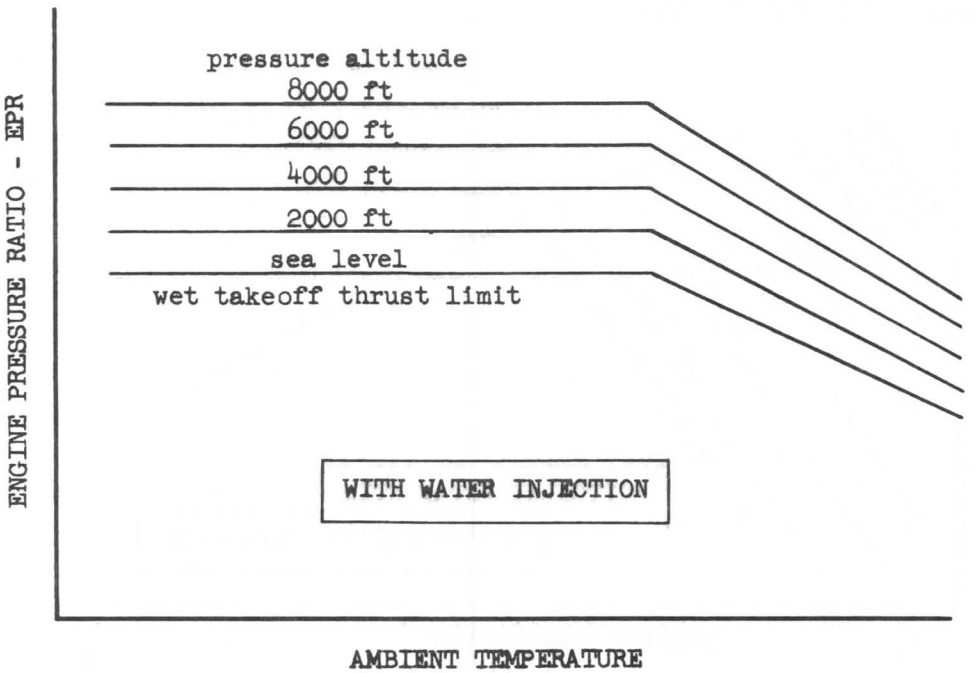

Figure 79.

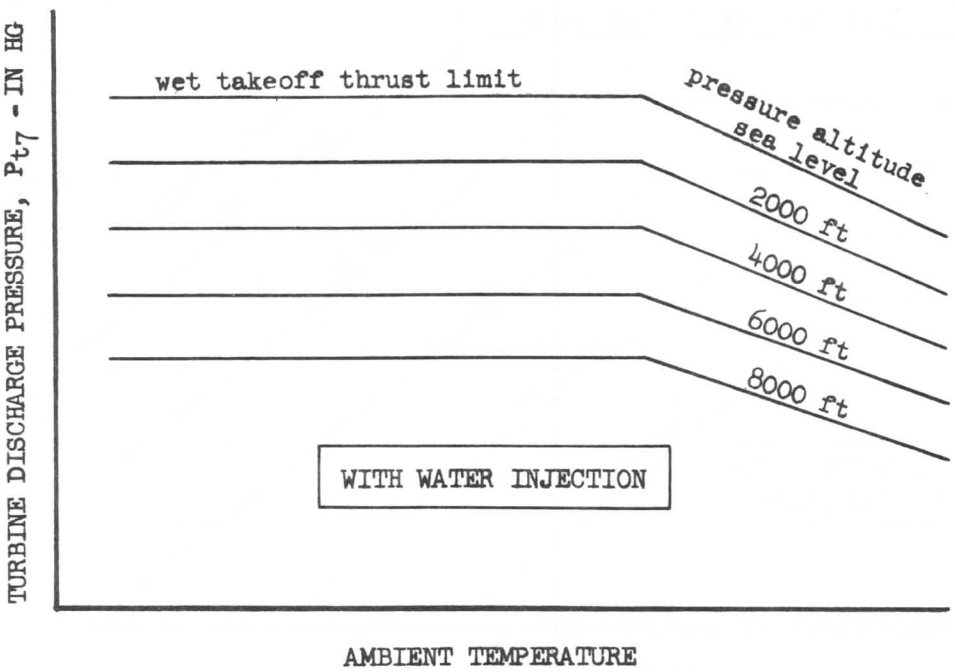

Figure 80.

In addition to the above EPR and P_{t_7} charts, another chart that is very handy for cross-referencing and preliminary setting of takeoff thrust is the N_1 check chart. Typical curves are shown in Figures 81 and 82. For some engines, it may be more advantageous to use N_2 rpm.

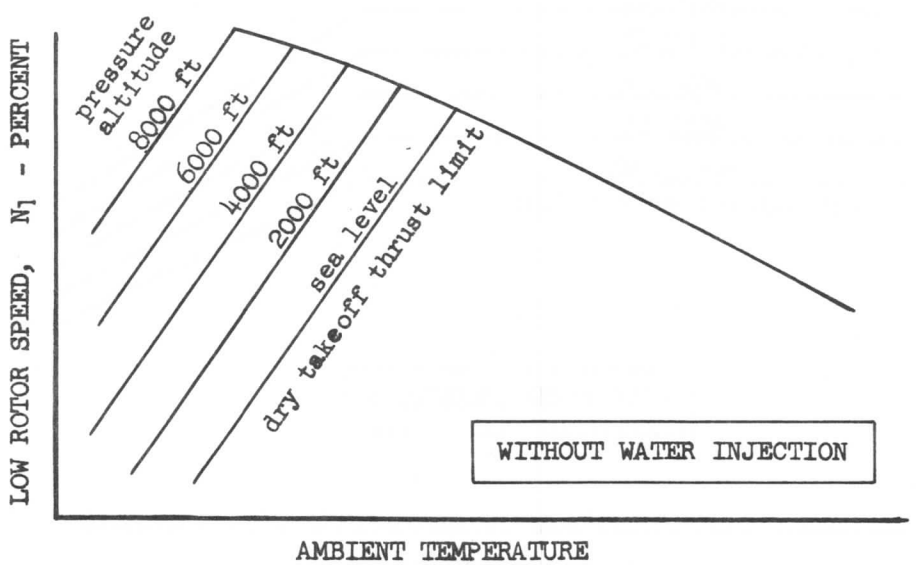

Figure 81.

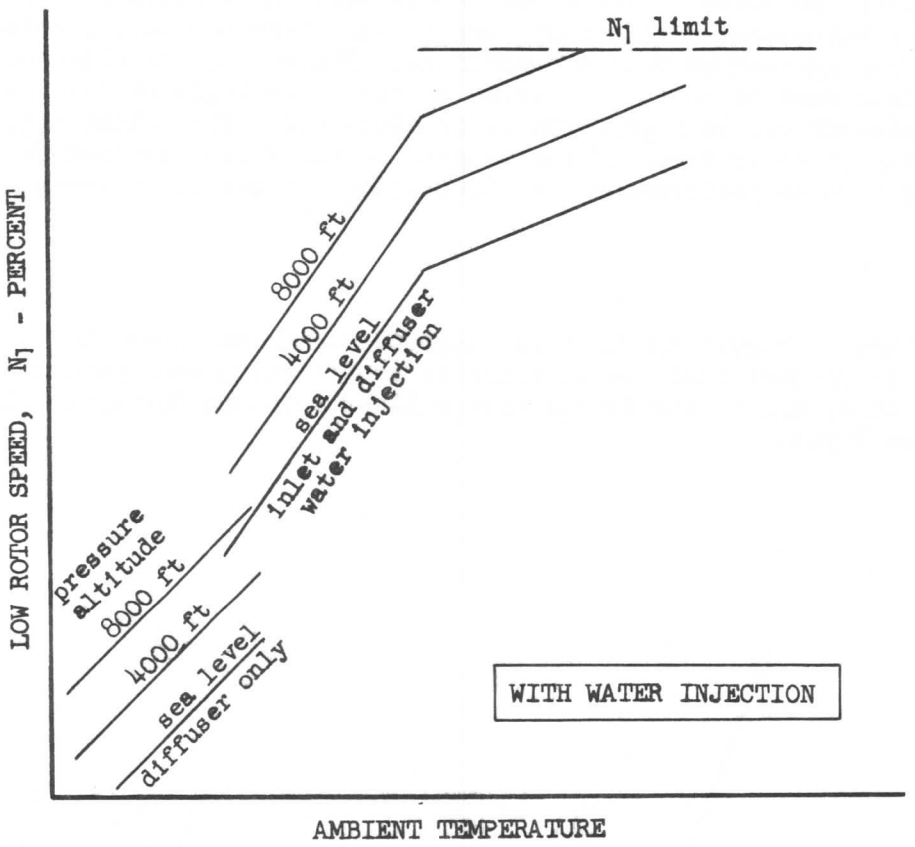
N1 limit
8000 ft
4000 ft
sea level
inlet and diffuser
water injection
pressure
altitude
8000 ft
4000 ft
sea level
diffuser only
WITH WATER INJECTION
LOW ROTOR SPEED, N1 - PERCENT
AMBIENT TEMPERATURE

Figure 82.

3-6 CLIMB

General

In straight and level flight at a given velocity, the thrust available from the engine is exactly equal to the thrust required to overcome the drag of the airplane. When the thrust available is less than this, the airplane will lose speed and perhaps altitude also. When the thrust available exceeds the thrust required, the airplane will be able to either accelerate in level flight or climb.

The two flight regimes in which climb is an important consideration are those associated with operation close to the ground where obstacle clearance is most important and those associated with enroute conditions where the only problem is the rate at which one approaches cruise conditions. Therefore, the climb performance of the airplane must be derived in terms of the climb angle or clearance capability when take-off climbout performance is discussed. This climb angle presentation is usually given in terms of the tangent of the angle, defined as climb gradient. But for enroute performance, the derivation and use is in terms of rate of climb.

Rate of Climb

Consider the airplane in Figure 83 which is climbing due to an excess of thrust over drag. If it is assumed that the airplane is accelerating and changing climb angle at the same time, all of the forces that will be involved during a climb can be shown on the Figure.

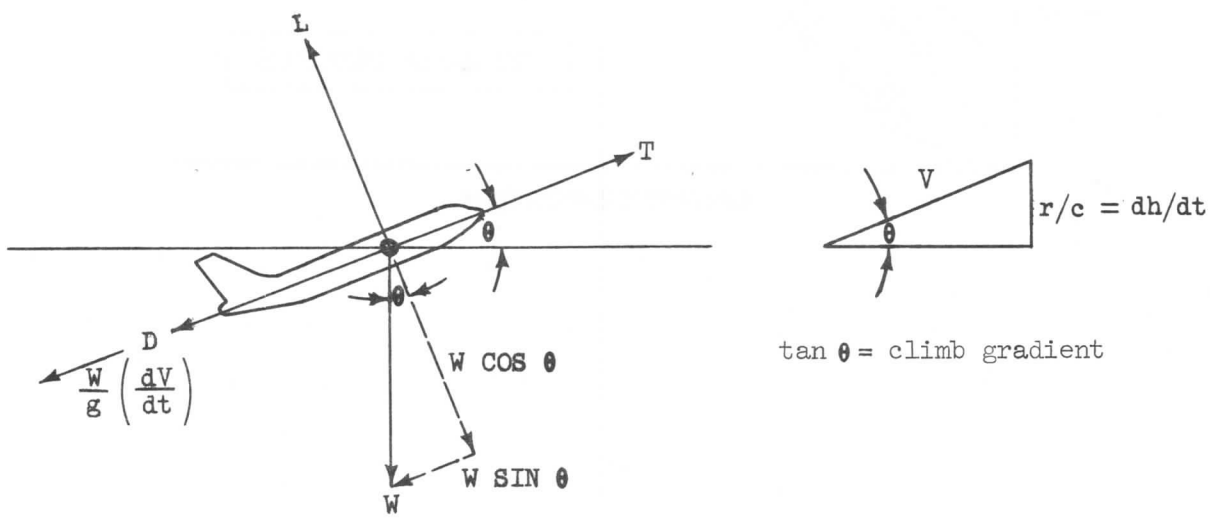

Figure 83.

The weight vector may be resolved into components parallel and perpendicular to the flight path, and the static equilibrium conditions may be applied in these

directions.

$$T - D - W \sin\theta - \frac{W}{g}\frac{dV}{dt} = 0 \qquad (96)$$

$$L + \frac{W}{g}\frac{d\theta}{dt} V - W\cos\theta = 0 \qquad (97)$$

Equation (96) may be written:

$$\sin\theta = \frac{1}{W}\left[T - D - \frac{W}{g}\frac{dV}{dt}\right]$$

$$= \frac{T-D}{W} - \frac{1}{g}\frac{dV}{dt} \qquad (98)$$

The rate of climb, r/c, will be equal to the vertical component of the flight velocity.

$$r/c = V \sin\theta$$

or,

$$r/c = \frac{(T-D)V}{W} - \frac{V}{g}\frac{dV}{dt} \qquad (99)$$

$\frac{dV}{dt}$ may be written as:

$$\frac{dV}{dt} = \frac{dV}{dh}\frac{dh}{dt}$$

so,

$$r/c = \frac{dh}{dt} = \frac{(T-D)V}{W} - \frac{V}{g}\frac{dV}{dh}\frac{dh}{dt}$$

$$\frac{dh}{dt}\left(1 + \frac{V}{g}\frac{dV}{dh}\right) = \frac{(T-D)V}{W}$$

$$r/c = \frac{dh}{dt} = \frac{\left(\frac{T-D}{W}\right)V}{1 + \frac{V}{g}\frac{dV}{dh}} \qquad (100)$$

The dimensionless term $\frac{V}{g}\frac{dV}{dh}$ is known as the acceleration factor, and values for use will be determined later. When the climb is being executed at a constant true airspeed, the acceleration factor equals zero and equation (100) for unaccelerated r/c becomes:

$$r/c \text{ (unaccelerated)} = \left(\frac{T-D}{W}\right)V \qquad (101)$$

The units of rate of climb are the same as those of velocity; in this case, ft/sec. If the rate of climb is to be expressed in ft/min and the velocity in knots, a conversion factor must be applied to equations (100) and (101). Since the velocity in ft/min is (1.688)(60) = 101.28 multiplied by the velocity in knots,

$$r/c = 101.28\frac{\left(\frac{T-D}{W}\right)V_k}{1+\frac{V}{g}\frac{dV}{dh}} = \frac{r/c\ (\text{unaccelerated})}{1+\frac{V}{g}\frac{dV}{dh}} \qquad (102)$$

where, r/c is rate of climb in ft/min,
V_k is velocity in knots, and
$\frac{V}{g}\frac{dV}{dh}$ is dimensionless.

In Section 1 it was shown that:

$$V\ (\text{knots}) = 661.5\ M\sqrt{\theta}$$

Therefore,

$$101.28V = 66{,}987\ M\sqrt{\theta} \qquad (103)$$

Substituting equation (103) into equation (102) and dividing both numerator and denominator by the pressure ratio, δ, results in:

$$r/c = \frac{66{,}987\ M\sqrt{\theta}}{1+\frac{V}{g}\frac{dV}{dh}}\left(\frac{T/\delta - D/\delta}{W/\delta}\right) = \frac{66{,}987\ M\sqrt{\theta}}{1+\frac{V}{g}\frac{dV}{dh}}\left(\frac{\Delta T/\delta}{W/\delta}\right) = \frac{r/c\ (\text{unaccelerated})}{1+\frac{V}{g}\frac{dV}{dh}} \qquad (104)$$

The division by δ is to put the force parameter in a form consistent with the presentation on the speed-thrust chart. Equation (104) states that to obtain rate of climb at a given Mach number, M, all that must be known is the available T/δ, and the airplane D/δ and W/δ. These quantities are obtainable from the speed-thrust chart, Figure 84. (This grid was discussed in detail above.)

The derivation of equation (104) takes care of the acceleration along the flight path. Equation (97) is the applicable equation for acceleration perpendicular to the flight path and may be written as:

$$L - W\cos\theta = -\frac{W}{g}V\frac{d\theta}{dt} \qquad (105)$$

where $V\,d\theta/dt$ is the centrifugal acceleration due to changing the flight path angle at a rate $d\theta/dt$ (see Chapter 3-4 in this section). It is found from experience that $d\theta/dt$ is very nearly zero at any point in the climb so that

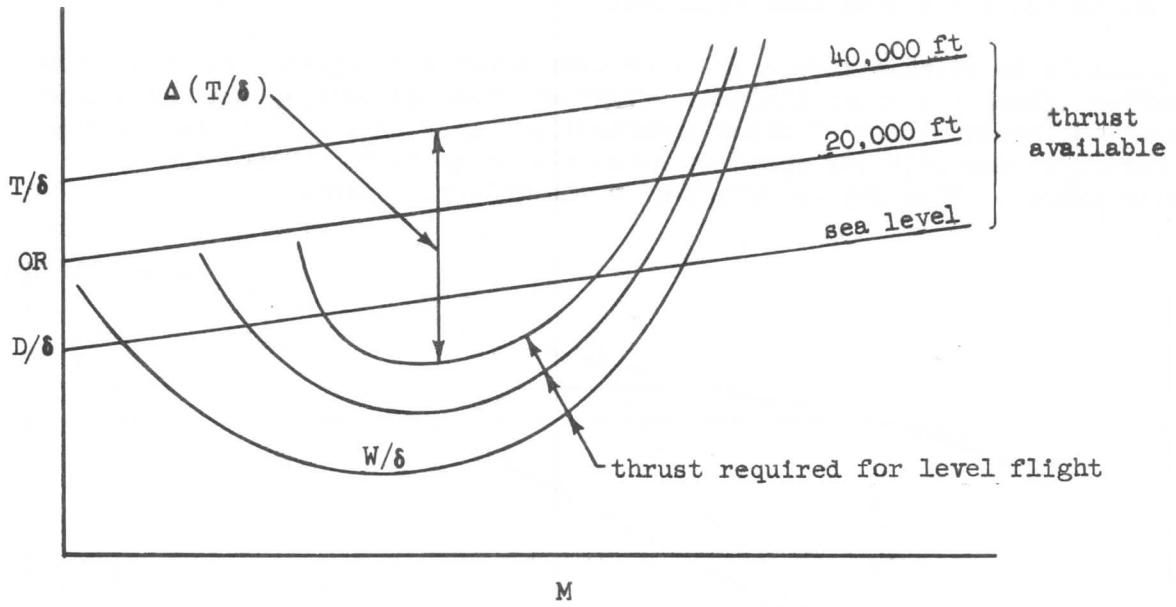

Figure 84.

equation (105) reduces to the form:

$$L - W \cos \theta = 0$$

or,

$$L = W \cos \theta \qquad (106)$$

This equation states that in a climb, the lift will be less than the weight (and thus the level flight lift) by the factor cos θ . This means that at a particular speed, the drag will be less than the drag at the same speed in level flight. The reduction in lift (and therefore drag) will be greater for larger climb angles. It will be found, however, that for most conditions on airplanes such as the 707, the climb angles will be small (below 15 degrees), so that cos θ will be very close to unity. Thus, the lift and drag during climb are practically identical to those existing under level flight conditions, which allows the level flight data for the airplane to be used. Of course, with airplanes having very large climb angles (interceptors, missiles, etc.), the climb angle effect on drag must be taken into consideration.

Maximum rate of climb for a given weight and altitude will occur at a speed where $\Delta T/\delta$ multiplied by the Mach number is greatest, as seen in equation (104). This will be at a speed slightly higher than where $(\Delta T/\delta)$ max is found. The maximum-rate-of-climb true velocity increases with altitude; therefore, the airplane must accelerate along the flight path to maintain the maximum rate of climb. If the thrust rating can not be increased, the rate of climb will be reduced to account for this acceleration, as seen from equation (104).

For one or two engines inoperative or any condition where extra drag is involved, equation (100) will be:

$$r/c \text{ (accelerated)} = \frac{\left(\frac{T-D-\Delta D}{W}\right) V}{1 + \frac{V}{g}\frac{dV}{dh}} \qquad (107)$$

where ΔD is the extra drag, when applicable.

It is possible to calculate rate of climb over a range of speeds that will give the maximum value at a given altitude. However, the following method determines the speed for maximum rate of climb immediately. In Figure 85, the best climb speed occurs at one half the speed at which the tangents to the D/δ and T/δ curves intersect. This may be verified in the following manner:

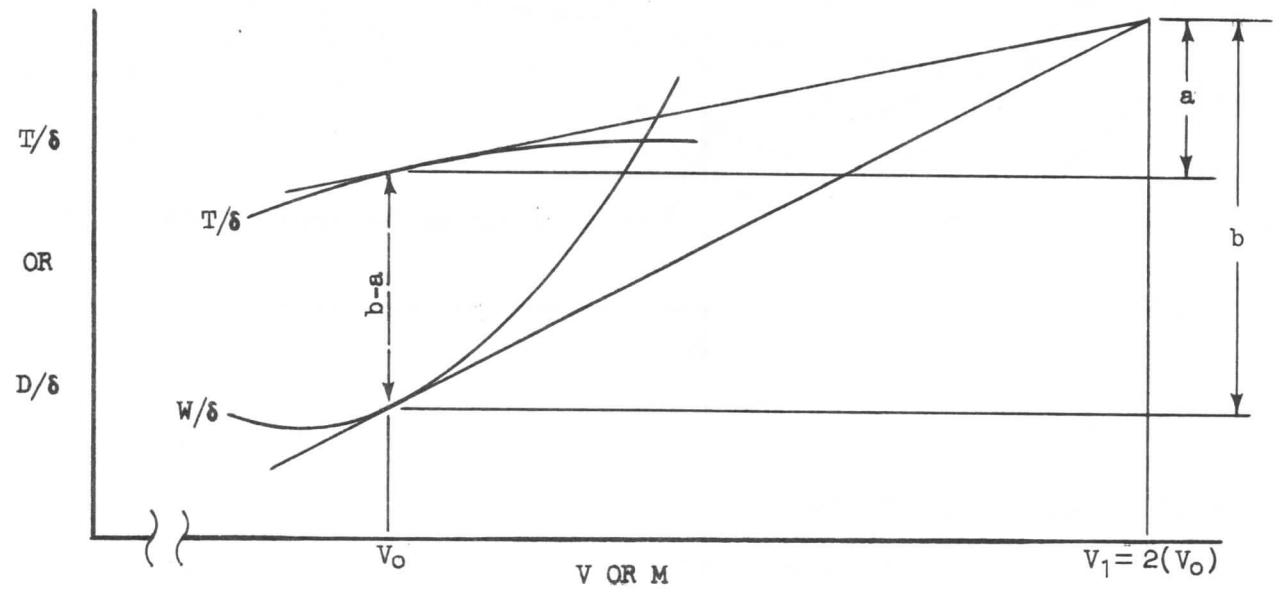

Figure 85.

$$a = \left(\frac{d(T/\delta)}{dV}\right)_{V_o} (V_1 - V_o)$$

$$b = \left(\frac{d(D/\delta)}{dV}\right)_{V_o} (V_1 - V_o)$$

$$b - a = \left(\frac{T}{\delta} - \frac{D}{\delta}\right)_{V_o} = - \left[\frac{d(T/\delta - D/\delta)}{dV}\right]_{V_o} (V_1 - V_o)$$

or,

$$\frac{\left(\frac{T - D}{\delta}\right)_{V_o}}{V_o} = - \left(\frac{V_1}{V_o} - 1\right) \left[\frac{d(T/\delta - D/\delta)}{dV}\right]_{V_o} \qquad (108)$$

From equation (101), it is known that:

$$r/c = C \left(\frac{T - D}{\delta}\right) V$$

For the rate of climb to be a maximum, the slope d(r/c)/dV has to equal zero as seen by Figure 86.

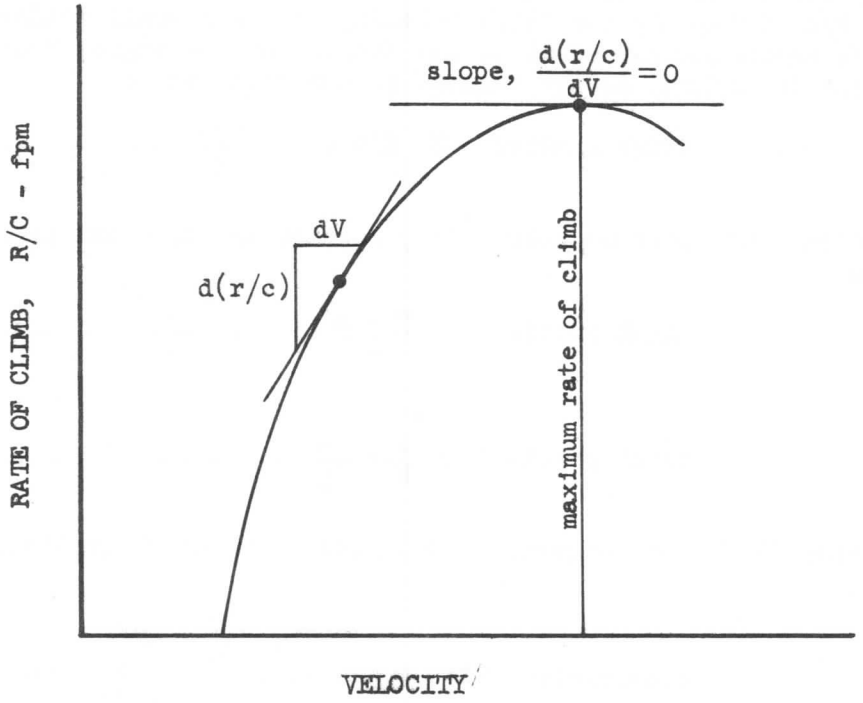

Figure 86.

Therefore,

$$\frac{d(r/c)}{dV} = 0 = \frac{d\left(\frac{T - D}{\delta}\right)}{dV}V + \frac{T - D}{\delta}$$

or,

$$\frac{\frac{T - D}{\delta}}{V} = -\frac{d\left(\frac{T - D}{\delta}\right)}{dV} \qquad (109)$$

If equations (108) and (109) are combined and simplified, the following results:

$$\frac{V_1}{V_o} - 1 = 1$$

$$\frac{V_1}{V_o} = 2$$

or,

$$V_1 = 2V_o$$

In the above analysis, the variation of speed with weight may be ignored, and a mean or average value may be used for each altitude for the 707 airplane.

Climb Gradient

Climb gradient may now be derived. Figure 83 shows that the sine of the climb angle is equal to r/c divided by the climb velocity, V. For small angles, the sine of an angle is approximately equal to the tangent of the angle; therefore, since climb gradient is defined as the tangent of the climb angle:

$$\text{climb gradient} \cong \text{Sin } \theta = \frac{r/c}{V} \qquad (110)$$

Substituting equation (101) into equation (110) results in the climb gradient for unaccelerated climb,

$$\text{climb gradient} = \frac{T - D}{W} \qquad (111)$$

or,

$$\text{climb gradient} = \frac{T}{W} - \frac{C_D}{C_L} \qquad (112)$$

Substituting equation (100) into equation (110) results in climb gradient for accelerated climb,

$$\text{accelerated climb gradient} = \frac{\frac{T}{W} - \frac{C_D}{C_L}}{1 + \frac{V\,dV}{g\,dh}} \qquad (113)$$

A chart showing climb performance traded for acceleration may now be discussed. The development of the chart, sketched in Figure 87, may be seen by analyzing the forces acting on an airplane in a climb at constant velocity (no acceleration) and the same airplane in accelerated level flight. This acceleration and climb trade chart is a general type chart and can be used for all aircraft. Considering the climb where

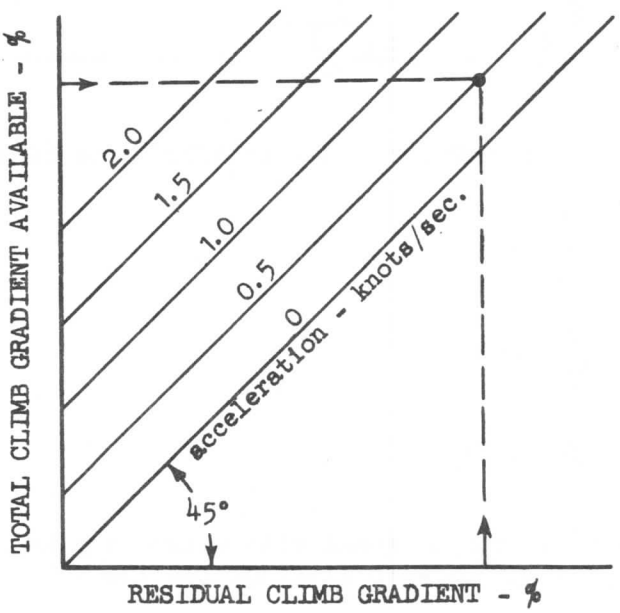

Figure 87.

there is no acceleration, equation (112) will apply. Considering acceleration in level flight as shown in Figure 88 and equating forces parallel to the flight path:

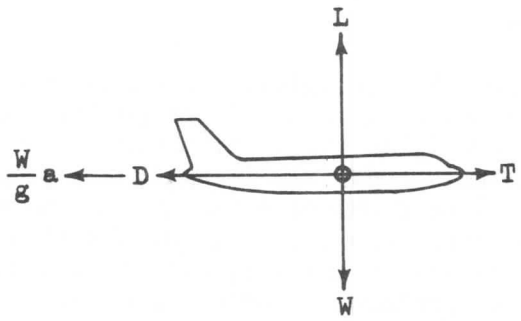

Figure 88.

$$T - D = \frac{W}{g}a$$

$$a = g\left(\frac{T - D}{W}\right)$$

$$\frac{a}{g} = \frac{T}{W} - \frac{C_D}{C_L} \qquad (114)$$

Since $T/W - C_D/C_L$ was defined as a gradient term, a/g may now be defined as acceleration gradient:

$$\text{acceleration gradient} = \frac{a}{g} \qquad (115)$$

and since part of the total climb gradient from equation (112) may be traded for acceleration, the following equation can now be written:

$$\left(\frac{T}{W} - \frac{C_D}{C_L}\right)_{total} = \left(\frac{T}{W} - \frac{C_D}{C_L}\right)_{residual} + \frac{a}{g}$$

or,

$$\left(\frac{T}{W} - \frac{C_D}{C_L}\right)_{residual} = \left(\frac{T}{W} - \frac{C_D}{C_L}\right)_{total} - \frac{a}{g} \qquad (116)$$

where $\left(\frac{T}{W} - \frac{C_D}{C_L}\right)_{Residual}$ is the climb gradient remaining.

Figure 87 is constructed with total climb gradient and residual climb gradient on the axes. At zero acceleration, the total gradient is equal to the residual gradient; therefore, the zero acceleration line is established at a 45° angle to the axes. Another constant acceleration value may be selected and divided by the

gravitational unit, g. The results, when expressed in percent and subtracted from various values of the total climb gradient, will determine values of the residual gradient, thus determining the location of the acceleration lines.

FAR Minimum Performance Requirements

Airplane performance potential is given in the Operations Manual and the FAA Flight Manual in terms of climb gradient available. These performance potentials are used to determine whether any flight plan meets the minimum performance requirements of the Federal Aviation Regulations. It is against regulations to plan a flight such that the airplane's performance capabilities, as measured in terms of its potential to climb, are less than the stipulated minima. Enroute minima, to be explained further in the cruise chapter, are stipulated in terms of total gross potential reduced by an arbitrary gradient factor. The minima during climb-out after takeoff, approach and landing are given in terms of the minimum gross gradient available. It should be emphasized that these regulations do not restrict operation; they merely set minimum standards of potential needed in case problems arise.

The regulations pertaining to climb gradients after takeoff, approach and landing for two, three, and four-engine transport airplanes are as follows:

Flight Condition	SR-422 Rules	FAR Part 25 and SR-422B Rules		
	4-engine airplanes	4-engine airplanes	3-engine airplanes	2-engine airplanes
(1) First takeoff climb segment	positive	0.5%	0.3%	positive
(2) Second takeoff climb segment	3.0%	3.0%	2.7%	2.4%
(3) Final takeoff climb segment (applies from the 400-foot level of second segment to end of takeoff pattern)	1.8%	1.7%	1.5%	1.2%
(4) Approach segment	2.8%	2.7%	2.4%	2.1%
(5) Landing segment	4.0%	3.2%	3.2%	3.2%

The flight conditions that are referred to are described below:

(1) First takeoff climb segment is with the critical engine inoperative, takeoff thrust, landing gear extended, flaps in takeoff position, takeoff speed ($V_2 \geq 1.20\ V_{S_1}$) under SR-422 or lift-off speed under SR-422B and part 25 of FAR, and the weight that exists at the time the gear retraction is started. (Under SR-422B and part 25 of FAR, $V_{S_1} = V_S$).

(2) Second takeoff climb segment is with the critical engine inoperative, takeoff thrust that exists at 400 feet above the takeoff surface, gear retracted, flaps in takeoff position, takeoff speed ($V_2 \geq 1.20\ V_{S_1}$), and the weight that exist at the time the gear is fully retracted. (Under SR-422B and part 25 of FAR, $V_{S_1} = V_S$). It should be noted that second segment extends to 400 feet or higher, if necessary, for terrain clearance.

(3) For purposes of definition and test, the climb-out above 400 feet is usually divided into two segments in addition to the final segment; the third

segment, in which the flaps are retracted while the airplane is accelerating in level flight, and a fourth segment, in which the airplane is in climb with takeoff thrust. The thrust and gross weight for each segment are those with which the airplane enters the segment.

Final takeoff climb segment is with the critical engine inoperative, maximum continuous thrust that exists at the higher altitude of either 1000 feet above takeoff surface under SR-422 (1500 feet under SR-422B and part 25 of FAR) or where transition to enroute configuration is completed, gear retracted, flaps retracted, speed $\geq 1.25\ V_{S_1}$; and weight is that existing at the time flap retraction is started under SR-422 or weight equal to that existing at the end of the takeoff path under SR-422B and part 25 of FAR. (Under SR-422B and part 25 of FAR, $V_{S_1} = V_S$).

(4) Approach climb segment is with the critical engine inoperative, takeoff thrust, gear retracted, flaps set so that $V_{S_1} \leq 1.10\ V_{S_o}$, speed $\leq 1.5\ V_{S_1}$, and at the landing weight. (Under SR-422B and part 25 of FAR, V_{S_1} and $V_{S_o} = V_S$).

(5) Landing climb segment is with all engines operating, takeoff thrust, gear extended, flaps in the landing configuration, speed $\leq 1.4\ V_{S_o}$ under SR-422 ($\leq 1.3\ V_S$ under SR-422B and part 25 of FAR), and at the landing weight. (Under SR-422B and part 25 of FAR, $V_{S_o} = V_S$)

During the flap retraction after takeoff, it may be possible to get the airplane into difficulties relative to the flap placard or the minimum speed allowable. Consider the airplane which is taking off at a light weight on a cold day and, rather than use its large excess thrust for climb during flap retraction, is allowed to accelerate in level flight. Due to the large excess thrust, the airplane will accelerate relatively rapidly and could conceivably overrun the flap placard, and cause structural damage to the flaps. Figure 89 shows the relationship of speed to flap extension. Consider now the opposite situation where the airplane is taken off on a very hot day. Assuming that there is now low excess thrust and that the airplane is allowed to use some of this excess to climb, it is possible that the acceleration is reduced so much that the speed increase is not sufficient to keep ahead of the minimum speed. Note that the minimum speed increases as the flaps are retracted. This is due to the reduction in available lift coefficient.

As in the calculations for water used during ground roll, the water requirements after unstick are calculated by first calculating the time and then multiplying this by the water flow rate. One engine is considered to be inoperative. Time is a function of the flight path selected, and speed maintained. For one-engine-inoperative operation, V_2 speed is maintained from the 35 foot height to the end of the second segment. For calculations for the all-engines-operating case, it is assumed that the airplane will accelerate to approximately V_2 + 10 Kts.

The gear is retracted as soon as safely practical after lift-off. For calculation purposes, it is assumed that the retraction is initiated 3 seconds after lift-off, and the retraction time is a conservative estimate based on tests run with one of the hydraulic pumps shut off (12.3 seconds for the 707-100 series). The airplane is flown without change in configuration or thrust to the end of second segment, at which time it is flown level and flaps are retracted.

In order to insure proper terrain clearance under all conditions, the regulations specify the determination of a minimum flight path which will give the necessary assurance. Under SR-422, the available gross takeoff path must clear all obstacles vertically by at least (35 + 0.01D) feet, where D is the distance from the end of the runway; it must clear horizontally by 200 feet if within the airport boundaries and 300 feet if beyond. The airplane may not be banked below 50 feet height and may not be banked beyond 15° until out of the takeoff segment of the flight (1000 feet or enroute climb condition, whichever is higher).

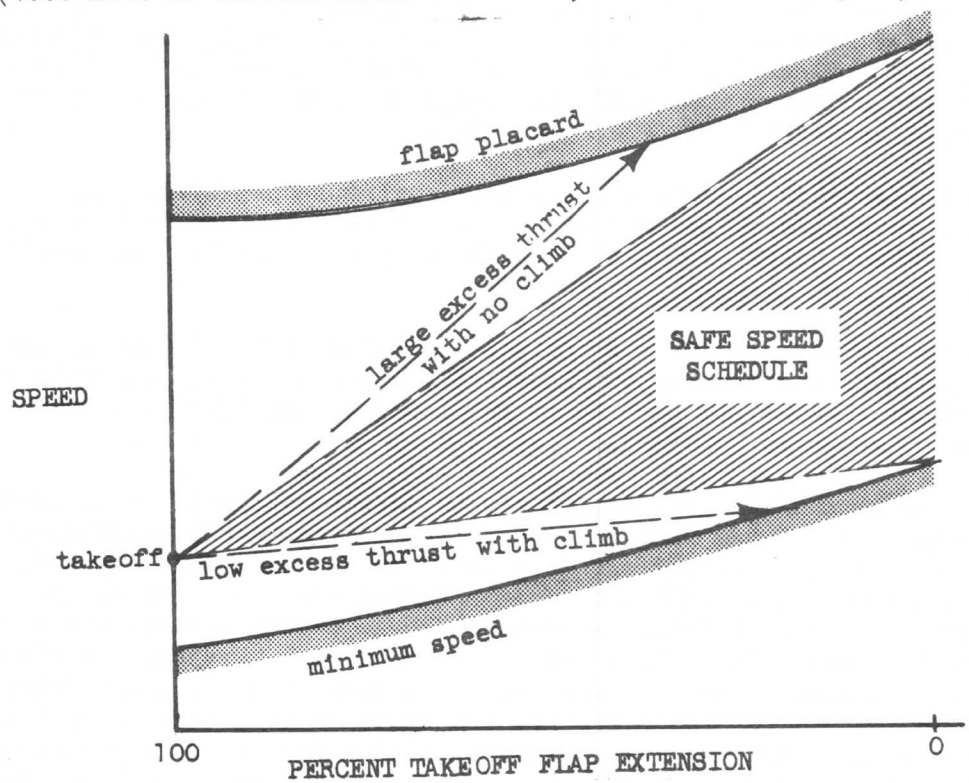

Figure 89.

Under SR-422B and FAR part 25, the net flight path must clear all obstacles in the takeoff segment by at least 35 feet, where the net flight path is defined as the gross path available reduced at each point by a gradient of climb equal to:

0.8 percent for two-engine airplanes;
0.9 percent for three-engine airplanes; and
1.0 percent for four-engine airplanes.

per FAR 25.115(b)

From calculations based on the solution to equation (112), the climb-out net flight path (vertical height versus horizontal distance) from the takeoff distance point (referred to as "reference zero") can be plotted as shown in Figure 90. This chart is used for checking obstacle clearance assuming failure of the most critical engine during takeoff. Note that the flight path starts at zero height. In order for the net flight path to clear any obstacle by the required 35 feet, the net flight path in Figure 90 has only to clear the obstacle. If the net flight path for a field-length limited weight does not clear the obstacle, the weight has to be reduced until the resulting flight path clears the obstacle. This reduction

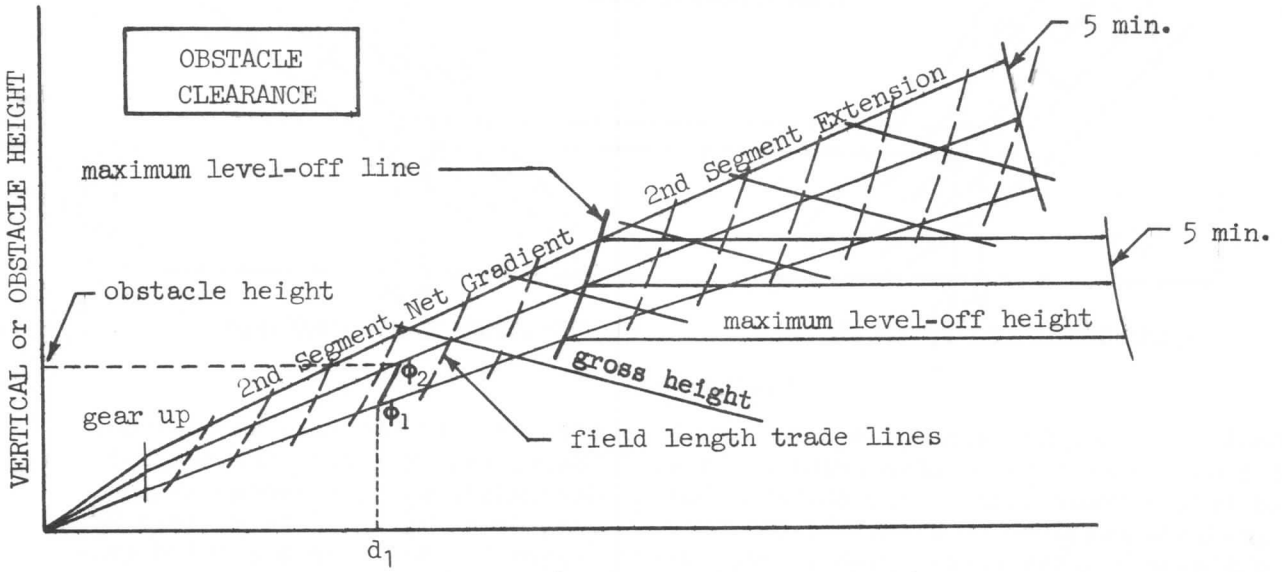

Figure 90.

in weight results in a reduction in takeoff distance which results in part of the flight path being over the runway, as shown in Figure 91. Taking advantage of this flight path over the runway keeps the weight reduction to a minimum.

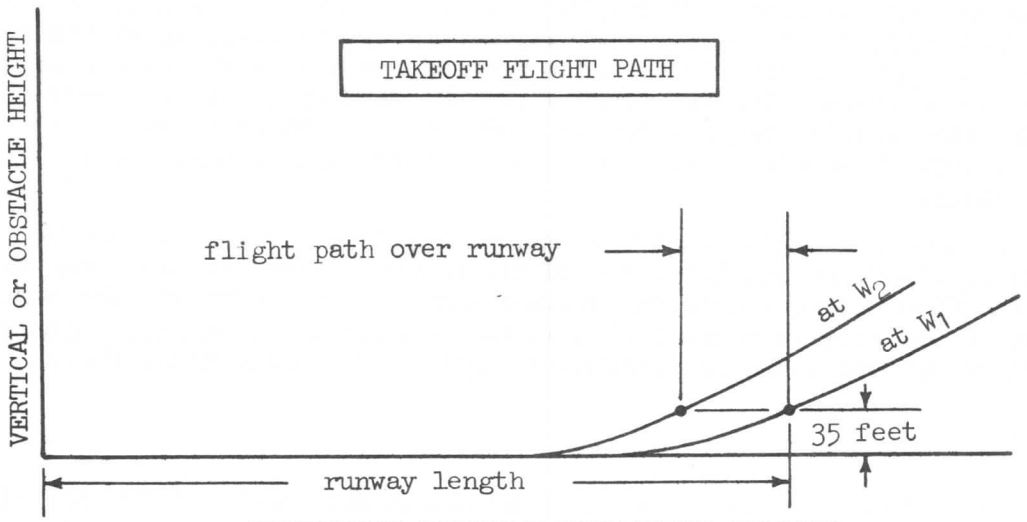

Figure 91.

By a iterative process one can with the help of Figure 92 (the second segment gradient chart) determine what the weight reduction would have to be. A much easier way of determining this reduction in weight is by adding some guide lines to Figure 90, known as "field length trade" lines, which eliminates the iterative method. For example, for a field length limiting weight, W_1, Figure 92 shows the second

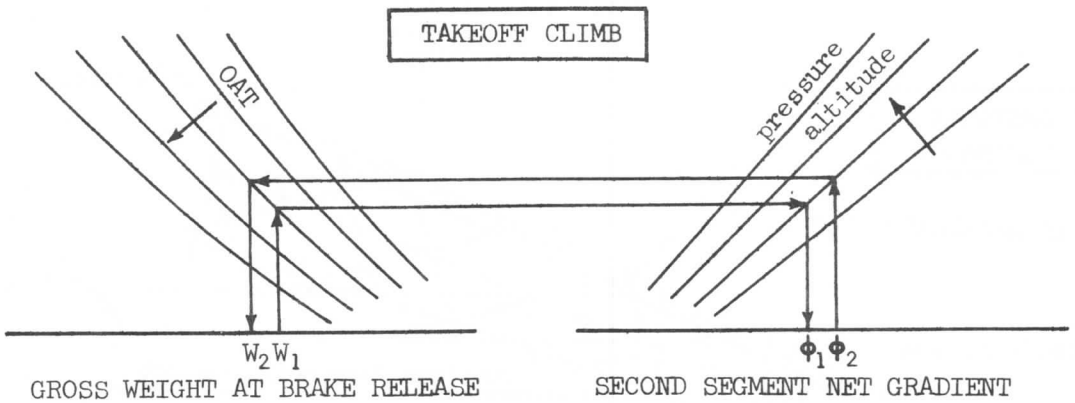

Figure 92.

segment net gradient equal to ϕ_1. Figure 90 shows that the obstacle at distance d_1 can not be cleared at this gradient of ϕ_1. Therefore, following the nearest field length trade line to the obstacle height determines ϕ_2, the second segment net gradient required to clear the obstacle; which, from Figure 92 determines W_2, the obstacle limited gross weight. When using Figure 90, the wind corrected gradient should be used.

When weight is reduced to achieve obstacle clearance, the horizontal distance between the obstacle and reference zero increases since takeoff distance required is less. The obstacle height also changes with respect to reference zero on a sloped runway, so a correction process is required to find the exact minimum profile and maximum weight for obstacle clearance.

Figure 90 also shows maximum level-off height values. At low climb gradients the airplane cannot take off, climb to 1500 feet and accelerate to flaps up within the 5 minute engine time limit at takeoff thrust. The maximum level-off heights shown in Figure 90 are the corresponding net heights for the maximum gross level-off heights where the acceleration segment can be scheduled at takeoff thrust. In addition, gross height lines are shown to assist in determining actual gross height at any instant.

If obstacles exist that are higher than the maximum level-off height and are beyond the maximum level-off height line, the second segment extension lines may be used, provided the final segment gradient exceeds a specified amount to take care of the acceleration and flap retraction at maximum continuous rather than takeoff thrust in the third segment since no performance data is scheduled under these conditions.

Climb Speeds

In practice, it is desirable to choose a climb speed schedule that a pilot can fly easily. Thus, the speed schedule will be established in terms of indicated airspeed, or indicated Mach number. From an examination of climb speed data as determined from the graphical means explained previously, it is found that the best rate of climb true airspeed varies with altitude, and is very close to a constant calibrated airspeed. This is nearly a constant indicated airspeed, since $V_C \cong V_I$. A comparison is made in Figure 93 of the best rate of climb speed and selection of a constant V_C.

Having established that the climb will be made at constant V_C up to the initial cruise Mach number, the rates of climb can be corrected for acceleration along

the flight path from equation (104) and Figure 96. A plot such as that of Figure 96 is based on flying constant calibrated airspeeds. At a given altitude, this will determine the acceleration factor, $1 + (V/g)(dV/dh)$, to be used in the equation. Actually, in a general case, the acceleration factor may be determined from a plot such as that in Figure 94 to get the velocity and slope, dh/dV, at any point. It should be noted here that dh/dV is the inverse of dV/dh as used in the acceleration factor.

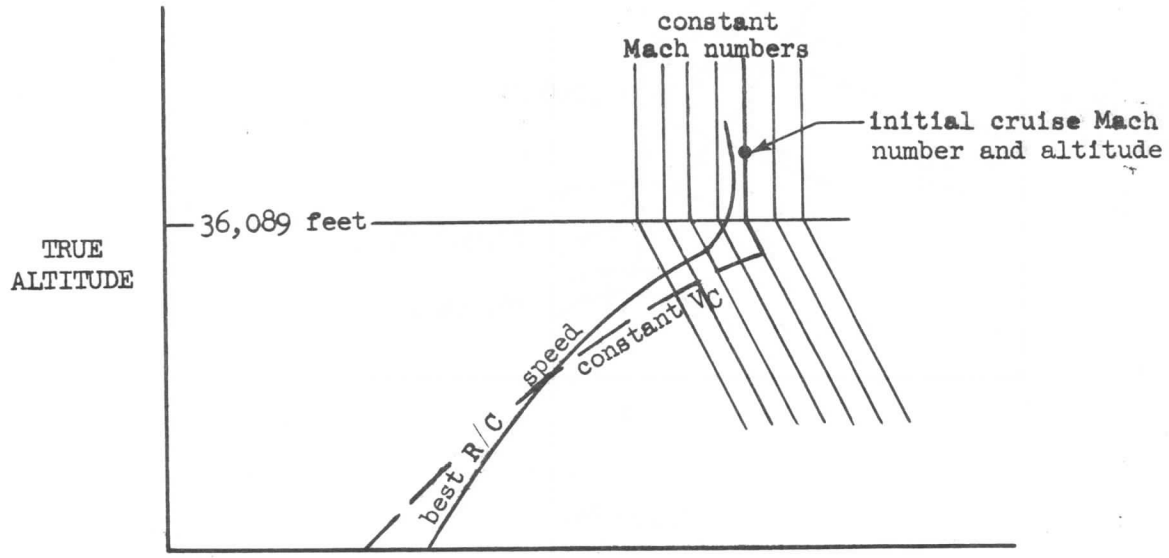

Figure 93.

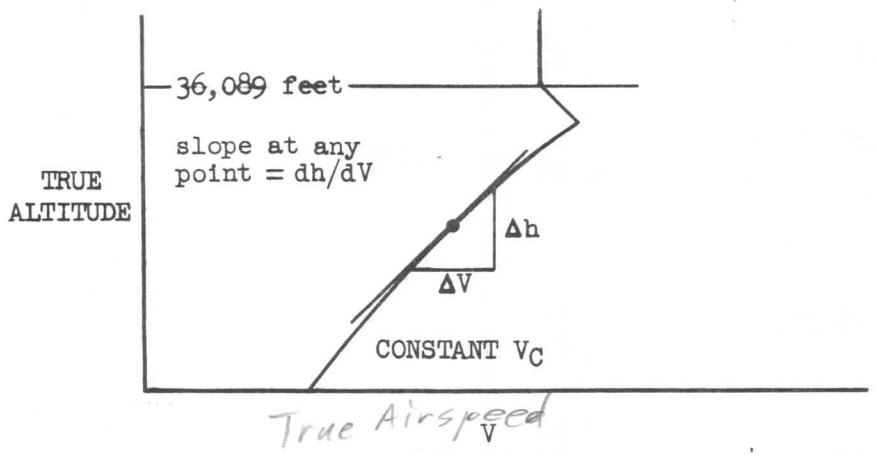

Figure 94.

When the uncorrected rate of climb values are corrected for acceleration, there may exist a shift in the velocity due to a shift in the peak of a rate of climb vs velocity relationship. This is shown in Figure 95. Because of the flatness of the curves, this speed change is not significant ordinarily, and the effect is not considered in the climb data shown for the 707 airplane.

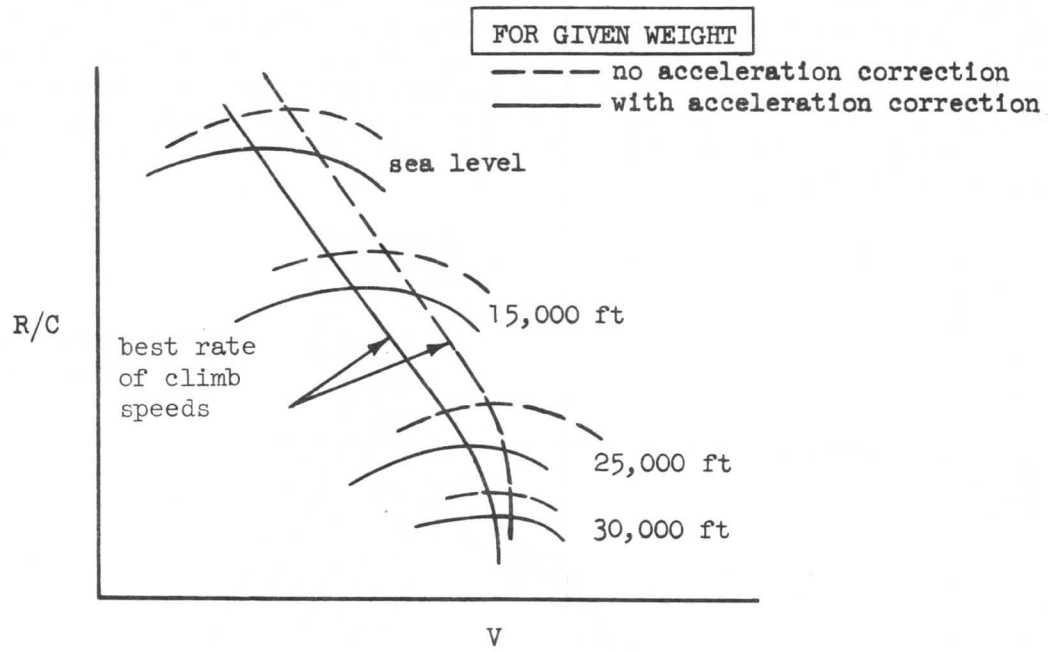

Figure 95.

At altitudes above 36,089 feet, it is found that most jet airplanes obtain maximum rate of climb at a constant true airspeed, thus constant Mach number. This means that no acceleration correction need by applied. The acceleration correction factor for other conditions is shown below:

(1) Constant M

Above 36,089 ft. $\frac{V\,dV}{g\,dh} = 0$

Below 36,089 ft. $\frac{V\,dV}{g\,dh} = -.133M^2$

(2) Constant V_E

Above 36,089 ft. $\frac{V\,dV}{g\,dh} = .7M^2$

Below 36,089 ft. $\frac{V\,dV}{g\,dh} = .567M^2$

It should be noted that the incremental altitude, dh, is a change in true altitude as shown by Figure 94 and not pressure altitude. Since the altimeter on any airplane reads pressure altitude, (pressure altitude is the same as true altitude on a standard day), this introduces an error. However, this effect is very small

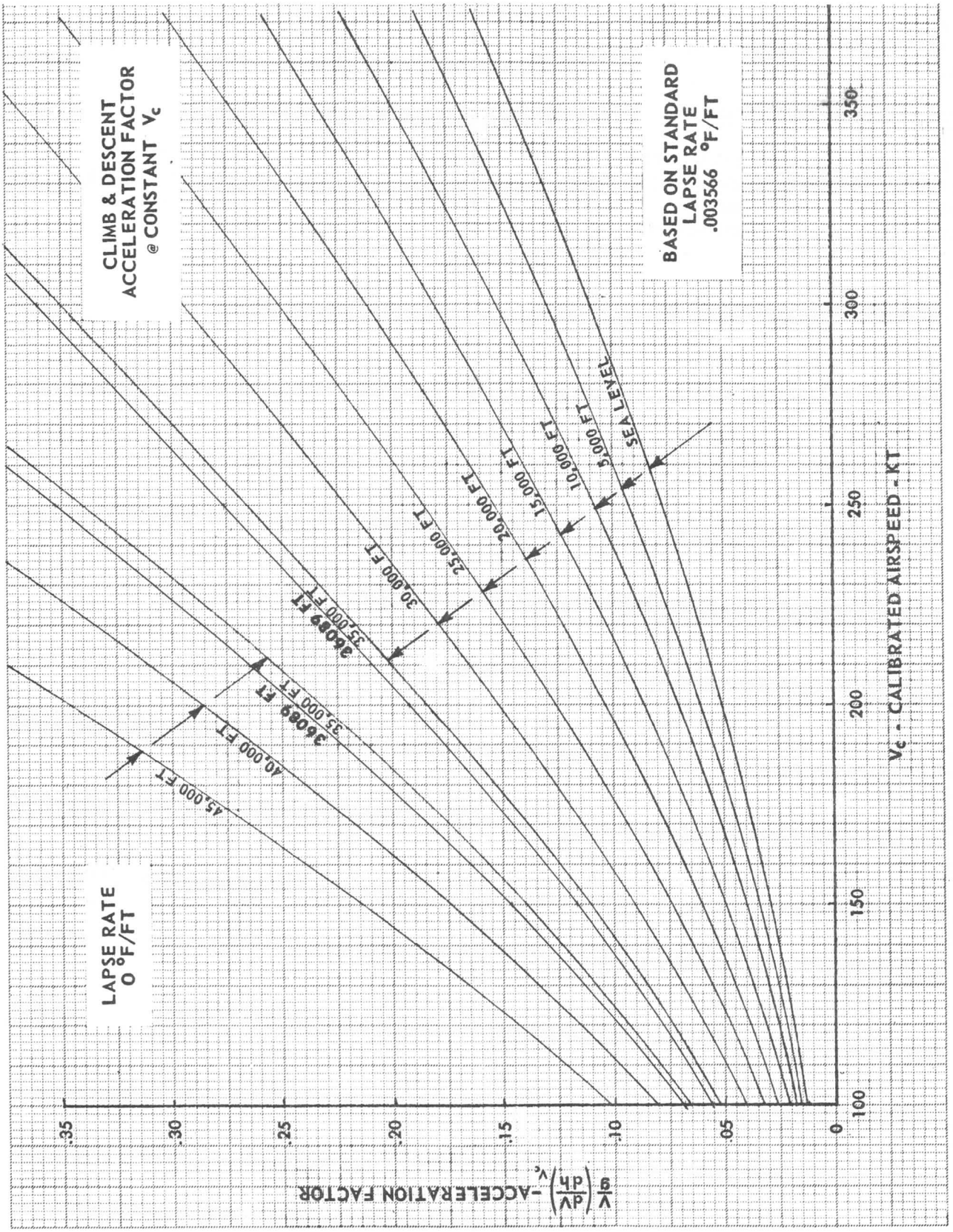
CLIMB & DESCENT
ACCELERATION FACTOR
@ CONSTANT V_c
BASED ON STANDARD
LAPSE RATE
.003566 °F/FT
LAPSE RATE
0 °F/FT
SEA LEVEL
5,000 FT
10,000 FT
15,000 FT
20,000 FT
25,000 FT
30,000 FT
35,000 FT
36089 FT
35,000 FT
40,000 FT
45,000 FT
V_c - CALIBRATED AIRSPEED - KT
$\frac{V}{g}\left(\frac{dV}{dh}\right)_{V_c}$ -ACCELERATION FACTOR

Figure 96.

and is usually ignored when obtaining the acceleration factor. It may be expedient under certain operating conditions to climb at other than best rate of climb speed.

Rate of Climb and Ceilings

From a series of calculations based on the solution to equation (104), the rates of climb and climb speeds for all weights and altitudes at a given engine rating can be plotted, see Figure 97. This figure shows the absolute ceilings for the weights considered, which are the points at which rate of climb is zero.

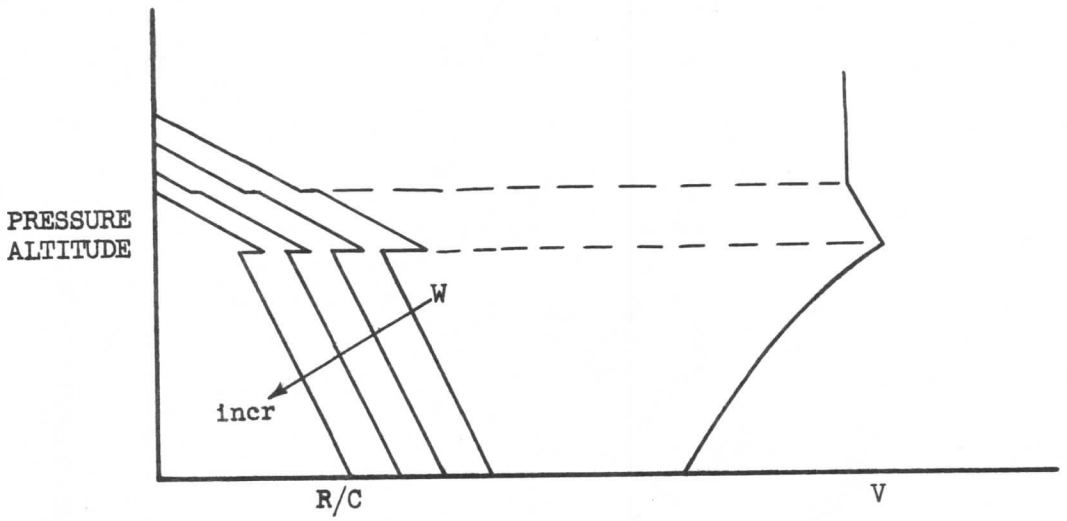

Figure 97.

Engine-inoperative climbs are calculated by the same methods as presented previously except that the T/δ available is reduced in proportion to the number of engines inoperative, and the T/δ required is increased to take into account the increased drag associated with the inoperative engine.

Climb Time, Fuel and Distance

After the rate of climb variation with pressure altitude has been established, the climb characteristics of time to climb, fuel consumed during climb, and climb distance may be derived. For non-standard days, the true altitudes must be determined from the selected pressure altitudes.

One of the methods to determine the time to climb is as follows:

$$r/c = \frac{dh}{dt}$$

where dh is the change in true altitude.

or,

$$dt = \frac{dh}{r/c}$$

Thus,

$$\int_{t_1}^{t_2} dt = \int_{h_1}^{h_2} \frac{dh}{r/c}$$

By integrating,

$$t_2 - t_1 = \Delta t = \frac{h_2 - h_1}{r/c_{avg}} \qquad (117)$$

where h_1 and h_2 are true altitudes and Δt is time to climb from altitude, h_1, to altitude, h_2, in minutes. Equation (117) is satisfactory throughout the entire altitude range, and especially at the lower altitudes. At the higher altitudes, where the ceiling is approached, the altitude increments chosen must be reduced for best results. As can be seen by equation (117), near the absolute ceiling, as the rate of climb decreases, the time to climb increases. Discriminate fairing of the rate of climb curves in this area provides satisfactory results.

For non-standard-day conditions, a correction has to be made. The correction to apply to obtain a true altitude increment due to non-standard-day temperatures is as follows:

$$\text{true altitude increment} = \text{Pressure altitude increment} \left(\frac{\text{absolute temp for non-std day}}{\text{absolute temp for std day}} \right)$$

or,

$$t_2 - t_1 = \Delta t = \frac{h_2 - h_1}{r/c_{avg}} \left(\frac{\text{absolute temp for non-std day}}{\text{absolute temp for std day}} \right) \qquad (118)$$

where, now h_1 and h_2 are pressure altitudes.

The normal method of obtaining time to climb is by integrating $1/(r/c)$ in a step by step process of small increments of altitude for each gross weight, allowing for changes in weight due to fuel consumption. A sample form, Figure 98, also shows how the incremental distance and fuel quantities are obtained.

PRESSURE ALTITUDES

h_{1_p} to h_{2_p}	h_{avg}	Δh_p	Δh_{true}	W_{avg}	r/c avg	Δt	$\Sigma \Delta t$
(1) Select	(2) Average	(3) $h_{2_p} - h_{1_p}$	(4)	(5) Assume	(6) Fig. 97	(7) (4) ÷ (6)	(8)

V_{avg}	Δs	$\Sigma \Delta s$	$W_{f_{avg}}$	ΔF	$\Sigma \Delta F$
(9) Fig. 97	(10) (9) x (7)	(11)	(12) From Engine Data	(13) (12) x (7)	(14)

Figure 98.

After the fuel quantity has been obtained, the assumed average weight for that step may be validated. Errors of up to 50 lb will not materially affect the time to climb. The size of Δh selected is a function of the rate of climb, as discussed before, and is usually in 5000 foot increments or less. When calculated, distance, fuel, and time are plotted as shown in Figure 99.

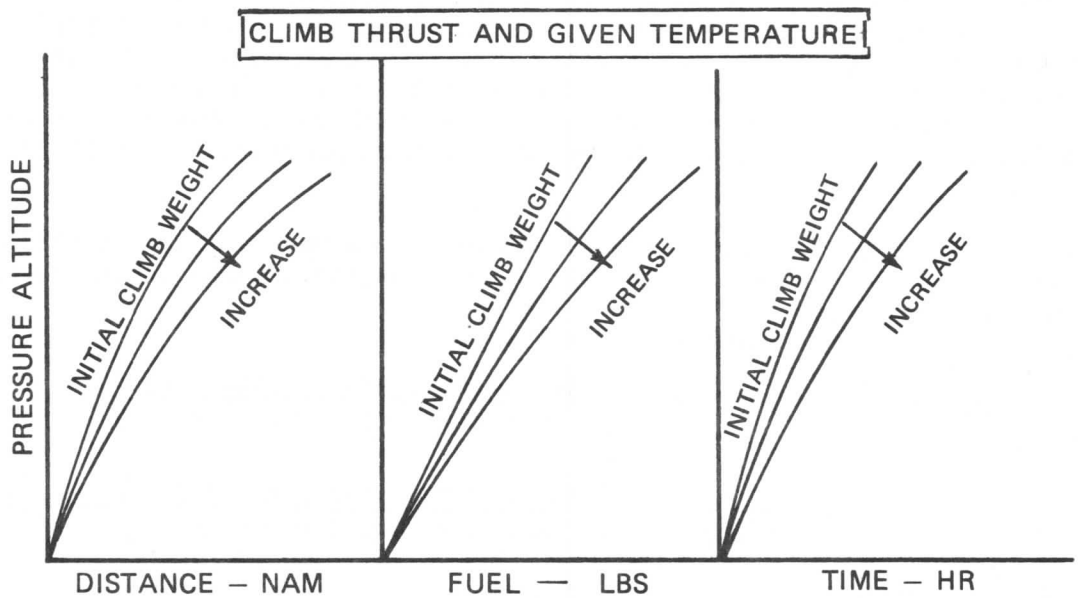

FIGURE 49

Figure 99.

Another form of presentation using the same data as in Figure 99 is shown in Figure 100. The figure plots time, fuel, and distance vs gross weight with altitude parameters. This type of chart is perhaps more useful to the flight crew. No particular technique need be used in constructing the plots, although as with Figure 99, the information is for particular temperature and thrust conditions. A change in temperature will vary the $\Delta T/\delta$ available for maximum rate of climb. See equation (104). Thus, the rate of climb is decreased for a hotter day and the time to climb, the range, and the fuel flow are increased. A colder day has the reverse effect.

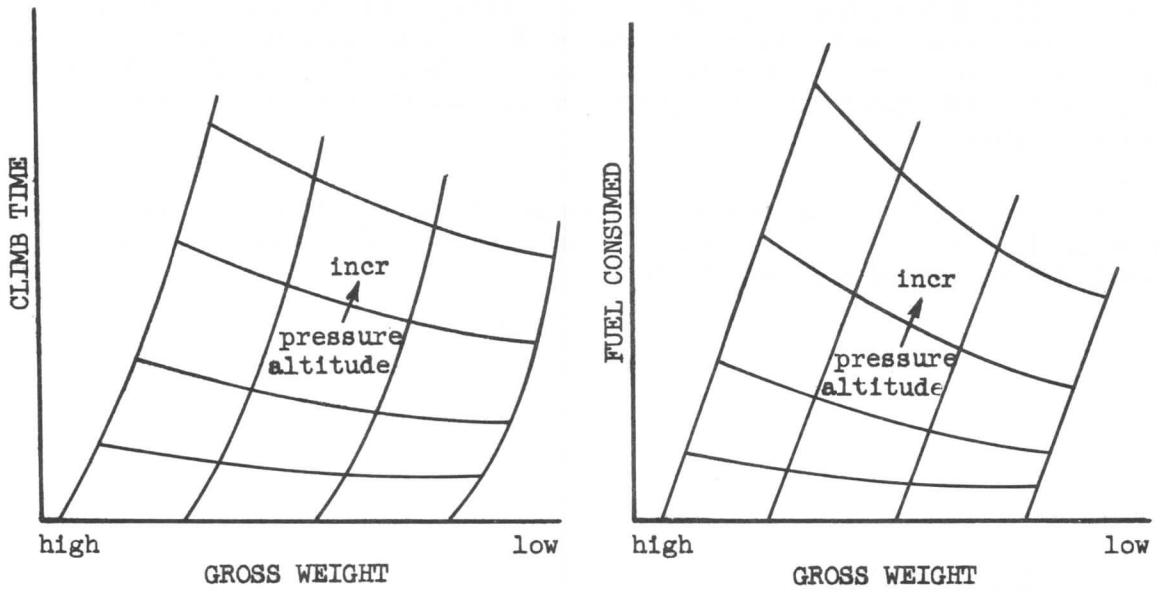
CLIMB TIME
incr
pressure altitude
high
low
GROSS WEIGHT
FUEL CONSUMED
incr
pressure altitude
high
low
GROSS WEIGHT

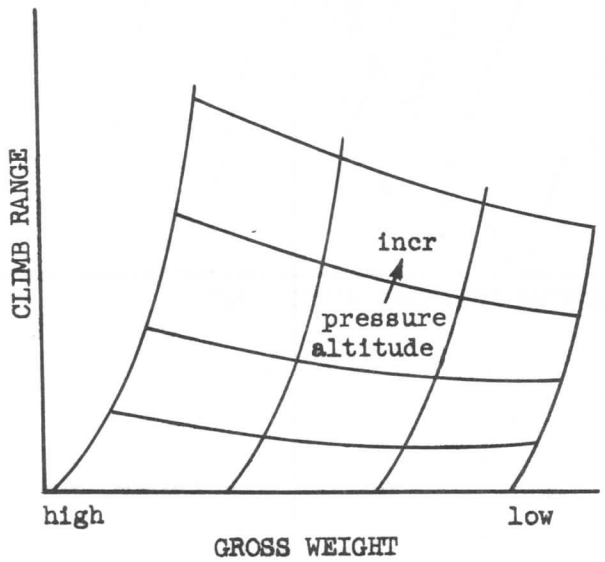
CLIMB RANGE
incr
pressure altitude
high
low
GROSS WEIGHT

Figure 100.

Thrust Presentation

Enroute climb thrust data in terms of EPR, or P_{t7}, is shown in Figures 101 and 102 Instead of plotting EPR versus temperature for constant values of altitude as was presented in takeoff performance, a plot of EPR versus altitude for constant values of temperature is made. The same is true for P_{t7}. Figures 101 and 102 are based on a fixed climb speed schedule (as shown in Figure 97) and at a given climb thrust rating.

Another chart that can be drawn is one independent of speed schedule. Such a chart is shown in Figure 103 This chart is very useful for obtaining a rated climb thrust for any speed and temperature.

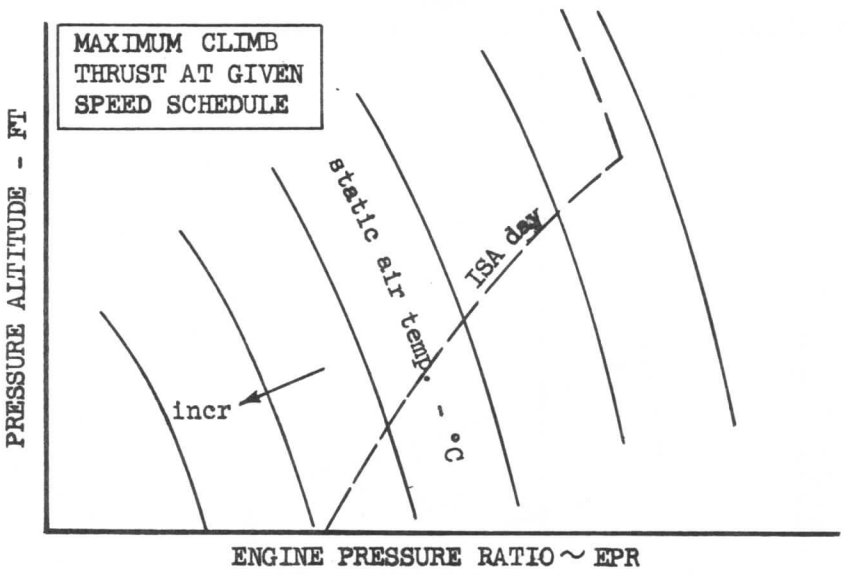

Figure 101.

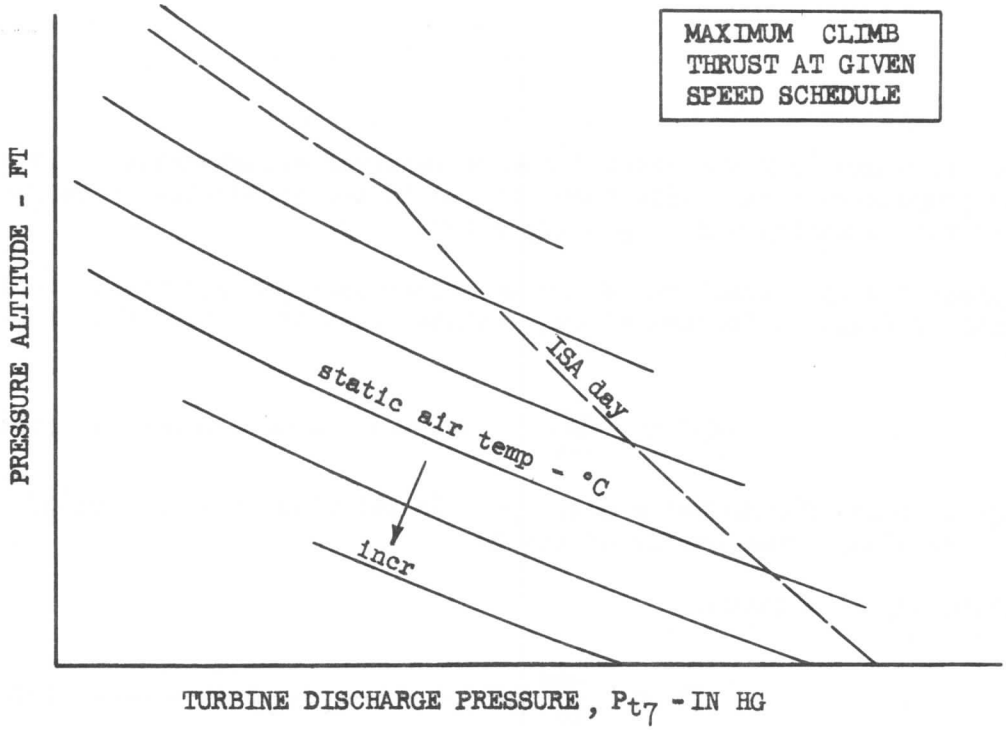

Figure 102.

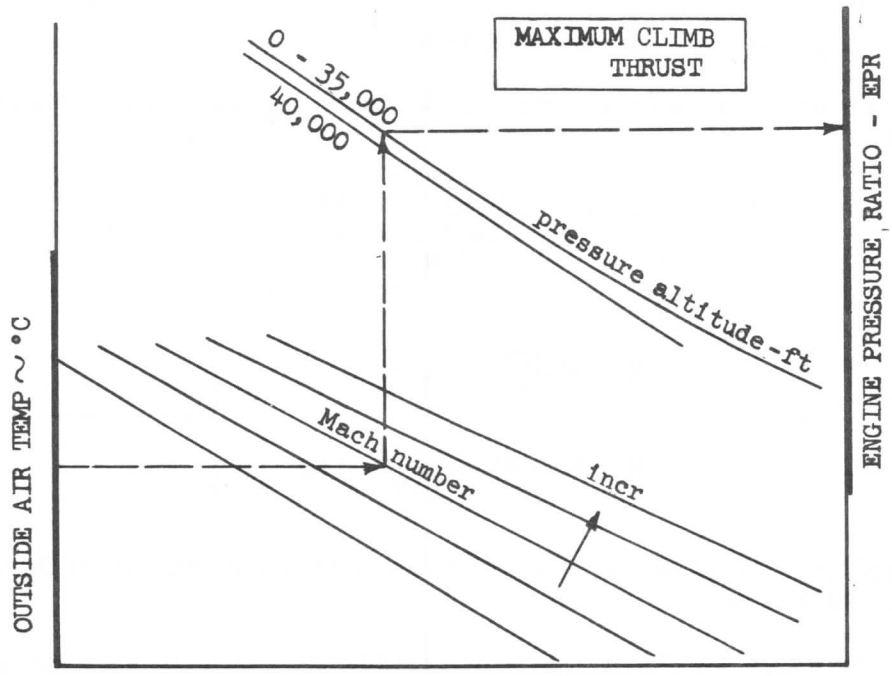

Figure 103.

3-7 RANGE

Range Equation

Basically, for an airplane to fly a given distance requires a conversion of its fuel energy into propulsive work. This then results in the production of range at the expense of fuel quantity and weight depletion.

Consider an airplane flying a small range increment, ΔR nautical air miles, while using up ΔW pounds of fuel. It's fuel mileage (miles flown per pound of fuel burned) will be:

$$\frac{\text{nam}}{\text{lb}} = -\frac{\Delta R}{\Delta W} \qquad (119)$$

The negative sign accounts for ΔW being negative. In calculus, when ΔR and ΔW approach zero in the limit, they become dR and dW.

Thus equation (119) may be written:

$$dR = -\frac{\text{nam}}{\text{lb}}\, dW \qquad (120)$$

Multiply the right hand side of equation (120) by W/W:

$$dR = -\left(W \frac{\text{nam}}{\text{lb}}\right) \frac{dW}{W} \qquad (121)$$

The factor W nam/lb is called the range factor.

Assuming for the moment that this factor can be made constant, the integration can be performed:

$$R = -W \frac{\text{nam}}{\text{lb}} \int_{W_1}^{W_2} \frac{dW}{W}$$

$$\left.\begin{aligned} R &= W \frac{\text{nam}}{\text{lb}} \ln \frac{W_1}{W_2} \\ R &= 2.30259\, W \frac{\text{nam}}{\text{lb}} \log \frac{W_1}{W_2} \end{aligned}\right\} \qquad (122)$$

The constant, 2.30259, accounts for the conversion from natural logarithms to logarithms to the base 10.

Another form of the range equation which is sometimes useful in preliminary design work, may be derived as follows: The term, nam/lb, which appears in equation (122), can be thought of as being composed of two terms, thus:

$$\frac{\text{nam}}{\text{lb}} = \frac{\text{nam}}{\text{hr}} \quad \frac{\text{hr}}{\text{lb}} \qquad \text{(123)}$$

$$\frac{\text{nam}}{\text{hr}} = \text{V (in knots)} \qquad \text{(124)}$$

and,

$$\frac{\text{hr}}{\text{lb}} = \frac{1}{\text{lb/hr}}$$

However, lb/hr will be recognized as the fuel consumption of the airplane and may be expressed as the thrust specific fuel consumption (lb fuel per hour per lb thrust) multiplied by the thrust being produced.

Thus,

$$\text{TSFC} = \frac{\text{lb/hr}}{\text{T}}$$

or,

$$\frac{\text{lb}}{\text{hr}} = \text{T(TSFC)}$$

Thus,

$$\frac{\text{hr}}{\text{lb}} = \frac{1}{\text{T (TSFC)}} \qquad \text{(125)}$$

Substituting equation (124) and (125) into equation (123):

$$\frac{\text{nam}}{\text{lb}} = \frac{\text{V}}{\text{T(TSFC)}} \qquad \text{(126)}$$

To put equation (126) into more familiar terms, it must be recognized that in level flight the engine thrust is exactly equal to the total airplane drag; therefore, the thrust term, T, in equation (126), may be replaced by the drag term, D. Also, if the numerator is multiplied by L, the airplane lift, and the denominator by W, the airplane weight, then the equality will be unchanged since the lift and weight are equal in level flight. Thus, equation (126) becomes:

$$\frac{\text{nam}}{\text{lb}} = \frac{\text{V}}{\text{(TSFC)}} \quad \frac{\text{L}}{\text{D}} \quad \frac{1}{\text{W}}$$

However, $V = a_o\sqrt{\theta}\,M$, from previous considerations. Thus,

$$\frac{\text{nam}}{\text{lb}} = \frac{a_o\sqrt{\theta}}{\text{(TSFC)}} \quad \text{M} \quad \frac{\text{L}}{\text{D}} \quad \frac{1}{\text{W}} \qquad \text{(127)}$$

Substituting equation (127) into equation (120):

$$dR = -\frac{a_o\sqrt{\theta}}{\text{(TSFC)}}\,\text{M}\,\frac{\text{L}}{\text{D}}\,\frac{dW}{W}$$

or,

$$R = -\frac{a_o\sqrt{\theta}}{(TSFC)} \; M \; \frac{L}{D}\int_{W_1}^{W_2} \frac{dW}{W}$$

Assuming that all quantities outside of the integral sign can be made constant,

$$R = \left(\frac{a_o\sqrt{\theta}}{(TSFC)}\right)\left(M\frac{L}{D}\right) \ln \frac{W_1}{W_2} \qquad (128)$$

This equation states that if the thrust specific fuel consumption, TSFC is considered to be nearly constant (which it usually is in the cruising region), a jet airplane will get the most range between any two weights, W_1 and W_2, by flying such as to make the quantity M L/D a maximum. This compares with the reciprocating engine airplane which must maximize the quantity $(\eta/C)(L/D)$.

In order to see how the maximum M L/D may be determined, consider Figure 104. This shows a C_L, C_D "polar" on which have been drawn tangent lines to each Mach number curve. These lines thus define the maximum L/D for each Mach number, and if L/D is a maximum, then M(L/D) must be a maximum for that Mach number. By plotting M(L/D) vs Mach number (Figure 104) the Mach number for maximum M(L/D) can be found. Now, since it is desirable to make M(L/D) a maximum, it will be seen that whereas L/D is a maximum on the "low-speed" polar, M(L/D) is not necessarily a maximum. This means that the maximum M(L/D) will occur at a slightly higher Mach number than that associated with the highest possible on the low-speed polar. In other words, maximum M(L/D) corresponds to cruising into the region where compressibility phenomena are becoming important; that is, the airplane actually is cruising into the drag rise.

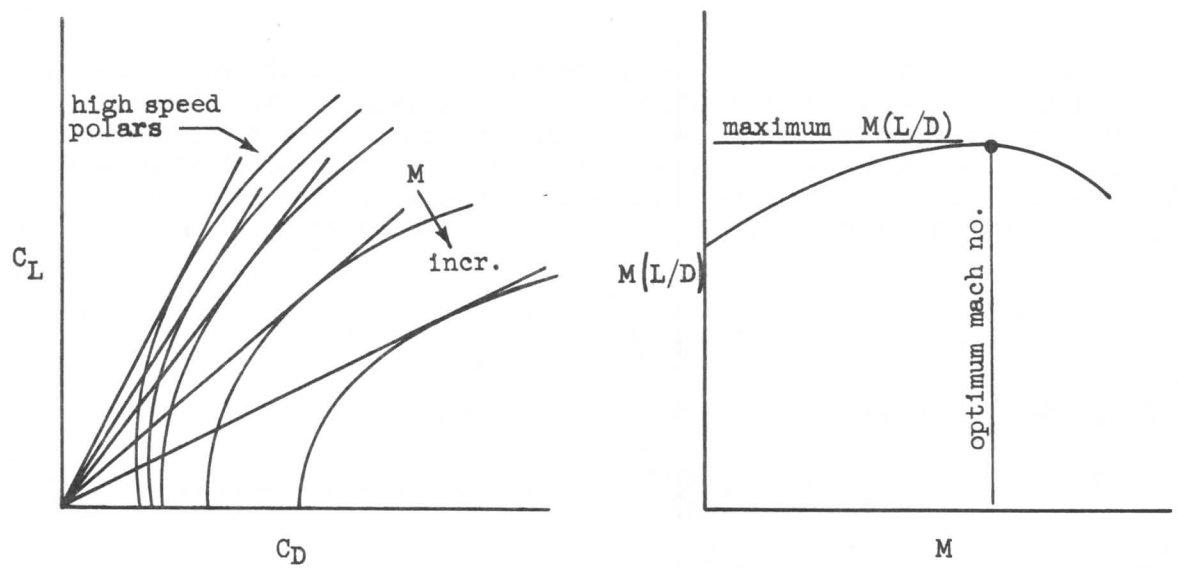

Figure 104.

This method of analysis is employed in preliminary work as a guide to establishing wing loading and thrust required for cruise. In the actual determination of

nautical miles per pound for a specific airplane, a different method is employed, with the above procedure used as a check to determine how close the design is to the optimum.

Turbojet Range Factor

It has been shown in the early part of this section how the engine fuel flow and thrust data may be referenced to standard sea-level condition. (This is known as "referring" or "generalizing" the data.) A plot of such generalized data, as given in Figure 105, is useful for preliminary design study and for range estimation. For a given W/δ , the Mach number determining maximum range will be found at the point where the D/δ and namδ/lb curves are tangent. A curve joining these tangent points represents the Mach number variation with weight for maximum range operation. By calculating range factor at each intersection and plotting as in Figure 106, one may determine the optimum W/δ for maximum range. And by drawing contour curves of constant range factor, $\frac{W}{\delta}$ namδ/lb, it is possible to show the relative change in range when operating at other than optimum range conditions.

It is important to remember that, as pointed out earlier, the engine data does not completely generalize to single curves of T/δ available and referred fuel flow. Thrust limits must be plotted for various altitudes even on the generalized speed-thrust plot as shown on Figure 105. The loss of range suffered by operation at a thrust limit below that thrust necessary for maximum range can be seen.

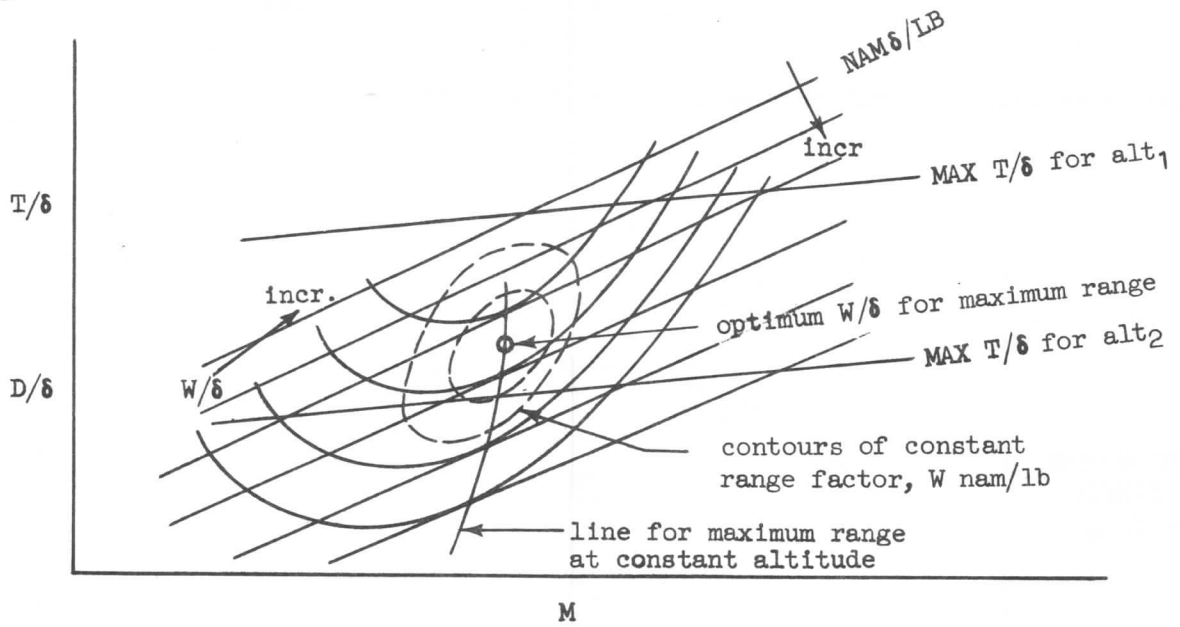

Figure 105.

Types of Cruise

As for takeoff and climb, the computation of nam/lb (range) is accomplished using IBM computers. The input data consists of the drag polar, engine data and the required altitudes, weights and Mach numbers. The final data are plotted as in

$W_f = \frac{lb}{hr}$

Figure 107 for constant altitudes in convenient increments. Both lines of maximum range and 99% maximum range, identified as "long range cruise," are presented as well as the maximum cruise thrust line. The effect of increasing temperature on the maximum thrust available is also shown. Constant Mach cruise lines may also be presented. The line identified as holding speed corresponds to almost minimum fuel flow. However, common practice restricts the holding speed from being any lower than the speed for minimum drag even though fuel flow is not quite minimum. For various reasons, it may be necessary, or even desirable, to hold at speeds and altitudes other than the values given in the manuals. The above types of cruise may be summarized in this way:

	Types of Cruise	Cruise Condition for Weight Decrease	Range Factor
1.	Constant M and W/δ;	increasing altitude	constant
2.	Constant altitude; (for maximum range or long range cruise)	decreasing M and decreasing thrust	varying
3.	Constant M and Altitude;	decreasing thrust	varying
4.	Rated thrust;	a. increasing altitude at constant M	varying
		b. increasing M at constant altitude	varying

These conditions may be confirmed by studying Figure 105.

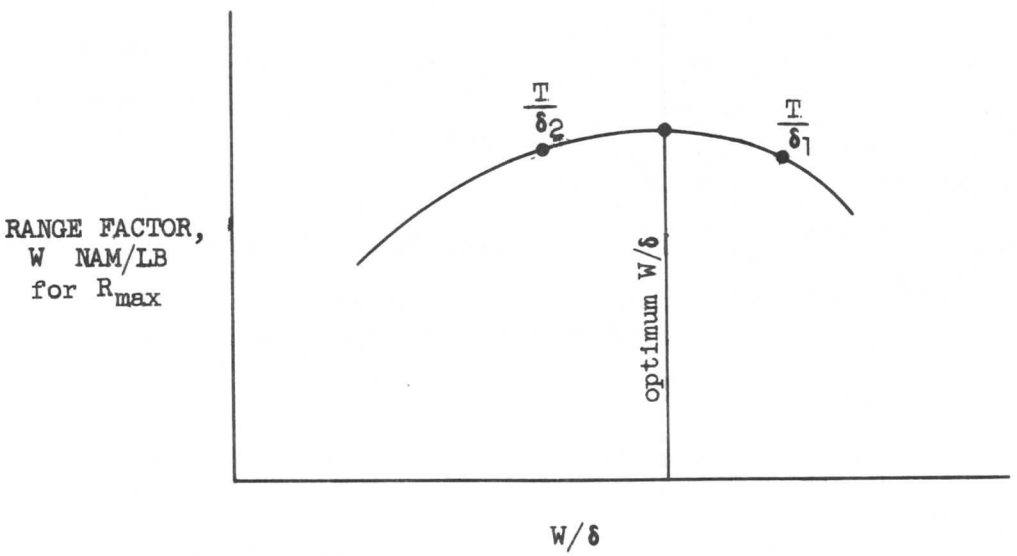

Figure 106.

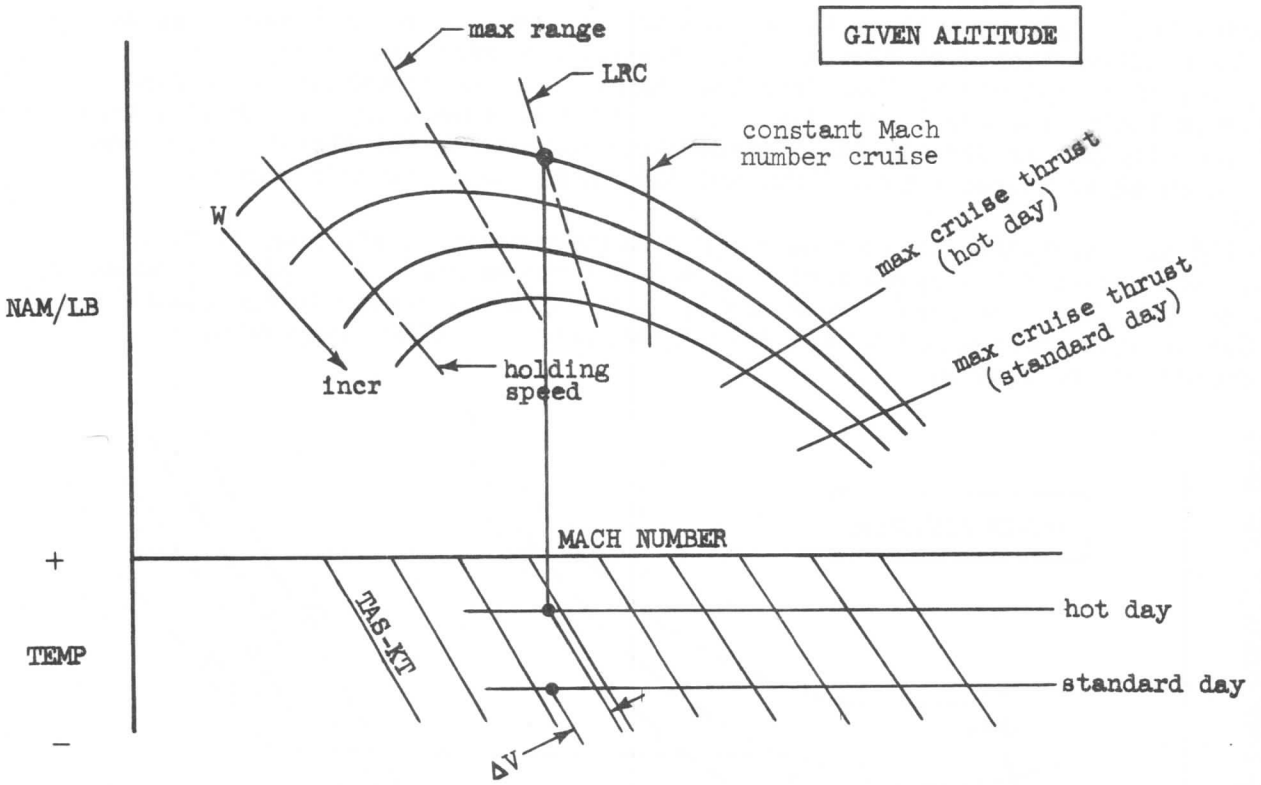

Figure 107.

To obtain the data necessary to plot curves like those shown in Figure 107, a procedure may be followed such as that outlined in Figure 108. For a given altitude, a table may be set up to facilitate the calculations.

GIVEN ALTITUDE

M	W	W/δ	D/δ	$\frac{F_N}{\delta}$	$(TSFC/\sqrt{\theta})^*$	W_f*	NAM/LB
(1)	(2)	(3)	(4)		(5)	(6)	(7)
Select	Select	Calculate	Speed-Thrust Data	$\frac{(4)}{\text{no. of eng.}}$	Engine Data	$(5) \times \frac{T}{\delta} \times \sqrt{\theta} \times \delta \times$ no. of eng.	$\frac{661.5\,M\sqrt{\theta}}{(6)}$

*Includes bleed correction

Repeat (3) - (7) for as many other weights as desired at given altitude.
Repeat complete procedure for other altitudes.

Figure 108.

Concerning the bleed corrections in calculating cruise data as in Figure 108, it should be recalled that fuel flow must be increased to maintain speed, i.e., thrust, any time that air is bled from the engine. If the operation is at less than thrust limit, the additional fuel may be added by advancing the thrust lever; but if the airplane is already in limited-thrust operation, the thrust lever cannot be advanced to increase fuel flow, and the speed cannot be maintained.

Figure 108 also provides the information for another useful plot, that of fuel flow vs Mach number for a given altitude, and for one engine. This plot is shown in Figure 109. Both the nam/lb vs M and W_f vs M plots may appear in the Operations Manual with the maximum cruise thrust ratings for various temperatures superimposed on the charts.

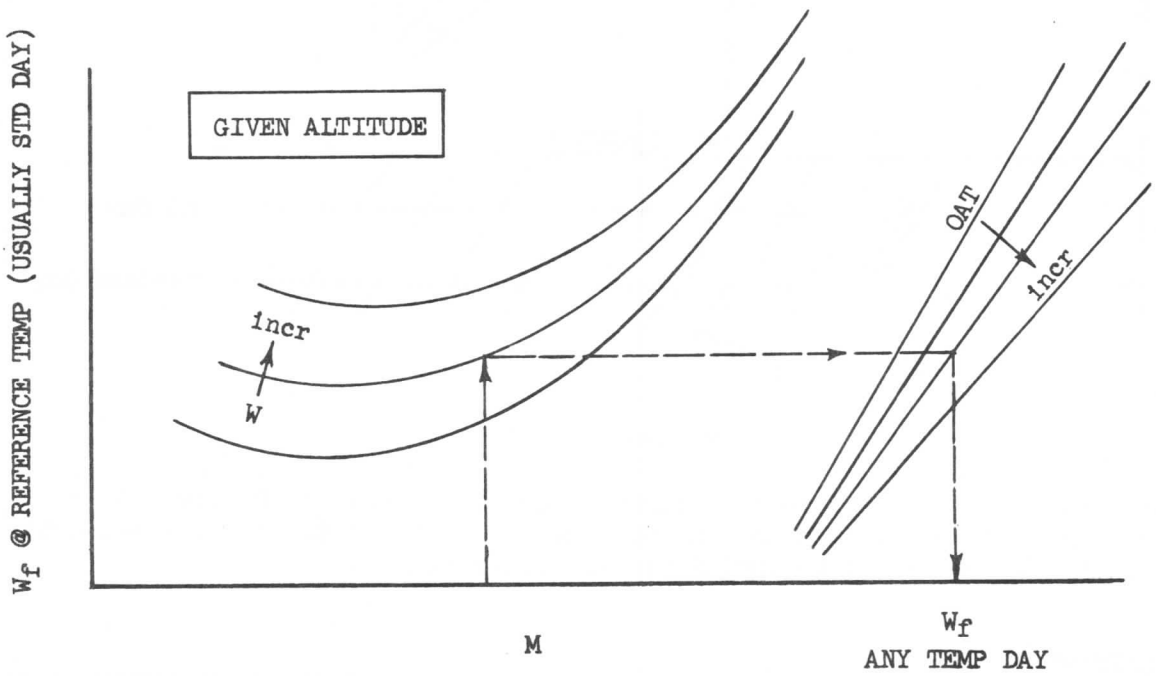

Figure 109.

These data may also be cross-plotted as a function of altitude, for specific cruise conditions. See Figure 110. Maximum cruise thrust ratings for various temperatures may be shown on the cross-plots also.

The effect of increasing altitude, generally, is to increase nam/lb. However, at heavy weights, the thrust requirements are such that a lower value of nam/lb is obtained at the higher altitudes. In other words, there exists for each weight an optimum altitude; increasing with decreasing weight. In order to fly at maximum range, an airplane must operate continuously at the optimum altitude. The 707 airplane shows improvement in fuel mileage at altitudes up to 42,000 feet. Above 35,000 feet, the Reynolds number effects on the engine contribute to a deterioration of the performance. Bleed requirements for pressurization also increase above 35,000 feet. The approved altitude limitation is 42,000 feet. The altitude associated with each weight condition may be determined by plotting range factor vs weight for several altitudes on a composite plot as in Figure 111. This type of plot is used to establish the maximum range or the long range cruise altitude schedule.

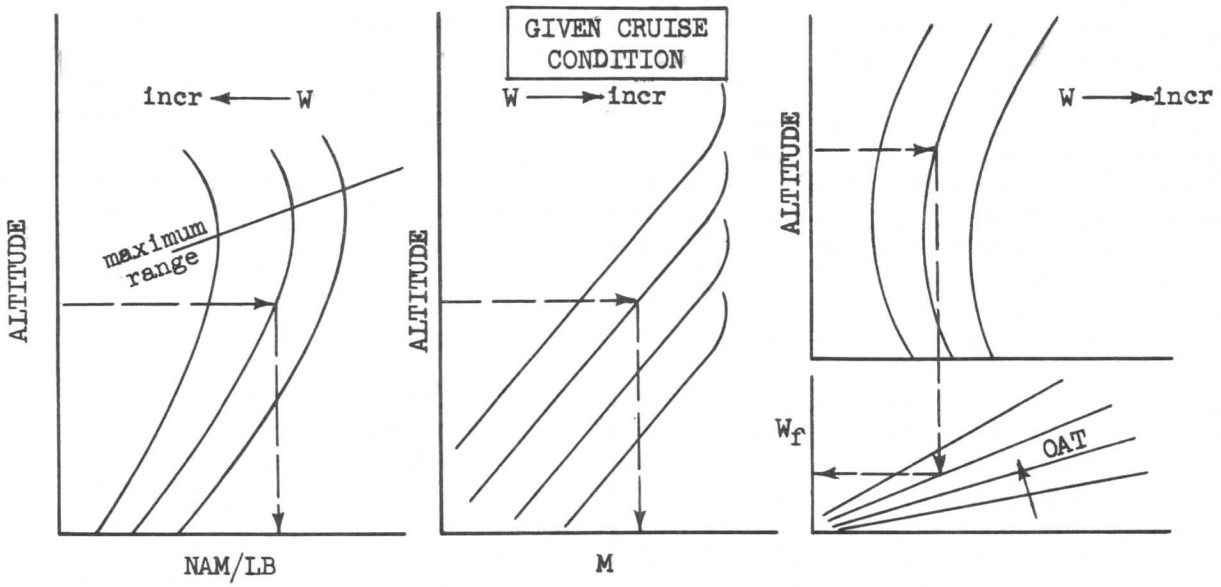

Figure 110.

It should be noted that the range factor is almost constant for maximum range or long range cruise in a climbing cruise operation. This fact justifies the simplified integration procedure in the early part of this chapter; however, for other types of cruise, the simplification may not be valid.

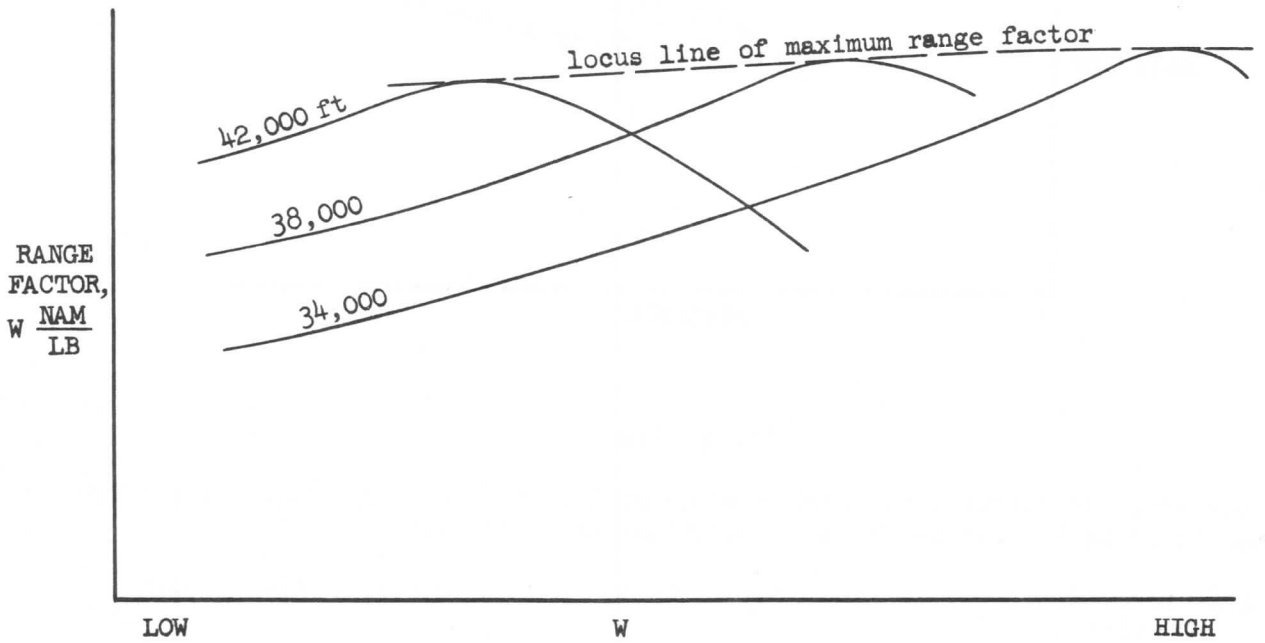

Figure 111.

AIRPLANE PERFORMANCE

All the calculations so far have assumed level flight conditions. The discussion concerning maximum range, and Figure 106, has shown that a constant W/δ should be maintained. Altitude must be increased so that δ is decreased at the same rate as the weight is decreased through fuel consumption. This will thus maintain a constant W/δ, but will require a finite rate of climb, which in turn will require a slightly higher thrust than that used in level flight. This may seem to be confusing since it may be argued that no excess thrust is needed for climb. The reasoning is that the engines are instantaneously adjusted to give the required T/δ to fly level at the given W/δ and M. Then, as fuel is consumed, the W/δ tends to decrease so that the T/δ required decreases. There is thus an excess thrust which tends to climb the airplane back to the proper W/δ where the engine T/δ available equals the T/δ required. This reasoning is in error primarily because it will take some finite time for a sufficient difference to exist between T/δ required and T/δ available.

Consider Figure 112. At any point A, the airplane is trimmed in level flight for optimum cruise conditions. It will not climb at the proper constant rate as shown in the figure until there exists a change in the W/δ such that the excess T/δ is properly related to the rate of fuel consumption to maintain a constant W/δ . There will thus exist a condition where the actual W/δ flown will be continually in error. To correct this situation, the thrust must be increased slightly at any given W/δ and Mach number so that a constant range factor can be maintained. For the 707 the reduction in W nam/lb due to the climb has been found from experience to be about 1% compared to level flight at the same W/δ and Mach number.

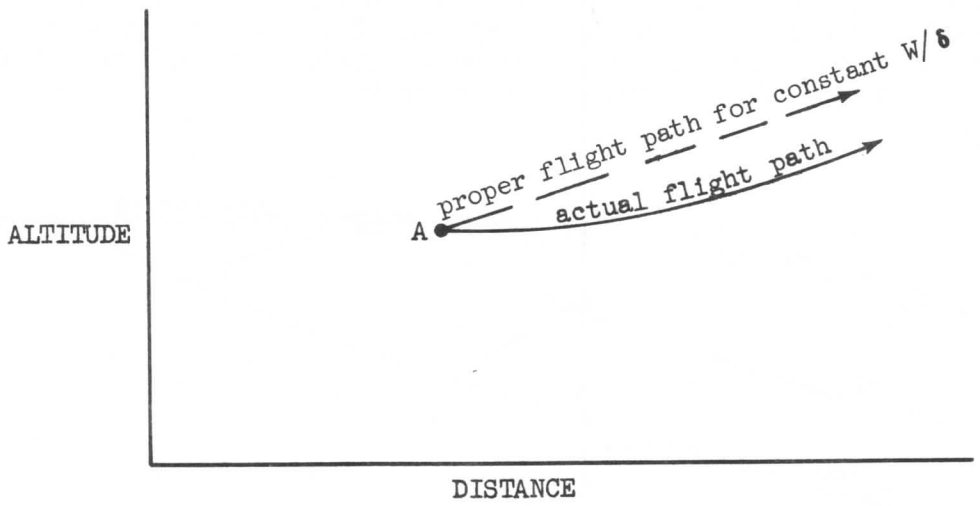

Figure 112.

In summary, the corrections which must be applied to the range factor for 100% range in order to account for all conditions discussed are:

(1) Reduction of 1% to allow for cruising at a higher speed (long range cruise).

*(2) Reduction due to accessory power and bleed requirements.

(3) Reduction of 1% due to climbing the airplane at a constant W/δ to the thrust limit, or a reduction in W/δ at the thrust limit.

*(4) Reduction due to thrust reverser-sound suppressor installation losses.

(*These items may be accounted for in the basic power plant data.)

Figure 113 shows the approximate reduction in fuel mileage for the constant W/δ cruise. A point which should be mentioned at this time is that when cruising at a given maximum rating and a constant W/δ and Mach number, it is not possible to increase the thrust to get an excess. For this condition, the T/δ is constant at a given Mach number and W/δ must be varied in order to vary D/δ.

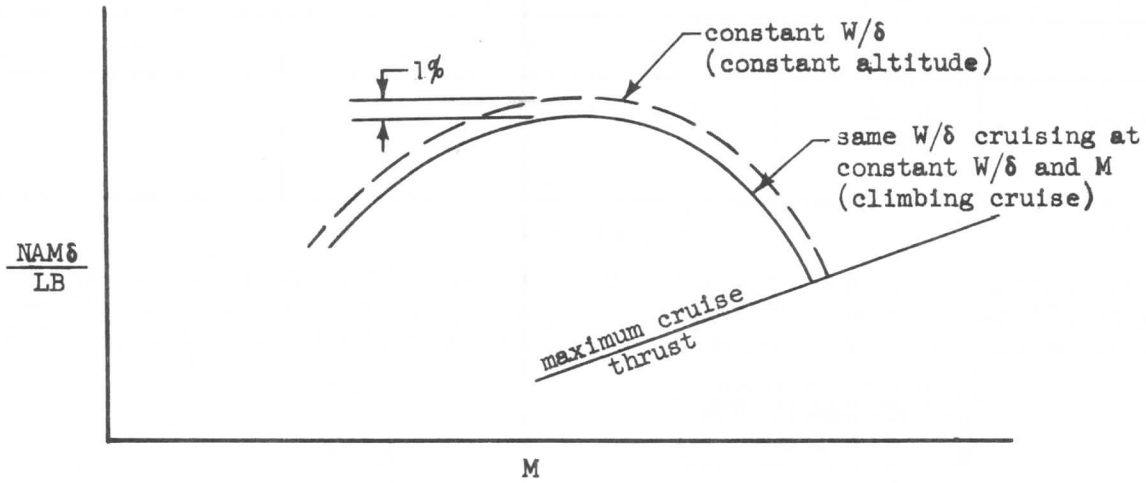

Figure 113.

Range Presentation

After the nam/lb has been established for the particular cruise condition desired, such as long range cruise at a constant altitude, the corresponding range for changes in weight can be determined.

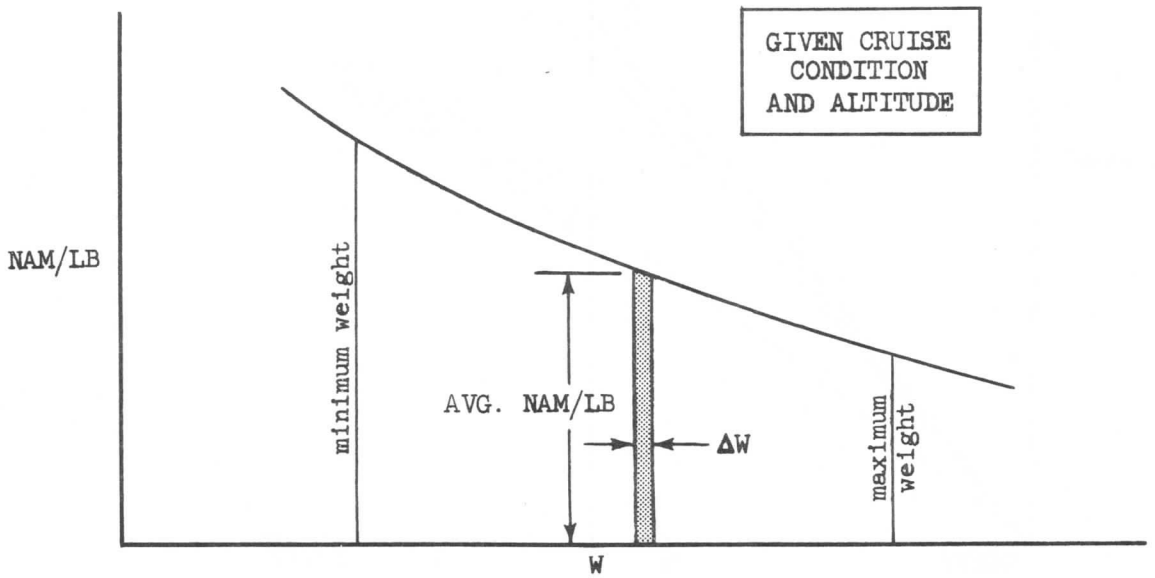

Figure 114.

In Figure 114 the shaded element represents an incremental range for a change in weight, ΔW. Integrating the area under the curve between the minimum and maximum weight limits gives the total range for the given condition. The integration may be done graphically by assuming small increments of weight, (about 10,000 lb for the 707), and assuming a constant average value of nam/lb for each of the increments; thus obtaining an incremental range. By adding up the areas, the total range between any two weights can be determined.

$$\Delta R = \left(\frac{nam}{lb}\right)_{avg} \Delta W \qquad (129)$$

and,

$$R = \Sigma \Delta R \qquad (130)$$

$\Delta W = W_1 - W_2$	W_{avg}	nam/lb_{avg}	ΔR	$\Sigma \Delta R$
(1)	(2)	(3)	(4)	(5)
Select	$\frac{W_1 + W_2}{2}$	Fig. 114	(1) x (3)	

Figure 115.

With the preceding two equations and Figure 114, a table similar to that shown in Figure 115 may be made. When data has been accumulated for all the desired cruise conditions, a plot of range vs weight can be made as shown in Figure 112.

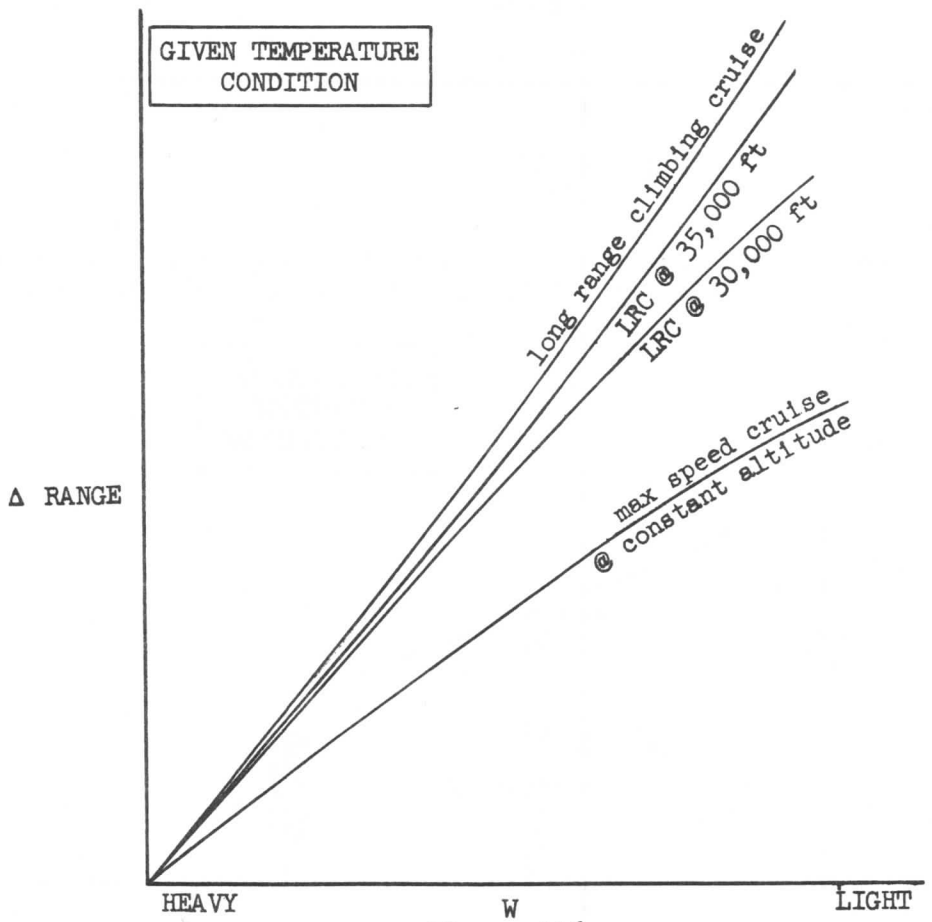

Figure 116.

Temperature Effects

The effect of air temperature on range under all conditions, except when operating at a rating, is negligible. Consider the case of operating under maximum long range conditions and assume that suddenly the temperature increases. Because of this temperature rise, the thrust, and thus T/δ, will decrease. However, to still maintain optimum conditions; that is, to hold the original W/δ and Mach number, the thrust (and T/δ) must be returned to its original value. This means that the thrust levers must be advanced. This advancement of the thrust levers will increase the engine RPM and will increase the specific fuel consumption because it requires additional work (and thus fuel) to turn the engine at a higher RPM. This effect can be seen in Figure 117, which shows the specific fuel consumption, TSFC, plotted against RPM for a typical jet engine.

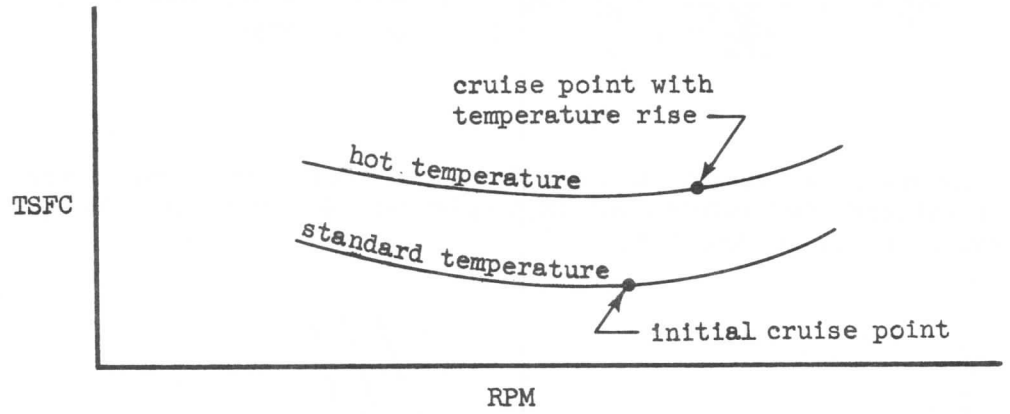

Figure 117.

This would seem to indicate that the fuel mileage of the airplane has deteriorated, until it is remembered that by maintaining a given Mach number under the increased temperature conditions the true airspeed has increased. The increase is due to the higher local speed of sound. The higher airspeed tends to counteract the increased fuel flow caused by the higher engine RPM. A more rigorous analysis shows that the effects exactly compensate except for secondary effects such as air conditioning bleed requirements varying with temperature which are usually ignored.

It will be remembered from equation (41) that:

$$W_f = \frac{V}{nam/lb}$$

but,

$$V = Ma_o\sqrt{\theta}$$

Therefore,

$$W_f = \frac{Ma_o\sqrt{\theta}}{nam/lb} \qquad (131)$$

Also,

$$W_f/eng. = \frac{TSFC}{\sqrt{\theta}} \times \frac{Fn}{\delta} \times \delta \times \sqrt{\theta} \qquad (132)$$

Therefore,

$$nam/lb = \frac{Ma_o\sqrt{\theta}}{\frac{TSFC}{\sqrt{\theta}} \times \frac{Fn}{\delta} \times \delta \times \sqrt{\theta} \times \text{no. of eng.}}$$

or,

$$nam/lb = \frac{Ma_o}{\frac{TSFC}{\sqrt{\theta}} \times \frac{Fn}{\delta} \times \delta \times \text{no. of eng.}} \qquad (133)$$

At a given Mach number, gross weight, and altitude, the thrust required (drag) of an airplane is constant and independent of temperature as previously shown in Figure 10 (redrawn here for convenience).

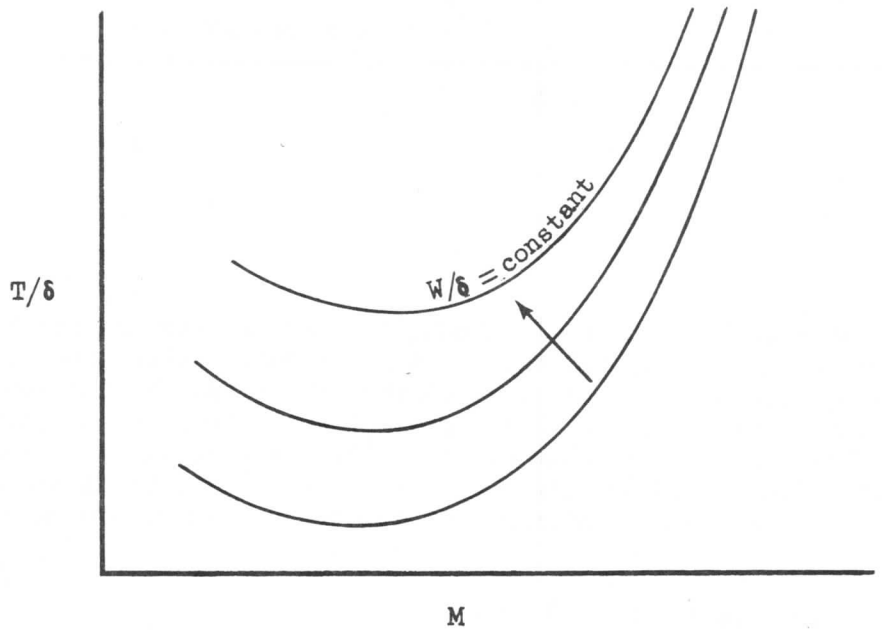

Figure 10.

Specific fuel consumption data is normally presented as previously shown in Figure 19 (redrawn here for convenience) with bleed requirements, power extraction and accessory drag allowances included.

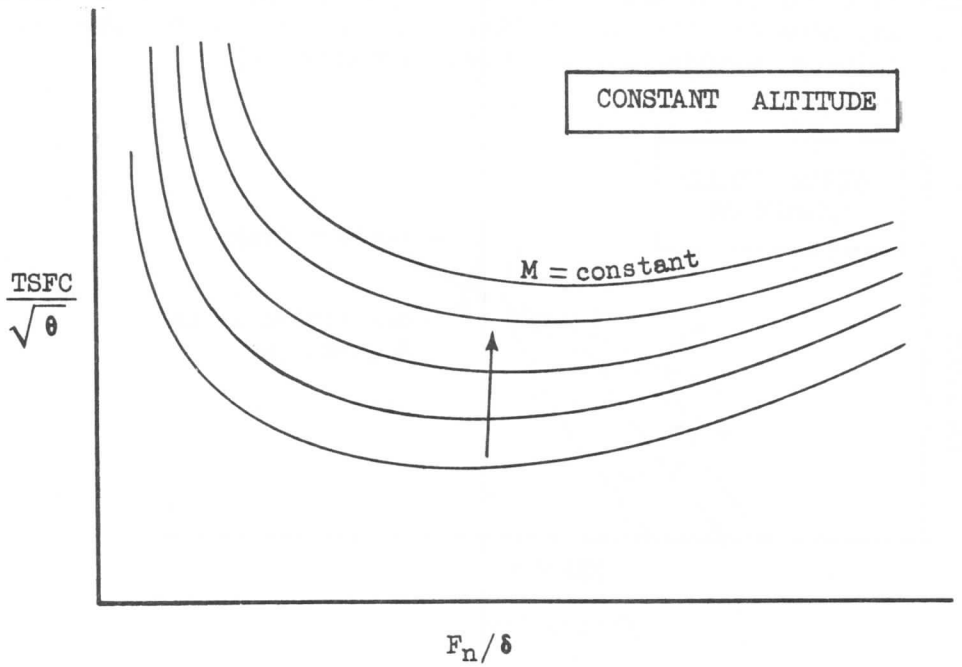

Figure 19.

As long as the variation of $TSFC/\sqrt{\theta}$ with Fn/δ and Mach number remains independent of temperature (which it does for most engines, again ignoring secondary effects such as air conditioning bleed requirements varying with temperature), any constant values of Fn/δ and Mach number obtained for all temperatures yield the same $TSFC/\sqrt{\theta}$. Therefore, from equation (133), nam/lb becomes independent of temperature.

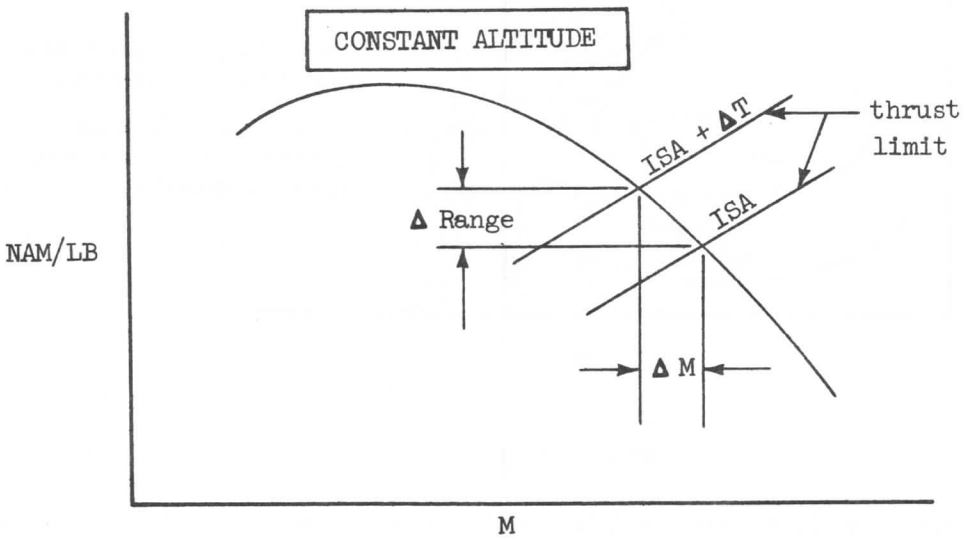

Figure 118.

When operating at a given rating (e.g. maximum cruise thrust) however, the effect of temperature changes will be felt. Since under these conditions the actual thrusts involved will be changed and the thrust lever cannot be advanced to compensate, the fuel consumptions and speeds will also be changed. This effect is illustrated in Figure 118.

Earlier, in Figure 110, curves of nam/lb vs altitude were shown with the maximum range line drawn. If, however, the thrust limited situation occurs, the maximum range altitude is no longer attainable, as shown in Figure 119.

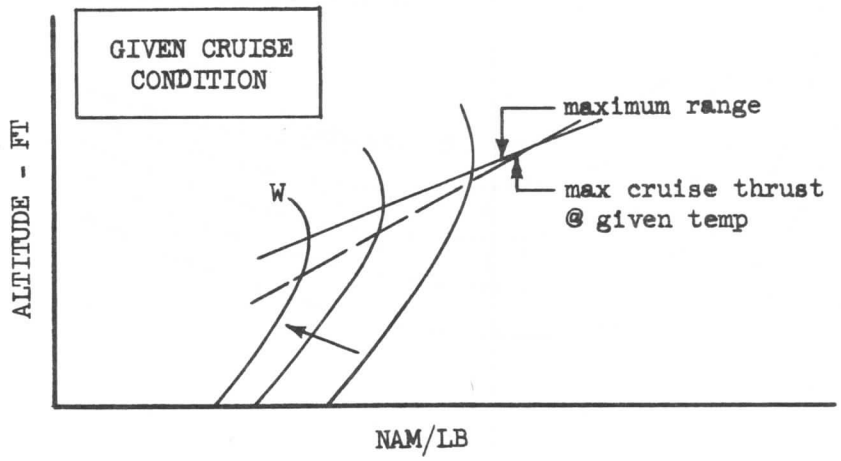

Figure 119.

When this situation occurs, a trade of speed for altitude may be made with a subsequent improvement in nam/lb from that shown at the thrust limit in Figure 119. This is shown in Figure 120.

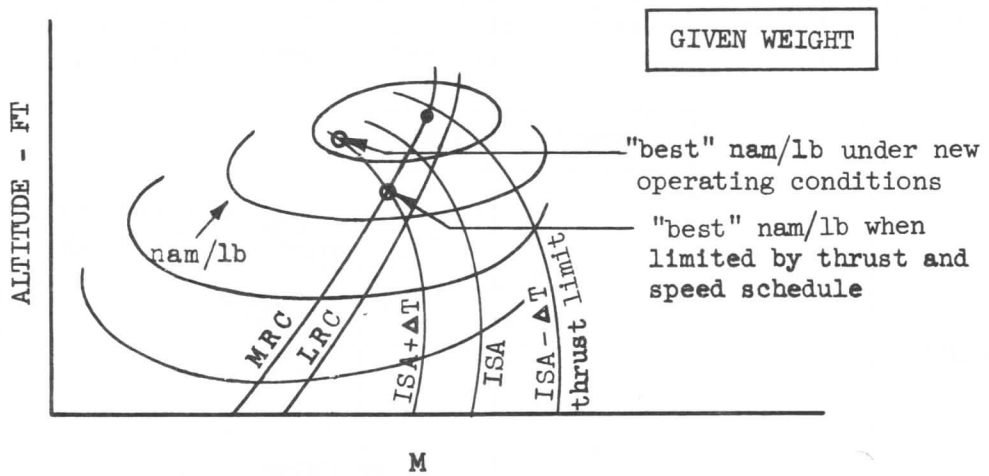

Figure 120.

To obtain the "best" nam/lb at the maximum cruise thrust rating for a series of weights at a given temperature, the following procedure is employed:

(1) At each weight, read the nam/lb and Mach number from the intersection of the fuel mileage curve and the thrust limit curve (Figure 118) for several altitudes.

(2) Plot nam/lb and Mach number vs weight for each altitude as shown in Figure 121.

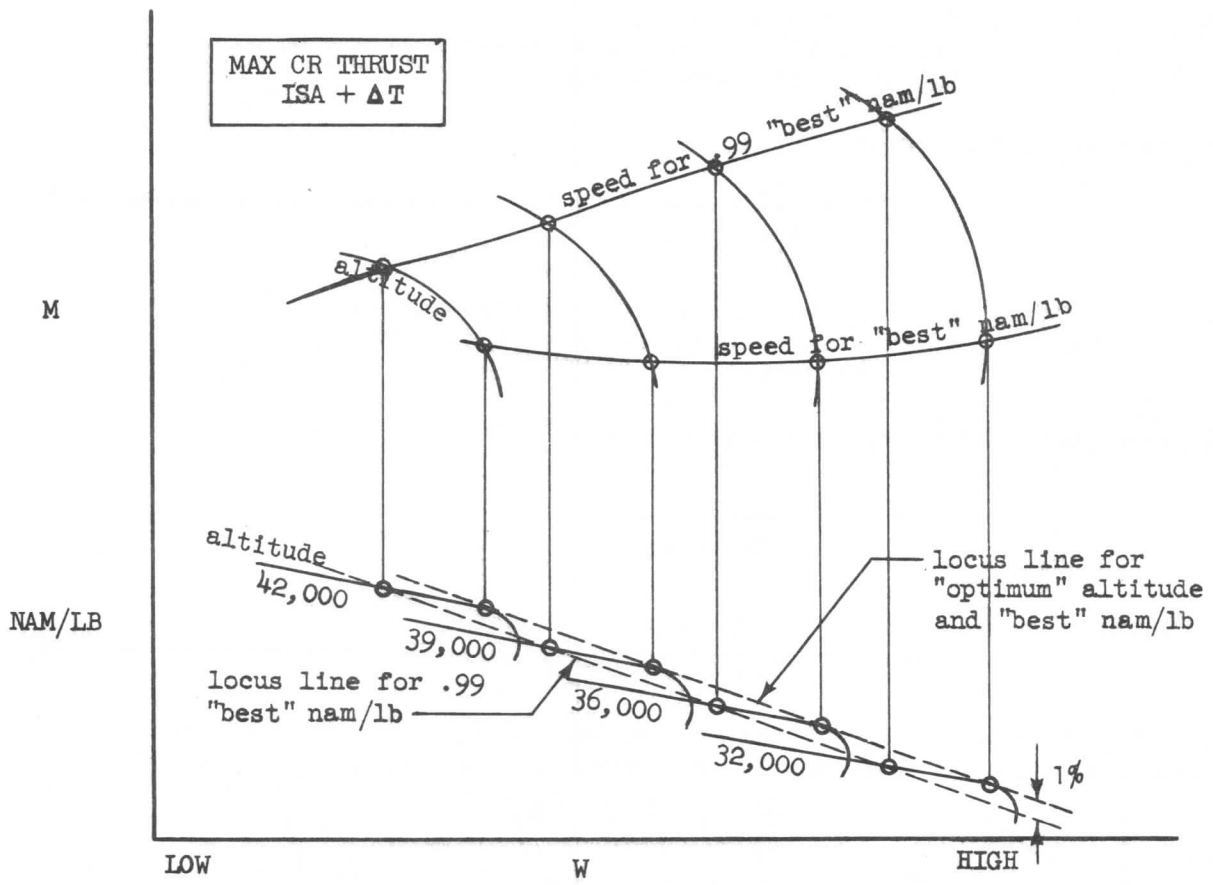

Figure 121.

(3) From Figure 121, integrated range curves such as shown in Figure 116 may be calculated and presented for either "best" or .99 "best" range.

Wind and Off-Altitude Effects

If an airplane is required to fly at a constant W/δ, (for maximum range, for example), then its altitude at any weight is specified. For various reasons it may be desired to fly at an altitude which is not optimum. Such a condition might exist when a strong tail wind is known to be present at some lower or higher altitude. It might then be advantageous to go to this altitude if the wind effect more than off-sets the loss in range due to flying at the off-optimum altitude. Also, it may be required to fly at other than desired altitudes due to air traffic conditions.

The effect of wind at a given altitude is to change the ground speed, thus changing the time to travel a given ground distance. Effectively, this is the same as travelling a different air distance. The correction for the wind effect is determined as follows:

Time to fly through the air mass is

$$t = \frac{nam}{V_{cr}} \qquad (134)$$

where, t is time in hours
nam is still air distance in nautical air miles
V_{cr} is cruise speed in knots

But referenced to the ground,

$$t = \frac{nm}{V_{cr} \pm V_w} \qquad (135)$$

where, nm is ground distance in nautical miles
V_w is windspeed component in knots. Tailwind is positive

For a given period of time, equation (134) equals equation (135).

$$\frac{nam}{V_{cr}} = \frac{nm}{V_{cr} \pm V_w}$$

or,

$$nam = nm\left(\frac{V_{cr}}{V_{cr} \pm V_w}\right) \qquad (136)$$

Equation (136) is used in presenting the effect of wind on ground distance in the Operations Manual. The form of presentation is as shown in Figure 122.

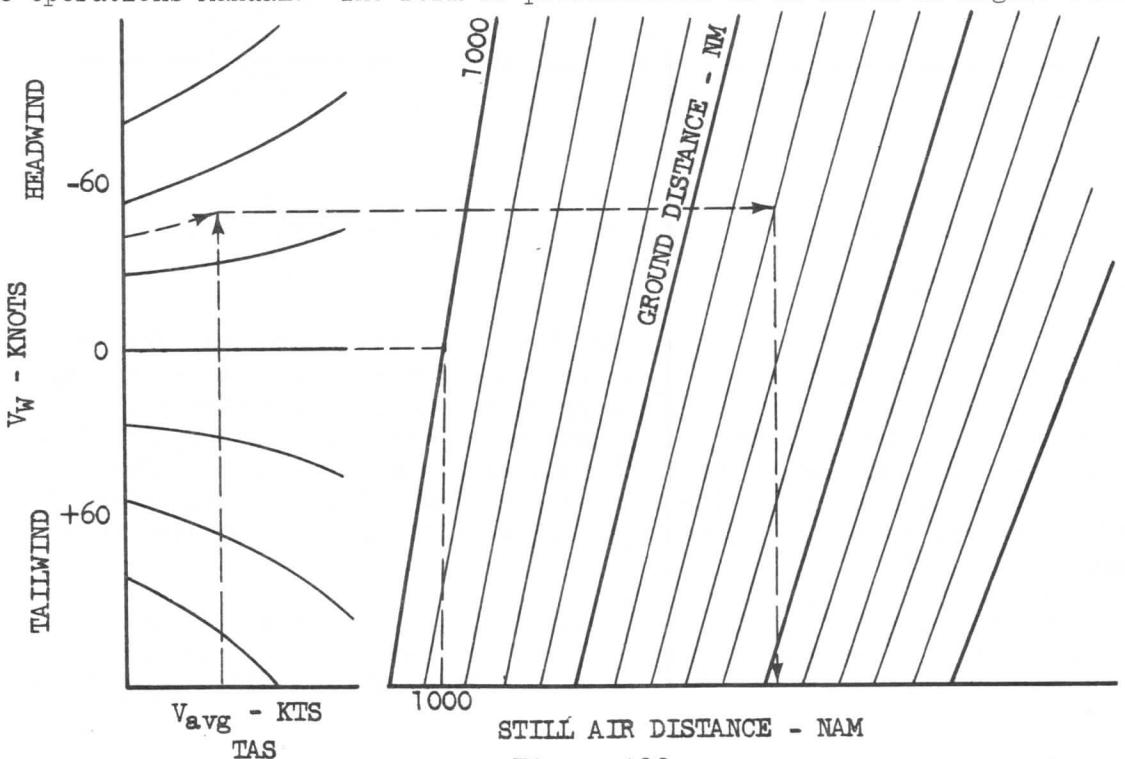

Figure 122

To construct the chart, selected values of headwinds and tailwinds for assumed values of cruise speed are substituted into equation (136) and the relative values of ground distance to still air distance are established. Note that, in Figure 122, the dashed lines demonstrate that at a zero wind condition, still air distances are equal to ground distances.

If the wind conditions at the cruising altitude indicate a desirability to change altitude either to reduce the losses of a headwind, or to increase the benefits of a tailwind, then the combined wind effect and the change in nam/lb at another altitude must be considered.

Emphasis must be placed on the fact that a small change in wind may not be adequate to compensate for the loss due to change in altitude in an effort to gain the wind effect. Only a major gain due to wind can be considered if a large change in altitude is involved. Also to be considered is the fact that commercial airplanes must fly specified altitudes, and the potential gain in changing altitude must be weighed against any inconvenience involved in seeking approval for a change.

It is of interest to consider the plight of the pilot on an overseas flight faced with the decision of turning back when an emergency arises. In order to help answer his question, he usually calculates two points: a point-of-no-return and an equi-time point. The PNR, point-of-no-return, is the greatest distance to which he could fly, lose the thrust of his most critical engine, and return without running out of fuel. The equi-time point is the greatest distance from which he could elect after engine failure to either return to departure point or fly on to destination, both decisions taking the same amount of time (or fuel).

To calculate the PNR, one could proceed as follows:

(1) Enter the all-engines-operating integrated range chart, Figure 116, with departure gross weight and a weight increment equal to one-half the weight of the fuel. Read the air distance increment corresponding to the planned type of cruise and correct for wind to obtain the ground distance out-bound.

(2) Enter the one-engine-inoperative integrated range chart with zero-fuel weight and a weight increment equal to one-half the fuel weight. Obtain the air distance corresponding to maximum range operation and correct for wind to obtain the ground distance in-bound.

(3) Plot the two ground distances obtained above against the air distance out-bound as shown in Figure 123.

(4) Repeat steps 1, 2, and 3 using a larger weight increment for the out-bound leg and the corresponding smaller increment in-bound.

(5) After enough pairs of nm points have been plotted to define an intersection of the out-bound and in-bound ground distance lines, obtain the location of the PNR both in ground distance and in air distance at this intersection.

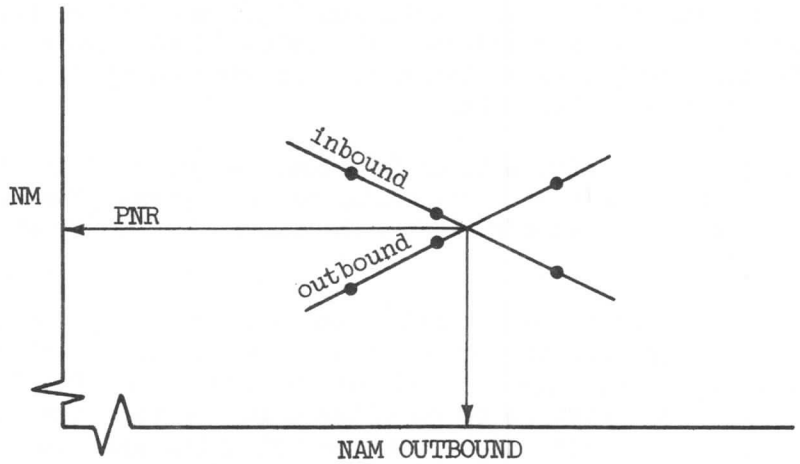

Figure 123.

Of course, one might locate the PNR by calculating range increments for the outbound and in-bound (backward) legs simultaneously, using more basic cruise fuel flow and speed data, and summing increments to the point of definition. Or one could calculate a no-wind PNR and apply a pre-calculated wind-correction factor.

The equi-time point calculation is based upon the assumption that the same type of one-engine-inoperative cruise is used for both legs; i.e., the same airspeed, V, applies for both. As a consequence of the use of the same airspeed and time in both legs of the flight, the fuel consumptions and air distances also will be equal.

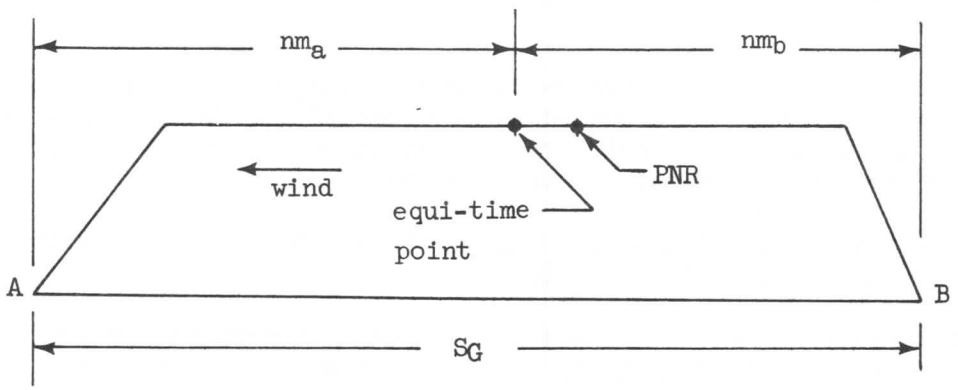

Figure 124.

In the nomenclature of Figure 124,

$$(nam)_a = (nam)_b$$

The wind correction, equation (136), shows that

$$\left(\frac{nam}{nm}\right)_b = \frac{V}{V - V_w} \quad \text{(headwind)}$$

and

$$\left(\frac{nam}{nm}\right)_a = \frac{V}{V + V_w} \quad \text{(tailwind)}$$

Therefore,

$$\frac{nm_a\ V}{V + V_w} = \frac{nm_b\ V}{V - V_w}$$

$$\frac{nm_a}{V + V_w} = \frac{nm_b}{V - V_w} \qquad (137)$$

From Figure 124, it is seen that

$$S_G = (nm)_a + (nm)_b \qquad (138)$$

Therefore, $(nm)_a$ can be determined by combining equation (137) and equation (138).

$$(nm)_a = S_G - (nm)_b$$

$$(nm)_a = S_G - \frac{(nm)_a\ (V - V_w)}{V + V_w}$$

$$S_G = (nm)_a \left[\ 1 + \frac{V - V_w}{V + V_w}\ \right]$$

$$(nm)_a = \frac{S_G}{\frac{2V}{V + V_w}}$$

$$(nm)_a = \frac{S_G\ (V + V_w)}{2V} \qquad (139)$$

Solving for $(nm)_b$ in like manner, one obtains the result,

$$(nm)_b = \frac{S_G\ (V - V_w)}{2V} \qquad (140)$$

For the above analysis it should be noted that only cruise flight was being considered. The descent to A or B under actual flight conditions changes the results slightly, but this is usually ignored.

Minimum Cost Operation

Because competition has become very aggressive, the determination of minimum-cost operation is occupying more time and effort than ever before. But the establishment of total cost is very difficult since it must include everything from airplane and engine purchase costs to crew day/night pay factors. Each airline seems to have its own specific way of calculating "direct operating costs," most of them adapted from the ATA formula. The formula is in the form:

$$D.O.C. = \frac{K_1}{V} + \frac{K_2}{nam/lb} + K_3 \qquad (141)$$

Minimum cost cruise could be defined by plotting cost factor, D.O.C./nautical air mile, vs weight as in Figure 125. The envelope of the constant altitude curves establishes the best weight-altitude operation.

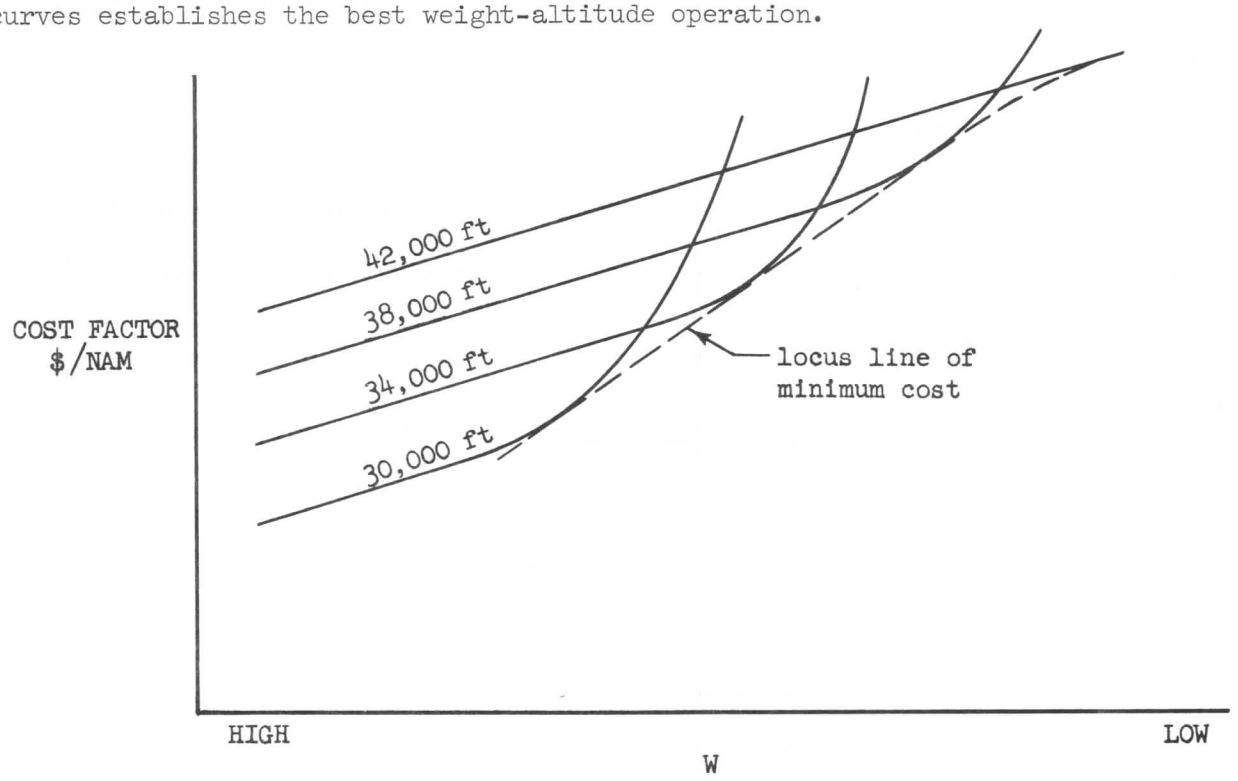

Figure 125.

If equation (141) were plotted on Figure 107, a plot such as shown in Figure 126 results. The locus of the tangents of the $/nam curves on the nam/lb curves determines the speed for minimum cost cruise at that altitude.

A summary of the range and speed values for minimum cost cruise at a number of altitudes may be drawn on a single plot, Figure 127. The altitude schedule may be read from Figure 125 and the speed and range from Figure 126. It should be noted that minimum cost cruise calls for low altitudes when at high weights and high altitudes when at low weights. Thus minimum cost cruise is obtained in a climbing cruise operation at a fixed speed schedule.

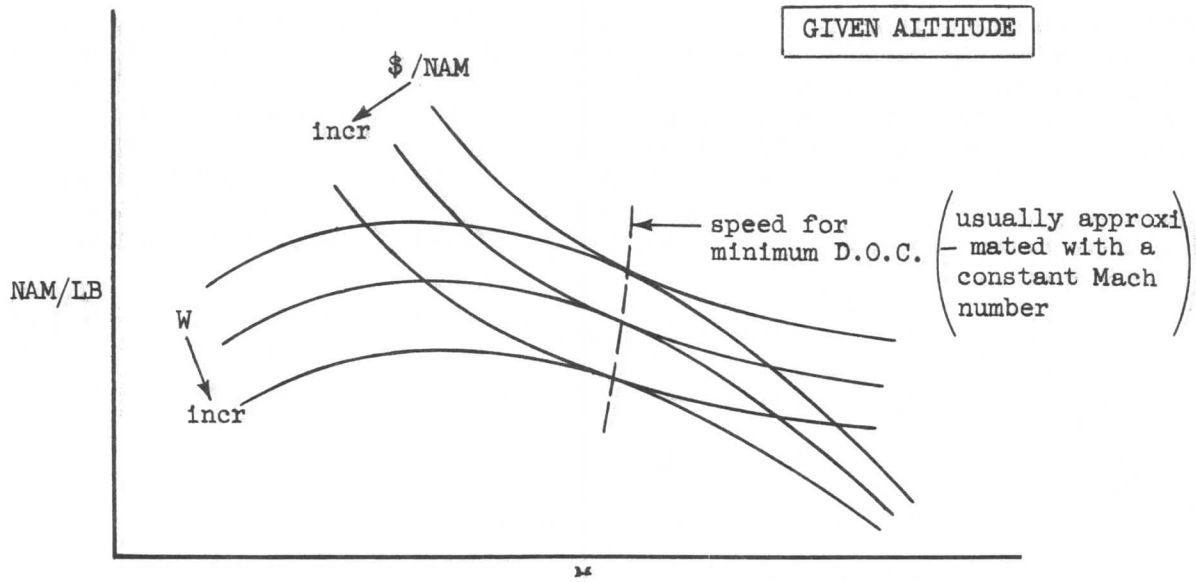

Figure 126.

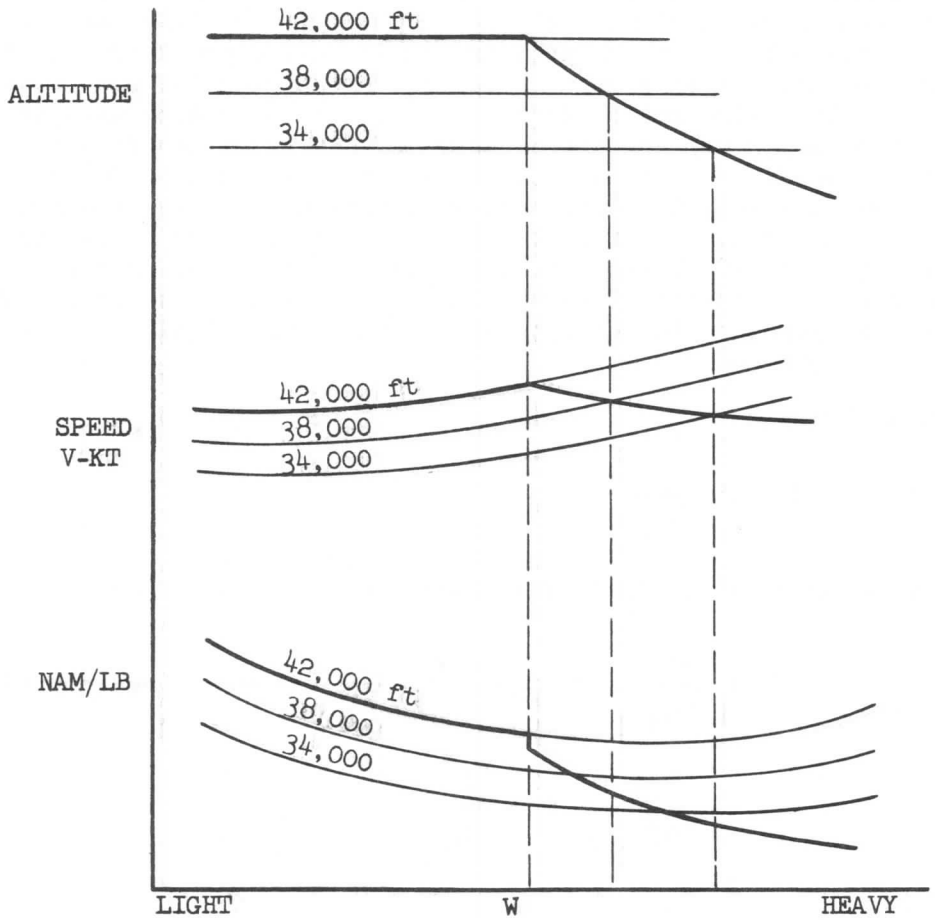

Figure 127.

SECTION 3

AIRPLANE PERFORMANCE

Dispatching personnel and flight crews have two problems which they would like to be able to solve easily without being exposed to cost accounting. The first involves flight planning to minimize cost. It is the question of how to find the least costly of a number of possible flight plans. The second problem is met in flight and involves making a decision as to whether it is possible to save by changing operation from the pre-planned flight to a different operating condition. The problem may arise because of unforeseen weather conditions, equipment malfunction, or other contingency outside the normal, planned condition of flight.

Let

C = total trip cost, \$

C_{hr} = fixed cost (fuel cost excluded), \$/hr

C_{lb} = fuel cost, ¢/lb

T = total flight time, hr

F = total flight fuel, lb

In defining hourly costs, C_{hr}, it should be noted that certain of the ATA direct operating costs should not be included. Only those cost items which would be affected by block speed or block time should be included in the calculation. For example, once the airplane has been accepted and is in use, depreciation charges may not necessarily be included as a cost factor in determining the most economical speed for flight. If a time saving does not result in increased utilization of the aircraft, depreciation charges are usually assumed to be independent of speed of operation and should not be included in the cost formula to determine minimum-cost airspeed. However, if additional utilization could be realized from higher cruising speed, there may be an influence upon depreciation cost, and its effect on operating speed might be included. Similarly, crew costs are not always included; insurance and passenger service items are seldom included. Considerable care must be exercised in interpretation of the cost analysis if a valid conclusion is to be drawn.

A flight index can be defined:

$$I = \frac{C_{hr}}{C_{lb}}$$

Total trip cost can be given in terms of fixed cost and fuel cost thus,

$$C = \frac{C_{lb}}{100} F + C_{hr} T \qquad (142)$$

$$T = -\frac{C_{lb}}{100\, C_{hr}} F + \frac{C}{C_{hr}}$$

Therefore,

$$T = -\frac{1}{100\, I} F + \frac{C}{C_{hr}} \qquad (143)$$

One can see that equation (143) represents a family of lines in the T-F plane whose slope is

$$m = -\frac{1}{100\ I} \qquad (144)$$

and whose intercepts on any time axis represent increasing total cost. Each line represents a constant total cost, increasing up and to the right.

In plotting these relationships, it is most convenient to put the slope into trigonometric form,

$$\alpha = \tan^{-1}\left(-\frac{1}{100\ I}\right)$$

This definition is valid only if the axes have the same unit-length value. However, it is not convenient to plot these data in such a system; so the scales are defined for convenient plotting and the slope is redefined to read,

$$\alpha = \tan^{-1}\left(\frac{-K}{100\ I}\right) \qquad (145)$$

$$K = \frac{\text{unit length on T scale}}{\text{unit length on F scale}} \qquad (146)$$

A circular nomogram constructed from equation (145) to overlay the basic T-F grid can be used to define the slope for any given cost index value. Thus, one obtains Figure 128.

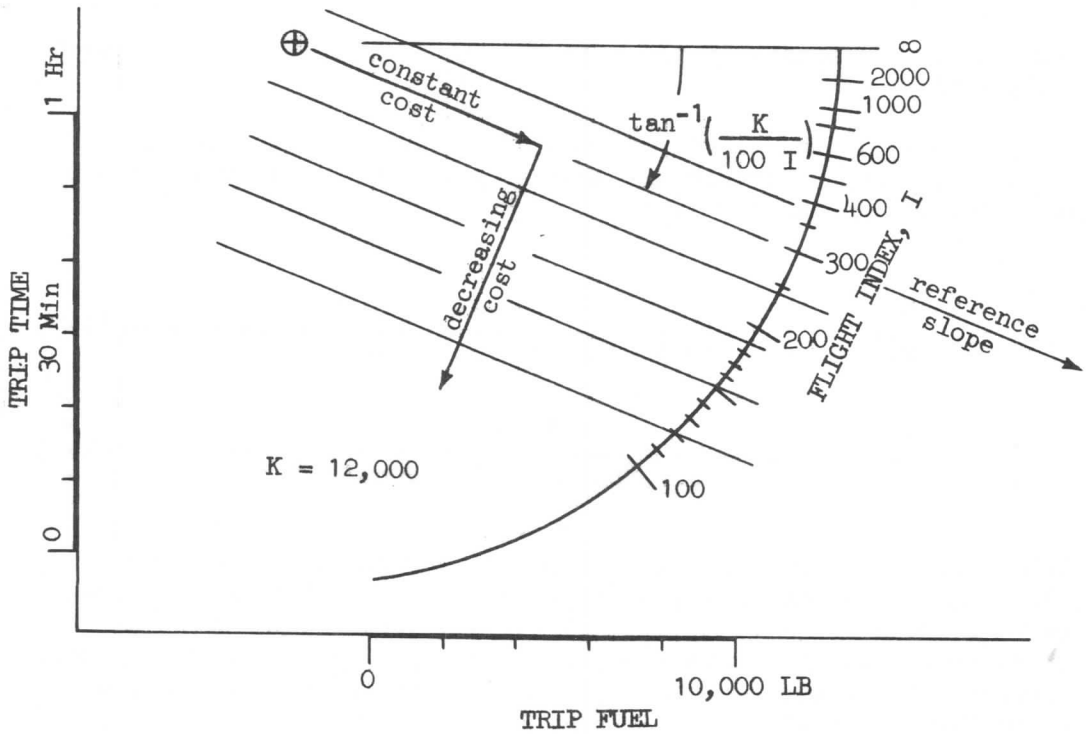

Figure 128.

The index value for any given route is determined by a cost analysis, and is used to determine the slope of a family of guide lines on the planning grid. The positions of any two plans represented on the grid shows the relative cost of each with respect to the other. Obviously, the larger the grid, the more accurate the analysis. But since very large grids are hard to work with, it is proposed to use only the portion of the large grid in which one is interested. Thus, if one is working on a short route, one may label the scales from 1 to 4 hours and 10,000 to 50,000 pounds; if on a long route, one may use 10 to 13 hours and 120,000 to 150,000 pounds.

An example worked out on Figure 129 is used to show this situation:

$$I = 300$$

Plan	Alt.	Schedule	Time	Fuel
A	31,000	LRC	11:33	135,106
B	35,000	LRC	11:30	128,166
C	31,000	.82M	11:08	142,291
D	35,000	.82M	11:16	133,299

These are possible flights drawn from tabulated or plotted flight-planning data in the Operations Manual.

The solution ranks the plans in order of increasing total cost:

D, B, C, A

Of the plans considered, the least expensive is a flight at 35,000' on a constant Mach number schedule of .82.

To develop an inflight chart for use in problems of the second type, let us divide through equation (143) by ground distance in nautical miles, nm. Ground distance is considered to account for wind.

$$\frac{T}{nm} = -\frac{1}{100\ I}\frac{F}{nm} + \frac{1}{C_{hr}}\frac{C}{nm} \qquad (147)$$

Therefore,

$$\frac{1}{V_G} = -\frac{1}{100\ I}\frac{1}{nm/lb} + \frac{1}{C_{hr}}\frac{C}{nm} \qquad (148)$$

Equation (148) shows that cost per mile is related to ground speed and range factor through the same index parameter, $-\frac{K}{100\ I}$, as in the flight planning analysis. Thus, the cost index could be used to define the slope of a family of constant cost lines on a grid of $1/V_G$ vs $\frac{1}{nm/lb}$. However, since the range factor, nm/lb, being referenced to ground distance, is hard to determine in flight, a better flight parameter is sought.

FLIGHT INDEX
PLANNING CHART

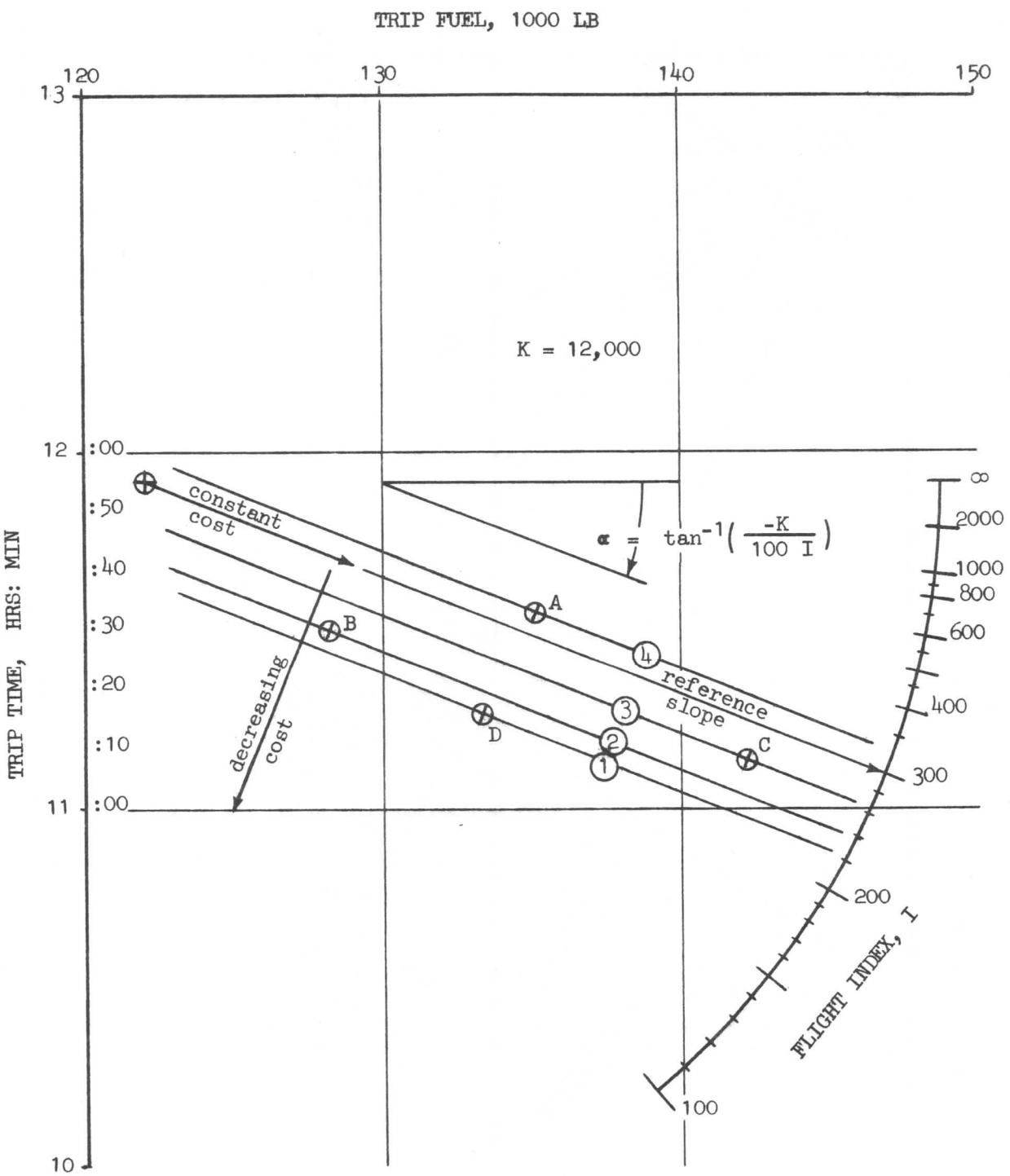

Figure 129.

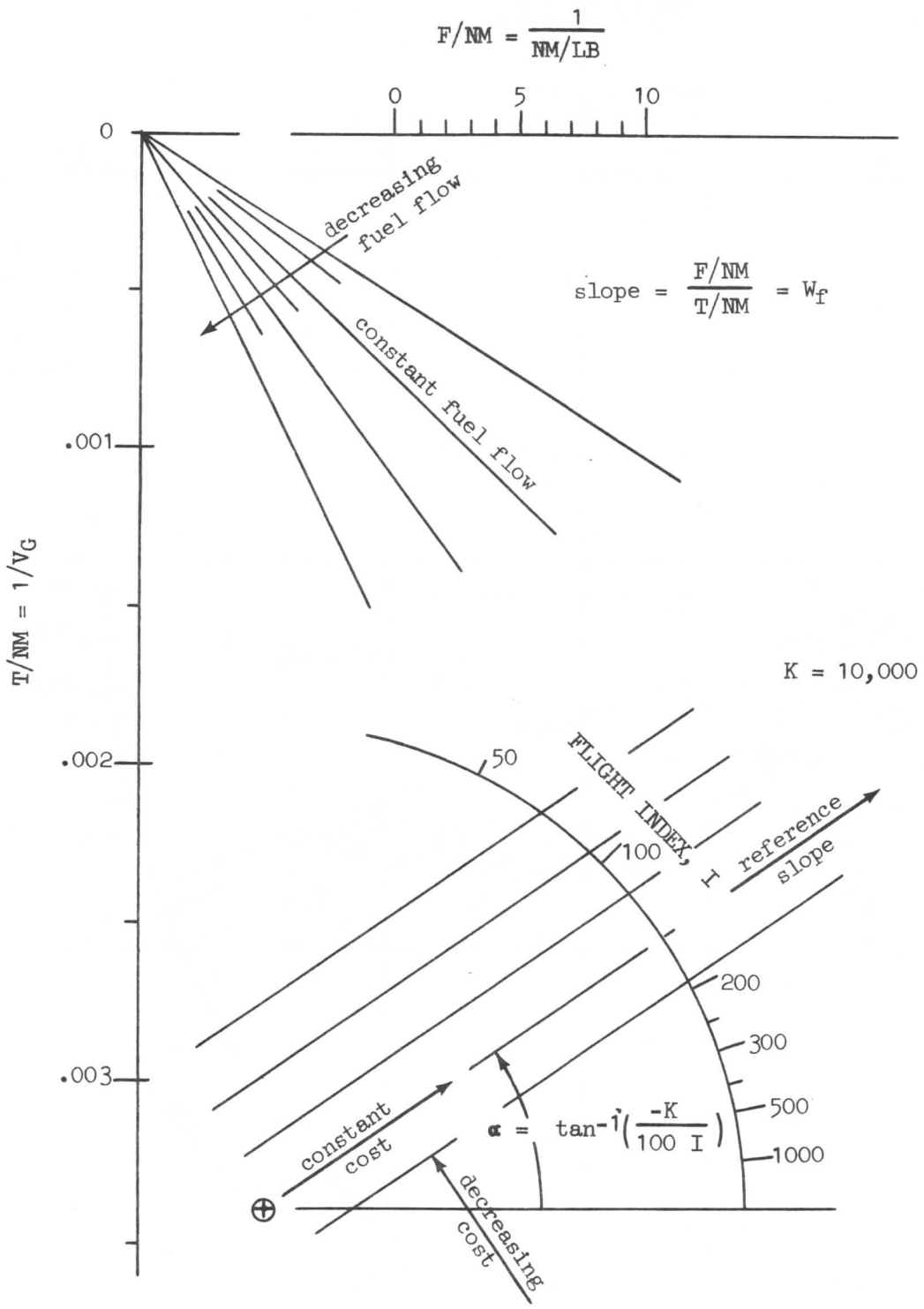
F/NM = 1 / NM/LB
0
5
10
0
decreasing fuel flow
slope = F/NM / T/NM = W_f
constant fuel flow
.001
T/NM = 1/V_G
K = 10,000
.002
50
FLIGHT INDEX, I
100
reference slope
200
300
.003
constant cost
$\alpha = \tan^{-1}\left(\frac{-K}{100\ I}\right)$
500
1000
decreasing cost

Figure 130.

In fact, in many cases, the determination of nm/lb may be one part of the solution sought. By considering fuel flow, it is realized that

$$W_f = \frac{F}{T}$$

$$W_f = \frac{F/nm}{T/nm}$$

which reduces to

$$\frac{1}{nm/lb} = W_f\left(\frac{1}{V_G}\right) \qquad (149)$$

Equation (149) defines a family of constant fuel flow lines in a fan from the origin of the $\frac{1}{nm/lb}$ vs $\frac{1}{V_G}$ grid. These can be used in flight since fuel flow is readily available. Thus, an inflight chart, Figure 130, is defined. To make the flight crew chart more adaptable to flight use, it is usually labeled in terms of V_G rather than in $1/V_G$, as in Figure 131. Figure 131 is referenced to 4-engine operation; therefore, for 3- or 2-engine applicability, the values on the abscissa scale have to be factored by three-fourths or one-half, respectively.

An example, shown on Figure 131, may be worked out from the following data:

I = 300

Condition	Alt.	Temp.	Ind. Mach.	TAS	Wind	V_{gr}	W_f
A	35,000	-55°C	.84	486K	-50K	436K	3430
B	30,000	-45	.84	496	-35	461	3660
C	39,000	-55	.807 (MC_rT)	468	-65	403	2926

The conditions, ranked in increasing cost, rate

B, A, C,

so from a total cost standpoint, the best flight condition of the three is found at 30,000 feet. However, from a range standpoint the three rank

$$C = 29.2\ \frac{lb}{nm} \qquad A = 31.3\ \frac{lb}{nm} \qquad B = 31.8\ \frac{lb}{nm}$$

and the best condition is found at 39,000 feet. Condition A requires 2.1 lb/nm and B, 2.6 lb/nm more than condition C. In 1000 nautical miles, conditions A and B respectively require 2100 and 2600 pounds more fuel than condition C, and it may be necessary to fly the more costly condition in order to have enough fuel to finish the flight with enough reserve on board.

Another point to consider is that it will always cost something extra to change flight condition to a higher altitude. If a change from 35,000 feet at condition A to 39,000 feet at condition C were to be considered, since these large transports take about 100 pounds of fuel extra for each 1000 feet climbed, some of the advantage of the higher altitude is lost.

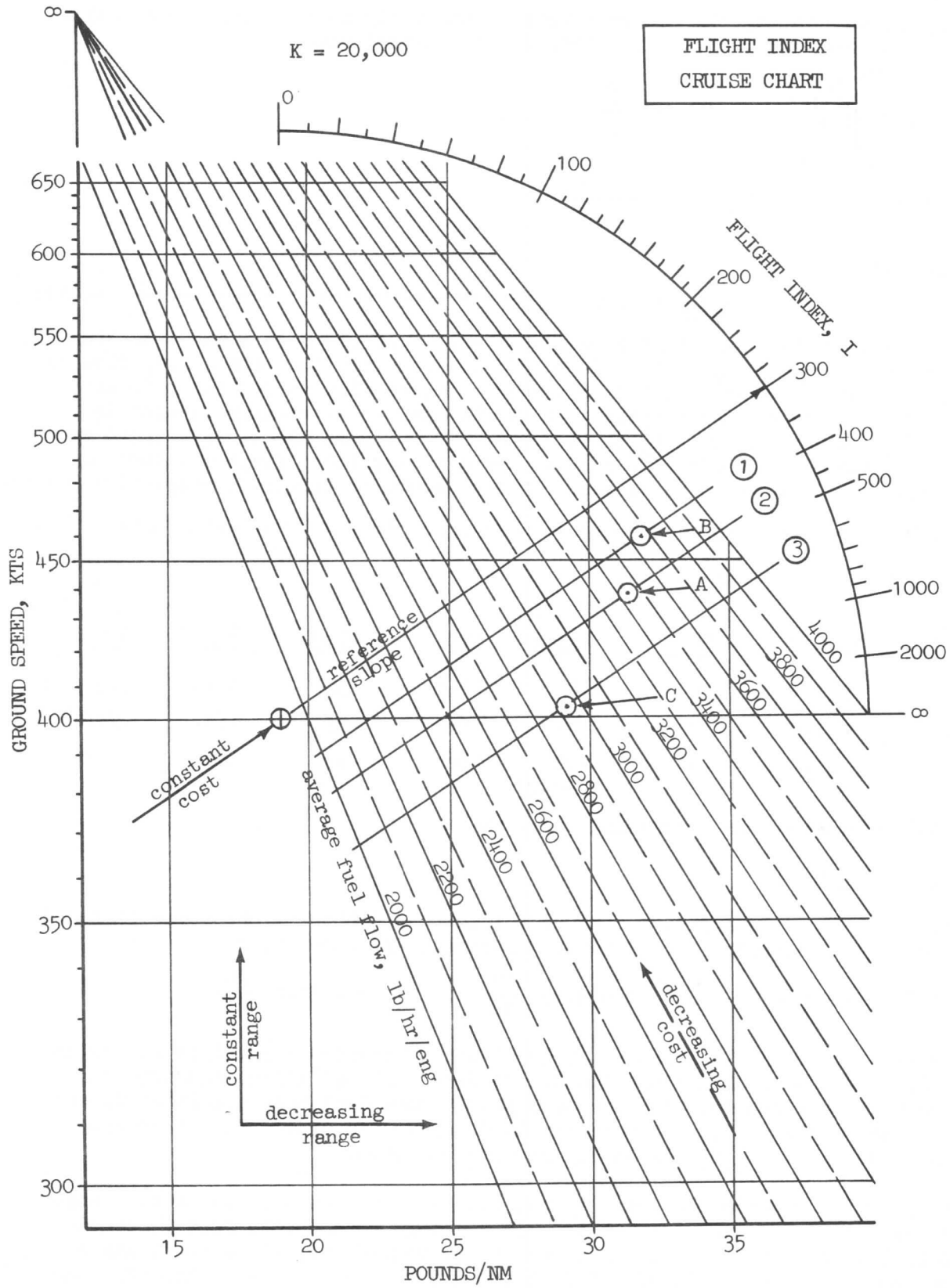
FLIGHT INDEX
CRUISE CHART
K = 20,000
FLIGHT INDEX, I
0
100
200
300
400
500
1000
2000
∞
GROUND SPEED, KTS
650
600
550
500
450
400
350
300
POUNDS/NM
15
20
25
30
35
reference slope
constant cost
average fuel flow, lb/hr/eng
2000
2200
2400
2600
2800
3000
3200
3400
3600
3800
4000
A
B
C
1
2
3
constant range
decreasing range
decreasing cost

Figure 131.

Since $\frac{400}{2.1} = 190.5$

at least 190.5 NM must be flown at the new altitude just to make up for the fuel used to climb. And an extra amount of fuel over and above this may be needed for pressurization and to compensate for the additional descent at the end of cruise.

Optimum Minimum Cost Cruise Speed

The relationship between minimum cost cruise speed and flight index, I, based on the fuel mileage curves is derived from equation (142) as follows:

$$C = C_{hr} T + \frac{C_{lb}}{100} F$$

Let $C_{hr} = C_t$ and $C_{lb/100} = C_f$, then,

$$C = C_t T + C_f F$$

Since T is range divided by velocity and F is range divided by fuel mileage, equation (142) can be written as:

$$C = C_t \frac{R}{aM} + C_f \frac{R}{FM}$$

where, R is cruise range, nam
FM is fuel mileage, nam/lb

Minimum cost cruise Mach number is the Mach number where the sum of the variable costs and the fuel costs is a minimum. For a given altitude and weight, minimum cost cruise occurs when $dC/dM = 0$, therefore,

$$\frac{dC}{dM} = \frac{C_t R}{a}\left(\frac{-1}{M^2}\right) + C_f R \left(\frac{-1}{(FM)2}\right) \frac{d\ FM}{dM}$$

$$\frac{dC}{dM} = -R\left[\frac{C_t}{aM^2} + \frac{C_f}{(FM)^2}\frac{d\ FM}{dM}\right] = 0$$

and, $$\frac{C_t}{aM^2} = -\frac{C_f}{(FM)^2}\frac{d\ FM}{dM}$$

or, $$\frac{C_t}{C_f} = -\frac{a_o\sqrt{\theta}\ M^2}{(FM)^2}\frac{d\ FM}{dM} = I \qquad \text{(150)}$$

Equation (150) yields curves of the form shown in Figure 132 which shows that as the flight index increases the speed for a minimum cost cruise increases. For example, an increase in variable costs or a decrease in fuel costs. Since fuel

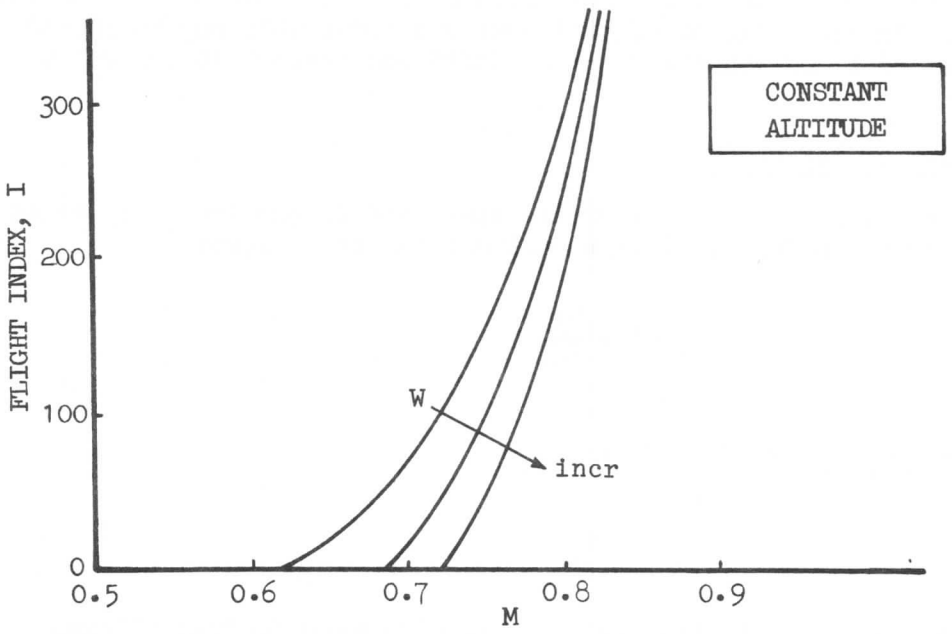

Figure 132

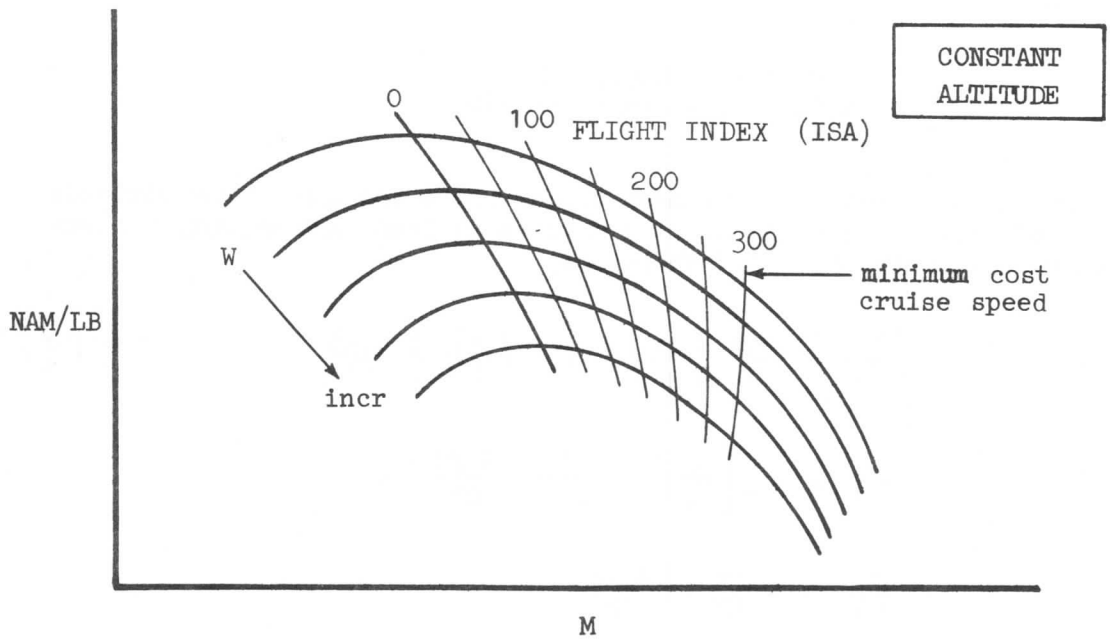

Figure 133

mileage, FM, and the change in fuel mileage with change in Mach number, d FM/dM, are obtained from Figure 126, flight index values can also be drawn on Figure 126, as shown on Figure 133.

The minimum cost flight index values in Figures 132 and 133 are for a given temperature at a given altitude since equation (150) shows that temperature is one of the variables. Also for a given flight index, it can be seen that the Mach number for minimum cost either increases or decreases as weight is increased.

Engine-Inoperative Cruise

When one or more engines are inoperative, the maximum range at the optimum altitude will always be less than for all-engine operation. The reason for this is that with engines inoperative, the airplane drag will increase due to the additional drag of the dead engine. This means that the L/D of the airplane will be lower than with all engines operating, so that with no better fuel consumption characteristics than were exhibited with all engines operating, the range must be less. This may be seen from equation (128).

$$R = \left(\frac{a_o\sqrt{\theta}}{TSFC}\right)\left(M\frac{L}{D}\right) \ln \frac{W_1}{W_2}$$

At low altitudes, however, where the thrust required per engine is low, and consequently the $TSFC/\sqrt{\theta}$ value is high, a more beneficial engine specific fuel consumption is available with less engines operating so thrust required per engine is higher. This is illustrated in Figure 134.

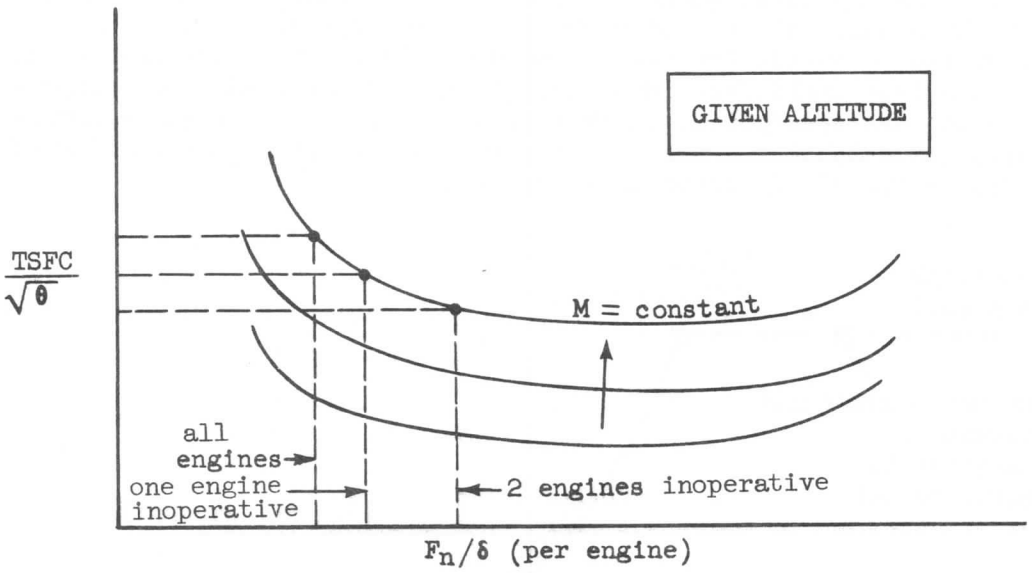

Figure 134.

The result of this is to improve nam/lb at low altitudes with one or two engines inoperative. However, the best range, if no altitude ceiling exists, is obtained with all engines operating as shown in Figure 135.

The way that engine-inoperative range performance is estimated is to modify the airplane drag polar, C_L vs C_D, by the addition of the drag coefficient associated with the engine-inoperative operation.

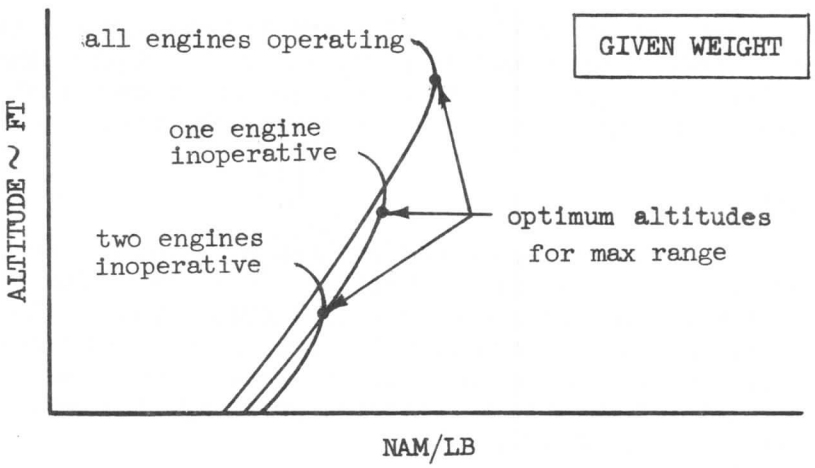

Figure 135.

Driftdown

In the event of engine failure or other radical loss of thrust in cruise, a descent to a lower altitude and an adjustment in speed may be necessary. A driftdown procedure designed to minimize loss of range is given. The thrust levers on the operating engines are advanced to obtain maximum continuous thrust and the airplane is allowed to descend at a specified speed which is compatible with the speed at which the engine-inoperative cruise will be flown. The speed is fixed such that there need not be a deceleration to descend and a subsequent acceleration required to attain the new cruise condition. While the descent is made and as the airplane stabilizes into level flight at a new altitude compatible with the thrust and speed, time is available to consult the engine-inoperative cruise data and establish a new flight plan. A schematic presentation of a possible driftdown profile is shown in Figure 136.

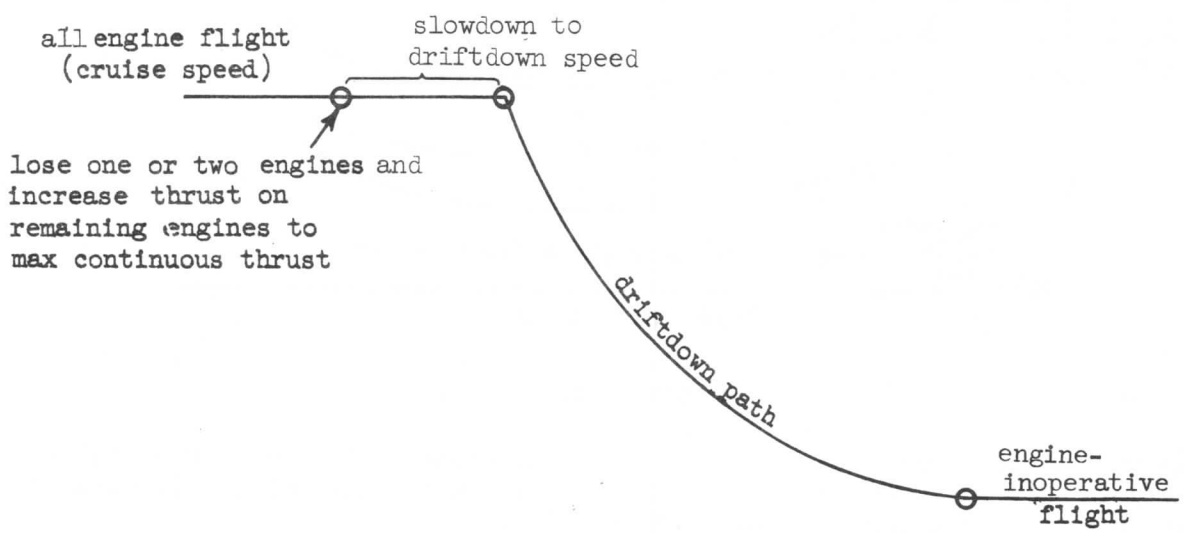

Figure 136.

Engine-inoperative cruise must satisfy the civil air regulations regarding terrain clearance. SR-422 4T.121 (a) and (b) states that in the most critical engine-inoperative condition the airplane must be capable of clearing all terrain by 2000 feet with a net flight path defined to be 1.8% less than actual gross climb gradient available if in one-engine-inoperative flight and 0.6% less in two-engine-inoperative flight (4-engine airplanes). The corresponding regulation in SR-422B and part 25 of FAR requires net flight path capabilities corresponding to reductions of 1.6%, 1.4%, and 1.1% for 4-, 3-, and 2-engine airplanes in one-engine-inoperative flight; and 0.5% and 0.3% for 4- and 3-engine airplanes in two-engine-inoperative flight. per FAR 25.123 (b) and (c)

Not only must the airplane be flown at or below its cruise ceiling; it must be flown above the minimum altitude to meet the above clearance regulations. If conditions are such that the cruise ceiling is below the clearance minimum altitude, the airplane weight must be reduced by dumping fuel, as shown in Figure 137, until it can satisfy the requirements.

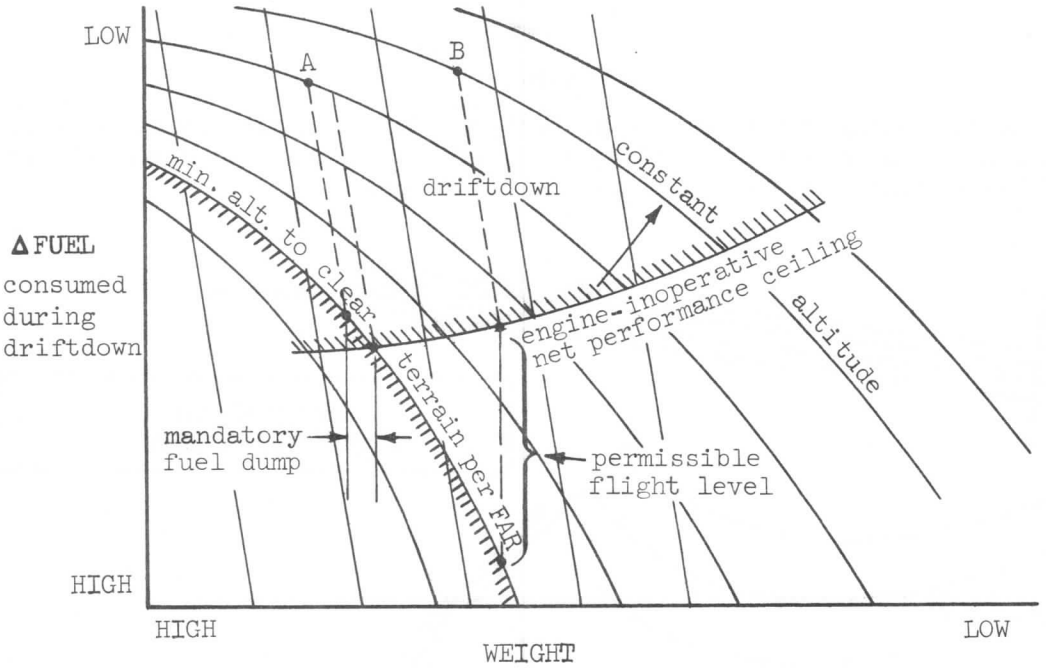

Figure 137.

Endurance

The problem of determining the best endurance performance from an airplane is very similar to that of obtaining best range. To obtain best range, it was desirable to maximize the quantity nam/lb. To obtain the greatest endurance, the pertinent quantity to be maximized is hrs/lb. If the engine fuel flow data completely generalizes, the problem of determining best endurance is quite simple.

An inspection of the basic fuel flow data, as developed previously (3-3) for Figure 14, provides the clue as to the best endurance. These data with the thrust required curves superimposed look similar to Figure 138. The lines of constant $W_f/\delta\sqrt{\theta}$ increase in the direction of the higher values of T/δ. Thus, a minimum fuel flow at a given W/δ (considering for the moment that δ and $\sqrt{\theta}$ are constant) will occur at the point of tangency between the two sets of curves.

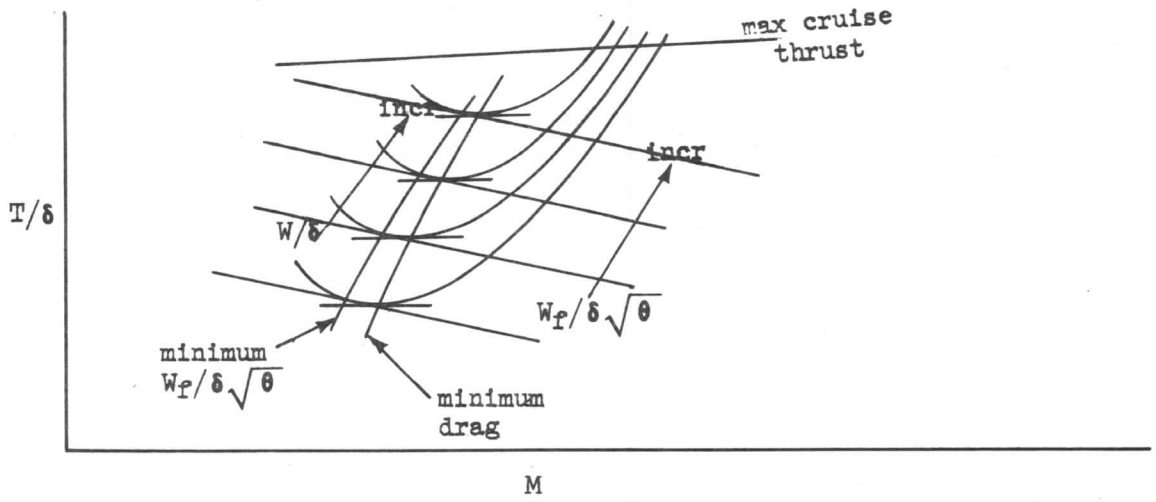

Figure 138.

At the point of tangency, for a given W/δ, $W_f/\delta\sqrt{\theta}$ will be a minimum or $\delta\sqrt{\theta}/W_f$ will be a maximum. Since the units of W_f are lb/hr, it is obvious that $1/W_f$ has the units of hr/lb which may be recognized as endurance.

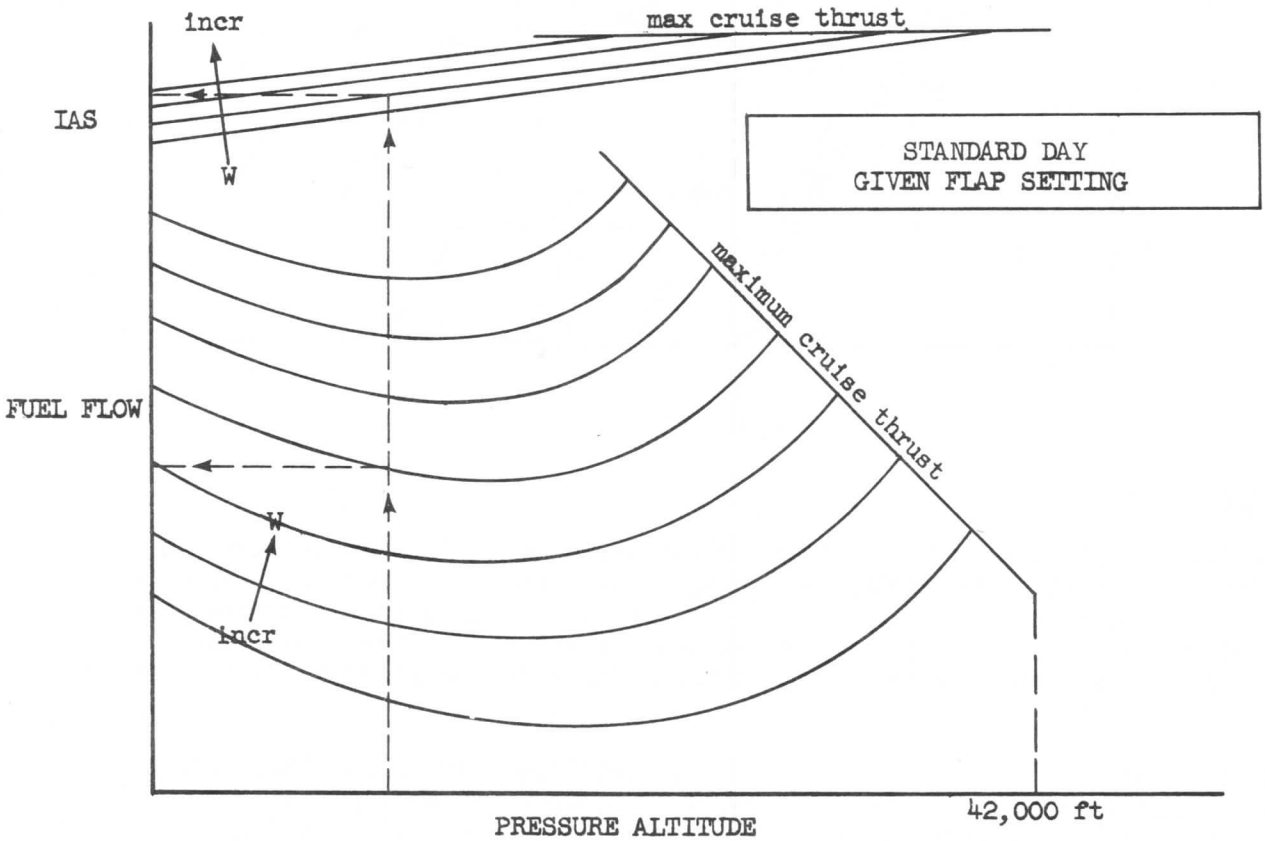

Figure 139.

In practice, it is found that the control of the airplane is much easier at a speed somewhat higher than that associated with minimum fuel flow. Again, referring to Figure 138, it can be seen that for all practical purposes, the speed schedule for holding (or endurance) may be that associated with minimum drag, at very little sacrifice in fuel economy.

For practically all holding practices, constant altitude operation is of primary interest. The technique used in obtaining the best endurance at constant altitude is similar to that explained above. Initially, the speed schedule is determined from a thrust vs velocity or Mach number plot at minimum drag for a series of selected constant altitudes. Using this speed schedule, the fuel flow for the corresponding weight values and for the selected altitudes is determined. From an inspection of the data available thus far, it is revealed that for a given weight, the best endurance for constant altitude operation would occur at a particular altitude. A plot of the data, as shown in Figure 139 may now be made based on a given flap setting and standard day conditions.

A correction graph for differences in temperature, shown in Figure 140, is merely the effect of $\sqrt{\theta}$ on the fuel flow.

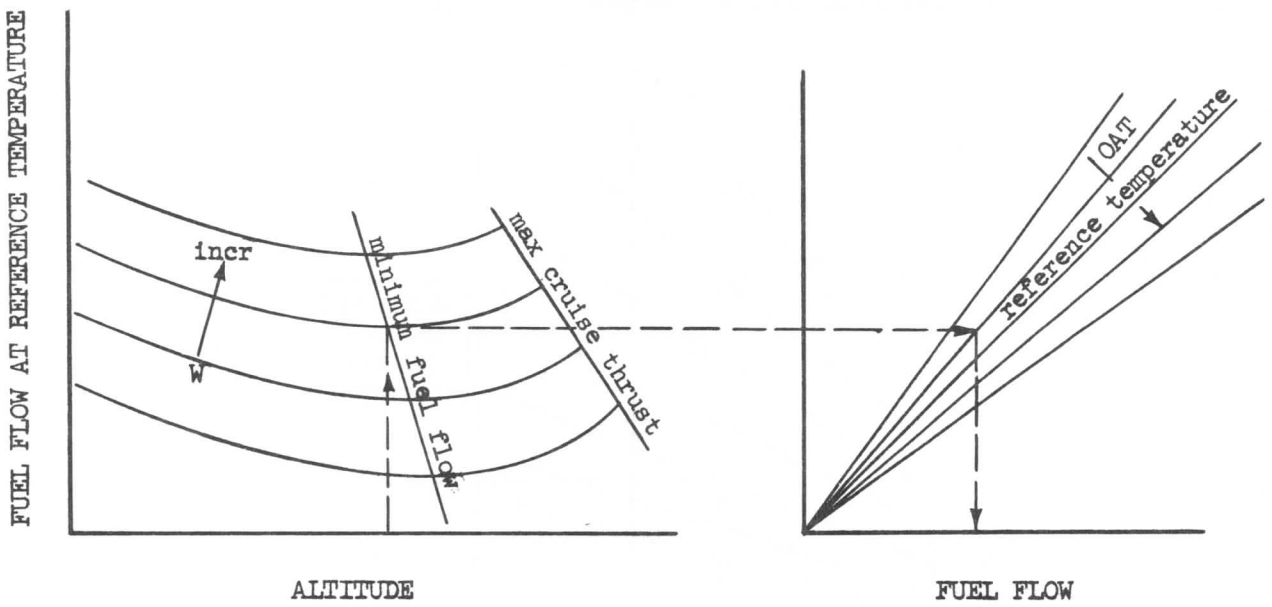

Figure 140.

Thrust Presentation

During cruise operations, care must be exercised not to exceed the maximum cruise thrust rating allowed by the engine manufacturer. Normally, the limiting thrust is defined in terms of Engine Pressure Ratio (EPR) or Turbine Discharge Pressure (P_{t_7}) and is shown as in Figures 141 and 142.

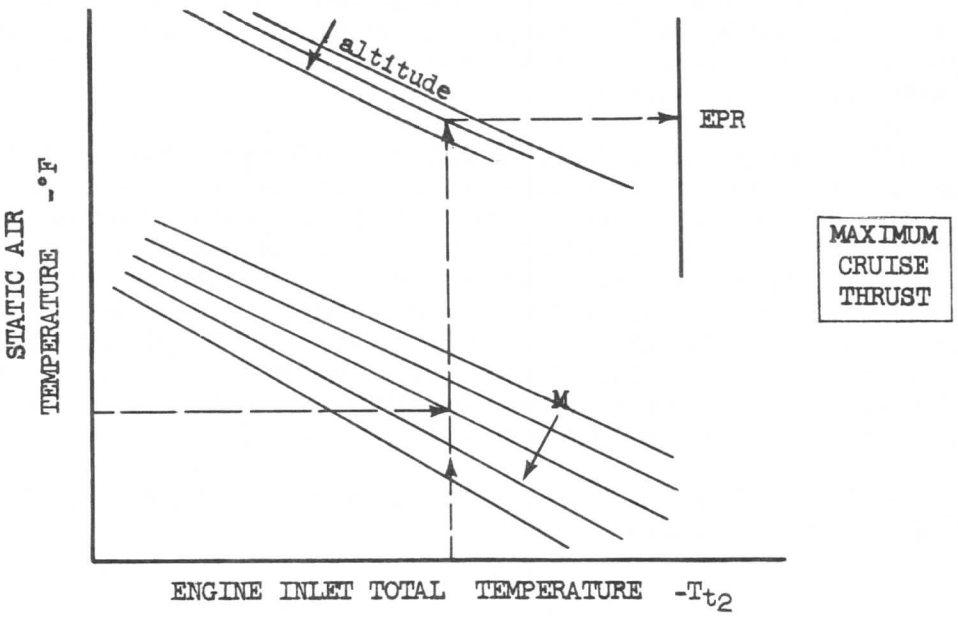

Figure 141.

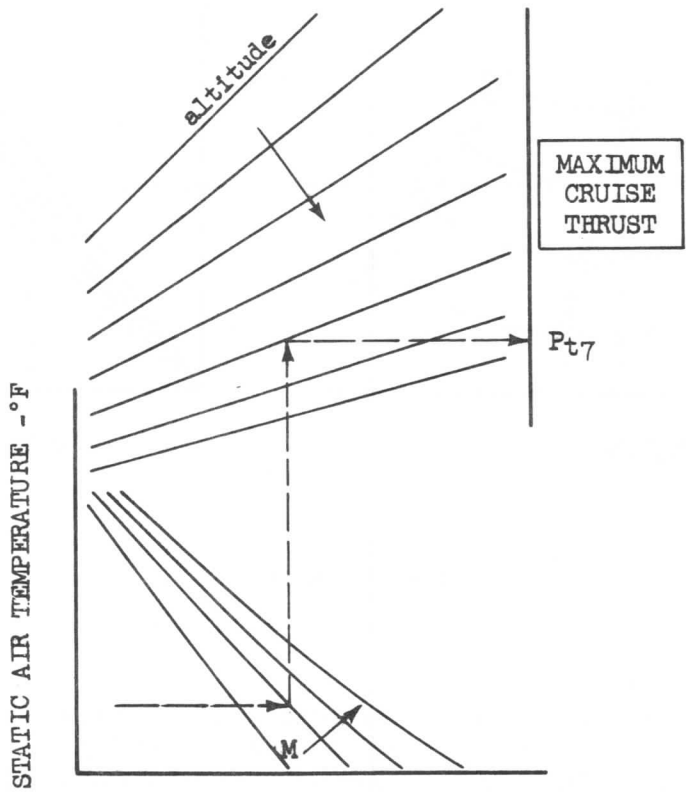

Figure 142.

However, when cruising at a thrust setting lower than the maximum permissible, it is necessary to use Figure 143 or 144 to set power.

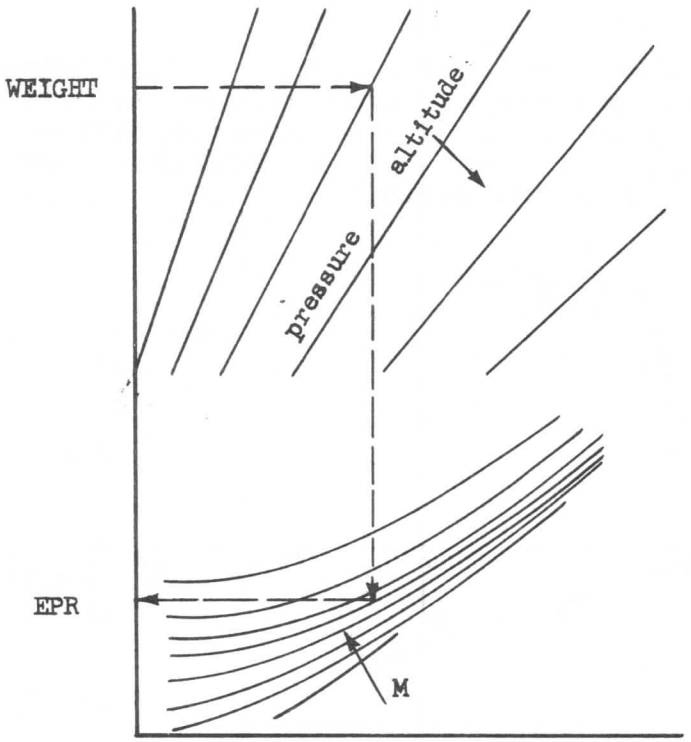

Figure 143.

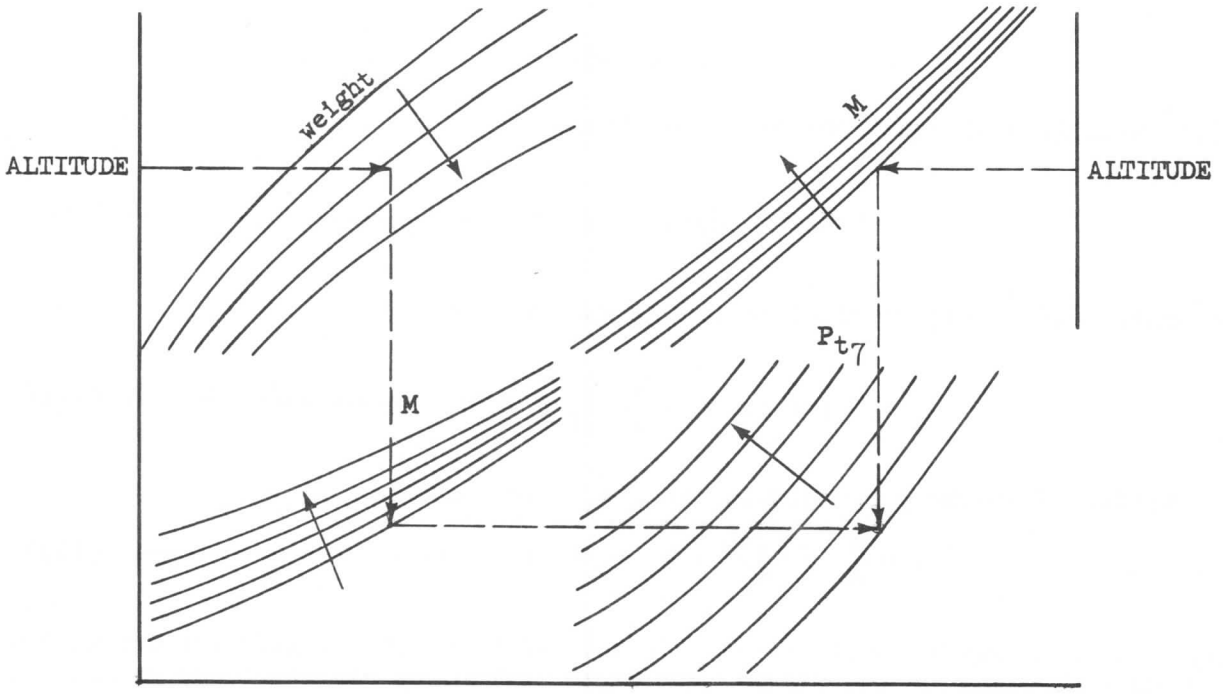

Figure 144.

3-8 DESCENT

Rate of Descent - General

Descent derivations and calculations are very similar to climb performance . When the thrust available is greater than the thrust required for level flight, the airplane must either accelerate or climb. When the thrust available is less than the thrust required, the airplane must decelerate or descend. The general equations for descent may be derived from Figure 145.

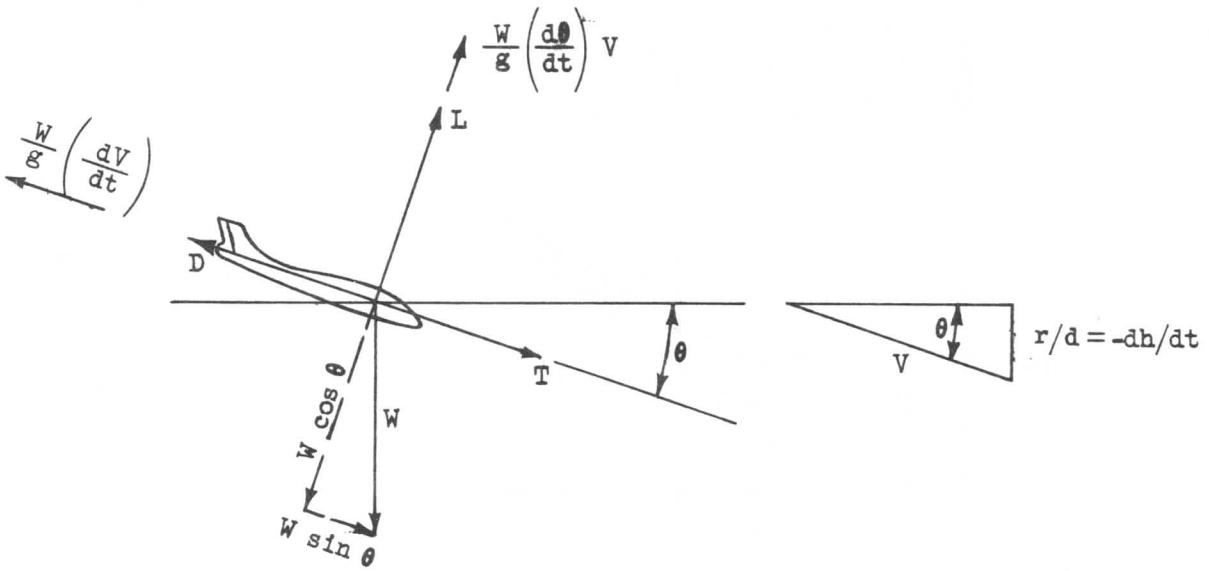

Figure 145.

The following general equations can be written:

$$r/d = -\frac{dh}{dt} = V \sin\theta \qquad (151)$$

The summation of forces parallel to the flight path is:

$$T - D + W \sin\theta - \frac{W}{g}\frac{(dV)}{(dt)} = 0 \qquad (152)$$

The summation of forces perpendicular to the flight path is:

$$L + \frac{W}{g} V\left(\frac{d\theta}{dt}\right) - W \cos\theta = 0 \qquad (153)$$

Again, if the assumption that was made in the climb section is made here; that is, if the rate of change of the flight path angle, $d\theta/dt$, is assumed to be small; then equation (153) becomes:

$$L = W \cos\theta \qquad (154)$$

During normal descents, θ is small and $\cos\theta$ may be considered unity. Equation (153) then reduces to L = W. However, if θ is large, such as during an emergency descent, the relationship expressed in equation (154) must be used to obtain accurate results.

From equation (151),

$$\sin\theta = -\frac{1}{V}\frac{dh}{dt}$$

Substituting the above equation into equation (152), results in:

$$T - D - \frac{W}{V}\frac{(dh)}{(dt)} - \frac{W}{g}\frac{(dV)}{(dt)} = 0$$

This equation may be rearranged and each term multiplied by V/W.

$$\frac{V\,(T-D)}{W} = \frac{V}{g}\frac{(dV)}{(dt)} + \frac{dh}{dt} \qquad (155)$$

But,

$$\frac{dV}{dt} = \frac{(dV)}{(dh)}\frac{(dh)}{(dt)}$$

Substituting this relationship into equation (155), the following expression is written:

$$\frac{V\,(T-D)}{W} = \frac{V}{g}\frac{(dV)}{(dh)}\frac{(dh)}{(dt)} + \frac{dh}{dt}$$

or,

$$\frac{V\,(T-D)}{W} = \frac{dh}{dt}\left[\frac{V}{g}\frac{(dV)}{(dh)} + 1\right]$$

Rewriting,

$$\frac{dh}{dt} = \frac{V\,(T-D)}{W\left[1 + \frac{V}{g}\frac{(dV)}{(dh)}\right]} \qquad (156)$$

This is the same equation as was derived in the climb section. However, from equation (151),

$$r/d = -\frac{dh}{dt}$$

Thus, when equation (151) is substituted into equation (156), the general descent equation becomes:

$$r/d = \frac{V\,(D-T)}{W\left[1 + \frac{V}{g}\frac{(dV)}{(dh)}\right]} \qquad (157)$$

In equation (157), r/d and V are expressed in terms of ft/min. To make this more usable with available data, the velocity, V, may be expressed in knots and the equation adjusted by the conversion factor 101.28. The resulting equation is:

$$r/d = \frac{101.28\ V_k\ (D-T)}{W\left[1+\frac{V}{g}\frac{dV}{dh}\right]} \qquad (158)$$

or,

$$r/d = \frac{66{,}987\ \sqrt{\theta}\ M\ (D/\delta - T/\delta)}{\left[1+\frac{V}{g}\frac{dV}{dh}\right](W/\delta)} \qquad (159)$$

From equation (158), it can be seen that to obtain the rate of descent at a constant true airspeed, the thrust available and required for a given altitude and speed condition must be known. These data can be obtained from the speed-thrust grids as shown in Figure 146.

Maximum rate of descent will occur at a speed where $\Delta(D/\delta)$ multiplied by M is largest. From Figure 146, it can be seen that maximum descent rates will be obtained by flying at maximum speeds.

To obtain the greatest range while in descent, the descent glide angle, θ, must be minimum. From equation (151),

$$\sin\theta = \frac{r/d}{V} \qquad (160)$$

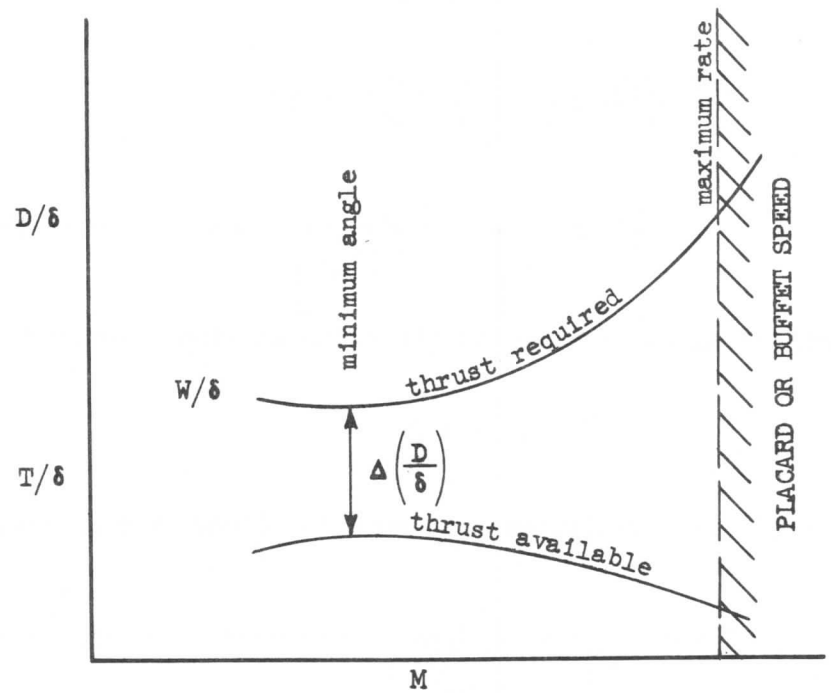

Figure 146.

Therefore, for θ to be minimum, $\frac{r/d}{V}$ must be a minimum. Considering $dV/dh = 0$, equation (157) can be written:

$$r/d = \frac{V\ (D\ -T)}{W}$$

Substituting the above in equation (160):

$$\sin \theta = \frac{r/d}{V} = \frac{V}{V}\ \frac{(D-T)}{W} = \frac{D-T}{W} \qquad (161)$$

This equation states that the minimum glide angle, θ, will occur at a speed where D-T (or $D/\delta - T/\delta$) is minimum. In Figure 146, this is the point where the thrust available and thrust required lines are parallel.

Using data obtained from the speed-thrust grids, rate of descent may be calculated and plotted as shown in Figure 147. This figure shows variation in descent rate for varying speed and weight at a given altitude and thrust setting.

Several interesting facts are apparent from Figure 147:

(1) Minimum glide angle at a given altitude is approximately the same for all weights. If thrust were zero, minimum glide angle would be exactly the same for all weights and would occur by gliding at the maximum lift/drag ratio.

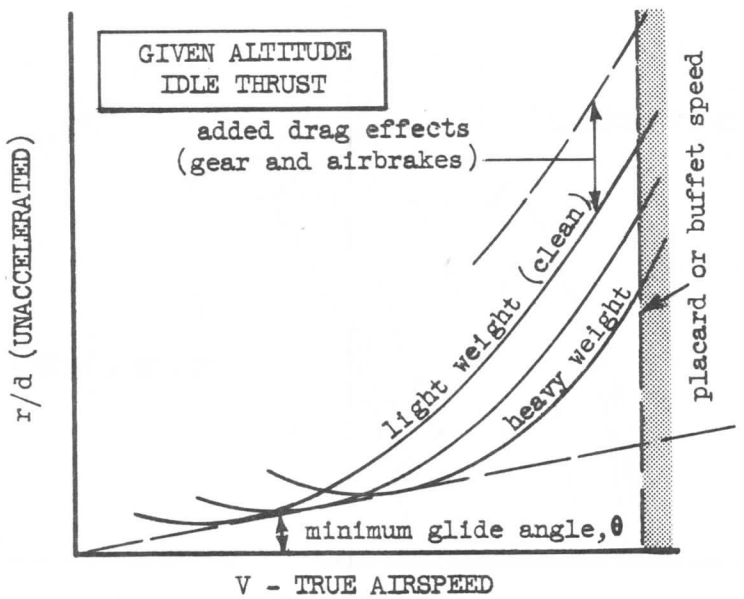

Figure 147.

(2) The speed to maintain a minimum glide angle increases with weight. This is necessary to be consistent with the statement in item (1), since as weight is increased a higher speed is required to keep the same lift/drag ratio.

(3) Maximum rate of descent will be obtained at highest possible airspeed.

(4) At any constant high speed, the rate of descent is higher for light weights than for heavy weights. This, again, is a function of the lift/drag ratio of the airplane.

(5) The effect of adding drag by lowering the landing gear or raising the speed brakes is to increase the rate of descent. This technique is used for emergency descent.

Operating a jet airplane at low altitude imposes a large penalty in fuel consumption and range. Therefore, it is desirable to remain at cruise altitude until it is definitely determined that a landing can be made shortly after descent. High rate descents introduce pressurization considerations which will be discussed later.

Minimum glide angle descent curves may be obtained by calculating rate of descent for varying airspeeds, altitudes, and weights, and plotting these as in Figure 147. The speed schedule and rates of descent are then determined by the points of tangency on each curve with a straight line drawn through the origin. Flying the speed schedule for minimum glide angle in descent does not necessarily yield maximum over-all range except in the special case of all engines inoperative (T = 0).

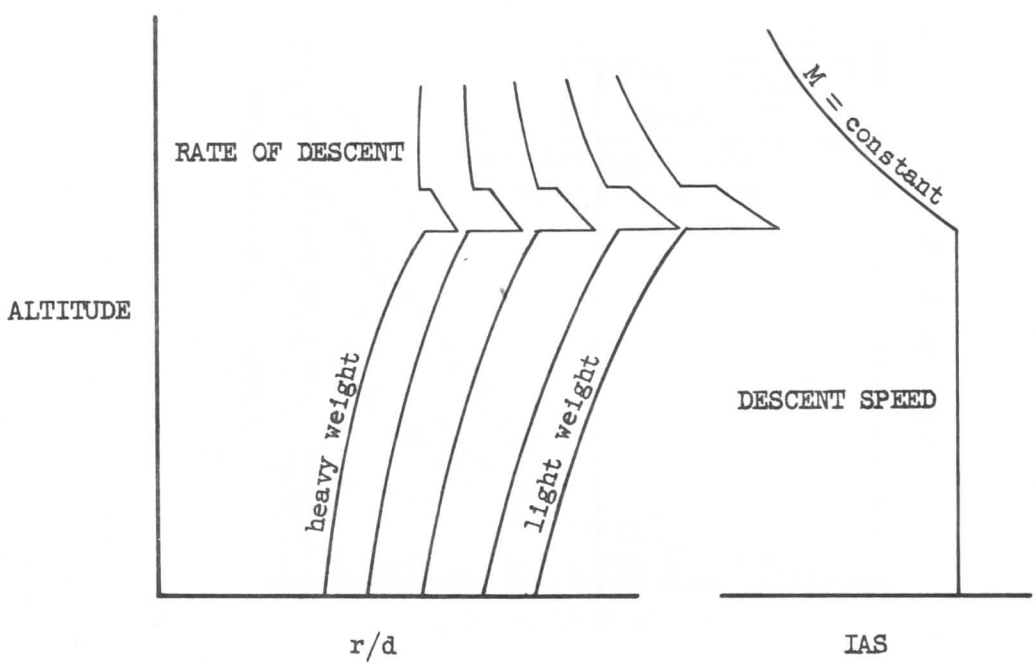

Figure 148.

Descent Range, Time, and Fuel Used

For flight planning purposes, plots which show descent prediction data (such as range, time, and fuel used) are required. Since rates of descent are known and plotted versus altitude as in Figure 148, the time in descent may be obtained by step integration in the same manner as time to climb. The descent range is merely average velocity times the time in descent. Fuel used is fuel flow multiplied by the time in descent. Below is a typical tabulation for determination of these data.

h_1 to h_2	h_{avg}	Δh	r/d_{avg}	Δt	$\Sigma\Delta t$	V_{avg}	ΔR
(1)	(2)	(3)	(4)	(5)	(6)	(7)	(8)
Select	average	$h_2 - h_1$	Fig. 148	(3) ÷ (4)		Fig. 147	$\frac{(5)x(7)}{60}$

$\Sigma\Delta R$	$W_{f_{avg}}$	ΔF	$\Sigma\Delta F$
(9)	(10)	(11)	(12)
	Engine Data	$\frac{(5)x(10)}{60}$	

Given Weight (initial)
Given Speed Schedule
Clean Configuration

Figure 149.

Final data may appear as shown in Figure 150. The weights shown are those existing at the start of the descent.

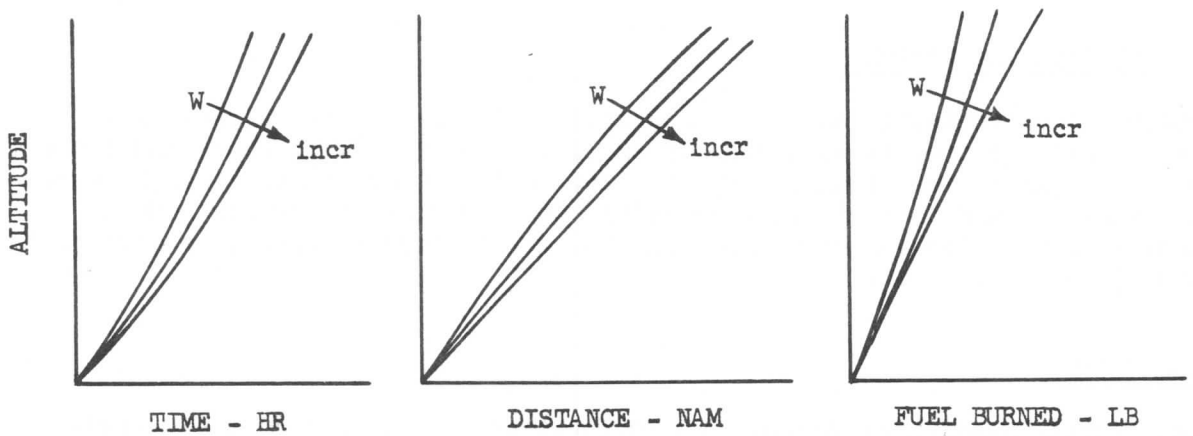

Figure 150.

High Rate Descents

Normal high rate descents will be made at high airspeeds with the rate of descent limited by cabin pressurization requirements. The cabin pressurization requirement is that change in cabin pressure equal to a rate of descent considered acceptable for passenger comfort. Since a sea level cabin altitude can be maintained at all airplane altitudes up to approximately 22,500 feet, it follows that the airplane rate of descent is limited only by the airplane structural and performance limits at these low altitudes. However, when the cabin altitude is not that of the field to which the airplane is descending, as would occur at high altitudes, the rate of descent will be governed by the time it takes to reduce the cabin altitude at a particular rate. A pressure change in the cabin equivalent to a rate of descent of 300 feet per minute at sea level has been selected. To maintain this pressure change at high altitudes requires a decrease in rate of descent with a corresponding increase in thrust required. These thrust requirements are high enough to make it necessary to operate the engines at thrust ratings above idle. This increase in thrust affects the time, range, and fuel burned.

The speed schedule chosen is one of either constant Mach number at the higher altitudes or a constant indicated airspeed at the lower altitudes. The exact speed schedule selected is of necessity determined by the cabin pressurization requirements establishing the maximum rate of descent.

Thrust Presentation

During emergency descents, the thrust levers will be in the idle position. The same is true for normal descents except that at high altitudes some engines require a small increase in thrust to take care of cabin pressurization requirements. These are usually given on the descent charts as constant values of EPR. Therefore, thrust setting charts are not required. If, however, thrust EPR's or P_{t_7}'s are required for power-on descents, they may be obtained from the climb or cruise thrust setting charts.

3 - 9 APPROACH AND LANDING

The problem of determining landing performance is in most respects similar to the takeoff calculation, varying only in the treatment of the approach and flare and in the consideration of auxiliary stopping devices such as the speed brakes. Detailed analysis and derivation of equations will be omitted for portions of the landing calculations which are similar to takeoff except perhaps in algebraic sign and limits.

Approach Climb

When calculating landing performance, consideration must be given to a missed-approach where a go-around has to be performed with the airplane in the approach configuration. FAR 25.121(d) requires calculation of climb gradient where V_S in this approach configuration does not exceed 110% of the V_S for the related landing configuration; the steady gradient of climb may not be less than:

2.1 percent for two-engine airplanes,

2.4 percent for three-engine airplanes, and

2.7 percent for four-engine airplanes,

with, (1) the critical engine inoperative, the remaining engines at takeoff thrust, (2) the maximum landing weight, (3) a climb speed not exceeding $1.5V_S$, and (4) landing gear retracted. Normal all-engines-operating procedure has to be considered. A climb speed near the maximum gradient of climb is selected, approximately 145% V_S.

Landing Climb

Landing-climb gradient charts have to be calculated for go-around with the airplane in the landing configuration where all engines are considered to be operating and the landing gear is extended. FAR 25.119 requires the steady gradient of climb not to be less than 3.2 percent with: (1) The engines at the thrust that is available 8 seconds after initiation of the thrust control from the minimum flight idle to the takeoff position, and (2) a climb speed of not more than 1.3 V_S. A climb speed near the maximum gradient of climb speed is selected, approximately equal to 120% V_S.

Chart presentation of climb gradient is similar to the climb gradient charts that were discussed during takeoff and climbout.

Approach and Flare

The term "approach", as used here, applies only to the air distance from an altitude of 50 feet to touchdown. This air distance consists of two parts:

(1) A steady-state glide path where the airplane is in the final landing configuration prior to touchdown, and

(2) the flare.

it would be said to have elevator-free stability. And if the floating angle were to exceed the requirement such that the pilot would find it necessary to supply a push force, the plane would be unstable in elevator-free flight.

Figure 151 is a sketch of the glide path and shows that the flare is assumed to be a circular arc of radius R. Remembering that γ is a small angle:

$$S_A = \frac{50}{\gamma} + \frac{R\gamma}{2} \qquad (162)$$

since for small angles $\cos\gamma = 1$ and $\sin\gamma \approx \tan\gamma \approx \gamma$ in radians. V is assumed to be constant during the approach glide. An expression for γ and R has to be determined.

$$D = T + W\sin\gamma$$

$$L = W\cos\gamma$$

$$\sin\gamma = \frac{D-T}{W}$$

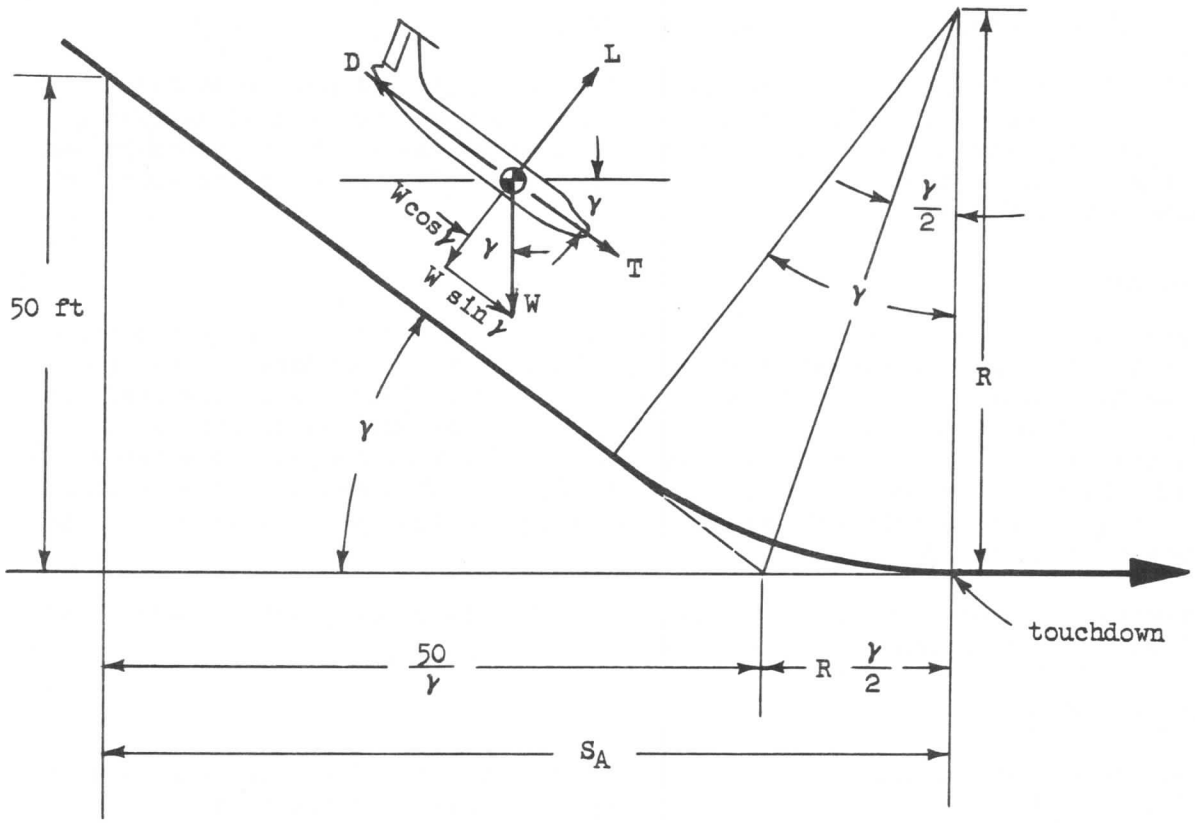

Figure 151.

The acceleration normal to the flight path needed to flare is attained by rotating the airplane to a higher C_L value, say C_L'. The lift force during flare is,

$$L' = C_L' \frac{\rho_o \sigma}{2} SV^2$$

The force normal to the flight path is,

$$F_N = L' - W \cos \gamma = L' - W$$

But during the glide,

$$W \cong L = C_L \frac{\rho_o \sigma}{2} SV^2$$

Therefore,

$$\frac{L'}{W} = \frac{C_L'}{C_L}$$

and,

$$F_N = W \frac{C_L'}{C_L} - W$$

$$F_N = W\,(n-1)$$

since $C_L'/C_L = n$, where n is load factor. The maximum value of n which may be applied to C_L is dictated by stall or buffet limits.

Acceleration normal to the glide path is:

$$a_N = V\,\frac{d\gamma}{dt}$$

and,

$$V = R\,\frac{d\gamma}{dt}$$

therefore,

$$a_N = \frac{V^2}{R}$$

$$F_N = \frac{W}{g}\,a_N$$

Thus,

$$F_N = W(n-1) = \frac{W}{g}\,\frac{V^2}{R}$$

or,

$$R = \frac{V^2}{g(n-1)}$$

But,

$$V^2 = \frac{L'}{S}\;\frac{2}{\sigma\rho_o\,C_L'}$$

or,

$$V^2 = \frac{nW}{S}\;\frac{2}{\sigma\rho_o\,C_L'}$$

Therefore,

$$R = \frac{W}{S}\;\frac{2n}{\sigma\rho_o\,C_L'}\;\frac{1}{g(n-1)} \qquad (164)$$

Collecting the information in equations (162), (163) and (164), and remembering that:

$$C_L' = nC_L$$

$$S_A = \frac{50}{\left(\frac{C_D}{C_L} - \frac{T}{W}\right)} + \frac{W/S\;\left(\frac{C_D}{C_L} - \frac{T}{W}\right)}{\sigma\rho_o\;g(n-1)\;C_L} \qquad (165)$$

The distance S_A can be varied by assuming values of n from 1 to that corresponding to $C_{L_{MAX}}$ or $C_{L_{buffet}}$ (which will affect the flare) and varying the rate of descent or γ (which will affect both approach and flare). Many rates of descent

can be selected and distances calculated from the minimum at $C_{L_{MAX}}$ to large values in a very flat approach. A 707 airplane, with high rates of descent available due to aerodynamic characteristics, can approach and land at very high angles and in very short "over the fence" distances. F.A.R. rules permit such profiles in the authorized performance manual but provide for increasing the field lengths by a factor of 1.667 to allow for more normal service operation to destination airports. The 707 can land with a final approach descent rate of over 20 ft/sec but a nominal value as demonstrated is used in landing calculations. The normal value of n used in flare is approximately 1.2.

The above method for analyzing the landing air distance has been used on all Boeing jet transports since the 707-120 certification. A simpler method which will give the same answers has recently been developed. This method is to average the demonstrated times from 50 feet to touchdown (essentially an average rate of descent). Distance is the product of average time and average velocity.

$$S_A = 1.688 \frac{V_{app} + V_{T.D.}}{2} \Delta t_{air}$$

$$S_A = .844\, V_{app} \left[1 + \frac{V_{T.D.}}{V_{app}}\right] \Delta t_{air} \qquad (166)$$

where,

V_{app} = approach ground speed at 50 feet, knots.

$\frac{V_{TD}}{V_{app}}$ = ratio of touchdown to approach speed for all air distances with a given flap setting.

Δt_{air} = the average time from 50 feet to touchdown for all air distances with a given flap setting, sec.

During past airplane certification, the touchdown speed was specified to be the same as the approach speed, 1.3 V_S. Since actual flight conditions show a speed decrease of approximately 5 knots during landing flare, this reduction in touchdown speed is now being accounted for in the landing distance calculations.

Ground Run

Derivation of the expression for ground run is not included because it is given for takeoff ground run in Chapter 3.5. The analysis is very similar except that the ground run consists of two parts:

(1) A short ground run (approx. 2 seconds) immediately following touchdown while the airplane is being changed from landing configuration to braking configuration. During this period the airplane is in normal ground attitude in the landing configuration, no brakes. This landing transition distance, using the average transition speed, becomes:

$$S_{TRAN} = 1.688 \frac{V_{TD} + V_B}{2} \Delta t_{TRAN} \qquad (167)$$

where,

V_{TD} = speed at touchdown, knots.

V_B = speed at full braking configuration, knots.

Δt_{TRAN} = the transition time from touchdown to full braking configuration, sec.

(2) The remaining ground run which brings the airplane to a complete stop The C_L and C_D values used include the use of stopping devices such as air brakes and the friction coefficient which corresponds to full wheel brakes as established from flight test. For estimated performance, $\mu = 0.3$ is used. Full ground effects on lift and drag are used.

The calculation of the ground-run braking distance is:

$$S_B = 2.849 \int_{V_B}^{V_W} \frac{(V - V_W)}{a} \, dV \qquad (168)$$

where,

V_B = initial braking speed in knots.

V_W = headwind in knots.

a = deceleration rate in ft/sec^2.

The acceleration formula, as derived in the takeoff section, may be used.

$$a = \frac{g}{W}\left((T - \mu_B W) - (C_D - \mu_B C_L)\frac{\sigma V^2 S_W}{295.37} - W\phi\right) \qquad (169)$$

where T is idle thrust, V is in knots, and ϕ (in radians) is positive for uphill slope.

The calculating procedure is identical with that used for segment E of the takeoff run. In fact, a study of the expressions used in the analysis of the takeoff ground run will suggest the application of the same analysis to the landing technique.

The total distance from a 50-ft clearance to touchdown, plus the rolling distance on the ground before braking, plus the rolling distance after braking forms the landing distance from a 50-ft clearance height. This distance multiplied by 1.667 determines the F.A.R. field length for a destination airport for a standard-day condition. The F.A.R. field length is used as one of the criteria to establish the landing weight, and a presentation is shown in Figure 152. A similar presentation for the distance from a 50-ft clearance height can be presented.

Wet FAR Landing Field Length

The FAR Landing Field Length for wet runways is equal to 115% of the FAR Landing Field Length for dry runways unless it can be demonstrated to be less, but never less than the dry FAR Landing Field Length. The demonstrated values will be equal to 115% of the wet stopping distance subject to the following conditions:

(1) The landing is preceded by a steady gliding approach not to exceed an angle of 3 degrees down to the 50-foot height and at a calibrated airspeed not less than 1.4 V_S.

(2) The time lapse between the 50-foot height and touchdown is not less than seven seconds.

(3) The landing is made on a level, smooth, hard-surfaced, wet, well-soaked runway.

(4) The wheels are fitted with tires that have been worn to a point where no more than 20 percent of the original tread remains.

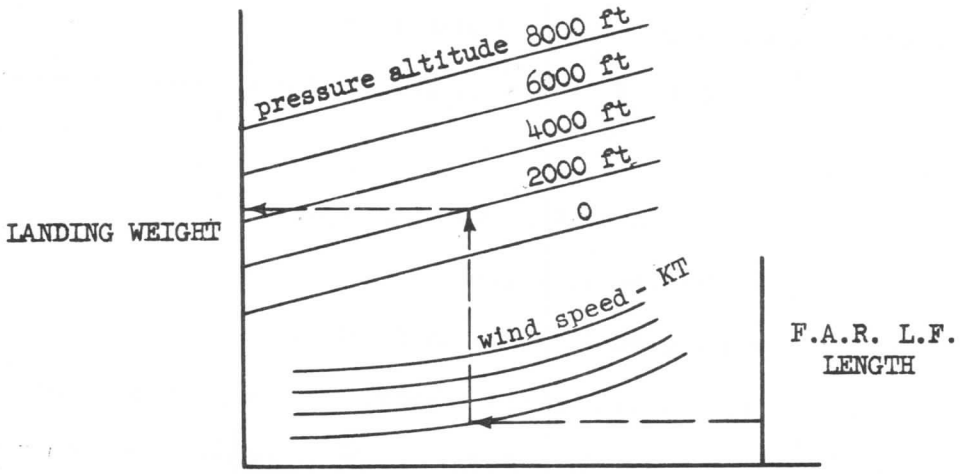

Figure 152.

SECTION 4

STABILITY AND CONTROL

SECTION 4

STABILITY AND CONTROL

4-1 INTRODUCTION

When thinking about flying qualities, the general aspects of stability and control, one must consider a much wider spectrum of concern than he normally does when thinking of performance. In general, he is concerned with two things:

1. Once a flight pattern is established, how often and to what degree must the pilot interfere or adjust the controls to maintain the original flight condition?

2. What type of action and what degree of action is needed by the pilot to change to a new flight condition?

The first of these questions is a very brief and simple statement of the stability problem. It asks whether the aircraft has a tendency to follow a prescribed straight and level course without pilot interference. This we usually call stability. However, there is also the consideration of how much of an outside influence is needed to cause an upset, or, put another way, how large a change in the condition will a given influence produce. Also, we must consider how long it takes to restore the equilibrium condition after it is upset. The designer is interested in studying what hinders or facilitates ease of maintaining the prescribed course. He must know if the inherent flying qualities of his craft are such as to induce structural stresses of unacceptable magnitude. Nor can he overlook the possibility that inept pilot interference could reduce stability instead of helping.

The second question deals with the possibility of maneuvering an aircraft into and along a chosen flight path; what types of control mechanisms are needed, their size and adequacy, and the compatibility of their demands upon the pilot with his abilities to meet these demands.

Relative stability and adequacy of control are of much more imminent concern in the design and operation of flying craft than in most other transport vehicles. While the airplane flies in a 3-dimensional space and is free to translate parallel to 3 axes and to rotate in 3 planes, the automobile, for example, can be steered with respect to only 2 axes and rotate in only 1 plane. In fact, some vehicles such as trains and other rail-guided equipment have no steering at all! The aircraft flies, is supported, and is even controlled in response to dynamic reactions to the controlled movement through the air. This reaction is much more complex than the more simple concepts of bouyancy and road reaction. Also, the speeds of most modern aircraft are so high as to impose very severe demands upon both the craft and the pilot, whether human or otherwise.

It is only natural that the study of flying qualities of aircraft occupies a very large place in the development of flight sciences. The subject is not complete, and its presentation is usually simplified. Even to define the movements of the airplane in an adequate way is very difficult. For this involves describing the movements through a non-stationary airmass of an elastic body of variable configuration and mass subject to aerodynamic, propulsive and gravitational forces. There is no reason to believe that such a task would be possible without the use of the most complex mathematics available. Nor is it valid to assume that standard simplifications can be applied to the calculations until they have been validated by experimental techniques.

SECTION 4

STABILITY AND CONTROL

The mathematics involved requires the development of (1) force equations to relate translations of the total mass to the external forces applied to it, (2) moment equations to relate its rotational motions to the moments evolved by the interaction of the external forces, and (3) elastic equations to relate the effects of deformations of the structure to the loading imposed upon it. The first category is of primary interest in the calculation of performance where the emphasis is directed toward defining large-scale, long-period translational effects; where moments and elastic deformations are of interest only in so far as they interact to impose secondary changes in the force equations. All three of the categories above lie within the scope of stability and control problems as they apply over short time periods compatible with the reaction times of the pilot-control systems involved. Moment effects and body rotations are of dominant interest. Aeroelasticity is concerned with vibration, flutter, and other short period motions which are usually best defined by elastic equations but may involve the others also. Thus the three fields and their studies are not independent and separately defined; the areas of overlap demand that the study of stability and control involve such topics as steady turning flight, normally a performance problem, and the response to air turbulence, normally considered to be an aeroelastic problem.

Relative stability and adequate control are designed into modern aircraft by using a number of analytic and experimental techniques. First, the complex behavior of the proposed craft is analytically defined in terms of systems of mathematical equations determined by theory, past experience, and analog computation. Next, wind tunnel testing defines the various parameters and coefficients needed as input data to solve the mathematical systems for the specific configuration proposal. And finally, the airplane is rigorously flight tested to verify the flying qualities expected, to eliminate any imperfections or unforseen problems, and to point out areas of improvement in design.

All of this discussion so far has centered on the airplane system as an isolated mechanical unit handled in a uniform manner by a control device. However, no aircraft being complete without its pilot, the extreme variation in human pilots and their flying techniques make it impossible to completely define the machine-man combination. For this reason as much as because of the inadequacy of our abilities to understand all of the fundamental reactions themselves, regulatory and monitoring agencies have set up only a few minimum standards in the form of criteria for response to command and force necessary to control. The flying qualities and properties of an aircraft are quite subjectively defined; in many cases the criteria for determining such things have no more firm bases then the opinion of the test pilot. Even though very precise instruments may be available to measure certain effects, there may be no agreement as to the value of the reading to be sought. Until there is available a more complete understanding of the total force-response complex of flight, of the mathematical tools and equations needed to define it, and of the human reactions to the demands of controlling it, the study of the stability and control of aircraft will continue to be a matter of opinion and debate as much as one of scientific definition.

The subject of stability is generally divided into two regimes: static stability, and dynamic stability. An example of static stability is shown in Figure 1 which shows a ball placed on three types of surfaces.

On the concave surface if the ball is displaced from the center it will tend to return to its original position of equilibrium. This condition is known as stable. If the ball is placed on a flat surface and displaced as before it will exhibit no

tendency to roll either back to or away from its original position. It is then said to be neutrally stable. Finally, if the ball is placed on the convex surface and displaced it will tend to move away from its original position. It is then said to be unstable.

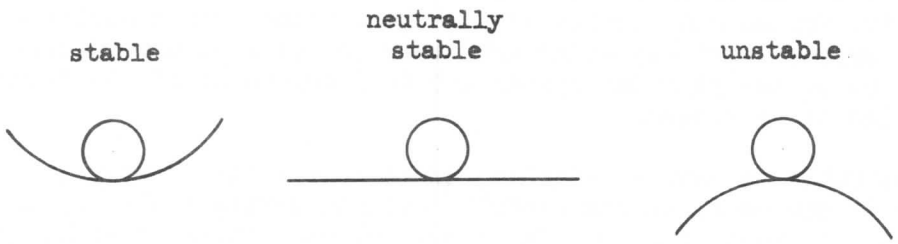

Figure 1.

Dynamic stability is associated with continued motion of the body and, in particular, with just how this motion varies with time. In the case of the ball on the concave surface after an initial displacement has been made, if there were no frictional forces acting, the ball would theoretically oscillate forever. It would then be said to have neutral dynamic stability. If there were frictional forces between the ball and the surface (which forces always oppose the motion), the motion would be found to "damp out" (that is, subside with time), and the ball would be dynamically stable. If there were some other force acting on the ball which would overcome the friction force (such as blowing on the ball in the direction of motion), the ball would either depart from or oscillate with ever-increasing amplitude about its neutral position. It would be said to be in dynamically divergent oscillation. The plot in Figure 2 shows the time history of these dynamic situations. It should be noted that although curves (a), (b) and (d) are different from a dynamic standpoint, they are all statically stable since their displacements do come back to zero at some time. Curve (c) shows static instability as well as divergence since at no time does the displacement tend towards zero again after the initial displacement.

The above physical example, so simple in its concept, should not confuse the student into thinking that static stability is defined only in terms of static equilibrium. The initial equilibrium condition may be one of uniform motion in a straight line such as that of a trimmed airplane flying at constant speed along a straight-line course. If after being upset from this uniform flight condition, the airplane tends to return to the same flight path and speed without pilot action, it is statically stable.

SECTION 4

STABILITY AND CONTROL

In considering the stability of an airplane it is convenient to break down the over-all stability picture into three types of stability. These are associated with the three principal axes of the airplane which are defined by three mutually perpendicular planes passed through some convenient point, often the center of gravity of the airplane, since this choice tends to simplify the mathematical development. See Figure 3. These axes are: (1) The Longitudinal Axis (also called the X-axis or Roll Axis) which passes fore and aft through the fuselage; (2) The Lateral Axis (also called the Y-axis or the Pitch Axis) which passes through the airplane from one side to the other; (3) The Vertical Axis (also called the Z-axis or the Yaw Axis) which passes through the airplane from top to bottom. If it is found that the forces and moments acting about these axes describe a stable system, stability exists about any other arbitrary set of axes also, since stability is a function of the physical system and is independent of the frame of reference from which it is viewed.

Although it is desirable to have an airplane quite stable for safety, it is not essential in that it can be flown successfully without having stability in all degrees of freedom. In fact, the very factors which contribute to stability preclude ease in maneuvering. For this reason, some light airplanes meant for racing and aerobatic work have been deliberately designed with neutral stability, or even to be statically unstable in certain areas. Sometimes it is more important to have superior control than it is to have stability. It is a matter of compromise, choosing a balance of the two to suit the job.

To maintain flight within reasonable aerodynamic regimes and the structural limits of the airplane, the pilot must have control over the flight parameters. He must be master of the rates of change in flight attitude, velocity and course heading. Control, then, is the ability to exert the necessary influence over pitch, sideslip, roll and speed by manipulation of elevators, stabilizer, rudder, ailerons, spoilers, flaps and thrust lever.

The pilot's linkages to the control surfaces are always designed to be as simple and direct as possible for the sake of safety and ease of maintenance. They must be coordinated one with the other. They must be effective enough for maximum utility and ample in all planes of motion, and they must be sensitive enough to give the pilot a "feel" for the relative amount of control being exerted. Yet, at the same time, there must be only such forces needed that the pilot may be able to do his job without unduly taxing his strength and endurance. The greater the demands upon the airplane in terms of speed, size and versatility, the more acute these control problems become.

4-2 STATIC STABILITY

Longitudinal Stability

Longitudinal stability is concerned with the motion of the airplane about the Y- or pitch-axis. If an angular displacement from equilibrium is made about this axis, stability requires that a resulting pitching moment must be generated in a direction to cause equilibrium to be restored. That is, a displacement in a climbing direction must be resisted by a diving moment and diving by a climbing moment.

Previously, in Section 1, the general equation for aerodynamic pitching moment was

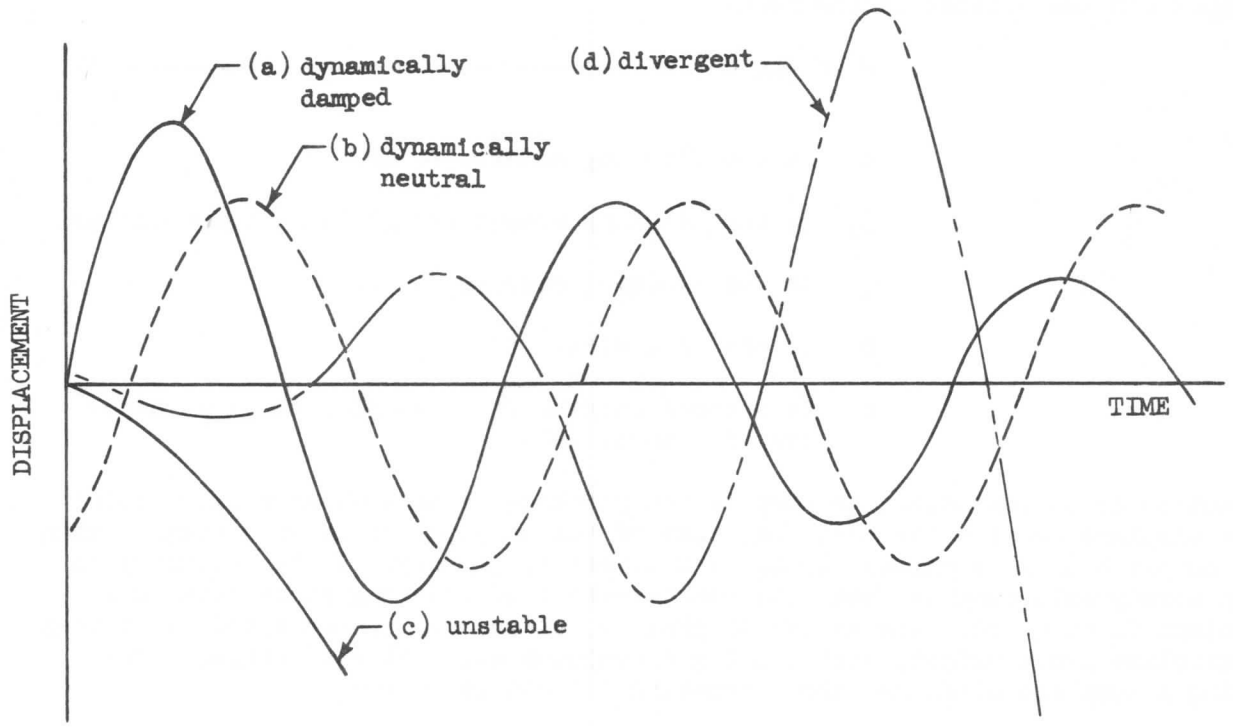

Figure 2.

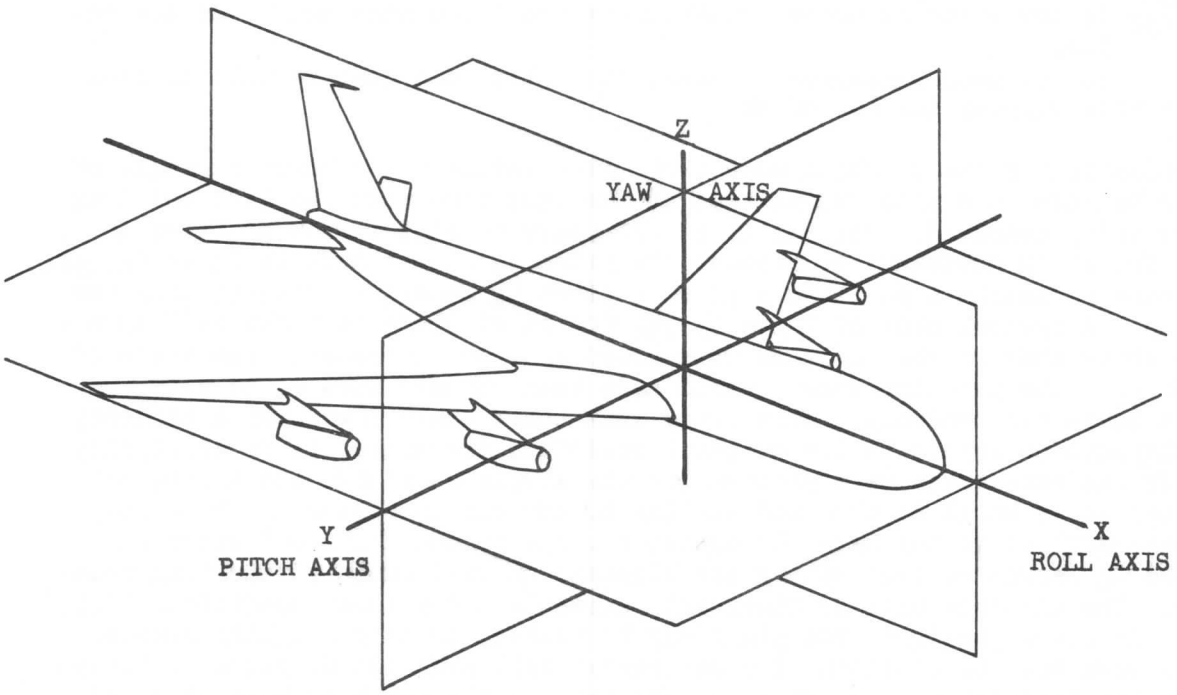

Figure 3.

developed and was written in the form:

$$M = C_m q S c \qquad (1)$$

where,

M is the pitching moment, ft lb,

C_m is the pitching moment coefficient, dimensionless

q is the dynamic pressure, lb/ft^2

S is the wing area, ft^2

c is a chord length, ft., (usually the mean aerodynamic chord, MAC.)

In practice it is convenient to compute the pitching moments about a fixed point on the airplane despite the fact that some of the computation is more complex than when the pitch axis is passed through the center of gravity. It is customary to sum up aerodynamic moments about the quarter-chord of the wing since this is a convenient fixed point. The center of gravity, of course, is not fixed; it varies with airplane gross weight, with loading techniques and with fuel usage. Considering a complete airplane, then, equation (1) can be written:

$$M_{.25\bar{c}} = C_{m.25\bar{c}}\ q S \bar{c} \qquad (2)$$

where $M_{.25\bar{c}}$ is the aerodynamic pitching moment about the quarter MAC point, ft lb
$C_{m.25\bar{c}}$ is the pitching moment coefficient about the same point, dimensionless
$\bar{c}$ is the mean aerodynamic chord, ft. This nomenclature will be used throughout this chapter instead of MAC.

The determination of the pitching moment characteristics with change in angle of attack can be made in a wind tunnel test at the same time that the lift and drag forces are being measured. Whereas it is customary to plot curves of C_L vs α, and C_L vs C_D, it is customary to present the pitching moment data as C_L vs $C_{m.25\bar{c}}$. By convention we assign a positive sign to a pitching moment tending to nose the airplane up. A typical plot of C_L vs $C_{m.25\bar{c}}$ for an airplane is shown in Figure 4. This plot shows that if the airplane were nosed up (thus increasing the angle of attack, or C_L), the pitching moment would have been changed such as to give the airplane a nose-down tendency. This means that there would have been a tendency for the airplane to return to its original position; therefore, it is statically stable. If the same curve were plotted for the airplane without its horizontal tail, another curve would be obtained similar to the one in Figure 4. This so-called "tail-off" curve may have the opposite slope to the "tail-on" curve in some of the C_L regime so that nosing the airplane up will cause a resulting nose-up moment. The airplane will be statically unstable under these conditions (C.G. at $.25\bar{c}$). In other portions, the plane may be neutral or only slightly stable. Thus it is seen how the addition of a horizontal tail aids the airplane in becoming stable longitudinally. In addition, the tail is the means of balancing and controlling the airplane, as will be shown later.

In order to investigate the stability of an airplane about the pitch axis it is

conventional to set up an equation expressing the relationship between the moments acting about this axis. If the airplane is studied in a steady-state equilibrium condition, forces in the other two planes, being symmetrically equal, can be neglected. Even in dynamic maneuvering conditions, the interacting lift and pitch effects of the symmetrical plane forces and moments are quite small. Consider Figure 5 which depicts the pertinent forces, moments and geometry.

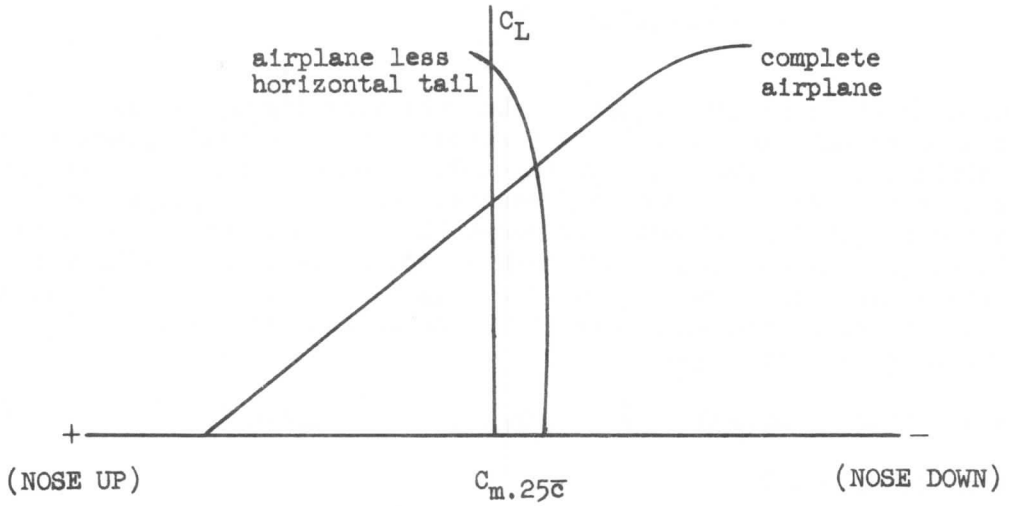

Figure 4.

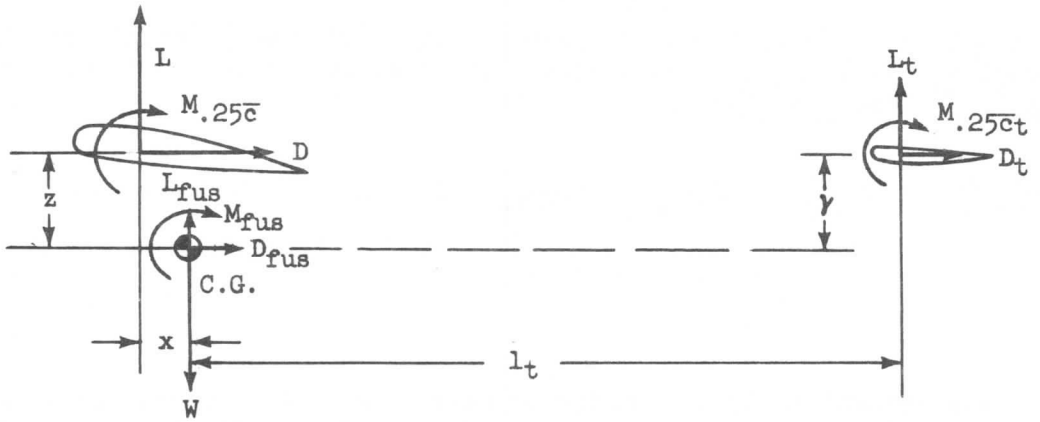

Figure 5.

The aerodynamic characteristics are shown as the lift, drag and pitching moment acting on the body about the C.G., the wing about the $.25\bar{c}$, and the tail about the $.25\bar{c}_t$. The forces, W, L_{fus} and D_{fus} do not contribute to the moment about the C.G. since they act through it. Also, the components involving D_t and $M.25\bar{c}_t$ are small enough to be neglected without significant error. So, summing the remaining moments about the C.G., airplane nose up positive, one may obtain:

$$M_{cg} = Lx + Dz + M_{.25\bar{c}} + M_{fus} - L_t l_t \qquad (3)$$

However,

$$\left.\begin{aligned} L &= C_L S q \\ D &= C_D S q \\ L_t &= C_{L_t} S_t q_t \\ M_{.25\bar{c}} &= C_{m.25\bar{c}}\, qS\, \bar{c} \\ M_{fus} &= C_{m_{fus}}\, qS\, \bar{c} \end{aligned}\right\} \qquad (4)$$

It should be noted in the tail lift equation that the quantity q_t is used. This is to take into account the fact that it is possible for the dynamic pressure at the tail to be different from that at the wing. On a jet airplane there is very little difference between the two dynamic pressures, whereas on a propeller-driven airplane the slipstream can actually cause the q at the tail to be greater than that at the wing. Disregarding slipstream effects, however, q_t will generally be less than q since the inboard portion of the tail can be buried in the boundary layer of the fuselage and in the wing wake, a region of reduced energy, or q. Substituting equations (4) into equation (3):

$$M_{cg} = C_L S q x + C_D S q z + C_{m.25\bar{c}}\, qS\, \bar{c} + C_{m_{fus}}\, q\, S\, \bar{c} - C_{L_t} S_t q_t l_t \qquad (5)$$

Dividing equation (5) by q S $\bar{c}$.

$$C_{mcg} = C_L \frac{x}{\bar{c}} + C_D \frac{z}{\bar{c}} + C_{m.25\bar{c}} + C_{m_{fus}} - C_{L_t} \frac{S_t\, l_t}{S\ \bar{c}} \frac{q_t}{q} \qquad (6)$$

The ratio of the terms q_t/q is given the name of "tail efficiency factor" and is given the symbol η_t. Also $S_t\, l_t/S\ \bar{c}$ is called "tail volume coefficient" and is designated by $\bar{V}$. Thus equation (6) is:

$$C_{mcg} = C_L \frac{x}{\bar{c}} + C_D \frac{z}{\bar{c}} + C_{m.25\bar{c}} + C_{m_{fus}} - C_{L_t}\, \eta_t\, \bar{V} \qquad (7)$$

$$(\eta_t \approx 96\%)$$

$$(\bar{V} \approx .60)$$

We have previously determined that in order to have longitudinal stability an increase in C_L must produce an increase in down (or negative) pitching moment. The slope of the curve, Figure 4, must be negative to produce stability. The slope of the pitching moment curve, rather than being expressed as dC_L/dC_m (which would be conventional, corresponding to dy/dx) is always written as dC_m/dC_L. By differentiating equation (7) with respect to C_L the slope dC_m/dC_L can be found.

$$\frac{dC_{mcg}}{dC_L} = \frac{x}{\bar{c}} + \frac{dC_D}{dC_L}\frac{z}{\bar{c}} + \frac{dC_{m.25\bar{c}}}{dC_L} + \frac{dC_{m_{fus}}}{dC_L} - \frac{dC_{l_t}}{dC_L}\, \eta_t\, \bar{V} \qquad (8)$$

At this point it will be convenient to consider those terms in equation (8) which are small enough to be dropped. Only those items which have a major effect on

stability will be retained. The first term which is found to be small is $dC_{Dz}/dC_L\ \bar{c}$. The reason for this is that dC_D/dC_L is itself a small quantity. Secondly, $dC_{m.25\bar{c}}/dC_L$ will be very small, if not zero, because it is found that in general the 1/4-chord point of the mean aerodynamic chord is very close to the aerodynamic center of the wing. It may be noted that by definition the aerodynamic center is the point about which the pitching moment coefficient is constant with lift coefficient, $dC_{m_{ac}}/dC_L = 0$.

Generally dC_{mfus}/dC_L will be found to be an appreciable quantity, but will also be found to be approximately constant for a given configuration. It is quite likely to be positive in sign, which means that it will destablize the airplane.

Common practice is to combine the wing and body effects into one term $\frac{dC_{mwb}}{dC_L}$; thus, if the moment center is not close to the quarter chord, the effects are still included. Also, it is easiest in the normal testing procedure to combine the two into one parameter.

Equation (8) can now be expressed as follows by dropping out the second term and combining the third and fourth terms on the right hand side.

$$\frac{dC_{mcg}}{dC_L} = \frac{x}{\bar{c}} + \frac{dC_{mwb}}{dC_L} - \frac{dC_{L_t}}{dC_L}\ \eta_t\ \bar{V} \qquad \text{——————} \qquad (9)$$

Let us now consider the term $x/\bar{c}$ in equation (9). By reference to Figure 5 it will be noted that x is the distance from the center of gravity to the 1/4 chord point of the mean aerodynamic chord. The farther aft the center of gravity moves, the more unstable the airplane will become since for positive stability it is required that dC_{mcg}/dC_L be negative. When the center of gravity is in a position aft of the 1/4 MAC, definite assurance of stability can come only from the last term in equation (9). If each quantity in this term has a positive sign, the term itself will be stabilizing since it enters the equation with a negative sign in front of it. We may thus say that the stabilizing influence is produced by this term, that due to horizontal tail.

It is convenient to write the last term of equation (9), in a different form. Consider Figure 6 which shows the tail angle of attack as related to the geometry of the airplane and wing angle of attack. In terms of these quantities it will be found that:

$$\alpha_t = i_t + \kappa$$

$$\kappa = \alpha_w - i_w - \epsilon$$

$$\alpha_t = \alpha_w - \epsilon + i_t - i_w$$

Note that the downwash, ϵ, is used to define conditions at the tail; so it is measured there, not at the wing.

Since, $$C_{Lt} = \frac{dC_{Lt}}{d\alpha_t}\ (\alpha_t - \alpha_{L_{ot}})$$

$$C_{Lt} = \frac{dC_{Lt}}{d\alpha_t}\ (\alpha_w - \epsilon + i_t - i_w - \alpha_{L_{ot}}) \qquad \text——————} \qquad (10)$$

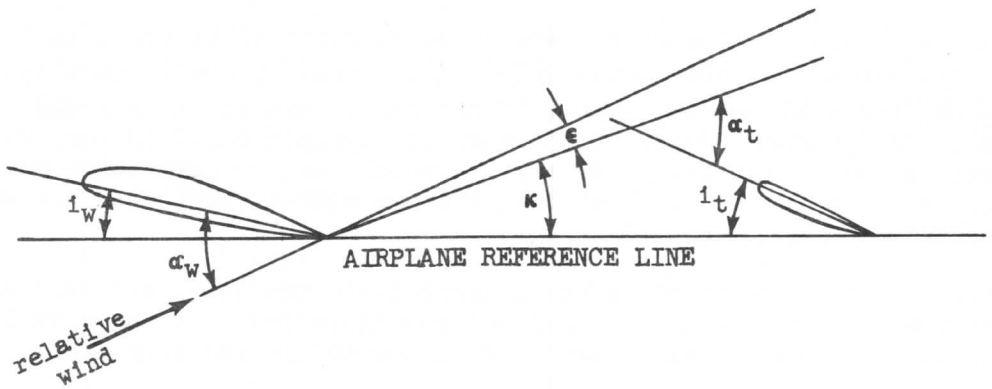

Figure 6.

The last term of equation (9) contains an expression for dC_{Lt}/dC_L; this term may be evaluated by differentiating equation (10) with respect to C_L.

$$\frac{dC_{Lt}}{dC_L} = \frac{dC_{Lt}}{d\alpha_t}\left(\frac{d\alpha_w}{dC_L} - \frac{d\epsilon}{dC_L} + 0 - 0 - 0\right) \qquad (11)$$

(Note that the tail angle of zero lift, and i_t and i_w, the incidence angles of the tail and wing, are constant for any given application.) Equation (11) can now be simplified as follows:

$$\frac{dC_{Lt}}{dC_L} = \frac{dC_{Lt}}{d\alpha_t}\left(\frac{d\alpha_w}{dC_L} - \frac{d\epsilon}{d\alpha_w}\frac{d\alpha_w}{dC_L}\right)$$

$$= \frac{dC_{Lt}}{d\alpha_t}\frac{d\alpha_w}{dC_L}\left(1 - \frac{d\epsilon}{d\alpha_w}\right)$$

$$= a_t \frac{1}{a_w}\left(1 - \frac{d\epsilon}{d\alpha_w}\right)$$

$$\frac{dC_{Lt}}{dC_L} = \frac{a_t}{a_w}\left(1 - \frac{d\epsilon}{d\alpha}\right) \qquad (12)$$

$$\left[1 - \frac{d\epsilon}{d\alpha}\right] \approx .60$$

It is customary to drop the subscript "w" from α in the expression $d\epsilon/d\alpha_w$, recognizing that the α being referred to is that of the wing.

Equation (12) can now be substituted back into equation (9) with the following result:

$$\frac{dC_{mcg}}{dC_L} = \frac{x}{\bar{c}} + \frac{dC_{mwb}}{dC_L} - \frac{a_t}{a_w}\eta_t \bar{V}\left(1 - \frac{d\epsilon}{d\alpha}\right) \qquad (13)$$

Examine the last term in this equation to find out just how each item affects the stability of the airplane, remembering that since the term is stabilizing, the larger it is the more stabilizing it will be. The first item is a_t/a_w, the ratio of the slopes of the tail and wing lift curves. If the wing lift curve slope is already fixed, then the greater the slope of the tail lift curve, the greater will be the airplane stability. The slope can be increased by making the aspect ratio larger, or by effectively making it larger by end-plating the tail with two vertical tails (as in the B-24). The second item is η_t, which is the ratio of the q at the tail to the q at the wing. Increasing q at the tail with respect to q at the wing will increase stability. The next item is $\overline{V}$ which is the tail volume coefficient $S_t l_t/S\bar{c}$. To make this larger, assuming that the wing geometry (S, and MAC) is fixed, either S_t, the tail area, or l_t the tail length can be increased, (or both increased). Finally, to improve stability, the item $d\varepsilon/d\alpha$ should be made as small as possible since it is making the quantity in brackets smaller. $d\varepsilon/d\alpha$ is the rate of change of downwash at the tail with angle of attack of the wing. This item for a given wing is fixed at any given location behind the wing. However, above or below the wing the downwash influences will be less, so $d\varepsilon/d\alpha$ will get smaller. This fact is sometimes made use of by mounting the horizontal tail on top of the vertical tail where it is a maximum distance possible above the wing.

Static Neutral Point

Once the airplane geometry is established, every item in equation (13) is fixed except quantities x and l_t, which relate the position of the center of gravity to the 1/4 chord of the MAC. Since we are at liberty to shift the center of gravity of an airplane, we will affect its stability by doing so. In particular, if we shift the center of gravity aft, making $x/\bar{c}$ larger, we will begin to overcome the stabilizing effect of the tail. If we move the center of gravity far enough aft to just make the right hand side of equation (13) zero, then of course $dC_{mcg}/dC_L = 0$. In this condition there is no change in pitching moment coefficient with lift coefficient (or angle of attack), so there is no tendency for the airplane to either return to an equilibrium position or diverge from it. The airplane is thus neutrally stable, and is said to have reached its "neutral point." (On the other hand, if the center of gravity is moved farther and farther forward, the airplane becomes more and more stable.)

The actual magnitude of the effect of center of gravity position is of interest. Consider Figure 7.

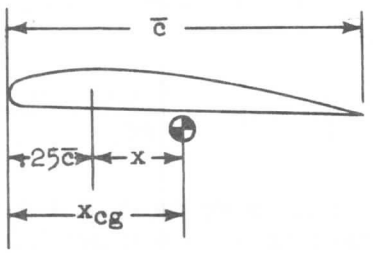

Figure 7.

Instead of writing the term $x/\bar{c}$, we write:

$$\frac{x}{\bar{c}} = \frac{x_{cg} - .25\bar{c}}{\bar{c}}$$

or,

$$\frac{x}{\bar{c}} = \frac{x_{cg}}{\bar{c}} - .25$$

This is done so that the longitudinal position of the center of gravity can be expressed as a fraction of the mean aerodynamic chord; it is usually expressed in percentage. Thus, equation (13) will become:

$$\frac{dC_{mcg}}{dC_L} = \left(\frac{x_{cg}}{\bar{c}} - .25\right) + \frac{dC_{m_{wb}}}{dC_L} - \frac{a_t}{a_w}\,\eta_t\,\bar{V}\left(1 - \frac{d\epsilon}{d\alpha}\right) \quad (14)$$

Let us assume that x_{cg} is changed by 1% of the $\bar{c}$ without any change in aerodynamic configuration. Then the change in $x_{cg}/\bar{c}$ is .01, and since all the other terms are constant, dC_{mcg}/dC_L changes by .01 also. In other words, if dC_{mcg}/dC_L were originally equal to -.10, an aft C.G. shift of 1% would result in a dC_{mcg}/dC_L of -.09. If the shift were 10%, dC_{mcg}/dC_L would be zero and the neutral point would have been reached. (This latter shift of 10% could have been, say, from 40% of $\bar{c}$ to 50% of $\bar{c}$). Such a condition can be illustrated by graph as in Figure 8, for the slope of the C_{mcg} vs C_L curve is dC_{mcg}/dC_L.

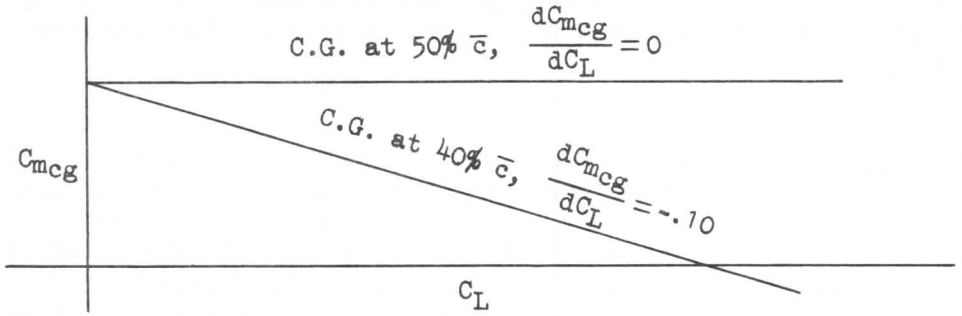

Figure 8.

Since the neutral point corresponds to $dC_{mcg}/dC_L = 0$, this fact can be inserted into equation (14) with the following results:

$$0 = \frac{x_{cg}}{\bar{c}} - .25 + \frac{dC_{mwb}}{dC_L} - \frac{a_t}{a_w}\,\eta_t\,\bar{V}\left(1 - \frac{d\epsilon}{d\alpha}\right)$$

Solving for the center of gravity position corresponding to this condition, and calling this the neutral point, N_o,

$$N_o = \frac{x_{cg}}{\bar{c}} = .25 - \frac{dC_{mwb}}{dC_L} + \frac{a_t}{a_w}\,\eta_t\bar{V}\left(1 - \frac{d\epsilon}{d\alpha}\right) \text{———} (15)$$

If the interactions of the yaw and roll effects upon the pitch characteristics of the airplane are neglected, and these effects are usually very small, the elevator hinge moment can be written as,

$$C_{he} = C_{h_o} + \frac{\partial C_{he}}{\partial \alpha_t}\,\alpha_t + \frac{\partial C_{he}}{\partial \delta_e}\,\delta_e + \frac{\partial C_{he}}{\partial \delta_{tab}}\,\delta_{tab} + \cdots \text{———} (16)$$

where C_{he} is the hinge moment coefficient,

$$C_{he} = \frac{(HM)_e}{qS_e c_e}$$

HM is moment of the elevator about its hinge line,

q is the dynamic pressure at the elevator, and S_e and c_e are the area and chord of the elevator behind the hinge line,

C_{ho} is the residual value of C_{he} at zero tail angle of attack and zero elevator and tab deflection,

δ_{tab} refers to the deflection of the tab with respect to the elevator, and

δ_e refers to the deflection of the elevator with respect to the horizontal stabilizer surface.

By setting $C_{he} = 0$ and solving for δ_e, one can determine the angle at which the elevator will tend to float when the controls are free to seek their own equilibrium position. For the case where $\delta_{tab} = 0$,

$$\delta_{e_{float}} = \delta_{e_o} - \frac{dC_{he}/d\alpha_t}{dC_{he}/d\delta_e} \alpha_t \qquad (17)$$

where δ_{e_o} is the elevator trim deflection necessary for airplane zero lift.

If the elevator floating angle at each lift condition were just equal to that needed to trim the airplane to equilibrium, the pilot would need to apply no stick force, and the airplane would be neutrally stable. However, if, with increasing lift, the elevator were to float up to an angle less than that needed to trim and the pilot had to apply a pull force to hold the airplane in equilibrium, it would be said to have stick-free stability. And if the floating angle were to exceed the requirement such that the pilot would find it necessary to supply a push force, the plane would be unstable in stick-free flight.

To evaluate the static longitudinal stability under elevator-free conditions, one must add the destabilizing effect of the free elevator and controls to the basic stability of the fixed system:

$$\left(\frac{dC_m}{dC_L}\right)_{free} = \left(\frac{dC_m}{dC_L}\right)_{fix} + \left(\Delta\frac{dC_m}{dC_L}\right)_{float}$$

From equation (7) it can be seen that the elevator-influenced tail component of the moment coefficient is given by:

$$C_{mt} = - C_{Lt}\, \eta_t\, \overline{V}$$

and,

$$\Delta \frac{dC_m}{d\delta_e} = - \frac{dC_{Lt}}{d\delta_e} \eta_t \bar{V}$$

The stability contribution of the free elevator is, then,

$$\left(\frac{dC_m}{dC_L}\right)_{float} = \left(\frac{d\delta_e}{dC_L}\right)_{C_{he}=0} \left(\frac{dC_m}{d\delta_e}\right)$$

The value of $(d\delta_e/dC_L)_{C_{he}=0}$ can be found by differentiating equation (17) with respect to C_L and evaluating α_t in terms of the wing- and tail-flow parameters:

$$\left(\frac{dC_m}{dC_L}\right)_{float} = \frac{dC_h/d\alpha}{dC_h/d\delta_e} \frac{a_t}{a_w} \bar{V} \eta_t \frac{d\alpha_t}{d\delta_e} \left(1 - \frac{d\varepsilon}{d\alpha}\right)$$

The elevator-free stability equation which corresponds to equation (14) is:

$$\left(\frac{dC_m}{dC_L}\right)_{free} = \frac{x_{cg}}{\bar{c}} - .25 + \left(\frac{dC_m}{dC_L}\right)_{wb} - \frac{a_t}{a_w} \eta_t \bar{V} \left(1 - \frac{d\varepsilon}{d\alpha}\right)\left(1 - \frac{dC_h/d\alpha}{dC_L/d\delta} \frac{d\alpha_t}{d\delta}\right) \quad (18)$$

The last factor in equation (18) determines the stability effect of the floating elevator. If there is no floating tendency, that is, if $\partial C_{he}/\partial\alpha = 0$, the elevator-fixed and elevator-free stabilities are equal. However, if the floating tendencies were large enough, they could conceivably overbalance the whole tail contribution to the airplane stability.

The elevator-free neutral point,

$$N_o' = .25 - \left(\frac{dC_m}{dC_L}\right)_{wb} + \frac{a_t}{a_w} \eta_t \bar{V} \left(1 - \frac{d\varepsilon}{d\alpha}\right)\left(1 - \frac{dC_h/d\alpha}{dC_h/d\delta} \frac{d\alpha_t}{d\delta}\right) \quad (19)$$

will be different from the elevator-fixed neutral point by the degree of the elevator floating tendency. The difference on the typical airplane may be in the order of 2 to 5% of the mean aerodynamic chord. The reduction in stability can be shown as in Figure 9.

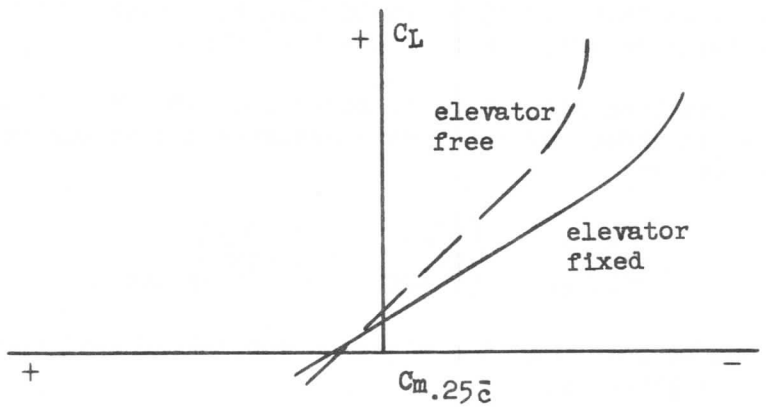

Figure 9.

Figure 8 shows the effect of a C.G. shift on the pitching moment characteristics about the center of gravity. Rather than make such a plot where a new curve must be drawn for each center of gravity position, it is conventional to plot a single curve considering that the center of gravity is at the quarter chord point of the mean aerodynamic chord. (See Figure 10.) To find the effects of center of gravity shift, the vertical axis is imagined to rotate about the origin as is shown. In other words, rather than the curve being rotated, the axis is rotated, accomplishing the same relative motion.

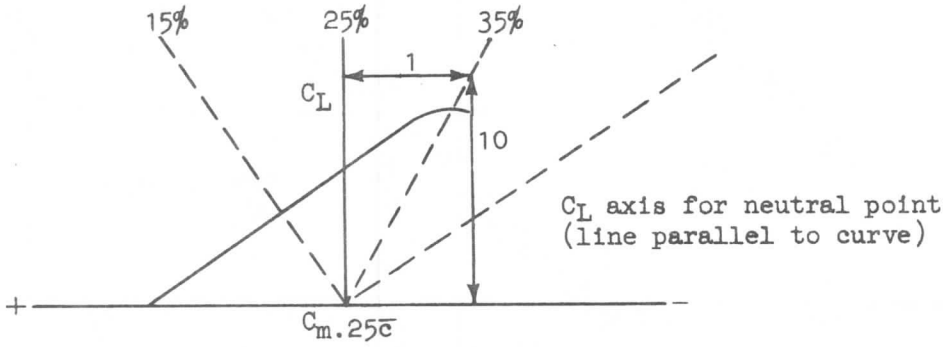

Figure 10.

The positioning of these new axes is made considering that for, say, a 10% change in center of gravity shift the pitching moment curve will change slope by .10. Thus, the slopes of the 15% and 35% axis in Figure 10 (both 10% shifts) will be -.10 and .10, respectively. Also in Figure 10 is shown the C_L axis corresponding to the neutral point. This line is located by drawing it in parallel to the C_L vs $C_{m.25\bar{c}}$ curve. Thus, relative to this new axis the curve could be considered vertical, and therefore dC_m/dC_L is zero.

The neutral point is of interest because it defines the center of gravity position at which static neutral stability exists. Flight at the neutral point requires continuous control; so our next concern is to determine how close to the neutral point the center of gravity can be located. The airplane must possess some positive stability to be easy to fly, so a stability "margin" is usually maintained. The amount of margin required is a function of a number of variables and will in general change from one airplane type to another.

The tool which is of particular value in estimating the neutral point of an airplane is the wind tunnel. It provides us with a preknowledge of the stability characteristics of the airplane which would be practically impossible to estimate by purely theoretical means. A sample of this wind tunnel data is shown on Figure 11. Shown are curves for flaps up and down, complete model and model without horizontal tail. Of most interest at this time are the complete model curves. It will be noted, however, that the complete model is much more stable than the model with the tail off. The stabilizing influence of the horizontal tail is thus clearly seen.

To illustrate the calculation of the static neutral point of an airplane, consider the full-plane flaps-up curve of Figure 11. The linear portion of the curve has the slope, $\frac{dC_m}{dC_L} = -.22$; this, added to the basic $.25\bar{c}$ at the reference point gives

the neutral point location at 47%$\bar{c}$.

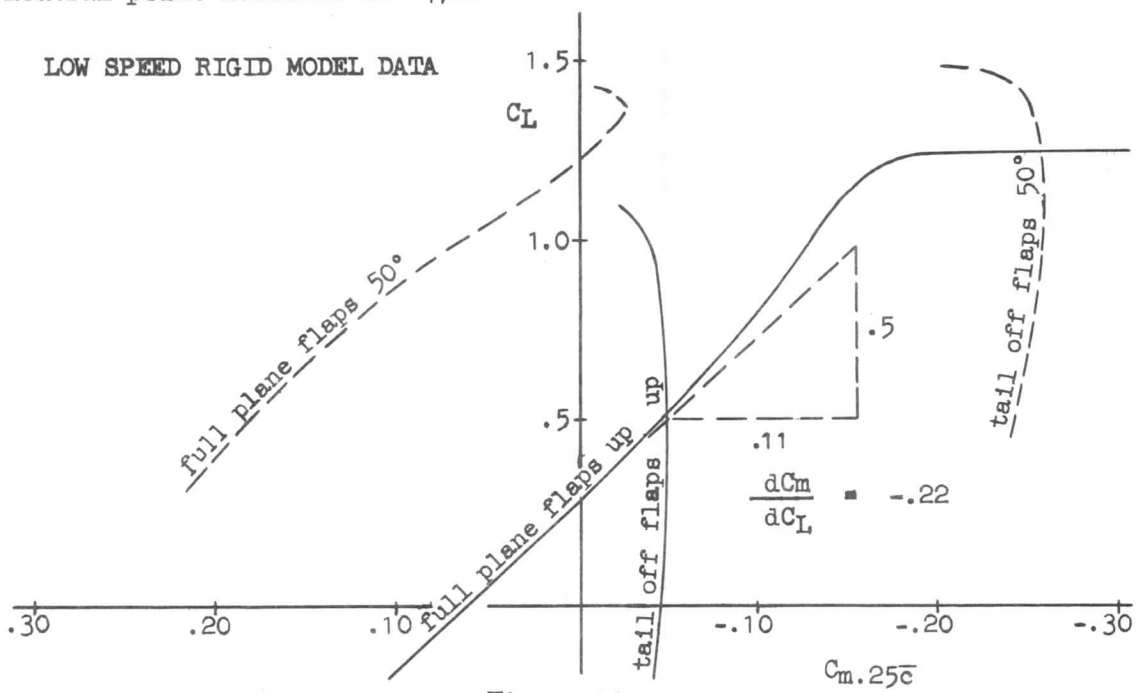

Figure 11.

It is erroneous to think of the static neutral point as being fixed even for a fixed C.G. position. The character and value of almost every one of the parameters in the stability equation change with Mach number; therefore, the neutral point tends to shift. Aeroelastic effects may also tend to aggravate the normal forward shift tendency. The static neutral point location on the 707 series airplanes is generally close to 50%$\bar{c}$ at low speeds and moves forward at high speeds (high Mach numbers). The "tuck" tendency discussed later is an example of this effect.

An unusual practical application of longitudinal stability occurs during the take-off of airplanes with bicycle gears such as the B-47 and B-52. On occasion, the take-off distance is shortened by pulling the airplane off the ground with the elevator in contrast to the normal procedure of letting it fly off in a level attitude. This procedure increases the angle of attack (and thus C_L) and results in a lower lift-off speed and a shorter takeoff run. This procedure should be used with caution because momentarily the airplane is in an unstable condition. To see how the previous statement is possible, consider Figure 12 which shows an airplane in the process of being pulled off the ground with the elevator. Momentarily the airplane is resting on only the rear gear and is rotating about the gear. In free flight, the rotation is about a point near the aerodynamic center of the airplane. If the airplane is rotating about the rear gear, it can be said that it will react as if it were in flight with the center-of-gravity moved aft to the vicinity of the rear gear. Since the rear gear on a bicycle-gear airplane is relatively far aft, this of course means that a relatively far aft center of gravity position is being duplicated. If the airplane is unstable about the rear gear it will tend to rotate in the direction in which it is originally displaced. Very soon, however, sufficient lift will have been developed to raise the whole airplane off the ground, at which time it is no longer rotating about the rear gear and is once again stable. Between the times when the nose gear lifts off and the rear gear lifts off, however, sufficient angular momentum may have been built up that, following unstick, the

airplane may continue to rotate to a greater nose-high attitude and eventually stall out. Several B-47 accidents have been caused by the pilot, not realizing that this phenomenon could take place, causing the airplane to pitch up so violently that recovery from the steep climb resulting was impossible before flying speed was lost and a stall-out occurred. The Boeing commercial airplane series, however, is stable enough about the gear that although the tendency is present, it is much reduced; for the main gear is located much closer to the aerodynamic center.

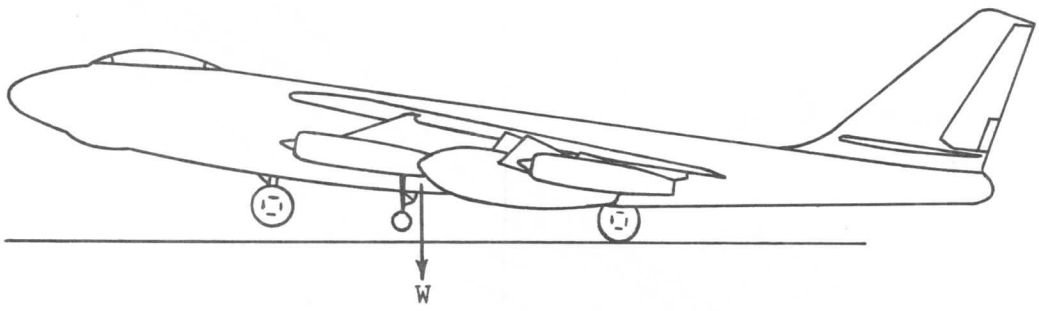

Figure 12.

The condition which limits the forward position of the C.G. is dictated by elevator power. The landing requirements on the elevator are more severe than any other. The elevator must be able to achieve power-on trim at $C_{L_{max}}$ in the landing configuration in ground effect with the C.G. in the most forward position. To allow for differences in pilot technique in flare procedure, a margin of about 5° of elevator travel is usually subtracted from the maximum elevator deflection when the forward C.G. limit is calculated.

Mach Number and Aeroelastic Effects

Up to this point no consideration has been given to the effects of Mach number or aeroelasticity on the stability of the airplane. Mach number was a major factor to be considered in performance work and is found to be important in stability work also. Aeroelasticity was scarcely mentioned in connection with performance and its influence there can thus be assumed to be negligible. Its influence on stability however, is far from negligible and must be taken into consideration. With reference to Figure 11, which shows the longitudinal stability characteristics of a wind tunnel model, what is presented are the characteristics without either Mach number or aeroelastic effects. Because of this, the curves are sometimes referred to as "low-speed" data for a "rigid" airplane. The data are obtained by testing at low Mach numbers on a model which is very rigid relative to the full scale airplane. Other testing at high Mach numbers and with less-rigid models yields different curves. Considering first the Mach number effects, it will be found that instead of having just a single curve of C_L vs C_m (as on Figure 11) for a given configuration, a different curve for each Mach number will be obtained. The difference between curves will be most noticeable at higher Mach numbers. Figure 13 shows a typical plot of C_L vs $C_{m.25\bar{c}}$ with curves for various Mach numbers.

Two reasons for the shift of the curves with Mach number will be discussed briefly. It should be noted that the pitching moment characteristics of an airplane are to a large degree a function of the distribution of lift over the airplane. This is

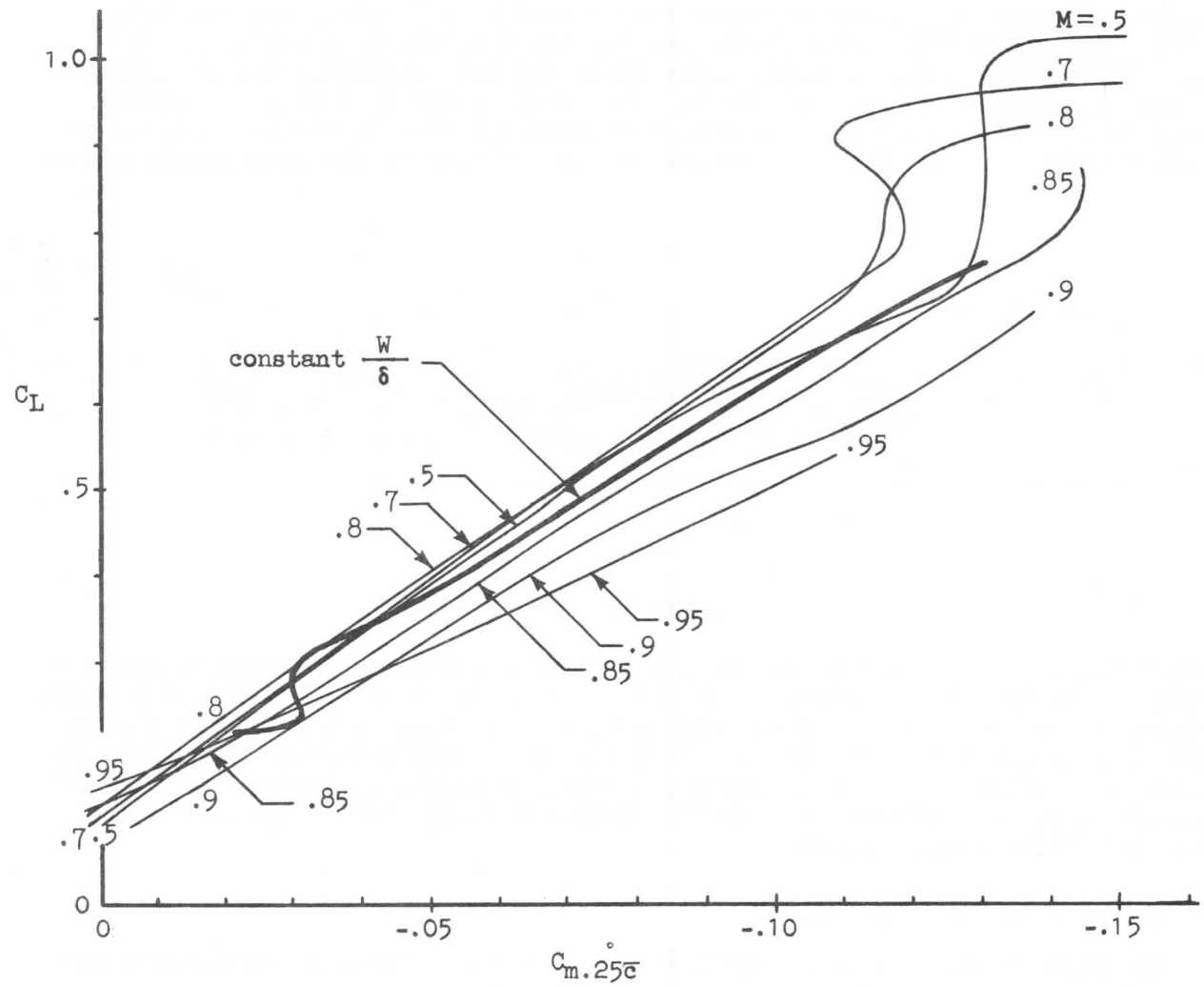

Figure 13.

particularly true in the case of a swept wing airplane. Since the wing actually covers a considerable longitudinal distance, changes in wing lift distribution can have a larger pitching moment effect than with a straight wing. The first Mach number effect is the same as that which was discussed in Section 1 wherein the increase in Mach number affected the pressure distribution on the airfoil sections and resulted in an increase in lift coefficient at any angle of attack, an increase in the slope of the lift curve, and an increase in downwash behind the wing into the tail. In the case of the pitching moments, this Mach number effect will be present on both the wing and the tail, and a change in stability will then be expected since the slopes of the wing and tail-lift curves enter the stability picture in equation (15). The net effect from this cause will in general be a change in longitudinal stability (either toward more stability or less stability, depending on the relative magnitude of the effects on the wing and tail). The second Mach number effect is felt when a sufficiently high Mach number is reached to cause airflow separation. If this separation occurs on a swept wing at the tip, for example, the resulting loss of lift in this region will have a considerable pitch effect near the aerodynamic center since the aero-

dynamic center will be forward of the wing tip. In this case the airplane would tend to pitch up. These effects can be seen in the typical "pitch-up" moment curves shown in Figure 14. Conversely, airflow separation near the root of the wing will cause a nose down pitching tendency. At low C_L values, increasing Mach number changes the pitching moment by shifting the center of pressure. At high C_L's, separation due to high angle of attack causes the curve to shift from stable through neutral to unstable as Mach number increases. The design of the wing on the 707 airplane has been tailored to eliminate the pitch-up "hook" shown in these curves.

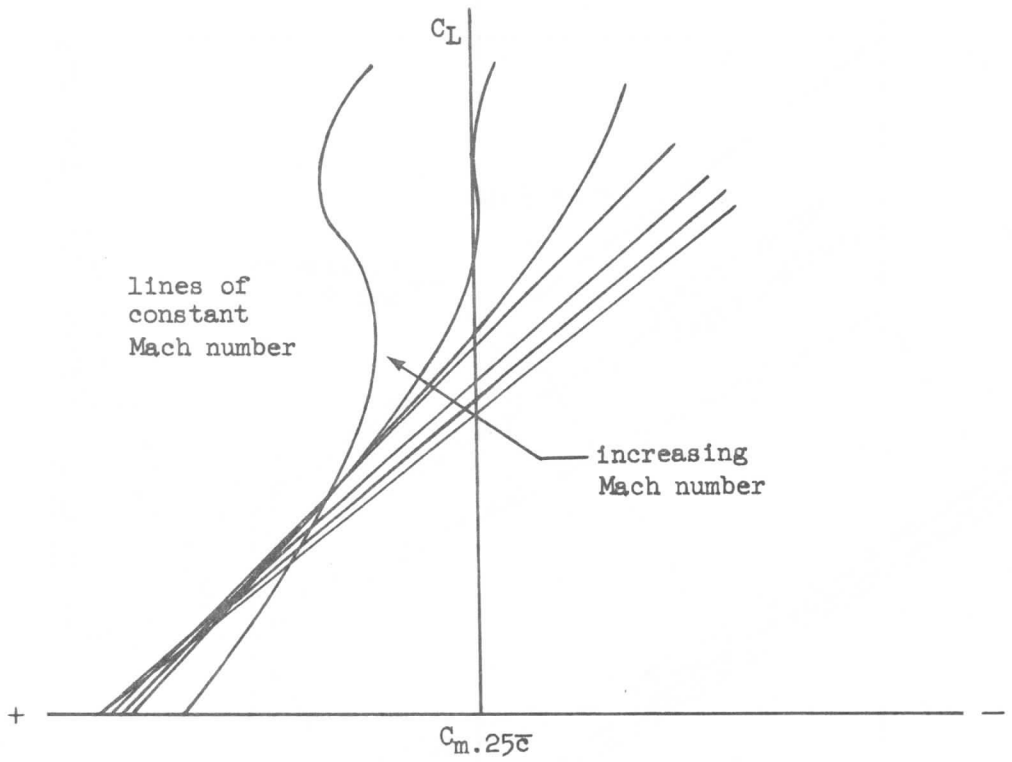

Figure 14.

Aeroelastic effects are as important as Mach number effects in longitudinal stability and must also be considered. By "aeroelastic" is meant the elastic deformations of the structure caused by the imposed aerodynamic loads. Of particular interest is the deformation of the wing. When a wing is generating lift, it flexes upward. On an unswept wing this bending does not have side effects; but on a swept wing it has. Consider Figure 15 which shows the plan and elevation views of a swept wing under load. Note that each elevation view is taken perpendicular to the center line of the wing. This is done for the reason that when the wing bends it will still appear as a line in edge view when seen from a direction perpendicular to the center line. In passing over the wing, however, the air does not move perpendicular to the center line of the wing. Looking at Figure 15 to note what occurs along a streamwise wing section, it is seen that the leading edge of this section is actually slightly lower than the trailing edge when viewed in elevation. If the leading edge is now lower than the trailing edge, as compared to the undeflected wing where the leading and trailing edges were at the same height, this can only mean that this airfoil section has under-gone a reduction in angle of attack. As can be seen from Figure 15, the greater the deflection,

the greater the change in angle of attack. Thus, at the wing root there is no angle of attack change since there is no deflection; on the other hand, at the tip there is a maximum deflection so that there will be a maximum reduction in angle of attack.

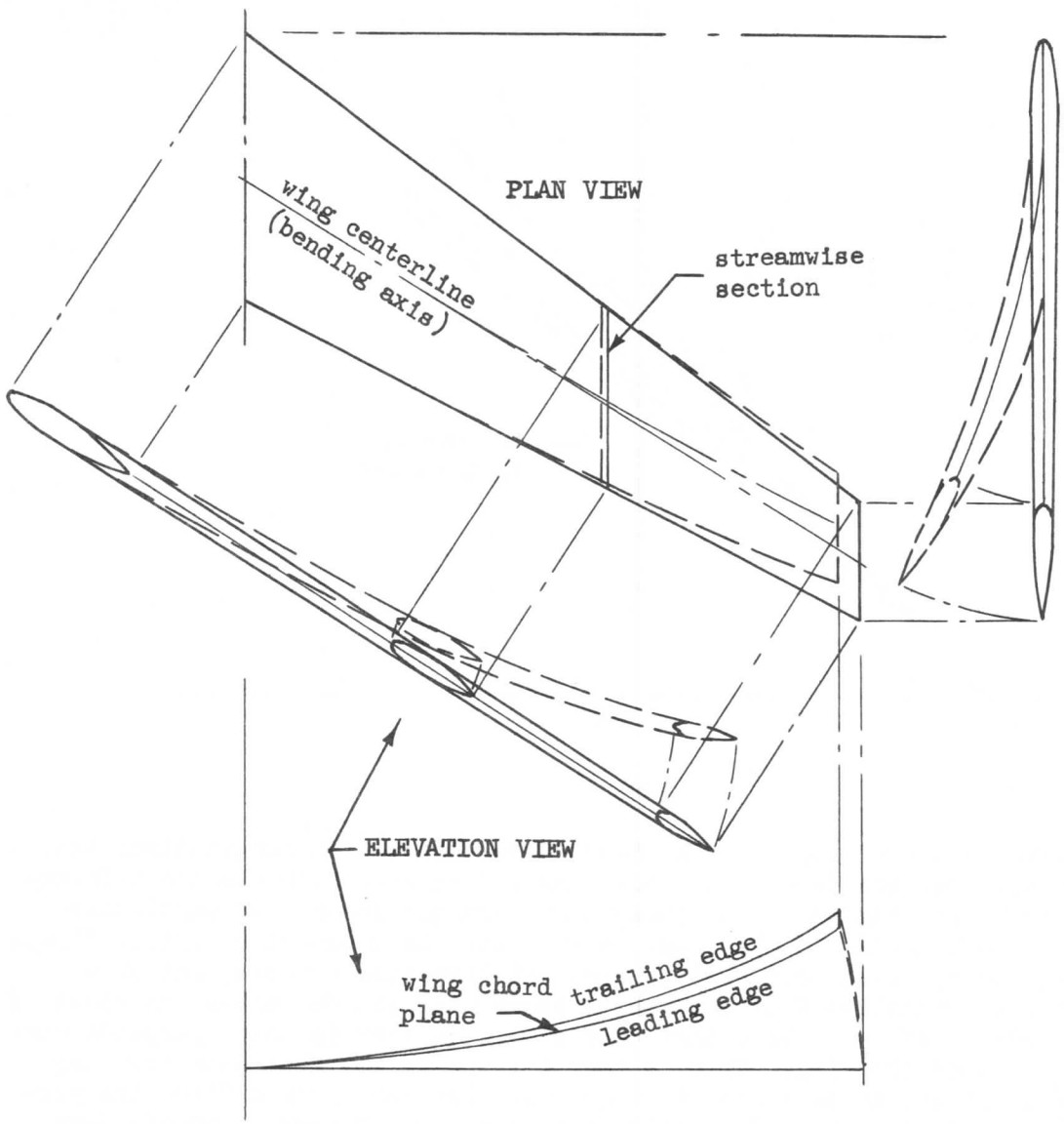

Figure 15.

From preceding discussion it can be seen that, although the wing actually does not twist very much in relation to the axis about which it bends, aerodynamically it has twisted, for the air does not pass over the wing perpendicular to the bending axis. (When the wing is twisted so as to reduce its angle it is said to be "washed out".) This aerodynamic twisting will obviously affect the load being applied to the wing since the load is a function of angle of attack. With the angle of attack being reduced all along the span, the load will be reduced, the greatest reduction occurring at the tip. Since the tip is now unloaded relative to the root, the spanwise load distribution and thus spanwise center of pressure is changed in comparison to that of the undeflected wing. But on a swept wing any change in spanwise load distribution will change the fore and aft location of the center of pressure. In the case where the tips unload on a swept wing, the center of pressure, in moving inboard, will move forward, A forward movement in center of pressure can be thought of as an effective rearward movement of the center of gravity since there is now a greater longitudinal distance between the lift and weight vectors (see Figure 5). As was shown previously, an aft movement of the center of gravity makes the airplane more unstable; thus this aero-elastic effect is a destabilizing one.

To show how this aeroelastic effect will cause changes in stability it would be interesting to examine wind tunnel data which include these effects. To obtain these data it is necessary to conduct the test with a model which duplicates both the elastic and aerodynamic characteristics of the actual airplane. This is done by building a full model to scale not only dimensionally, but also elastically. These tests will obviously record all aeroelastic effects, including body deflection due to horizontal tail loads. Since the air load on the wing is causing it to bend (and thus twist), and since the load is a function of C_L (and thus α), wing area, and dynamic pressure ($L = C_L S q$), it is reasonable to assume that the dynamic pressure, q, will be an important variable in aeroelastic phenomena. The wind tunnel tests are therefore conducted at various constant values of q. (Analogous to testing at various constant values of Mach number in obtaining compressibility effects). When the results of these tests are plotted, a series of curves similar to Figure 16 will be obtained. If it is assumed that the airplane operates on one of the higher q lines, it can be seen that its stability (as indicated by the slope of the curve) is poorer than at some lower q.

However, what is important in the final analysis is a determination of how the Mach number and aeroelastic effects combine in the full scale airplane to produce a resulting set of pitching moment curves. An airplane might have Mach number characteristics as represented by the low C_L portion of Figure 13 and aeroelastic characteristics as in Figure 16, since with increasing Mach number there is also increasing q. It is reasonable that the two sets of curves might combine as in Figure 17. (In this figure Mach number is retained as the variable distinguishing the curves.) The final position of the curves depends on the relative magnitude of the Mach number and aeroelastic effects. In this case, the two effects tend to cancel each other since on one hand there is a shift to a greater nose up tendency with increasing speed (aeroelastic), and on the other a nose down tendency with increasing speed (Mach number).

The resulting effects of Mach number and aeroelasticity on the longitudinal stability must now be examined. Consider an airplane which is flying at a constant altitude at a given weight. It is obviously, then, at some particular W/δ which will be considered constant. It will be remembered that:

$$W/\delta = 1481 M^2 C_L S$$

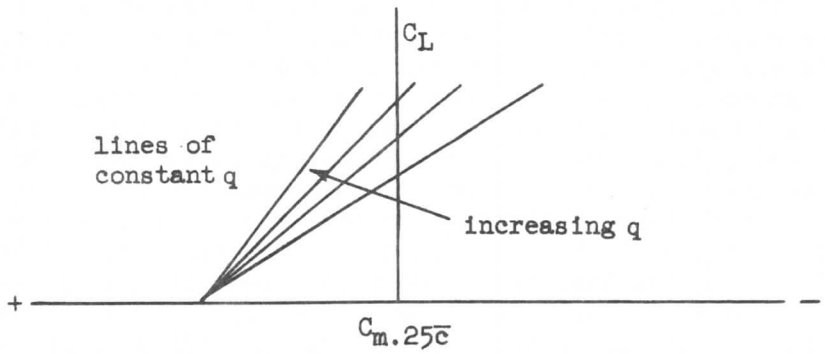

Figure 16.

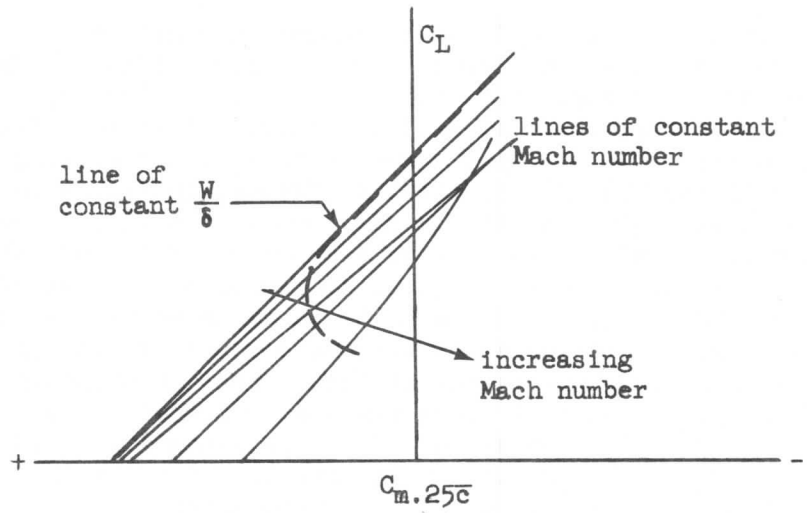

Figure 17.

Knowing the W/δ will thus enable one to establish the relationship between Mach number and C_L. This means that a line of constant W/δ can be drawn on Figure 17; this curve defines the variation of pitching moment coefficient with lift coefficient or speed change. It can be seen that even though the airplane may be stable with respect to pitch as shown by the constant M lines, it can be unstable with respect to constant W/δ . The positive slope of this curve at low C_L (high Mach number) values indicates a speed instability. Since the curve shows a tendency for the airplane to nose down with increase in speed, this effect is often called "tuck-under." Usually an airplane which demonstrates this characteristic need not cause the pilot any difficulty since it occurs only at relatively high Mach number where speed gradient is low and the period is very long. It is easily controlled by normal pilot reaction if the elevator control design is compatible with the wing design.

In the tuck-under regime, the airplane tends to nose down as Mach number is increased, and the control forces required of the pilot to change speed may be

different from those in the low-speed region. The change in force gradient may lead to over- or under-control in turbulent conditions or during rapid acceleration. The control aspects of tuck-under will be discussed more fully in a later section on longitudinal control. Pitch-up tendencies also will be discussed there.

Static Directional Stability

Static directional stability may be defined as the tendency of an airplane to return to its equilibrium sideslip angle (usually zero) after being displaced from this position. This is analogous to the longitudinal stability case in which changes in angle of attack are assumed.

The terms "sideslip" and "yaw" are usually used as though they meant the same thing. Actually, sideslip is the displacement of the airplane centerline from the relative wind direction, and yaw is the angular displacement of the airplane from some reference heading. If, however, a straight flight path is assumed (see Figure 18), then sideslip and yaw are equal in magnitude (but opposite in sign) and may be used as equivalent terms.

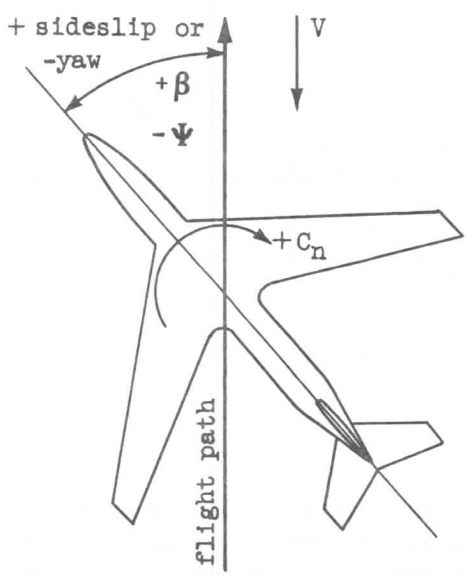

Figure 18.

When an airplane is placed in a side-slipped attitude, its various components (fuselage, nacelles, tail, etc.) will develop moments about the vertical axis (yawing moments) which will tend to either increase or decrease the side slip. If the 707 airplane less the vertical tail is considered, it will be found to be slightly unstable; that is, a displacement from equilibrium will develop a yawing moment which will tend to increase the displacement. With the addition of the vertical tail, however, a stable configuration is obtained. The curves presenting these data are shown in Figure 19, which plots the dimensionless yawing moment coeffi-

cient, C_n vs sideslip angle, β, where:

$$C_n = \frac{N}{qSb}$$

N = yawing moment, ft lb

q = 1/2 ρV^2, dynamic pressure, lb/ft^2

S = wing area, ft^2

b = wing span, ft

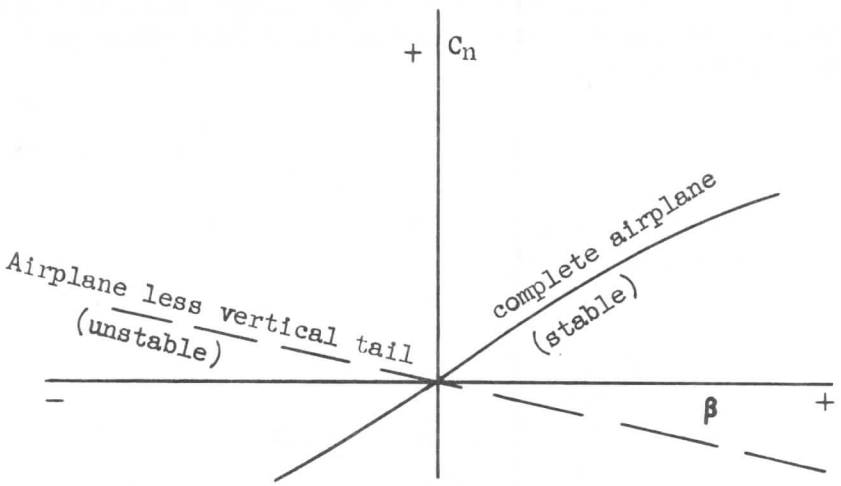

Figure 19.

Although a change in sideslip (yaw) is always accompanied by an interacting roll effect, it is possible to analyse the yaw components as if they could be made independent and thereby gain some insight into the directional stability of the airplane. Such application of the static stability principle to rotation about the yaw axis shows that to be stable, the airplane must have "weathercock stability": Flight at a sideslip angle relative to the flight path must generate a yawing moment such as to tend to restore it to a zero sideslip operation. Hence, $\partial C_n/\partial \beta$ must be positive if C_n is in the direction to rotate nose right and β is the sideslip angle defined positive if the relative wind on the nose is from the right.

The principle contributions to this stability are from the body and the vertical tail. The wing is only slightly stabilizing, and C.G. location is a relatively weak parameter.

However, on airplanes which use wing-mounted spoilers for lateral control, as does

the 707 series airplanes, the unsymmetrical drag condition induced by spoiler deflection can exert a noticeable yaw effect. This drag-induced yaw tends to turn the airplane in the direction in which it is banked and reduces the need for rudder deflection.

The fin contribution can be written in terms of the vertical tail volume, fin lift slope, velocity across the fin (if affected by prop wash or jet induction), and side wash angle induced by the wing wake vortex pattern. Thus a stability equation similar to that for the longitudinal case and of the same form can be developed.

Static Lateral Stability

Static stability may be provided about the yaw and pitch axes since a displacement from equilibrium can be made to generate a restoring moment. But a pure displacement in roll does not in itself generate any such counter-rolling moment. So in this sense there is no hope of static lateral stability. On the other hand, however, a rolling velocity component can be combined with other velocity components to generate forces and moments which may manifest themselves as moments about the roll axis. Specifically, a rolling velocity added vectorially with the forward velocity of the airplane changes the flow across the wing in both magnitude and direction. The result of this change is usually felt as a damping moment tending to resist the roll which generated it. The pilot thinks of this damping as a stabilizing effect, so the relative change in wing angle of attack, which is obviously related to the damping effect, is taken as a measure of the static lateral stability. (See Figure 41)

Using the angle of attack change at the wing tip as the index of roll damping, consider that the linear velocity normal to the wing at the tip is:

$$V_n = p\frac{b}{2}, \text{ feet per second}$$

where, $$p = \frac{d\phi}{dt}, \text{ the rolling velocity in radians per second}$$

The angle defined by the sum of this linear velocity and the forward velocity along the flight path defines the change in angle of attack at the tip. The parameter, pb/2V, the tangent of this angle, defines the helix traced by the wing tip. This is the recognized lateral stability and control parameter.

Actually, the total roll excitation and damping is the result of a rather complicated interaction of both pitch and yaw effects with roll. The tendency of the airplane to maintain flight on an even keel is so very intimately tied to the dynamic reaction and interactions with pitch and yaw that it is difficult to define it adequately except in terms of dynamic analysis.

4-3 CONTROL

Basic Longitudinal Aspects

For an airplane to maintain level flight it must be trimmed properly; its stabilizer or elevator must be adjusted to hold the airplane at whatever speed is

desired and the thrust levers must be set such as to provide enough thrust to overcome the drag and maintain the altitude. Thrust limitation or improper handling of the controls can induce pitch effects and change trim conditions. However, it is necessarily assumed that there is enough thrust available for the intended flight and that the pilot flies the aircraft in a normal way.

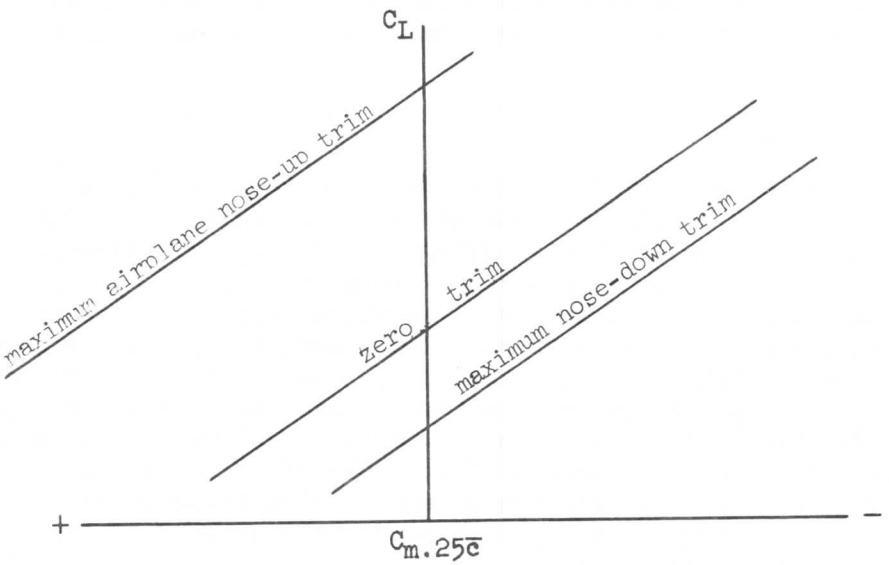

Figure 20.

When a stabilized trim situation has been achieved, there will be no pitching effect. Referring to Figure 20, one sees that zero pitching moment, along the C_L axis, is possible at only one C_L for each trim configuration. For example, the flaps-up model shown in Figure 11 is trimmed to fly at $C_L = 0.3$ and could fly at only the speed corresponding to this C_L unless the configuration were changed. It will be noted that it is possible to trim the airplane over a large range of C_L's and thus accommodate a large range of speeds. The lowest speed at which the airplane can be trimmed corresponds to the maximum airplane nose-up trim; i.e. maximum stabilizer nose down and maximum up elevator. On the other hand, the highest trim speed corresponds to maximum airplane nose-down trim. Since it is mandatory to save some elevator for maneuvering, it is not recommended that the elevator be used for trimming; the stabilizer only is used for that purpose. With surfaces of the sizes used on Boeing airplanes, one degree of rotation of the stabilizer is as effective as 2.5 to 3.5 degrees of elevator.

Generally, it is found to be true that the change in lift coefficient is proportional to the change in elevator (or stabilizer) angle:

$$\delta_e \propto C_L$$

$$\delta_e = K_1 C_L \qquad (20)$$

where δ_e is the elevator deflection. But we know that:

$$W = C_L S \frac{V^2 \sigma}{295}, \quad V \text{ in knots}$$

or,

$$V^2 = \frac{295W}{C_L S \sigma}$$

so for fixed values of W, S, and σ,

$$V^2 = \frac{K_2}{C_L} \qquad (21)$$

where,

$$K_2 = \frac{295W}{S\sigma}$$

From equation (20),

$$C_L = \frac{\delta_e}{K_1}$$

Substituting for C_L in equation (21):

$$V^2 = \frac{K_2 K_1}{\delta_e}$$

$$V^2 = \frac{K}{\delta_e}$$

$$V = \sqrt{\frac{K}{\delta_e}} \qquad (22)$$

This equation establishes the variation of elevator angle with velocity. When the two quantities are plotted against each other a curve similar to Figure 21 is obtained. This plot shows that relatively large elevator angle changes are required to effect small speed changes in the low speed region, whereas the opposite is true in the high speed region. The same general analysis and plot could be used for the stabilizer except that the values of the K constants and the deflection scale would be different.

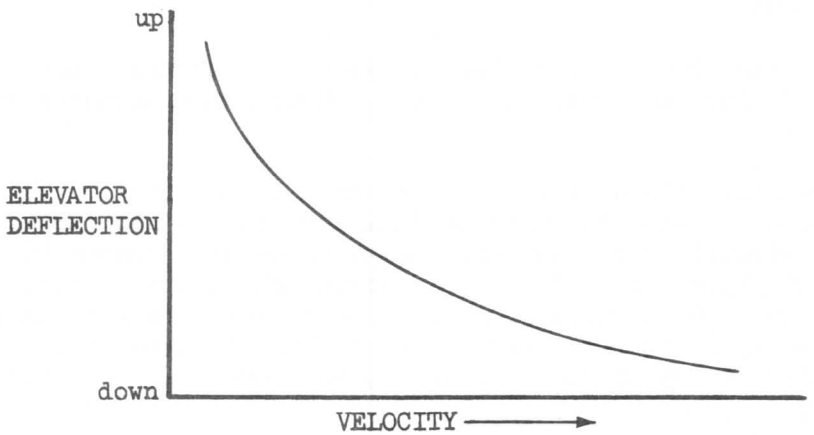

Figure 21.

STABILITY AND CONTROL

It will now be interesting to show the effect of airplane center of gravity on the ability to trim. Consider first the case of moving the center of gravity aft. As was shown in Figure 10, a center of gravity shift can be shown by merely rotating the vertical axis of the C_L vs $C_{m.25\bar{c}}$ curve. If this is done for curves at various elevator (or stabilizer) angles, the result will appear as in Figure 22. The aft center of gravity causes the curves representing the 3 elevator (or stabilizer) positions to intersect the axis at high values of C_L, which of course corresponds to lower speeds than in the previous (25% C.G.) case. Note also that now a greater C_L spread between the maximum up and the maximum down elevator positions is possible than before. This means that a greater speed range is possible than before, although not quite as high a speed (low C_L) can be attained. The big difference is thus on the high C_L end of the curves where an appreciably higher C_L can be attained. The same trends result from use of the stabilizer or both stabilizer and elevator together.

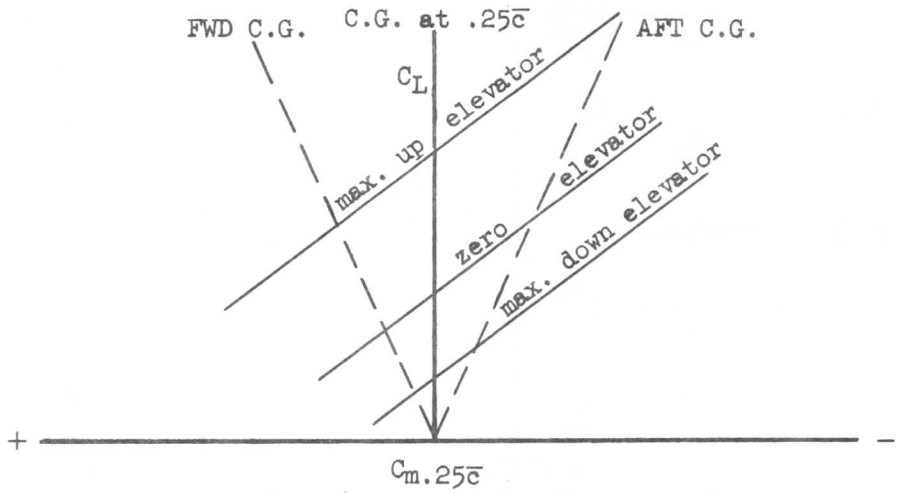

Figure 22.

In contrast, the forward C.G. positions limit the C_L (and thus velocity) range of the airplane with a significant reduction in the ability to get to low speeds. The airplane with most forward C.G. is the most stable. However, it is possible to make it so stable that it is difficult to control. As a matter of fact, the limits on forward C.G. position are commonly set by the landing situation in which low speeds (high C_L's) are required. If with forward C.G. lack of sufficient stabilizer and elevator "power" make it impossible to maneuver at sufficiently low speeds, the C.G. must be moved aft until the airplane can be flown acceptably at the desired speeds.

To further clarify the effects of center of gravity on control, Figure 20 is cross-plotted in Figure 23 for the three C.G. cases, showing the comparative speeds which can be achieved.

With regard to the limitations on aft C.G. movement, when the neutral point of the airplane is reached, when the axis becomes parallel to the curves in Figure 22, it takes zero stabilizer or elevator change to cause a change in trim. In other words, the airplane has no fixed trim speed, and requires continuous control. Therefore, the C.G. is usually maintained at some "margin" ahead of the neutral point. The value of this margin varies with the type of airplane, but numbers in the order of 10% of the mean aerodynamic chord are not uncommon in transport aircraft.

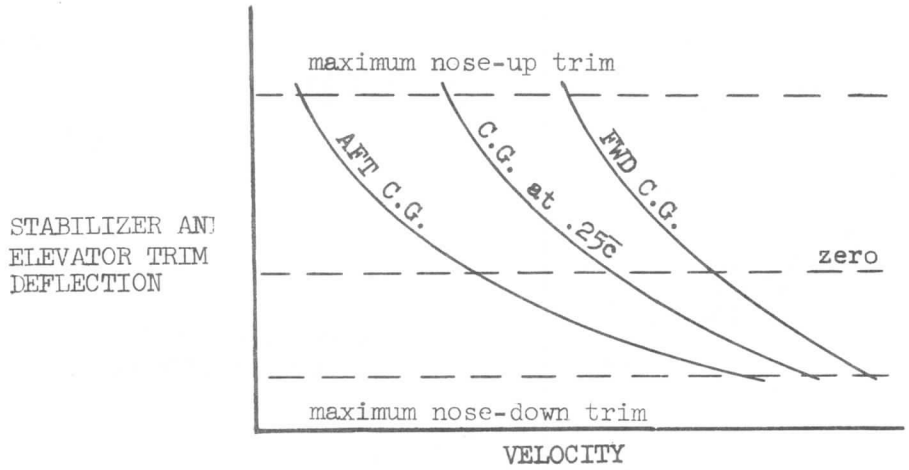

Figure 23.

Regardless of the type of trim used, the elevator effectiveness under all trim conditions must be great enough to allow for adequate changes in flight speed. This could be shown in terms of the speed range attainable by the elevator for the most adverse trim setting or the amount of erroneous trim setting that can be counter-controlled by the elevator. One of the reasons for using a different device for trim is to allow full movement of the elevator in all trim conditions.

Many other reasons have been given for using a movable stabilizer for trim rather than preset of the elevator. Since relative movement of the whole surface is more effective, a smaller empennage can do the total job. The installation is a lower drag configuration, for there is less wetted area and skin friction, and there is a smaller projected frontal area since the deflection from stream direction is less and the orientation is more streamlined. The rigging and mechanisms can be simpler, a single actuator being involved and its placement being more central. The torsional stresses on the surface can be reduced since it can be hinged closer to its natural rotation center. And this will allow rotation with fairly light actuators.

Aeroelastic and Mach Number Effects

Consider the case of "tuck-under" as shown in Figure 17. If the data were plotted as in Figure 24, it becomes obvious that as Mach number increases, more down elevator or nose up stabilizer is needed to trim the airplane until the point where tuck-under is felt. At this point the pitching moment curve starts to diverge from the low-speed curve. As Mach number increases further the divergence becomes so great as to change the slope direction and require up elevator or nose-down stabilizer. This represents "trim reversal." In this speed region and beyond, it is mandatory that longitudinal trim in the direction opposite to that normally used in flight be used. But, unless the airplane is accelerating very rapidly or the wing design is such that the reversal is very sharply defined, the transition is gradual and presents no difficulty. As the curve indicates, the rate of trim change is not abrupt. The situation normally follows so smoothly that the pilot can rely upon his automatic reaction to take care of it. Many pilots have gone in and out of the region without realizing it.

However, when "tuck-under" might be severe, in order not to confuse the pilot, and

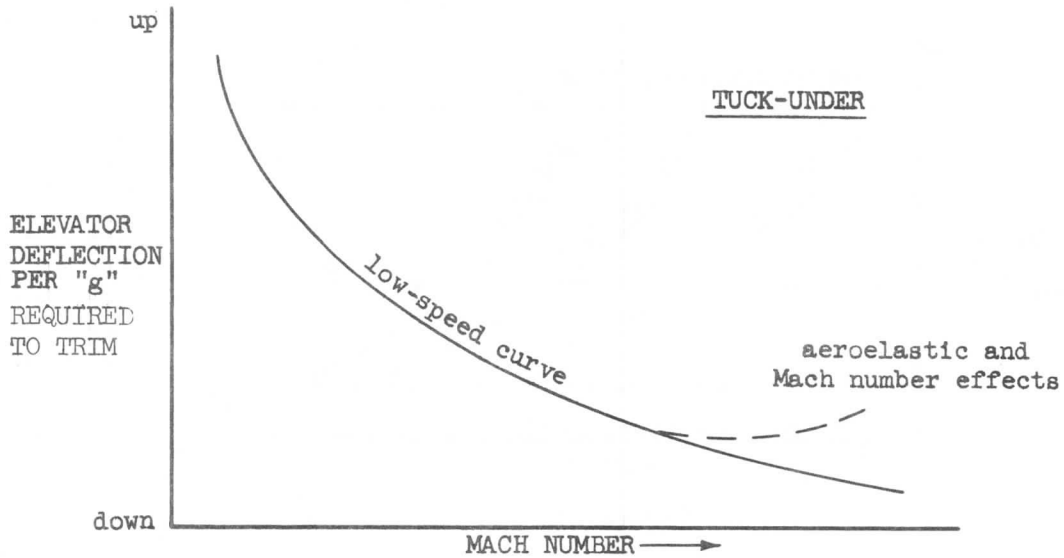

Figure 24.

to give positive feel to the controls, it is customary to provide artificial control force and to trim the airplane automatically in the Mach number regime where the effects are to be expected. These compensating devices can be triggered and powered by any of a number of methods - electrical, pneumatic, hydraulic, gyroscopic or a combination of these. A Mach number sensor modulates the system and automatically changes the trim when the airplane is in the tuck-under region since the necessary trim compensation is a function of Mach number. A similar device might monitor the trim forces needed and automatically adjust the stabilizer angle. The ultimate result desired is a system which will afford the pilot a stick force gradient with speed which is consistently stable throughout his full flight regime.

Pitch-up tendencies are characteristic of high C_L values. They are associated with "hooked" moment curves such as shown in Figure 14. If the slope change were to occur at low enough C_L to be within the anticipated cruise Mach number range, the airplane might be accelerated directly into an unstable condition. As Mach number picks up or as C_L is increased at a given Mach number (due to maneuver or gust, for instance) the nose suddenly comes up and the elevator force falls off as in Figure 25. Although the effect is stable in the sense that the increase in angle of attack is in the direction to reduce speed and bring the airplane back out of the pitch-up regime, it is possible that the change may be so violent as to bring on very severe buffeting and even complete wing stall. Since the airplane is presumed to be fairly heavily loaded (flying at relatively high C_L) and at high speed, the stresses upon the structure are usually found to be high enough to cause concern for the safety of the airplane structure. The wing of the Boeing airplane has undergone very careful design studies to insure that there will be no tendency towards pitch-up during normal high-speed operation.

General Control Aspects

A very unorthodox type of control which has been investigated in experimental aircraft involves changes in trim, especially in the longitudinal sense, by shifting the center of gravity of the airplane with respect to the center of pressure.

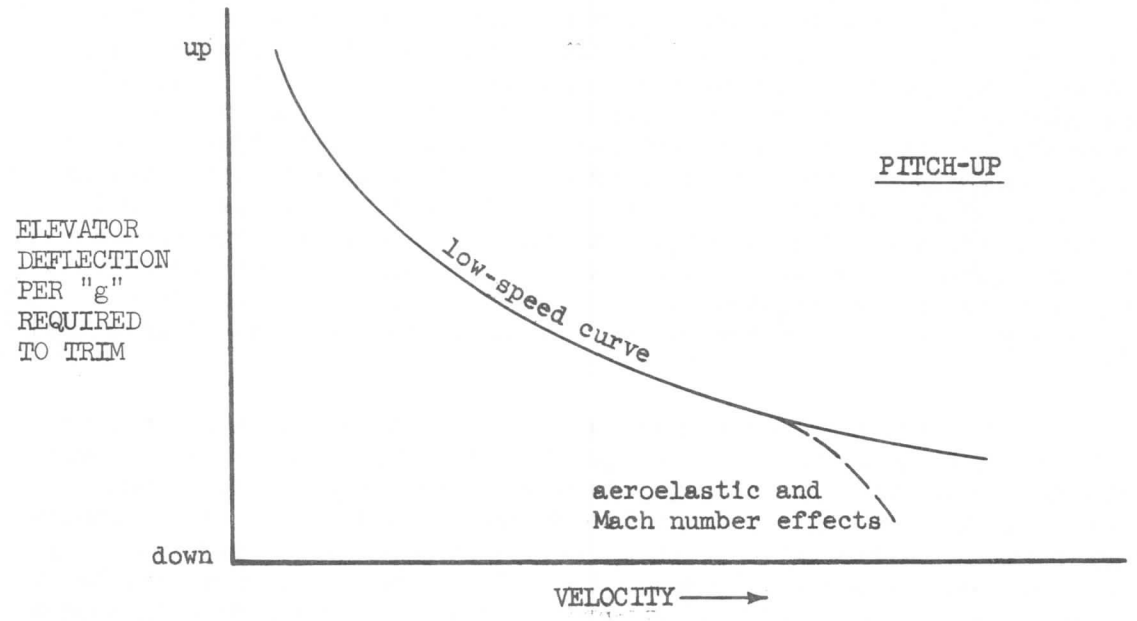

Figure 25.

This can be done by shifting such fixed loads as the crew or the fuel or cargo containers, or by mechanically moving the lifting surfaces with respect to the fuselage. As can be seen, the mechanical problems involved in obtaining rapid enough movement safely are very difficult. And the changes in stability of the airplane are highly undesirable. It seems to be much more practical to maintain a relatively fixed structure and load distribution, to control by means of changes in the lift on aerodynamic surfaces fixed in position on the airplane.

In the study of performance and stability of an aircraft, it is tacitly assumed that the control surface deflection necessary to place the craft in a given flight condition and to hold it there can be attained. However, the aerodynamic forces on a large deflected surface can exert such great hinge moments as to make it a major engineering problem to find methods for countering them. A study of the hinge moment of an unbalanced control surface,

$$HM = C_h \, 1/2 \, \rho \, V^2 \, S_c c_c \qquad (23)$$

indicates that the moment to be overcome is directly proportional to the square of the speed and the cube of the size (linear dimension). If the area, S_c, and chord, c_c, are measured behind the hinge line, any balancing devices used will affect the values as they modify the coefficient C_h. In the analysis, then, the major problem is resolved into the determination of the coefficients "b" of the major variables in the moment coefficient equation,

$$C_h = b_0 + b_1 \alpha + b_2 \delta_c + b_3 \delta_{tab} + \cdots \qquad (24)$$

The use of such a linear definition is usually good enough, at least for early approximation.

Hinge moment coefficients are most difficult to determine. Since a very large number of geometric parameters influence the coefficients, a very wide range of designs is in current use. Scale effects can nullify model tests, for boundary layer effects are often large. Some of the variables which may affect the calculations are chord ratio of control to surface, hinge location, balance type and ratio, nose shape, trailing edge angle, planform, gap or slot, type and size of tab, springs, bob weights, etc. Most of these devices have been developed in an attempt to lower or adjust the hinge moment, for the pilot force is directly proportional to the adjusted hinge moment; and such forces must be kept within the range of human capabilities unless the load is to be taken out of the pilot's hands entirely and the forces supplied by fully-powered units. In this latter case, it may be necessary to introduce rather complex accessory units to give the pilot "feel."

A point very often overlooked in the consideration of mechanical control is that the total work needed to overcome the hinge loads must equal that unbalanced work exerted by the airstream effects. This involves not only control forces, but also moment arm and the distance through which the force is applied. It is possible that hinge moments of very large proportions can be balanced through suitably designed mechanical lever gearing; the mechanical advantage can be made very large. But the space required to move the small control forces through adequate distances may be more than the control cabin can afford. This need for space in which to work is as acute a part of the total problem as is the force requirement. Both considerations must be studied when one must decide how much of the total surface hinge load is to be carried by the pilot.

The reduction of hinge moment requirements is accomplished by various means. In some cases it may be possible to rotate the whole flight surface about a point close to the aerodynamic center, the change in angle of attack of the surface producing the necessary change in lift. Since the control rotation is about a point close to the natural rotation center of the surface, the hinge moment can be quite small. Also, the total angular deflection needed is much less than that for most other control types. Examples of this type of control are the "slab" tails currently found on some aircraft and the movable horizontal stabilizer used for trim on Boeing Transport airplanes.

A more usual type of control changes the lift on a surface by changing the camber of the surface by means of a flap on the trailing edge. Most modern controls are of this type, conventional elevators, ailerons, rudders, and flaps. With the advent of very large high-speed airplanes, the hinge moment requirements for moving the surfaces have risen to such values as to present serious problems. Much development work has gone into attempts to arrive at solutions which use the dynamics of the airstream itself to relieve the pilot by balancing out part of the load. Even fixed balance weights and springs have been employed. The more closely balanced the control, however, the more sensitive the control becomes with regard to such things as nose shape, clearances, and shift in surface center of gravity with flight attitude which can change radically with manufacturing variations. The current trend is to relieve the pilot of some or all of the load by using power controls, but often various aerodynamic balances are employed along with the powered controls.

Where power is applied to the control in such a way as not to reflect feel forces back to the pilot, the control is called an irreversible control system. This system must be provided with artificial control forces so that the pilot may feel

changes in force requirement proportional to both degree of deflection and speed.

The pilot may obtain feel while supplying all the control force through a direct mechanical connection, Figure 26a; as feed-back through a "ratio-type" partial-power system such as shown in Figure 26b; or as direct control force to a supplementary feel surface deflected in parallel with the power control as in the 707 rudder system, Figure 26c. Most operators seem to prefer reversibility in controls. It is typical of human behavior that an operator likes to have as direct connection as possible with that which he controls. It might be noted in passing that in Figure 26c, the feel tab represented there has been isolated from the control surface to indicate that it serves only to give feel and that the power unit controls the surface. In the actual 707 installation, the tab is placed on the surface such that in case of power loss it can be used as a control tab.

Where the control power system is irreversible, the feel must be artificially supplied. The force should be proportional to deflection and to velocity squared. By proper selection, a mechanical spring deflection can be fitted to the deflection feel, but the speed feel is most accurately duplicated by a speed-pressure device such as the "Q" bellows. An example of the use of both devices on a single control system is on the 707 rudder installation, Figure 27. Pilot action deflects the push-rod system in proportion to the signal to the power unit. The push-rod deflection is transmitted through the crank-cable system to deflection of the bellows-spring combination which resists the original pilot action. This resistance "feel" is proportional to the amount of deflection, calibrated by control of the spring constant, and to velocity squared as felt through the dynamic pressure sensed into the bellows.

It is of interest to note that the feel systems of both Figure 26c and 27 are incorporated in the same rudder control system on the 707 airplanes. In order to retain the tab control back-up feature of the design and also to be able to operate the rudder to deflections beyond the tab capability, two systems operating over two distinct deflection regimes are used. The shift from one to the other is accomplished by differential mechanical linkages and stops in the control push-rod system which has been shown in simplified form in the given figures. In that portion of the control regime where the feel is controlled by the "Q" system, the tab is anti-balanced to give increased rudder effectiveness.

It is important that the control linkages and devices be mass balanced such that accelerations and changes in attitude do not feed false signals into the airplane controls. An example might be drawn from use of a long, heavy elevator column without proper mass balance below the hinge line. Acceleration or high nose attitude would introduce false nose-up signals into the elevator due to the gravitational effects.

Most of the aerodynamic control balances used to relieve pilot force requirements involve tabs or nose balances. Several forms of aerodynamic nose balance are in current use, but all are based upon the same fundamental principle of the use of the dynamics of the airstream to develop hinge moments counter to those developed on the main control surface.

The simple "horn" balance consists of a forward extension of the control surface, carrying the lifting surface beyond the hinge line and affording a counter moment in proportion to the surface moment, see Figure 28. The major problem involved with its use is that in order for the horn balance to produce large enough moments for large deflections the horn must be made so large that it gives too much

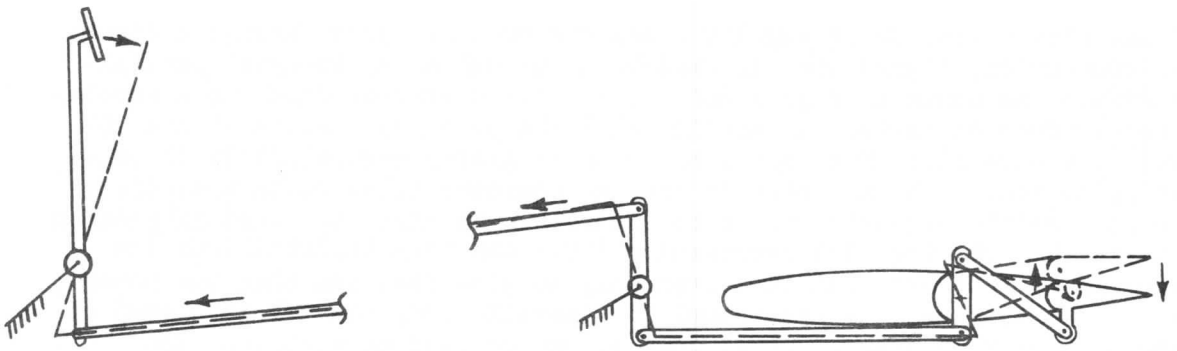

a

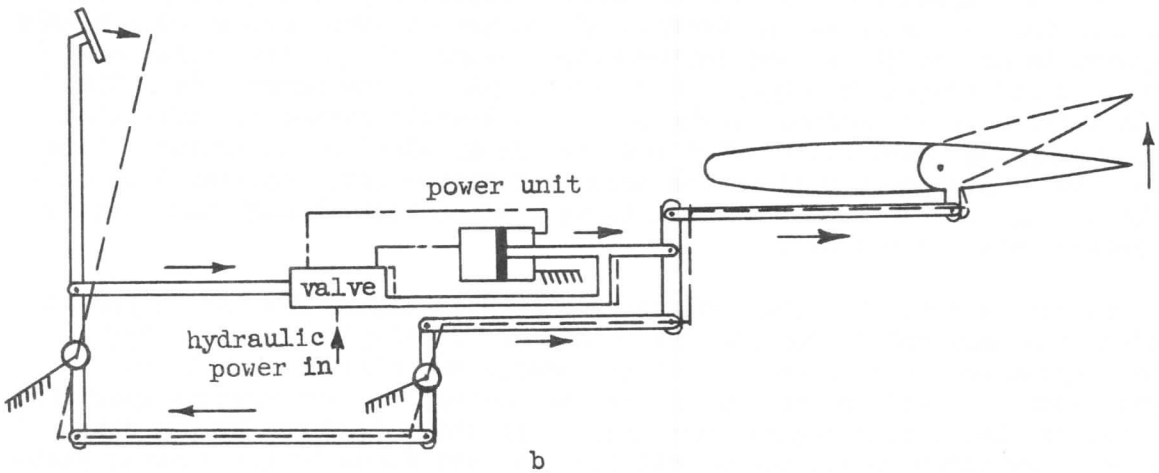

b

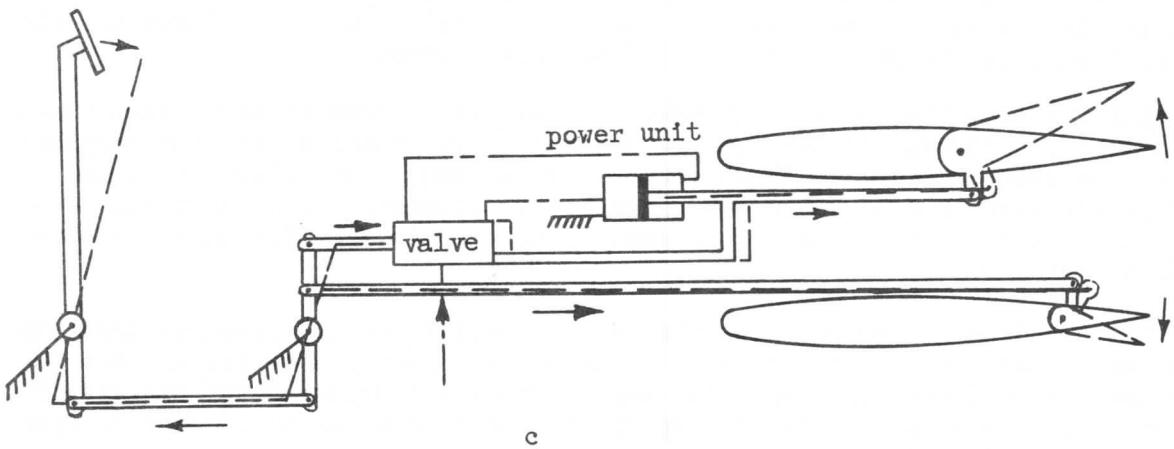

c

Figure 26.

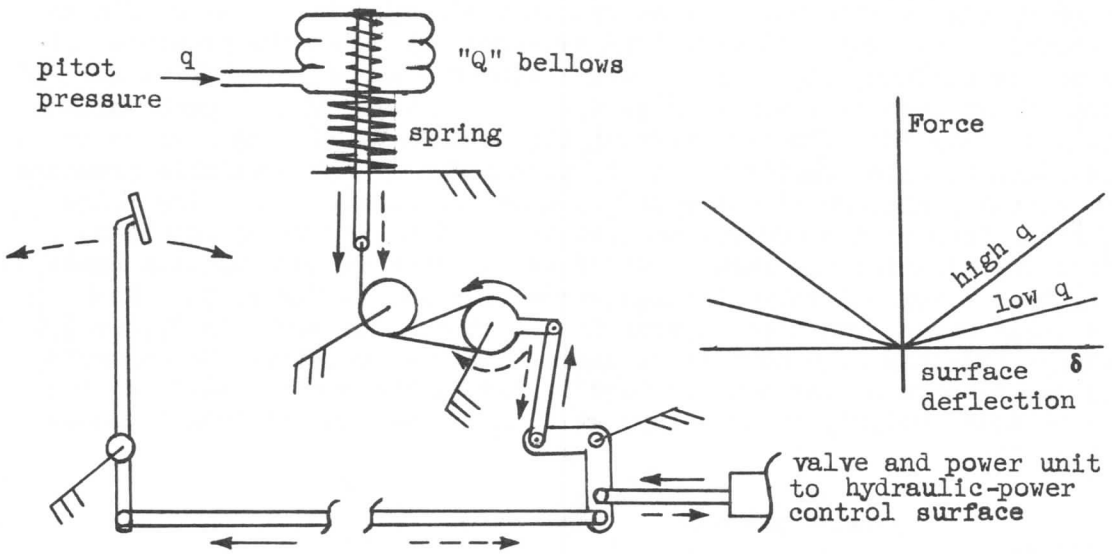

Figure 27.

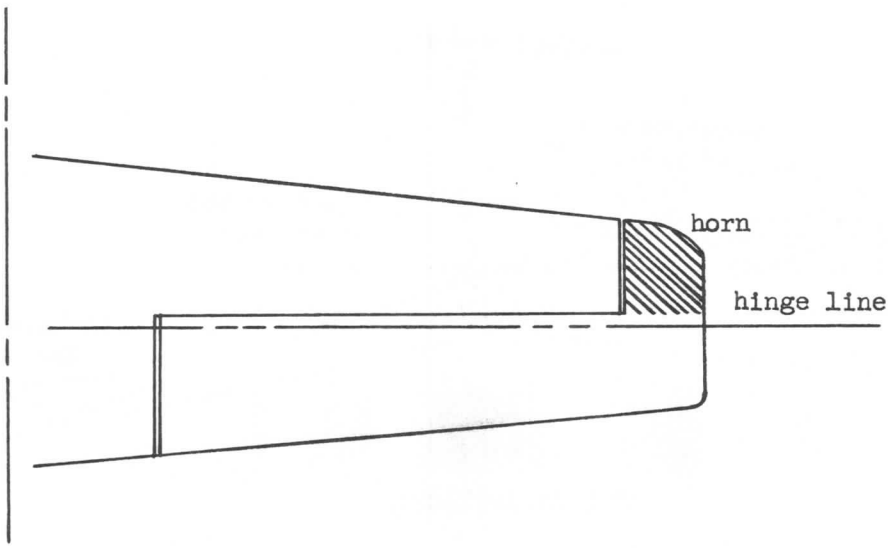

Figure 28.

moment at lower deflections. Also, there is an undesirably large drag increment associated with a large horn or a radically set-back hinge which lifts the nose far into the airstream.

A method for using the nose balance without the drag problems has been developed. If there is room, the balance panel is buried in the wing, stabilizer or fin to avoid the exposed horn. The lift effect is developed by using the pressure difference across the surface, bleeding it into a closed chamber in which is located the extension of the nose as shown in Figure 29. With this type of nose balance, it is possible to vary the effective size of the balance by placing a valve in the pressure plate to allow variation in the percentage of the available pressure differential actually allowed to act upon the nose extension. Since the valve position is a function of the control surface deflection, the valve may be a simple, static installation, as shown. Other valve types include various cone-in-orifice kinds. A typical valve leakage curve is shown in Figure 30. The reduction in hinge moment can then be seen in a plot such as shown in Figure 31. It is not always possible or practical to use an internal balance. For example, a small horn may provide a platform for mass balancing the control surface with less penalty in total weight, an advantage which may outweigh the drag increase in a given situation.

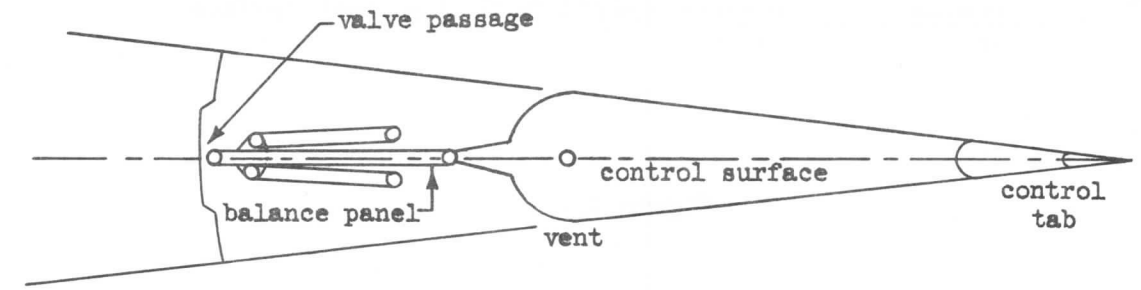

CONTROL NEUTRAL

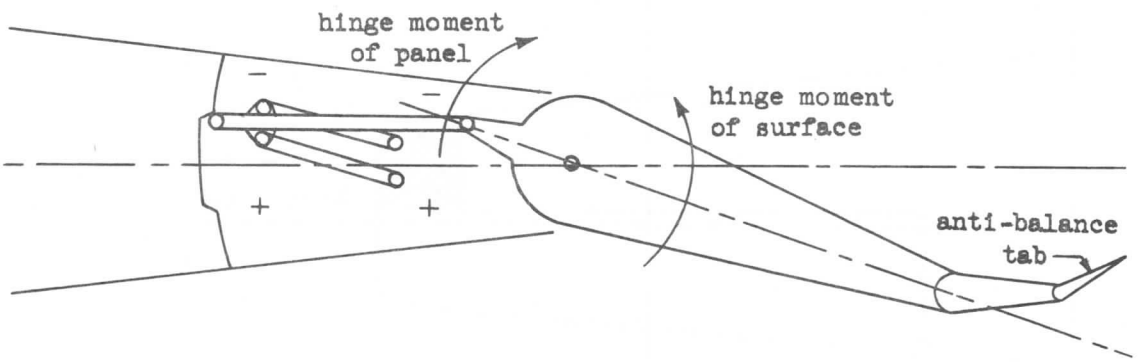

CONTROL DEFLECTED

Figure 29.

The tab is a secondary control surface placed on the primary control surface in much the same way as the primary control surface is placed on the lifting surface. Thus the tab can exert a hinge moment on the primary control surface to balance the surface at the necessary deflection to produce the desired control lift change. Since the area of the tab is small with respect to that of the control surface, the primary control effect is small. However, the control surface moment effect is relatively large. Thus, a small tab hinge moment can furnish the large control hinge moment requirement, enabling a pilot to move a much larger control

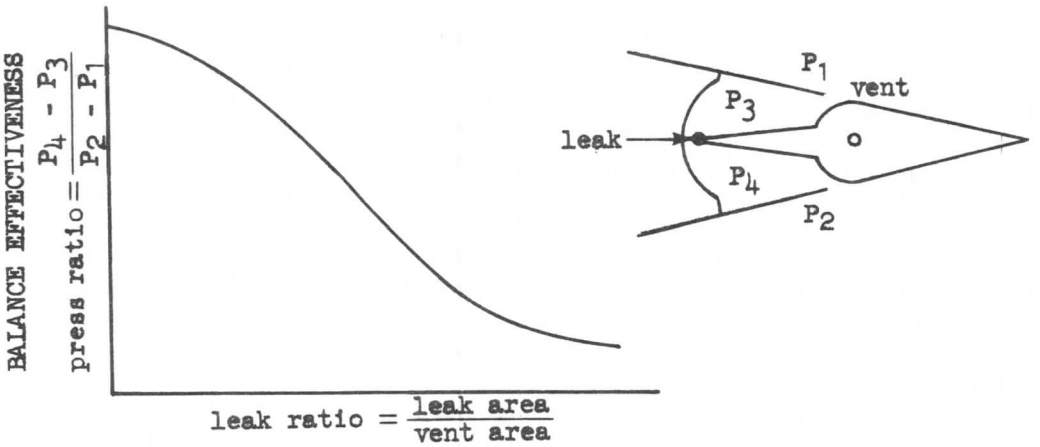

Figure 30.

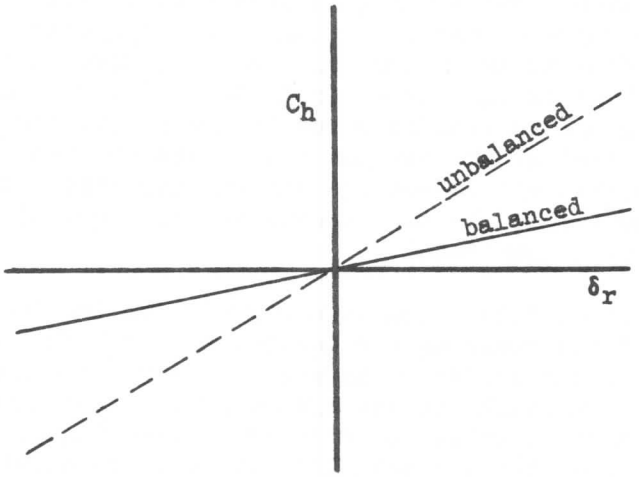

Figure 31.

surface than he could if he were to attempt to supply the control hinge moment directly. Or a small amount of the energy output of a control surface may be used to provide enough hinge moment on a tab to help control the surface itself. The tab to control surface relationship may be shown as in Figure 32. Often the relationship is linear enough that it may be stated in terms of a simple ratio.

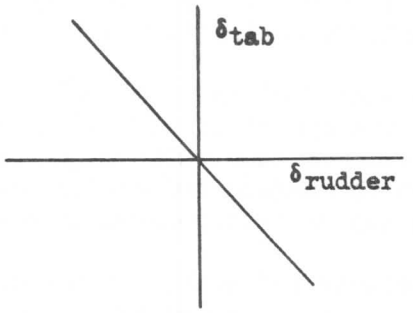

Figure 32.

Many control surfaces are free-floating trailing edge flaps moved by means of control tabs. The tab in such a situation is deflected by the pilot through direct linkage and held in position as long as needed, or it is held in position by some kind of trim control. Thus, the hinge moment needed to deflect the surface to a new trim condition can be obtained by the application of small forces on tab controls. The trim tab is in very wide use even on powered-control surfaces. The use of the tab for maneuvering control is losing favor since the increase in size and speed of aircraft makes the tab requirements much more critical and because separation, boundary layer and Mach number effects often cause radical changes in tab operation which can change the pilot feel in a very undesirable manner. Servo tabs used for maneuvering control or trim are rigged such that the tab deflection assists the control surface to increase the lift or help to relieve the moment created by the blow-back action of the airstream against the surface. Thus the deflection of the tab with respect to the surface must be opposite in direction to the deflection of the surface it is to help move.

It may be necessary to design a tab and rig it such that it will deflect in the direction to increase the surface moment (antibalance the system). In this case, the tab must lead the surface it is to control, that is, move in the same direction. It will be noted, that though the control tab in Figure 33a deflects downward to a large angle when the control is moved by the pilot, the reaction of the surface with the "stick" fixed at the new position moves the tab relative to the surface such as to antibalance and reduce the controlling effect of the tab. This negative follow-up motion of the tab cancels out the control command as the desired surface response is accomplished.

If a system similar to that in Figure 33a were rigged with the tab push rod connected to the same side of the crank as the control pushrod, the follow-up would be positive. In this case, the surface response to the tab command would initiate further command signals through the tab system in the same direction. The positive follow-up would help to boost the surface to even higher deflection until the tab-produced moment on the surface might balance the airstream moment.

The same effects as fixing the control at the pilot's station can be obtained from a tab "geared" to fixed structure as in Figure 33b. This kind of tab could be used for such purposes as to resist "floating" tendencies of a surface or to assist motion initiated by some other motivation. The way in which it is geared will determine whether it acts as a servo tab or as an antibalance tab. An example of a geared servo or balance tab is the one used on the outboard aileron on the 707 series airplanes. The stabilizer-actuated elevator tab on the 720 airplanes is a geared tab the gearing of which is rigged in such a way as to give balance action to the elevator in part of the stabilizer-elevator regime, no action at all in part, and antibalance action to provide better feel in part.

It is thought in some quarters that feel is enhanced by the use of springs in a geared tab linkage to change the amount of control movement required as speed increases. The effect is the same as that which might be obtained by increasing the gearing, the tab deflection to surface deflection ratio. Figure 34 shows a simple example of how a spring may be incorporated in a simple control system.

Many other types of springs, weights and biases have been incorporated in tab systems to give special effects. As the speed and versatility of airplanes increases, the sophistication of the control system will undoubtedly grow in proportion.

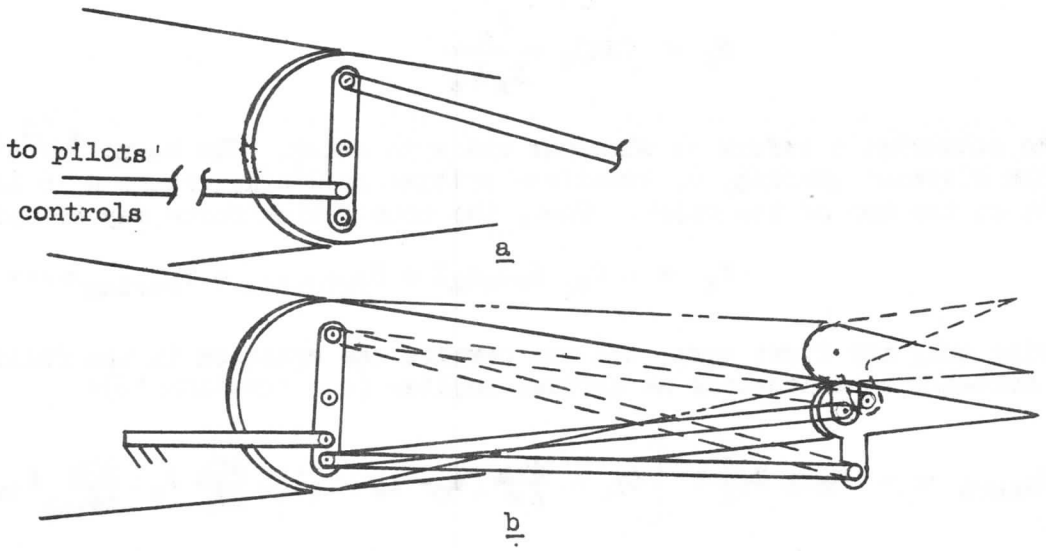

Figure 33.

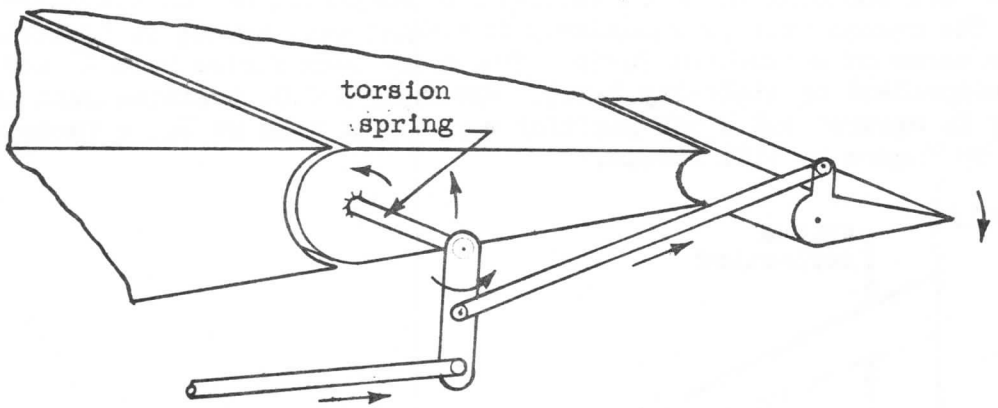

Figure 34.

Stick Force and Gradient in Unaccelerated Flight

The study of the floating tendency of the elevator and its effect upon the stability is of interest chiefly because of its influence upon the variation in stick force required of the pilot in changing trim speed. The stick force at the top of the column is required to overcome the hinge moment at the elevator, so it is determined by this moment and the mechanical advantage of the control system. System position and the effects of any force bias devices such as centering springs also influence forces. To determine the force necessary to balance the aerodynamic moment, one recalls that the work expended at the stick must equal the work accomplished at the elevator. In a simple stick-to-elevator system

$$F_s l_s \delta_s = (HM)_e \delta_e$$

$$F_s = (HM)_e \frac{\delta_e}{l_s \delta_s}$$

where the subscript e refers to elevator and s to stick. The term, $\delta_e / l_s \delta_s$ is called the elevator gearing, G, sometimes written as $d\delta e/ds$, where s is linear movement at the top of the stick. Thus, the total stick force may be written as

$$F_s = - C_{h_e} S_e c_e q_t G + F_{friction} + F_{spring} + \cdots \quad —(25)$$

Considering only the first term, one can rewrite the equation in the following form by suitable substitutions as defined earlier (see equation 16):

$$F_{s_{aero}} = - GS_e c_e \eta_t \frac{\rho}{2} V^2 \left[C_{h_o} + \frac{\partial C_h}{\partial \alpha} (\alpha_o - i_w + i_t) + \frac{\partial C_h}{\partial \delta_e} \delta_e + \frac{\partial C_h}{\partial \delta_{tab}} \delta_{tab} \right]$$

$$+ GS_e c_e \eta_t \frac{W}{S} \frac{\partial C_h / \partial \delta_e}{\partial C_m / \partial \delta_e} \left(\frac{dC_m}{dC_L} \right)_{free} \qquad (26)$$

The forces are composed of an elevator-fixed component and an elevator-float component. The second term is relatively invariant with speed; it reflects the stability in terms of a constant force. The first term varies with V^2 and is relatively independent of stability level. Assuming a C.G. position such that basic stability is assured and a tab position such as to trim at V_t, a force curve such as shown in Figure 35 will result.

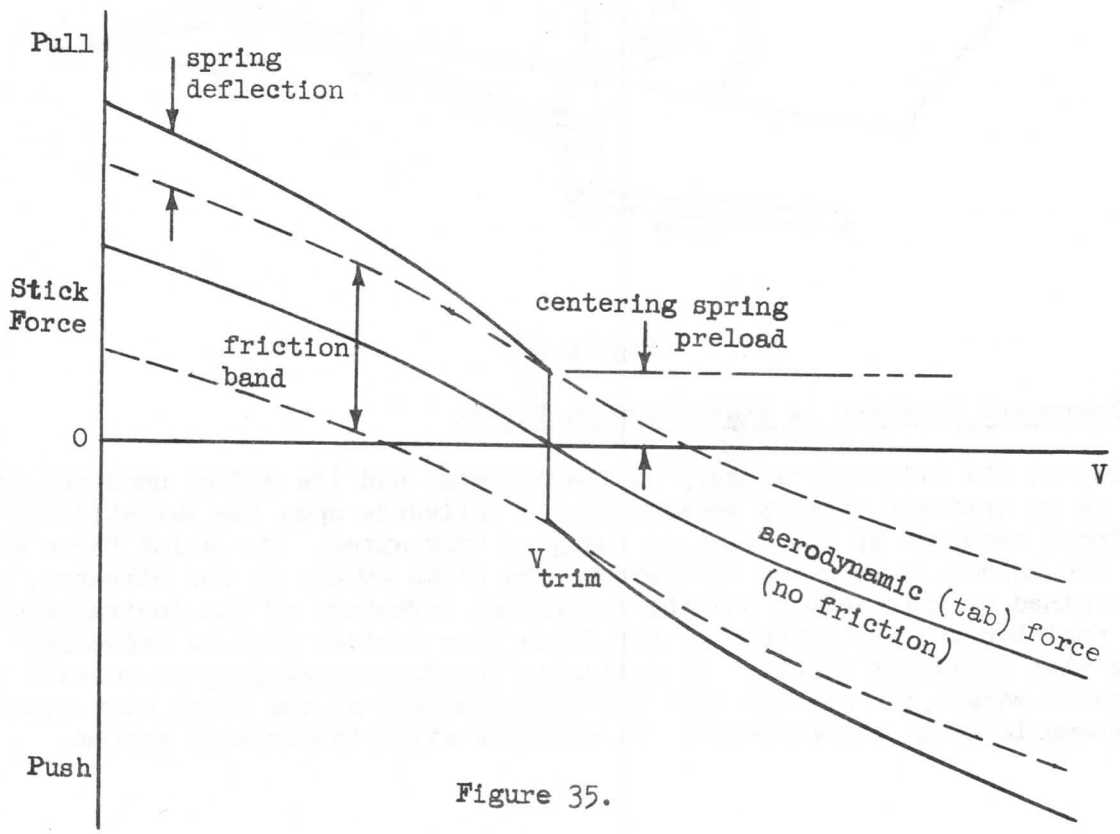

Figure 35.

If the friction band is large and no centering force is designed into the system, the airplane does not tend to return to a single trim speed when the stick is released after a speed change. The new trim condition could be anywhere within the speed range covered by the friction band. To eliminate this problem it is common practice to preload the system on both sides at the trim condition with a spring force great enough to overcome the friction, as shown. Now the spring load brings the speed back to within a very narrow range. A typical centering spring installation might be as shown in Figure 36.

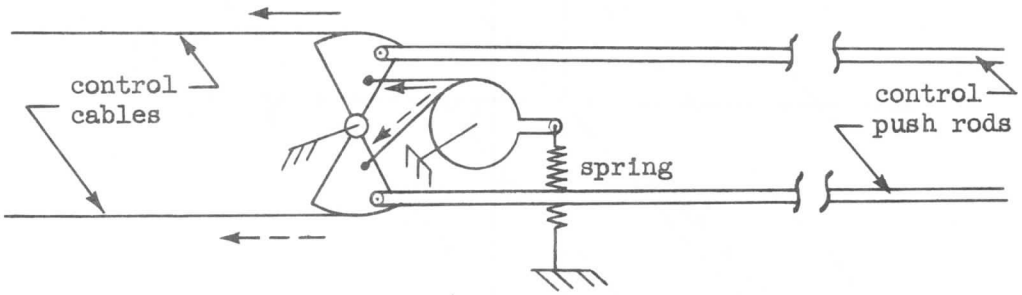

Figure 36.

A second function of the spring in the system might be to increase the force gradient in systems where the tab force requirement is not suitable. By choosing the correct spring and linkage, one may compensate for non-linearity or even hook in tab hinge moments. A hinge moment curve is said to hook if it bends in such a way as to indicate the same moment for two or more speeds or control surface deflections.

The stick force gradient, the slope of the force curve, is of great importance since it is the index of the pilot's feel for speed change. A steep gradient, especially close to the trim speed, will tend to keep the airplane flying at trim speed with a minimum of pilot interference, and it will enable him to trim to a given speed very easily.

Rudder pedal forces and control wheel forces may be analysed in a similar way.

Directional Control

If the rudder is deflected, a yawing moment will be generated which will cause the airplane to seek a new equilibrium side slip angle where the yawing moment is zero, as shown in Figure 37.

As mentioned before, this yaw will cause a rolling moment which must be counteracted by the application of lateral control (crossed controls) if a steady side slip is desired. Since there is the interaction of yaw and roll effects on the aircraft, it is possible to balance the lateral effects upon yaw against the rudder-induced yaw. In this way rudder and aileron control can be applied to cause the airplane to fly in a steady sideslip condition. The yaw effects due to roll can be shown as in Figure 38.

Although the combined yaw-roll side-slip is sometimes used as a drag device to increase the descent rate, it is not normally used on transport planes. A more usual use of the rudder in the landing pattern is its use to yaw the airplane

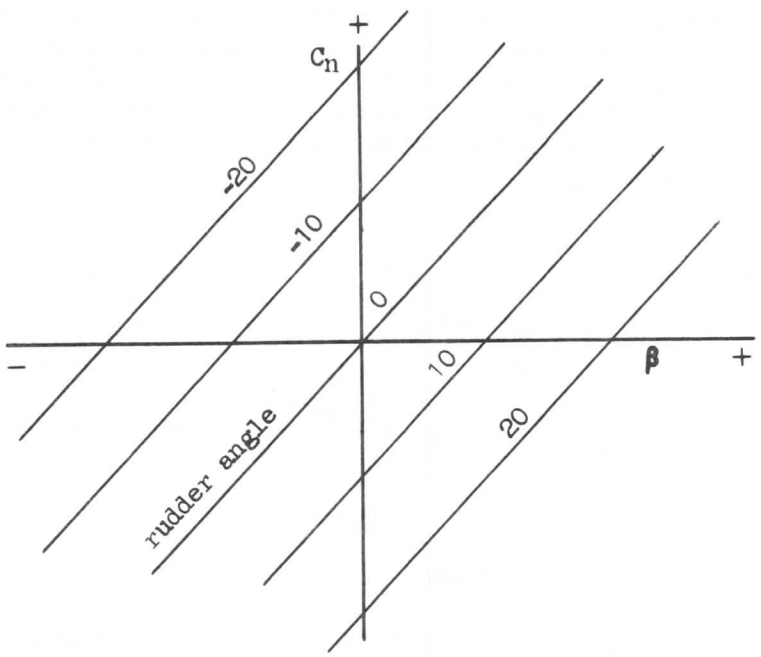

Figure 37.

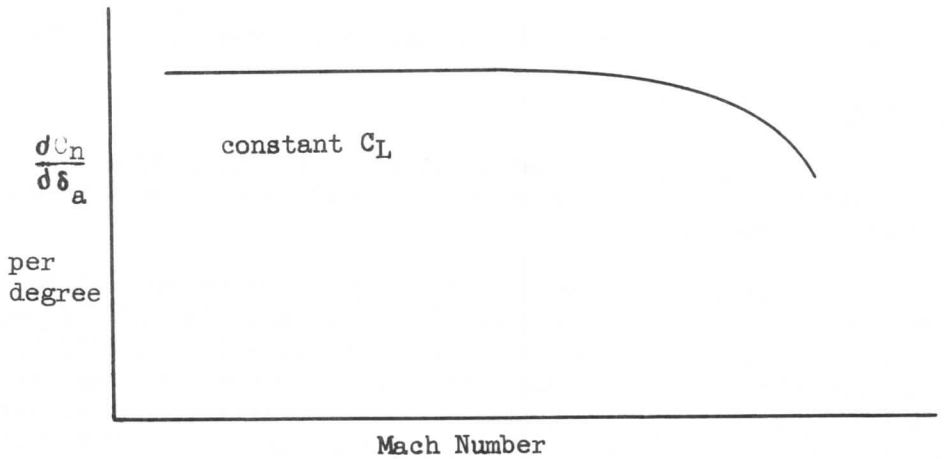

Figure 38.

into the crab angle necessary to compensate for cross-wind and to allow the airplane to maintain its flight path on the runway heading as shown in Figure 39. Since the plane is headed into the relative wind, it is necessary to take out the yaw at touchdown so as to line up the fuselage and the wheels for the roll down the runway. It is possible to maintain heading and alignment both by using the lateral control system to compensate for the wind yaw; however, the aileron is more sensitive, requiring more attention and technique, so it is usually necessary to use some rudder with the aileron. Also, the wing-down attitude is less desirable than the crab angle, and the lift-drag-thrust relationship is upset more.

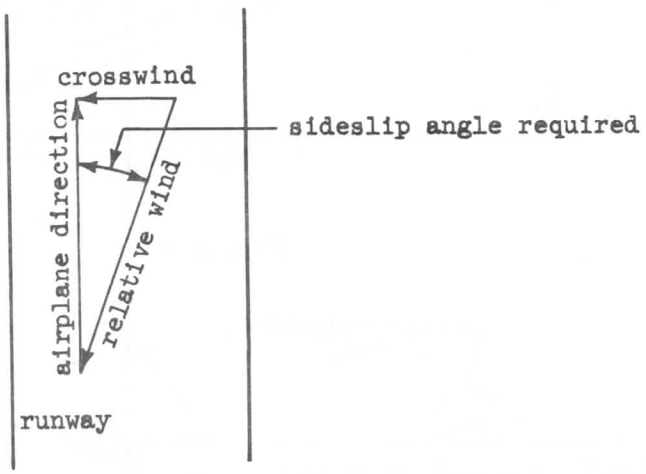

Figure 39.

The most critical requirement for the rudder is in counteracting the yawing effect of unsymmetrical engine thrust. The most critical conditions for unsymmetrical power occur at low speeds and high powers, such as just following takeoff. The requirements for rudder deflection are shown in Figure 40 for one and two engines out along with the maximum available rudder and maximum trim. The points where the maximum available rudder line intersects the engine-out lines define the speeds below which zero sideslip cannot be maintained. Below these speeds, however, no difficulty should be experienced since some of the additional yaw requirement can be counteracted by lateral control down to below "minimum control speed", V_{MC}.

Another place where the rudder is used is for turn coordination. When lateral control for a turn is applied and a roll rate is established, a yaw condition is set up which tends to oppose the roll. This "adverse" yaw is caused basically by the rotation of the lift vectors as indicated in Figure 41. To counteract this effect, some rudder deflection in the direction of the roll (left rudder for left roll) may be required. On the 707, however, this requirement is reduced because the spoilers which are raised to produce the roll produce drag, and thus a yawing moment, in a favorable or coordinating direction. Rudder deflection is required at low speeds, but the requirement drops off to where very little is used at cruise speed.

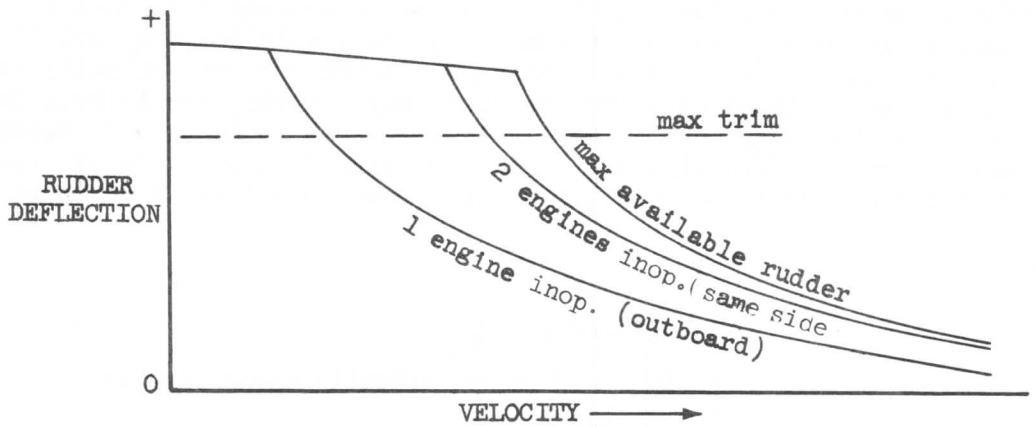

Figure 40.

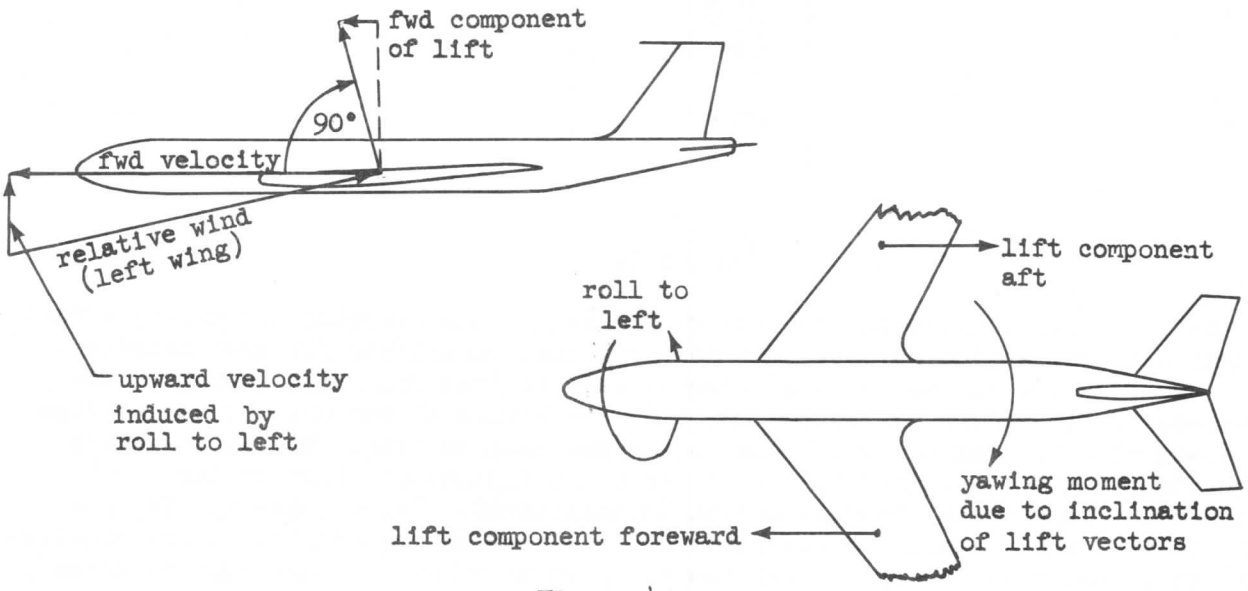

Figure 41.

Minimum control speed, V_{MC}, is defined in Section 3. Many of the civil air regulations are based upon this speed parameter. It must be possible to control the airplane with the most critical engine out and to maintain straight flight with zero yaw and bank angle not to exceed 5°. The speed shall not exceed $1.2\ V_{S_1}$ with take-off power, rear C.G., take-off flaps and landing gear retracted. per FAR 25.149

To analyze minimum control speed, consider the forces as shown in Figure 42. The sum of the moments about the C.G. must be zero.

$$\Sigma M_{CG} = 0$$

$$(T_e + D_{wm})l_e = F_r l_r = N_{design}$$

where, $$N = C_n S_{wing} q b \qquad (27)$$

and N_{design} is a value somewhat less than N_{max}, the difference being to allow for some dynamic overyaw capability.

Therefore, $$(T_e + D_{wm})_{avail} = \frac{C_{n\ design} S_w q b}{l_e}$$

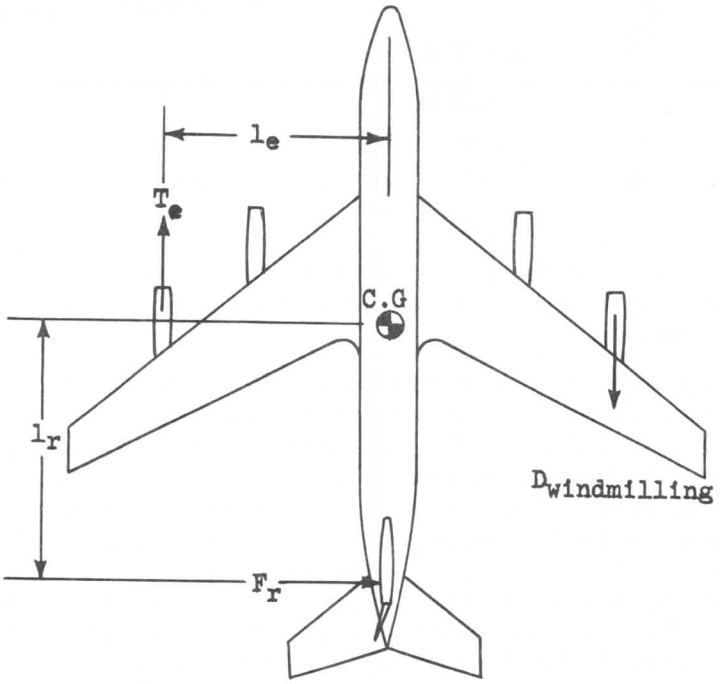

Figure 42.

Wind tunnel or flight test is used to determine C_{nMAX}, and equation (27) used to calculate $(T_e + D_{WM})$ and therefore thrust in terms of equivalent airspeed:

V_e	q	$T_e + D_{WM}$	T_e
assume	calculate	calculate	

Note that the single curve of V_e versus T_e is independent of altitude and temperature; it represents performance in all flight conditions. It is a definition of the rudder capacity.

If curves of thrust available from the engine for given altitude and temperature conditions are superimposed on the plot, a series of points are defined by the intersections. These are the minimum control speeds under those conditions. See Figure 43.

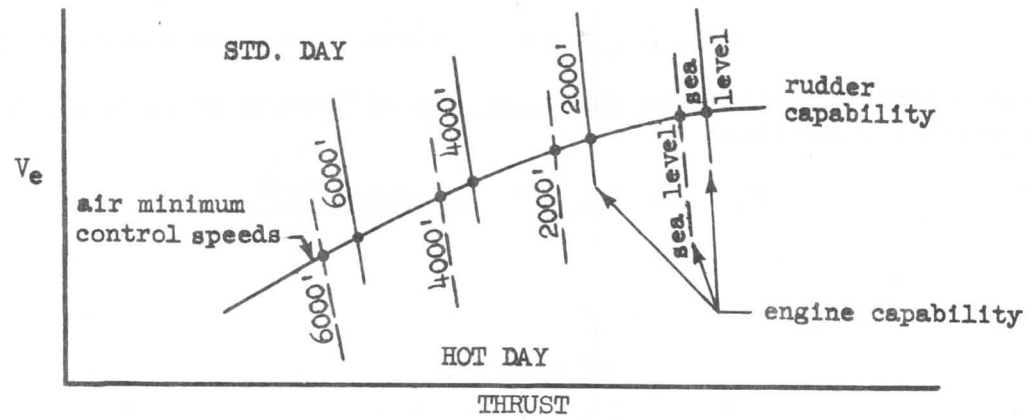

Figure 43.

Often, in actual practice, the tail yaw to be used is calculated by means of the formula,

$$C_n = C_{L_{vt}} \overline{V}_v$$

where $\overline{V}_v$ is the vertical tail volume coefficient analogous to $\overline{V}$ for the horizontol, and $C_{L_{vt}}$ is a reasonably high value of the vertical tail lift coefficient, but somewhat less than maximum.

On the ground, the minimum control speed may be lower since the rudder is assisted by the friction of the landing gear on the runway. The speeds are usually established by actual taxi tests. Although the friction of the nose wheel may lower V_{MC}, steering may not be employed to establish the published value. In addition, the ground minimum control speed is affected by crosswinds. It may increase or decrease. It will increase when the inoperative outboard engine and the crosswind are on the same side of the airplane. Separate analysis of Figure 42 has to be made to determine the magnitude of speed correction per knot of crosswind. For most airplanes, the correction is approximately 1.5 knots per knot of crosswind. The air minimum control speed is not affected by crosswinds since the airplane is flying within the moving air mass.

Lateral Control

The primary problem of lateral control is to provide a means of control which allows the pilot to hold wings level or at some desired bank angle, and to vary the bank angle as required. This means that the lateral control should ideally produce a pure rolling moment. This ideal lateral control has yet to be developed however, since there will always be some additional yawing effect.

The rolling control may be ailerons, spoilers, or a combination of both. In any case, deflection of the lateral control surface causes a spanwise asymmetry in wing lift distribution and results in a rolling moment being produced as shown in Figure 44a. As soon as the airplane starts to roll there is a second change in the spanwise lift distribution caused by the rolling velocity, as shown in Figure 44b.

The reason for this spanwise distribution is that the down-going wing has its angle of attack increased by the roll rate whereas the up-going wing has its angle reduced. At a given speed this angle of attack change is proportional to the roll rate as well as the spanwise station on the wing. When the lateral controls are deflected and a roll rate is generated, this rate will continue to increase until the rolling moment due to control deflection is exactly equalized by the resisting moment caused by the roll rate. (Note in Figures 44a and b that the rolling

moments are in opposite direction.) This rolling moment due to roll rate is usually called "damping in roll."

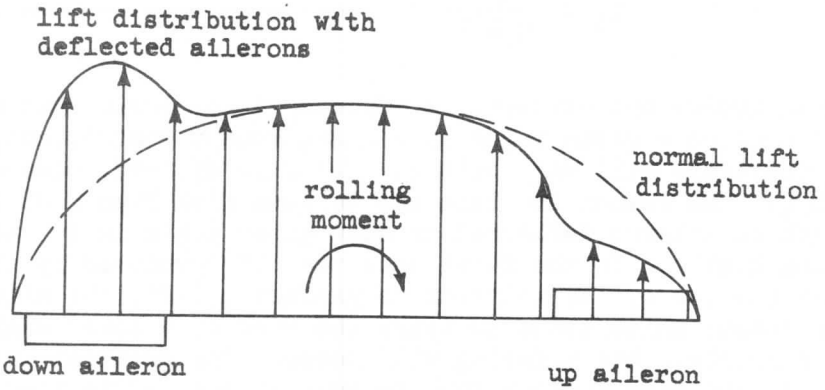

a

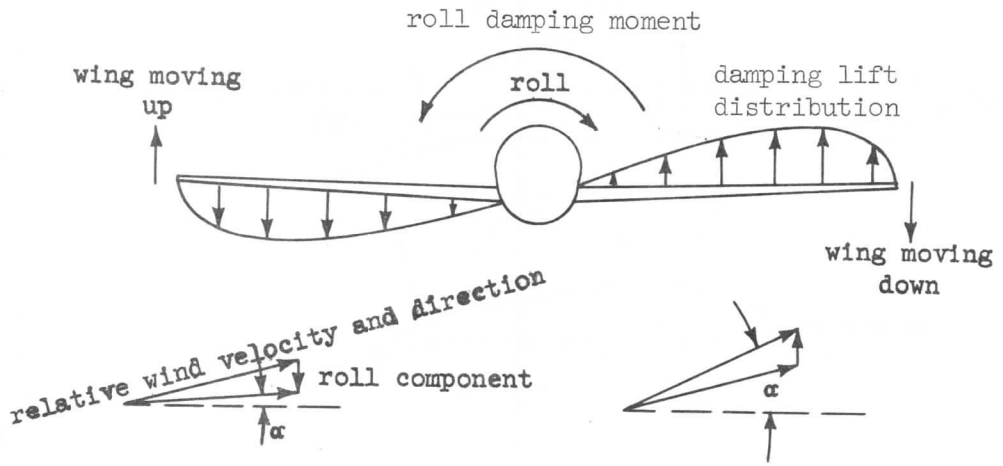

b

Figure 44.

There are several types of lateral controls used on airplanes. The first is the conventional wing-tip aileron such as used on the B-47. The reason for the wing tip selection is that it will produce the greatest rolling moment about the roll axis due to the large moment arm. The 707 makes use of inboard ailerons and spoilers also. In order to describe these control surfaces it is necessary to introduce the basic rolling moment equation which is identical in form to the pitching moment and yawing moment equations:

$$\mathscr{L} = C_l \, q \, S \, b \qquad (28)$$

where,

$\mathscr{L}$ is the rolling moment, ft lb

C_l is the rolling moment coefficient

q is the dynamic pressure, lb/ft^2

S is the wing area, ft^2

b is the wing span, ft

Solving for C_l,

$$C_l = \frac{\mathscr{L}}{q\ S\ b} \qquad (29)$$

Disregarding Mach number and aeroelastic effects, it is found that a given aileron deflection will produce a given value of rolling moment coefficient, C_l. (The rolling moment therefore will vary with q.) Elastic effects, however, will cause C_l to vary with q. The reason for this can be seen from Figure 45 in which a wing section with an aileron deflected to some given angle is subjected to air flow at low q and high q. In the first case the lift produced by the aileron is small because of the low q. In addition to producing lift, the aileron also produces a torsion moment which tends to twist the wing to a lower angle of attack. If the wing is flexible, this twisting will occur. The greatest twisting will occur, however, at the high q since for the same aileron deflection the torsion will be greatest.

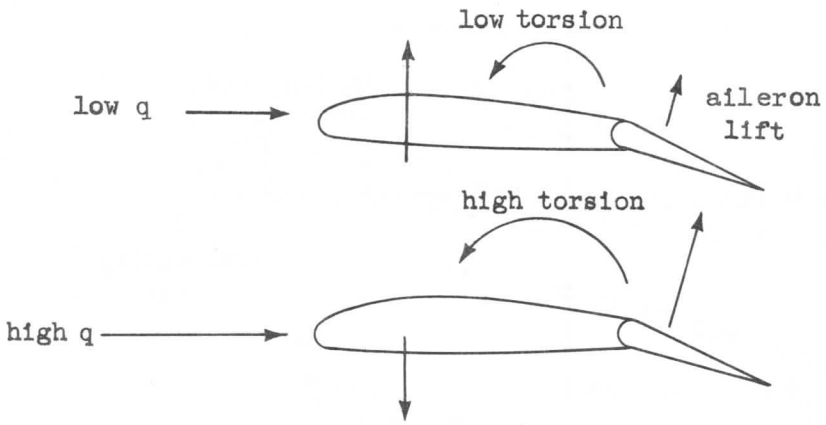

Figure 45.

The torsion being felt all along the wing span, the effect is additive; the twisting is increased linearly outward. Also, since the wing is most flexible at the tip, the twist is even more pronounced in the outboard sections. This twisting will be seen to be detrimental since it is reducing the angle of attack and thus unloading that portion of the wing. But the purpose of deflecting the aileron in the first place was to increase the load.

Eventually, if the q is increased to a high enough value, the increase in load due to the aileron will be exactly counteracted by the reduction in load due to the wing twisting. At this speed, deflecting the aileron will cause no roll response. To see this situation graphically, consider Figure 46, which plots rolling moment coefficient, C_l, vs q. The outboard aileron reaches what is called the "aileron reversal speed" beyond which the response of the aileron is actually reversed in sense. (Left wheel rotation will cause right roll.)

The inboard aileron, on the other hand, displays less reversal tendency since it has less wing span to work on torsionally. There is some loss of effectiveness, however. Also because of the shorter moment arm, the low speed rolling effectiveness will be less than that of the outboard aileron.

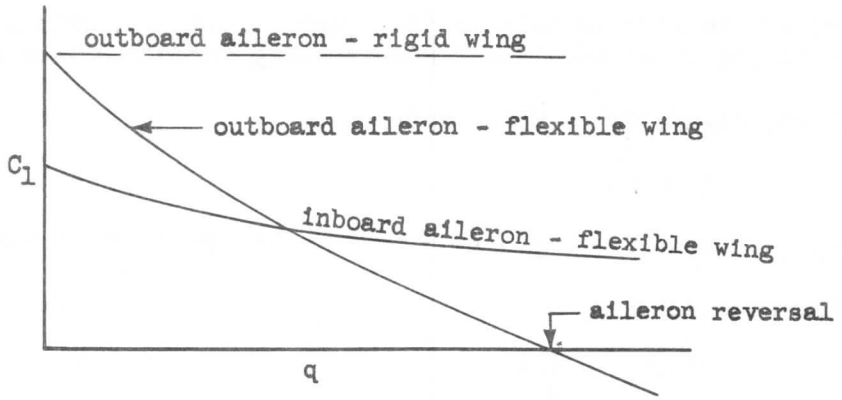

Figure 46.

The spoiler, which is actually an upper surface split flap, causes a loss in lift on the wing locally. Since the spoilers are used on one wing only or at least in laterally unsymmetrical configuration, they cause a rolling moment. However, they produce relatively minor elastic deflections of the wing because their lift increment is near wing elastic axis, and thus they are superior to the outboard aileron. In addition, spoilers are valuable as drag-producing items when deflected symmetrically on both wings. Used in this manner, they are called "speed-brakes."

The 707 airplane uses a combination of all the lateral controls discussed but programs the usage to gain the maximum utility. Outboard ailerons are provided to give the large rolling moment needed at low speed, but these surfaces are locked out when the airplane is flying at such speeds as to give excessive torsional bending and aileron reversal tendencies. The outboard ailerons are mechanically locked out of operation when the wing flaps are retracted; otherwise, they operate with the inboard ailerons. The spoilers are actuated by the same control linkage as the ailerons and work in conjunction with them. The aileron actuation is mechanical; the spoiler actuation hydraulic. The outboard and inboard spoilers are fed from separate hydraulic sources to insure against the loss of both sets at once.

Maneuvering Flight

When the airplane is in straight, unaccelerated flight, all the forces are in equilibrium; the system of moments is static. Therefore, the study of static stability and the location of the neutral points is of prime importance. But despite the fact that over 90% of flight is in a dynamic equilibrium condition, it is necessary to consider stability and control along curved paths and in maneuvers.

To accelerate or curve the flight path in the pitch plane, that is, to pull up or nose over, the force equilibrium must be unbalanced. The lift coefficient must be changed so rapidly that the speed cannot keep up with the change, and the equilibrium condition, $C_L V^2 = K$, is no longer satisfied. Thus an unbalanced force acts to create acceleration normal to the flight path. Or the speed change is induced more rapidly than α (or C_L) can compensate, producing the same effects. Unbalance in the vertical plane is induced also by rolling the airplane into a normal turn. Banking the wings rotates the lift vector out of the vertical plane.

This leaves only part of the lift to balance the weight vector and allows the horizontal component to act as an unbalanced accelerating force for lateral turn.

Let us assume a pull-up, Figure 47 in which lift is

$$L = nW$$

The unbalanced force, $\Delta L = nW - W = W(n-1)$ ——————————— (30)

produces a centripetal acceleration, a:

$$W(n-1) = \frac{W}{g} a$$

$$a = g(n-1) \text{ ——————————————} \quad (31)$$

However, centripetal acceleration in mechanics is given in terms of radius and tangential velocity as

$$a = \frac{V^2}{R} = g(n-1)$$

and angular velocity, in radians per second, is given as

$$\frac{d\theta}{dt} = \frac{V}{R} = \frac{g(n-1)}{V} \text{ ——— (pull-up)——————} \quad (32)$$

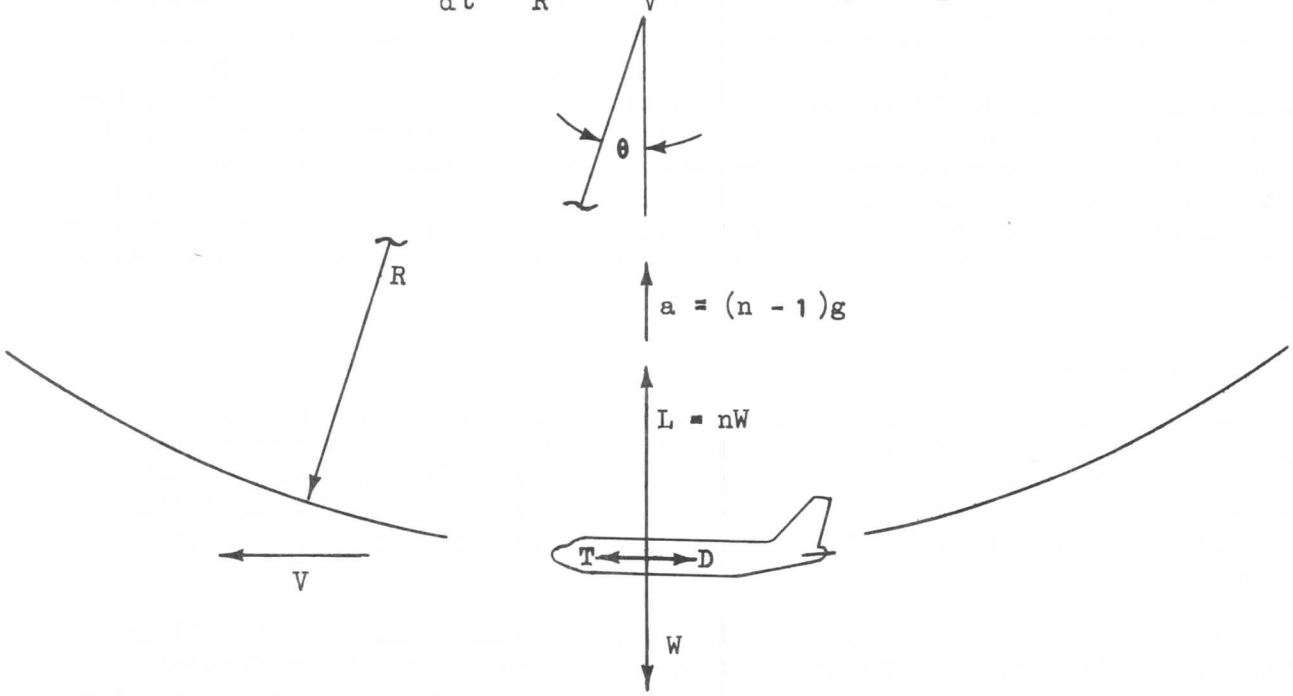

Figure 47.

In a steady state level turn, however, the unbalanced radial force is $L \sin\phi$, as shown in Figure 48. So rotation Ω in a horizontal plane at radius R' takes place. As shown in Section 3 (page 3.37), it can be proved that $R' = V^2/g \tan\phi$ and the pitch acceleration necessary to coordinate the turn is $n = 1/\cos\phi$.

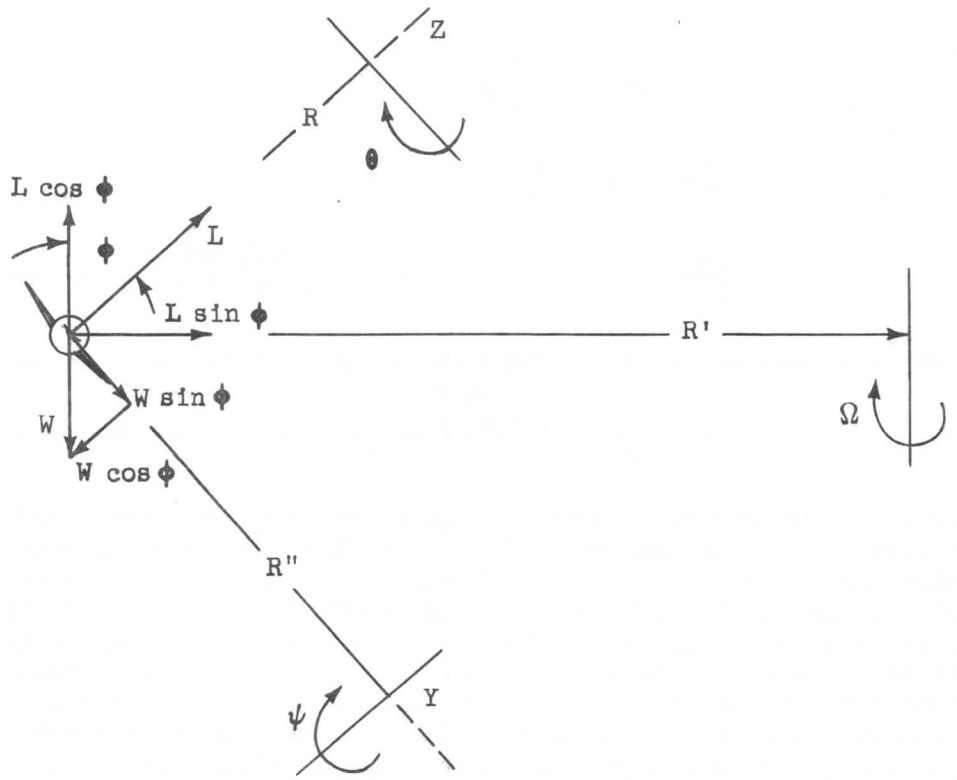

Figure 48.

In the horizontal plane,

$$L \sin\phi = \frac{W}{g}\frac{V^2}{R'}$$

$$ng \sin\phi = \frac{V^2}{R'}$$

but,
$$\sin\phi = \frac{\sqrt{n^2 - 1}}{n}$$

so,
$$\frac{d\Omega}{dt} = \frac{V}{R'} = \frac{g}{V}\sqrt{n^2 - 1} \qquad (33)$$

However, in order to study the needed airplane maneuvers, the motion must be resolved into components in the stability axis system related to the airplane itself. For the pilot can feel and react to only those forces which are felt upon the airframe and referenced to an axis system in which he can properly relate himself.

In the pitch plane, the unbalanced force is

$$L - W\cos\phi = \frac{W}{g}a_z$$

$$L - W\cos\phi = \frac{W}{g}\frac{V^2}{R},$$

and,

$$n - \cos\phi = \frac{V}{g}\frac{V}{R}$$

So,

$$\frac{d\theta}{dt} = \frac{V}{R} = \frac{g}{V}(n - \cos\phi)$$

$$\frac{d\theta}{dt} = \frac{g}{V}\left(n - \frac{1}{n}\right) \quad \text{—} \left(\begin{matrix}\text{steady-state} \\ \text{level turn}\end{matrix}\right) \text{———} \quad (34)$$

In a similar way the angular velocity component in yaw can be shown to be:

$$\frac{d\psi}{dt} = \frac{V}{R''} = \frac{g}{V}\frac{\sqrt{n^2 - 1}}{n} \quad \text{———————} \quad (35)$$

The angular velocity introduced by maneuvers produces damping moments which tend to oppose the rotation. This damping is felt as a false increase in stability and will require additional control moments over those normally needed to overcome the stability moments themselves. In maneuvering flight, then, it is necessary to increase the stick forces and deflect the elevator in order to increase lift even when the airplane is balanced at the neutral point, stick-fixed or free. The fact is that the C.G. may be moved aft of the neutral point and the airplane still retain stable feel. But eventually, a C.G. position will be reached such that the elevator angle required will be zero; this is called the stick-fixed maneuver point, N_m. The C.G. position where the stick force is zero is called the stick-free maneuver point, N'_m.

Since the elevator angle and stick force required for steady state maneuvering flight are determined by the load factor, n, it is convenient to use n as an independent variable and to express relative stability and control in terms of the deflection angle per g and force per g.

The angular rotation of the airplane in steady state maneuver imparts a change in flow around the stabilizer and, therefore, a change in angle of attack. This change creates a moment in such a direction as to damp the rotation as shown in Figure 49. The change in angle of attack at the stabilizer is

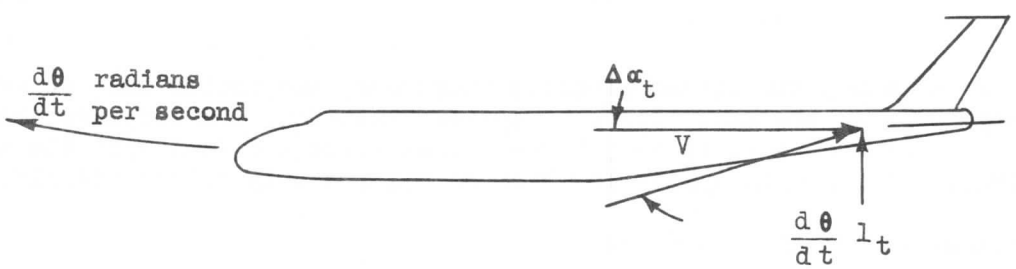

Figure 49.

$$\Delta\alpha_t = \frac{(d\theta/dt)l_t}{V} \quad \text{in radians} \qquad (36)$$

and the effective change in angle of attack due to the necessary change in elevator angle to compensate is

$$\Delta\alpha_t = \left(\frac{d\alpha_t}{d\delta_e}\right)\delta_e \qquad (37)$$

Thus,
$$\delta_{e_{req'd}} = \frac{(d\theta/dt)\,l_t}{(d\alpha_t/d\delta_e)V}(57.3) \quad \text{in degrees} \qquad (38)$$

but (in the pull-up),
$$\frac{d\theta}{dt} = \frac{g}{V}(n-1)$$

so,
$$\delta_e = \frac{g\,l_t}{(d\alpha_t/d\delta_e)V^2}(n-1)(57.3) \qquad (39)$$

For lack of a better criterion for judging the damping of the rest of the airplane, the δ_e required of the tail contribution is multiplied by 110% to obtain the total airplane damping requirement in maneuvers:

$$\delta_{e_{damp}} = \frac{63\,g\,l_t}{(d\alpha_t/d\delta_e)V^2}(n-1) \qquad (40)$$

The elevator deflection can then be written as

$$\delta_e = \delta_{eo} - \frac{C_L}{(dC_m/d\delta_e)}\left(\frac{dC_m}{dC_L}\right)_{Fix} - \frac{63\,g\,l_t\,(n-1)}{(d\alpha_t/d\delta_e)\,V^2}$$

which may be reduced to

$$\delta_e = \delta_{e_o} - \frac{2n(W/S)}{\rho V^2(dC_m/d\delta_e)}\left(\frac{dC_m}{dC_L}\right)_{fix} - \frac{63\,g\,l_t\,(n-1)}{(d\alpha_t/d\delta_e)\,V^2} \qquad (41)$$

The gradient of elevator angle can then be expressed in elevator angle per g by differentiation.

$$\left(\frac{d\delta_e}{dn}\right)_{pull\text{-}up} = -\frac{1}{V^2}\left[\frac{63g\,l_t}{(d\alpha_t/d\delta_e)} + \frac{2(W/S)}{\rho(dC_m/d\delta_e)}\left(\frac{dC_m}{dC_L}\right)_{fix}\right] \qquad (42)$$

The corresponding equations for steady-state level turn maneuver, found by substituting equation (34) instead of equation (32), are

$$\delta_{e\,turn} = \delta_{e_o} - \frac{2n(W/S)}{\rho V^2(dC_m/d\delta_e)}\left(\frac{dC_m}{dC_L}\right)_{fix} - \frac{63g\,l_t}{V^2(d\alpha_t/d\delta_e)}\left(n - \frac{1}{n}\right) \qquad (41a)$$

and
$$\left(\frac{d\delta_e}{dn}\right)_{turn} = -\frac{1}{V^2}\left[\frac{63g\,l_t}{(d\alpha_t/d\delta_e)}\left(1 - \frac{1}{n^2}\right) + \frac{2(W/S)}{\rho(dC_m/d\delta_e)}\left(\frac{dC_m}{dC_L}\right)_{fix}\right] \qquad (42a)$$

The gradient component sensed at the neutral point is only that portion contributed by the damping in pitch. Thus if the gradient (42) or (42a) is equated to zero, the resulting expression solved for $\left(\frac{dCm}{dCL}\right)_{fix}$, and that value added to N_o, the stick-fixed maneuver point is defined:

$$N_m = N_o - \frac{63\rho g l_t}{2(W/S)} \frac{(\partial C_m/\partial \delta_e)}{(d\alpha_t/d\delta_e)} \qquad (43)$$

This maneuver point is aft of the stick-fixed neutral point, the difference between the two being a function of altitude (density) and wing loading on a given configuration.

The pilot's most valid index of his maneuverability is the force required of him to produce the necessary acceleration to maneuver, the stick force per g. This stick force includes the airplane's maneuver damping and the effects of elevator floating tendencies. Too high a force gradient makes the control too fatigueing to the pilot; too low a gradient makes the airplane too sensitive to handle properly.

The angle of attack of the tail in accelerated flight may be written as,

$$\alpha_t = \alpha_o + \frac{2n(W/S)}{\rho V^2 a_w}\left(1 - \frac{d\varepsilon}{d\alpha}\right) - i_w + i_t + \frac{g l_t}{V^2}(n-1)\,57.3 \qquad (44)$$

and δ_e is defined by equation (41).

If these are substituted into the general stick force equation,

$$F_s = -GS_e c_e \rho/2\, V^2 \eta_t \left[C_{h_o} + \frac{\partial C_h}{\partial \alpha_t}\alpha_t + \frac{\partial C_h}{\partial \delta_e}\delta_e + \frac{\partial C_h}{\partial \delta}_{tab}\delta_{tab}\right]$$

the following force equation results:

$$F_s = -G S_e c_e \rho/2\, V^2 \eta_t \left[C_{ho} + \frac{\partial C_{he}}{\partial \delta_{tab}}\delta_{tab} + \frac{\partial C_{he}}{\partial \alpha}\left[\alpha_o + \frac{2n(W/S)}{\rho V^2 a_w}\left(1 - \frac{d\varepsilon}{d\alpha}\right) - i_w + i_t + \frac{g l_t}{V^2}(n-1)\,57.3\right] + \frac{\partial C_{he}}{\partial \delta_e}\left[\delta_{eo} - \frac{2n(W/S)}{\rho V^2(\partial C_m/\partial \delta_e)}\left(\frac{dC_m}{dC_L}\right)_{fix} - \frac{63 g l_t}{V^2(d\alpha_t/d\delta_e)}(n-1)\right]\right]$$

$$F_s = -G S_e c_e \rho/2\, V^2 \eta_t \left[C_{ho} + \frac{\partial C_{he}}{\partial \alpha}(\alpha_o - i_w + i_t) + \frac{\partial C_{he}}{\partial \delta_e}\delta_{e_o} + \frac{\partial C_{he}}{\partial \delta_{tab}}\delta_{tab} + \frac{2n(W/S)}{\rho V^2}\left[\frac{1}{a_w}\frac{\partial C_{he}}{\partial \alpha}\left(1 - \frac{d\varepsilon}{d\alpha}\right) - \frac{\partial C_{he}/\partial \delta_e}{\partial C_m/\partial \delta_e}\left(\frac{dC_m}{dC_L}\right)_{fix}\right] + \frac{57.3\, g l_t}{V^2}(n-1)\left[\frac{\partial C_{he}}{\partial \alpha} - \frac{1.1}{d\alpha_t/d\delta_e}\frac{\partial C_{he}}{\partial \delta_e}\right]\right]$$

But, $\left(\frac{dC_m}{dC_L}\right)_{free} = \left(\frac{dC_m}{dC_L}\right)_{fix} - \frac{\partial C_m/\partial \delta_e}{\partial C_h/\partial \delta_e}\frac{\partial C_{he}/\partial \alpha}{\partial C_L/\partial \alpha}\left(1 - \frac{d\varepsilon}{d\alpha}\right)$,

$$\text{so,}\quad F_s = -G\,S_e\,c_e\,\rho/2\,V^2\,\eta_t\left[C_{h_o} + \cdots + \frac{\partial C_{he}}{\partial \delta_{tab}}\,\delta_{tab} - \frac{2n(W/S)}{\rho V^2}\right.$$

$$\left.\frac{\partial Ch/\partial \delta_e}{\partial Cm/\partial \delta_e}\left(\frac{dC_m}{dC_L}\right)_{free} + \frac{57.3\,g l_t}{V^2}\cdots\right]$$

$$F_s = -G\,S_e\,c_e\,1/2\,\rho V^2\,\eta_t\left[C_{h_o} + \frac{\partial Che}{\partial \delta_e}\,\delta_e + \frac{\partial Che}{\partial \delta_{tab}}\,\delta_{tab} + \right.$$

$$\frac{\partial Che}{\partial \alpha_t}\,(\alpha_o - i_w + i_t) - \frac{2n(W/S)}{\rho V^2}\,\frac{\partial Che/\partial \delta_e}{\partial Cm/\partial \delta_e}\left(\frac{dCm}{dC_L}\right)_{free} +$$

$$\left.\frac{57.3\,g l_t}{V^2}\,(n-1)\left(\frac{\partial C_{he}}{\partial \alpha} - \frac{1.1\,\partial Che/\partial \delta_e}{d\alpha_t/d\delta_e}\right)\right] \qquad (45)$$

Let us evaluate this equation for the condition in which the airplane is trimmed to $F_s = 0$ at V_{trim} in $n = 1$ flight.

$$0 = -G\,S_e\,c_e\,1/2\,\rho\,V_{trim}^2\,\eta_t\left[C_{h_o} + \frac{\partial Che}{\partial \delta_e}\,\delta_e + \frac{\partial Che}{\partial \delta_{tab}}\,\delta_{tab} + \right.$$

$$\left.\frac{\partial Che}{\partial \alpha_t}\,(\alpha_o - i_w + i_t) - \frac{2(W/S)}{\rho V_{trim}^2}\,\frac{\partial Che/\partial \delta_e}{\partial Cm/\partial \delta_e}\left(\frac{dCm}{dC_L}\right)_{free}\right]$$

This yields,

$$C_{h_o} + \frac{\partial Che}{\partial \delta_e}\,\delta_e + \frac{\partial Che}{\partial \delta_{tab}}\,\delta_{tab} + \frac{\partial Che}{\partial \alpha_t}\,(\alpha_o + i_t - i_w) = \frac{2(W/S)}{\rho V_{trim}^2}\,\frac{\partial Che/\partial \delta_e}{\partial Cm/\partial \delta_e}\left(\frac{dCm}{dC_L}\right)_{free}$$

which can now be substituted into the force equation:

$$F_s = G\,S_e\,c_e\,\eta_t\;W/S\;\frac{\partial Che/\partial \delta_e}{\partial Cm/\partial \delta_e}\left(\frac{dCm}{dC_L}\right)_{free}\left(n - \frac{V^2}{V_{trim}^2}\right) -$$

$$57.3\,G\,S_e\,c_e\,\rho/2\,\eta_t g l_t\,(n-1)\left(\frac{\partial Che}{\partial \alpha} - \frac{1.1\,\partial Che/\partial \delta_e}{\partial \alpha_t/\partial \delta_e}\right)$$

The maneuvering stick force gradient is obtained by simple differentiation with respect to n; therefore, stick force per g is:

$$\frac{dFs}{dn} = G\,S_e\,c_e\eta_t\;W/S\;\frac{\partial Che/\partial \delta_e}{\partial Cm/\partial \delta_e}\left(\frac{dCm}{C_L}\right)_{free} -$$

$$57.3\,G\,S_e\,c_e\,\eta_t\;\rho/2\,g l_t\left(\frac{\partial Che}{\partial \alpha} - \frac{1.1\,\partial Che/\partial \delta_e}{\partial \alpha_t/\partial \delta_e}\right) \qquad (46)$$

The first term of this expression is the stability contribution; the second, the airplane damping. Any artificial damping device or static weight in the airplane system will add its contribution to the force and force gradient equations.

Note that the stick force gradient does not vanish at the stick-free neutral point, for if $(dCm/dCL)_{free} = 0$, there is still the damping component of gradient. However, if the C.G. is moved sufficiently far aft, dFs/dn will vanish at a position N'_m which we define as the stick free maneuver point. If the C.G. were aft of this point, the gradient would be negative. By solving the gradient expression at the dFs/dn = 0 condition, the following equation is found:

$$N'_m = N'_o + \frac{57.3\ \rho/2\ g\ l_t}{W/S\ \frac{\partial Che/\partial \delta e}{\partial Cm/\partial \delta e}} \left(\frac{\partial Che}{\partial \alpha} - \frac{1.1\ \partial Che/\partial \delta e}{\partial \alpha_t/\partial \delta e} \right) \quad \text{——— (47)}$$

Obviously, stick forces and stick force gradients increase with airplane size and wing loading. But the gradient is a function of altitude also. The force per g is greatest in maneuvers at low altitude and decreases as altitude is increased. This decrease in damping at altitude manifests itself in an apparent decrease in stability when maneuvering in high-altitude flight. The stick force per g is independent of speed except for compressibility and Reynolds number effects upon the lift and control effectiveness.

It is not within the province of this discussion to deal with transient or non-steady-state accelerations of the airplane. But it should be said that in rapid maneuvers the relationships may be quite different due to the fact that the relative lag in control and feel relationships depends very largely upon the type of balance, the response rate in the control linkage, the relative rigidity of the surfaces, and many other factors.

Since the maneuvering deflection and force requirements may be limiting upon the C.G. position, it is advisable to review the restrictions on C.G. location. In terms of aft limit, the two limiting factors would be stability as measured by the stick-free neutral point and maneuvering control as measured by the minimum acceptable force gradient. Generally, the stability requirement is most critical and the aft C.G. location will be determined at such a position as to allow a small safety margin ahead of the neutral point. The forward position is limited by control requirements as measured in terms of the total control deflection available and the stick forces necessary. The maximum stick force per g must not exceed the average pilot's abilities; the stick force gradient with speed at the trim velocity must be adequate to give good centering, but cannot be so great as to unduly restrict the ability to change speed. The stick force required to change speed and to flare in the landing procedure must not exceed a specified maximum value, and the elevator deflection required by this maneuver must not be limited by the structural limit of the elevator design. In most cases of transport type airplanes, the elevator requirement in landing is most restrictive.

Center of Gravity Control

Since the center of gravity location is of very great importance in the longitudinal stability and control characteristics of the airplane, it is imperative that there be efficient means of locating it for any loading condition. This can be accomplished quite simply even though there may be a great many various conditions to be considered. Standard practice is to find the sum of all moments about a fixed reference and to calculate the C.G. from the total weight and moment at that point: for example, total moment about the .25$\bar{c}$ point is the total weight times the distance from the C.G. to that reference point.

Since all structure and fixed equipment are of given weights and in fixed location, the moment of each component can be calculated once and tabulated or plotted for future use. Then the effects of passengers, cargo and incidentals can be calculated and tabulated in terms of various weights placed in various probable positions. Fairly complete tabulations of this kind are always made up for each transport plane. Thus the total moment sum can be found easily. And if the moment-weight curves are calculated for the C.G. limits specified by the aerodynamic design, there is an easy way to test any specific loading proposal against design limitations, to find the optimum location for any given load, or to determine the proper trim setting for a given loading condition.

The C.G. grid provides a simple graphical method for determing the center of gravity from the weight-moment relationship about a point within the C.G. range of the airplane.

The weight-moment relationship about any given reference axis is:

$$M = k\,W \qquad (48)$$

where,

M = moment
k = distance from the reference axis
W = gross weight

This equation represents a family of lines when plotted as M vs W for constant k (or C.G. location) as in Figure 50.

Usually the reference axis is arbitrarily set near the center of the C.G. range of the airplane, and the lines are drawn along convenient load C.G. locations from the forward to the aft limits established by the design.

Since the weight range of interest does not extend beyond operational weights, the grid may be cut off below W_{min} and above W_{max}. Any operational weight - C.G. condition can be located as a point on the remaining grid. The accuracy with which values may be read is dependent upon grid size and accuracy, and upon the care with which it is used.

The major problem in weight and balance is the determination of the resulting C.G. location when a given weight increment is added (or subtracted) at a given location on the airplane. For example, knowing the total gross weight and relative C.G. location at the initial cruise operation, one needs to find the C.G. location, and thereby the stability, after a given weight of fuel located in a fixed tank has been burned off.

If a given weight increment is imposed at a given distance from the reference point, a given moment is generated, and this moment, when added to the original total moment, will determine the resulting total moment. The slope of the moment weight relationship is a function of the location only and is independent of the airplane balance. However, the stability effect of C.G. shift is a function of the original C.G. position also. Once the C.G. grid is overlaid upon the moment-weight grid and the slopes representing loading station locations are established, it is possible to trace the C.G. through the full loading and unloading sequences by a purely graphical method. The basic rectangular moment-weight grid is often erased to simplify the plotting grid.

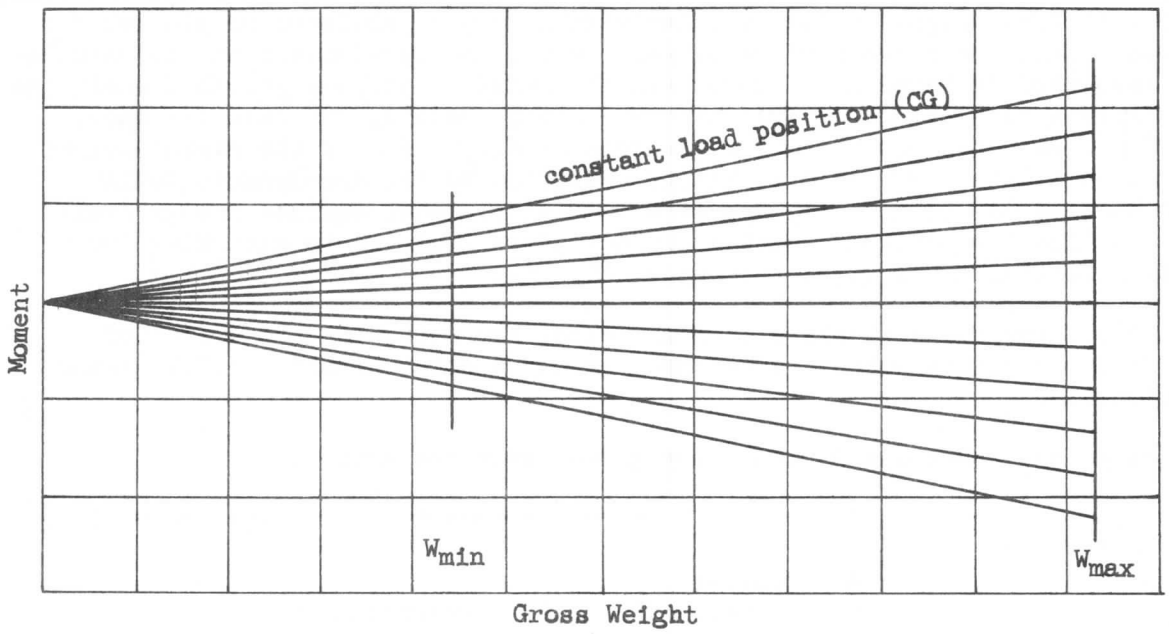

Figure 50.

One may prove the validity of such a process and also show how the slopes may be established geometrically by establishing a relationship between the moment-weight-C.G. grid and a convenient body station scale thus:

Beside a C.G. grid such as Figure 51, lay out a convenient body station scale as shown, parallel to the gross weight axis.

Define the moment scale factor,

$$m = \frac{M}{\text{C.G. scale length}} = \frac{\bar{c}(\text{in})}{100\%} \; W_{max}(\text{lb}) \; \frac{\text{C.G. range in } \% \; \bar{c}}{\text{C.G. scale length (in)}}$$

in lb/in,

the body station scale factor

$$s = \frac{\text{Fuselage length (in)}}{\text{body scale length (in)}} \qquad \text{in/in,}$$

and the weight scale factor

$$w = \frac{W_{max}(\text{lb}) - W_{min}(\text{lb})}{\text{Weight scale length (in)}} \qquad \text{lb/in}$$

Locate the reference point of the design C.G. range on the body scale by adding to the body station of the leading edge of the mean aerodynamic chord (inches) the $\bar{c}$ (inches) multiplied by the percentage of the $\bar{c}$ to the reference point, which is usually given in $\%\bar{c}$. This is point H. Erect a perpendicular at point H to J of the length

$$HJ = \frac{m}{sw}$$

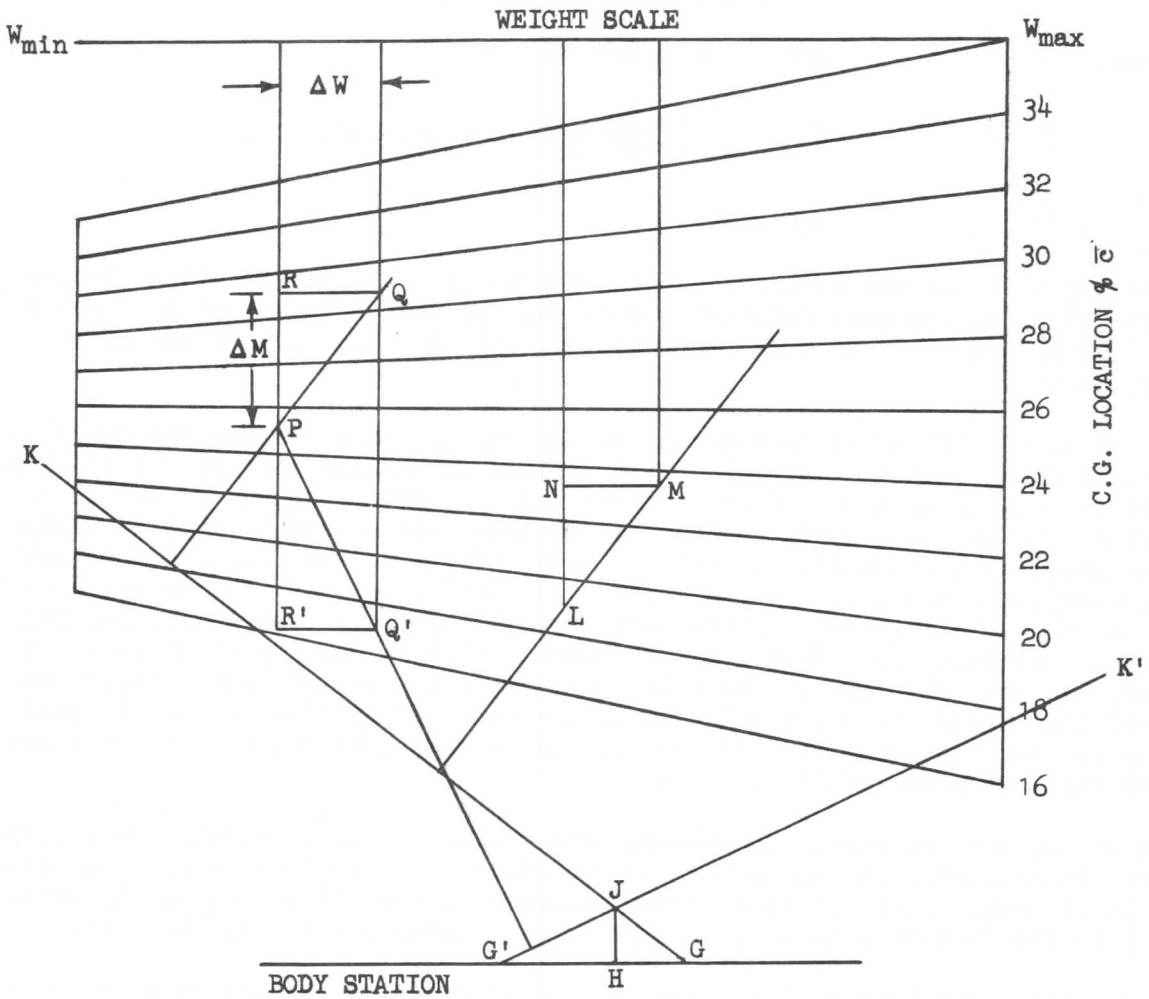

Figure 51.

If a weight, ΔW, is to be added at station G of the body, draw line GJK. Thru the known original loading point P drop a perpendicular to GJK and project to Q, the new weight point determined by adding ΔW to the original weight.

The line PR represents the change in moment, ΔM. For since triangles GJH and PQR are similar,

$$GH = \frac{(PR)\ (JH)}{QR}$$

But by construction

$$JH = \frac{m}{(s)\ (w)} \quad ,$$

so,

$$GH = \frac{(PR)\ m}{(QR)\ (s)\ (w)} \quad .$$

The distance of the load from the reference is D = (s) (GH), and the change in moment is ΔM = D (ΔW).

Therefore,

$$\Delta M = (s)\,(GH)\,(w)\,(QR)$$

$$\Delta M = (s)\,\frac{(PR)\ (m)}{(QR)\ (s)\ (w)}\,(w)\,(QR)$$

$$\Delta M = (PR)\ m$$

If, starting with any new original loading condition, L, the same weight increment were added at the same location, as above, the same moment increment would result. LM and PQ would be equal in magnitude and direction regardless of the starting points.

It will be noted that HJ is independent of the weight increment and the position where it is to be placed. In fact, HJ is defined by the geometry of the grid and is fixed for all conditions. G is a function of position only, so direction or slope of PQ (or LM) is defined by position or body station only. Thus if weight is to be added at a given station (the centroid of the forward cargo compartment, for instance), the slope of the line which will define any Q or M from any P or L is defined from the station. In the same way, the slope is defined for loading at any other station, G'. Thus a fan of slopes defining loading at various stations can be drawn anywhere on the grid paper or an overlay and each transfered by translation along the principal axes to the point of application on the grid. By doing so, one may trace the full loading or unloading sequence, step by step, and know the C.G. location at any time.

The use of the grid in obtaining balance data results in time-saving. By a simple graphical construction one can obtain a full picture of the loading and C.G. placement. It is common practice in military planning to use the grid directly or indirectly in the form of a slide-rule type load adjuster based upon the grid.

For commercial operations each airline is furnished with a loading document which gives complete details in tabular form. There are listed moment arms, weights and moments for all structure and components, both fixed and expendable. Passenger and cargo loadings in various combinations are given, and allowances for crew and passenger moment as well as fleet variations are made.

Many other graphical and tabular methods for calculating C.G. and trim setting are in current use.

4-4 DYNAMIC CONSIDERATIONS

Dihedral Effects

An airplane wing will create roll disturbances whenever it is disturbed in yaw. This roll due to yaw is called dihedral effect because dihedral (wing tip higher than wing root) can be shown to be one of the major causes. In order to study the yaw-dihedral effect independent of angle of attack, consider a wing with dihedral flying at zero angle of attack and yawed. See Figure 52.

The velocity of the wing panel normal to the airplane x-axis, measured at point P, the center of pressure, is:

$$V_n = V_y \sin \gamma \qquad (49)$$

where γ is the dihedral angle. For small angles, γ, this can be approximated closely by

$$V_n = V_y \gamma \quad (\gamma \text{ in radians})$$

The change in angle of attack due to dihedral and yaw only is

$$\Delta\alpha_{\text{dihedral}} = \frac{V_n}{V} = \frac{V_y \gamma}{V}$$

But, $V_y = V\beta$

so, $\Delta\alpha = \beta\gamma$

The lift effect could be indicated thus:

$$\Delta C_L = a\Delta\alpha = a\beta\gamma,$$

and

$$\left(\frac{\partial C_L}{\partial \beta}\right)_{\text{dihedral}} = a\gamma \qquad (50)$$

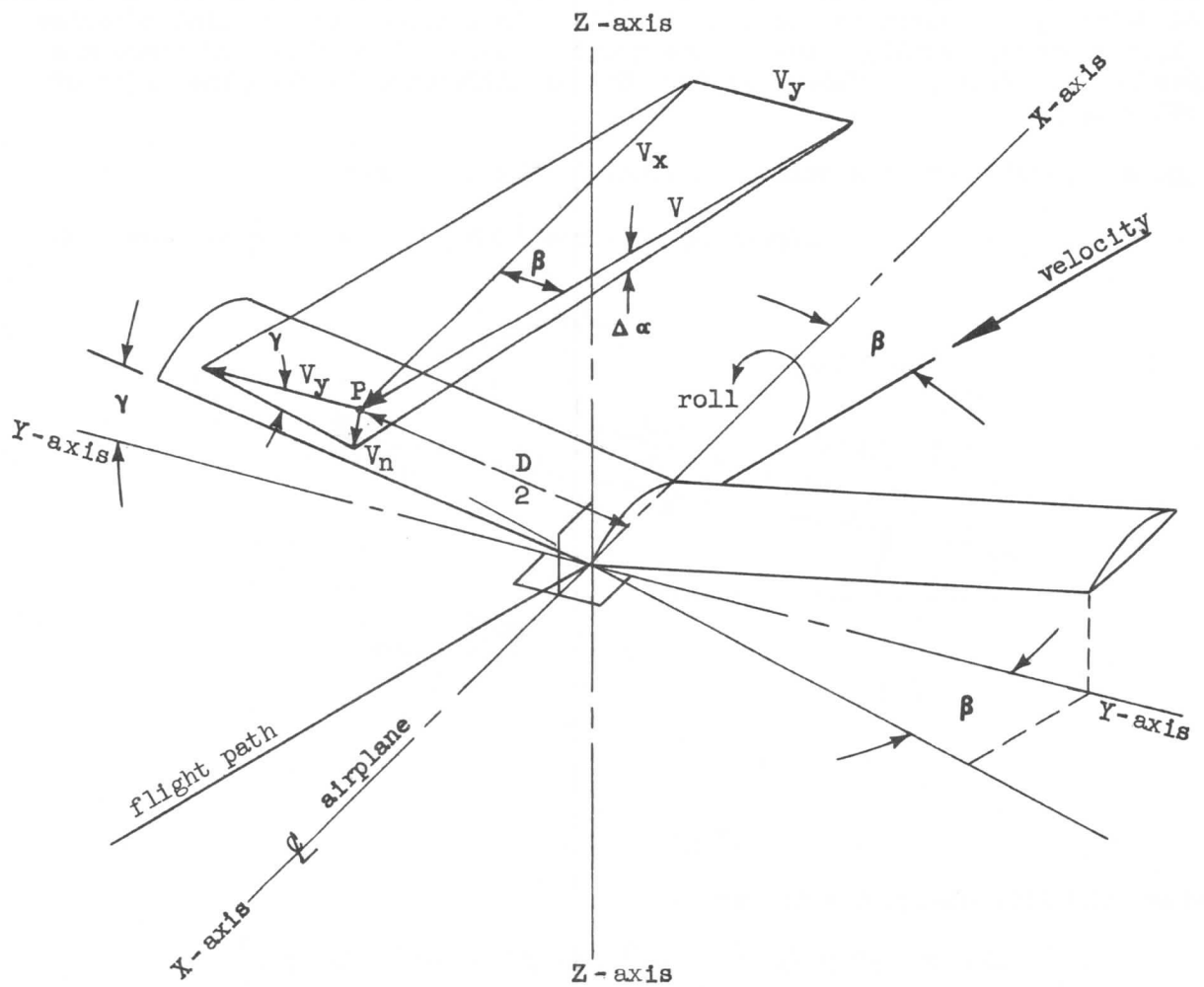

Figure 52.

The roll effect of each wing panel, in terms of the rolling moment coefficient, could be written as

$$\left(\frac{\partial C_l}{\partial \beta}\right)_{\text{dihedral}} = \left(\frac{\partial C_L}{\partial \beta}\right)_{\text{dihedral}} \frac{D}{2b} = \frac{aD\gamma}{2b}$$

and the total dihedral effect is the sum of the effects on the two wing panels:

$$\left(\frac{\partial C_l}{\partial \beta}\right)_{\text{dihedral}} = \frac{aD\gamma}{b} \qquad (51)$$

D is the distance between lift centers and b is the wing span.

The interaction of yaw upon roll is also affected by other factors; principally the sweepback angle. In fact, the effects are so like those of dihedral, that they are usually added and the combination of all the interactions called "dihedral effects." To study and approximate the dihedral effects of sweepback, recall that, as shown in section 1, the lift of the swept wing is proportional to and determined by the velocity component in the X-Y stability plane normal to the line of effective lift centers, usually close to the quarter chord. Therefore, if there are changes in lift with yaw, their sum must be the difference between the lifts of the two wing panels.

In Figure 53, note that the velocity normal to the .25 chord

$$V_{\text{effective}} = V \cos(\Lambda \pm \beta) \qquad (52)$$

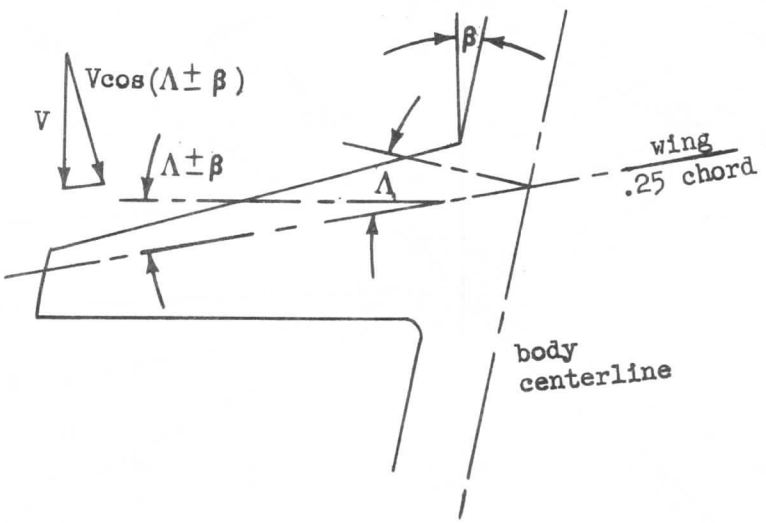

Figure 53.

Therefore the lift change due to yaw is

$$\Delta L = C_L \rho/2 S/2 \, V^2 \left[\cos^2(\Lambda - \beta) - \cos^2(\Lambda + \beta) \right]$$

but, $\cos^2 x - \cos^2 y = -\sin(x+y)\sin(x-y)$,

so, $$\Delta L = C_L \frac{\rho}{2} \frac{S}{2} V^2 \left[-\sin 2\Lambda \sin(-2\beta) \right]$$

$$\Delta L = C_L \frac{\rho}{2} \frac{S}{2} V^2 \left[\sin 2\Lambda \sin 2\beta \right] \qquad (53)$$

Since β is always small in the practical case, we may set $\sin 2\beta = 2\beta$ and

$$\Delta L = \beta\, C_L \frac{\rho}{2} V^2\, S \sin 2\Lambda \qquad (54)$$

If one assumes that one half of this lift acts on each panel at a distance D/2 from the roll center,

$$(C_l)_{sweep} = \frac{\Delta L\ D}{q\ S\ b\ 2} \qquad (55)$$

and differentiating,

$$\left(\frac{dC_l}{d\beta}\right)_{sweep} = \frac{D}{2b} C_L \sin 2\Lambda \qquad (56)$$

There may be other influences upon $dC_l/d\beta$ beside dihedral and sweep. The fuselage interferes with flow over the wings and thus may induce roll effects. The effects of up or down-wash on the upstream side and corresponding wake effects on the downstream side of a yawed fuselage are dependent upon the size and cross-section of the fuselage ahead of and beside the wing and the wing location on the body. Side forces developed by the vertical tail of the sideslipping airplane give rise to rolling tendencies since the tail aerodynamic center is above the normal rolling axis.

A simplified picture of dihedral effects might be obtained by considering roll and yaw with respect to the flight path, as in Figure 54. The wing moving forward in the yaw is not only travelling at greater speed than the other; it is also at greater angle of attack. This will result in a rolling moment in the same direction as the yawing motion. If the wing is also swept, it will contribute still more moment due to the increase of the moment arm of the wing moving forward and the decrease of the moment arm on the aft-moving wing.

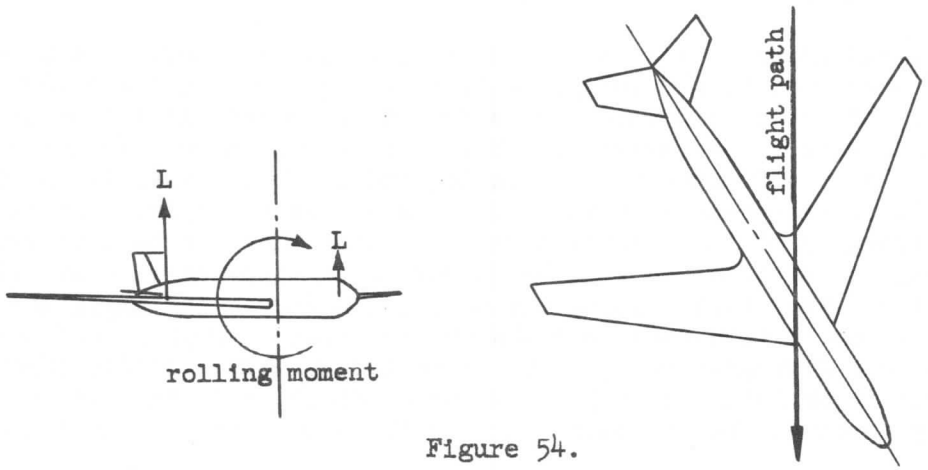

Figure 54.

STABILITY AND CONTROL

Dutch Roll

When an airplane is rolled, the inclination of the lift vector and the resulting unbalanced side component produce side slip due to roll. This side slip on a wing with dihedral causes a rolling moment tending to lift the down wing since the lift will be greater on that side than on the other. The effect upon the vertical tail is to produce a yawing moment, nose to the down side. If the tail effects are large compared to the dihedral effect, the airplane goes into an ever-tightening spiral dive and is said to be spirally unstable. If the dihedral effect is large with respect to the spiral effect, the airplane rolls back, producing slip in the opposite direction to start the cycle over again. The result of the lag in this yaw-roll compensation is a type of pendulum-like motion akin to that of a person waltzing on skates, Figure 55. The name "Dutch Roll" given to it is taken from a classical skating maneuver. The physical discomfort accompanying Dutch Roll has led to much study of "yaw dampers" and other devices to increase stability in coupled yaw and roll.

Since wing sweep induces large dihedral effects, all swept-wing airplanes face the Dutch Roll problem. Spiral instability is not particularly undesirable, for the excursion is very slow and easily controlled, so the attack is usually made in the direction of increasing the tail components of dynamic stability. To do this by enlarging the tail or lengthening the tail moment arm to make the yawing moment large would add large weight and drag penalties. So a method of effectively mass over-balancing the rudder with yaw damping devices is sought. The effect is to make the deflection of the rudder lag the oscillation - producing forces to such a degree as to provide large damping effects. A number of dampers to accomplish this purpose have been developed. There is a yaw-damper effect built into the autopilot which serves to care for the yaw-damping requirements on the 707 airplanes and special electronic yaw dampers on the 727.

Flutter

The phenomenon of flutter and related aeroelastic problems are extremely important and very difficult. Most problems of this type involve aerodynamic forces, inertial effects and elasticity in combination with each other in very complex patterns. Every part of the structure of the modern aircraft is elastic in some degree and has a natural period of oscillation when disturbed and then released. Such oscillations may be in bending or torsion and may involve a large spectrum of related modes or "overtones."

The frequency of oscillation of the wing, for example, is well defined and is relatively fixed; there are slight changes with airspeed, but these are very small. However, if the wing is fitted with a free surface such as a flap or aileron or the tail, with a free elevator, this surface will have a tendency to oscillate elastically at a frequency which is determined by its inertia and the airspeed. The natural frequency increases with the airspeed and can vary rather widely. If the frequency of the surface should coincide with the natural frequency of the wing, its oscillation will be in resonance with the wing and will excite it to vibrate. When this occurs, the excitation forces and amplitudes may be of such magnitude as to completely overshadow the natural damping tendencies of each and to cause a divergent oscillation to be set up. The surface takes energy from the airstream into the wing to excite an oscillation instead of damping it. This wing movement then orients the control surface into an attitude

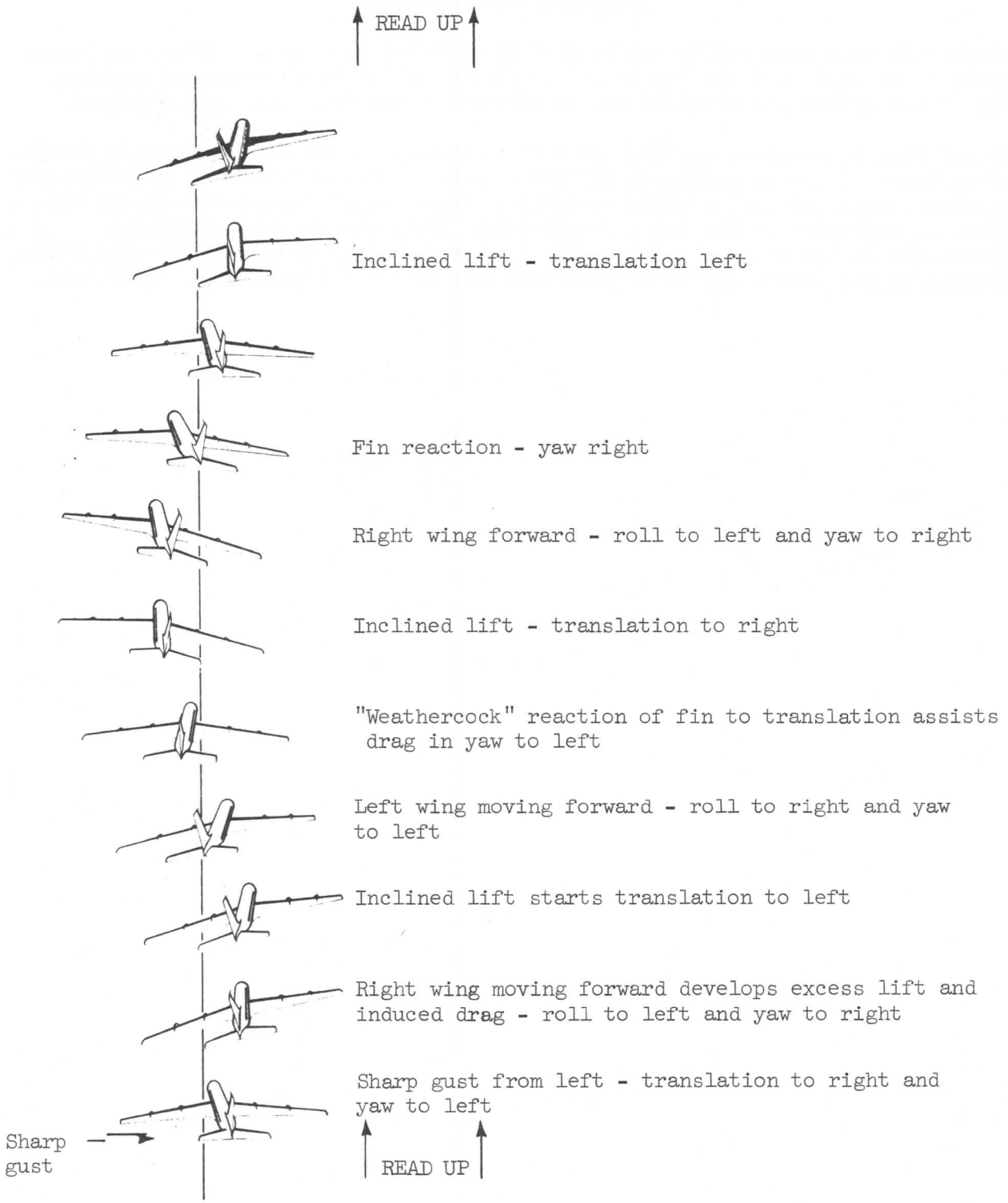

First cycle of a typical Dutch Roll development as viewed from aft and above the airplane.

Figure 55.

which will once more excite the wing to even higher amplitude. Often the divergence is so rapid and the forces are so large that serious structural problems can be met before the airspeed can be changed or adequate damping introduced.

Actual flutter problems are usually much more complicated than the simple example cited here. Coupling resonance may occur between many combinations of bending or torsional oscillations, surface movements, "organ pipe" frequencies in air columns, or multiples of the basic frequencies. Many aeronautical engineers specialize in the study of such problems, and the study is one of the most challenging in the modern fields of practical analysis and experimental techniques.